

Biological evaluation of halogenated flavone derivatives as antiangiogenic and anticancer agents



A thesis submitted to the University of Reading in partial fulfilment
for the degree of Doctor of Philosophy

School of Pharmacy

by

Mai Khater

July 2024

Declaration

I confirm that this is my own work and the use of all material from other sources has been properly and fully acknowledged.

MAI KHATER

“My success lies with Allah.

In Him I trust; and to Him, I turn”

Dedicated to my parents & my beloved husband

Acknowledgments

First, I would like to express my gratitude to my supervisors Prof Helen Osborn and Prof Francesca Greco for their constant support and valuable guidance throughout my PhD journey. I am truly thankful for the level of academic depth and understanding that I've gained from them during this PhD.

I would like to thank the Newton-Mosharafa Fund, British Council, Egypt for granting me this scholarship and funding my PhD studies at the University of Reading.

I would also like to thank Prof Kim Watson, Dr Sam Boateng and Dr John Brazier for their expertise and support in the fruitful collaborations we had during this project.

I am grateful for all the technical and administrative staff at the School of Pharmacy especially, Dr Radek Kowalczyk and Nicholas Michael (CAF lab) and Phillip Mason (Stores) for their valuable services.

My most sincere thanks go to fellow postgraduate students at the University of Reading especially my former and present lab and office mates (Esmie Wescott, Jack Cheesman, Sultan Ilyada, Ahmed Alhajmi, Tai Diep, Anum Sultana and Camilla Pergaro) where we shared our hopes, dreams and frustrations.

I would like to particularly thank my colleagues and dearest friends Az Alddien Natfji, Madonna Mitry, Ibrahim Shah, and Jamila Almahroogy for their technical, mental and emotional support throughout this journey. Your company is more than appreciated and it's a privilege knowing you on both the professional and the personal levels.

My most heartfelt thanks go to my close and extended family, particularly my brother, Ahmed Khater for his constant encouragement and being my role model in taking courageous decisions in life.

My beloved husband, Mahmoud Shahin, I can not thank you enough for your love and endless support and for putting up with lots of ups and downs and tolerating the encountered hardships with such grace.

To the best parents one could have, Ali Khater and Nawal Sobeih, I can not express with words how much I am grateful for the unconditional love and support you have showered me with. You have sacrificed a lot and endured many difficulties for me to achieve my goals and dreams. I would have never got this far without you.

Abstract

The key role of angiogenesis in the growth and metastasis of cancer has led to the inclusion of antiangiogenic therapy in cancer treatments, which has proved clinically beneficial when combined with cytotoxic effects in a multi-targeting approach (e.g. sunitinib is first line therapy for renal cancer). However, current multi-targeting therapies (administered as drug combinations or single drug) suffer from increased adverse events. Flavonoids present advantageous polypharmacological anticancer properties and are well tolerated. Hence, this study explores the bi-modal antiangiogenic and cytotoxic efficacy of a group of synthetic flavonoids as potential anticancer agents.

First, reported data on the antiangiogenic activities of flavonoids was analyzed via systematic and quantitative analyses, establishing their antiangiogenic effectiveness. Antiangiogenic structure activity relationship (SAR) data was extracted from the conducted analysis. Cytotoxic SARs were gathered from reported studies and combined with the antiangiogenic SAR, resulting in the design of two sets of 5,7/7,8-disubstituted-4'-chloro/bromophenyl flavones (**Chapter 2**). The designed flavones (**7-14**) were synthesized and spectroscopically characterized with good yields (60-97%) and purities (>90%). Compounds **9**, **11**, **12** and **14** particularly showed significant *in vitro* angiogenic inhibition against endothelial cell (EC) vascular endothelial growth factor (VEGF)-induced tube formation and migration (>50% and 25-37%, respectively, at 10 μM). The 4-thio derivatives **11** and **12** inhibited VEGFR2 phosphorylation (57 and 37% at 10 μM , respectively) in western blotting and were oriented in a favorable position inside its ATP binding site in a molecular docking study (**Chapter 3**).

Further optimization of the test compounds was investigated through ruthenium (Ru) or iridium (Ir) metal complexation based on their reported antiangiogenic/cytotoxic effectiveness. The novel Ru(II)-*p*-cymene complexes (**19** and **20**) of flavones **11** and **13** were successfully synthesized and spectroscopically confirmed with 46 and 30% yields, respectively (**Chapter 4**). The bi-modal anticancer effects of **11** and **13** in addition to the impact of Ru complexation on the measured effects were evaluated *in vitro* (**Chapter 5**). The lead thioflavone **11** displayed strong cytotoxic ($\text{IC}_{50}=1.2 \pm 0.8$ and $43.06 \pm 1.29 \mu\text{M}$ on MCF-7 and MDA-MB-231, respectively) and antimigratory activities (43% inhibition at 1 μM on MDA-MB-231) on breast cancer cells, in addition to the notable antiangiogenic effects on EC (e.g. 42% tube formation inhibition at 1 μM). These effects were comparable to reported values for the drug sunitinib in the same assays (e.g. $\text{IC}_{50}=5 \mu\text{M}$ on MCF-7, 50% tube formation inhibition at 10 μM). Complexation with Ru negatively impacted the tube formation inhibitory effects of **11** and **13**. Ru chelation diminished **11**'s cytotoxicity against MCF-7 and MDA-MB-231 breast cancer cells whereas the antimigratory activity against MDA-MB-231 was equivalent to the parent flavone. In contrast, Ru complexation enhanced the cytotoxic and antimigratory effects of the oxoflavone **13** against breast cancer cells (e.g. 50 versus 33% inhibition of MCF-7 migration, $p<0.05$). Finally, the test derivatives showed a presumably non-intercalative binding with VEGF and c-myc i-motif DNA, as novel anticancer targets, in UV-Vis spectroscopic studies (**Chapter 5**).

This work identified compound **11** as a promising anticancer agent with dual antiangiogenic and cytotoxic activities. Its structural features and interaction with the VEGF/VEGFR2 pathway provides a suitable base for extension towards novel anticancer applications in the future, such as the development of dual antiangiogenic and immunomodulatory agents (**Chapter 6**).

List of Publications

Khater, M.; Ravishankar, D.; Greco, F.; Osborn, H. M. I. Metal Complexes of Flavonoids: Their Synthesis, Characterization and Enhanced Antioxidant and Anticancer Activities. *Future Med. Chem.* 2019, 11 (21), 2845–2867.

Khater, M.; Greco, F.; Osborn, H. M. I. Antiangiogenic Activity of Flavonoids: A Systematic Review and Meta-Analysis. *Molecules* 2020, 25 (20), 4712–4742.

Khater, M.; Watson, K. A.; Boateng, S. Y.; Greco, F.; Osborn, H. M. I. Halogenated Flavonoid Derivatives Display Antiangiogenic Activity. *Molecules* 2022, 27 (15), 4757–4778.

Khater, M.; Brazier, J. A.; Greco, F.; Osborn, H. M. I. Anticancer evaluation of new organometallic ruthenium(II) flavone complexes. *RSC Med Chem* 2023, 14 (2), 253–267.

List of Conferences

M2M Science Plus Networking Event III, 2019, Thames Valley Science Park, UK.

Pharmacy PhD Showcase, 2019, University of Reading UK, Poster presentation: Exploring the antiproliferative and antiangiogenic activities of novel flavone derivatives.

M. Khater, F. Greco and H.M.I. Osborn

Annual GP2A Medicinal Chemistry Conference, 2019, Nottingham UK, Poster presentation: Design and synthesis of novel flavone derivatives as anticancer agents.

M. Khater, F. Greco and H.M.I. Osborn

10th APS International PharmSci Conference, 2019, Greenwich UK, Poster presentation: Synthesis of novel selenium and ruthenium flavone derivatives as anticancer agents.

M. Khater, F. Greco and H.M.I. Osborn

Pharmacy PhD Showcase, 2020, University of Reading UK, Winner of the best oral presentation: Exploring the antiproliferative activities of novel flavone derivatives.

M. Khater, F. Greco and H.M.I. Osborn

Pharmacy PhD Showcase, 2021, University of Reading UK, Oral presentation: Synthesis and cytotoxic activities of flavonoid metal complexes.

M. Khater, F. Greco and H.M.I. Osborn

Annual GP2A Medicinal Chemistry Online Conference, 2021

Table of contents

Chapter 1: General introduction	1
1.1. Current prospects in cancer therapy	3
1.2. Angiogenesis	7
1.2.1. Physiological angiogenesis	7
1.2.2. Tumor angiogenesis	8
1.2.3. Antiangiogenic targeted therapy	9
1.3. Flavonoids	15
1.3.1. Cytotoxic activity of flavonoids	17
1.3.2. Antiangiogenic activity of flavonoids	19
1.3.3. Clinical progression of flavonoids as anticancer agents	20
1.3.4. Improving flavonoids' bioavailabilities	22
1.4. Anticancer activity of ruthenium and iridium metal complexes	26
1.4.1. Anticancer activity of ruthenium metal complexes	26
1.4.2. Anticancer activity of iridium metal complexes	28
1.4.3. Anticancer activity of flavonoid ruthenium and iridium metal complexes	29
1.5. Project aim	30
Chapter 2: Design of lead flavonoids based on systematic review, meta-analysis, and structure activity relationship data	32
2.1. Introduction	33
2.2. Results and discussion	36
2.2.1. Systematic analysis of literature relating to the angiogenic activity of flavonoids	36
2.2.1.1. Search and selection of studies	36
2.2.1.2. Analysis of the involved studies	37
2.2.2. Meta-analysis of the antiangiogenic activity of flavonoids	42
2.2.2.1. Search and selection of studies	42
2.2.2.2. Characteristics and meta-analysis of the involved studies	43
2.2.2.3. Quality assessment	53
2.2.3. SAR studies	59
2.2.3.1. Antiangiogenic SAR study	59
2.2.3.2. Cytotoxic SAR study	62
2.2.4. Design of lead flavonoids	62
2.3. Conclusions and future perspectives	68

Chapter 3: Synthesis and <i>in vitro</i> evaluation of the antiangiogenic properties of halogenated flavones	69
3.1. Introduction	70
3.2. Results and discussion	75
3.2.1. Synthesis and structural characterization of the designed flavones	75
3.2.1.1. Synthesis and structural characterization of 4-oxo and 4-thio flavones	75
3.2.1.2. Attempted synthesis and structural characterization of 4-seleno flavones	80
3.2.2. <i>In vitro</i> evaluation of the antiangiogenic properties of the synthesized flavones	85
3.2.2.1. Cytotoxicity against endothelial cells	85
3.2.2.2. Inhibition of endothelial cells tube formation	86
3.2.2.3. Inhibition of endothelial cells migration	93
3.2.2.4. Exploring VEGFR2 as an antiangiogenic target	95
3.3. Conclusions and future perspectives	105
Chapter 4: Design, synthesis and characterization of flavone metal complexes	107
4.1. Introduction	108
4.2. Results and discussion	114
4.2.1. Synthesis and structural characterization of Ru(II)- <i>p</i> -cymene flavone complexes	114
4.2.1.1. 5,7-Dihydroxyl-4'-chlorophenyl Ru(II) complexes (19 and 20)	114
4.2.1.2. 7,8-Dihydroxyl-4'-bromophenyl Ru(II) complexes (21 and 22)	119
4.2.2. Attempted synthesis and structural characterization of Ir(III) Cp* flavone complexes	123
4.2.2.1. 5,7-Dihydroxyl-4'-chlorophenyl Ir(III) complexes (23 and 24)	123
4.2.2.2. 7,8-Dihydroxyl-4'-bromophenyl Ir(III) complexes (25 and 26)	125
4.3. Conclusions and future perspectives	126
Chapter 5: Antiangiogenic and cytotoxic evaluation of halogenated flavones and their Ru-complexes against breast cancer	127
5.1. Introduction	128
5.2. Results and discussion	131
5.2.1. <i>In vitro</i> antiangiogenic evaluation of Ru(II) complexes (19 and 20)	131
5.2.1.1. Cytotoxicity against endothelial cells	131
5.2.1.2. Inhibition of endothelial cells tube formation	132
5.2.2. <i>In vitro</i> anticancer evaluation on breast cancer cell lines	136
5.2.2.1. Cytotoxicity against breast cancer cells	136
5.2.2.2. Inhibition of breast cancer cells migration	138

5.2.3. I-motif DNA binding	141
5.3. Conclusions and future perspectives	144
Chapter 6: General discussion and future work	148
6.1. Introduction	149
6.2. Summary of the thesis	149
6.3. General discussion and future work	152
6.3.1. Clinical prospects for the use of flavonoids in cancer therapy	152
6.3.2. Clinical prospects for the use of antiangiogenic agents in cancer therapy	154
Chapter 7: Experimental	165
7.1. Materials	166
7.1.1. Chemistry	166
7.1.2. Cell culture	166
7.1.3. I-motif DNA binding	167
7.2. Equipment	167
7.2.1. Chemistry	167
7.2.2. Cell culture	168
7.2.3. I-motif DNA binding	168
7.3. Methods	168
7.3.1. Systematic review and meta-analysis	168
7.3.1.1. Search strategy	171
7.3.1.2. Inclusion and exclusion criteria	172
7.3.1.3. Data extraction	173
7.3.1.4. Data analysis	173
7.3.1.5. Quality assessment	175
7.3.2. Chemistry	178
7.3.2.1. Structural characterization	178
7.3.2.2. Synthesis	178
7.3.2.2.1. Synthesis of 4-oxo/thioflavones (7-14)	178
7.3.2.2.2. Attempted synthesis of 4-selenoflavones (15-18)	187
7.3.2.2.3. Synthesis of ruthenium and iridium metal complexes (19-26)	188
7.3.2.3. Stability of complexes (19 and 20)	191
7.3.3. Cell culture	192
7.3.3.1. General methods	192
7.3.3.1.1. Preparation of phosphate buffer saline (PBS)	192
7.3.3.1.2. Preparation of EGM-2 medium	192
7.3.3.1.3. Preparation of VEGF and VEGF enriched medium	193
7.3.3.1.4. Maintenance of cell lines	193
7.3.3.2. Antiangiogenic evaluation	196

7.3.3.2.1. Cytotoxicity on endothelial cells (trypan blue exclusion assay)	196
7.3.3.2.2. Endothelial cell Matrigel tube formation assay	197
7.3.3.2.3. Endothelial cell scratch assay	199
7.3.3.2.4. Western blotting	200
7.3.3.3. Anticancer evaluation against breast cancer cells	207
7.3.3.3.1. Cytotoxicity on breast cancer cells (MTT assay)	207
7.3.3.3.2. Breast cancer cells scratch assay	207
7.3.3.4. Molecular docking	208
7.3.3.5. I-motif DNA binding	209
7.3.3.6. Statistical analysis	211
References	212
Appendix A	241
Appendix B	314

List of Figures

Chapter 1

Figure 1.1. The VEGF family signaling pathways	8
Figure 1.2. A) Schematic diagram representing a turned on angiogenic-switch during tumorigenesis. (B) Tumor cells recruit different stromal cells (e.g. myeloid cells and fibroblasts) to the tumor site, together they release different growth factors and cytokines that induce angiogenesis	9
Figure 1.3. Schematic representation of antiangiogenic resistance mechanisms	10
Figure 1.4. Basic chemical structures of flavonoid subclasses	15
Figure 1.5. Chemical structures of flavonoids mentioned in this chapter	16
Figure 1.6. Schematic representation of the main anticancer mechanisms of action of flavonoids	17
Figure 1.7. Schematic presentation of the main routes of flavonoids absorption and metabolism in the human body	23
Figure 1.8. Schematic representation of the main cytotoxic mechanisms of action of Ru compounds	27
Figure 1.9. Outline of the presented PhD thesis	31

Chapter 2

Figure 2.1. PRISMA flow diagram of study search and selection process of the systematic review	37
Figure 2.2. Number of papers retrieved with respect to chemical subclass of flavonoid from the year 1997 to 2020. (A) Chemical structures of flavonoid subclasses; (B) Absolute number of studies; (C) Percentage of studies for each subclass relative to the total number of studies	39
Figure 2.3. Number of papers retrieved with respect to pharmacological application from the year 1997 to 2020. (A) Percentage of studies focusing on cancer, angiogenesis or other application relative to the total number of studies; (B) Absolute number of studies focusing on different types of cancer	40
Figure 2.4. Profiling of types of assays used for antiangiogenic evaluation of flavonoids from the year 1997 to 2020. (A) Percentage of studies using <i>in vitro</i> , <i>in vivo</i> assays or a combination of both; (B) Percentage of studies using different types of <i>in vivo</i> assays	41
Figure 2.5. PRISMA flow diagram of search and selection of study process for the meta-analysis	43

Figure 2.6. Schematic diagram of the CAM assay procedure for the 2 sets of involved studies	44
Figure 2.7. (A) Dose-response relationship at 3 concentration ranges: 10-20, 40-50 and 100 μM expressed as % of CAM vasculature inhibition relative to untreated control \pm SEM; (B) Forest plots of means ratio and 95% confidence interval (CI) of number of CAM blood vessels relative to untreated control at 10-20, 40-50 and 100 μM	49
Figure 2.8. Forest plot of means ratio and 95% confidence interval (CI) of number of CAM blood vessels of flavonoids at 10-20 μM relative to control on OVCAR-3 cell lines	52
Figure 2.9. Quality assessment of studies included in set 1 of meta-analysis	56
Figure 2.10. Quality assessment of studies included in set 2 of meta-analysis	57
Figure 2.11. Summary of the antiangiogenic SAR of flavonoids derived from set 1 of the meta-analysis	60
Figure 2.12. Schematic diagram of the design process of the lead flavonoids used in this project. Log P values were predicted using ADMET lab 3.0 web-server	63
 Chapter 3	
Figure 3.1. Structures of the designed compounds. Panel (B), 5,7-disubstituted-4'-chlorophenyl flavones; Panel (C), 7,8-disubstituted-4'-bromophenyl flavones	70
Figure 3.2. Percentage of studies using different types of <i>in vitro</i> assays used for antiangiogenic evaluation of flavonoids from the year 1997 to 2020	72
Figure 3.3. ^1H NMR spectrum of 3 showing double-doublet peaks of the 4'-chlorophenyl ring	79
Figure 3.4. (A) ^1H NMR spectra of compounds 7 and 9 showing downfield shift of H3; (B) ^{13}C NMR spectra of compounds 7 and 9 showing (4-C=O) and (4-C=S) peaks, respectively	79
Figure 3.5. (A) ^1H NMR spectra of compounds 8 and 10 showing downfield shift of H3; (B) ^{13}C NMR spectra of compounds 8 and 10 showing (4-C=O) and (4-C=S) peaks, respectively	80
Figure 3.6. Chemical structures of Lawesson's and Woollin's reagents	81
Figure 3.7. Stacked ^1H NMR spectra of 8 (black) and product of trial 1 for synthesis of 16 (blue)	82
Figure 3.8. Stacked ^1H NMR spectra of 8 (black) and product of trial 2 of 16 (blue) synthesis	83
Figure 3.9. ^1H and ^{13}C NMR spectra of reaction product of 15 synthesis	84

- Figure 3.10. Cell viability of HUVECs after 24 h of treatment with 40 μ M of the tested flavones (**7-14**). Data are expressed as mean \pm standard error of the mean (SEM), n = 3 86
- Figure 3.11. Antiangiogenic activity of the tested flavones (**7-14**) on *in vitro* HUVEC tube formation after 12 h of treatment with 1 μ M, expressed as a ratio to the +ve control (10 ng/mL VEGF-enriched media). (**A**) Representative images of tube formation assay at 4X magnification. Images were analyzed using Angiogenesis Analyzer macro in ImageJ software; (**B**) number of junctions, (**C**) number of meshes, (**D**) number and length of master segments and (**E**) number and length of segments. Data are expressed as mean \pm standard error of the mean (SEM), n = 3. Statistical significance was estimated with respect to the +ve control by one-way ANOVA, followed by Dunnett's multiple comparison test (* $p < 0.05$, ** $p < 0.01$, *** $p < 0.001$) 89
- Figure 3.12. Antiangiogenic activity of the tested flavones (**7-14**) on *in vitro* HUVEC tube formation after 12 h of treatment with 10 μ M, expressed as a ratio to the +ve control (10 ng/mL VEGF-enriched media). (**A**) Representative images of tube formation assay at 4X magnification. Images were analyzed using Angiogenesis Analyzer macro in ImageJ software; (**B**) number of junctions, (**C**) number of meshes, (**D**) number and length of master segments and (**E**) number and length of segments. Data are expressed as mean \pm standard error of the mean (SEM), n = 3. Statistical significance was estimated with respect to the +ve control by one-way ANOVA, followed by Dunnett's multiple comparison test (* $p < 0.05$, ** $p < 0.01$, *** $p < 0.001$) 91
- Figure 3.13. Summary of SAR considerations observed for the test flavones (**7-14**) on tube formation (TF) activity 92
- Figure 3.14. *In vitro* HUVEC wound closure (migration) inhibition activity of flavones (**9, 11, 12** and **14**) expressed as a ratio to the +ve control (10 ng/mL VEGF-enriched media). (**A**) Representative images of scratch assay at 0 h and 12 h at 10X magnification. Images were analyzed using ImageJ software; (**B**) Migration after 12 h as a ratio to +ve control. Data are expressed as mean \pm standard error of the mean (SEM), n = 3. Statistical significance was estimated with respect to the +ve control by one-way ANOVA, followed by Dunnett's multiple comparison test (* $p < 0.05$, ** $p < 0.01$, *** $p < 0.001$) 94

- Figure 3.15. VEGFR2 induced phosphorylation inhibition activity of flavones (**9**, **12**, **11** and **14**) on HUVEC cell lysates. (A) Representative western blot images of the HUVECs proteins; T-VEGFR2, P-VEGFR2 and β -Actin. Full blots are presented in **Figure 7.3, Chapter 7**. Images were analyzed using ImageJ software; (B) T-VEGFR2 quantification relative to β -actin; (C) VEGFR2-induced phosphorylation inhibition expressed as a ratio to the +ve control (10 ng/mL VEGF-enriched media). Data are expressed as mean \pm standard error of the mean (SEM), $n = 3$ except for **14** (1 μ M) where $n = 2$. (B) Statistical difference between the individual groups was estimated by one-way ANOVA, followed by Tukey's multiple comparison test, as recommended for pairwise comparisons (ns; non-significant, $p > 0.05$); (C) Statistical significance was estimated with respect to the +ve control by one-way ANOVA, followed by Dunnett's multiple comparison test, (* $p < 0.05$, *** $p < 0.001$) 96
- Figure 3.16. Schematic representation of the catalytic binding site of VEGFR2 /KDR. (A) ATP binding mode in active conformation; (B) Type I inhibitors binding mode, represented by sunitinib, in active conformation; (C) Type II inhibitors binding mode, represented by sorafenib, in inactive conformation 99
- Figure 3.17. Docking of the original co-crystallized ligand (N-{4-[4-amino-6-(4-methoxyphenyl)furo[2,3-d]pyrimidin-5-yl]phenyl}-n'-[2-fluoro-5-(trifluoromethyl)phenyl]urea) with VEGFR2 (1YWN). (A) 2D interaction of ligand with binding pocket; (B) 3D interaction of ligand with binding pocket showing key amino acids 100
- Figure 3.18. Interaction of flavones **11** and **12** (green) with VEGFR2 binding pocket compared to co-crystallized ligand (pink). (A) 3D of all 20 conformers of **11**; (B) 3D of all 20 conformers of **12**; (C) 3D of **11** top conformer; (D) 3D of **12** top conformer; (E) 2D of **11** top conformer; (F) 2D of **12** top conformer; (G) mesh representation of active vertical orientation of **11** (blue) and **12** (green) showing different regions of the catalytic site 102
- Figure 3.19. Comparison of the 3D interactions of flavones (**9**, **11**, **12** and **14**) in ATP-binding pocket of VEGFR2. (A) **9** (salmon) versus **11** (green); (B) **14** (salmon) versus **12** (green). HBs are represented by yellow dashed lines, clashes are represented by orange dashed lines 104

Figure 3.20. 3D interaction of all 20 conformers of flavones (green) with VEGFR2 binding site compared to co-crystallized ligand (pink). (A) 9 ; (B) 14 ; (C) 7 ; (D) 8 ; (E), 13	105
--	-----

Chapter 4

Figure 4.1. Schematic representation of the proposed metal complexation optimization strategies	108
Figure 4.2. Chemical structures of flavonoids from which organometallic derivatives have been prepared	110
Figure 4.3. Stacked ¹ H NMR spectra of (A) 11 and 19 ; (B) 13 and 20	116
Figure 4.4. ¹³ C NMR spectra of complexes (A) 19 ; (B) 20	117
Figure 4.5. Temperature dependent UV-Vis spectra of (A) 19 and (B) 20 in 0.1%DMSO/ddH ₂ O solution recorded over a 6 h time interval	118
Figure 4.6. MALDI-TOF MS of 21	120
Figure 4.7. ¹ H NMR spectrum of attempted Ru(II)- <i>p</i> -cymene complexation of 14 with 2.1 eq. NaOMe	122
Figure 4.8. ¹ H NMR spectrum of attempted Ru(II)- <i>p</i> -cymene complexation of 14 without NaOMe	123
Figure 4.9. ¹ H NMR spectra of attempted Ir(III)Cp* complexation of (A) 11 and (B) 13	125

Chapter 5

Figure 5.1. Standard double helix DNA and non-canonical i-motif structures	131
Figure 5.2. Cell viability of HUVECs after 24 h of treatment with 40 μM of the flavone Ru(II) complexes (19 and 20). Data are expressed as mean ± standard error of the mean (SEM), n = 3	132
Figure 5.3. Antiangiogenic activity of flavone Ru(II) complexes (19 and 20) and their free flavones 11 and 13 (added for comparison) on <i>in vitro</i> HUVEC tube formation after 12 h of treatment with 1 μM, expressed as a ratio to the +ve control (10 ng/mL VEGF-enriched media). (A) Representative images of tube formation assay at 4X magnification. Images were analyzed using Angiogenesis Analyzer macro in ImageJ software; (B) number of junctions, (C) number of meshes, (D) number and length of master segments and (E) number and length of segments. Data are expressed as mean ± standard error of the mean (SEM), n = 3. Statistical significance was estimated with respect to the +ve control (*) by one-way ANOVA, followed by Dunnett's multiple comparison test (*, <i>p</i> <0.05, ** <i>p</i> <0.01). Statistical pairwise significance (11 versus 19 and 13 versus 20) was estimated by one-way ANOVA (#),	133

followed by Tukey's multiple comparison test, as recommended for pairwise comparisons (# $p < 0.05$, ## $p < 0.01$)

- Figure 5.4. Antiangiogenic activity of flavone Ru(II) complexes (**19** and **20**) and their free flavones (added for comparison) on *in vitro* HUVEC tube formation after 12 h of treatment with 10 μ M, expressed as a ratio to the +ve control (10 ng/mL VEGF-enriched media). (A) Representative images of tube formation assay at 4X magnification. Images were analyzed using Angiogenesis Analyzer macro in ImageJ software; (B) number of junctions, (C) number of meshes, (D) number and length of master segments and (E) number and length of segments. Data are expressed as mean \pm standard error of the mean (SEM), $n = 3$. Statistical significance was estimated with respect to the +ve control (*) by one-way ANOVA, followed by Dunnett's multiple comparison test (* $p < 0.05$, ** $p < 0.01$, *** $p < 0.001$). Statistical pairwise significance (**11** versus **19** and **13** versus **20**) was estimated by one-way ANOVA (#), followed by Tukey's multiple comparison test, as recommended for pairwise comparisons (# $p < 0.05$) 135
- Figure 5.5. Cytotoxic activity of flavone **11** and its Ru(II) complex **19** against (A) MCF-7 and (B) MDA-MB-231 cancer cell lines. Data are expressed as mean \pm standard error of the mean (SEM), $n = 3$ 137
- Figure 5.6. Cytotoxic activity of flavone derivative **13** and its Ru(II) complex **20** against (A) MCF-7 and (B) MDA-MB-231 cancer cell lines. Data are expressed as mean \pm standard error of the mean (SEM), $n = 3$ 137
- Figure 5.7. *In vitro* MCF-7 migration (wound closure) inhibition activity of flavone derivative (**13**) and the Ru(II) complexes (**19** and **20**) expressed as a ratio to control. (A) Representative images of scratch assay at 0 h and 24 h at 4X Magnification. Images were analyzed using ImageJ software; (B) Migration after 24 h as a ratio to the control. Data are expressed as mean \pm standard error of the mean (SEM), $n = 3$. Statistical significance was estimated with respect to the control (*) by one-way ANOVA, followed by Dunnett's multiple comparison test (** $p < 0.01$, *** $p < 0.001$). Statistical pairwise significance for **13** versus **20** was estimated by one-way ANOVA (#), followed by Tukey's multiple comparison test, as recommended for pairwise comparisons (# $p < 0.05$) 139
- Figure 5.8. *In vitro* MDA-MB-231 migration (wound closure) inhibition activity of flavone derivatives (**11** and **13**) and the Ru(II) complexes (**19** and **20**) expressed as a ratio to control. (A) Representative images of scratch assay at 0 h and 24 h at 4X Magnification. Images were 141

analyzed using ImageJ software; (B) Migration after 24 h as a ratio to the control. Data are expressed as mean \pm standard error of the mean (SEM), n = 3. Statistical significance was estimated with respect to the +ve control (*) by one-way ANOVA, followed by Dunnett's multiple comparison test (* p <0.05, ** p <0.01, *** p <0.001). Statistical pairwise significance (**11** versus **19** and **13** versus **20**) was estimated by one-way ANOVA (#), followed by Tukey's multiple comparison test, as recommended for pairwise comparisons (## p <0.01)

- Figure 5.9. Absorption spectra of VEGF and c-myc i-motif DNA with the flavone derivatives (**11** and **13**) and their Ru(II) complexes (**19** and **20**) in 1:1 ratio. (A) VEGF i-motif interactions; (B) C-myc i-motif interactions 142
- Figure 5.10. Normalized UV melting curves for VEGF and c-myc i-motif DNA the flavone derivatives (**11** and **13**) and their Ru(II) complexes (**19** and **20**) at 295 nm at 1:1 ratio. (A) VEGF i-motif melt; (B) C-myc i-motif melt 143
- Figure 5.11. Summary of SARs for the anticancer effects of the flavone derivatives (**11** and **13**) and the Ru(II) complexes (**19** and **20**) 145

Chapter 6

- Figure 6.1. Summary of the key findings of the thesis 151
- Figure 6.2. Schematic diagram of the angiogenic-immune crosstalk 158

Chapter 7

- Figure 7.1. Representative images of *in vitro* HUVEC tube formation assay optimization after 12 h in VEGF enriched media (10 ng/mL) at 4X magnification. (A) 1 x10⁴ cells/well density; (B) 1.5 x10⁴ cells/well density; (C) 2 x10⁴ cells/well density 198
- Figure 7.2. BSA standard calibration curve used for HUVEC lysate protein content determination 201
- Figure 7.3. Raw western blot membrane for trials N1- N3 206

List of Schemes

Chapter 3

Scheme 3.1. Synthesis of flavones via Baker-Venkataraman rearrangement	71
Scheme 3.2. Synthesis of flavones via Claisen-Schmidt condensation	71
Scheme 3.3. Synthesis of flavones via Kostanecki-Robinson method	72
Scheme 3.4. Synthesis of 4-oxo and 4-thio- <i>p</i> -halophenyl flavone derivatives	75
Scheme 3.5. Keto-enol tautomerism of the β -diketone intermediates	78
Scheme 3.6. Attempted synthesis of 4-Seflavone derivatives (15-18)	81

Chapter 4

Scheme 4.1. Synthesis of Ru(II) complexes 19 and 20	114
Scheme 4.2. Attempted synthesis of Ru(II) complex 21	119
Scheme 4.3. Attempted synthesis of Ru(II) complexes 22a and 22b	120
Scheme 4.4. Attempted synthesis of Ir(III) complexes 23 and 24	124
Scheme 4.5. Attempted synthesis of Ir(III) complexes 25 and 26	125

List of Tables

Chapter 1

Table 1.1. Current cancer therapeutic approaches	5
Table 1.2. Main angiogenic factors	7
Table 1.3. Multi-target antiangiogenic therapy in clinical trials	13
Table 1.4. Anticancer effects of combined chemo and antiangiogenic therapies	14
Table 1.5. Reported <i>in vitro</i> VEGFR2 activity of flavonoids on ECs	19
Table 1.6. Overview of flavonoids registered at www.clinicaltrials.gov as anticancer agents since 2010	21
Table 1.7. Structural factors affecting flavonoids bioavailability and selected approaches to address them	24
Table 1.8. Advantages and disadvantages of selected flavonoid bioavailability enhancement approaches	25

Chapter 2

Table 2.1. Summary of systematic reviews relevant to the topic of flavonoids and angiogenesis	34
Table 2.2. Summary of SAR studies on the antiangiogenic activity of flavonoids	35
Table 2.3. Summary of antiangiogenic activity of flavonoids on tumor induced CAM vasculature	51
Table 2.4. Critical criteria included in the CAM assay methodological quality and risk of bias assessment checklist	54

Chapter 3

Table 3.1. Comparison of the most common <i>in vitro</i> angiogenesis assays	73
Table 3.2. Comparison of synthetic methods reported (Rep) for compounds (3 -14) by Ravashinkar <i>et al</i> and methods applied in this project (App)	77
Table 3.3. Reaction conditions for the attempted synthesis of 16	82
Table 3.4. Column chromatography optimization for purification of 15	83
Table 3.5. Amino acid residues defining the catalytic kinase domain of VEGFR2	98
Table 3.6. Amino acid residues interacting with different type I VEGFR2 inhibitors compared to leads 11 and 12 . The adenine mimicking scaffold of each molecule is highlighted in blue, while the shared amino acids between 11 and 12 and the included inhibitors are highlighted in bold	102

Chapter 4	
Table 4.1. Summary of synthetic conditions and characterization methods for flavonoid metal complexes	111
Table 4.2. λ_{260}^a and $\Delta \lambda_{260}^b$ of complexes 19 and 20 at 20 – 80 °C	118
Table 4.3. Attempted optimization of the deprotonation step for the synthesis of 22a or 22b	121
Chapter 5	
Table 5.1. Summary of antiangiogenic and cytotoxic activities reported for Ru(II) complexes against breast cancer	129
Table 5.2. Determined IC ₅₀ for flavone derivatives (11 and 13) and their Ru(II) complexes (19 and 20) against MCF-7 and MDA-MB-231. Data are expressed as mean \pm standard error of the mean (SEM), n =3	137
Table 5.3. Summary of UV-Vis data of VEGF and c-myc i-motifs in the presence of the flavone derivatives (11 and 13) and their Ru(II) complexes (19 and 20) at 1:1 ratio	143
Table 5.4. Anticancer effects of lead 11 as evaluated in this study compared to reported data for sunitinib and sorafenib taken from references as indicated	146
Chapter 6	
Table 6.1. Summary of antiangiogenic SAR conclusions of flavonoids available in the literature compared to SAR findings of this project	154
Table 6.2. Statistical significance (expressed as <i>p</i> -values) of levels of VEGF, PDGF and ICAM-1 factors in tumor (T) and serum (S) of primary breast cancer relative to T and S of benign breast lesions	155
Chapter 7	
Table 7.1. PRISMA-P 2015 Checklist. This checklist has been adapted for use with protocol submissions to Systematic Reviews from Table 3 in Moher D <i>et al</i> : Preferred reporting items for systematic review and meta-analysis protocols (PRISMA-P) 2015 statement. Systematic Reviews 2015 4:1	169
Table 7.2. Search strategy used to conduct the systematic review on ScienceDirect, PubMed and Web of Science electronic databases	171
Table 7.3. Search strategy used to conduct the meta-analysis on ScienceDirect, PubMed, Web of Science and Google Scholar electronic databases	172
Table 7.4. CAM assay methodological quality and risk of bias assessment checklist	176

Table 7.5. Components of media used for HUVECs culture and antiangiogenic evaluation	192
Table 7.6. Culture conditions for the cell lines used in this project	
Table 7.7. Composition of 7% resolving gel	195
Table 7.8. Composition of 3% stacking gel	202
Table 7.9. Composition of 10X running buffer	202
Table 7.10. Composition of 10X transfer buffer	202
Table 7.11. Composition of 10X tris buffer	203
Table 7.12. Composition of stripping buffer (pH 2.2)	204
Table 7.13. Supplier's data for VEGF and c-myc i-motif oligonucleotides	204
	210

Abbreviations

A2780	Ovarian cancer cell line
A375	Melanoma cell line
A431	Cervical cancer cell line
A549	Lung cancer cell line
Akt	Protein kinase B
Ala	Alanine
AML	Acute myeloid leukemia
ANOVA	Analysis of variance
Asp	Aspartic acid
ATP	Adenosine triphosphate
Bcl-2	B-cell lymphoma 2
br	Broad
BMS	Bristol Myers Squibb
BSA	Bovine serum albumin
C13*	Ovarian cancer cell line
CAM	Chick chorioallantoic membrane assay
CDK	Cyclin dependent kinase
CH1	Ovarian cancer cell line
CI	Confidence interval
CLL	Chronic lymphocytic leukemia
c-myc	Cellular myc oncogene
CONSORT	Consolidated standards of reporting trials
CR	Complete remission
CRC	Colorectal cancer
Cys	Cysteine
d	Doublet
dd	Double distilled
DNA	Deoxyribonucleic acid
DSF	Differential scanning fluorimetry
EC	Endothelial cell
ECL	Enhanced chemiluminescence
ECM	Extracellular matrix
EGF	Epidermal growth factor
ELISA	Enzyme linked immunosorbent assay
ERK	Extracellular signal-related kinase
ESI-MS	Electrospray ionization-mass spectrometry
FBS	Foetal bovine serum
FDA	Food and drug administration
FGF	Fibroblast growth factor
FT-IR	Fourier transform-infrared
GFR	Growth factor reduced
GI ₅₀	The half maximal growth inhibitory concentration
Glu	Glutamine

Gly	Glycine
GSK3R	Glycogen synthase kinase
HB	Hydrogen bond
HBA	Hydrogen bond acceptor
HCC	Hepatocellular carcinoma
HCC1954	Breast cancer cell line
HCT-15	Colon cancer cell line
HEK293	Non-transformed human embryonic kidney cell line
Hela	Cervical cancer cell line
HepG2	Hepatic cancer cell line
HIF	Hypoxia inducible factor
HPLC	High performance liquid chromatography
HTRF	Homogenous time-resolved fluorescence
HUVECs	Human umbilical vein endothelial cells
f	Higgin's heterogeneity measure
IC ₅₀	The half maximal inhibitory concentration
ICB	Immune checkpoint blockade
IFN- γ	Interferon- γ
Ileu	Isoleucine
ILs	Interleukins
IMR-90	Normal lung cell line
IV	Inverse variance
J	Coupling constant
Jurkat E6-1	Human leukemia cell line
K _d	Dissociation constant
K _i	Inhibition constant
LR	Lawesson's reagent
LD ₅₀	The half maximal lethal concentration
Leu	Leucine
log P	Logarithm of the octanol–water partition coefficient
Log β	Logarithm of the equilibrium constant for the formation of complex in solution
Lys	Lysine
m	Multiplet
m/z	Mass/charge ratio
mAb	Monoclonal antibody
MALDI-TOF	Matrix-assisted laser desorption ionization time-of-flight
MAPK	Mitogen activated protein kinase
MCF-7	Estrogen receptor positive breast cancer cell line
MDA-MB-231	Triple negative breast cancer cell line
Met	Methionine
MMPs	Matrix metalloproteinases
m.p	Melting point
mTOR	Mammalian target of rapamycin
NCI	National cancer institute

NCI-H460	National cancer institute non-small cell lung cancer cell line
NFAT	Nuclear factor of activated T-cells
NMR	Nuclear magnetic resonance
OHAT	Oral health assessment tool
OS	Overall survival
OVCAR-3	Ovarian cancer cell line
PBMC	Peripheral blood mononuclear cells
PBS	Phosphate buffer saline
PC-3	Prostatic cancer cell line
PD-1	Programmed cell death receptor 1
PDB	Protein data bank
PDGF	Platelet derived growth factor
PD-L1	Programmed cell death ligand 1
PDT	Photodynamic therapy
PFS	Progression free survival
Phe	Phenylalanine
PI3K	Phosphoinositide 3-kinase
Pin1	Peptide isomerase
PLGF	Placental growth factor
PRISMA	Preferred reporting items for systematic reviews and meta analyses
PVDF	Polyvinylidene difluoride
R ²	Coefficient of determination
Raf	Rapidly accelerated fibrosarcoma
RCC	Renal cell carcinoma
RIPA	Radioimmunoprecipitation assay
RMSD	Root mean square deviation
RoB	Risk of bias
ROS	Reactive oxygen species
s	Singlet
SARs	Structure activity relationships
SBE	Salvia plebeia extract
SD	Standard deviation
SDS-PAGE	Sodium dodecyl-sulfate polyacrylamide gel electrophoresis
SEM	Standard error of mean
SGC-7901	Gastric cancer cell line
SI	Selectivity index
SK-OV-3	Ovarian cancer cell line
SMIs	Small molecule inhibitors
SPR	Surface plasmon resonance
STAT3	Signal transducer and activator of transcription 3
SW480	Colon cancer cell line
SYRCLE	Systematic review centre for laboratory animal experimentation
T47D	Breast cancer cell line
TAMR-MCF-7	Tamoxifen resistant breast cancer cell line

TKIs	Tyrosine kinase inhibitors
T_m	Transition temperature
TNBC	Triple negative breast cancer
TNF- α	Tumor necrosis factor alpha
ToxRtool	Toxicological data reliability assessment tool
TrxR	Thioredoxin reductase
Tyr	Tyrosine
UV	Ultraviolet
v/v	Volume/volume
VCAM-1	Vascular cell adhesion molecule-1
VE-Cadherin	Vascular endothelial cadherin
VEGF	Vascular endothelial growth factor
VEGFR2	Vascular endothelial growth factor receptor 2
WR	Wollin's reagent
λ_{max}	Absorbance maximum

Chapter 1

General introduction

Overview

Tumors arise from malfunctioning cells and as such hold histological similarities with normal tissues despite their distinctive microscopic features [1]. This resemblance poses a challenge for chemotherapeutic drugs to differentiate between cancerous and normal cells which leads to severe systemic side effects. Efforts have therefore been directed towards selective therapeutic approaches, targeting specific features or conditions in the tumor microenvironment [2]. The relationships between tumor growth and metastasis and angiogenesis were first introduced by Judah Folkman in 1971. During tumorigenesis the angiogenic switch is turned on, tipping towards a proangiogenic state which drives the growth and invasion of cancer cells. In that context, the co-targeting of cytotoxic and angiogenic proteins/pathways by either combining different drugs in one regimen or using a single multi-targeting molecule has shown clinical benefits. For example, the addition of the anti-vascular endothelial growth factor (VEGF) antibody bevacizumab to fluorouracil/leucovorin/irinotecan colorectal cancer (CRC) treatment regimen increased the overall and progression free survivals (OS, PFS) from 15.6 and 6.2 months to 20.3 and 10.6 months, respectively ($p < 0.001$), in a phase III clinical trial [3]. Multi-target tyrosine kinase inhibitors (TKIs) such as sunitinib, sorafenib and axitinib target the proangiogenic vascular endothelial growth factor receptor 2 (VEGFR2) among others, and are currently used as first line therapy for renal cell (RCC) and hepatocellular (HCC) carcinomas [4]. Nevertheless, the available antiangiogenic/cytotoxic drug combinations or monotherapies are associated with high toxicity and susceptibility to resistance which greatly limits their pharmacological effectiveness [5].

Flavonoids are chemical compounds of natural origin that are well tolerated by the human body [6]. They are reported to elicit multi-targeting effects, involving key proliferative and angiogenesis regulators such as the phosphoinositide 3-kinase (PI3K) and mitogen activated protein kinase (MAPK) pathways, VEGF and matrix metalloproteinases (MMPs) [7–9]. These attributes suggest that flavonoids can provide pharmacological benefits, in terms of potency, along with the potential to overcome resistance and safety, as bi-modal antiangiogenic/cytotoxic anticancer agents. However, natural flavonoids suffer from poor bioavailability that incapacitates their clinical progression [10]. In that regard, synthetic

flavonoids can be strategically designed in a manner that augments flavonoids' desired biological properties and addresses their pharmacokinetic challenges. Hence, this study aims to explore the potential of synthetic flavonoids as bi-modal antiangiogenic/cytotoxic anticancer agents.

In order to clarify the rationale of this project, this chapter will provide background information on current cancer treatment approaches (**Section 1.1**). The role of angiogenesis in tumor development will then be discussed (**Section 1.2**) in light of the use of targeted antiangiogenic therapy in cancer treatment (**Section 1.2.3**). The challenges and opportunities of combining antiangiogenic and cytotoxic effects as a multi-targeting cancer therapeutic strategy will also be reviewed in **Section 1.2.3**. The proposed bi-modal anticancer effects of flavonoids will then be rationalized in terms of their reported cytotoxic and antiangiogenic activities (**Section 1.3**). Flavonoids' limited bioavailability which poses a significant challenge for their development for clinical usage, as well as possible ways to overcome this, will be discussed in **Section 1.3.4**. Anticancer activities of ruthenium (Ru) and iridium (Ir) metal compounds will finally be presented as an explored structure activity optimization strategy for enhancing the pharmacological and pharmacokinetic properties of the target flavonoids (**Section 1.4**).

1.1. Current prospects in cancer therapy

Ranking second in worldwide causes of death, cancer was responsible for 10 million deaths in 2020 [11]. In 2040, 27.5 million new annual cases are expected worldwide [12]. The advances in the comprehension of the molecular alterations associated with cancer progression have not been matched to the same extent by advancements of cancer treatment. For instance, mortality rates for all cancers in the UK have decreased by 19% since the 1970s [13]. In the United States, the age-standardized death rates from malignant neoplasms changed from 194 per 100,00 in 1950 to 146 per 100,000 in 2019 [14]. These improved statistics are arguably low especially that they are not wholly due to improvement in treatment options, for example they can be partly attributed to earlier detection by improved diagnostic techniques, increasing the time span between first diagnosis and end-stage disease. Hence, traditional therapeutic approaches of surgery, radio and chemotherapy need to be complemented by alternative approaches to realize

a step change in cancer therapy. Accordingly, significant improvements in cancer treatment can be accelerated via research into novel therapeutics. **Table 1. 1** summarizes the available conventional and advanced cancer therapeutic approaches and provides an overview of their most important advantages and drawbacks [2,15].

Conventional anticancer therapy includes surgery, radiotherapy and chemotherapy or a combination of those. While surgery and radiotherapy target localized tumors [1,2,15], chemotherapy involves the systemic treatment of cancer via the administration of chemical agents. These agents target malfunctioning proteins and cellular cascades, that would normally promote tumor's growth and progression [1]. However, chemotherapy often results in debilitating side effects due to the lack of specificity for cancer cells over normal ones. The development of resistance is another major limitation of conventional chemotherapy that renders the treatment ineffective after an initial cytotoxic response [2]. Hence, novel anticancer approaches have focused on targeted therapy or precision medicines, in order to achieve higher selectivity that translates into fewer side effects. Of particular interest are agents targeting the tumor vascularization, discussed in the following section.

Table 1. 1. Current cancer therapeutic approaches [2,15]

Strategy	Remarks	Advantages	Disadvantages	FDA approved example
Surgery	Suitable for localized solid tumors	<ul style="list-style-type: none"> • Curative in case of removal of the whole tumor mass • Instant relief of symptoms 	<ul style="list-style-type: none"> • May not remove all cancer cells • Surgical risks such as bleeding and damage to nearby tissues 	n/a
Radiotherapy	Given at different stages either alone or combined with surgery and/or chemotherapy	<ul style="list-style-type: none"> • Eradicates large proportion of cancer cells • Shrinks tumor's size 	<ul style="list-style-type: none"> • Damage to surrounding healthy tissues and organs • Inability to target all cancer cells (e.g. cells that do not appear on the imaging scan) 	n/a
Conventional chemotherapy	Given at different stages either alone or combined with surgery and/or radiotherapy	<ul style="list-style-type: none"> • Highly effective in reaching cancer cells throughout different parts of the body • Slows tumor's growth • Shrinks tumor's size 	<ul style="list-style-type: none"> • High toxicity to healthy tissues and organs • Resistance may develop 	Paclitaxel for breast, ovarian, lung cancer and others
Stem cells	<ul style="list-style-type: none"> • Do not usually directly affect cancer cells • Help the body regenerate bone marrow cells destroyed during other treatments • Types: embryonic, pluripotent, hematopoietic, neural, mesenchymal and cancer stem cells 	<ul style="list-style-type: none"> • Effective • Extend survival 	<ul style="list-style-type: none"> • Tumorigenesis • Adverse events during transplantation • Drug toxicity and resistance • Increased immune responses and autoimmunity 	Sipuleucel-T (pluripotent stem cells) for prostatic cancer

Targeted therapy	<ul style="list-style-type: none"> • Interferes with specific targets blocking tumor's growth or propagation • Types: monoclonal antibodies (mAb) and small molecule inhibitors (SMIs) 	<ul style="list-style-type: none"> • Selective • Less toxicity and side effects 	<ul style="list-style-type: none"> • Unknown long-term side effects • Resistance may develop • Efficacy subject to tumor type and isoform 	<p>Nivolumab (mAb) and sunitinib (SMI) for renal cell carcinoma</p>
Gene therapy	<ul style="list-style-type: none"> • Introduction of pro-apoptotic, chemosensitizing, tumor suppressor, immune response eliciting genes or silencing of oncogenes • New generation based on small interfering RNAs (siRNAs) for targeted gene silencing 	<ul style="list-style-type: none"> • Effective • For siRNAs: <ul style="list-style-type: none"> • High efficacy • Safe 	<ul style="list-style-type: none"> • Immune system neutralization • Drug delivery limitations • Genome integration • For siRNAs: <ul style="list-style-type: none"> • <i>in vivo</i> instability • Off-target effects 	<p>Genicine (induces p53 expression) for neck and head squamous cell carcinoma</p>
Ablation	<ul style="list-style-type: none"> • Destroys tumors via exposure to thermal or electromagnetic changes • Types: thermal, radiofrequency, microwave, ultrasound and cryoablation 	<ul style="list-style-type: none"> • Non-invasive • Higher precision compared to surgery 	<ul style="list-style-type: none"> • Local effect • Needs technical expertise 	<p>n/a</p>

n/a, not applicable.

1.2. Angiogenesis

1.2.1. Physiological angiogenesis

Angiogenesis (the formation of new blood vessels from existing ones) is a highly complex process that is regulated by different types of cells and a plethora of signaling pathways. A monolayer of endothelial cells (ECs) forms the internal lining of blood vessels, bordered by pericytes and a basement membrane (i.e. mural tissue) [16]. The surrounding extracellular matrix (ECM) is rich in fibrillar proteins such as collagen and elastin in addition to other types of cells such as fibroblasts. In order for new vessels to sprout, ECs convert to an actively proliferating phenotype, breaking the junctions with neighboring cells and migrating through the ECM towards chemotactic and angiogenic stimuli [16]. At physiological conditions, angiogenesis is balanced by the counteracting effects of endogenous pro and antiangiogenic factors. The many cytokines and growth factors regulating angiogenesis include VEGF, fibroblast growth factor (FGF), platelet derived growth factor (PDGF), epidermal growth factor (EGF), angiopoietins and thrombospondins (**Table 1. 2**). Different cell types, such as ECs, fibroblasts, platelets and cancer cells, are capable of secreting these angiogenic factors [16]. However, its the VEGF family that predominantly regulates angiogenesis (**Figure 1. 1**). VEGF's activation of its main receptor VEGFR2 is highly correlated with sustaining normal vasculature and also to the pathogenesis of complex diseases like cancer [17]. VEGFR2 governs EC survival via the PI3K/Akt pathway, which modulates the apoptotic proteins B-cell lymphoma 2 (Bcl-2) and caspase-9 [17]. VEGFR2 also guides EC proliferation through the rapidly accelerated fibrosarcoma (Raf-MEK-ERK) cascade, activating DNA synthesis. Furthermore, VEGFR2 phosphorylation regulates EC migration via the activation of PI3K and the upstream protein SHB [17].

Table 1. 2. Main angiogenic factors

Angiogenic factor	Role in angiogenesis
VEGFA-E, PLGF	Induce angiogenesis, permeability and adhesion
PDGFA-D	Recruit pericytes
FGF1, 2, HIF	Induce angiogenesis
MMPs	Remodel BM and ECM, liberate growth factors

Angiopoietins	Regulate vessel maturation/destabilization and permeability
Endostatin	Inhibit EC survival and migration

VEGF, vascular endothelial growth factor; PLGF, placental growth factor; PDGF, placental derived growth factor; FGF, fibroblast growth factor; HIF, hypoxia-inducible factor; MMPs, matrix metalloproteinases; BM, basement membrane; ECM, extracellular cell matrix; EC, endothelial cell.

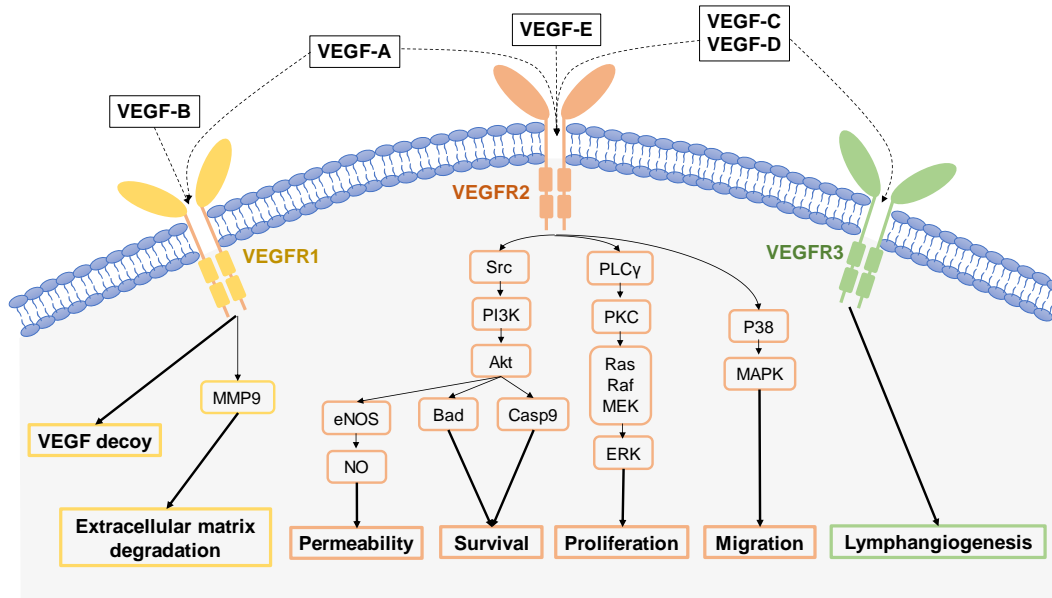


Figure 1. 1. The VEGF family signaling pathways [18]

VEGF, vascular endothelial growth factor; VEGFR1 to 3, vascular endothelial growth factor receptors 1 to 3; MMP9, matrix metalloproteinase 9; Src, cytoplasmic protein tyrosine kinase; PI3K, phosphatidylinositol-3-kinase; Akt, protein kinase B; eNOS, endothelial nitric oxide synthase; NO, nitric oxide; Bad, BCL2 associated agonist of cell death, Casp9, caspase 9; PLCγ, phospholipase C; PKC, protein kinase C; Ras, rat sarcoma; Raf, rapidly accelerated fibrosarcoma; MEK, mitogen-activated protein kinase; ERK, extracellular signal-regulated kinase; MAPK, mitogen-activated protein kinase.

1.2.2. Tumor angiogenesis

Tumors, like normal tissues, require nutrients and oxygen for their growth and survival. Tumors were observed to preferentially grow next to blood vessels since the 1950s [1]. Indeed, tumor cells located more than 0.2 mm (the effective range for oxygen transport through tissues) away from the blood supply exhibited no growth [1]. Judah Folkman first made the observation that tumors rely on angiogenesis to grow and metastasize. In that regard, a study of cancer evolving in the pancreatic islets of transgenic mice showed intriguing results. At early stages, hyperplastic islets grew to a maximum diameter of 0.1 to 0.2 mm [19]. The formed islets then entered a temporary phase of a sustained size achieved by the balance between uncontrolled cell proliferation and cell attrition via apoptosis (programmed cell death). Once these preneoplastic cells gained the ability to

induce angiogenesis, they broke the attained size and formed larger cancerous tumor masses. In this case, the so called “angiogenic-switch” is turned on where the tumor acquires a proangiogenic state [19] (**Figure 1. 2**). Additionally, high tumor vascularity is strongly related to enhanced metastatic potential. The increased proportion of newly formed leaky and permeable vessels after angiogenesis provides an escape route for cancer cells into the blood stream (intravasation) to reach distant organs [20].

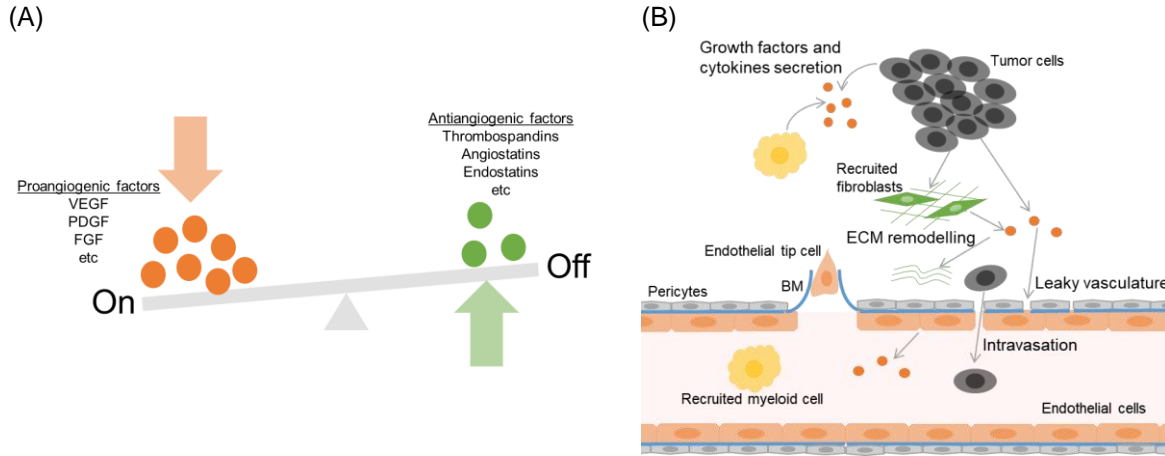


Figure 1. 2. (A) Schematic diagram representing a turned on angiogenic-switch during tumorigenesis. (B) Tumor cells recruit different stromal cells (e.g. myeloid cells and fibroblasts) to the tumor site, together they release different growth factors and cytokines that induce angiogenesis.

Similar to its crucial role in physiological angiogenesis, the VEGF/VEGFR2 system plays a critical role in tumor survival, growth and metastasis [21]. VEGFR2 is highly overexpressed in many cancers such as ovarian (100%), pancreatic (80%), colon (71.4%), breast (64.5%) and bladder (50%) cancers [22]. This upregulation results in an escalation in the tumor vascularization by means of increased EC sprouting, permeability, MMPs expression and matrix degradation [22]. Accordingly, VEGF/VEGFR2 targeted therapy is widely explored in cancer treatment clinical applications.

1.2.3. Antiangiogenic targeted therapy

The dependence of cancer growth and propagation on angiogenesis makes it an attractive target as an anticancer therapeutic approach. Furthermore, the complexity of the angiogenic process provides multiple target cells and signaling pathways for anticancer intervention [1,23]. As a result, a category of anticancer medications specifically blocking angiogenesis (i.e. antiangiogenic agents) as a targeted therapeutic

strategy has emerged. Currently, multiple antiangiogenic agents are used as first and second line therapies in the treatment of several cancers such as CRC, ovarian and advanced gastric carcinomas [24]. These agents are mostly monoclonal antibodies (mAb) or small molecule inhibitors (SMIs) targeting the VEGF pathway. However, tumors are able to circumvent the antiangiogenic actions of the used agents by acquiring resistance. As summarized in **Figure 1. 3**, tumors adopt different neovascularization strategies after an initial period of vessel regression which in some cases leads to less than expected clinical outcomes, disease relapse and increased metastasis [21,25–28]. For instance, ramucirumab (mAb with high affinity to VEGFR2) resulted in significant improvement in PFS (2.8 versus 2.1 months for placebo, $p<0.001$) of HCC patients while no improvements were observed for the OS (9.2 versus 7.6 months for placebo, $p=0.1391$) in a phase III trial [29]. In a phase II study, sunitinib discontinuation elicited a compensatory 4-fold increase in EC proliferation in RCC patients compared to non-treated controls ($p<0.003$) which positively correlated with the time of treatment discontinuation ($p<0.001$) [30].

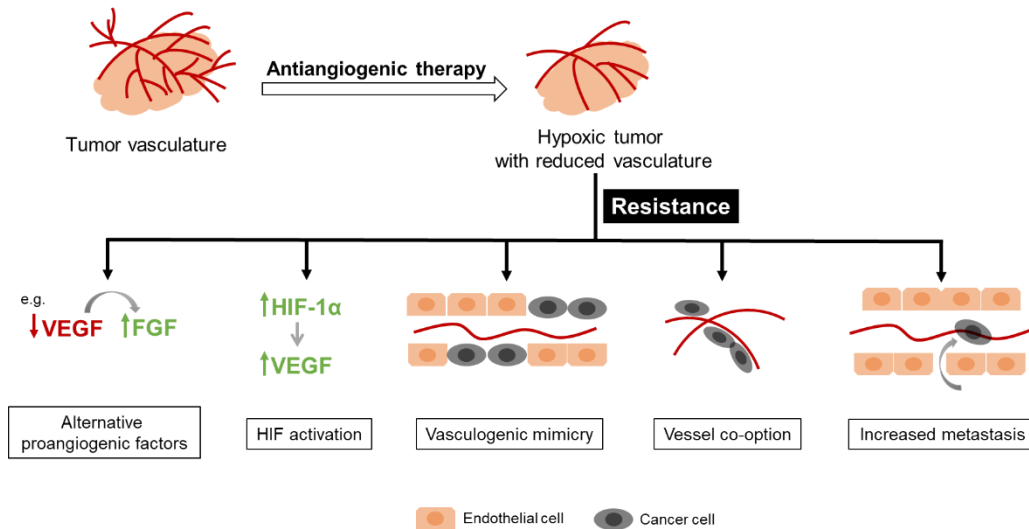


Figure 1. 3. Schematic representation of antiangiogenic resistance mechanisms. Tumors can shift their reliance on one proangiogenic factor to another in order to maintain proangiogenic conditions [25]. The tumor hypoxic environment created by antiangiogenic therapy can upregulate the hypoxia-inducible factor (HIF-1 α) that results in VEGF upregulation [21]. Tumors adopt neovascularization models, like vasculogenic mimicry and vessel co-option [21]. Cancer cells either adopt endothelial properties and form endothelial like vascular assemblies [26,27] or hijack existing vasculature and expand along its sides [21]. Antiangiogenic therapy can increase cancer cell metastasis and invasion through increased vasculature leakiness [28].

Consequently, antiangiogenic multi-targeting strategies have been exploited in preclinical and clinical settings in order to simultaneously block some of the tumors' angiogenic

escape routes. As shown in **Table 1. 3**, the concurrent inhibition of different proangiogenic factors, administered as mono or combined therapies, has demonstrated promising clinical efficacy against several metastatic and advanced cancers [31]. The combination of chemotherapeutic and antiangiogenic treatments represents yet another multi-targeting avenue. As outlined in **Table 1. 4**, such a combination is motivated by the enhanced delivery of cytotoxic agents to tumors due to the transient normalization of the tumor's vasculature and the decrease in intratumoral pressure [25]. Additionally, the cytotoxic effects of chemotherapeutic agents can alleviate some of the antiangiogenic tumor resistance mechanisms manifested in adopting neovascularization models like vascular mimicry and vessel co-option [21]. Moreover, cytotoxic agents can mitigate the increase in cancer cell metastasis and invasion resulting from the increased vasculature leakiness due to antiangiogenic therapy [28]. In fact, chemotherapeutic and antiangiogenic co-targeting exhibited good anticancer clinical outcomes. A phase II study for example, showed that 58 and 72% of inflammatory breast cancer (highly aggressive form) patients reached a 5-year disease free survival and OS, respectively, after receiving a combined treatment of bevacizumab with carboplatin, paclitaxel and cyclophosphamide [32]. In that regard, antiangiogenic drugs such as bevacizumab, aflibercept and ramucirumab are approved for use against cervical cancer, CRC and non-small cell lung carcinoma, respectively, in combination with paclitaxel/cisplatin, fluorouracil/leucovorin/irinotecan and erlotinib regimens, respectively [24].

Despite the reported therapeutic benefits of antiangiogenic and/or cytotoxic multi-targeting, treatment related grade 3 or higher adverse events are often induced [31]. Vascular toxicities from antiangiogenic therapy manifest as severe hypertension, and hand and foot syndrome, as well as elevated levels of thyroid stimulating hormone and cholesterol. Combined with chemotherapeutic side effects, patients' tolerance for these regimens poses challenges. In a recent phase II clinical study combining apatinib with etoposide against resistant ovarian cancer, 20% of the enrolled patients discontinued the treatment due to adverse events such as neutropenia, thrombocytopenia and hypertension [33]. Besides toxicity, the co-administration of chemotherapeutic and antiangiogenic drugs is clinically complicated with regards to dosage scheduling and the occurrence of drug-drug interactions [5,34]. In this context, the use of phytochemical

flavonoids is emerging as an attractive alternative multi-targeting approach [31]. The polypharmacological effects of these dietary agents alongside their tolerability presents opportune anticancer modalities [31].

Table 1. 3. Multi-target antiangiogenic therapy in clinical trials. Table adapted from Vafopoulou, P.; Kourti, M. *J. Cancer Metastasis Treat.* 2022, 8 [31].

Antiangiogenic agent [Ref]	Cancer	Targets	Clinical phase	OS (months)	PFS (months)	Side effects (grade \geq 3)
Anlotinib [35]	Refractory metastatic soft tissue sarcoma	VEGFR, PDGFR EGFR, FGFR RET, Aurora-B c-KIT, c-FMS DDR1	II	12	5.6	Hypertension, hypertriglyceridemia, pneumothorax, no deaths
Anlotinib [36]	Advanced NSCLC		III	9.6 (placebo=6.3)	5.4 (placebo=1.4)	Hypertension, hyponatremia, no deaths
Surufatinib [37]	Advanced pancreatic neuroendocrine cancer	VEGFR1-3, FGFR1	III	n/r	10.9 (placebo=3.7)	Hypertension, proteinuria, hypertriglyceridemia, 3 deaths
Regorafenib [38]	Advanced CRC	VEGFR1-3, PDGFR- β , FGFR TIE2, KIT, RET RAF	II	7.4	3.5	Hypertension, hand-foot skin reaction, hypophosphataemia, no deaths
Lenvatinib + pembrolizumab [39]	Metastatic RCC Endometrial cancer NSCLC SCCHN Urothelial cancer Melanoma	<u>Len</u> : VEGFR1-3 FGFR1-4, PDGFR α , KIT RET <u>Pem</u> : PD-1R	I/II	n/r	19.8 9.7 5.9 4.7 5.4 5.5	Fatigue, diarrhea, hypertension, hypothyroidism, 2 deaths
Axitinib + pembrolizumab [40]	Advanced RCC	<u>Ax</u> : VEGFR1-3 PDGFR, c-KIT <u>Pem</u> : PD-1R	I	n/r	20.9	Hypertension, diarrhea, fatigue, elevated alanine aminotransferase levels, no deaths
Axitinib + pembrolizumab [41]	Advanced RCC		III	n/r	15.4 (sunitinib=11.1)	Hypertension, alanine aminotransferase increase, diarrhea, no deaths

NSCLC, non-small cell lung carcinoma; CRC, colorectal carcinoma; RCC, renal cell carcinoma; SCCHN, Squamous cell carcinoma of the head and neck; VEGFR, vascular endothelial growth factor receptor; PDGFR, platelet-derived growth factor receptor; EGFR, epidermal growth factor receptor; FGFR, fibroblast growth factor receptor; RET, rearranged during transfection; c-KIT: tyrosine-protein kinase KIT or mast/stem cell growth factor receptor; c-FMS, colony stimulating factor; DDR1, discoidin domain receptor1; TIE2, angiopoietin-1 receptor; RAF, rapidly accelerated fibrosarcoma; PD-1R, programmed cell death protein 1 receptor; OS, overall survival; PFS, progression-free survival; n/r, not reported.

Table 1. 4. Anticancer effects of combined chemo and antiangiogenic therapies

Activity	Effect	Example
Antiangiogenic		
Vascular normalization	Enhanced tumor delivery of chemotherapeutic agents	Anti-VEGFR2 antibody DC101 normalized tumor vessels demonstrated a significant change in vessel diameter distribution and perivascular coverage compared to control ($p < 0.001$) in murine mammary carcinoma [42]. DC101 significantly increased the tumor penetration length of bovine serum albumin compared to control ($p < 0.05$) in murine mammary carcinoma [42].
Decreased intratumoral pressure		Anti-VEGFR2 antibody DC101 lowered intratumoral pressure by 50% compared to control in murine mammary carcinoma [42].
Chemotherapeutic		
Cancer cell cytotoxicity	Alleviate vascular mimicry and vessel co-option antiangiogenic tumor resistance mechanisms	Vincristine and dasatinib liposomes reduced vascular mimicry in MDA-MB-231 xenografted mice via induction of apoptosis, resulting in 66% inhibition of tumor volume compared to 19% for control ($p < 0.05$) [43].
	Decrease cancer cell metastasis and invasion resulting from the increased vasculature leakiness due to antiangiogenic therapy	Doxorubicin, topotecan and gemcitabine combination reversed sunitinib-induced lung carcinoma metastasis in xenograft models [44].

MDA-MB-231, triple negative breast cancer cell line.

1.3. Flavonoids

Research on the nature-derived flavonoids first gained momentum in the 1990s, fueled by their association with a lower incidence of coronary heart disease, stroke and cancer in several studies [45–47]. To date, the number of publications on the pharmacological activities of flavonoids have reached around 2000 articles/year with more than 10,000 identified flavonoids [48].

Flavonoids are polyphenolic compounds with a 15 carbon skeleton which is comprised of two phenyl rings (A and B) connected by a 4H-pyran ring (C ring) as shown in **Figure 1. 4**. They are classified into subgroups based on their degree of oxidation, C ring substitutions and the position of the B ring (**Figure 1. 4**) [49].

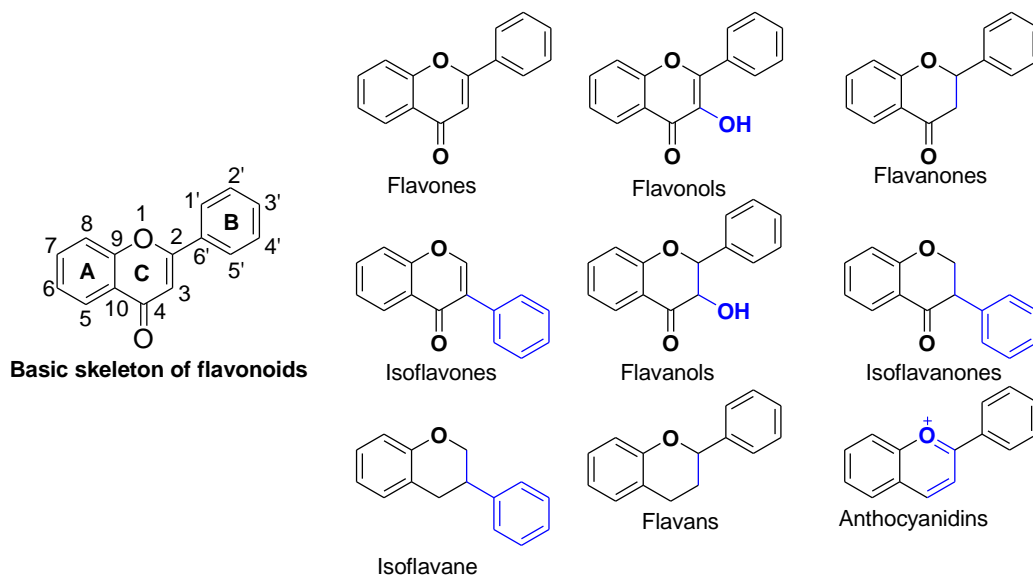


Figure 1. 4. Basic chemical structures of flavonoid subclasses

In general, flavonoids exhibit low toxicity with examples such as naringenin, apigenin and luteolin (**Figure 1. 5**) having LD₅₀ (the half maximal lethal concentration) values of >5000 mg/kg in mice [50]. In a pilot investigation of 32 men with chronic prostatitis, the flavonol quercetin showed no adverse events when administered orally at a dose of 1 g/day [51]. In another study, 47 healthy overweight individuals showed no statistical differences in blood safety parameters such as kidney and liver function after consuming 900 mg/day of a citrus fruit extract containing at least 90% catechin (of total polyphenols) and 20% naringenin (of total flavanones) for 12 weeks [52]. Similarly, a systematic study of 30

randomized controlled trials (n=5166) on the effects of flavonoids on viral acute respiratory tract infections reported no difference in the incidence of adverse events between the flavonoid and control groups [53].

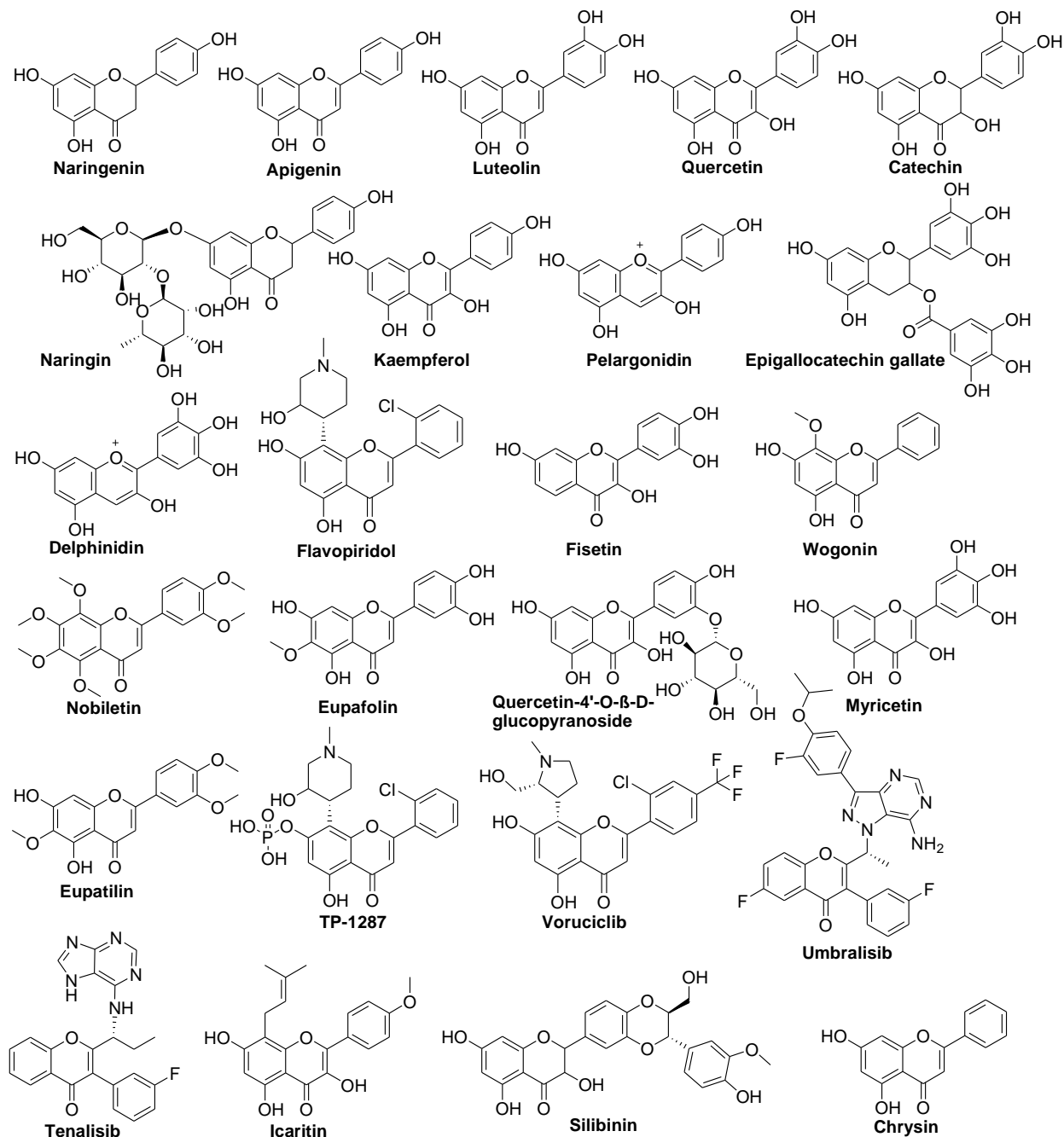


Figure 1. 5. Chemical structures of flavonoids mentioned in this chapter

The wide range of biological activities that have been attributed to flavonoids include but are not limited to antioxidant [54], antiinflammatory [55], antimicrobial [56],

cardioprotective [57], neuroprotective [58] and anticancer activities [59]. Besides their inherent pharmacological activities, flavonoids offer other advantages such as structural diversity and ready availability that make them attractive candidates for the development of bioactive lead compounds. Of relevance to this project are the cytotoxic and antiangiogenic anticancer effects of flavonoids that are reviewed next.

1.3.1. Cytotoxic activity of flavonoids

Flavonoids are known to inhibit cancer by interfering with an array of targets affecting cancer growth and progression. The cytotoxic mechanisms of action of flavonoids include induction of apoptosis and cell cycle arrest as well as proliferation inhibition as shown in **Figure 1. 6.**

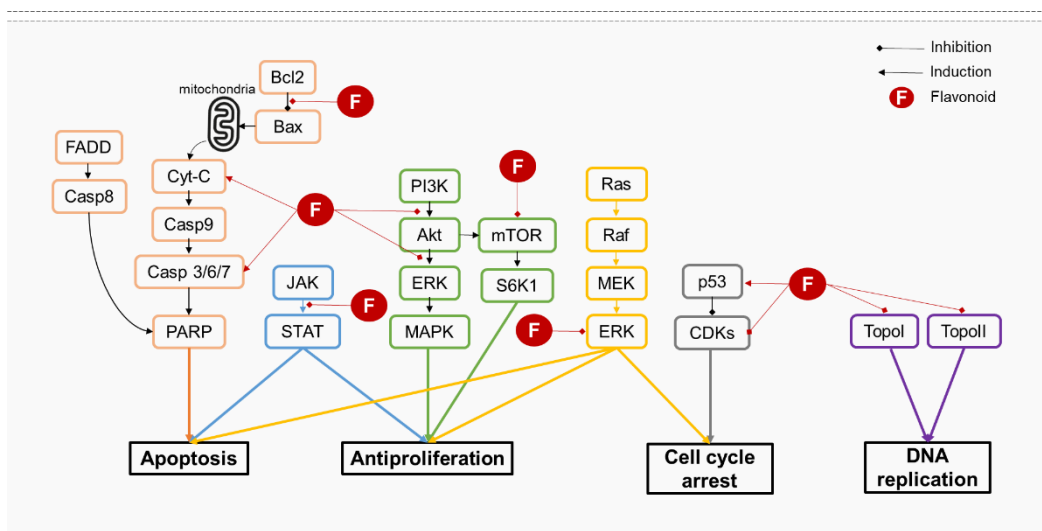


Figure 1. 6. Schematic representation of the main anticancer mechanisms of action of flavonoids. FADD, Fas-associated protein with death domain; Casp, caspase; Bcl2, B-cell lymphoma; BAX, Bcl2-associated X protein; Cyt-C, cytochrome complex; PARP, poly ADP-ribose polymerase; JAK, janus kinase; STAT, signal transducer and activator of transcription; PI3K, phosphoinositide 3-kinase; Akt, protein kinase B; ERK, extracellular signal-regulated kinase; MAPK, MEK, mitogen-activated protein kinase; mTOR, mechanistic target of rapamycin; S6K1, ribosomal S6 kinase, Ras, reticular activating system; Raf, rapidly accelerated fibrosarcoma; CDK, cyclin-dependent kinase; Topo I, II, topoisomerases I, II.

Flavonoids like quercetin, kaempferol, luteolin, and naringenin have shown proapoptotic activities by upregulating p53, Bax, and caspase proteins and downregulating the antiapoptotic Bcl2 protein in breast, ovarian, hepatic and gastric cancer cell lines among others [60]. For instance, naringenin increased Bax and caspase 3 expression by 2-fold ($p < 0.05$) and decreased that of Bcl2 ($p < 0.05$) at 20 μM , inducing a 50% rise in apoptotic rates of gastric cancer cells SGC-7901 compared to control ($p < 0.05$) [61]. In another

study, luteolin showed a dose dependent increase in levels of p53 and tumor cell apoptosis in lung cancer mice xenografts ($p < 0.05$) at 50, 100 and 200 mg/kg [62].

Multiple flavonoids were also shown to modulate PI3K, which regulates several oncogenic processes, such as protein synthesis, cell growth and cell cycle progression, by interfering with signaling proteins such as mammalian target of rapamycin (mTOR), extracellular signal regulated kinase (ERK) and signal transducer and activator of transcription 3 (STAT3), via protein kinase B (Akt) phosphorylation [63]. Quercetin is reported to function as a dual PI3K and mTOR inhibitor [64]. Granato *et al* showed the ability of quercetin to reduce the phosphorylation of Akt (40-78%), mTOR (58-67%) and STAT3 (50%) relative to control in primary effusion lymphoma cells at 50 μ M [65]. Apigenin and pelargonidine decreased PI3K and Akt phosphorylation at 20 and 15 μ M in bladder and osteosarcoma cancer cell lines, respectively [66,67]. Apigenin also reduced STAT3 phosphorylation by 45% relative to control in colon cancer mice tissues at 200 mg/kg [68]. Other flavonoids such as epigallocatechin galate and delphinidin inhibited the PI3K/Akt pathway in breast and ovarian cancer cell lines, respectively [60]. Furthermore, delphinidin caused a significant decline in ERK phosphorylation compared to control (40%, $p < 0.01$) at 0.1 μ M in the SKOV3 ovarian cancer cell line [69].

Flavopiridol is an 8-piperidine substituted flavone that was the first cyclin dependent kinase (CDK) inhibitor to enter clinical trials and was approved by the food and drug administration (FDA) as an orphan drug (drug used for the management of a rare disease) for the treatment of chronic lymphocytic leukemia (CLL) [70,71]. The CDK family regulates cell cycle progression where CDK1, 2, 4 and 6 are recognized as active during the cell cycle and are inhibited by flavopiridol with IC_{50} (half maximal inhibitory concentration) ranging from 20 to 60 nM. Flavopiridol additionally inhibits CDK9 ($IC_{50}=20$ nM) that is involved in transcriptional regulation, consequently inducing cell cycle arrest and apoptosis [71,72]. While flavopiridol's cell cycle arrest is p53 independent, other flavonoids such as fisetin and apigenin can regulate CDKs' function and promote cell cycle arrest via p53 activation in bladder and breast cancer cells [73,74]. P53 can downregulate CDKs through the upregulation of p21 expression [75].

Flavonoids are reported to interact with other important anticancer targets such as DNA topoisomerases. Topoisomerases have key roles during DNA transcription and replication. Luteolin and apigenin inhibited topoisomerase I DNA re-ligation in a human leukemia cell line [76]. Moreover, luteolin demonstrated rat liver topoisomerase I inhibition with an IC₅₀ of 5 μ M [77].

1.3.2. Antiangiogenic activity of flavonoids

The multifaceted antiangiogenic effects of flavonoids in cancer were recently reviewed by Wei *et al* [78]. On a preclinical level, flavonoids were able to modulate several angiogenic pathways and mediators such as hypoxia inducible factor (HIF), VEGF/VEGFR2 pathway, interleukins (ILs) and MMPs [8]. Hypoxic conditions are quite common in tumor microenvironments. In that regard, the HIF-1 α plays a key role in the adaptation of cells with reduced oxygen by inducing the expression of several proangiogenic factors like VEGF, angiopoietins 1 and 2 and PDGF [79]. Wogonin for example notably decreased VEGF levels ($p < 0.05$, relative to control) in breast, liver and colon cancer cell lines under both normoxic (20% O₂) and hypoxic (1% O₂) conditions at 20 μ M. Wogonin also reduced VEGF expression by 40% relative to control ($p < 0.05$) in the estrogen receptor positive breast cancer cell line MCF-7 [80]. Similarly, nobiletin showed 30 and 43% decline in VEGF levels and HIF-1 α expression ($p < 0.01$, relative to control) at 20 and 40 μ M, respectively, in OVCAR-3 ovarian cancer cells [81]. As shown in **Table 1. 5**, a number of flavonoids were reported to directly interact with VEGFR2's phosphorylation and activation in ECs.

Table 1. 5. Reported *in vitro* anti-VEGFR2 activity of flavonoids on ECs

Flavonoid	Evaluated VEGFR2 activity	Reported activity	Ref
Wogonin	VEGFR2 phosphorylation	50% decrease relative to control ($p < 0.05$) at 10 μ M	[82]
Eupafolin	VEGFR2 phosphorylation	Decreased phosphorylation relative to control (qualitative) at 5, 10 and 20 μ M	[83]
Quercetin	VEGFR2 phosphorylation	Decreased phosphorylation relative to control (qualitative) at 40 μ M	[84]
Luteolin	VEGFR2 phosphorylation	Decreased phosphorylation relative to control (qualitative) at 40 μ M	[85]

Quercetin-4'-O-β-D-glucopyranoside	VEGFR2 phosphorylation	Decreased phosphorylation relative to control (qualitative) at 5 and 20 μM	[86]
	VEGFR2 kinase activity	IC ₅₀ =20.12 nM	
Kaempferol	VEGFR2 kinase activity	30% decrease relative to control ($p<0.001$) at 100 μM	[87]
Naringenin	VEGFR2 kinase activity	25% decrease relative to control ($p<0.05$) at 30 μM	[88]

The proinflammatory cytokine IL-6 mainly mediates its angiogenic effects via STAT3 resulting in VEGF upregulation [7]. Luteolin is reported to decrease levels of ILs 1, 6 and 8 and tumor necrosis factor α (TNF- α) by 67, 27, 37 and 32%, respectively, compared to control ($p<0.05$) in prostatic cancer cells (PC-3) at 40 μM [85]. Apigenin significantly reduced IL-6 and VEGF expression (89 and 62%, respectively, at 10 μM) in esophageal cancer cells. Esophageal cancer mice xenografts showed 87% reduction in tumor weight at an apigenin dose of 10 mg/kg [89].

The flavonoids luteolin, wogonin, myricetin, eupatilin and nobiletin are all reported to inhibit the activity of the proteolytic enzymes MMPs particularly MMP-2 and 9 in breast, liver, prostatic and bone cancer cells [90–92]. In particular, nobiletin elicited a dose dependent impairment of MMPs 2 and 9 function in osteosarcoma cells with the highest dose of 100 μM causing 70 to 90% reductions in MMPs 2 and 9 enzyme activity and mRNA expression ($p<0.001$, relative to control) [91].

1.3.3. Clinical progression of flavonoids as anticancer agents

As outlined in **Table 1. 6**, several flavonoids have progressed into clinical trials. The broad spectrum CDK inhibitor, flavopiridol, has gained an FDA orphan approval in 2007 for the treatment of CLL, which was revoked in 2022 as it did not prove efficacious as a single agent against this indication [93,94]. Flavopiridol is now mostly explored in combination therapies where it demonstrated good efficacy. In a phase II trial, flavopiridol combined with mitoxantrone and cytosine arabinose resulted in high complete remission (CR) (67%) and OS (12.6 months) rates in the treatment of acute myeloid leukemia (AML) patients with poor prognosis risk factors [95]. Individuals with such disease normally have <30% CR rates and <10% 3-5-year survival. Since flavopiridol can only be administered intravenously, due to its poor bioavailability [96], TP-1287 was developed as its oral

phosphate prodrug. TP-1287 received FDA approval as an orphan drug against ewing sarcoma in 2023 [97], yet, it showed high toxicity in a phase I study where the majority of patients with advanced solid tumors (98%) suffered from treatment related adverse events with 55% being of grade 3 or higher [98]. Voruciclib is a flavopiridol based CDK inhibitor with higher selectivity to the CDK family over related kinases such as MAK (inhibition constant (K_i)=259 nM versus 1.08 nM for flavopiridol) [99]. Voruciclib's selectivity has been attributed to its structural variation from flavopiridol (4'-CF₃ substitution and a hydroxymethyl pyrrolidine ring instead of the hydroxypiperidine at C8, **Figure 1. 5**) [99]. Voruciclib is therefore expected to show better tolerability than flavopiridol due to the reduced off-target interactions. Its safety is currently being evaluated against several lymphomas and AML in a phase I trial [99].

Table 1. 6. Overview of flavonoids registered at *www.clinical trials.gov* as anticancer agents since 2010

Flavonoid	No of trials	Monotherapy (M) or Combined (C)	Main indication/s	Clinical Phase/s
Flavopiridol (alvocidib®)	4	C	AML	I-II
TP-1287	1	M	Ewing sarcoma, advanced solid tumors	I
Voruciclib	1	M, C	B-cell malignancies, AML	I
Umbralisib (Ukoniq®)	24	M, C	CLL, lymphomas	I-II
Tenalisib (RP6530)	11	M, C	BC, lymphoma	I-II
Icaritin	9	M, C	HCC	I-III
Quercetin	3	C	SCCHN, BC	I-II
Silibinin	5	M, C	Solid tumors	I-III

AML, acute myeloid leukemia; HCC, hepatocellular carcinoma; CLL, chronic lymphocytic leukemia; BC, breast cancer; SCCHN, squamous cell carcinoma of the head and neck; CRC, colorectal carcinoma.

The synthetic flavonoid, umbralisib, was approved by the FDA for the treatment of marginal zone and follicular lymphomas in 2021 acting as a dual PI3K δ and casein kinase-1 ϵ inhibitor [48]. Umbralisib was later voluntarily withdrawn from the market by the manufacturing company (TG Therapeutics) due to an imbalance in OS relative to the control arm that outweighed umbralisib's benefits [100]. Tenalisib is a selective inhibitor for the δ and γ isoforms of PI3K and is being assessed for its safety and efficacy primarily

as a single drug against lymphoid malignancies in several phase I and II trials [48]. In addition to the aforementioned synthetic flavonoids that are mainly indicated for hematological malignancies, the natural flavonoids icaritin, quercetin and silibinin are undergoing multiple clinical trials against solid tumors acting via a multi-targeting mechanism of action. Icaritin has been approved for use against liver cancer in China since 2022 [48]. Icaritin is reported to inhibit various anticancer targets including estrogen receptor- α , Akt and STAT3 signaling [101]. Moreover, the immunomodulatory effects of icaritin play an essential role in its anticancer activity through the inhibition of inflammatory cascades and the activation of both the innate and adaptive immunity against the tumor microenvironment [102].

Despite the reviewed clinical evaluations, flavonoids' anticancer clinical progression remains limited relative to their well-established preclinical effectiveness. No clinical trials have yet looked into the activity of flavonoids as antiangiogenic agents in cancer therapy. The multi-target effects of flavonoids present challenges with regards to low target specificity and off-target interactions that could lead to increased systemic toxicity. However, if tuned by mechanistic precision, the pharmacological promiscuity of flavonoids can still offer advantageous qualities, such as increased effectiveness and overcoming drug resistance. In that scope, specific anticancer targets of flavonoids need to be identified followed by extrapolation of relevant structure activity relationship (SAR) data in order to optimize the design of target-specific active compounds suitable for clinical translation [103]. On the other hand, the poor pharmacokinetic properties of flavonoids remain a big hurdle towards achieving their full therapeutic potential and hence is briefly discussed in the upcoming section [104].

1.3.4. Improving flavonoids' bioavailabilities

As demonstrated in **Figure 1. 7**, the small intestines is the main site of absorption of flavonoids. Once hydrolyzed by the lactase phlorizin hydrolase, flavonoid aglycons can be passively transported into the enterocytes where they are subjected to extensive phase I and II metabolism. The absorbed flavonoids and/or their metabolites then reach the liver via the hepatic portal circulation where they are exposed to further metabolism, leading to their rapid excretion from the body. **Table 1. 7** outlines the impact of the

different structural features of flavonoids on their bioavailabilities and potential approaches that can be used to address their shortcomings.

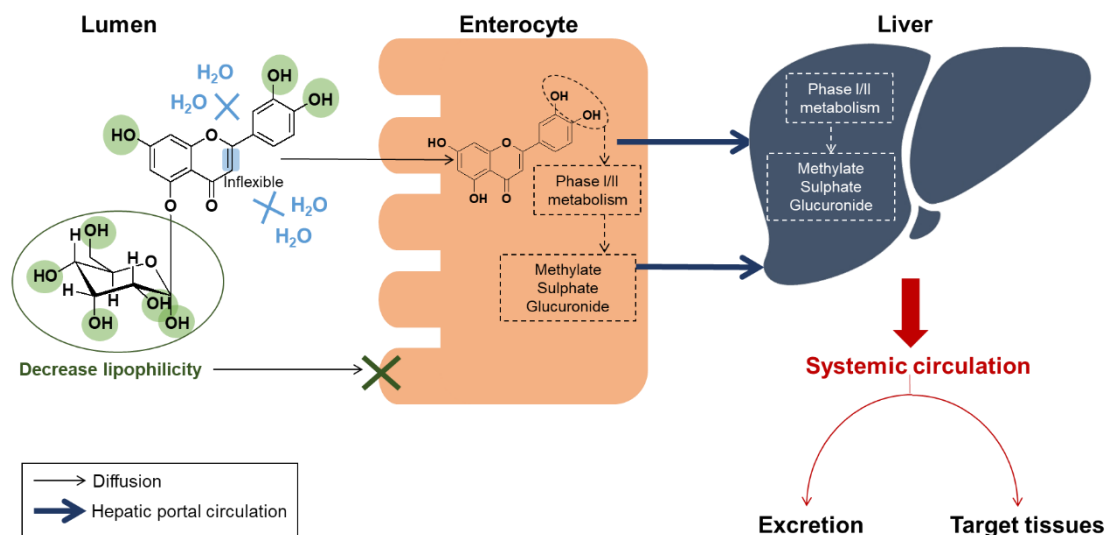


Figure 1. 7. Schematic presentation of the main routes of flavonoids absorption and metabolism in the human body

Multiple bioavailability improving strategies including structural modification and nanoformulation have been applied to flavonoids as reviewed by Zhao *et al* [54] and Teng *et al* [105]. As shown in **Table 1. 8**, the structural modification strategy offers a low cost bioavailability enhancing method that does not infer the use of toxic or unstable external modifiers. Metal complexation, particularly with transition metals, is a structural modification strategy that proved effective in enhancing the aqueous solubility of poorly soluble drugs [106]. Several quinolone antibiotics such as lomefloxacin as well as taxol and other bioactive molecules such as curcumin have shown significantly better solubility in water after metal chelation [107–109]. For example, curcumin's aqueous solubility increased by 1.5 to 2-folds upon complexation with the zinc cation (Zn^{2+}). Metal chelation did not only improve aqueous solubility but also enhanced biological activities of the binding drugs/bioactive compounds [109]. The copper (Cu)II taxol complex showed average GI_{50} (half maximal growth inhibitory concentration) values that were 44% better than that of taxol on the National Cancer Institute's (NCI) panel of 60 cancer cell lines [108].

Table 1. 7. Structural factors affecting flavonoids bioavailability and selected approaches to address them

Structural feature	Impact on bioavailability	Bioavailability enhancement approach		
		Structural modification	Absorption enhancers	Nanoformulation
C2-C3 unsaturation	Keeps the molecule in a planar form, decreasing accessibility to solvent molecules and consequently dissolution [10] (e.g. aqueous solubility of myricetin is 16.6 µg/mL resulting in 9.62% oral bioavailability in rats [10])	Complexation with organometallic derivatives to increase aqueous solubility and gastro-intestinal dissolution (e.g. Ru(II)- <i>p</i> -cymene complexation enhances aqueous solubility of flavonoids by 10-fold [110])	Apple pectin dietary intake to increase gastro-intestinal dissolution and permeability (e.g. quercetin plasma concentration in rats increased from 3.45 ± 0.67 to 5.84 ± 1.60 µM (<i>p</i> <0.05) [111])	Self-nanoemulsifying drug delivery system (SNEDDS) to increase gastrointestinal solubility and permeability and protect from gastro-intestinal enzymatic degradation (e.g. myricetin AUC _{0-24h} in rats plasma increased by 5.13-, 6.33-, 4.69- and 2.53-fold [112]; quercetin oral bioavailability in rats increased by 5-fold [113])
Excess OH groups in main structure and attached glycosides	<ul style="list-style-type: none"> Decrease lipophilicity of the molecule, preventing its diffusion through the hydrophobic cell membrane (e.g. catechin, a flavonoid with 5 OH groups, showed a 5% oral bioavailability in rats which was attributed to its poor apparent permeability (P_{app}) of 6×10^{-7} cm/s [10].) Susceptible to intestinal and hepatic metabolism via methylation, sulfation and glucourinidation leading to rapid excretion of the flavonoid from the body (e.g. quercetin was undetected in plasma of subjects receiving 4 g orally. Conjugated flavonoids are the predominantly detected forms in human specimens, while the amounts of unconjugated flavonoids in human plasma and urine are usually reported to be below the analytical detection limits [114]) 	<ul style="list-style-type: none"> Replacement of OH group/s in B ring with halogen atom to increase lipophilicity and gastrointestinal permeability. Methylation of free OH groups in A ring to protect from intestinal and hepatic metabolism (e.g. 5, 7-diOCH₃ chrysin was detected in the plasma and in liver, lungs and kidney tissues of rats after 1 hour with peak concentrations of 2.5, 16.5, 7.5 and 5 µM, respectively, while chrysin was not systemically detected [115]) 		

Table 1. 8. Advantages and disadvantages of selected flavonoid bioavailability enhancement approaches

Bioavailability enhancement approach	Advantages	Disadvantages
Structural modification	<ul style="list-style-type: none"> • Low cost • Enhance biological activity by incorporation of bioactive moieties 	Biological activity might be suppressed by masking certain functional groups [116]
Absorption enhancers	<ul style="list-style-type: none"> • Easy to formulate • Low cost • Natural origin • Safe 	Poor thermal and mechanical stability [116]
Nanoformulation	Thermodynamically and thermokinetically stable	<ul style="list-style-type: none"> • High cost • Low drug loading • Toxicity due to off-target accumulation [10]

Flavonoids possess metal chelating abilities by virtue of their hydroxyl and oxo groups, which can enhance their pharmacokinetic and pharmacological properties [117]. As mentioned in **Table 1. 7**, Ru(II) chelation with flavonol derivatives resulted in a 10-fold rise in water solubility relative to the free flavonols [110]. Moreover, the majority of Ru complexes are positively charged and lipophilic which enhances their diffusion through the negatively charged lipophilic cell membrane [118]. Arene-Ru(II) complexes have particularly gained interest because of their beneficial structural features. The arene ring not only stabilizes the complex, but also enhances its cellular uptake by increasing the lipophilicity [118]. Complexes of the related transition metal, Ir, with a cyclopentadienyl ligand (Cp*) display similar properties. In that regard, the lipophilic nature of the Cp* ligand would result in increased cellular absorption and improved pharmacokinetic properties. In general, organometallic Ru and Ir complexes including flavonoid ones have demonstrated interesting anticancer properties. Therefore, it was postulated that Ru or Ir complexation of the flavonoids involved in this project would present opportune characteristics that are useful for the anticancer applications targeted herein. The anticancer properties of Ru and Ir complexes in general and those of flavonoids in particular are hence critically appraised next.

1.4. Anticancer activity of ruthenium and iridium metal complexes

1.4.1. Anticancer activity of ruthenium metal complexes

Ru based complexes are often explored as an alternative to the widely used platinum (Pt) based anticancer agents, cisplatin and carboplatin. The favorable pharmacological properties of Ru complexes are demonstrated by their high potency, low toxicity and low predisposition to resistance developing compared to Pt based drugs [119,120]. Ru similarity to iron (Fe), is viewed as a reason for its higher selectivity towards cancer cells since it can exploit the overexpressed Fe transferrin or albumin tumor transport mechanisms [121]. Additionally, Ru complexes are preferentially activated to their reduced Ru(II) form by the acidic and hypoxic tumor environment [118,122].

The cytotoxicity profiles of various Ru complexes on cervical, ovarian, breast, lung and other cancer cell lines were reviewed by Das *et al*, displaying IC₅₀ values that ranged from 0.04 to 10 μ M in the majority of cases [122]. **Figure 1. 8** summarizes the main anticancer effects of Ru complexes. DNA binding is one of the main mechanisms of cytotoxic action of Ru compounds. Upon hydrolysis of the bound ligand, the electron deficient metal atom can bind to nucleophilic regions of DNA. In addition, the aromatic ligands of Ru complexes can covalently bind to DNA base pairs [118]. Sadler *et al* demonstrated the high covalent binding of Ru-arene-ethylenediamine complexes to N7 of guanosine and inosine mononucleosides (>97 and 59.4% Ru bound species, respectively) by ¹H NMR studies at neutral pH [123]. The covalent Ru-DNA binding results in irreversible Ru-DNA adducts that impair DNA transcription and replication. Non-covalent types of DNA interaction are also possible either via intercalation (the insertion of planar aromatic compounds between DNA base pairs) or groove binding by electrostatic interactions [118].

Ru compounds preferentially accumulate in the mitochondria, endoplasmic reticulum and lysosomes, eliciting apoptotic cascades. The negatively charged mitochondrial membrane (-160 to -180 mV) as well as the acidic lumen of lysosomes (pH=4.6-5) attract the positively charged metal ion, inducing mitochondrial dysfunction, autophagy, cell necrosis and apoptosis [118]. Increased generation of reactive oxygen species (ROS) in cancer cells by Ru compounds also contributes to their apoptotic abilities. This is achieved either through the metal's oxidizing and DNA damaging effects or via the

inhibition of redox enzymes such as thioredoxin reductase (TrxR). Luo *et al* reported a significant 60% TrxR inhibition ($p < 0.01$, relative to control) by their Ru(II) polypyridyl complex at 4 μM in melanoma A375 cell line with an IC_{50} of 0.9 μM on the same cell line compared to 7.3 μM for cisplatin [124]. The Ru based organic compounds are also reported to bind through their ligands to a number of protein kinases regulating cancer cell proliferation and death such as the proto-oncogene, Pim-1 and the glycogen synthase kinase, GSK3R [125,126].

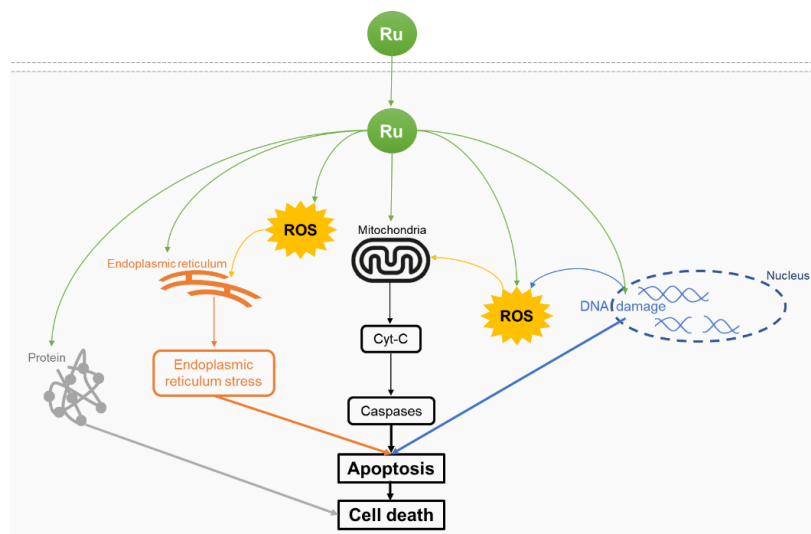


Figure 1. 8. Schematic representation of the main cytotoxic mechanisms of action of Ru compounds

The specific antimetastatic activity of the clinical Ru agent NAMI-A attracted researchers' attention towards the antiangiogenic and antimetastatic abilities of Ru complexes. NAMI-A significantly reduced the numbers (40-100%) and weights (70-100%) of lung and brain metastases of several malignancies (e.g. lung and mammary carcinoma, melanoma and leukemia) xenografted in nude mice [127]. However, clinical progression of NAMI-A was halted at the phase II stage due to insufficient effectiveness of its gemcitabine combination in the treatment of non-small cell lung carcinoma. RM175 is one of the early developed Ru complexes demonstrating strong inhibition of metastasis in mice models. RM175 primarily suppressed the lung metastatic mass of mammary carcinoma by 85 to 95% at 10 mg/kg/day [128]. Generally, Ru complexes are reported to target angiogenic factors, including c-myc, VEGF, EGF, and MMP proteins, impacting tumor invasion, migration, and proliferation processes [118,129–131].

The diverse anticancer modes of action reported for Ru compounds raise concerns that their mechanisms are not yet fully understood [118]. These reported activities highly suggest that Ru molecules elicit a multifactorial mode of action which may be considered a disadvantage with regards to selectivity [127]. In that context, novel approaches such as photodynamic therapy (PDT) has shown promising anticancer effectiveness by selectively activating tumor-infiltrating Ru agents, with compound TLD1433 undergoing phase I/II clinical trials for bladder cancer treatment using PDT [118,132]. However, further research on the mechanisms of action, cellular uptake, metabolism and SAR aspects of Ru complexes is still needed in order to exploit their full clinical potential [133].

1.4.2. Anticancer activity of iridium metal complexes

Ir complexes have gained recent interest as anticancer agents due to their resemblance to Pt. Ir complexes were regarded as inert with very low ligand exchange rates until experiments reported a significant increase in their ligand exchange rates when attached to a Cp* ligand [134,135]. Consequently, a number of Ir(III) half-sandwich pseudo-octahedral Cp* complexes were developed with N/N, N/O, O/O or C/N bidentate donor atoms as potential anticancer agents [136]. The Cp* moiety stabilizes the complex and plays a role in target interactions (e.g. DNA intercalation) [137]. The developed Ir(III) complexes are reported to have high selectivity and cytotoxicity to cancer cells over normal cells. Liu *et al* reported the synthesis of several Cp-Ir(III) complexes with *N,N* or *C,N* phenanthrene or bipyridine ligands that showed higher activity than the Pt drugs oxaliplatin and cisplatin on the NCI's panel of 60 cancer cell lines [138]. The synthesized complexes mainly acted as DNA binding agents via both DNA intercalation and directly binding to base pairs, particularly guanine, blocking DNA replication [136]. Ouyang's group developed a number of Ir(III) with imidazophenanthroline that showed higher selectivity than cisplatin with the most potent compound having an IC₅₀ ranging from 0.5 to 1.5 μM on cervical (Hela), hepatic (HepG2) and lung (A549) cancer cell lines. These complexes were shown to target mitochondrial mediated apoptosis by the release of cytochrome C [139].

Studies have shown that organometallic Ir(III) Cp* compounds can hinder angiogenesis by suppressing EC tube formation *in vitro* [140]. Additionally, these compounds have

been found to prevent the sprouting of blood vessels in *in vivo* zebrafish models [141,142]. These activities were attributed to the downregulation of the VEGF system, achieved either through the down expression of VEGF or the inhibition of VEGFR3 [141,142].

Ir metal complexes exhibit promising anticancer properties, however they are still in the early stages of development and hence require extensive preclinical evaluations for their modes of action and pharmacodynamics [133].

1.4.3. Anticancer activity of flavonoid ruthenium and iridium complexes

The strong cytotoxic and antiangiogenic activities displayed by Ru and Ir based organic compounds suggest potential synergistic anticancer effects upon fusion with the bioactive flavonoids. Accordingly, a number of Ru and Ir flavonoid complexes have been developed for anticancer applications.

Arene-Ru(II) complexes with the $[\eta^6\text{-arene-Ru(II)-XYZ}]$ formula have gained much interest because of their beneficial structural features. X and Y represent either a two mono-dentate or one bi-dentate ligand, for example with the O, O chelation of flavonoids. Z is a leaving group, often a chlorine (Cl), that is preferentially displaced by H₂O inside the cell due to lower Cl concentrations (~ 22 mM) compared to the blood (~104 mM). The formed $[\text{Ru-OH}_2]^{2+}$ species are more reactive towards biological targets, for example enabling DNA intercalation via guanine substitution [143].

A series of Ru(II)-*p*-cymene-flavonol complexes showed antiproliferative activities on ovarian (CH1), colon (SW480) and lung (A549) cancer cell lines with IC₅₀ values ranging from 0.86 to 20 μM [144]. The measured activities of the Ru(II) compounds were largely equivalent to that of their free flavonols and lower than that of cisplatin. Nevertheless, two Ru(II) complexes were more active than their parents on the A549 cell line (IC₅₀=17 and 18 versus 81 and 37 μM) and one showed similar activity to cisplatin on SW480 cells (IC₅₀=3.8 versus 3.3 μM) [144]. Similarly, a panel of dimethyl sulfoxide (DMSO) Ru(II) flavone complexes displayed comparable cytotoxic activities to their precursor flavones on MCF-7 cells [145]. However, the most potent complex of the examined DMSO Ru(II) compounds (IC₅₀=16 μM) increased the percentage of apoptotic MCF-7 cells of the control and free ligand from 0.18 and 1.85%, respectively, to 6.28% [145]. The study by Rubio *et al* examined the cytotoxic potential of Ru(II)-*p*-cymene and Ir(III) Cp* complexes

of 7-substituted derivatives of the flavone chrysin on SW480 and A549 cancer cell lines [146]. The metal complexes generally exhibited higher cytotoxic activities compared to their unbound counterparts. In particular, the 7-butyl piperidine chrysin-Ru(II) or Ir(III) organometallic complexes exhibited superior activity compared to cisplatin on the specified cell lines, with IC₅₀ values of 28.5, 31, 16 and 19 μ M, respectively (cisplatin IC₅₀ =46.7 and 37.6 μ M on SW480 and A549 cell lines, respectively) [146]. Furthermore, the Ru(II) and Ir(III) complexes demonstrated stronger selectivity for cancerous lung cells compared to normal lung cells (IMR-90) with selectivity indices (SI) of 1.8, surpassing both their flavonoid precursor and cisplatin (SI=0.2 and 1.5, respectively). Additionally, the metal complexes were able to overcome cisplatin resistance on the ovarian cancer cell line A2780 with resistance factors of 0.6 and 1 compared to 8.6 for cisplatin. The Ru(II) and Ir(III) chelates showed significant effects on ROS production and cell cycle progression ($p < 0.01$, relative to control), whereas the free chrysin derivative did not have any effects [146].

1.5. Project aim

The combination of one or more drugs with antiangiogenic and cytotoxic properties led to significant improvements in OS and PFS rates in clinical trials, however, their general use is restricted by the frequency of grade 3 or higher treatment-related adverse events, including hypertension and, in certain cases, death (**Section 1.2.3**). The multi-targeting antiangiogenic and cytotoxic properties attributed to flavonoids together with their generally favorable safety and tolerability profiles mean they are excellent leads for clinical development (**Section 1.3**). Nonetheless, the development of flavonoids for antiangiogenic application has not progressed beyond the preclinical stage. The poor selectivity and pharmacokinetic features of flavonoids have presumably hampered their clinical progression so far (**Section 1.3.4**).

This project aims to develop synthetic flavonoid lead compounds that are able to elicit combined antiangiogenic, cytotoxic and antimetastatic activities. Additionally, this study aims to extrapolate the key SARs required for the proposed activities which can be adopted for the future design of flavonoids optimum for anticancer clinical applications.

The outline of this thesis is presented in **Figure 1. 9**. The first objective was to establish the preclinical antiangiogenic effectiveness of flavonoids on qualitative and quantitative levels via a robust systematic analysis study (**Chapter 2**). The second was to design a library of flavonoids capable of eliciting antiangiogenic and cytotoxic activities and with enhanced pharmacokinetic features by combining the SAR outcomes relevant to each of these components (**Chapter 2**). The goal was thereafter to synthesize and characterize the designed flavonoids in order to assess their *in vitro* antiangiogenic activities (inhibition of VEGF-induced EC tube formation and migration), initiating investigations on the mechanisms of action of the most active compounds (*in vitro* and *in silico* VEGFR2 interaction) (**Chapter 3**). Our focus was then directed towards maximizing the antiangiogenic and cytotoxic properties of the test flavonoids via their complexation with Ru(II) and Ir(III) metal ligands (**Chapter 4**). The final objective was to test the combined *in vitro* antiangiogenic (inhibition of EC tube formation), cytotoxic (breast cancer cell viability) and antimetastatic (inhibition of breast cancer cell migration) activities of the most active flavonoid (a 4-thioflavone), its 4-oxo derivative and their modified Ru(II) metal complexes, culminating the different elements of the conducted work into the main goal of the project (**Chapter 5**).

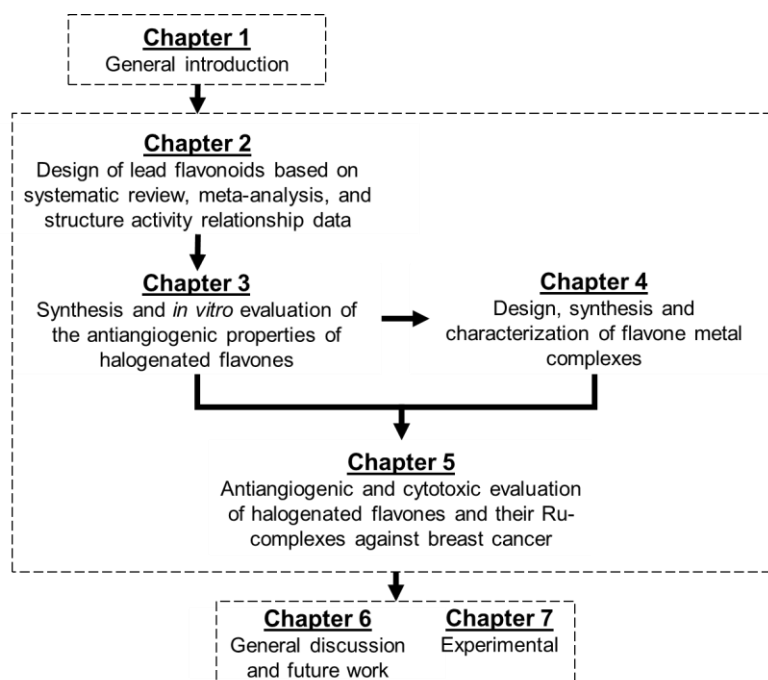
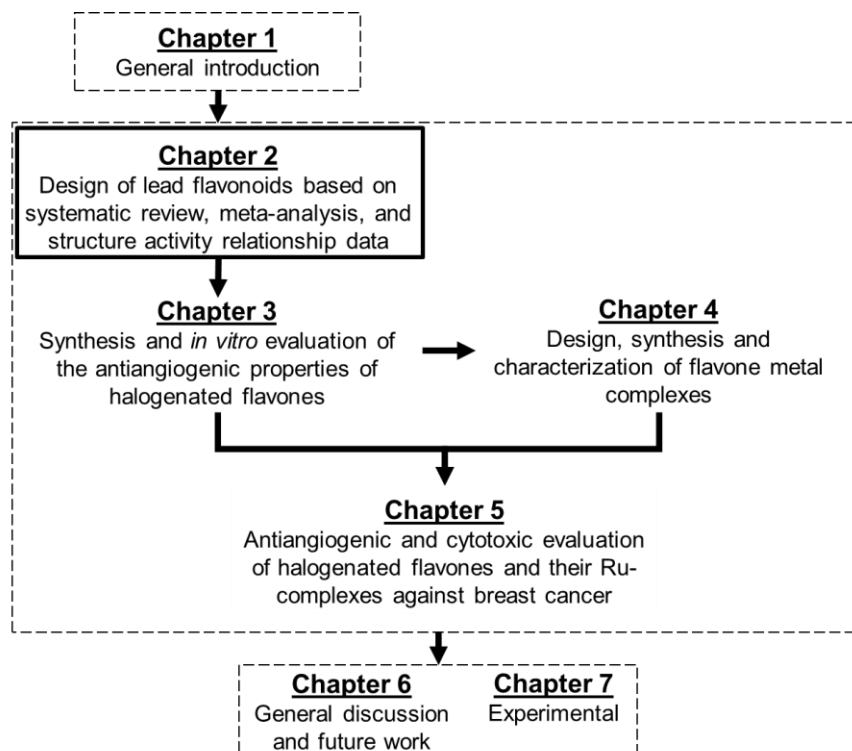


Figure 1. 9. Outline of the presented PhD thesis

Chapter 2

Design of lead flavonoids based on systematic review, meta-analysis, and structure activity relationship data



2.1. Introduction

The polypharmacological antiangiogenic and cytotoxic properties [9,49,147] of flavonoids, as well as their favorable safety profiles [6], have been demonstrated in **Section 1.3, Chapter 1**. However, no flavonoids have reached clinical trials as antiangiogenic agents (**Section 1.3.3, Chapter 1**). Hence, the aim of this chapter is to design lead flavonoids combining dual antiangiogenic and cytotoxic properties for future clinical development. Accordingly, this chapter comprises three main components: a) investigating the preclinical effectiveness of flavonoids as antiangiogenic agents through systematic and quantitative statistical analyses of literature data studying the antiangiogenic activities of flavonoids (**Sections 2.2.1 and 2.2.2**), b) extrapolating antiangiogenic (as described in this chapter) and cytotoxic (gathered from SAR studies conducted in prior research) flavonoid SAR studies (**Section 2.2.3**), and c) design of lead flavonoids combining antiangiogenic and cytotoxic SARs with pharmacokinetic enhancing structural features (**Section 2.2.4**).

The systematic and meta-analysis approach presents a suitable methodology for objectively evaluating the extensive body of literature data and individual studies concerning the angiogenic effects of flavonoids. Being conducted in a methodical, replicable and transparent manner, with minimum subjectivity and bias, systematic studies can provide evidence-based conclusions, addressing existing gaps [148–151]. Since systematic studies combine the findings of several independent investigations looking into their consistency and reproducibility, they have more power than any single study [152,153]. As shown in **Table 2. 1**, few systematic studies have already shown insight for the antiangiogenic activities of specific flavonoids from the scope of their anticancer effects. However, none has looked collectively at the antiangiogenic effects of flavonoids as a class of chemical compounds, hence this chapter had the potential to bring novel insight for determining their preclinical effectiveness as antiangiogenic agents. Antiangiogenic SAR studies for flavonoids are scarce as well, with only two studies [154,155] reporting antiangiogenic SAR evaluations using a rather limited library of flavonoids (**Table 2. 2**). Therefore, the need for a meaningful large scale antiangiogenic SAR study was recognized herein, which could provide important knowledge to be used in the design of effective antiangiogenic flavonoids.

Table 2. 1. Summary of systematic reviews relevant to the topic of flavonoids and angiogenesis

Title of study	General scope	Types of evaluated studies	No of evaluated studies	Time limit	Ref
Wound healing properties of flavonoids: a systematic review highlighting the mechanisms of action	Healing properties of flavonoids on skin wounds	<i>In vivo</i>	55	May 2020 - June 2020	[156]
A systematic review of anticancer effects of radix astragali	Anticancer effects of the herb radix astragali	<i>In vitro, in vivo</i>	92	Inception - November 2013	[157]
A systematic review of the preventive and therapeutic effects of naringin against human malignancies	Anticancer effects of naringin	<i>In vitro, in vivo</i>	87	Inception - September 2020	[158]
Quercetin and ovarian cancer An evaluation based on a systematic review	Chemopreventive and antiproliferative effects of quercetin on ovarian cancer	<i>In vitro, in vivo</i>	13	Inception - May 2015	[159]
Potential role of phytochemicals against matrix metalloproteinase induced breast cancer; an explanatory review	Phytochemicals' modulating effects on matrix metalloproteinase induced breast cancer	<i>In vitro</i>	44	Inception - January 2020	[160]
Anticancer activities of polygonum odoratum Lour.: a systematic review	Anticancer effects of the plant polygonum odoratum Lour.	<i>In vitro</i>	8	Inception - March 2022	[161]
Antiangiogenic Activity of Flavonoids: A Systematic Review and Meta-Analysis	Antiangiogenic activities of flavonoids	<i>In vitro, in vivo</i>	402	Inception - May 2020	[162]

Search was conducted using the keywords (flavonoids AND angiogenesis AND systematic) in the title and/or abstract fields in ScienceDirect, PubMed and Web of Science databases. The study conducted herein is highlighted in blue color.

Table 2. 2. Summary of SAR studies on the antiangiogenic activity of flavonoids

Title of Study	Assay/s used to derive SAR conclusions	Subclasses of evaluated flavonoids	No of evaluated flavonoids	Studied structural features	Ref
<i>In vitro</i> and <i>in vivo</i> structure and activity relationship analysis of polymethoxylated flavonoids: Identifying sinensetin as a novel antiangiogenesis agent	<ul style="list-style-type: none"> • <i>In vitro</i> HUVECs proliferation • <i>In vivo</i> zebrafish vessel formation 	<ul style="list-style-type: none"> • Flavanones • Flavones 	7	<ul style="list-style-type: none"> • 7-O glycosylation • 3'-H to OH • 4'-OH to OCH₃ • 8-H to OCH₃ • 3'-H to OCH₃ • 5, 6, 7, 4'-OH to OCH₃ 	[154]
Exploring quercetin and luteolin derivatives as antiangiogenic agents	<i>In vitro</i> HUVECs scratch assay	<ul style="list-style-type: none"> • Flavonols • Flavones 	8	<ul style="list-style-type: none"> • 3, 5, 7, 3', 4'-OH to OCH₃ • 4-C=O to C=S 	[155]
Antiangiogenic Activity of Flavonoids: A Systematic Review and Meta-Analysis	<i>In vivo</i> CAM assay	<ul style="list-style-type: none"> • Flavonols • Flavanols • Flavanones • Flavones • Isoflavones • Anthocyanidins 	36	<ul style="list-style-type: none"> • C2-C3 unsaturation • Number of OHs • Position of OHs • 3-H to OH • 7-OH to OCH₃ • 7-H to OCH₃ • 3, 7-O glycosylation 	[162]

HUVECs, human umbilical vein endothelial cells; CAM, chick chorioallantoic membrane. The study conducted herein is highlighted in blue color.

2.2. Results and discussion

2.2.1. Systematic analysis of literature relating to the angiogenic activity of flavonoids [162]

This systematic review was conducted according to the Preferred Reporting Items for Systematic reviews and Meta Analyses (PRISMA) guidelines (**Table 7.1, Section 7.3.1, Chapter 7**) [163].

2.2.1.1. Search and selection of studies

For the first section of this chapter, 3708 records were initially identified in three electronic databases (1555 from ScienceDirect, 1984 from PubMed and 169 from Web of Science), using all possible combinations of the keywords (flavonoid, flavone, flavonol, flavanol, anthocyanidin, polyphenol) and (angiogenesis, antiangiogenic, proangiogenic, “cell migration”, “wound healing”) (**Table 7.2, Section 7.3.1.1, Chapter 7**). Search results were then limited to research articles, review articles, short communications and systematic reviews and the remaining 3380 articles were subjected to title and abstract screening. 2556 records were found to be irrelevant to the subject in focus or did not fulfill the inclusion criteria outlined in **Section 7.3.1.2, Chapter 7**. After the removal of duplicates (422), 402 articles were finally included in this systematic analysis as shown in **Figure 2.1**.

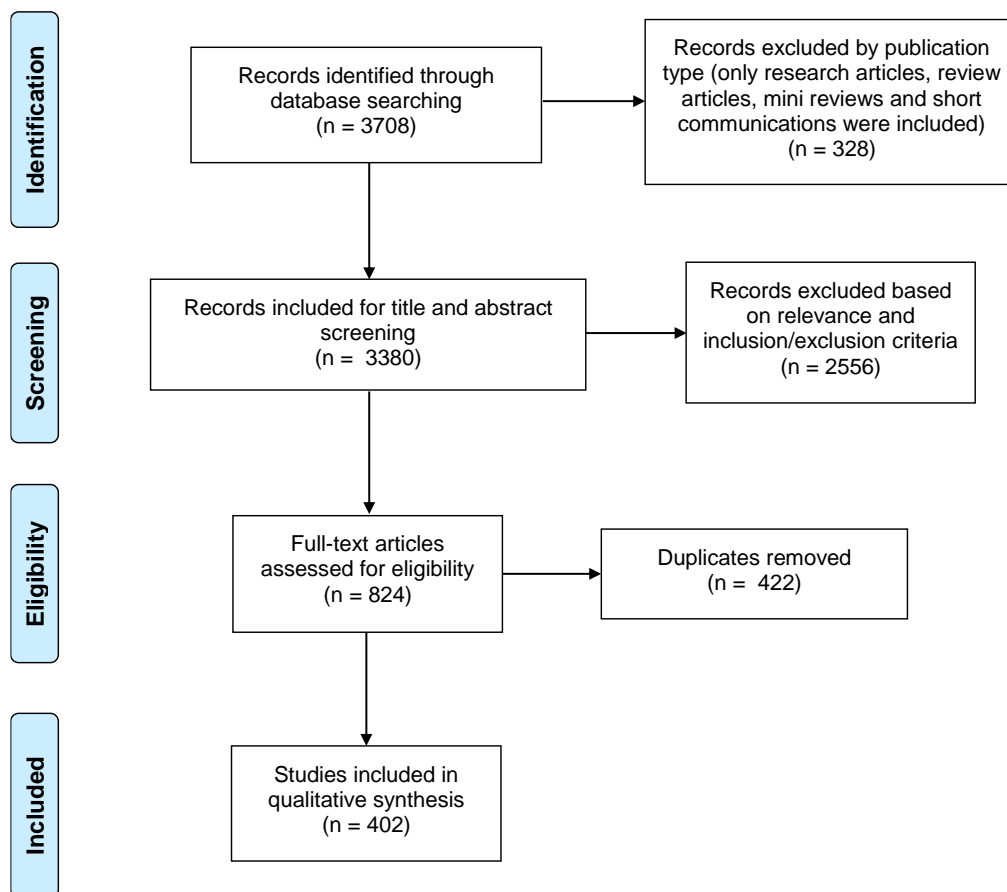


Figure 2. 1. PRISMA flow diagram of study search and selection process of the systematic review [162]

2.2.1.2. Analysis of the involved studies

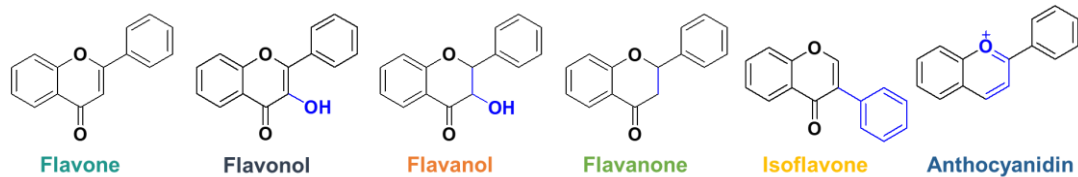
402 Research and review articles reporting angiogenesis related *in vitro* and/or *in/ex vivo* assays for different subclasses of flavonoids were included in this systematic review. The following data was extracted from the studies: year of publication, flavonoid subclass, flavonoid name, disease, *in vitro* tests and *in/ex vivo* tests as summarized in **Table 1, Appendix A**. These characteristics generated a large database of around 96 natural and synthetic flavonoids from 9 different flavonoid subclasses that was used in the subsequent data analysis.

Flavonoid subclasses analysis

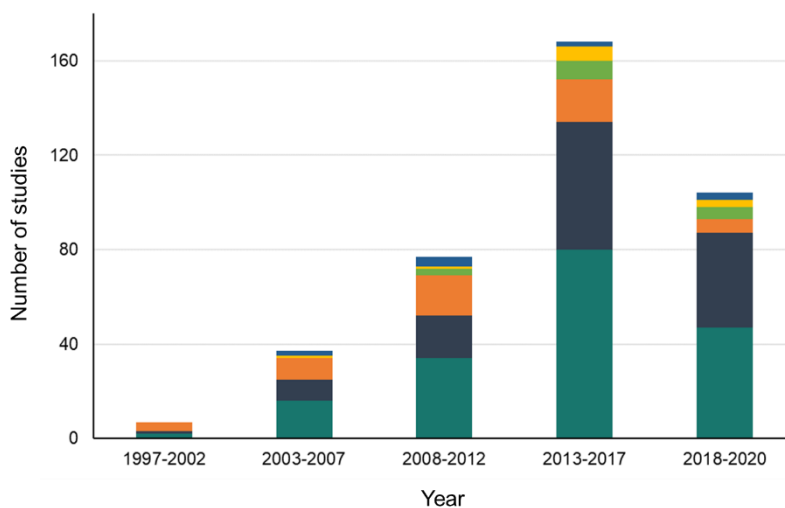
As shown in **Figure 2. 2A**, there has been a notable increase in the overall volume of research dedicated to investigating the impact of flavonoids on angiogenesis, particularly during the period spanning 2013 to 2017. The flavone chemical subclass, featuring a

carbonyl group in position number 4 with C2-C3 unsaturation and no hydroxyl groups on ring C, represented the most studied subclass of flavonoids throughout the investigated period, accounting for 40% of the total research conducted (**Figure 2. 2B**). The subclass of flavonols constituted an additional 29% of the total articles examined within this analysis. Flavones and flavonols are considered to be highly active subclasses of flavonoids, making them particularly promising for the development of efficacious treatments.

(A)



(B)



(C)

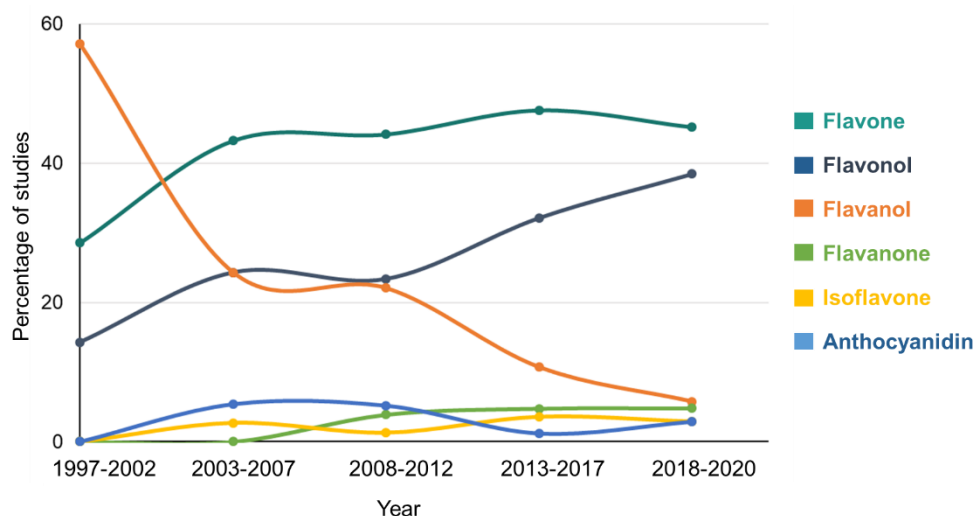


Figure 2. 2. Number of papers retrieved with respect to chemical subclass of flavonoid from the year 1997 to 2020. (A) Chemical structures of flavonoid subclasses; (B) Absolute number of studies; (C) Percentage of studies for each subclass relative to the total number of studies. Data for flavane, isoflavane and isoflavanone subclasses were not shown due to the limited number of papers retrieved for them (1, 2 and 3, respectively).

Biological applications of the reported studies

With regards to the principal objective of the research, studies reported a significant proportion of articles (332, 82%) consistently focused on the implications of angiogenesis on cancer growth and metastasis (**Figure 2. 3A**). Breast cancer dominated the cancer type with 45 articles (13.5%) followed by glioma (35 articles, 10.5%) and lung cancer (30 articles, 9%) (**Figure 2. 3B**). Only 7% of the articles studied angiogenic effects of flavonoids on other diseases such as diabetes, bone and eye diseases, whereas 11% focused on the angiogenic activity of flavonoids without application to a specific pathology. These data suggest that the indicated research trends generally focused on cancer in the context of types with the highest incidence and mortality rates (e.g. breast and lung cancers were the second highest cancer types in terms of worldwide incidence and mortality, respectively, from 2003 to 2017 [164]).

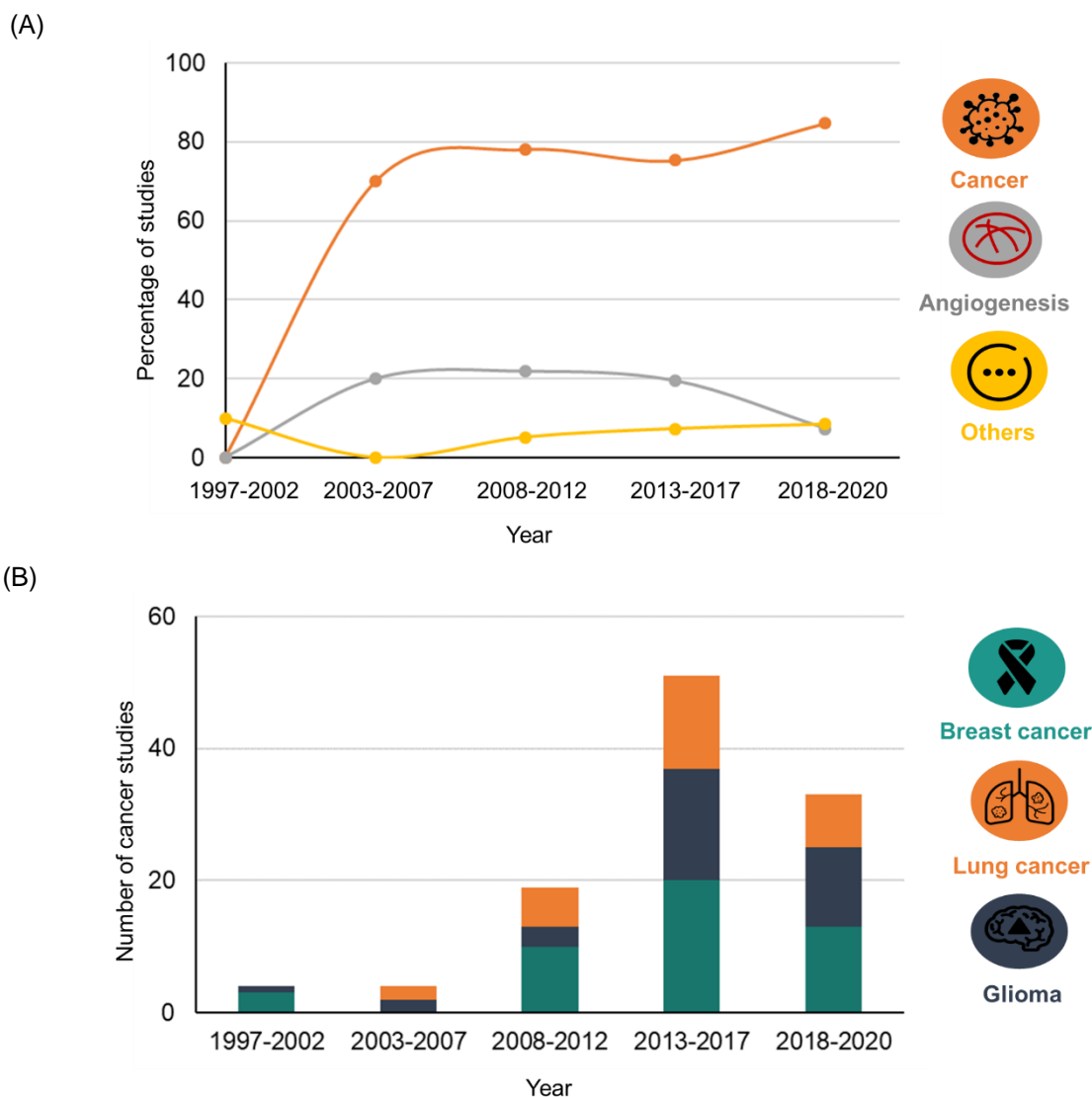


Figure 2. 3. Number of papers retrieved with respect to pharmacological application from the year 1997 to 2020. (A) Percentage of studies focusing on cancer, angiogenesis or other application relative to the total number of studies; (B) Absolute number of studies focusing on breast, lung and glioma cancer types

Types of assays used in the evaluation of the antiangiogenic activity of flavonoids

With regards to the types of assays used within the pool of studies, almost 50% of researchers exclusively conducted *in vitro* assays whereas approximately 45% utilized a combination of both *in vitro* and *in vivo* models (**Figure 2. 4A**). Findings on *in vitro* studies are presented in **Figure 3.2, Section 3.1, Chapter 3**. The use of a combination of *in vitro* and *in vivo* assays is usually recommended as it provides complementary results [165]. Upon further examination of the presented data, it is evident that the number of research papers that relied only on *in vivo* tests was consistently low.

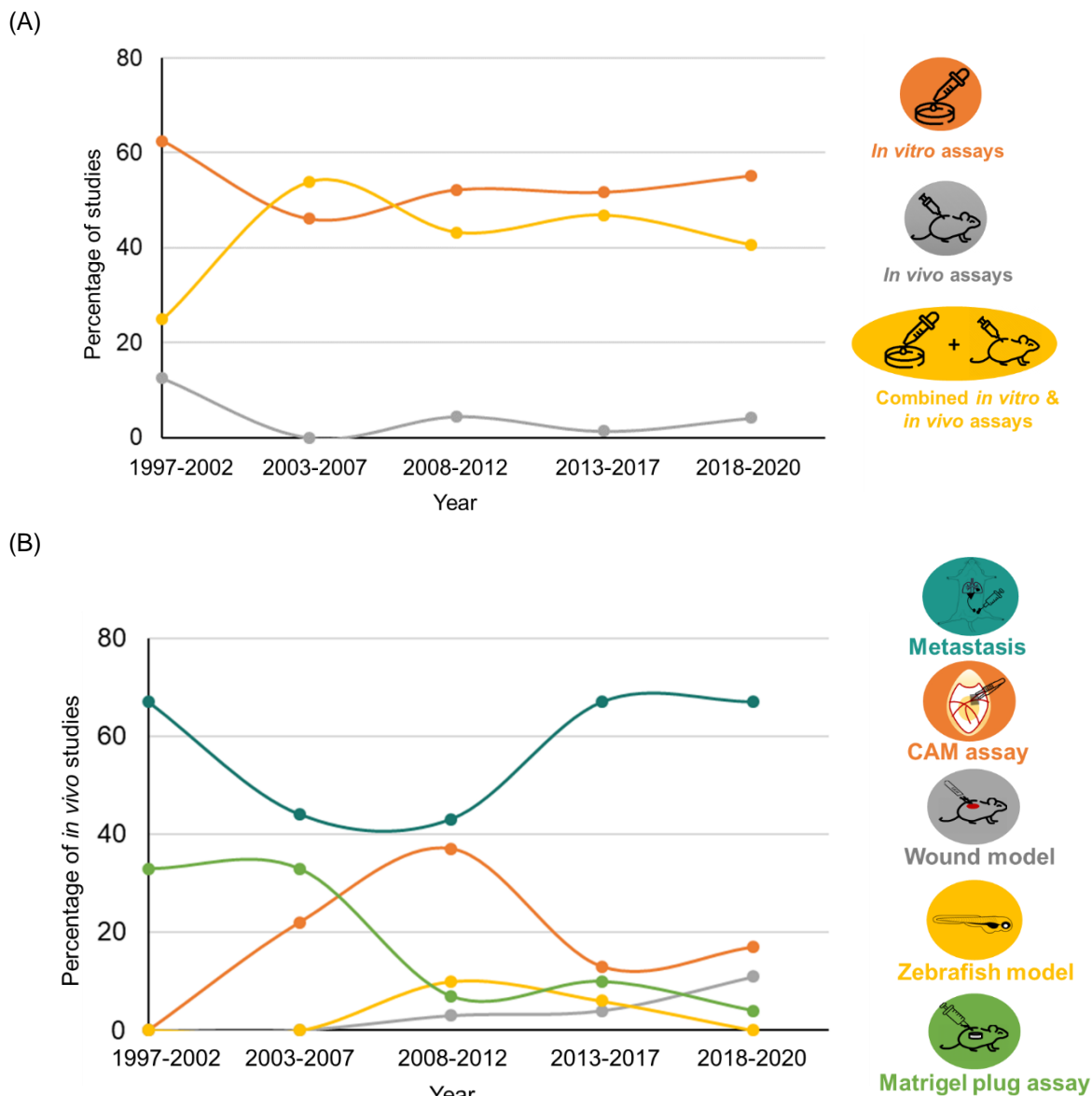


Figure 2. 4. Profiling of types of assays used for antiangiogenic evaluation of flavonoids from the year 1997 to 2020. (A) Percentage of studies using *in vitro*, *in vivo* assays or a combination of both; (B) Percentage of studies using different types of *in vivo* assays

As shown in **Figure 2. 4B**, most of the *in vivo* reports measured the effects of flavonoids on the inhibition of metastasis of tumor xenografts (37% of the total conducted *in vivo* assays). Interestingly, the chick chorioallantoic membrane (CAM) assay witnessed a continuous increase in usage up until 2012 (37%). However, subsequent years revealed a decrease in its application for the *in vivo* assessment of flavonoids, with preference being displayed for studies on mammalian metastasis. In spite of the importance of murine models in the preclinical assessment of therapeutic agents, the CAM model has

several benefits to offer particularly in the early drug screening stage as is the case with the studies included herein. For instance, the CAM assay is fairly simple, inexpensive and has a shorter treatment duration in comparison to mouse models [165–168]. Therefore, it is more appropriate for large scale screening. Furthermore, CAMs can express almost all of the known angiogenic factors [169,170], besides lacking a mature immune system which allows for the study of tumor induced angiogenesis in addition to the normal conditions evaluations [171]. The application of the CAM model therefore has the potential to yield novel insights on the antiangiogenic properties of flavonoids.

Analysis of the 402 included studies from a variety of perspectives (i.e. flavonoid subclass, biological application and types of assays) showed useful insights. Specifically, the flavone and flavonol subclasses were the most researched presumably because of their reported high activity relative to the other subclasses. Anticancer applications dominated the intended application of the conducted antiangiogenic research (82%), with preclinical data being presented, but no compounds progressing to the clinic. Hence, this field could benefit from a comprehensive quantitative meta-analysis, given their role in guiding clinical research [172]. Accordingly, the *in vivo* CAM assay was selected as a base for conducting a quantitative meta-analysis herein. The abovementioned technical advantages of the CAM assay coupled with its ability to provide comparable sets of data across different subclasses of flavonoids can yield robust conclusions on the antiangiogenic properties of flavonoids. The conducted meta-analysis would therefore ascertain the flavonoid structural framework for the design of this project's lead compounds, supporting the aim of this chapter.

2.2.2. Meta-analysis of the antiangiogenic activity of flavonoids [162]

This meta-analysis was conducted according to PRISMA guidelines (**Table 7.1, Section 7.3.1, Chapter 7**) [163].

2.2.2.1. Search and selection of studies

The second search, which is the basis of the meta-analysis, followed the same general methodology as detailed in the systematic review section. Two sets of keywords (flavonoid, flavone, flavonol, flavanol, anthocyanidin, polyphenol) and (angiogenesis, “chick chorioallantoic membrane”, “in vivo angiogenesis”) were systematically combined

(Table 7.3, Section 7.3.1.1, Chapter 7). 960 records were identified from the four electronic databases (381 from ScienceDirect, 496 from PubMed, 65 from Web of Science and 18 from Google Scholar) (Section 7.3.1.1, Chapter 7). 25 research articles were included in the quantitative analysis after the sequential steps of screening and sifting, as shown in Figure 2. 5 and described in Section 7.3.1.2, Chapter 7.

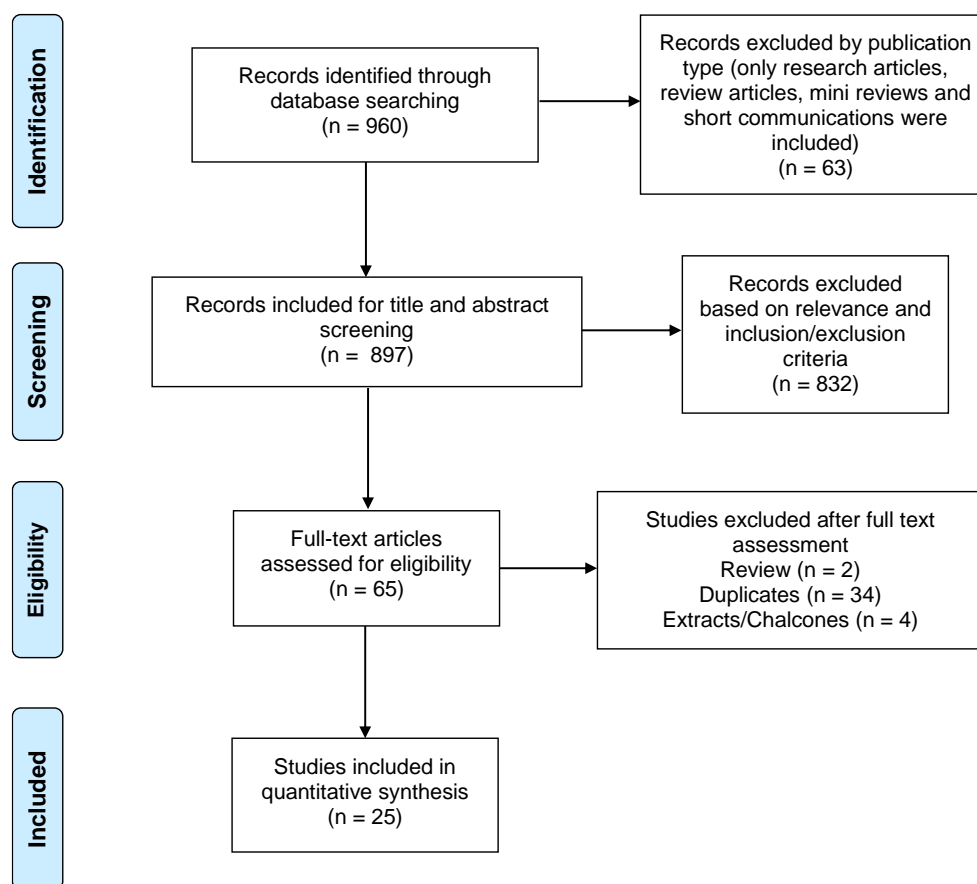


Figure 2. 5. PRISMA flow diagram of search and selection of study process for the meta-analysis

2.2.2.2. Characteristics and meta-analysis of the involved studies

In order to ensure proper quantification of the angiogenic activity of flavonoids, the following study characteristics were extracted from the included studies: (a) author and year of publication, (b) studied flavonoids, (c) angiogenesis promoters used, (d) cell line, (e) concentration of flavonoid, (f) time and duration of treatment, (g) how the results were represented and (h) number of trials (n) (Table 2, Appendix A).

To better understand attributes of the included studies, the general set-up of the CAM assay is described in Figure 2. 6. Fertilized chicken eggs are incubated at 37 °C for 3

days then a small hole is made in the egg shell to remove some of the albumin in order to facilitate detachment of the CAM from the shell. Across the different studies, compounds under investigation are added to approximately 5 to 10 days old chicks on specific carriers, such as matrigel or sterile filter/plastic discs, through a small window cut in the egg shell. After 2 to 8 days, existing blood vessels can be visualized and evaluated by light or electron microscopy.

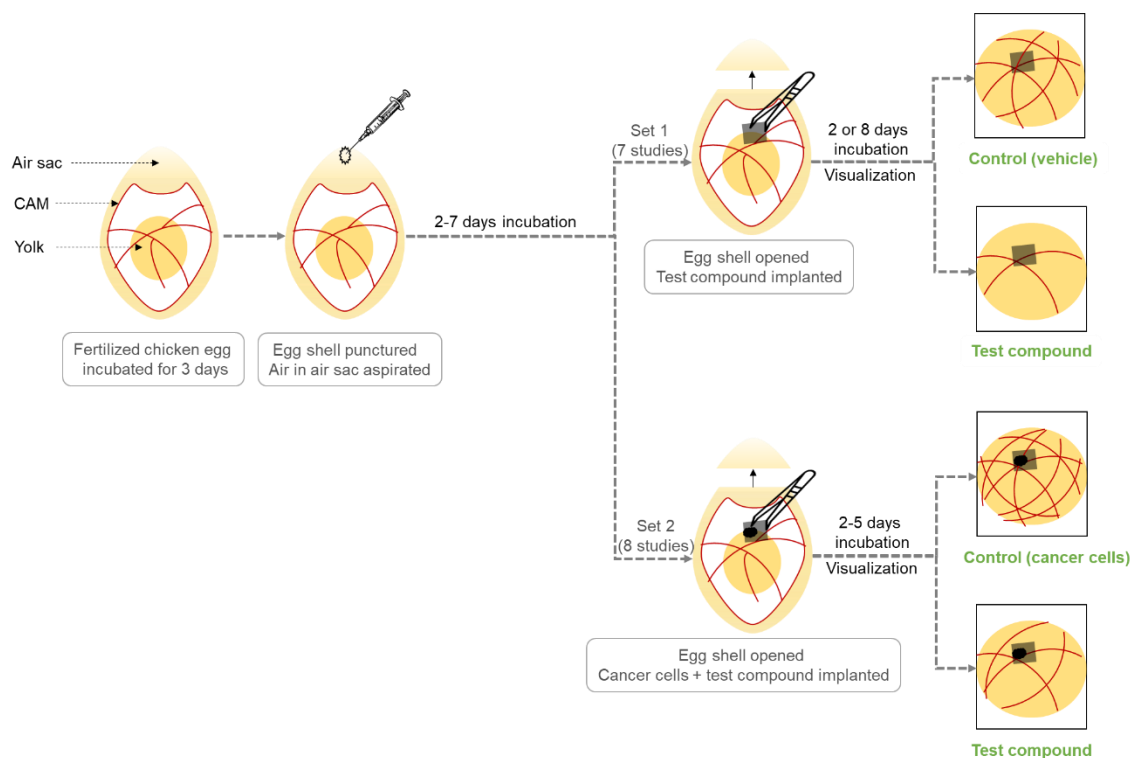


Figure 2. 6. Schematic diagram of the CAM assay procedure for the 2 sets of involved studies

6 Studies [173–178] were not included in the conducted analysis as they failed to report the required data outcomes. Authors of the studies that did not report the data required for analysis herein were contacted via email but this did not provide further insight [37–39]. The remaining 19 studies were grouped into 3 sets based on the controls used to ensure a more meaningful comparison. In the first set (7 studies [85,180–185]), the normal vasculature of the CAM was used as a control without any interventions that would induce angiogenesis (**Figure 2. 6**). The second set tested the antiangiogenic activity of flavonoids on CAMs with abnormal angiogenesis using cancer cell lines (8 studies [81,186–192]). The third group had 4 publications [179,193–195] that primarily investigated the antiangiogenic properties of wogonoside on lipopolysaccharide or IL-6

induced CAMs. However, these reports did not offer data relevant to the scope of this study and hence were not presented.

Set 1: Antiangiogenic effects of flavonoids on CAMs' normal vasculature (normal conditions)

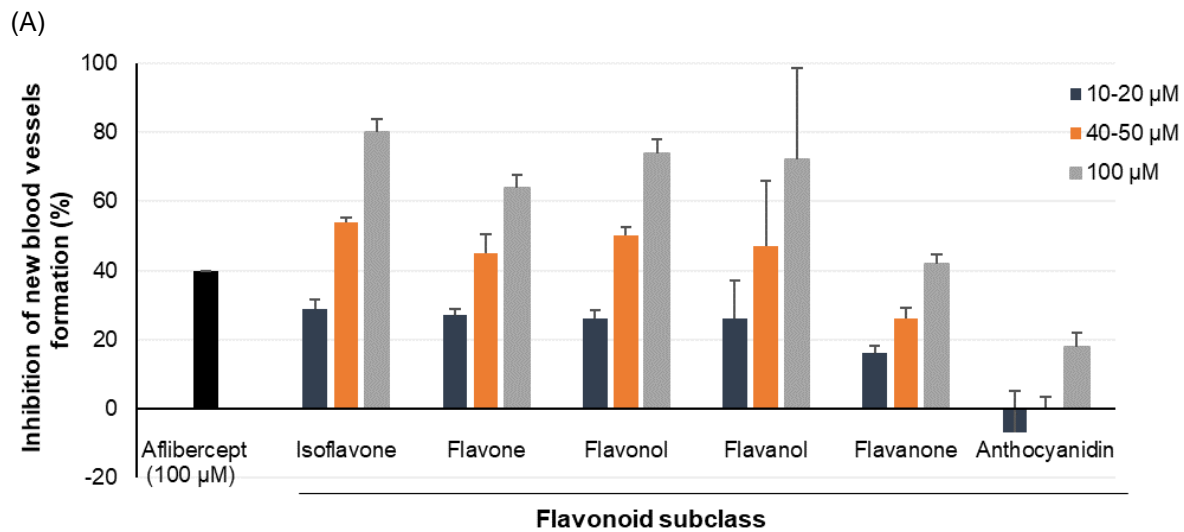
The number of blood vessels relative to the control was used as the outcome measure to ensure comparability across studies, the lower the ratio the higher the antiangiogenic activity (for full details on data preparation and generation, see **Section 7.3.1.4, Chapter 7**). The antiangiogenic VEGF inhibitor drug aflibercept (zaltrap®) was used in this study, as a benchmark to evaluate the significance of flavonoids' antiangiogenic activity in comparison to commercially available treatments. Aflibercept has a higher affinity to VEGF than both its endogenous VEGF receptors and the anti-VEGFR antibody bevacizumab (avastin®) [196]. Aflibercept can additionally target placental growth factors (PLGF-1 and 2), which makes it more effective than bevacizumab in tackling tumor's reliance on alternative proangiogenic factors as a resistance mechanism [196].

Flavonoids were sub grouped based on their chemical subclass. Three dose ranges of 10-20 (low), 40-50 (medium) and 100 μM (high) were used in the meta-analysis of set 1 to ensure consistency in the conducted comparison. Moreover, these ranges aligned with the reported dose range for the cytotoxic effects of flavonoids (10-100 μM against solid tumors such as bladder, breast and lung cancers [197]). This is of importance as the aim of this project is to combine both antiangiogenic and cytotoxic activities in a single molecule.

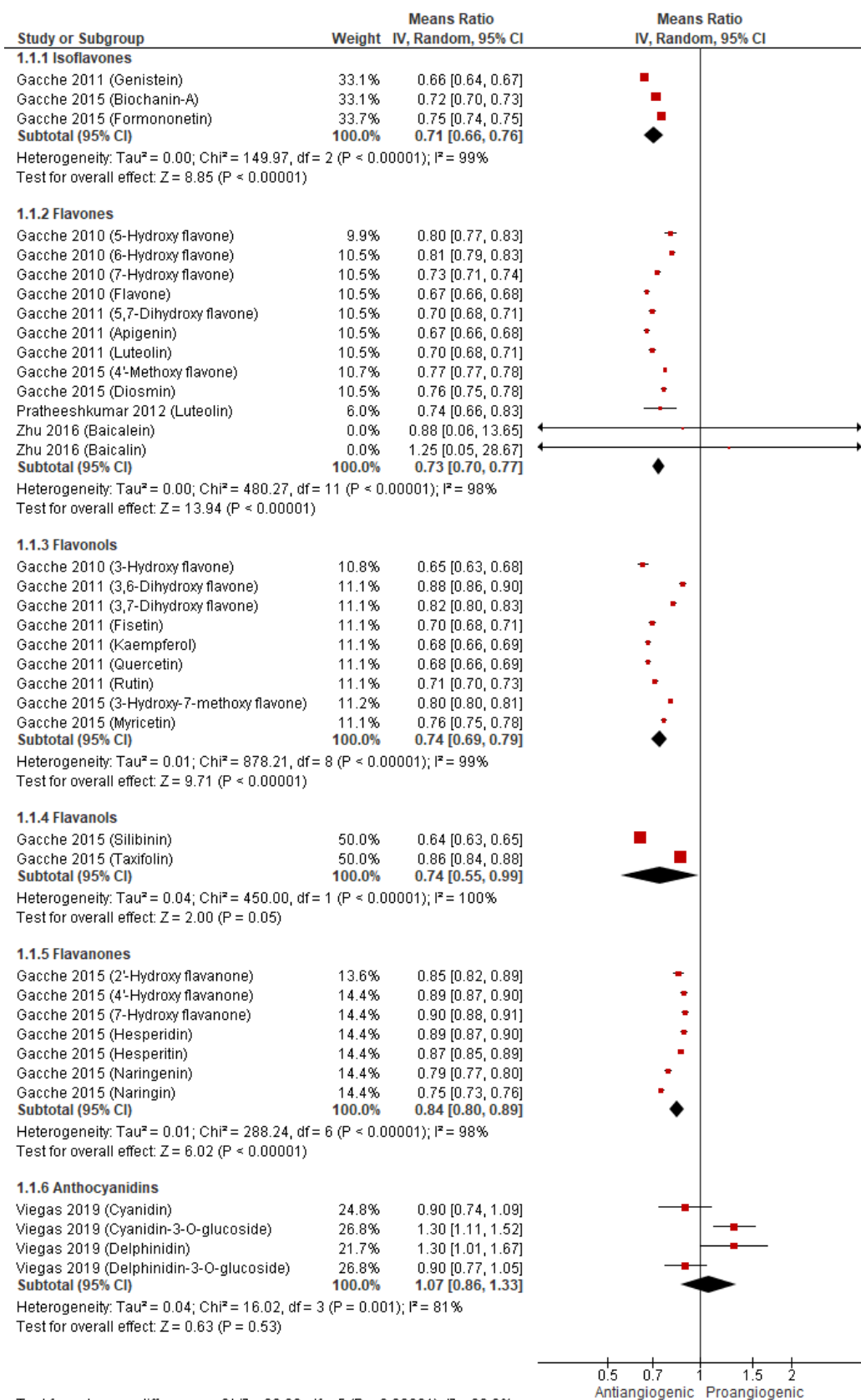
As summarized in **Figure 2. 7A**, all of the tested subclasses, except for anthocyanidins, demonstrated a concentration dependent antiangiogenic activity. The majority of subclasses were more potent than the positive control, aflibercept at 100 μM . The suppressive effects of isoflavones, flavones, and flavonols on the development of CAM vessels at 100 μM were found to be 80, 64, and 74%, respectively. In comparison, aflibercept exhibited a 40% inhibition at the same concentration.

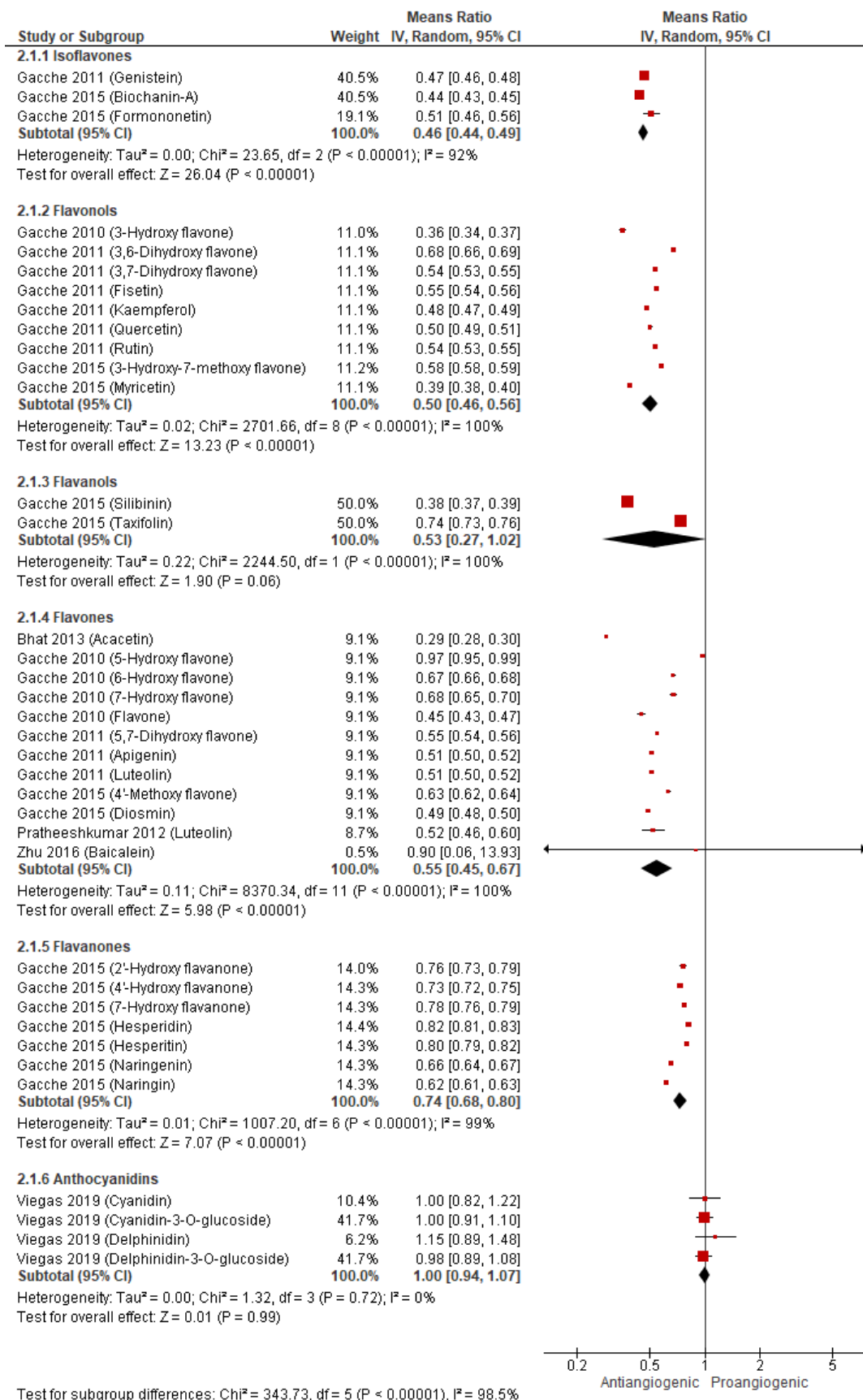
Looking at the detailed forest plots, most of the subclasses exhibited similar activity at 10-20 μM (**Figure 2. 7B**). The overall means ratios (summary estimates of antiangiogenic activity of a subgroup of flavonoids relative to control) ranged from 0.71 to 0.74 for

isoflavones, flavones, flavonols and flavanols subclasses (29-26% reduction in blood vessels, $p < 0.001$). The majority of flavonoid subclasses significantly suppressed CAM vasculature by 70-80% at 100 μM ($p < 0.001$). This corresponds to a 30-40% rise in antiangiogenic inhibition when compared to the activities recorded at 10-20 μM . The flavanone subgroup showed a lower yet still significant inhibition of 42% ($p < 0.001$) at 100 μM . In contrast, anthocyanidins demonstrated a comparatively smaller reduction of 18% at the same concentration.



(B)

10-20 μM 

40-50 μM 

100 μ M

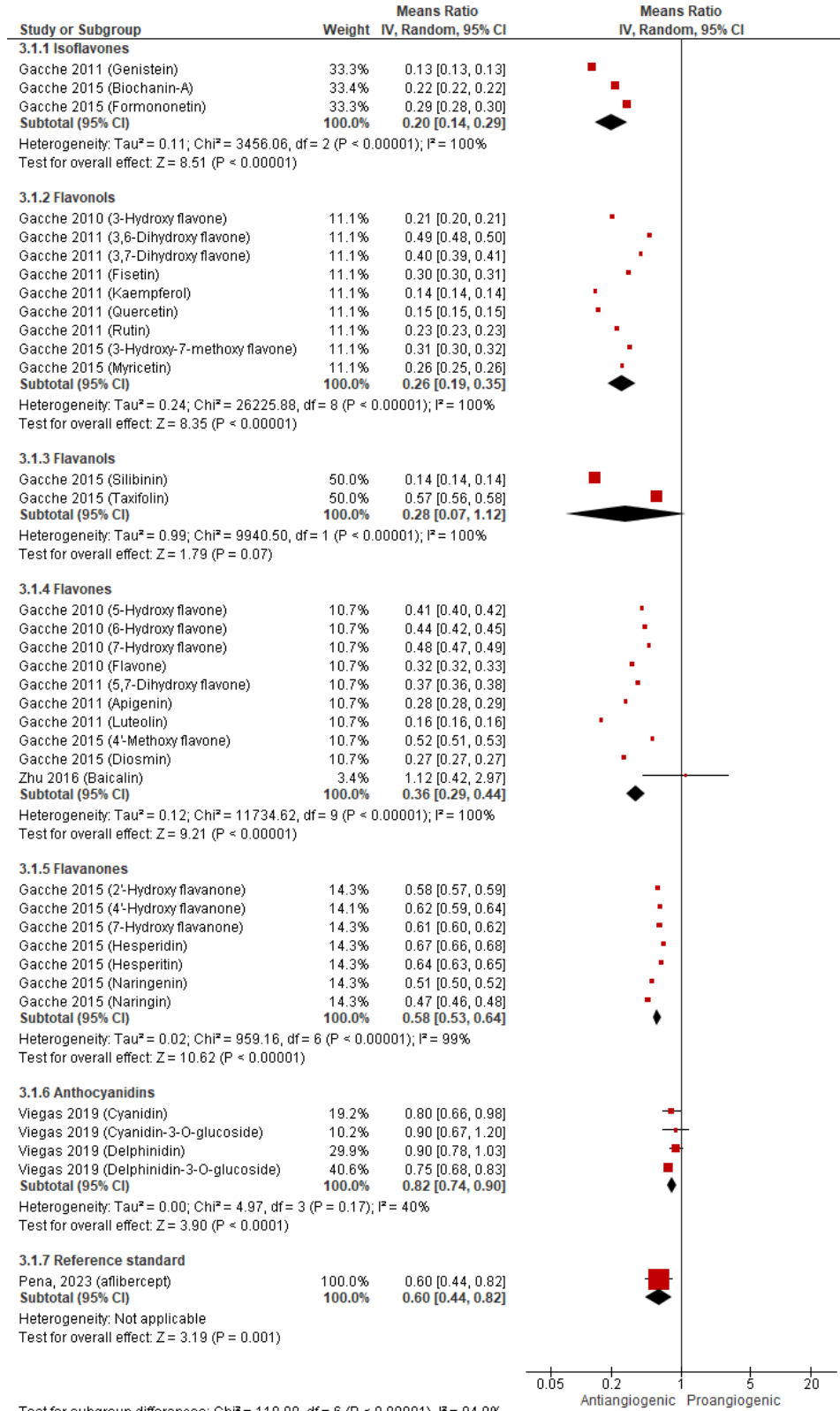


Figure 2. 7. (A) Dose-response relationship at 3 concentration ranges: 10-20, 40-50 and 100 μ M expressed as % of CAM vasculature inhibition relative to untreated control \pm SEM; **(B)** Forest plots of means ratio and 95% confidence interval (CI) of number of CAM blood vessels relative to untreated control at 10-20, 40-50 and 100 μ M

Generally, the meta-analysis conducted on this dataset has revealed significant *in vivo* antiangiogenic activity exhibited by flavonoids in the CAM assay. This highlights the viability of the chemical group of flavonoids for further preclinical and clinical advancement as prospective antiangiogenic agents. The isoflavones, flavones and flavonols subgroups have shown the strongest antiangiogenic effects. This finding aligns with previous data derived from the systematic investigation, wherein flavones and flavonols emerged as the most extensively studied subclasses (**Section 2.2.1.2**). Indeed, the activities for these subgroups surpassed that of the antiangiogenic agent aflibercept. Furthermore, the detected antiangiogenic action was in line with the dosage range at which flavonoids exert their cytotoxic effects. This suggests that flavonoids can be considered an appropriate starting point for the development of dual antiangiogenic/cytotoxic anticancer agents.

Set 2: Antiangiogenic effect of flavonoids on tumor induced CAM vasculature

This set investigated the inhibitory activities of several flavonoids on CAM vasculature implanted with different breast, ovarian and prostatic cancer cell lines. Due to the variability in the used cancer cell lines, the antiangiogenic effects and modes of action of the studied flavonoids are presented as individual studies in **Table 2. 3**. The tested flavonoids showed good inhibitory activity of >40% in most cases at concentrations ranging from 3 to 40 μM . The flavone nobiletin, for example, showed a significant level of vessel inhibition (79%, $p < 0.01$) on the ovarian cancer cell line A2780 at 20 μM [81]. For reference, the multi-target antiangiogenic/cytotoxic drug sunitinib is reported to cause 51% reduction of branching in A2780-implanted CAMs at 700 μM [198]. Quercetin, on the other hand, exhibited promising activity on the tamoxifen resistant breast cancer cell line (TAMR-MCF-7) reaching 46% reduction in vasculature at 30 μM ($p < 0.05$) [186]. A comparative subset of data was drawn from the antiangiogenic effects of the four flavonoids apigenin, myricetin, acacetin and kaempferol on the ovarian cancer cell line (OVCAR-3) at 10-20 μM . **Figure 2. 8** shows a significant overall means ratio for the four flavonoids (0.35, 95%CI: 0.27, 0.45; $p < 0.001$) in which the flavone apigenin exhibited the highest reduction in the number of CAM blood vessels (70%, $p < 0.001$).

Table 2. 3. Summary of antiangiogenic activity of flavonoids on tumor induced CAM vasculature

Flavonoid	Cell line	No of CAM blood vessels relative to control (%)	Mechanism	Ref
Quercetin	MCF-7 [§] TAMR-MCF-7*	54% (30 μ M)* 60% (10 μ M)* 79% (3 μ M)*	<ul style="list-style-type: none"> • Suppresses Pin1 VEGF gene transcription[§] • Inhibits VEGF production* • Inhibits HIF-1α and C-jun/Ap-1* • Inhibits Pin1 expression* • Inhibits Akt phosphorylation* 	Soo Jin Oh, 2010 [186]
Acacetin	OVCAR-3 [^] A2780 [†]	50% (10 μ M) [^]	<ul style="list-style-type: none"> • Inhibits VEGF transcription^{^†} • Inhibits HIF-1α expression^{^†} • Inhibits Akt phosphorylation^{^†} 	Ling-Zhi Liu, 2011 [187]
Galangin	OVCAR-3 [^] A2780 [†]	48% (40 μ M) [^]	<ul style="list-style-type: none"> • Reduces VEGF^{^†} • Downregulates HIF-1α^{^†} • Inhibits Akt phosphorylation^{^†} 	Haizhi Huang, 2015 [188]
Myricetin	OVCAR-3 [^] A2780 [†]	40% (20 μ M) [^]	<ul style="list-style-type: none"> • Reduces VEGF^{^†} • Downregulates HIF-1α^{^†} • Inhibits Akt phosphorylation^{^†} • Downregulates c-myc[^] 	Haizhi Huang, 2015 [188]
Apigenin	OVCAR-3 [^] PC-3 [#]	56% (7.5 μ M) [^] 27% (15 μ M) [^] 62% (10 μ M) [#] 47% (20 μ M) [#]	<ul style="list-style-type: none"> • Inhibits VEGF expression[#] • Inhibits HIF-1α expression[#] • Inhibits Akt phosphorylation^{^#} 	Jing Fang, 2007 [191]
Nobiletin	A2780	19% (20 μ M)	<ul style="list-style-type: none"> • Inhibits VEGF expression • Inhibits HIF-1α expression • Inhibits Akt phosphorylation • Inhibits NF-κB 	Jianchu Chen, 2015 [81]
Kaempferol	OVCAR-3 [^] A2780 [†]	61% (20 μ M)	<ul style="list-style-type: none"> • Inhibits VEGF expression^{^†} • Inhibits HIF-1α expression^{^†} • Inhibits Akt phosphorylation^{^†} 	Haitao Luo, 2009 [192]

MCF-7, breast cancer cell line; TAMR-MCF-7, tamoxifen breast cancer resistant cell line; OVCAR-3, A2780, ovarian cancer cell lines; PC-3, prostatic cancer cell line.

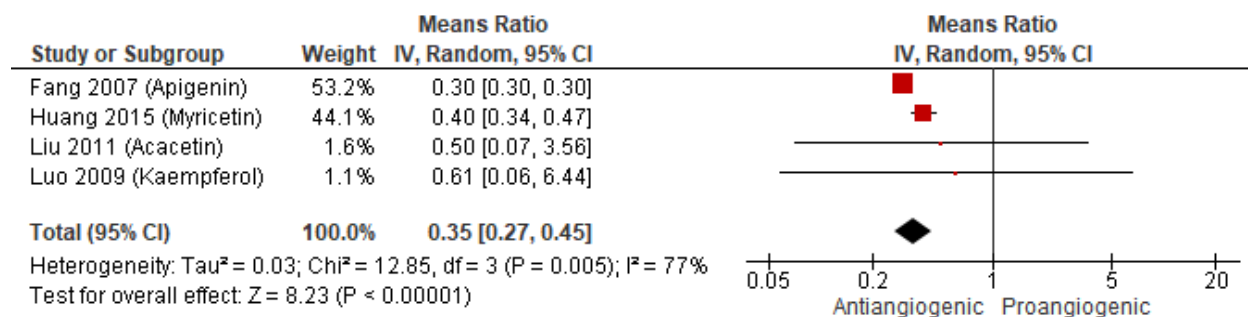


Figure 2. 8. Forest plot of means ratio and 95% confidence interval (CI) of number of CAM blood vessels of flavonoids at 10-20 μ M relative to control on OVCAR-3 cell lines

With regards to the antiangiogenic mode of action of the flavonoids included in this set (2), the authors reported the inhibition or downregulation of a number of key signaling proteins and cascades (**Table 2. 3**). This indeed underpins the required antiangiogenic polypharmacological effect of flavonoids that could circumvent some of tumors' antiangiogenic resistance mechanisms. Herein, all of the tested flavonoids caused a reduction in VEGF levels that in the majority of cases resulted from downregulation of HIF-1 α . For example, acacetin decreased HIF-1 α expression by almost 60% in OVCAR-3 treated CAMs at 10 μ M [187]. In another study, kaempferol resulted in 25 ($p < 0.01$) and 30% ($p < 0.05$) reduction in HIF-1 α protein levels in OVCAR-3 and A2780 cells at 5 and 10 μ M, respectively [192]. HIF-1 α is often overexpressed in tumors especially under the intratumoral hypoxic conditions created by antiangiogenic agents and in turn activates VEGF transcription and production as a counter mechanism [79]. The inhibition of Akt phosphorylation and activation was also heavily reported for the included flavonoids (**Table 2. 3**). For instance, 20 μ M of kaempferol reduced phosphorylated Akt from 21.8 ng/mg total protein for the control to 11.2 ng/mg ($p < 0.05$) in OVCAR-3 cells [192]. The Akt pathway among other signaling cascades can activate the synthesis of HIF-1 α protein and is thus considered an upstream regulator of HIF-1 α and subsequently VEGF [199]. Other angiogenesis regulators were also affected by the flavonoid treatments as shown in **Table 2. 3**. The overexpression of peptide isomerase (Pin1) in many tumors, such as breast and prostatic cancers, leads to VEGF upregulation via the activation of HIF-1 α and increased angiogenesis [200]. In that context, Jin Oh *et al* reported a more than 2-fold decrease in the Pin1 expression by quercetin at 30 μ M in TAMR-MCF-7 cell lines [186].

It is important to note that the reported modes of action were derived from a small set of data (6 studies) from cancer cell line-implanted CAM experiments. The included studies examined these mechanisms from the authors' views. Thus, other interactions may contribute to flavonoids' antiangiogenic and resistance-overcoming properties that were not highlighted in this meta-analysis. For example, flavonoids have been shown to disrupt MAPK, FGF, and MMPs pathways [7–9] in addition to exhibiting immunomodulatory effects [201]. These interactions could be useful as a means to bypass the tumor's dependence on alternative proangiogenic pathways.

In summary, analysis of this set has shown the robust capacity of flavonoids to disrupt the angiogenic switch of several tumors and commence an antiangiogenic trajectory. The modes of antiangiogenic action of these further confirmed their suitability as a basic framework for multi-target antiangiogenic agents where all of the included flavonoids had detrimental effects on the key proangiogenic protein VEGF via different routes.

2.2.2.3. Quality assessment

The reliability and robustness of the presented findings were evaluated on two levels. First, the methodological rigor and risk of bias (RoB) of the studies included in the meta-analysis were evaluated via a specifically designed checklist. Secondly, the robustness of the meta-analysis findings of set 1 was verified by a sensitivity analysis.

Methodological quality of included studies and risk of bias evaluation

The standard formats and guidelines utilized for the critical evaluation of studies in systematic analyses, such as the Cochrane risk of bias [202], exclusively apply to randomized clinical trials. Novel quality and RoB assessment tools for preclinical systematic analyses that rely on primary research are available. However, these prestructured checklists are specifically tailored for particular types of investigations, such as the Toxicological data Reliability Assessment Tool (ToxRtool) [203] or the Oral Health Assessment Tool (OHAT) [204]. In the absence of a universally accepted critical appraisal instrument for preclinical studies, researchers often resort to a tool that may not align with the experimental design, or they construct their own approach [205,206]. Herein, a novel checklist, that is mainly customized to the technical aspects of the CAM assay, was devised to effectively evaluate the methodological quality and RoB of the papers included

in this meta-analysis. The checklist presented in **Table 7.4, Section 7.3.1.5, Chapter 7** incorporates the relevant criteria derived from established prestructured tools such as the Systematic Review Centre for Laboratory Animal Experimentation (SYRCLE) [207] and the Consolidated Standards of Reporting Trials (CONSORT) [208]. Additionally, important factors that have the potential to influence the quality of the CAM assay [167–169,171,209] were included. Elements presented in **Table 2. 4** of the developed checklist were considered to be crucial for a high-quality CAM test. In this context, research from set 1 that did not adhere to any of these critical criteria but presented a low RoB underwent additional examination in the sensitivity analysis (**Section 7.3.1.5, Chapter 7**). For set 2, studies that failed to comply with the critical criteria were excluded from the reported results since further sensitivity analysis examinations could not be applied.

Table 2. 4. Critical criteria included in the CAM assay methodological quality and risk of bias assessment checklist

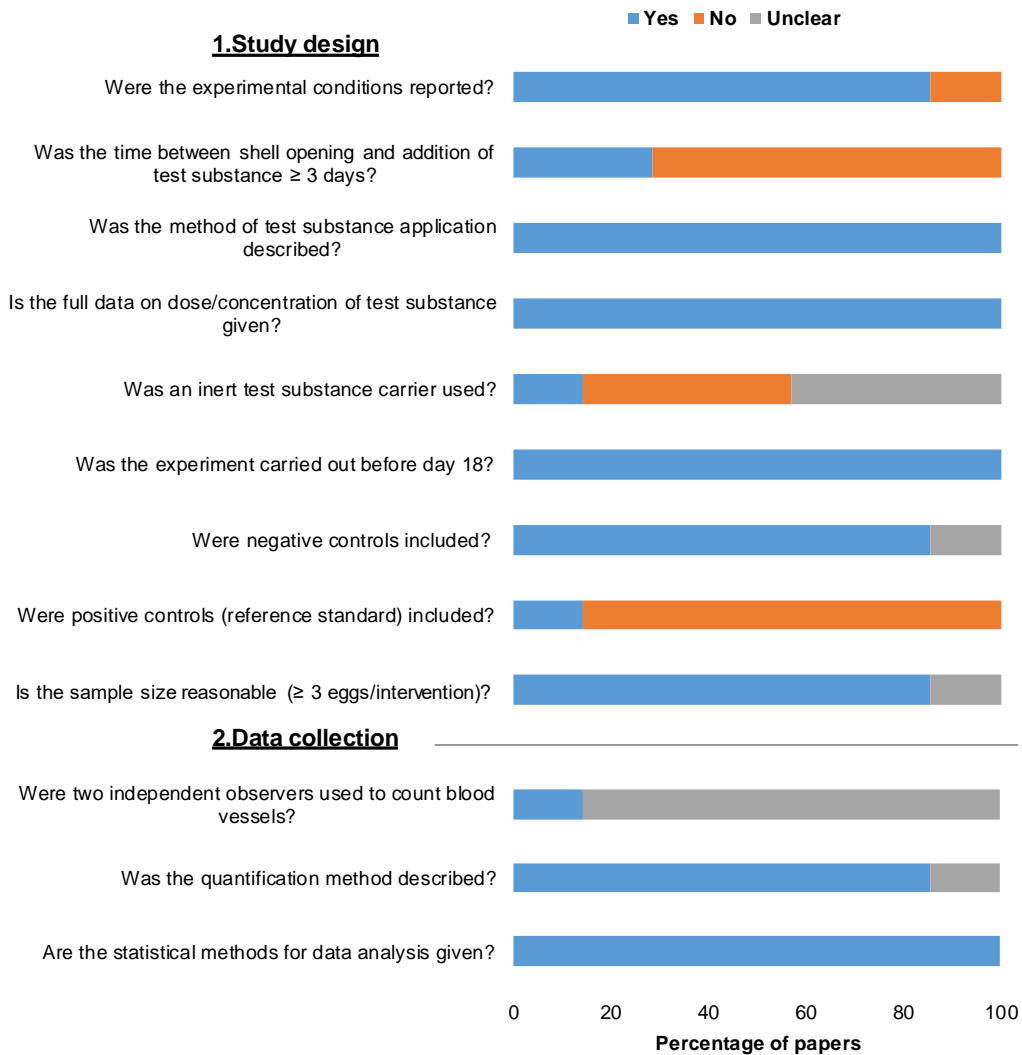
Critical criteria	Comments	Ref
Was the time between shell opening and addition of test substance ≥ 3 days? OR Were negative controls included?	Provides time to check for any inflammatory reaction resulting from the shell opening Ensures experimental conditions do not cause CAM irritation and provides a common baseline for all interventions	[169,171] [171,209]
Is the sample size reasonable (≥ 3 eggs/intervention)?	Increases the reliability and reproducibility of the results and ensures the statistical significance of the observed effects	[209]
Was the quantification method described?	Ensures quality of outcomes	[168,171]
Is the time between tumor implantation and vessel quantification ≥ 72 h?*	Tumors vascular infiltration starts 72 h after implantation. Hence, imaging of vessel development becomes challenging due to inadequate tumor vascularization	[168,171]
Was the experiment carried out before day 18?*	CAM lacks a fully developed immune system until day 18 which avoids immune reactions that can trigger angiogenesis. Additionally, this helps the implanted cells to preserve their immunogenic characteristics	[168,169]

*, criteria specific to set 2 (angiogenesis under tumor conditions).

Generally, the investigations covered by both sets 1 and 2 complied with the proposed criteria, demonstrating good methodological quality and low RoB (**Figure 2. 9** and **2.10**). Although a significant proportion of the studies (71% of set 1 and 100% of set 2) did not adhere to the recommended 3-days period between the shell opening and application of the test substance, the majority of articles (86% of set 1 and 100% of set 2) included a

negative control in their studies which mitigated against a risk of undetected CAM inflammation. Only the Pratheeshkumar *et al* study [85] failed to address one of these two items besides not fully describing how they quantified the CAM vasculature. In addition, Bhat *et al* [185] were unclear on how many eggs were used per treatment and hence did not meet the sample size criteria. Given the low RoB demonstrated by both studies, they were included in the sensitivity analysis to check their impact on the reliability of findings. The two set 2 studies by Huang *et al* investigating the effects of wogonoside on breast cancer cell lines [189,190], reported only 48 hours between tumor implantation and the evaluation of antiangiogenic effects. Consequently, both investigations were not included in the findings of set 2. The remaining studies from set 2 (75%) examined the antiangiogenic effects of flavonoids 3-5 days after the addition of both the tumor and the treatment, which allows an appropriate period of time for the tumor vasculature to grow. None of the included studies have shown a high and/or unclear RoB in more than one of the criteria (**Figure 2. 9B** and **2.10B**). Therefore, all of the included studies were recognized as low risk (**Section 7.3.1.5, Chapter 7**).

(A)



(B)

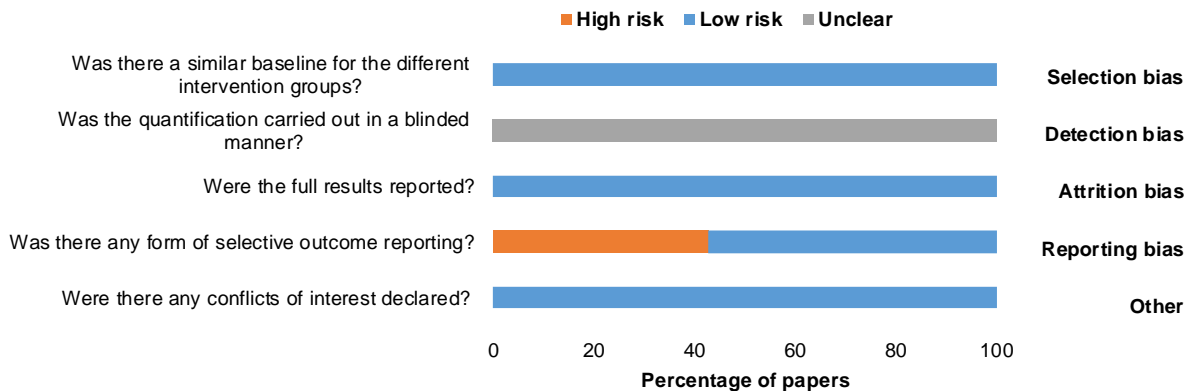
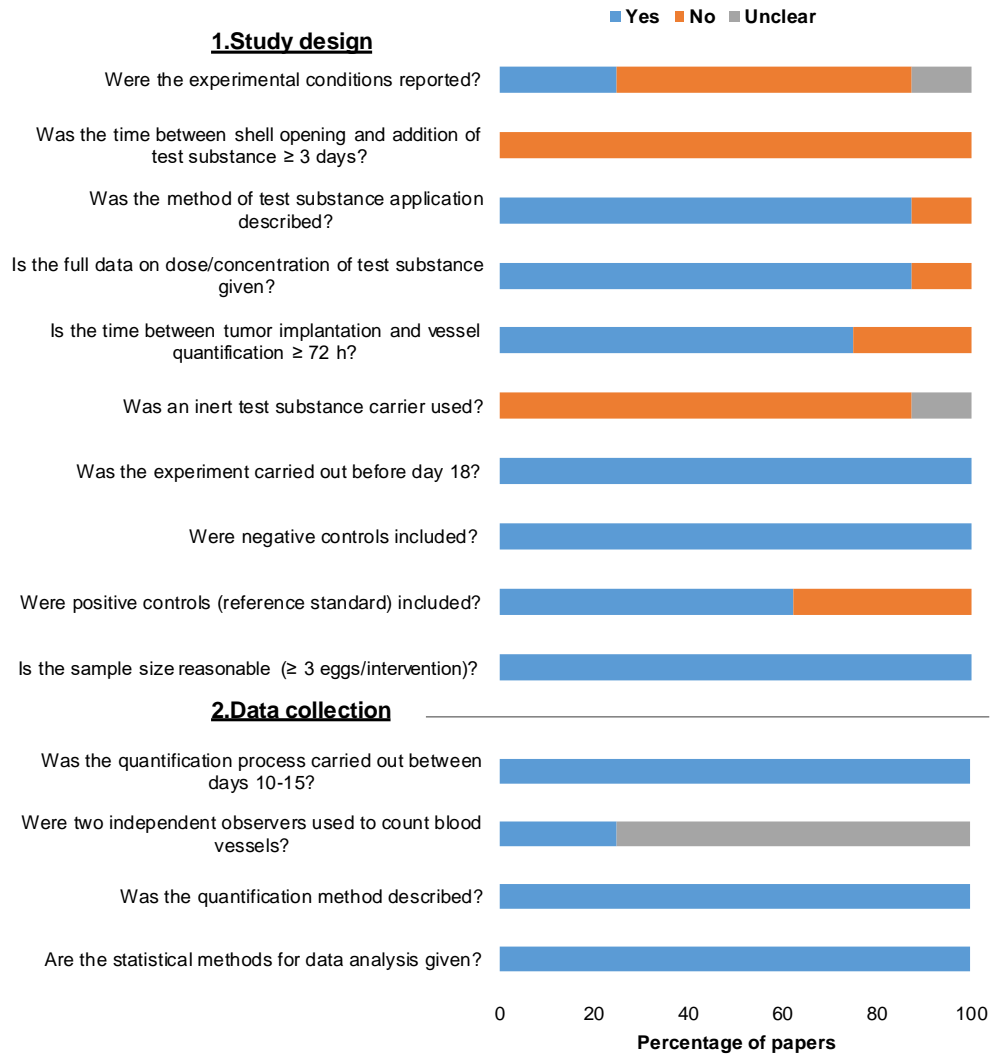


Figure 2. 9. Quality assessment of studies included in set 1 of meta-analysis

(A)



(B)

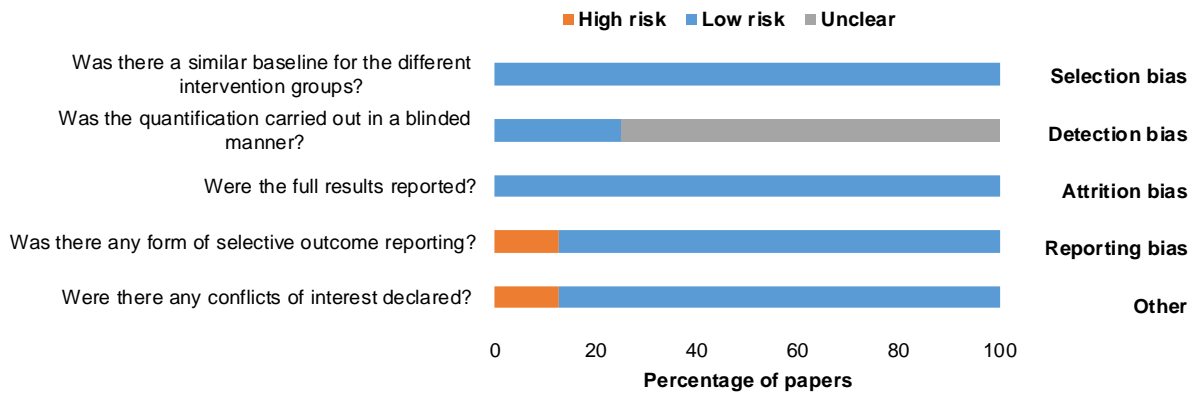


Figure 2. 10. Quality assessment of studies included in set 2 of meta-analysis

Sensitivity analysis

Although it was important to validate the meta-analysis results, it was recognized that the accuracy of heterogeneity estimates in small meta-analyses is a subject of debate, as it is uncertain if any statistical technique can effectively offer heterogeneity estimates. According to the Cochrane guidelines, an investigation of heterogeneity would yield limited informative outcomes unless there is a considerable number of interventions (studies) [210]. This is defined as at least 10 studies in the same guideline [210], a criterion that is not reached in meta-analysis studies including the one presented here. Indeed, the documented median quantity of studies per meta-analyses published in the Cochrane library varies between 3 and 7 [211]. Given the imprecision of heterogeneity estimates, such as the Higgins' (I^2) measure in small scale meta-analyses [211–213], the high heterogeneity ($I^2 > 80\%$) observed for all subgroups in the generated forest plots was not unexpected (**Figure 2. 7B**).

As an alternative approach, sensitivity analysis can be more appropriate, for providing insights into the reliability and stability of the obtained results [212]. Hence a sensitivity analysis was conducted herein by evaluating the effect of removing individual studies from the meta-analysis and determining if it significantly influenced the overall results [210].

To begin with, the impact of removing the studies by Pratheeshkumar *et al* [85] and Bhat *et al* [185], that have shown disputed methodological rigor as discussed earlier, were determined. This revealed that the removal of each caused insignificant changes in the overall summary estimates (**Tables 3 and 4, Appendix A**). The overall impact of the flavone subgroup remained consistent throughout the 10-20 and 40-50 μM range after the removal of the antiangiogenic effects of luteolin, reported by Pratheeshkumar *et al* [85]. Likewise, the exclusion of Bhat *et al* study's acacetin [185] from the flavone subgroup at 40-50 μM resulted in a minor shift in the summary estimate from 0.55 (95%CI: 0.45, 0.67) to 0.59 (95%CI: 0.51, 0.68). As a result, it was deemed appropriate to include the studies by Pratheeshkumar *et al* [85] and Bhat *et al* [185] in the meta-analysis.

Next, minimal variations were observed in the overall effects, upon the systematic removal of individual studies, across all subgroups except for the flavanol subgroup

(**Tables 3-5, Appendix A**). The flavanol subgroup, which comprises just two flavonoids (silibinin and taxifolin), is likely to be more sensitive to the removal of one flavonoid, thereby significantly affecting the overall outcome. At the 40-50 μM range for instance, the overall pooled means ratio shifted from 0.53 (95%CI: 0.27, 1.02) to 0.74 (95%CI: 0.73, 0.76) and 0.38 (95%CI: 0.37, 0.39) after excluding silibinin and taxifolin, respectively (**Table 4, Appendix A**). These results confirm the reliability of the conducted meta-analysis as a measure to assess the antiangiogenic activity of flavonoids. However, the available evidence pertaining to the subgroup of flavanols is insufficient to establish meaningful conclusions.

In summary, the included studies have shown high methodological quality and low RoB, as assessed by a specifically designed checklist. These results, along with the sensitivity analysis study, establish the reliability and robustness of the conclusions derived from the meta-analysis. Taken together, findings of the meta-analysis validated the selection of flavonoids as antiangiogenic compounds, suitable for the development of potent antiangiogenic/cytotoxic agents. Based on that, the relationship between flavonoids' chemical structure and antiangiogenic activity was explored to be incorporated in the design of the target antiangiogenic/cytotoxic agents.

2.2.3. SAR studies

2.2.3.1. Antiangiogenic SAR study

Despite the huge amount of research carried out on flavonoids' antiangiogenic activities, only Lam *et al* [154] and Ravashinkar *et al* [155] reported SAR evaluations. Both studies primarily investigated the impact of methylation of OH groups on a small set of compounds. Herein, a large scale antiangiogenic SAR study was conducted using CAM assay based data obtained from set 1 (**Section 2.2.2.2**) due to their comparability in terms of methodology, conditions and flavonoid concentrations. Additionally, set 1 included a diverse range of flavonoid subclasses, making it suitable for investigating the SAR from multiple angles. The SAR conclusions made herein (**Figure 2.11**) were derived from comparisons of structurally similar flavonoids, differing solely in the specific feature under evaluation, as noted below:

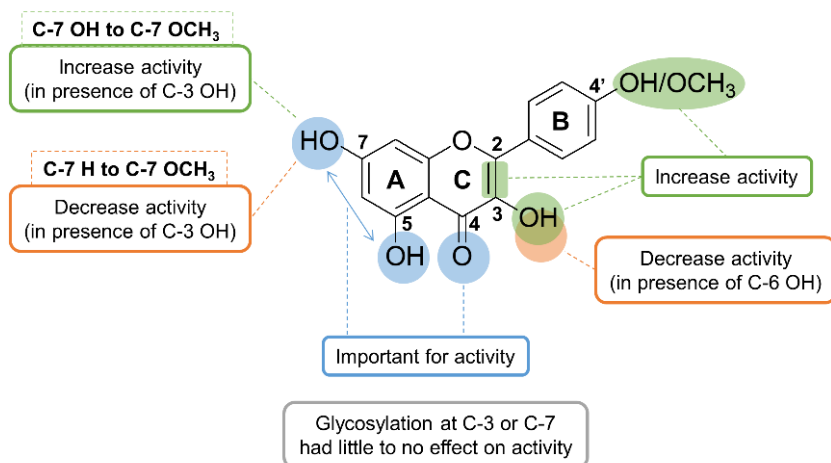


Figure 2. 11. Summary of the antiangiogenic SAR of flavonoids derived from set 1 of the meta-analysis
Unsaturation of the C2-C3 bond on ring C

It was noted that C2-C3 unsaturation increased the antiangiogenic activity. 7-OH flavone and 7-OH flavanone are two good examples that show this. At concentrations of 10, 50, and 100 μM , the vessel reduction for 7-OH flavone was 27, 32, and 52%, respectively, while the corresponding percentages for the saturated derivative (7-OH flavanone) were 10, 22, and 39%. It is worth noting that unsaturation of the C2 and C3 bond is a prevalent characteristic observed in many highly active flavonoids and is reported to be important for flavonoids' biological activities [59]. The C2=C3 together with the 4-C=O conjugation found in the flavone scaffold has been reported as crucial for interaction with several targets. These structural characteristics keep the planarity of the molecule and facilitate the electron delocalization between rings A and C [59,214].

Number and position of OH groups on rings A, B and C

A statistical regression analysis was conducted to examine the relationship between the number of OH groups and the antiangiogenic actions of flavonoids. The results indicated that there was no link between these two elements, as evidenced by the low coefficient of determination (R^2) values of 0.06, 0.04, and 0.03 for doses of 10-20, 40-50, and 100 μM , respectively. Although no clear correlation was observed between the number of OHs and activity, the position of the OH groups appeared to be of significance. Most of the highly active flavonoids had OH groups at positions 3, 5 and 7 and/or 4' (e.g. 3-OH flavone, acacetin, biochanin A, apigenin, silibinin and kaempferol). The 7-OH group can

be considered more important for activity since 7-OH flavone showed higher activity in the low and medium concentrations compared to the 5-OH analogue (e.g. 42 versus 3% vessel reduction at 50 μM). Absence of the 3-OH group resulted in a reduction in activity by as much as 14% at 50 and 100 μM . This was observed in several comparisons, such as between 3-OH flavone and flavone, kaempferol and apigenin, and 3,7-diOH flavone and 7-OH flavone. In contrast, this was not the case for 3,6-diOH flavone versus 6-OH flavone where removal of the 3-OH group marginally increased the activity by 1 to 5% at the mid and high concentrations.

Replacement of the H at positions 7 or 4' on rings A and B, respectively, with an OCH₃ group

Regarding the effect of OCH₃ groups, there were examples where the presence of a OCH₃ group at position 4' increased the activity (e.g. biochanin A, diosmin and formononetin). Nevertheless, the inclusion of an OCH₃ group at C7 resulted in a decrease in activity when compared to the unsubstituted counterpart. Specifically, in the case of the 3-OH flavone versus the 3-OH-7-OCH₃ flavone, the reduction in vessel count was 35 and 20% at a concentration of 10 μM , 64 and 42% at 50 μM , and 79 and 69% at 100 μM , respectively.

Replacement of the OH group at position 7 on ring A with an OCH₃ group

Presence of the 7-OCH₃ group in 3-OH-7-OCH₃ flavone slightly improved the activity (reduction of number of vessels) over the 3,7-di-OH derivative from 18 to 20% at 10 μM and from 63 to 69% at 100 μM , respectively. However, this was the only case of such replacement which therefore requires additional investigation.

Glycosylation of OH groups at positions 7 or 3 on rings A and C, respectively

Glycosylation at positions 7 or 3 showed neither a pronounced nor a consistent effect on the antiangiogenic activity of flavonoids. While a decrease in activity was observed with quercetin versus rutin, hesperitin versus hesperidin and cyanidin versus cyanidin-3-O-glucoside, an increase was observed in the cases of naringin versus naringenin and delphinidin versus delphinidin-3-O-glucoside.

2.2.3.2. Cytotoxic SAR study

As noted before, the main goal of this project is to maximize the therapeutic efficacy of antiangiogenic anticancer agents by combining dual and cytotoxic activities within a single molecule. Hence the design of the lead compounds was taken forward with reference to the extensive body of SAR data available for the cytotoxic profiles of flavonoids [6,59,214–219], with a focus on comparative investigations on the impact of flavonoids on human cancer cell lines. Relevant SAR conclusions deduced by literature reviews were also taken into consideration. The findings of these reports are summarized in (Table 6, Appendix A) and will be discussed in the following section as an integral component of the design of the lead compounds.

2.2.4. Design of lead flavonoids

Figure 2. 12 illustrates the sequential stages involved in the design process, which can be outlined as follows:

Structural framework (A):

The design of the first framework was based on combining the structural features that were reported as the most important for antiangiogenic and cytotoxic activities. These features are C2=C3, 4-C=O (i.e. flavone structure) in addition to OH substitutions at positions 5, 7 and 4'.

The importance of flavones was previously demonstrated by findings of the systematic review and meta-analysis (Sections 2.2.1 and 2.2.2). Results of the antiangiogenic and cytotoxic SAR analyses carried out in this chapter (Section 2.2.3), reinforced the significance of flavones' structural requisites for achieving biological efficacy. Consequently, flavones served as the primary structural foundation for the design of the dual antiangiogenic/cytotoxic anticancer lead compounds.

The 5, 7-diOH substitution pattern on ring A was also present in many active flavonoid structures [6]. In this context, the C5-OH and 4-C=O can act as bioisosteres for N1 and C6-NH₂ pharmacophores of the adenine molecule of adenosine triphosphate (ATP), facilitating the interaction with the ATP binding pocket of several target kinases such as PI3K, Pim1 kinase, CDK and P-glycoprotein [220–222].

The contribution of an OH group at the C4' position to the increased activity of flavonoids has been consistently observed in relation to their antiangiogenic and cytotoxic properties. This was demonstrated in the antiangiogenic SAR study carried out herein (Section 2.2.3.1) as well as in several reports on cytotoxic profiles [6,214,216,217,223] (Table 6, Appendix A). In that context, the C4'-OH group has been identified as a mutual characteristic of flavonoids exhibiting estrogenic and topoisomerase I and II inhibitory activities [224].

It is worth mentioning that structural framework (A) is the structure of the natural flavone apigenin which is one of the most bioactive flavonoids with multi-target antiangiogenic and cytotoxic activities (for a full review on apigenin's therapeutic potential, see ref [225]).

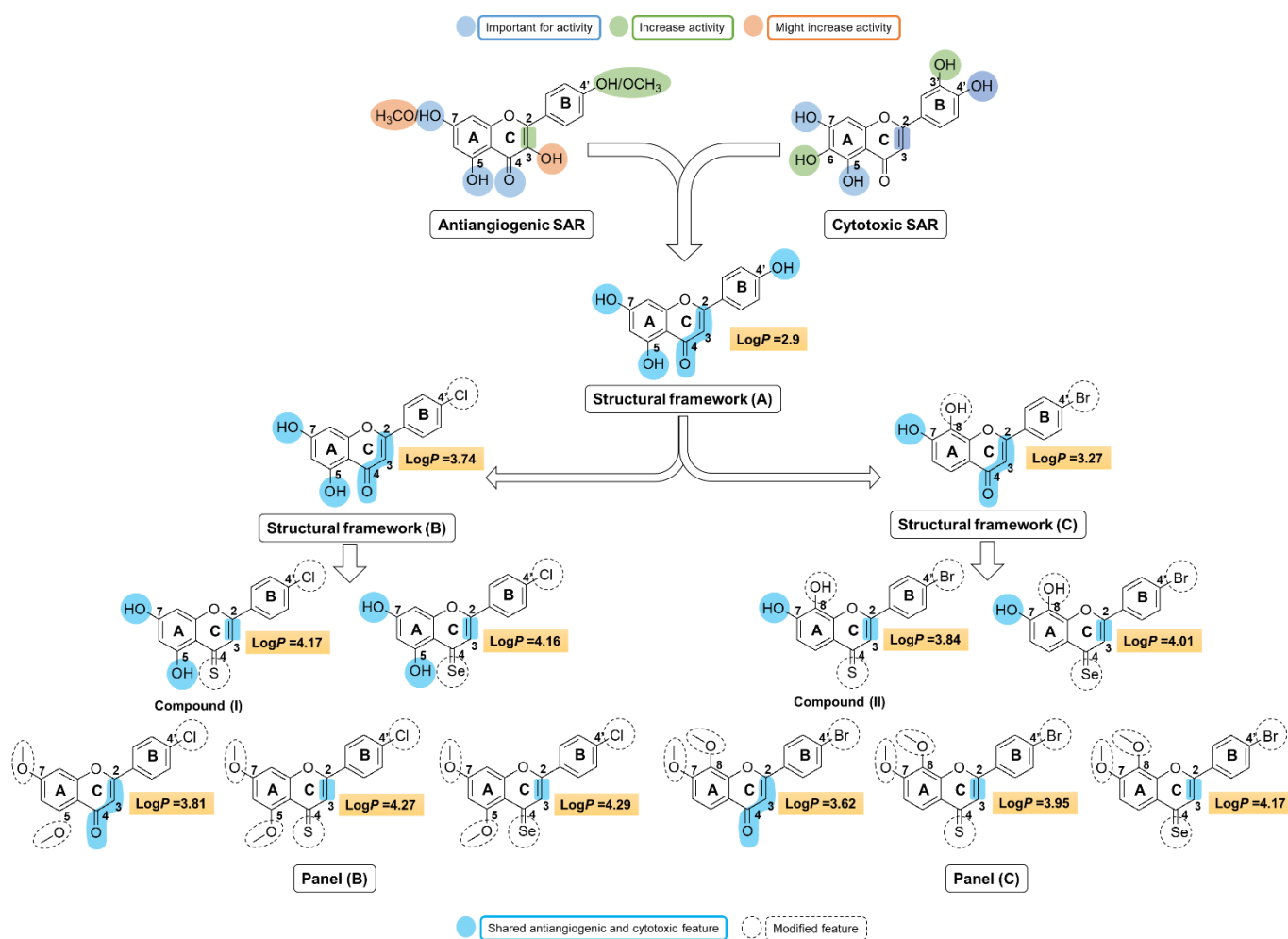


Figure 2. 12. Schematic diagram of the design process of the lead flavonoids used in this project. LogP values were predicted using ADMET lab 3.0 web-server [226].

Structural frameworks (B) and (C):

In this step, structural framework (A) was further developed into a better lead structure with the aims of a) enhancing the activity and b) enhancing the physicochemical properties. With regards to ring A, framework (B) still incorporated the 5,7-diOH substitution pattern. A 7,8-diOH functionality was alternatively introduced into framework (C). In a study by Ravishankar *et al*, the novel compounds (**I** and **II**) (**Figure 2. 12**) bearing 5,7-diOH and 7,8-diOH substitutions, respectively, were identified as the most cytotoxic on breast cancer cell lines MCF-7, MCF-7/DX and MDA-MB-231 (IC₅₀ ranging from 1 to 9 µM) amongst 76 synthetic flavone analogues [219]. Moreover, the mean inhibitory doses of **I** and **II** against the NCI's panel of 60 cancer cell lines were 2.81 and 2.39 µM, respectively. Leads **I** and **II** exhibited nanomolar range GI₅₀ values against several NCI cancer cell lines, such as breast cancer cell lines MCF-7 and T-47D for compound **I** (GI₅₀ =0.18 and 0.03 µM, respectively) and non-small cell lung (NCI-H460) and colon carcinoma (HCT-15) cells for compound **II** (GI₅₀=0.97 and 0.48 µM, respectively). As mentioned previously, the *meta*-diOH substitution pattern is important for both antiangiogenic and cytotoxic activities. However, as seen with active hit (**II**), the presence of an *ortho*-7, 8-diOH substitution showed promising cytotoxic activity. The presence of 7, 8-diOH was also reported to enhance the antiestrogenic effects of flavonoids by Le Bail *et al* [227]. Furthermore, to the best of our knowledge, the effects of such substitution on the antiangiogenic activity of flavonoids have not been described before. Thus, introducing a 7, 8-disubstituted analog not only holds potential for enhancing the biological activities of the test compounds but would also diversify the designed flavonoid library and introduce new insights on the effects of such substitution on activity (structural framework (C), **Figure 2. 12**).

For ring B, it was hypothesized that replacement of the 4'-OH group with a halogen atom would have a two-fold benefit. To begin with, it would enhance the activity by creating more hydrophobic interactions as well as increasing the electron delocalization through the flavonoid. According to Ravishankar *et al*, the presence of an electron withdrawing group at C-4', particularly Cl and Br substitutions, increased cytotoxicity by 2-7 fold on the MCF-7 and MCF-7/DX cell lines [219]. Previous studies have reported that the inclusion of a Cl group on ring B has a positive impact on the activity on several kinases,

such as Raf1 and c-Jun N-terminal Protein Kinase [214]. The Cl group at position 6' on ring B of flavopiridol is reported to increase the hydrophobicity of the molecule and bind to the hydrophobic pocket of CDK [222]. The second advantage of a 4'-halogen atom is improving the physicochemical properties by replacing the 4'-OH which is adversely related to gastrointestinal permeability due to low lipophilicity and high susceptibility to O-glucouronidation and sulfation metabolism [228]. According to Plochmann *et al*, the enhanced cell membrane permeability observed for more lipophilic flavonoids explains the negative correlation between their cytotoxic activity and maximum solubility in human leukemia cell line (Jurkat E6-1) [217]. In the structurally similar catechols, increasing the lipophilic character ($\log P$) caused enhanced cytotoxicity on isolated rat hepatocytes [229]. Consequently, Cl and Br atoms substituted the 4'-OH in structural framework (A) ($\log P = 2.9$) to give frameworks (B) ($\log P = 3.74$) and (C) ($\log P = 3.27$), respectively (**Figure 2.12**).

Replacement of the 4-carbonyl with 4-thiocarbonyl

Sulfur containing small molecules are commonly associated with beneficial biological effects. The observed effects can be related to their radical scavenging properties, metal chelating abilities, and interaction with crucial redox enzymes [230,231]. The substitution of flavonoids' oxygen atoms with sulfur has been linked with improved cytotoxic activity. The 1-thio analogue of a 1-oxo-2-aminophenyl flavone derivative has shown enhanced inhibition of ERK-MAPK pathway activation ($IC_{50} = 1.88$ and $2.95 \mu M$ versus 4.35 and $13.18 \mu M$ for MEK1 and ERK1/2 phosphorylation, respectively) [232]. As previously reported in the cytotoxic SAR study by Ravishankar *et al* [219], the 4-thio substitution significantly enhanced the cytotoxic activity against the breast cancer cell lines by more than 2-folds [219]. Similarly, Li *et al* showed a considerable improvement in the cytotoxic activity of dimethyl flavone derivatives upon the thionation of C-4 against cervical (HeLa), breast (HCC1954) and ovarian (SK-OV-3) cancer cell lines ($IC_{50} = 11$, 16 and $12 \mu M$, respectively, versus no activity for 4-oxoflavone) [233]. Moreover, our group demonstrated in an antiangiogenic SAR study that the 4-thio substitution enhances the antimigratory activity of flavonoids on ECs [155]. Therefore, the inclusion of 4-thioflavone moieties could greatly enhance the cytotoxic properties of our library of leads, while also offering novel information on the impact of such bioisosteric replacement on the

antiangiogenic activity. Finally, the 4-thio group would increase the lipophilicity of the flavonoid molecule (**Figure 2. 12**) which is favorable for the physicochemical properties as previously discussed.

Replacement of the 4-carbonyl with 4-selenocarbonyl

The essential trace element selenium (Se) has similar chemical properties to sulfur but higher reactivity [234]. Se displays higher nucleophilic character than S (and O) which is favorable for some chemical and biological processes such as metal chelation [234]. Organoselenium compounds generally demonstrate selective antiangiogenic and cytotoxic anticancer effects mediated by DNA damage, induction of apoptosis, and interaction with important proteins such as p53, VEGF and HIF-1 α [235,236]. Concerning flavonoids, the bioisosteric replacement of the 4-carbonyl of quercetin and chrysin derivatives with a 4-selenocarbonyl was reported by Martins *et al* to significantly enhance their cytotoxicity against nine different cancer cell lines including breast (MCF-7), cervical (A431), cisplatin-resistant cervical (A431/Pt) and ovarian (C13*) adenocarcinoma cells [237]. While polymethoxylated quercetin has shown negligible cytotoxicity, its Se derivative exhibited a 9-fold higher potency than quercetin and a 3-fold higher potency than cisplatin, on average. Se chrysin showed 18 and 3-fold lower IC₅₀ than chrysin and cisplatin, respectively. The evaluated Se flavonoids demonstrated better selectivity than their parent molecules, and cisplatin, towards cancer cells over non-transformed human embryonic kidney (HEK293) cells [237]. Therefore, it was hypothesized herein that 4-seleno (in addition to 4-thio) substitution could potentially afford compounds with higher activity. Moreover, literature reports on the biological evaluation of Se flavonoids are scarce which calls for more research in this area.

Replacement of OH groups with OCH₃ groups

Introduction of OCH₃ groups at positions 5 and 7 is commonly observed to improve the antiangiogenic activity of flavonoids [154,155,162] (**Section 2.2.3.1**). On the contrary, methylation of the 5 and 7 OH groups has been predominantly reported to exert an adverse effect on the cytotoxic activity of flavonoids. Zhang *et al* [238], Yun *et al* [239], Li *et al* [218] and Ravishankar *et al* [219] all reported a decrease in activity upon methylation of the 5 and/or 7-OH groups whilst Plochmann *et al* [217] and Wang *et al* [59] reported

the opposite (**Table 6, Appendix A**). The observed discrepancies in SAR might plausibly be attributed to variations in experimental procedures and flavonoid concentrations used in each study. Additionally, the different evaluated flavonoids exert their antiangiogenic or cytotoxic activities by interacting with distinct targets that necessitate specific structural features. Despite the inconclusive SAR findings on the impact of methylation of the free OH groups of a flavonoid, their positive influence on flavonoids bioavailability is well established. A number of studies by Wen and Walle [240,241], relating to the evaluation of the stability and bioavailability of fully methylated flavones in comparison with the free OH analogues, showed intriguing results. The methylated equivalents of chrysin (5, 7-diOH flavone) and apigenin (5, 7, 4'-OH flavone) showed a 5 to 8-fold increase in *in vitro* hepatic stability and intestinal permeability using human liver S9 fraction and Caco-2 intestinal absorption models, respectively [240]. Since the oxidative demethylation of the OCH₃ groups is much lower than OH conjugation, the metabolic stability of methyl protected analogues is much higher [242]. *In vivo* oral absorption studies in rats confirmed the previous results. While chrysin was not detected systemically, 5, 7-diOCH₃ flavone was detected in the plasma and in liver, lungs and kidney tissues after 1 hour with peak concentrations of 2.5, 16.5, 7.5 and 5 µM, respectively [115]. Accordingly, the incorporation of OCH₃ derivatives in the panel of lead compounds could provide novel SAR insight on their impact on the cytotoxic activities. Their inclusion is further warranted by enhancing the bioavailability of the test flavones based on the aforementioned studies. As a result, if methylation of free OHs did not negatively affect the anticancer activities of the target flavones, they would be of great value for future clinical translation.

In summary, the design of lead compounds in this work was influenced by two factors, namely; combining dual antiangiogenic/cytotoxic structural features, and enhancing the physicochemical properties. This was carried out in a systematic manner where first the most important antiangiogenic and cytotoxic pharmacophores were extracted from literature data and combined in one framework (A) bearing a C₂=C₃, 4-C=O (i.e. flavone structure) and 5, 7 and 4'-OH substitutions. This was followed by adding other modified features, as guided by published reports, that could enhance both the activity and physicochemical properties. These included 4'-Cl or Br, 4-C=S or Se and 5,7 or 7,8-diOCH₃ substitution. All in all, two lead panels (B and C) of 4-oxo/thio/seleno-4'-

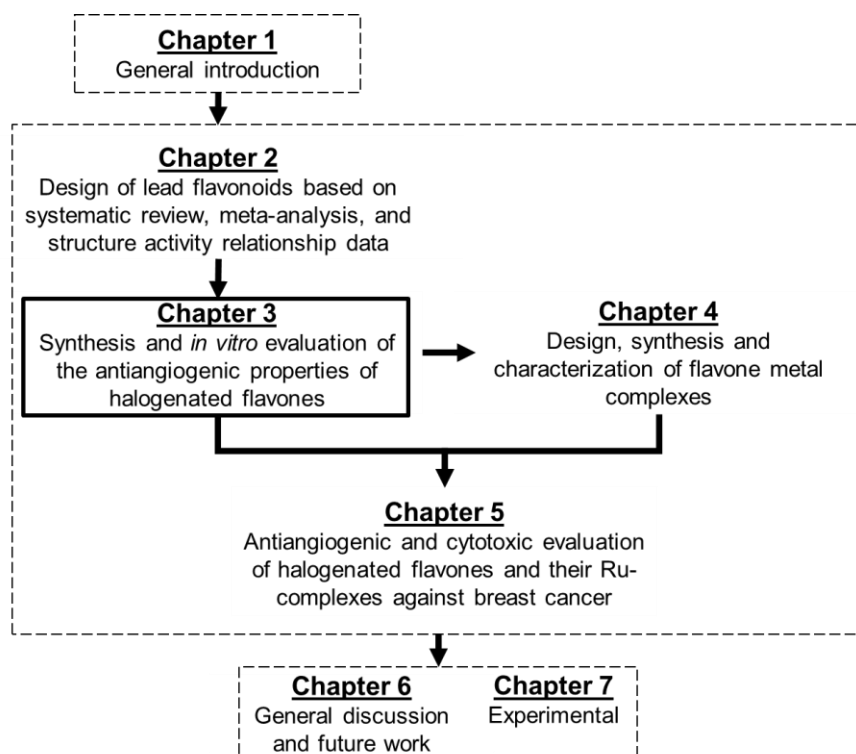
halogenated flavones with 5,7 or 7,8-diOH/OCH₃ substitutions were designed as potential anticancer leads with dual antiangiogenic and cytotoxic activities (**Figure 2. 12**).

2.3. Conclusions and future perspectives

The conducted systematic analysis revealed a focus on the flavones subclass (40%) and anticancer applications (82%) in addition to a lack of exclusive *in vivo* investigations (3% of 342 research studies) within the field of antiangiogenic activity of flavonoids. Thereby an *in vivo* quantitative meta-analysis was carried out utilizing the CAM assay, based on its technical value and comparability of data, to address the aforementioned gaps in the existing literature. Flavonoids have shown promising inhibition of CAM vessel formation that reached 80% (versus 40% for the antiangiogenic drug aflibercept) at the highest concentration of 100 μ M. Flavonoids also effected a significant drop of vasculature under different proangiogenic cancer conditions that ranged from 19 to 79% at concentrations as low as 3 μ M. Mechanistically, the majority of flavonoids resulted in the downregulation of VEGF and HIF-1 α which is a major contributor to tumor resistance in antiangiogenic therapy. The pool of gathered data was used to extract the key structural features required for the proposed antiangiogenic activity in a large scale SAR study. The extrapolated antiangiogenic structural features were finally combined with the cytotoxic structural features gathered from the literature in the design of the target dual activity flavonoid leads. The presence of unsaturation at C2-C3, a 4-carbonyl group, phenyl attachment at C2 and 5, 7-diOH substitution was considered important for both activities. Other features such as 4-thiocarbonyl and 4'-halogen substitutions were incorporated into the final library of leads with the aim of enhancing the activity and the pharmacokinetic properties of flavonoids. Although this study provided useful information regarding the preclinical antiangiogenic effectiveness of flavonoids and the relevant SAR data, further research into target-specific antiangiogenic SARs is needed to improve the future prospects of flavonoids as potentially clinically active antiangiogenic agents.

Chapter 3

Synthesis and *in vitro* evaluation of the antiangiogenic properties of halogenated flavones



3.1. Introduction

In the previous chapter, a library of halogenated flavones (**Figure 3. 1**) was designed for evaluation as antiangiogenic and cytotoxic anticancer agents. This chapter describes the synthesis of the designed flavones originating from framework A, namely 5,7-disubstituted-4'-chlorophenyl (panel B) and 7,8-disubstituted-4'-bromophenyl (panel C) flavones (**Figure 3. 1**), and reports their *in vitro* inhibitory activities against VEGF-induced EC angiogenesis. Therefore, an overview of the different pathways employed in the synthesis of flavonoids, as well as the methods used for their *in vitro* antiangiogenic evaluation, are provided herein.

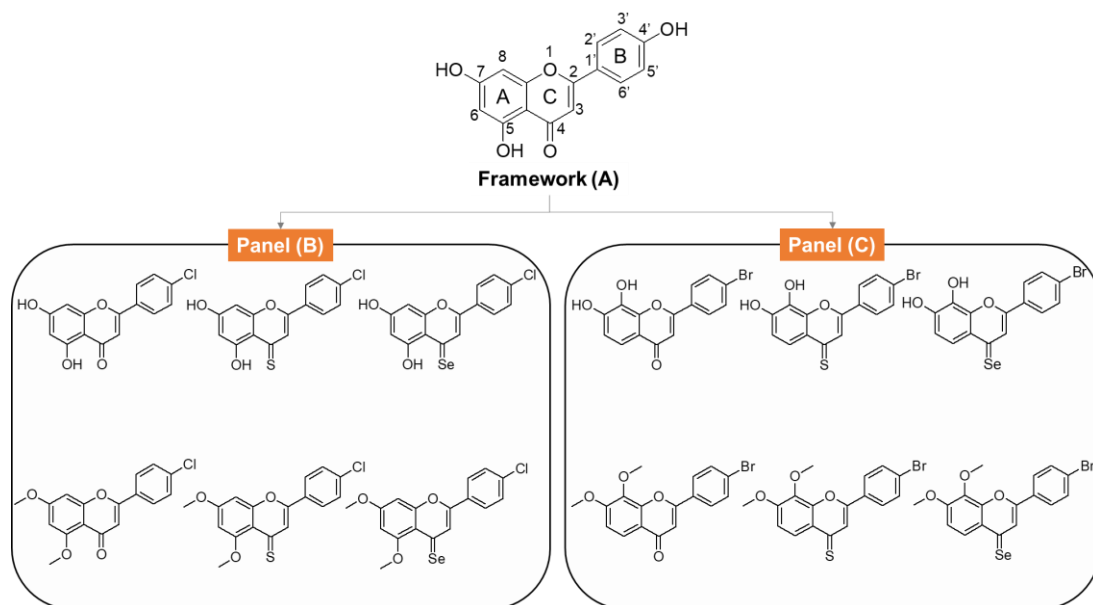
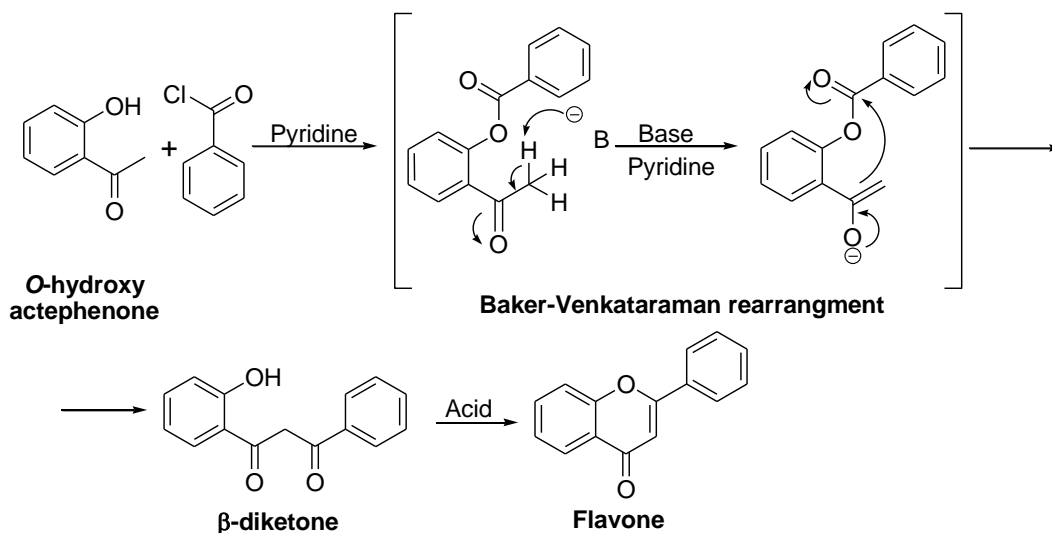


Figure 3. 1. Structures of the designed compounds. Panel (B), 5,7-disubstituted-4'-chlorophenyl flavones; Panel (C), 7,8-disubstituted-4'-bromophenyl flavones

Synthesis of flavones is mainly achieved via one of the following well-established methods:

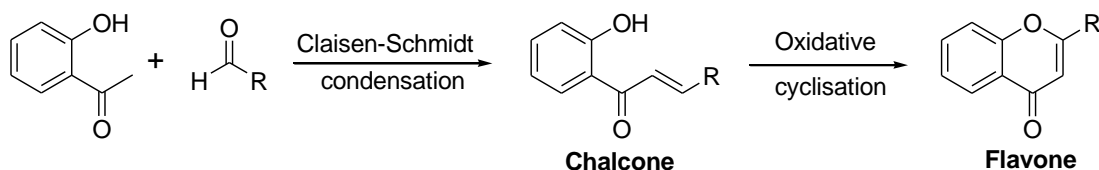
- a) Baker-Venkatarman method: This method starts with the conversion of *o*-hydroxyacetophenone to a phenolic ester followed by a rearrangement into a β -diketone in the presence of a strong base (**Scheme 3. 1**). The β -diketone is then cyclized under strongly acidic conditions to form the corresponding flavone [243,244]. The OH groups of the acetophenone derivative need to be protected before the esterification reaction [245]. Additionally, any substituents on either the A or B rings need to be introduced to the acetophenone or the aryl acid prior to the synthesis [246].

In general, this method affords the desired flavones using accessible starting materials with good yields and no side products [247].



Scheme 3. 1. Synthesis of flavones via Baker-Venkataraman rearrangement

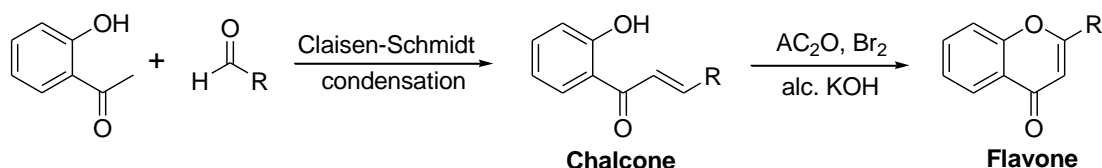
b) Claisen-Schmidt condensation: This method involves the formation of a chalcone intermediate by reacting benzaldehydes with acetophenones [246] (**Scheme 3. 2**). The chalcone is subjected to an oxidative cyclisation reaction using catalysts such as I_2 in DMSO or FeCl_3 [247]. These oxidative cyclization methods often result in low yields and formation of flavanone and aurone byproducts, and require long reaction times [248]. More efficient methods utilizing ICl /DMSO with ultrasound, or SeO_2 with microwave irradiation, have been reported for the oxidative cyclization step, affording flavones with high yields and purities [247,248].



Scheme 3. 2. Synthesis of flavones via Claisen-Schmidt condensation

c) Kostanecki-Robinson method: This technique is analogous to the Claisen-Schmidt pathway in relation to the first condensation step [247]. Herein the cyclized flavone is formed by 1,2 bromination of the chalcone followed by dehydrohalogenation using alcoholic KOH [247,248]. This method is not suitable for synthesizing flavones

substituted at positions 5 and 7, 4' or 5' due to the formation of aurones instead of the desired flavones [248].



Scheme 3. 3. Synthesis of flavones via Kostanecki-Robinson method

Generally, none of the used methods are absolute and each often needs optimization to afford specific flavone substructures. Herein, synthesis of the target flavones followed the Baker-Venkataraman method according to the reported procedure by Ravashinkar *et al* [219], affording the desired products in good yields and with excellent purities.

With regards to the biological evaluation of antiangiogenic effects, several *in vitro* models are currently in use as reviewed in **Table 3. 1** [165,249]. *In vitro* assays utilized to assess the antiangiogenic activities of flavonoids in particular are presented in **Figure 3. 2**, which is derived from the systematic analysis carried out in **Section 2.2.1.2, Chapter 2**.

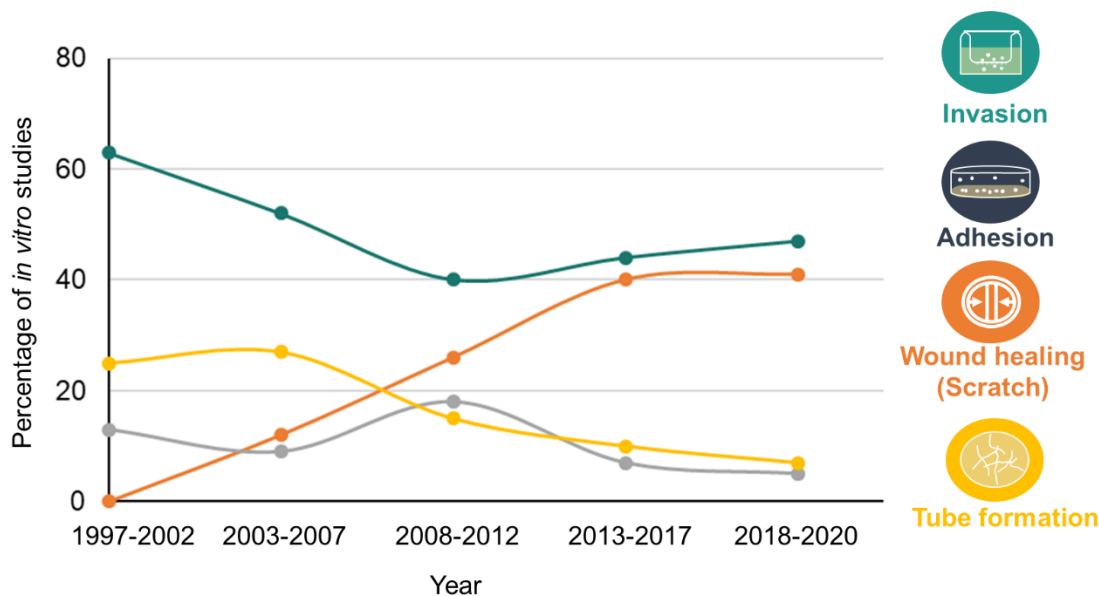


Figure 3. 2. Percentage of studies using different types of *in vitro* assays used for antiangiogenic evaluation of flavonoids from the year 1997 to 2020

Table 3. 1. Comparison of the most common *in vitro* angiogenesis assays [165,249]

<i>In vitro</i> assay	<i>In vitro</i> model	Parameter	Overview	Advantages	Limitations
Proliferation	Cell counting	Number of cells	ECs cultured and numbers with or without treatment are counted either manually using a hemacytometer or electronically using an automated cell counter	<ul style="list-style-type: none"> • Simple • Inexpensive 	<ul style="list-style-type: none"> • Time consuming • Prone to error
	Cell cycle kinetics	Cellular process	Measures cellular processes; <ul style="list-style-type: none"> • mitochondrial metabolism via colorimetric methods • DNA replication via radioactive methods 	<ul style="list-style-type: none"> • Fast • High reproducibility • Inexpensive • Accurate 	<ul style="list-style-type: none"> • Does not differentiate between cytostatic and cytotoxic effects (measures cell viability) • Expensive • Time consuming • Difficult to interpret
Migration	Boyden chamber (transwell)	Chemotactic cellular migration	ECs migrate from the top to the bottom, through a matrix protein, in response to a chemotactic factor. Migrated cells are then dyed and counted	<ul style="list-style-type: none"> • High sensitivity to concentration gradient changes 	<ul style="list-style-type: none"> • System equilibrium difficult to maintain • Expensive • Insensitive to small number of cells
	Scratch (wound healing)	Rate and extent of cellular migration	Confluent ECs monolayer is scraped and area recovered by migrating cells is determined microscopically	<ul style="list-style-type: none"> • Simple • Monitoring at different time intervals • Presence of cell-cell interaction • Inexpensive 	<ul style="list-style-type: none"> • Difficult to reproduce due to confluency inconsistencies
Differentiation	Tube formation assay	Differentiation of ECs into capillary like tubules	ECs are cultured on matrix protein stimulating attachment, migration and differentiation of cells	<ul style="list-style-type: none"> • Mirrors <i>in vivo</i> conditions • Suitable for large-scale screening 	<ul style="list-style-type: none"> • Lumen formation in differentiated tubules is debatable • Time consuming analysis • Expensive

Herein, the antiangiogenic effects of the test flavones were evaluated against the different components of angiogenesis, namely proliferation, differentiation and migration [250]. The cell counting, tube formation and scratch assay models were proposed as the most appropriate to use for measuring these effects based on their technical benefits, as well as their practicalities.

The percentage of studies evaluating flavonoids' antiangiogenic effects via the tube formation assay was relatively low with a decline from 25% during the period of 1997-2002 to 10% during 2013-2017 (**Figure 3. 2**). Although the tube formation assay is arguably technically difficult and time consuming [249], it offers a practical method to evaluate the overall antiangiogenic effects of potential leads as it covers the fundamental steps involved in the process of angiogenesis under controlled conditions (**Table 3. 1**). The tube formation assay is based on the culture of ECs on a matrix Matrigel that resembles the ECM in its constitution, containing several vital growth factors like the FGF and the transforming growth factor [251]. As such, it provides a two dimensional medium that promotes the fundamental steps of EC differentiation and morphogenesis into capillary like tubules, mimicking the *in vivo* situation [165,249]. Molecules that can disrupt such differentiation frequently possess potent antiangiogenic behaviors [249].

Regarding the scratch assay, this involves EC migration to recover a scraped (wounded) area as part of the natural wound healing process that involves angiogenesis [249]. Its ease of use and cost-effectiveness versus the invasion assay (**Table 3. 1**) may have contributed to the increase in its use over time (**Figure 3. 2**). Primary drawbacks associated with the invasion (i.e. transwell) model are the difficulty in sustaining the concentration gradient of chemotactic inducing factors across the two compartments, and the insensitivity to small numbers of migrating cells [165,249,252] (**Table 3. 1**). The scratch assay also has some disadvantages including the challenge of maintaining the same degree of confluency in every batch of the experiment. Nonetheless, this problem can be avoided by tight regulation and scheduling of the culture conditions throughout the experiment [165]. Additionally, increasing the number of trials can compensate for such minor errors.

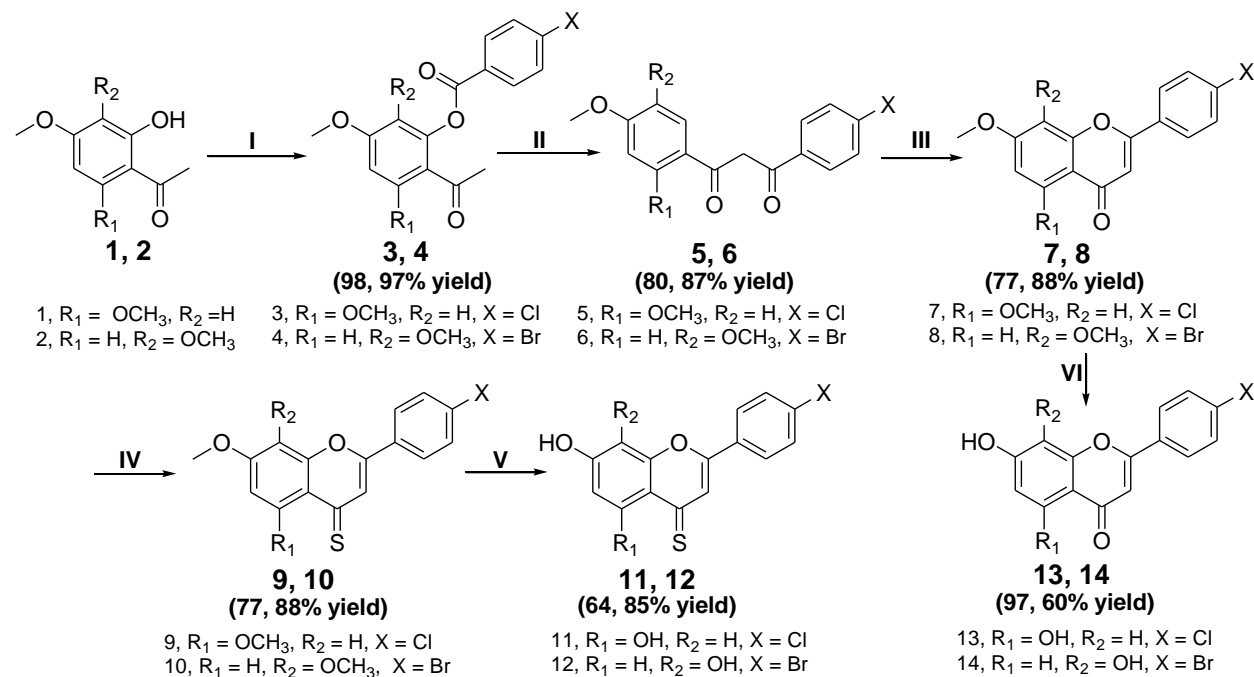
In **Chapter 2**, evidence from published work has demonstrated that several flavonoids can interfere with the VEGF pathway, eliciting antiangiogenic effects (**Table 2.3, Section 2.2.2.2**). Hence, the VEGF-mediated antiangiogenic effects of the flavones prepared in this thesis were evaluated to determine whether interacting with the VEGF pathway is feasible. To test this, the selected tube formation and scratch assays were conducted under VEGF-induced angiogenic conditions. Furthermore, interference with VEGFR2, as the predominant receptor of VEGF, was explored for the most active compounds via western blotting and molecular docking techniques.

3.2. Results and discussion

3.2.1. Synthesis and structural characterization of the designed flavones

3.2.1.1. Synthesis and structural characterization of 4-oxo and 4-thio flavones

Synthesis of the two series of 5,7-disubstituted-4'-chlorophenyl and 7,8-disubstituted 4'-bromophenyl flavones was carried out via Baker-Venkatarman rearrangement, following the reported method previously adopted by our laboratory [219] (**Scheme 3.4**) [253].

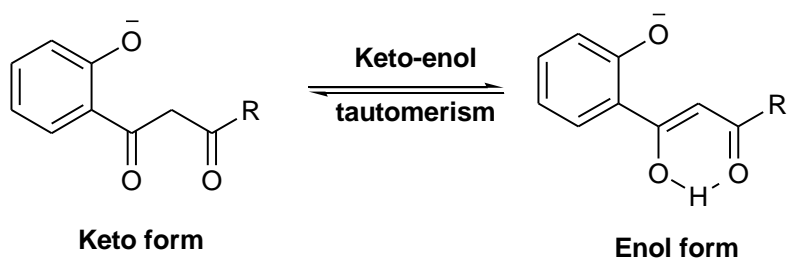


Scheme 3.4. Synthesis of 4-oxo and 4-thio-*p*-halophenyl flavone derivatives. (I) Halobenzoyl Chloride, DBU, pyridine, 75 °C, 2 h; (II) Pyridine, KOH, 50 °C, 2 h; (III) Glacial acetic acid, 1% H₂SO₄, 90–110 °C, 1 h; (IV) Dry toluene, Lawesson's reagent, 110 °C, 4 h; (V, VI) Dry DCM, BBr₃, room temp, 4 h

Some of the reactions' conditions as well as the column chromatography solvent systems were optimized in order to obtain the desired products as presented in **Table 3.2**. The

structures of the synthesized compounds were confirmed using ^1H and ^{13}C NMR spectroscopic analysis, mass spectrometry and IR spectroscopy, with data being in agreement with the reported data.

The first step involved esterification of the 4,6 or 3,4-diOCH₃ protected 2-OH-acetophenones and Cl or Br-benzoylchloride, respectively, in basic medium. Double-doublet signals for the phenyl halide rings appeared in the ^1H NMR spectra of **3** and **4** at δ 7.45, 8.06 ($J=8.0$ Hz) (**Figure 3. 3**) and 7.98, 8.08 ($J=8.0$ Hz) ppm, respectively. The C=O groups of the ester linkage were also present in the ^{13}C NMR spectra of **3** and **4** at δ 164.26 and 164.10 ppm, respectively, indicating successful esterification. The diketone intermediates (**5** and **6**) were obtained, in 80 and 87% yields, respectively, via the intramolecular rearrangement of esters (**3** and **4**) in strong basic conditions (KOH in pyridine) as described earlier for Baker-Venkataraman's reaction (**Scheme 3. 1**). The obtained intermediates were washed with acetic acid to remove the excess pyridine and taken to the next step without further purification. The β -diketones (**5** and **6**) existed as keto-enol tautomers (**Scheme 3. 5**). The OH protons of these intermediates appeared at δ 13.24 and 12.26 ppm whilst the singlet proton signals of the exocyclic C-H₂ appeared at δ 4.68 and 3.94 ppm, respectively, in the ^1H NMR spectra.



Scheme 3. 5. Keto-enol tautomerism of the β -diketone intermediates

Table 3. 2. Comparison of synthetic methods reported (Rep) for compounds (**3 -14**) by Ravashinkar *et al* [219] and methods applied in this project (App) [253]

Compound	Procedural modification	m.p (°C)		Yield (%)		Mobile phase for column chromatography		Purity determined by HPLC	
		App	Rep	App	Rep	App	Rep	App	Rep
3	No modification	112-4	124-6	98	91	Hexane:CHCl ₃ : EtOAc (6:3:1 v/v/v)	CHCl ₃ :Hexane: EtOAc (6:3:1 v/v/v)	n/a	n/a
4	No modification	101-2	117-9	97	88	Hexane:CHCl ₃ : EtOAc (5:4:1 v/v/v)	CHCl ₃ :Hexane: EtOAc (6:3:1 v/v/v)	n/a	n/a
5	No modification	n/a	n/a	80	85	No modification	No modification	n/a	n/a
6	No modification	n/a	n/a	87	85	No modification	No modification	n/a	n/a
7	No modification	174-5	188-92	77	66	EtOAc (100%) followed by 5% MeOH in EtOAc	CHCl ₃ :Hexane: EtOAc (8:1:1 v/v/v)	96.4%	99.8%
8	No modification	198-8.5	197-9	88	90	CHCl ₃ :Hexane: EtOAc (5:3:2 v/v/v)	CHCl ₃ :Hexane: EtOAc (6:3:1 v/v/v)	99.4%	99.7%
9	1 eq. lawesson's reagent instead of 0.6 eq.	173.1-3.8	170-2	77	83	No modification	No modification	93.5%	95.4%
10		214-6	216-8	88	82	No modification	No modification	92.3%	97.8%
11	2.5 eq. BBr ₃ for each OMe instead of 1.25 eq.	247.7-7.8	249-52	64	77	No modification	No modification	98.6%	98.7%
12	2.5 eq. BBr ₃ for each OMe instead of 1.25 eq. Time of reaction 4 h instead of overnight	223.8-24	235-7	85	68	EtOAc (100%)	CHCl ₃ :Hexane: EtOAc (8:1:1 v/v/v)	90.5%	95.0%
13	2.5 eq. BBr ₃ for each OMe instead of 1.25 eq.	250	294-6	97	61	No modification	No modification	99.4%	98.3%

	Time of reaction overnight instead of 4 h								
14	2.5 eq. BBr ₃ for each OMe instead of 1.25 eq.	275-80	285-90	60	58	No modification	No modification	98.8%	98.8%

m.p, melting point; n/a, not available; eq, equivalents.

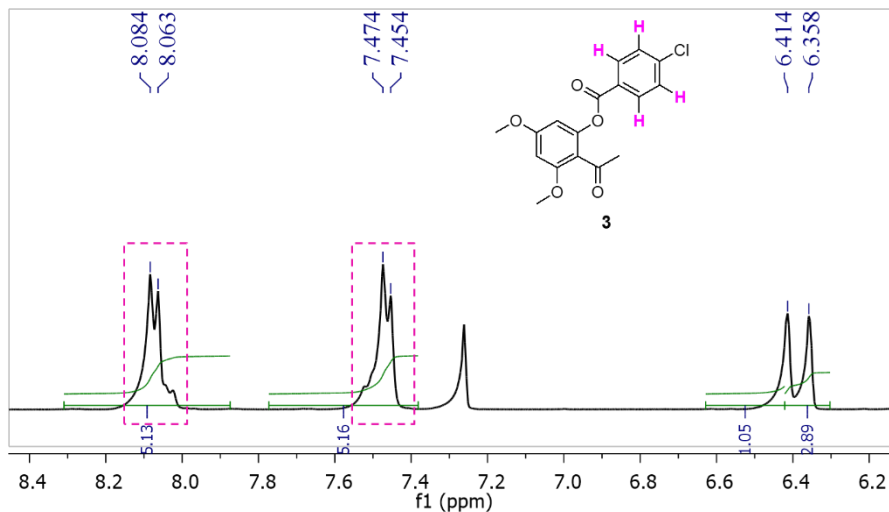


Figure 3. 3. ^1H NMR spectrum of **3** showing double-doublet peaks of the 4'-chlorophenyl ring

Intermediates **5** and **6** were subjected to acid assisted cyclic dehydration to afford the diOCH₃ flavones (**7** and **8**) in 77 and 88% yields, respectively. Cyclisation was evident from the presence of the olefinic –CH proton at δ 6.64 and 6.75 ppm for **7** and **8**, respectively, in their ^1H NMR spectra. The 4-C=S derivatives (**9** and **10**) were obtained from their 4-C=O parents (**7**, **8**), in 77% and 88% yields, respectively, using 1 equivalents Lawesson's reagent (LR) (instead of the reported 0.6 equivalents) in anhydrous toluene in accordance with studies reporting thionation of flavones or related chromones [254,255]. Replacement of the 4-C=O by a 4-C=S resulted in a downfield shift of both the olefinic –CH proton and the 4-C carbon of **7** and **8** by around 0.9 ppm and 23 ppm in the ^1H and ^{13}C NMR spectra, respectively (**Figure 3. 4** and **3.5**).

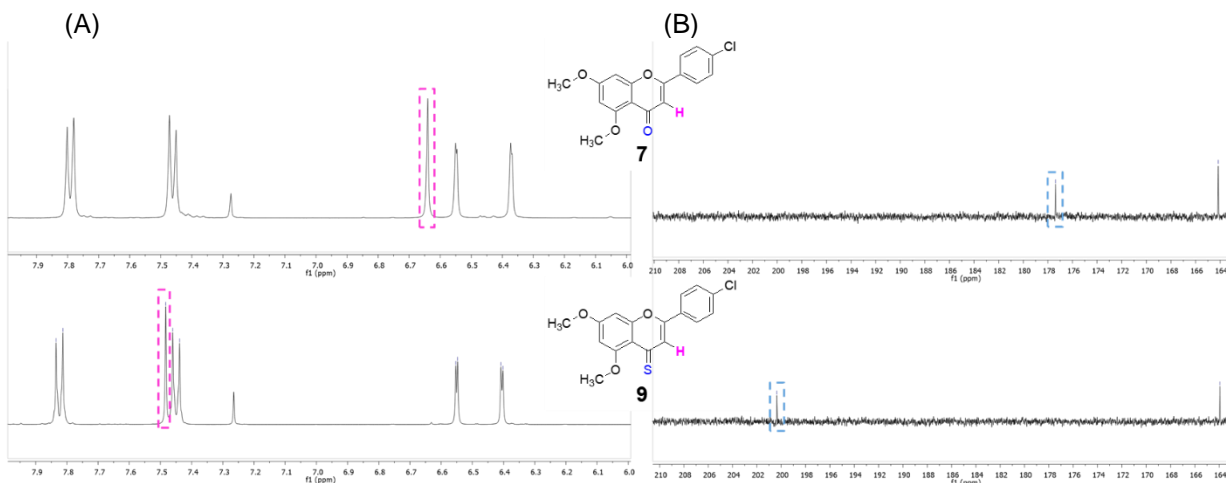


Figure 3. 4. (A) ^1H NMR spectra of compounds **7** and **9** showing downfield shift of H3; (B) ^{13}C NMR spectra of compounds **7** and **9** showing (4-C=O) and (4-C=S) peaks, respectively

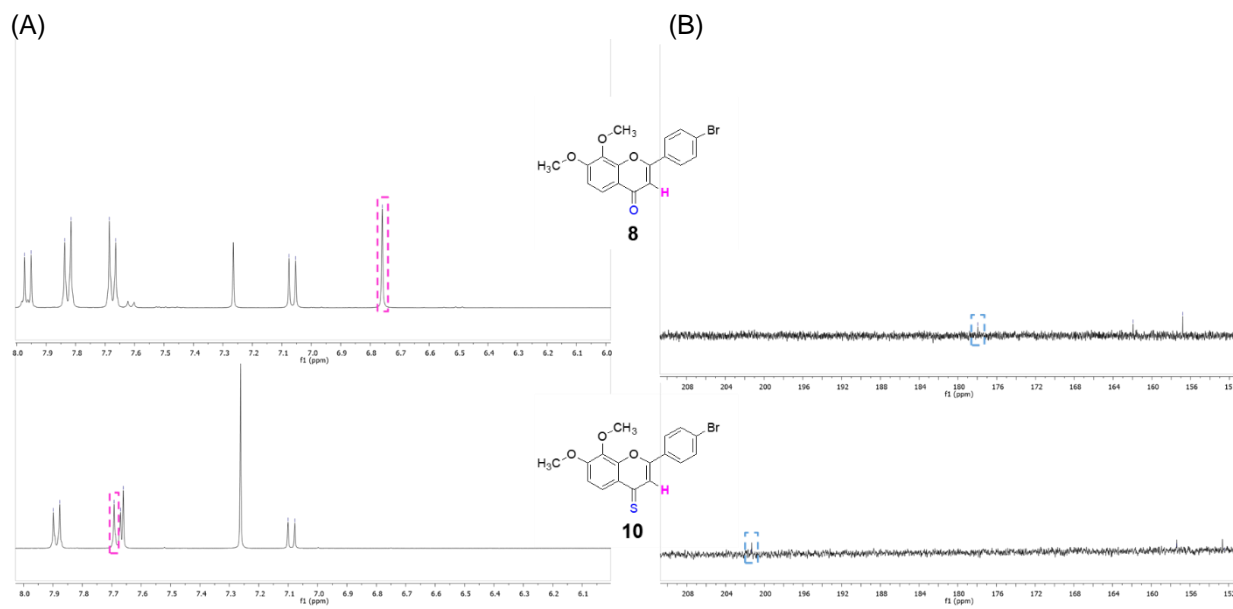


Figure 3. 5. (A) ¹H NMR spectra of compounds **8** and **10** showing downfield shift of H3; (B) ¹³C NMR spectra of compounds **8** and **10** showing (4-C=O) and (4-C=S) peaks, respectively

Subsequent demethylation of both the 4-C=O and 4-C=S OCH₃ flavones (**7**, **8** and **9**, **10**) was not achievable using 1.25 equivalents of the deprotecting reagent, BBr₃, for each OCH₃ group as in the reported method [219]. Consequently, 2.5 equivalents BBr₃ were used here, achieving full deprotection with generally favorable yields (60%–97%) and affording compounds with comparable purities to those reported (**Table 3. 2**). Accordingly, the two OCH₃ peaks were no longer present in the ¹H and ¹³C NMR spectra. IR spectra also showed the broad OH peaks of **11**, **12** and **13**, **14** at $\nu = 3358$, 3501, 3350 and 3365 cm⁻¹, respectively.

All of the synthesized flavones were purified by column chromatography (except for intermediates **5** and **6** as mentioned above). Purities of the final compounds **7-14** were >90% as determined by HPLC analysis (**Table 3. 2**).

3.2.1.2. Attempted synthesis and structural characterization of 4-seleno flavones

Effective methods for the direct selenation of carbonyl groups is rarely reported in the literature. Based on the analogous thiocarbonyl conversion, the selenating reagent (Woollin's) was discovered as a substitute for LR to achieve selenocarbonyl conversions [256] (**Figure 3. 6**). Woollin's reagent (WR) has several benefits compared to other Se

reagents used for this particular transformation including air stability and ease of preparation [256].

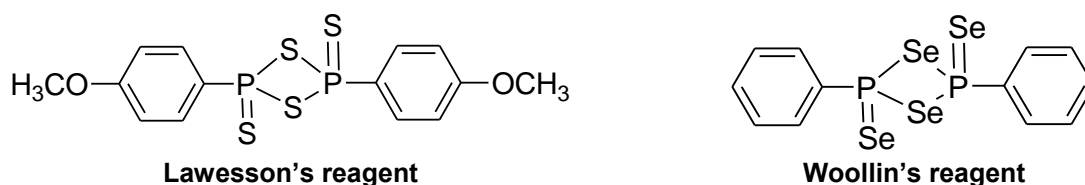
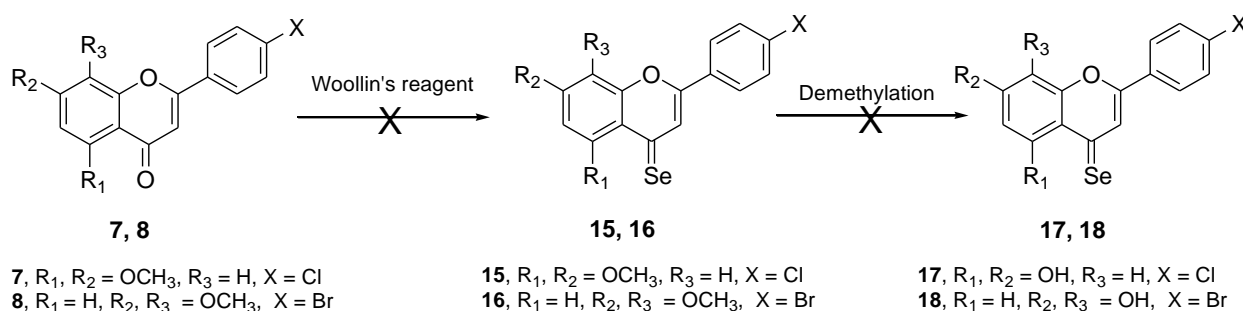


Figure 3. 6. Chemical structures of Lawesson's and Woollin's reagents

Recent reports by Martins *et al* expanded the successful use of microwave assisted synthesis, when preparing thioflavonoids using LR, for the selenation of carbonyl groups using WR [257]. Testing different experimental conditions, Martins and colleagues improved the synthesis of Se caffeine from a 2% yield upon using conventional heating conditions to 42% yield using WR and microwave assisted synthesis [257]. The authors successfully utilized the WR and microwave combination to synthesize flavonoid Se derivatives in another study [237].

Several attempts were conducted in this project, using varying reaction conditions, to produce the selenoflavones **15** and **16** from their respective parent flavones (**7** and **8**) (**Scheme 3. 6**).



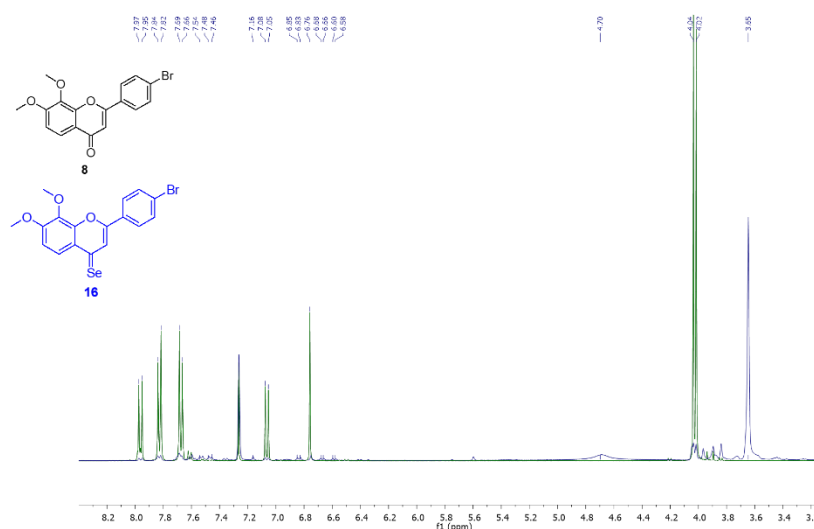
Scheme 3. 6. Attempted synthesis of 4-Se flavone derivatives (**15-18**)

Here, the synthesis of the 4'-bromophenyl flavone (**16**) was attempted by reacting compound **8** with 0.4 equivalents of WR in anhydrous acetonitrile (ACN) using microwave irradiation (175 W, 150 °C for 7 min) following the method reported by Martins *et al* for the synthesis of the related 4-Se chrysin [237]. Two fractions of the reaction product were separated by column chromatography [100% dichloromethane (DCM) followed by 1:1 DCM:methanol (MeOH) (v/v)].

Table 3. 3. Reaction conditions for the attempted synthesis of **16**

Method	Solvent	WR Equivalence	Conditions
Microwave	ACN	0.4	175 W, 150 °C, 7 min
Heating	Toluene	0.8	130 °C, 4 h

Their ^1H NMR spectroscopic analysis showed the first fraction to be devoid of any organic chemical compounds while the second to be a mixture of starting material (**8**) and another product. As shown in **Figure 3. 7**, the ^1H NMR spectrum of fraction 2 showed peaks corresponding to flavone **8** in addition to similar signals that were shifted upfield which is contradictory to the downfield shift expected upon selenation [237,257].

**Figure 3. 7.** Stacked ^1H NMR spectra of **8** (black) and product of trial 1 for synthesis of **16** (blue)

As shown in **Table 3. 3**, another trial to synthesize **16** was carried out by doubling the amount of WR (0.8 equivalents) in anhydrous toluene under conventional heating conditions (130 °C, 4 h) similar to the analogous thionation reactions using LR. ^1H NMR spectroscopic analysis of the product that was purified by column chromatography [100% DCM followed by 1:1 DCM:MeOH (v/v)] showed more promising results than that afforded using microwave irradiation. First, there were no proton signals corresponding to the starting material. Moreover, the ^1H NMR spectrum of the product exhibited an upfield shift for the $2\times\text{CH}_3$ proton peaks from δ 4.01-4.03 to δ 3.83-3.87 ppm (**Figure 3. 8**). Despite the presence of peaks that might correspond to H3, H5, H6 and *p*-bromophenyl ring

protons that are shifted downfield as a consequence of selenation, there were other unassigned peaks that indicate the presence of several impurities or byproducts that persisted even after purification with column chromatography.

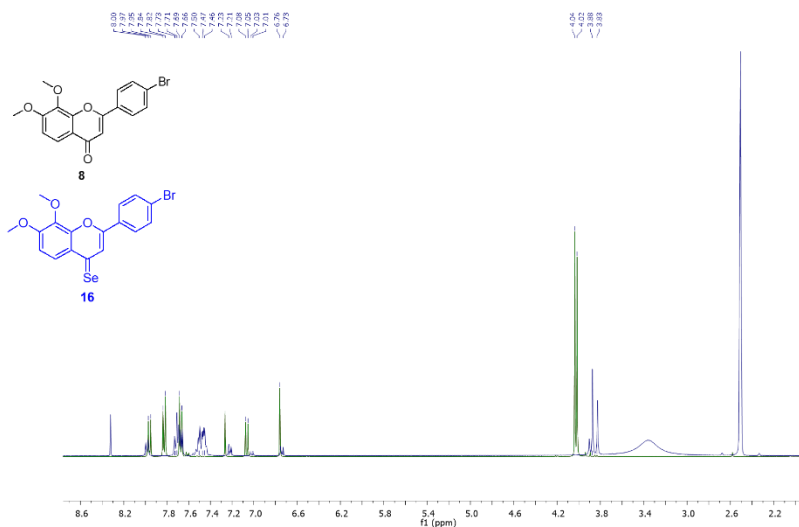


Figure 3. 8. Stacked ^1H NMR spectra of **8** (black) and product of trial 2 of **16** (blue) synthesis

Despite the unsuccessful attempts to obtain **16** as a product, conventional heating showed better evidence of conversion compared to microwave conditions. Consequently, synthesis of the related flavone **15** was tried using conventional heating. First, 0.6 equivalents of WR were reacted with compound **7** at 110 °C for 4 hours in anhydrous toluene. ^1H NMR spectroscopic analysis of the crude product showed signs for formation of a 4-Se derivative where the $2\times\text{CH}_3$ proton peaks were shifted upfield from δ 3.91-3.95 to δ 3.81-3.83 ppm and new signals appeared in the aromatic region that could correspond to H3, H6, H8 and *p*-chlorophenyl ring protons, so column chromatography was used in an attempt to obtain a pure product. Several eluents were tried in pursuit of obtaining a single product as summarized in **Table 3. 4**, but were unsuccessful.

Table 3. 4. Column chromatography optimization for purification of **15**

Mobile phase	Comment
100% CHCl_3	Low eluting speed with no separation of components
100% EtOAc	High eluting speed with no separation of components

As mentioned earlier, the literature has only a few examples of the interconversion between carbonyl and selenocarbonyl moieties [237,257–259]. Martins and colleagues have documented the screening of different microwave conditions, in terms of temperature, microwave power, and time, for the synthesis of selenocaffeine in several solvents and with varying equivalents of WR [257]. Selenation only succeeded in one case, with a 42% yield, using 0.6 equivalents of WR and irradiation for 180 min at 170 °C in *p*-xylene. This underpins the preciseness of conditions under which a successful conversion can be obtained in good yields. Herein, further screening of the various conditions required for the synthesis of the desired 4-selenoflavone derivatives was not possible within the project's time frame. Based on the available literature reports, future attempts could focus on increasing the equivalence of WR from 0.4 and 1.5, using temperatures ranging from 125 to 175 °C, microwave powers between 175 and 300 W, and a duration of 5 to 180 minutes. These reactions could be carried out in acetonitrile, toluene, *p*-xylene, or 1,4-dioxane [257–259].

3.2.2. *In vitro* evaluation of the antiangiogenic properties of the synthesized flavones

3.2.2.1. Cytotoxicity against endothelial cells

To ensure biocompatibility of the synthesized flavones (**7-14**) with the human umbilical vein ECs (HUVECs) used in the antiangiogenic evaluation, their direct cytotoxic effects, (except for compound **10** due to insolubility in a suitable organic solvent), were assessed using the trypan blue assay [260,261]. The natural flavone luteolin was selected as a reference standard due to its potent antiangiogenic activity as demonstrated in both *in vitro* and *in vivo* studies [85]. Furthermore, it offers a basis for comparison between the synthetic flavones developed for this project and other naturally occurring flavonoids that fall within the same subclass. Treatment with a concentration four times higher (i.e., 40 µM) than the highest concentration used for the antiangiogenic evaluation studies (i.e., 10 µM) for 24 h was chosen for this cytotoxicity assay. As shown in **Figure 3. 10**, ~100% viability of the cells was retained with compounds **7-14** with no observed cytotoxic activities (no statistically significant difference compared to control in all cases, $p > 0.05$). Hence, it may be inferred that any detectable antiangiogenic effects exhibited by the flavones under investigation are not attributable to the direct cytotoxicity on ECs, but

rather stem from the modulation of other EC functions, such as differentiation or migration.

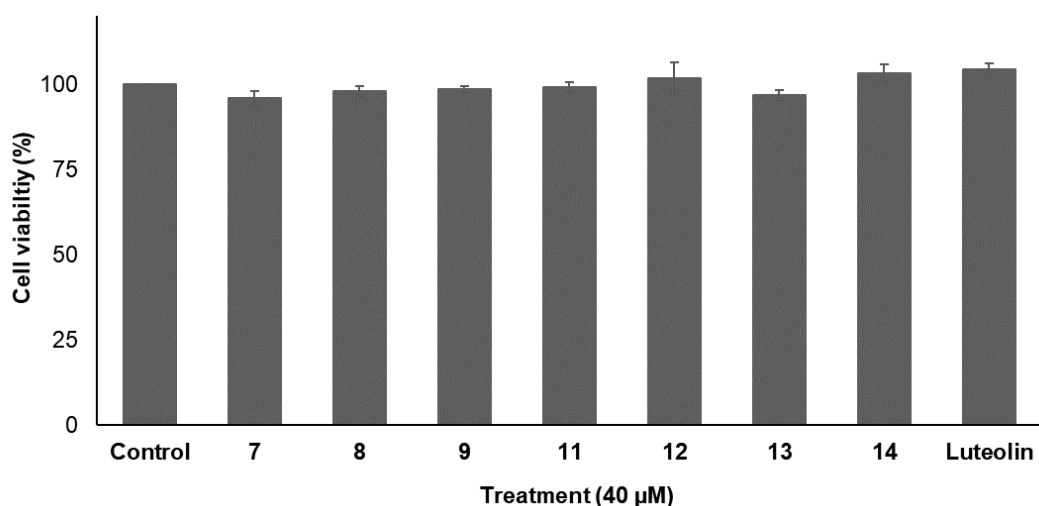


Figure 3. 10. Cell viability of HUVECs after 24 h of treatment with 40 μM of the tested flavones (**7-14**). Data are expressed as mean ± standard error of the mean (SEM), n = 3.

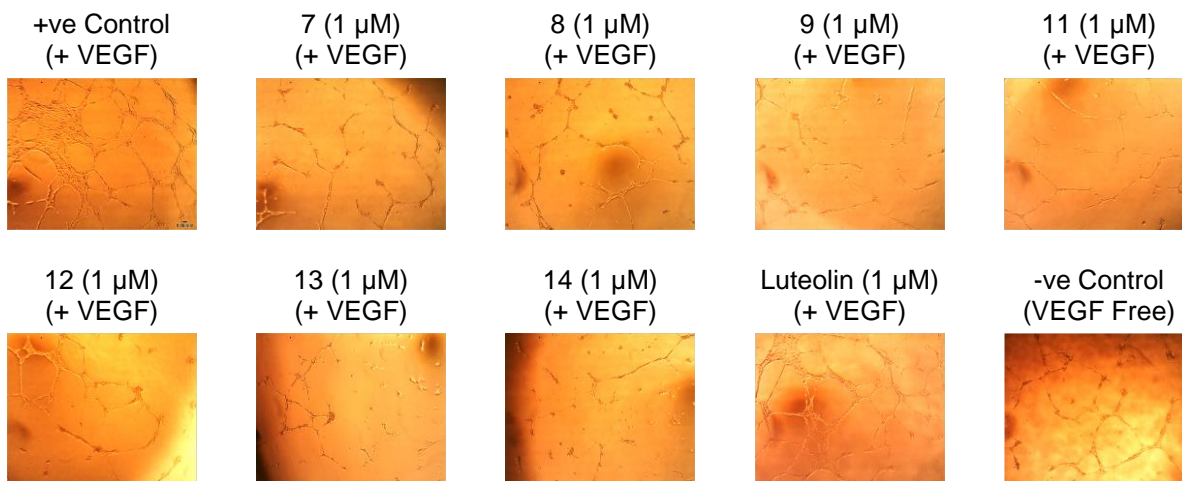
3.2.2.2. Inhibition of endothelial cells tube formation

The ability of flavones (**7-14**) to inhibit HUVEC tube formation was investigated at 1 and 10 μM. These dosages align with the published IC₅₀ range of compounds **11** and **12** against breast cancer cell lines (e.g., IC₅₀ against MCF-7=1 and 4.9 μM, respectively) [219] and hence were selected being mindful of the aim of this work for the compounds to be both antiangiogenic and cytotoxic. Additionally, lower doses are associated with reduced side effects [25,262]. The EC tube formation was stimulated by the addition of 10 ng/mL of VEGF, which is reported by Carpentier *et al* to induce angiogenesis more effectively ($p < 0.05$, relative to control) than other concentrations of 5, 25 and 50 ng/mL ($p > 0.05$) [263]. Tube formation was quantified after 12 hours using the Angiogenesis Analyzer plugin [264] in ImageJ software [265]. The measured parameters included the number of junctions and meshes, as well as the number and length of master segments and segments. These variables were selected as they offer high sensitivity in detecting different features of angiogenesis [263].

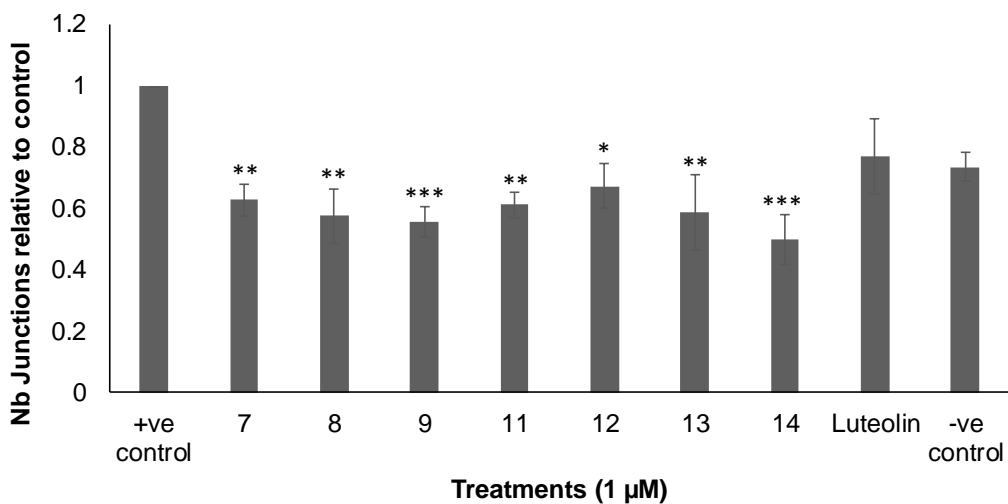
As shown in **Figure 3. 11**, the active reference luteolin showed around 30% decrease in tube formation relative to the control, in agreement with previous reports [85,195]. In that context, all of the evaluated flavones demonstrated more than 30% decrease in tube

formation relative to the control, indicating inhibitory activity. Indeed, all of the tested flavones exhibited considerable reduction of the measured tube formation parameters, namely, the number of junctions (33 - 51%, $p < 0.05$), the number of master segments (42 - 60%, $p < 0.01$), the total master segments length (32 - 50%, $p < 0.05$), the number of segments (40 - 58%, $p < 0.05$) and the total segments length (37 - 55%, $p < 0.05$), relative to the control at 1 μM . The 7,8-diOH-4'-bromophenyl flavone (**14**) demonstrated strong antiangiogenic inhibition against the control for all variables at 1 μM (50% inhibition of the number of junctions and total master segments length ($p < 0.001$), 57% inhibition of the number of meshes ($p < 0.05$), 60% inhibition of number of master segments, 58% of number of segments and 54% of total segments length ($p < 0.001$)). In the clinical context, the antiangiogenic activity observed for compound **14** in this assay is equivalent to that reported for the VEGFR inhibitor sunitinib (50%) in the same assay and at the same concentration of 1 μM yet after 48 hours of treatment [266].

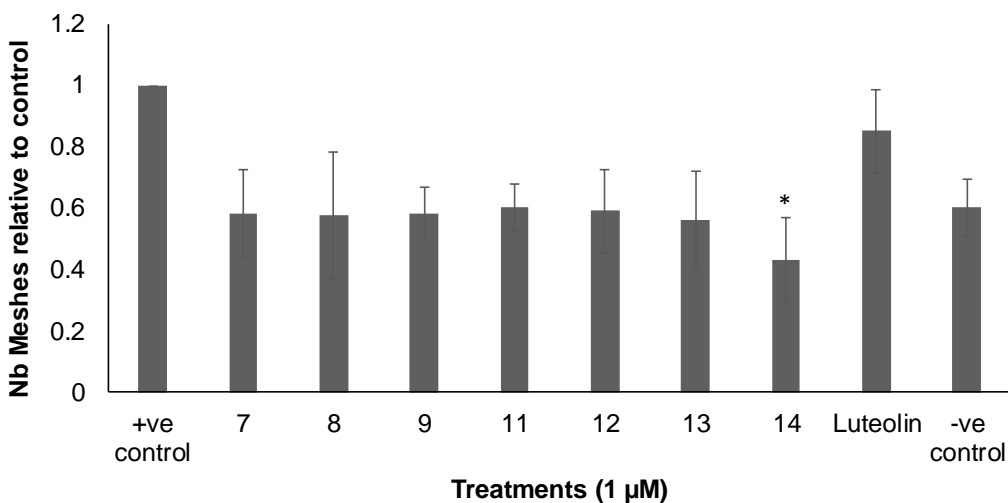
(A)



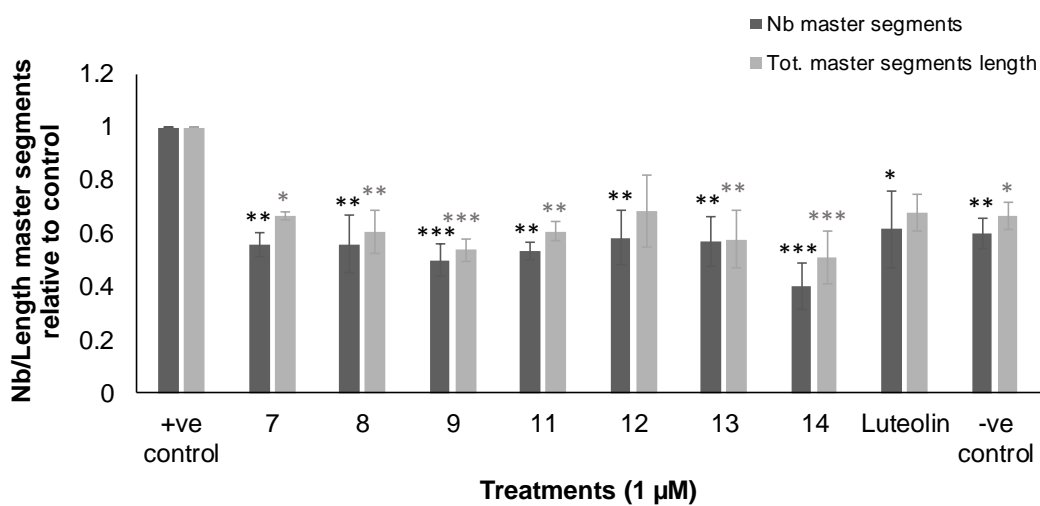
(B)



(C)



(D)



(E)

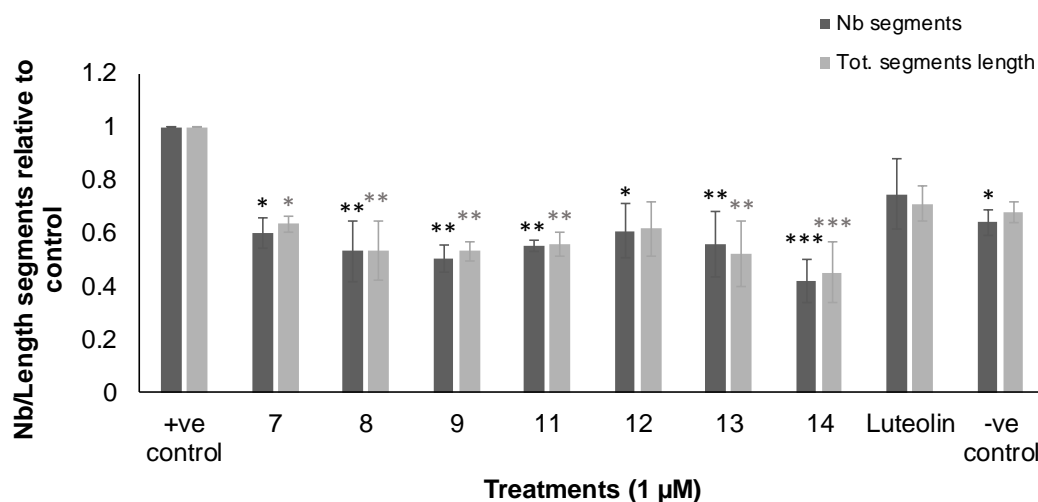
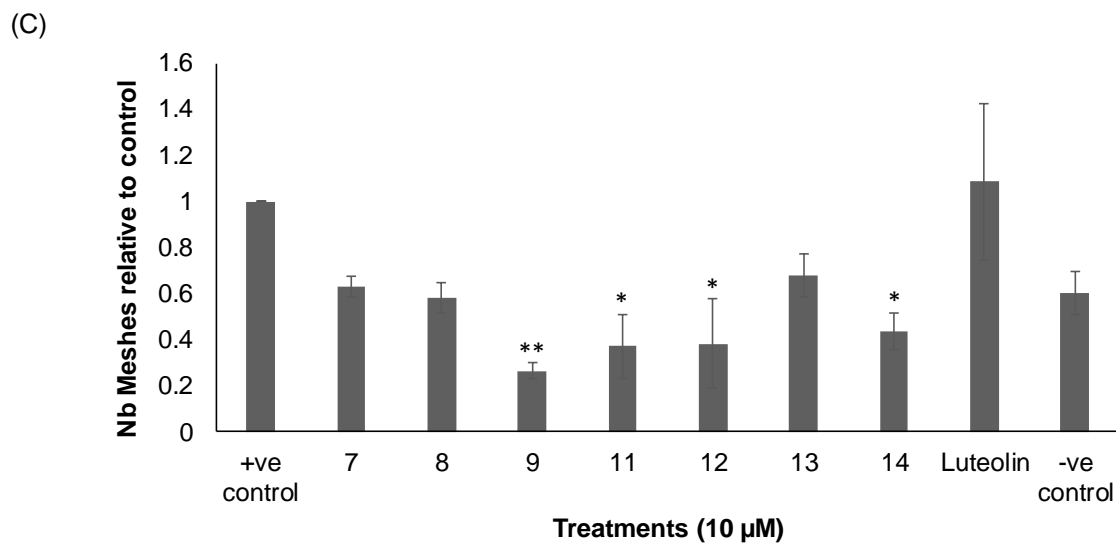
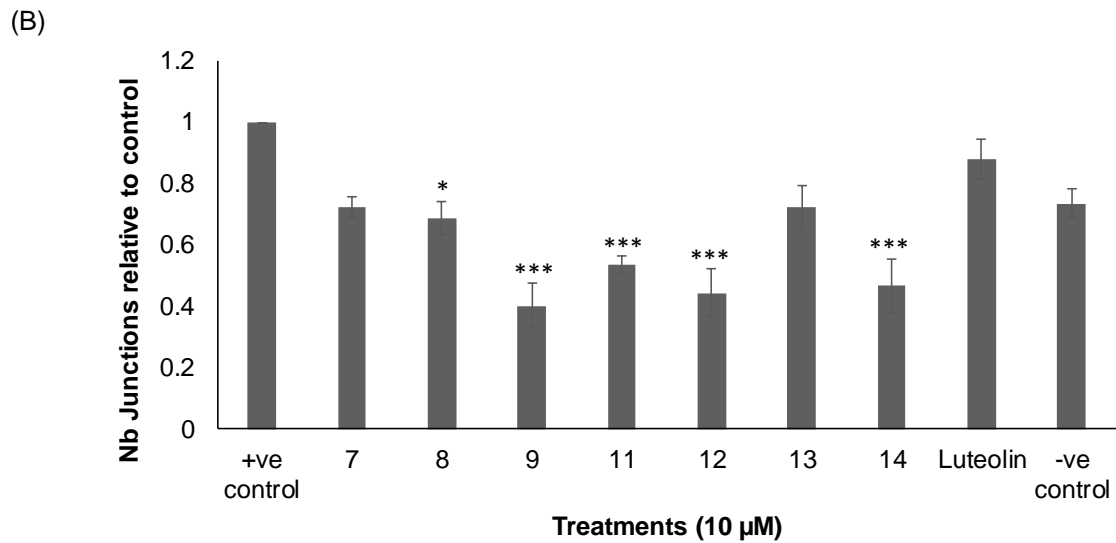
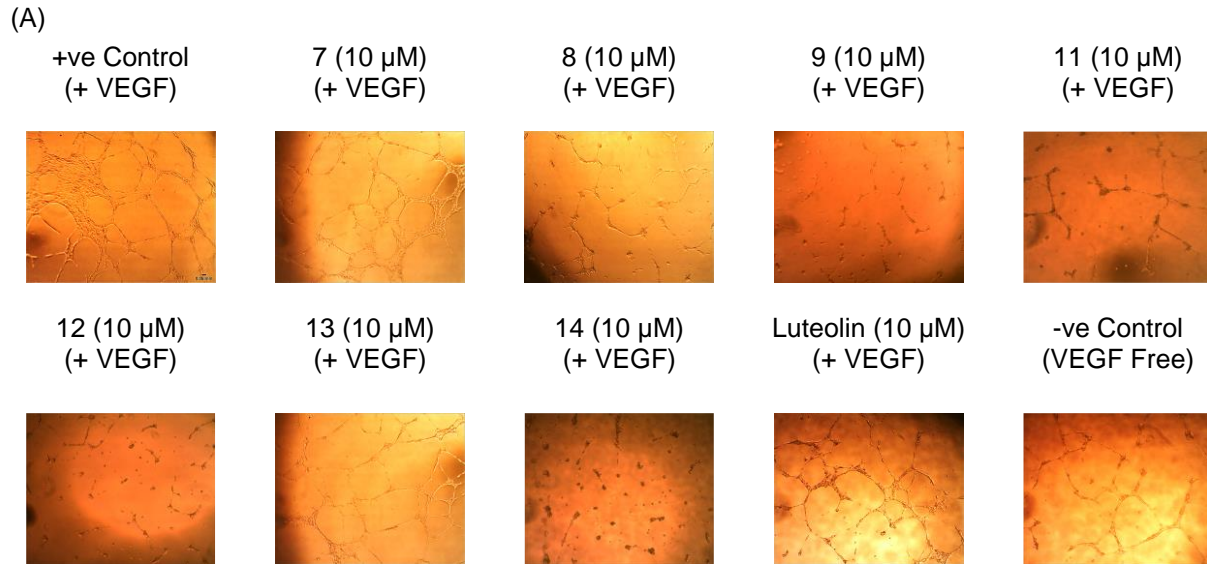
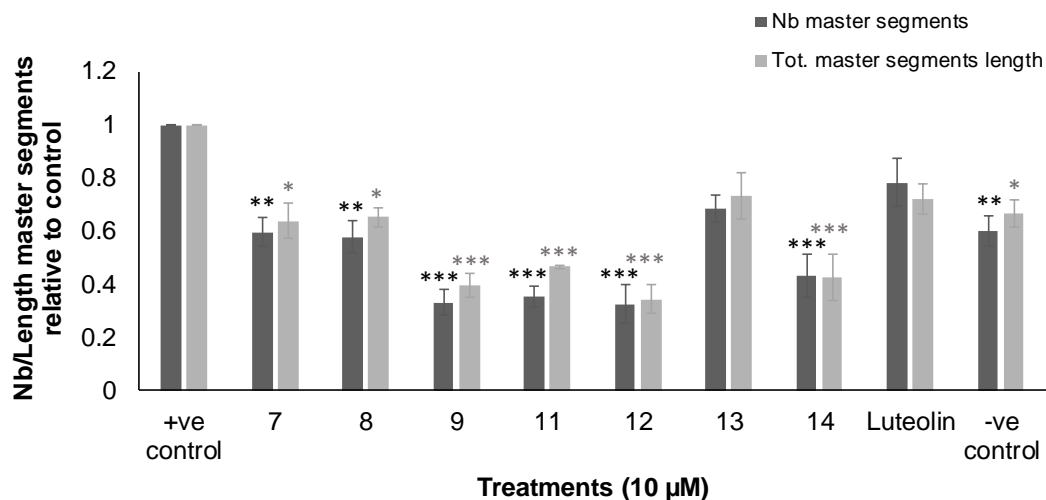


Figure 3. 11. Antiangiogenic activity of the tested flavones (**7-14**) on *in vitro* HUVEC tube formation after 12 h of treatment with 1 µM, expressed as a ratio to the +ve control (10 ng/mL VEGF-enriched media). (**A**) Representative images of tube formation assay at 4X magnification. Images were analyzed using Angiogenesis Analyzer macro in ImageJ software; (**B**) number of junctions, (**C**) number of meshes, (**D**) number and length of master segments and (**E**) number and length of segments. Data are expressed as mean ± standard error of the mean (SEM), n = 3. Statistical significance was estimated with respect to the +ve control by one-way ANOVA, followed by Dunnett's multiple comparison test (* $p < 0.05$, ** $p < 0.01$, *** $p < 0.001$).

At the 10 µM concentration, compounds **9**, **11**, **12**, and **14** exhibited the most pronounced antiangiogenic effects on the assessed components of angiogenesis (**Figure 3. 12**). The thioflavone (**9**) showed 60% inhibition of the number of junctions and total master segments length ($p < 0.001$), 70% inhibition of number of master segments, number and total segments length ($p < 0.001$), and 75% inhibition of number of meshes ($p < 0.001$) relative to the control. The two 4-thio-di-OH derivatives (**11** and **12**) followed **9**'s lead in eliciting strong reduction in tubule formation with an average tubule reduction of 55 ($p < 0.001$) and 66% ($p < 0.001$), respectively (**Figure 3. 12**). Compound **14**, that demonstrated high activity at 1 µM, also had a substantial overall inhibition of 57% when tested at a concentration of 10 µM.



(D)



(E)

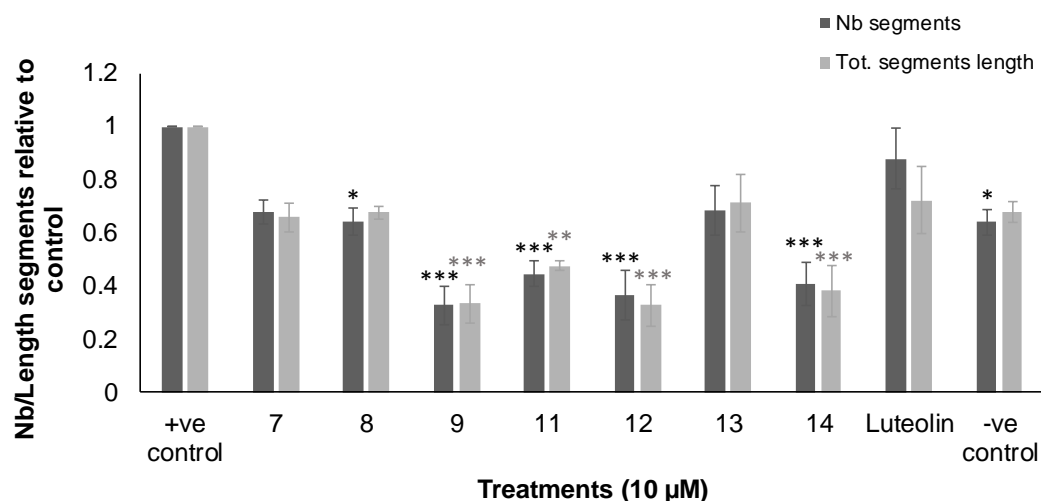


Figure 3. 12. Antiangiogenic activity of the tested flavones (**7-14**) on *in vitro* HUVEC tube formation after 12 h of treatment with 10 μM, expressed as a ratio to the +ve control (10 ng/mL VEGF-enriched media). (**A**) Representative images of tube formation assay at 4X magnification. Images were analyzed using Angiogenesis Analyzer macro in ImageJ software; (**B**) number of junctions, (**C**) number of meshes, (**D**) number and length of master segments and (**E**) number and length of segments. Data are expressed as mean ± standard error of the mean (SEM), n = 3. Statistical significance was estimated with respect to the +ve control by one-way ANOVA, followed by Dunnett's multiple comparison test (* $p < 0.05$, ** $p < 0.01$, *** $p < 0.001$).

In addition to the significant angiogenic inhibition demonstrated by the tested panel of flavones, several SAR observations (analyzed by one-way ANOVA, followed by Tukey's multiple comparison test as recommended for pairwise comparisons [267]) were noted as summarized in **Figure 3. 13**. First of all, the flavone derivatives bearing a 4-C=O group (**7, 8, 13** and **14**) exhibited a dose independent pattern of activity. In this case, the lower 1 μM concentration exhibited similar or increased levels (by 2 to 14%) of tube formation

inhibition compared with the 10 μM concentration. For example, 1 μM of compound **13** showed 44% inhibition compared to 30% inhibition at 10 μM ($p < 0.001$). This implies that 4-C=O flavones achieve saturation of their target protein and exhibit optimal reactivity at a concentration below 10 μM . Similar observations were reported by others for the quercetin metabolite (isorhamnetin-3-glucuronide) in which it suppressed the expression of vascular cell adhesion molecule-1 (VCAM-1) in HUVECs by approximately 30% at 2 μM and only 10% at 10 μM [268]. Interestingly, the 4-C=S derivatives (**9**, **11** and **12**) did not follow the same trend to the 4-C=O flavones and displayed concentration dependent antiangiogenic effects. Additionally, the 4-C=S flavones demonstrated higher inhibitory effects than their 4-C=O counterparts at the 10 μM concentration (**7** versus **9** $p < 0.001$, **11** versus **13** $p < 0.001$ and **12** versus **14** $p < 0.05$), highlighting the positive impact of the 4-C=S group on inhibitory activity. Overall, the distinct patterns of activity between the 4-C=O and the 4-C=S derivatives suggest that the two groups may have different antiangiogenic mechanisms of action. This hypothesis is further explored in **Section 3.2.2.4**.

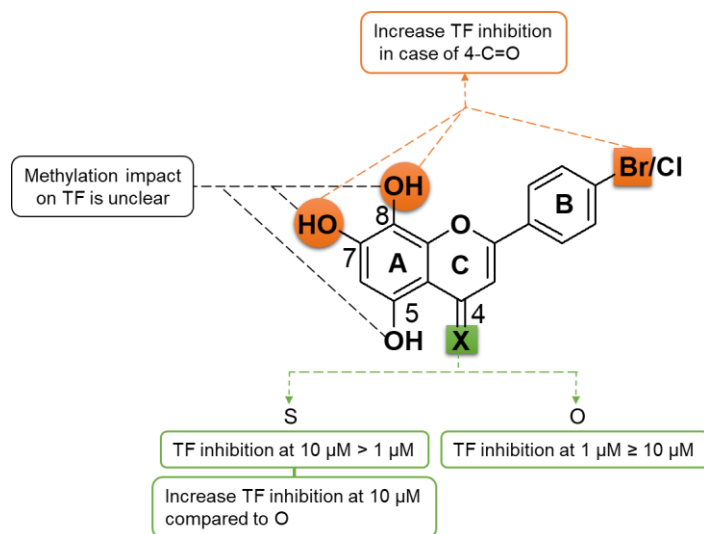


Figure 3.13. Summary of SAR considerations observed for the test flavones (**7-14**) on tube formation (TF) activity

Next, the *ortho*-7,8-disubstitution showed an advantageous role on the antiangiogenic activity of the di-OH-4-C=O derivative **14**. The 7,8-diOH flavone **14** exhibited higher activity compared to the corresponding 5,7-diOH flavone **13** at the 1 (55 versus 44% inhibition, $p < 0.01$) and 10 μM (58 versus 30% inhibition, $p < 0.001$) concentrations. The remaining 7,8-disubstituted derivatives **8** and **12** showed equivalent inhibitory activities to

their 5,7-disubstituted analogues **7** and **11** ($p>0.05$), respectively. While a beneficial role has been attributed to the 4-C=S and 7,8-disubstitution on the cytotoxic activities of flavonoids (see **Section 2.2.4, Chapter 2**), their impact on the antiangiogenic activity has been sparsely reported [155] or not elucidated in existing literature. Thereby, these outcomes reinforce the positive influence of the integration of the 4-C=S and the 7,8-disubstitution functionalities into the design of the target leads.

Finally, the role of OCH₃ substitution on activity was inconsistent. In some instances, methylation of the free OH groups led to a 5 to 21% decrease in the suppression of tube formation (e.g. **8** versus **14**, $p<0.01$) while in others it resulted in a 4 to 10 % increase in activity (e.g. **9** versus **11**, $p<0.05$). Nonetheless, the inclusion of methyl-capped flavonoids in this study was still viewed as beneficial given their potential advantages in terms of enhancing flavonoids bioavailabilities.

Overall, the test flavones **7-14** have shown prominent EC tube formation inhibitory activities in their primary *in vitro* antiangiogenic evaluation. Their pronounced effects at 1 μM ($\geq 37\%$ at 12 h) were similar to that of the multi-TKI drug sunitinib (50% at 48 h). The deliberate use of structural diversification strategies, such as 4-thionation and 5,7 or 7,8-disubstitution, led to distinct patterns of activity. These variations pertain to possibly distinct antiangiogenic targets for each functionality, necessitating further exploration.

3.2.2.3. Inhibition of endothelial cells migration

In order to evaluate how inhibition of the overall tube formation translates into suppression of the key steps involved in the process of angiogenesis, candidates showing more than 50% suppression of tube formation at 10 μM (i.e. compounds **9**, **11**, **12**, and **14**) were assessed for their abilities to inhibit VEGF-induced HUVECs migration.

As seen in **Figure 3. 14**, the four compounds displayed significant reduction of HUVEC migration at 10 μM , which aligns with their potent suppression of tube formation. The 4-C=O flavone **14** resulted in a high level of migration inhibition relative to the control at both the 10 μM and 1 μM concentrations (37%, $p<0.001$ and 20%, $p<0.05$, respectively). On the other hand, the 4-C=S derivatives (**9**, **11** and **12**) showed equivalent inhibition of HUVEC migration of around 25% at 10 μM ($p<0.01$, relative to the control). The analogy

of activity amongst the 4-C=S compounds, as well as their variation from the 4-C=O derivative, further support the hypothesis that the two groups exert their antiangiogenic activities via different VEGF pathways.

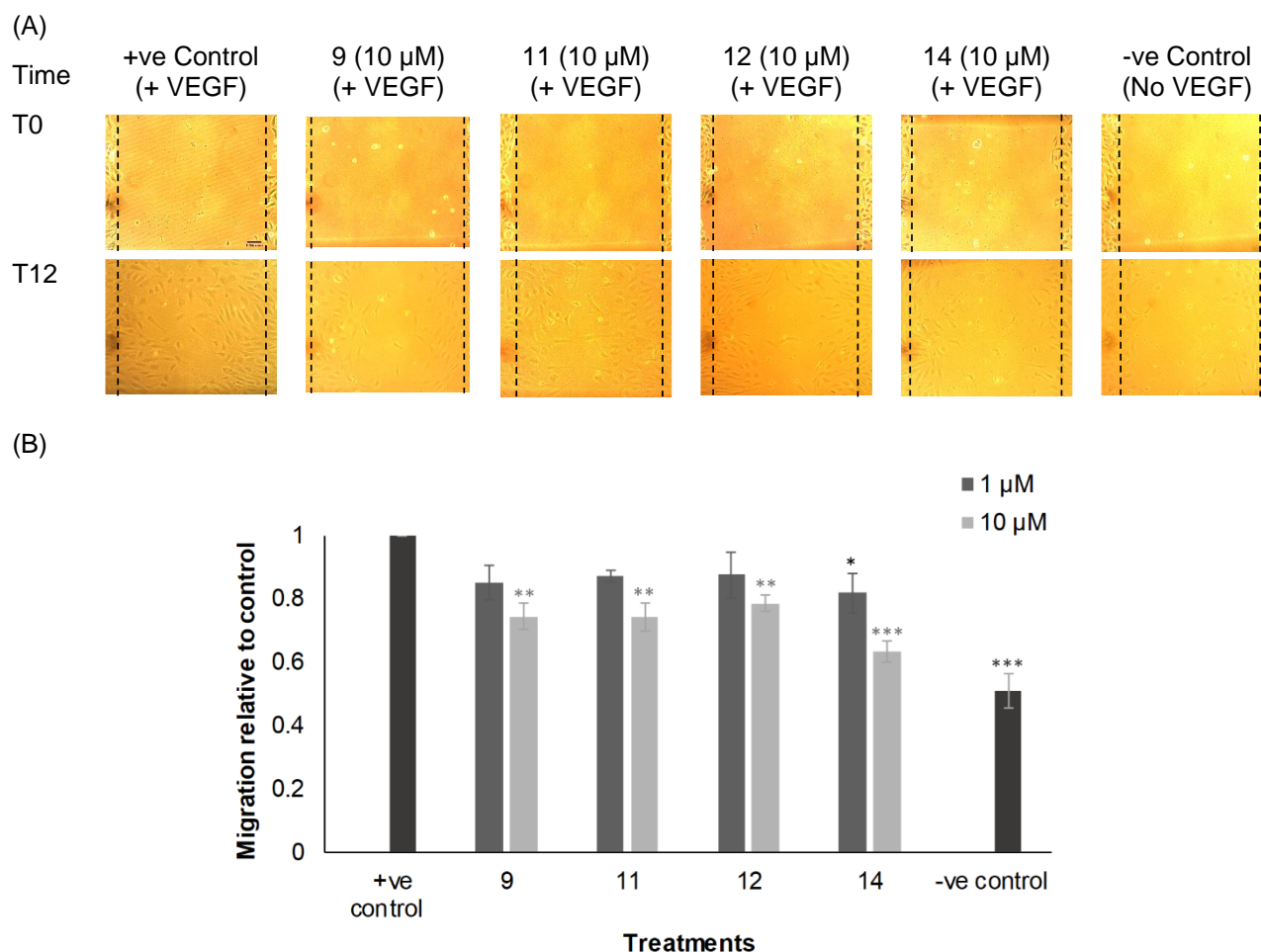


Figure 3. 14. *In vitro* HUVEC wound closure (migration) inhibition activity of flavones (**9**, **11**, **12** and **14**) expressed as a ratio to the +ve control (10 ng/mL VEGF-enriched media). (A) Representative images of scratch assay at 0 h and 12 h at 10X magnification. Images were analyzed using ImageJ software; (B) Migration after 12 h as a ratio to +ve control. Data are expressed as mean \pm standard error of the mean (SEM), $n = 3$. Statistical significance was estimated with respect to the +ve control by one-way ANOVA, followed by Dunnett's multiple comparison test (* $p < 0.05$, ** $p < 0.01$, *** $p < 0.001$).

In general, the active derivatives **9**, **11**, **12**, and **14** demonstrated strong suppression of VEGF-induced EC tube formation, ranging from 37 to 66% at 1 and 10 μ M concentrations (Section 3.2.2.2). They were furthermore able to suppress the VEGF-induced migration of ECs in a significant manner at 10 μ M (25 to 37%). Collectively, these results suggest that these compounds follow the general antiangiogenic behavior of flavonoids (Table 2.3, Chapter 2) by disrupting VEGF-associated signaling pathways, hence reducing the

differentiation and migration of ECs. Therefore, interaction of these compounds (**9**, **11**, **12**, and **14**) with VEGF's main receptor VEGFR2 was examined as a potential mode of action.

3.2.2.4. Exploring VEGFR2 as an antiangiogenic target

Inhibition of VEGFR2 phosphorylation in endothelial cells

At the molecular level, VEGFR2 is a tyrosine kinase receptor with an extracellular, a transmembrane, and an intracellular catalytic domain. The extracellular binding of VEGF leads to the dimerization and activation of the receptor via phosphorylation of the intracellular tyrosine residues [17,269]. VEGFR2 contains several phosphorylation sites, however only a few of them are considered important for its activity. The Tyr1175 site, in particular, has a critical role in mediating many of the cellular functions regulated by VEGFR2. The auto-phosphorylation of Tyr1175 triggers phospholipase C- γ , MAPK and PI3K/Akt pathways as well as the SHB and SCK adaptor proteins. These pathways modulate various EC activities, including permeability, survival and migration [17,269]. Herein, the capacity of the most active hits (**9**, **11**, **12**, and **14**) to impair Tyr1175 auto-phosphorylation and subsequently VEGFR2 activation, was investigated via western blotting. To begin with, the levels of total-VEGFR2 (T-VEGFR2) were calculated, relative to the in house protein β -actin, to investigate whether the test compounds affected the overall VEGFR2 expression. The tested compounds (**9**, **11**, **12**, and **14**) did not cause a variation of T-VEGFR2 levels compared to what was observed in presence of VEGF alone (i.e. positive control) ($p > 0.05$), as shown in **Figure 3. 15B**. The levels of VEGFR2 phosphorylation (P-VEGFR2) relative to the T-VEGFR2 were also measured for the target compounds at 1 and 10 μ M. The di-OH-4-thioflavones **11** and **12** demonstrated significant inhibition of 57 ($p < 0.001$) and 37% ($p < 0.05$), respectively at 10 μ M, compared to the positive control (**Figure 3. 15C**). On the other hand, the di-OCH₃-4-thioflavone (**9**) and the di-OH-4-oxoflavone (**14**), did not have notable effects on VEGFR2 phosphorylation at either of the examined concentrations ($p > 0.05$).

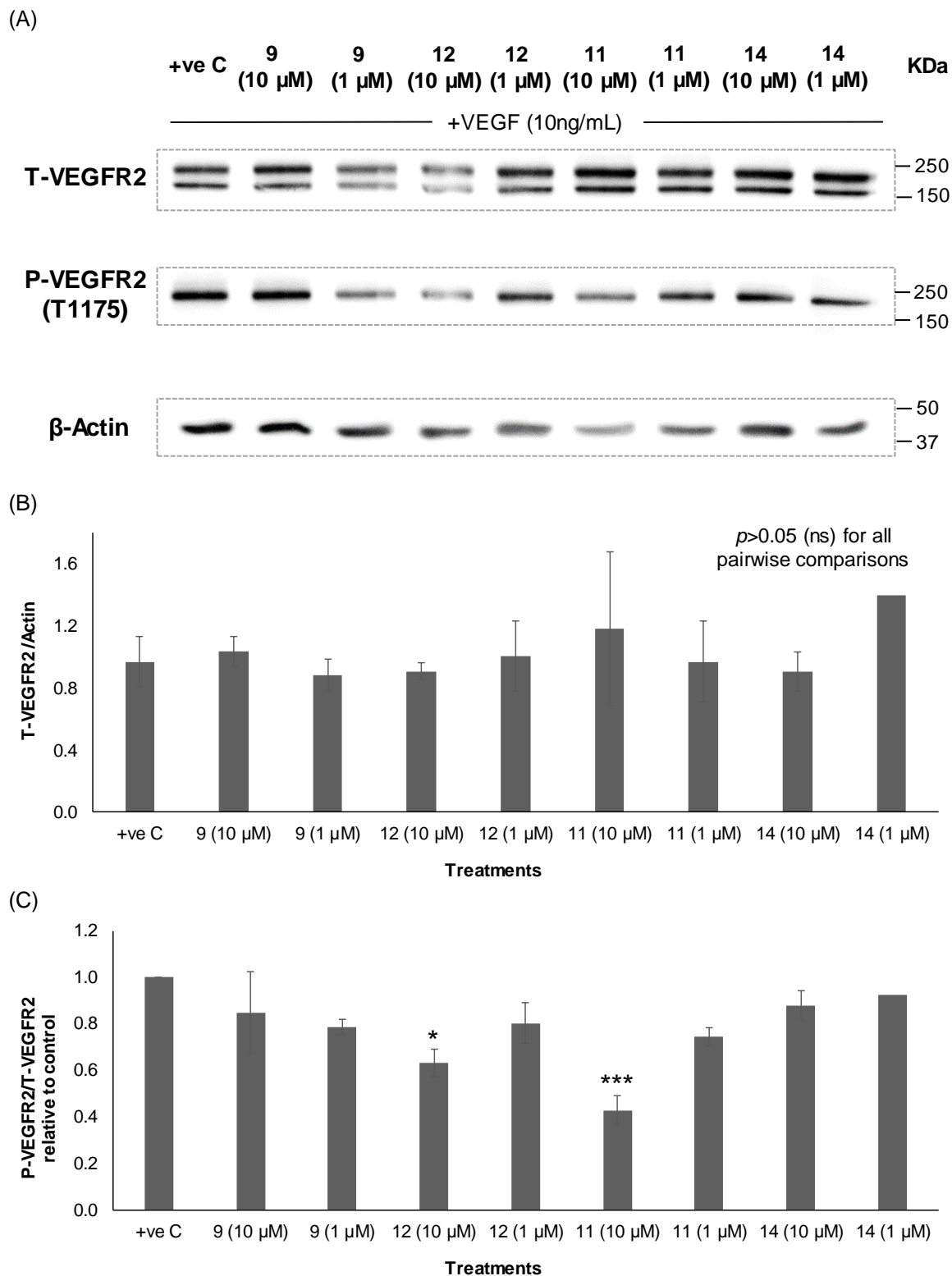


Figure 3. 15. VEGFR2 induced phosphorylation inhibition activity of flavones (**9,12, 11** and **14**) on HUVEC cell lysates. (A) Representative western blot images of the HUVECs proteins; T-VEGFR2, P-VEGFR2 and β -Actin. Full blots are presented in **Figure 7.3, Chapter 7**. Images were analyzed using ImageJ software; (B) T-VEGFR2 quantification relative to β -actin; (C) VEGFR2-induced phosphorylation inhibition expressed as a ratio to the +ve control (10 ng/mL VEGF-enriched media). Data are expressed as mean \pm standard

error of the mean (SEM), $n = 3$ except for **14** ($1 \mu\text{M}$) where $n = 2$. (B) Statistical difference between the individual groups was estimated by one-way ANOVA, followed by Tukey's multiple comparison test, as recommended for pairwise comparisons [267] (ns; non-significant, $p > 0.05$); (C) Statistical significance was estimated with respect to the +ve control by one-way ANOVA, followed by Dunnett's multiple comparison test, (* $p < 0.05$, *** $p < 0.001$).

Given the ability of active hits **11** and **12** to inhibit VEGFR2 phosphorylation, their interactions with VEGFR2 were further explored through molecular docking studies. Interactions of the remaining flavones (**7-9**, **13** and **14**) with VEGFR2 were also studied in order to understand the target-specific SAR dynamics of this library of synthesized flavones.

Interaction with VEGFR2's catalytic site

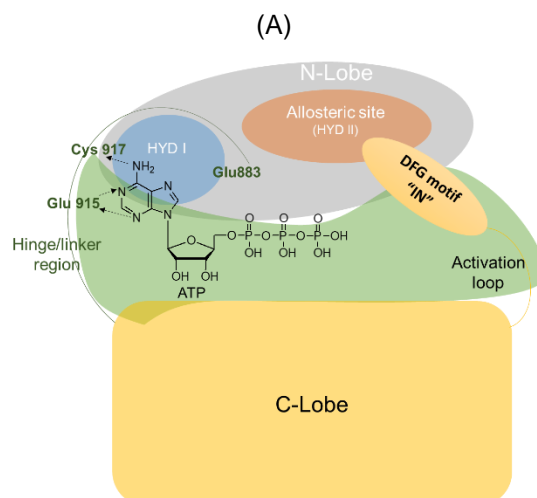
Evidence from the literature shows that the conserved catalytic kinase domain of VEGFR2 is the biologically relevant site for VEGFR2 ligands [22,270–272]. All of the currently approved small molecule RTKIs, including VEGFR2 inhibitors such as sunitinib, sorafenib and axitinib, elicit their kinase inhibitory effects by binding to the catalytic domain [269,270]. The kinase domain catalyzes the auto-phosphorylation of the receptor via ATP binding, activating VEGFR2 and triggering its signaling cascades. Hence, blocking the auto-phosphorylation step halts the receptor's activation and its dependent proangiogenic events [22]. With regards to flavonoids, data accumulated *in vitro*, *ex vivo* and through molecular modelling show that they can bind to the catalytic domain of several kinases, including VEGFR2, mostly by attaching to the ATP-binding site [273–277]. Flavonoids' structural features characterized by the heteroaromatic planar chromenone scaffold allow them to mimic the adenine moiety of ATP [273]. In that context, X-ray crystallographic analysis verified the binding of myricetin and quercetin in the conserved ATP-binding region of PI3K with dissociation constants (K_d) of 0.17 and 0.28 μM , respectively [278]. Based on the aforementioned data it is postulated herein that the synthesized halogenated flavones (**7-14**) could interact with the conserved catalytic kinase domain of VEGFR2.

Ligands **7-14** were docked in the ATP-binding site of VEGFR2 using its X-ray crystal structure (PDBid: 1YWN). The reported amino acids surrounding the catalytic domain were defined to create a protomol that accommodates all of the different binding pockets comprising the active site as outlined in **Table 3.5**.

Table 3. 5. Amino acid residues defining the catalytic kinase domain of VEGFR2 [269,271,272,279–282]

Catalytic domain region	Amino acids
ATP-binding site	Leu838, Gly841, Val846, Ala864, Lys866, Val912, Ileu913, Val914, Glu915, Phe916, Cys917, Lys918, Gly920, Leu1033, Cys1043
DFG region	Glu883, Asp1044, Phe1045, Gly1046
Allosteric site	Ileu886, Leu887, Ileu888, Ileu890, Val896, Val897, Leu1017, Ile1042

The catalytic domain is composed of a small N-lobe and a larger C-lobe joined by a hinge/linker region where the ATP docks [269,283,284] (**Figure 3. 16A**). VEGFR2 inhibitors generally bind to the catalytic site in two modes. Type I inhibitors, such as sunitinib, compete with ATP by interacting with residues in the hinge area during the active (DFG in) state of the binding site [269,271,283] (**Figure 3. 16B**). Type II inhibitors like sorafenib, stabilize the receptor's inactive state by extending through the hinge region and the allosteric pocket which is exposed by shifting of the DFG residue (Asp-Phe-Gly) towards the sugar/phosphate region, adopting an “out” conformation [269,271,281,283] (**Figure 3. 16C**).



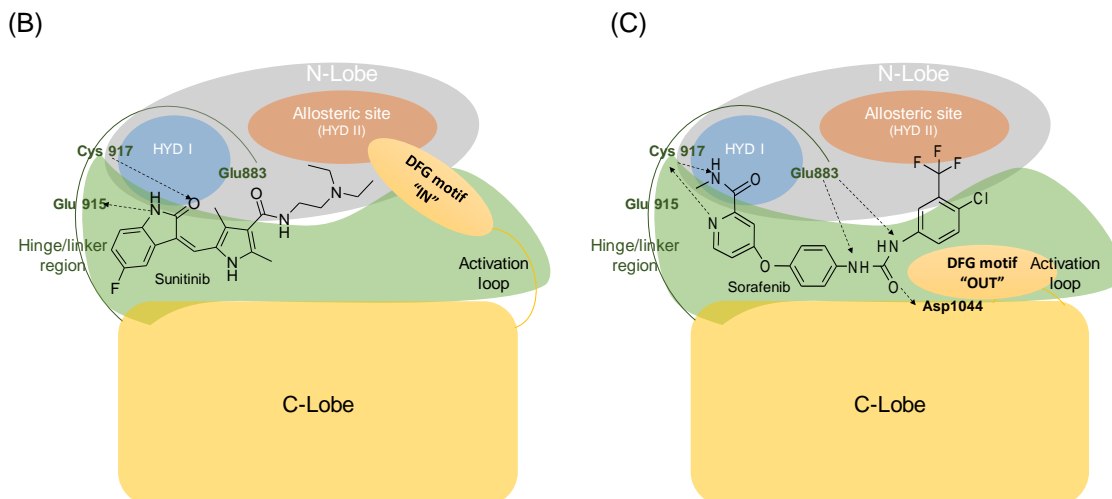


Figure 3. 16. Schematic representation of the catalytic binding site of VEGFR2/KDR. (A) ATP binding mode in active conformation; (B) Type I inhibitors binding mode, represented by sunitinib, in active conformation; (C) Type II inhibitors binding mode, represented by sorafenib, in inactive conformation

Ligands (**7-14**) were docked using a flexible mode algorithm (in Sybyl), enabling them to freely adopt different orientations and conformations within the binding site, as defined by the protomol. By default, twenty conformations were considered sufficient for each ligand due to the rigid nature of flavonoid molecules. In order to validate the docking procedure, the original ligand (4-amino-furo[2,3-d]pyrimidine) co-crystallized with VEGFR2 was removed from the receptor and re-docked with the prepared active site. Superimposition of both the original and re-docked ligand resulted in a root mean square deviation (RMSD) of 0.97 Å, which is well within the 2 Å grid resolution used for docking [285]. Moreover, the binding mode of the docked ligand was compared with the co-crystallized structure solution (PDBid: 1YWN) [279] and demonstrated the same interactions, typical of a type II inhibitor, as shown in **Figure 3. 17**.

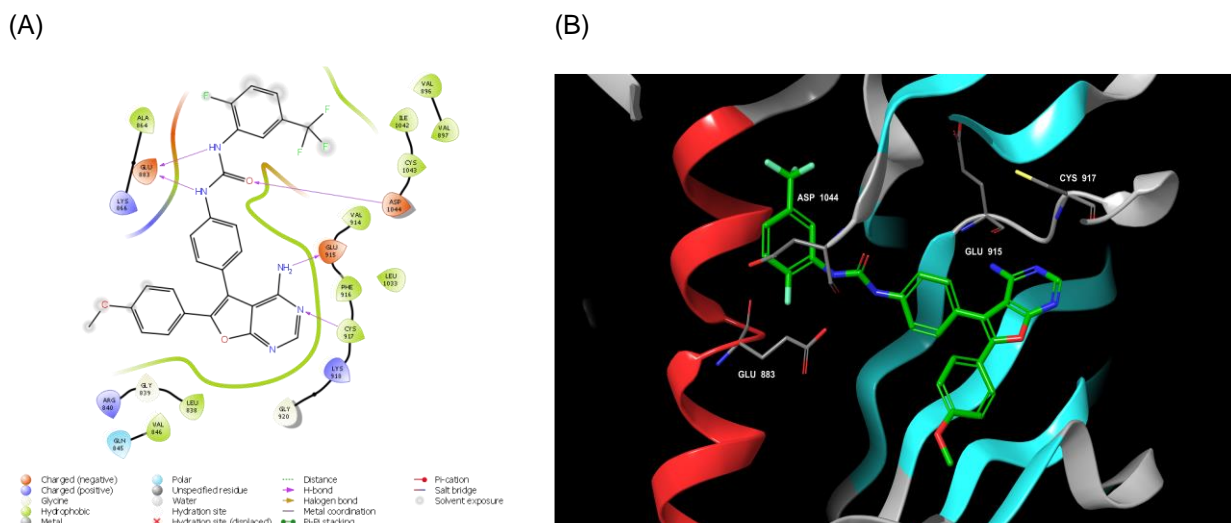
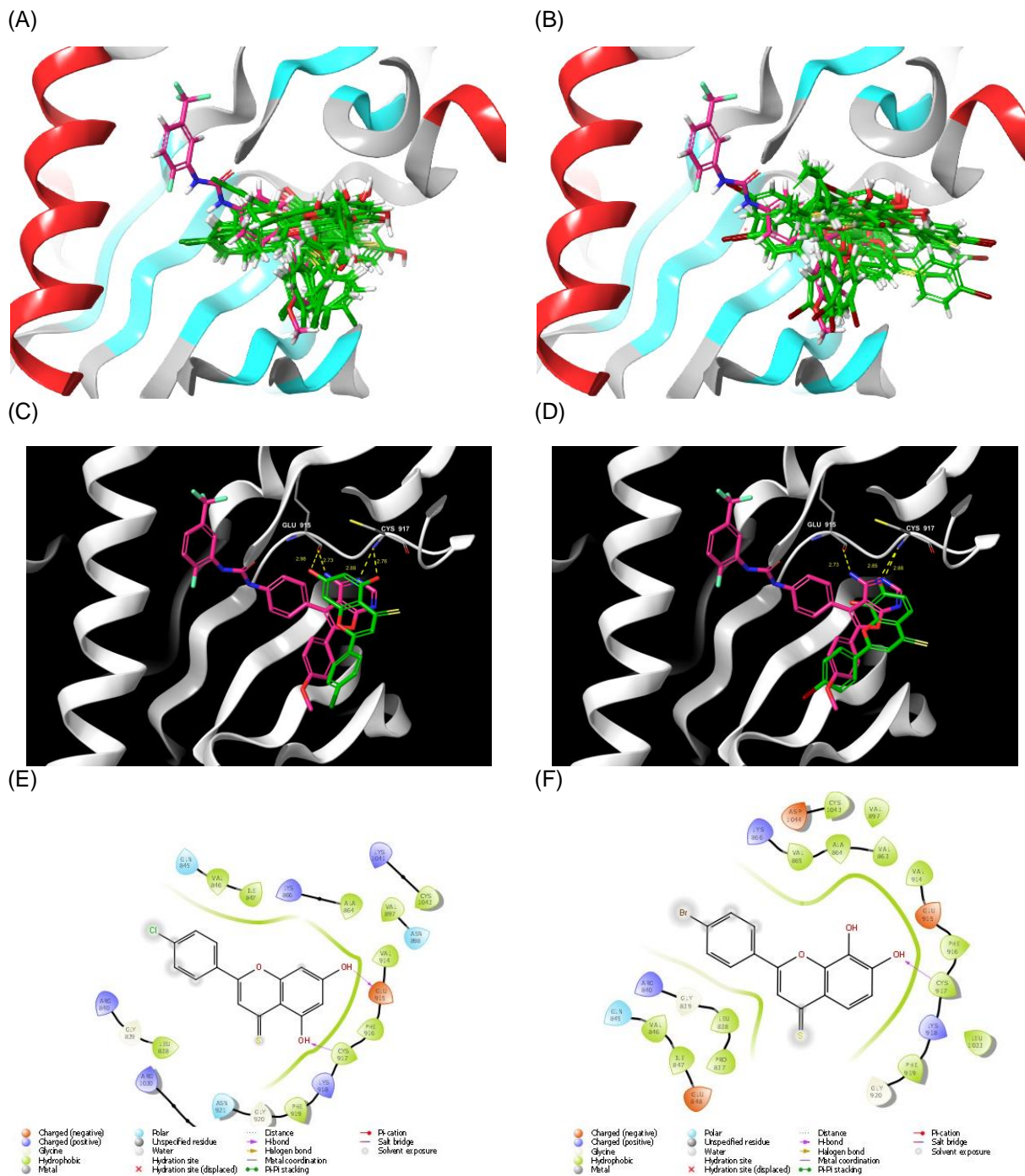


Figure 3. 17. Docking of the original co-crystallized ligand (N-{4-[4-amino-6-(4-methoxyphenyl)furo[2,3-d]pyrimidin-5-yl]phenyl}-n'-[2-fluoro-5-(trifluoromethyl)phenyl]urea) with VEGFR2 (1YWN). (A) 2D interaction of ligand with binding pocket; (B) 3D interaction of ligand with binding pocket showing key amino acids

The binding modes of flavones (**9**, **11**, **12** and **14**) explained their order of activity of VEGFR2 phosphorylation inhibition (**11** > **12** > **9** > **14**), as observed in the western blotting assay. The majority of lead **11**'s conformations adopted a pose that is largely aligned with the furopyrimidine-6-*p*-methoxyphenyl scaffold of the ligand (**Figure 3. 18A**). The top docked pose of **11** shows that ring A is closely stacked on the ligand's aminopyrimidine ring, where the OH groups at positions 5 and 7 act as bioisosteres for N and NH₂ of the ligand, respectively (**Figure 3. 18C**). In that regard, ring A mimics the adenine ring of ATP by occupying the hinge region and forming hydrogen bonds (HBs) with the key Glu915-O (2.98 Å) and Cys917-N (2.76 Å) residues. As for the thioflavone **12**, slightly more than half of the twenty generated conformations adopted a favorable vertical alignment, parallel to that of **11** (**Figure 3. 18B**). As shown in **Figure 3. 18D**, **12**'s top conformer was capable of forming one HB with Cys917-N (2.85 Å) via the O of the 7-OH group. In addition to interacting with the critical Glu915 and Cys917 amino acids, **11** and **12** showed several key hydrophobic interactions with residues in the adenine region (**Figure 3. 18E and F**), which are characteristic of type I VEGFR2 inhibitors as presented in **Table 3. 6**.



(G)

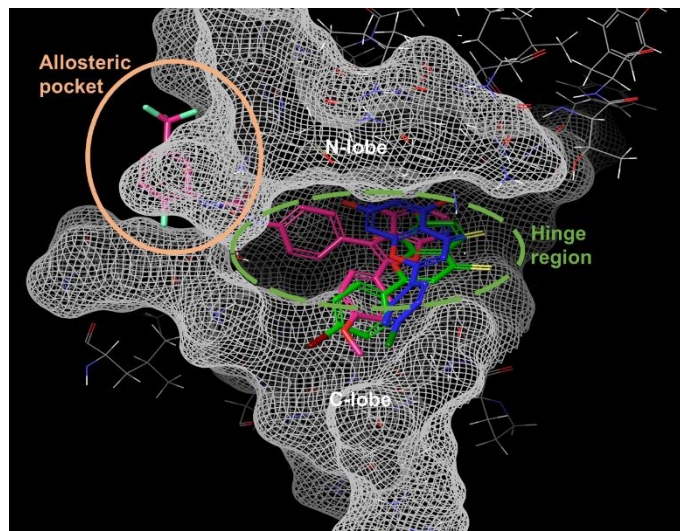
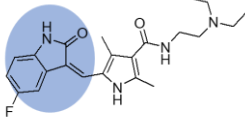
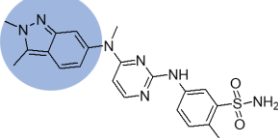
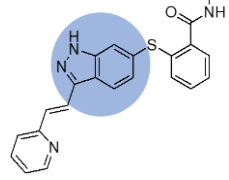
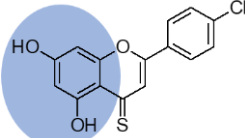
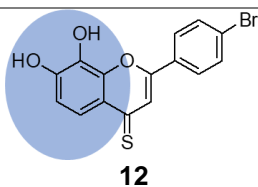


Figure 3. 18. Interaction of flavones **11** and **12** (green) with VEGFR2 binding pocket compared to co-crystallized ligand (pink). (A) 3D of all 20 conformers of **11**; (B) 3D of all 20 conformers of **12**; (C) 3D of **11** top conformer; (D) 3D of **12** top conformer; (E) 2D of **11** top conformer; (F) 2D of **12** top conformer; (G) mesh representation of active vertical orientation of **11** (blue) and **12** (green) showing different regions of the catalytic site

Table 3. 6. Amino acid residues interacting with different type I VEGFR2 inhibitors compared to leads **11** and **12**. The adenine mimicking scaffold of each molecule is highlighted in blue, while the shared amino acids between **11** and **12** and the included inhibitors are highlighted in bold.

Type I VEGFR2 inhibitor	HB	Hydrophobic interactions
 Sunitinib [286]	Glu915, Cys917	Leu838, Ala864, Val914, Phe916, Leu1033
 Pazopanib [287]	Lys866, Glu883, Cys917, Asp1044	Leu887, Ile890, Val896, Val897, Val912, Val914, Phe916, Leu1017, His1024, Cys1043, Phe1045
 Axitinib [288]	Glu883, Glu915, Cys917, Asp1044	Leu838, Ala864, Lys866, Val914, Phe916, Gly990, Leu1033, Phe1045
 11	Glu915, Cys917	Leu838, Val846, Ile847, Ala864, Val897, Val914, Phe916, Phe919, Leu1033, Leu1034, Cys1043

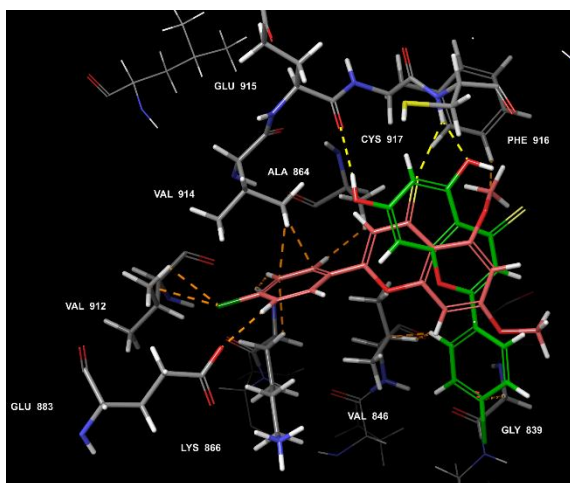
**Cys917**

Leu838, Pro837, Val846, Ile847, Val863,
Ala864, Val865, Val897, **Val914**, **Phe916**,
 Phe919, **Leu1033**, **Cys1043**,

Taken together with their ability to inhibit VEGFR2 phosphorylation, these findings suggest that lead compounds **11** and **12** could exert their antiangiogenic effects via type I VEGFR2 inhibition. However, additional research is required to determine if the lack of the linker component that forms HBs with Glu883 and Asp1044, in the DFG motif area, will adversely affect the binding affinities of **11** and **12** to VEGFR2 in comparison to type I inhibitors currently on the market.

In contrast to the active derivatives **11** and **12**, compounds **9** and **14** formed HBs with Cys917-N but with their 4-C=S (3.33 Å) and 4-C=O (3.04 Å) moieties, respectively, instead of the O in their OH groups. This resulted in a horizontal alignment for **9** and **14** in which their B and C rings extend into the adenine and DFG regions, forming undesirable clashes with important amino acids such as Glu883 and Ala864 (**Figure 3. 19**). The bulkiness and branching of 5-OCH₃ of **9** clashes with Phe916, hindering its ability to face residues Glu915 and Cys917. With regards to **14**, its horizontal pose possibly resulted from the better hydrogen bond acceptor (HBA) character of the carbonyl O over the hydroxyl O. This is manifested in the higher number of **14** conformations in which the C=O is facing the inside of VEGFR2 binding cavity where it can interact with several amino acids via HBs (**Figure 3. 20B**).

(A)



(B)

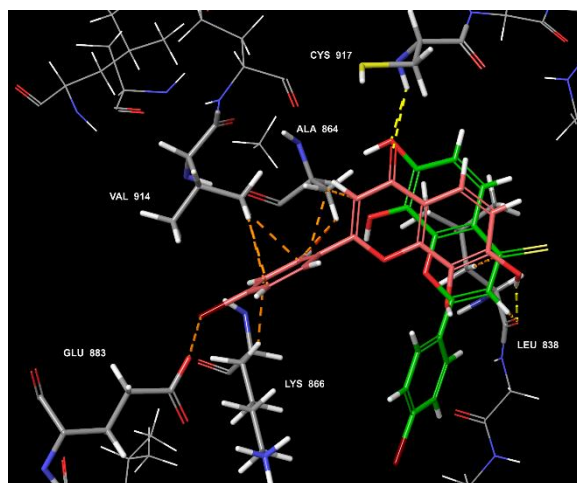
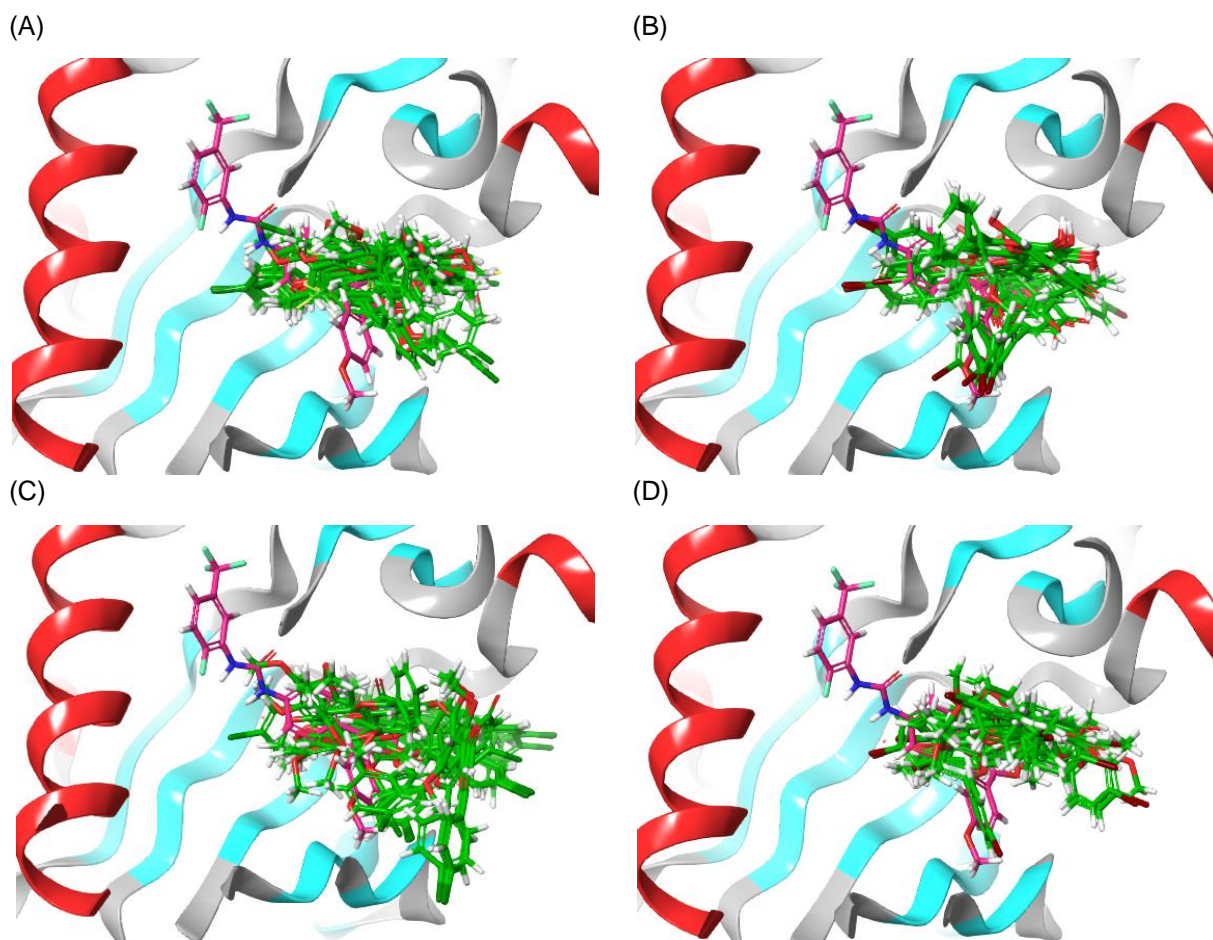


Figure 3. 19. Comparison of the 3D interactions of flavones (**9**, **11**, **12** and **14**) in ATP-binding pocket of VEGFR2. (A) **9** (salmon) versus **11** (green); (B) **14** (salmon) versus **12** (green). HBs are represented by yellow dashed lines, clashes are represented by orange dashed lines.

To further investigate the effect of the 4-C=O and the OCH₃ functionalities on VEGFR2, the binding modes of compounds (**7**, **8**, and **13**) were examined (Figure 3. 20C-E). None of the conformations adopted by these flavones showed the distinctive binding mode of the ATP-binding scaffold of the active compound **11**, with the exception of 3 out of 20 conformations for compound **13**. These results explain the lack of VEGFR2 inhibitory activities of the diOCH₃ derivative **9** and the 4-C=O derivative **14**, indicating that their strong antiangiogenic effects likely result from interactions with other angiogenic target/s reported for flavonoids.



(E)

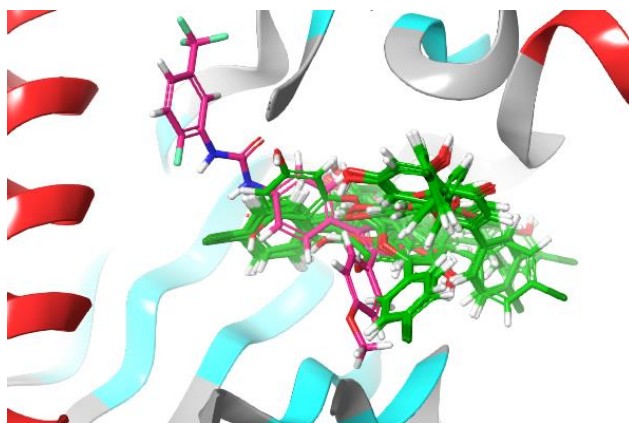


Figure 3. 20. 3D interaction of all 20 conformers of flavones (green) with VEGFR2 binding site compared to co-crystallized ligand (pink). (A) **9**; (B) **14**; (C) **7**; (D) **8**; (E), **13**

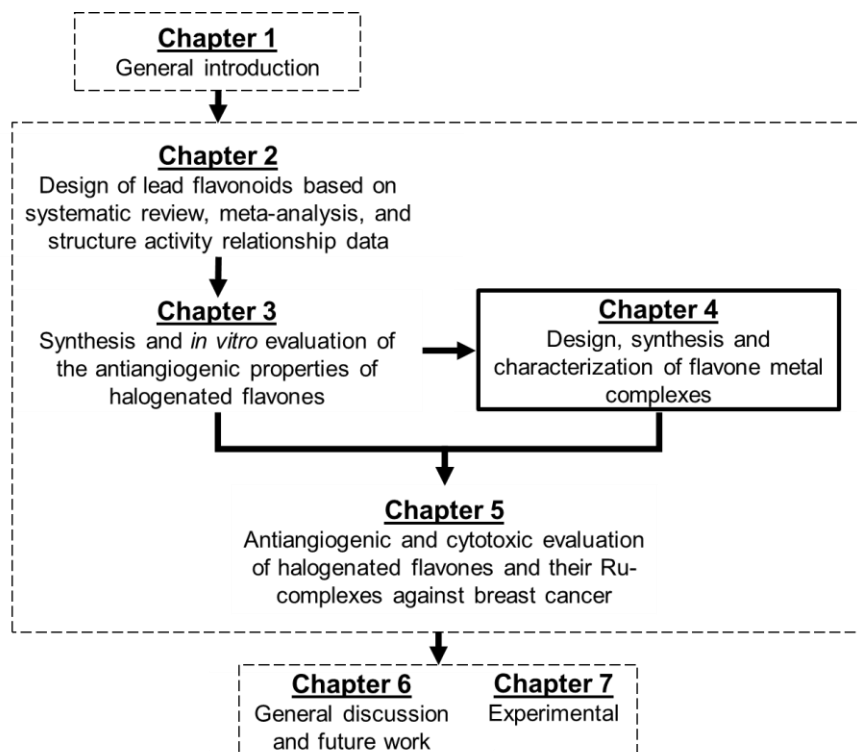
3.3. Conclusions and future perspectives

The designed 4-C=O and 4-C=S flavones (**7-14**) were synthesized via the Baker-Venkataraman pathway in good to excellent yields (60-97%) and with excellent purities (>90%). Synthesis of the 4-C=Se flavones (**15-18**) was explored via direct selenation of **7** and **8** using WR under either microwave assisted or standard heating conditions, however, neither approach produced the intended output. In that context, it was not possible to separate a pure product from the crude reaction product after consecutive column chromatography with different solvent systems. Evaluation of the *in vitro* antiangiogenic activities of **7-14** as part of their assessment as dual antiangiogenic/cytotoxic anticancer agents, revealed strong suppression of VEGF-induced angiogenic features. The tested compounds did not exhibit cytotoxic effects on ECs ($p > 0.05$, compared to control) at 40 μM . Flavones (**7-14**) inhibited EC tube formation in a significant manner (37-55% at 12 h) at low concentration of 1 μM . The effects were comparable to the reported tube formation inhibition of the anticancer drug sunitinib (50% at 48 h). The most active compounds (**9**, **11**, **12**, and **14**) identified from the tube formation assay notably suppressed EC migration by 25 and 37% at 10 μM . VEGFR2 interactions were explored as a potential antiangiogenic target for the active leads using western blotting and docking studies. Compounds **11** and **12**, possessing 7-OH and 4-C=S groups, relied on VEGFR2 inhibition to mediate their antiangiogenic effects, with 57 and 37% VEGFR2 phosphorylation inhibition at 10 μM , respectively ($p < 0.05$). This inhibition

is likely achieved by an ATP-competitive binding mode. Analogues **9** and **14** showed unfavorable binding modes with the VEGFR2 catalytic site due to the presence of the 5,7-diOCH₃ and 4-C=O structural characteristics, resulting in a lack of activity on VEGFR2 phosphorylation inhibition. Future investigations, such as X-ray crystallography, are recommended to confirm the proposed binding modes of flavones **11** and **12** with VEGFR2. However, the main target of the remaining set of flavones has not been elucidated. Moreover, the tested panels are expected to interact with several biological targets given the reported multi-target characteristics of flavonoids [59,289,290] and the conserved nature of protein kinases [273]. In that regard, the antiangiogenic targets of the structurally similar flavones apigenin, luteolin and chrysin, such as IL-6/STAT3 and MAPK pathways and MMPs-2 and 9 [291–293], can guide the future antiangiogenic evaluations of the flavones presented herein. High throughput screening strategies can be applied in order to develop a comprehensive profile of the biological targets affected by the tested flavones. This is not only important for shaping the beneficial therapeutic effects of these compounds, but also for determining off-target interactions that might result in undesired pharmacological effects.

Chapter 4

Design, synthesis and characterization of flavone metal complexes



4.1. Introduction

In **Chapter 2**, a library of halogenated flavone compounds was purposefully designed as a foundation for the development of bi-functional antiangiogenic and cytotoxic anticancer agents. The designed compounds were synthesized and biologically evaluated for their *in vitro* antiangiogenic activity, specifically targeting EC tube formation, migration and VEGFR2 activation (**Chapter 3**). The promising antiangiogenic activity demonstrated by the assessed candidates motivated additional structural refinement to further enhance their antiangiogenic and cytotoxic activities.

Based on the strong antineoplastic activity reported for Ru(II) arene and Ir(III)Cp* compounds in general, and their flavonoid derivatives in particular (**Section 1.4, Chapter 1**), it is hypothesized herein that their combination with the flavones synthesized in this study could result in synergistic antiangiogenic and cytotoxic effects (**Figure 4. 1**). The high tumor selectivity of the metal scaffolds means that they can enhance the antiangiogenic and cytotoxic effectiveness of the active leads and lower the probability of having off-target interactions that might result in toxicity. Additionally, the lipophilic nature of the arene and Cp* ligands could result in increased cellular absorption and improved pharmacokinetic properties of our compounds. Hence, this chapter explores the chemical challenges encountered, and the progress made, for the synthesis and spectroscopic characterization of the modified Ru(II)-*p*-cymene and Ir(III) Cp* halogenated flavone derivatives (**19-26**).

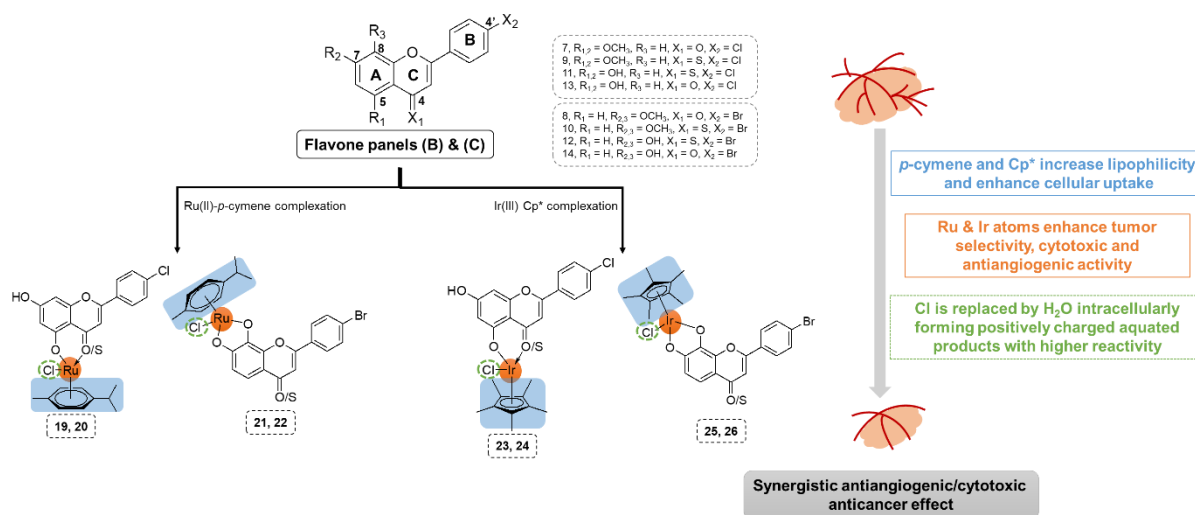


Figure 4. 1. Schematic representation of the proposed metal complexation optimization strategies

Flavonoid metal complexes are generally synthesized by reacting flavonoid and metal salts dissolved in an alcoholic or aqueous solution. The reaction can be carried out under different conditions of stirring and/or heating with the use of a base to deprotonate the OH groups and facilitate metal coordination. The complex usually precipitates from solution, and is then filtered and air dried. A range of spectroscopic and analytical methods have proved insightful for structural characterization of flavonoid metal complexes (**Figure 4. 2**), and the synthesis and analytical methods that have been used in the literature are summarized in **Table 4. 1** [117].

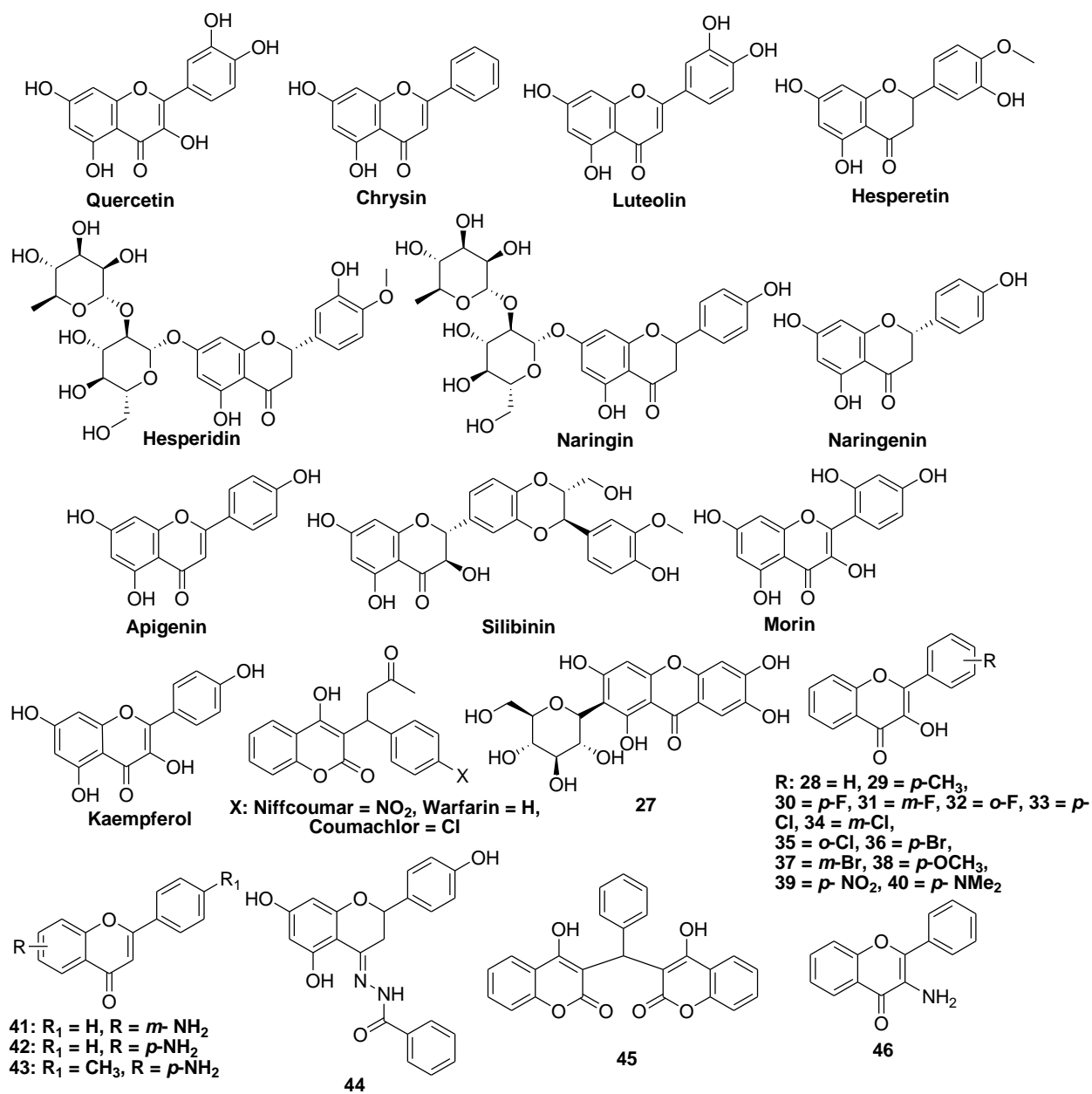


Figure 4. 2. Chemical structures of flavonoids from which organometallic derivatives have been prepared

Table 4. 1. Summary of synthetic conditions and characterization methods for flavonoid metal complexes

Flavonoid Solution	Metal	Base used and pH	Final product Formula	Characterization	Ref
Quercetin.2H₂O in EtOH	NiCl ₂ .6H ₂ O	NaOEt 6-7	Ni(Que) ₂ (H ₂ O) ₂	UV, IR, Elemental Analysis	[294]
	CuCl ₂ .2H ₂ O	NaOEt 6-7	Cu(Que) ₂ (H ₂ O) ₂	UV, IR, Elemental Analysis	[295]
	La acetate Nd acetate Eu acetate Gd acetate Tb acetate Dy acetate Tm acetate Y acetate	NaOEt n/a	La(Que) ₃ (H ₂ O) ₆ Nd(Que) ₃ (H ₂ O) ₆ Eu(Que) ₃ (H ₂ O) ₆ Gd(Que) ₃ (H ₂ O) ₆ Tb(Que) ₃ (H ₂ O) ₆ Dy(Que) ₃ (H ₂ O) ₆ Tm(Que) ₃ (H ₂ O) ₆ Y(Que) ₃ (H ₂ O) ₆	UV, IR, ¹ H NMR, TG-DTG, Fluorescence analysis, Electrochemistry, Elemental analysis	[296]
[Cu(Que)₂(H₂O)₂] in MeOH	SnCl ₄	n/a	[Cu(Que) ₂ (H ₂ O) ₆ -Sn ₂ Cl ₄]	IR, ¹ H, ¹³ C & ¹¹⁹ Sn NMR, EPR, ESI-MS, TG-DTG	[297]
[Zn(Que)₂(H₂O)₂] in MeOH	SnCl ₄	n/a	[Zn(Que) ₂ (H ₂ O) ₆ -Sn ₂ Cl ₄]	IR, ¹ H, ¹³ C & ¹¹⁹ Sn NMR, EPR, ESI-MS, TG-DTG	[297]
Chrysin in EtOH	Vanadyl acetylacetonate	n/a 5	VO(Chry) ₂ EtOH	UV-Vis, IR, EPR, Spectrophotometric titrations	[298]
	Ph ₃ GeBr	Na ₂ CO ₃ n/a	Chry-Ge. C ₂ H ₆ O	IR, ¹ H & ¹³ C NMR, Elemental analysis	[299]
	La acetate	NaOH n/a	La(Chry) ₂ .OAc(H ₂ O) ₇	IR, ¹ H NMR, Elemental analysis, TG-DTG, Spectrophotometric titrations	[300]
Luteolin in H₂O	VOSO ₄ .H ₂ O	NaOH 6	VO(Lut) ₂	UV-Vis, IR, ¹ H NMR, ESI-MS	[301]
Luteolin	50% aqueous solution of VOCl ₂	NaOH 5	[VO(Lut)(H ₂ O) ₂]Na·3H ₂ O	UV-Vis, IR, EPR, Elemental analysis	[302]
Luteolin in EtOH	Mn(CH ₃ COO) ₂	n/a 4	MnO-Lut	UV-Vis, IR, Elemental analysis, TG-DTG	[303]
Hesperidin in H₂O	50% aqueous solution of VOCl ₂	NaOH 12	[VO(Hesp)(OH) ₃]. Na ₄ (H ₂ O) ₃	UV-Vis, IR, EPR, Spectrophotometric titrations	[304]

Chapter 4: Design, synthesis and characterization of flavone metal complexes

Hesperetin in EtOH	CuCl ₂ ·2H ₂ O	NH ₃ solution 7-8	[Cu(Hespt) ₂ (H ₂ O) ₂]·H ₂ O	UV-Vis, IR, ESI-MS, TG-DTG	[305]
Naringin in MeOH	Cu acetate in distilled H ₂ O	n/a	[Cu (Nar)] ⁺ [CH ₃ COO] ⁻ ·(H ₂ O) ₅	UV-Vis, IR, ¹ H NMR, ESI-MS, Elemental analysis	[306]
Naringenin in EtOH	CuCl ₂ ·2H ₂ O	NH ₃ solution 7-8	[Cu(Narg) ₂ (H ₂ O) ₂]·H ₂ O	UV-Vis, IR, ESI-MS, TG-DTG	[305]
Apigenin in EtOH	CuCl ₂ ·2H ₂ O	NH ₃ solution 7-8	[Cu(Apg) ₂ (H ₂ O) ₂]·H ₂ O	UV-Vis, IR, ESI-MS, TG-DTG	[305]
Silibinin in EtOH	50% aqueous solution of VOCl ₂	NaOMe 9	Na ₂ [VO(Sil) ₂].(H ₂ O) ₆	IR, EPR, Spectrophotometric titrations	[307]
Morin in MeOH	50% aqueous solution of VOCl ₂	NaOMe 5	[VO(Mor) ₂ H ₂ O]. (H ₂ O) ₅	UV-Vis, IR, EPR, Spectrophotometric titrations	[308]
Kaempferol in EtOH	ZnCl ₂ ·2H ₂ O	NaCl 8-10	[Zn(Kaem) ₂ (H ₂ O) ₂]·H ₂ O	UV-Vis, IR, ¹ H NMR, ESI-MS, Elemental analysis	[309]
Nifflcoumar sodium salt in H₂O	Ce(NO ₃) ₃ ·6H ₂ O La(NO ₃) ₃ ·6H ₂ O Nd(NO ₃) ₃ ·6H ₂ O	n/a 4-5	Ce(NS) ₃ . (H ₂ O) ₄ La(NS) ₃ . (H ₂ O) ₄ Nd(NS) ₃ . (H ₂ O) ₆	IR, ¹ H NMR, Elemental analysis	[310]
Nifflcoumar in H₂O	Aqueous solution of ZrCl ₄	NaOH 5	Zr(Niff) ₂ (OH) ₄ (H ₂ O) ₅	IR, ¹ H NMR, Elemental analysis, TG-DTG	[311]
Warfarin in H₂O	Aqueous solution of ZrCl ₄	NaOH 5	Zr(War) ₂ (OH) ₄ (H ₂ O) ₂	IR, ¹ H NMR, Elemental analysis, TG-DTG	[311]
Coumachlor in H₂O	Aqueous solution of ZrCl ₄	NaOH 5	Zr(Coum) ₂ (OH) ₄ (H ₂ O) ₆	IR, ¹ H NMR, Elemental analysis, TG-DTG	[311]
27 in 50% EtOH	GeO ₂ in deionized H ₂ O	NaOH 7	n/a	UV-Vis, IR, ¹ H NMR, MS, Elemental analysis, TG-DTG	[312]
28-37 in MeOH	[Ru(η ⁶ - <i>p</i> - cymene)Cl ₂] ₂ in CH ₂ Cl ₂	NaOMe n/a	n/a	¹ H & ¹³ C NMR, Elemental analysis, X-ray	[110,144]
41-44 in CH₂Cl₂	[Ru(η ⁶ - <i>p</i> - cymene)Cl ₂] ₂ in CH ₂ Cl ₂	n/a	n/a	UV-Vis spectra, IR, ¹ H NMR, FAB/EI-MS, X-ray	[144,313, 314]

Chapter 4: Design, synthesis and characterization of flavone metal complexes

33, 38-40 in EtOH	[Ru(DMSO) ₄ Cl ₂] in EtOH	TEA n/a	[Ru(DMSO) ₂ (34) ₂] ₂ NaNO ₃ (H ₂ O) ₂ [Ru(DMSO) ₂ (38) ₂] ₂ NaNO ₃ . H ₂ O [Ru(DMSO) ₂ (39) ₂]. (NO ₃) ₂ (H ₂ O) ₂ [Ru(DMSO) ₂ (40) ₂] ₂ NaNO ₃ (H ₂ O) ₅	IR, ¹ H NMR, ESI-MS, Elemental analysis	[145]
44 in EtOH	La(NO ₃) ₃ .6H ₂ O	TEA n/a	n/a	UV-Vis, IR, ¹ H NMR, Elemental analysis, TG-DTA	[315]
45 in H₂O	Aqueous solution of Ce La Nd	NaOH 5	Ce(45)(OH)(H ₂ O) ₂ La(45)(OH).H ₂ O Nd(45)(OH).H ₂ O	IR, ¹ H & ¹³ C NMR, Elemental analysis	[316]
46 in EtOH	Aqueous solution of K ₂ PtCl ₄	n/a	cis - [Pt(46) ₂ Cl ₂]	IR, ¹ H & ¹⁹⁵ Pt NMR	[317]

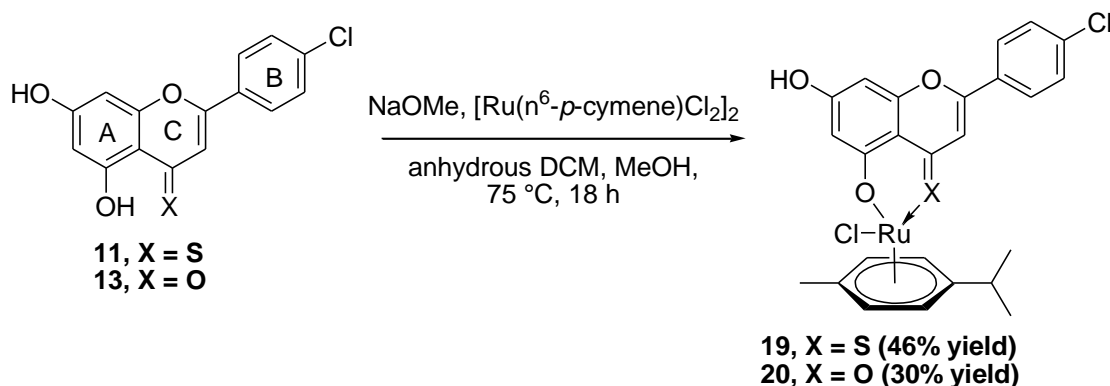
UV, ultraviolet; IR, infrared; NMR, nuclear magnetic resonance; TG, thermogravimetry; DTG, differential thermogravimetry; EPR, electron paramagnetic resonance; ESI-MS, electron spray ionization mass spectrometry; DTA, differential thermal analysis; n/a, not available.

4.2. Results and discussion

4.2.1. Synthesis and structural characterization of Ru(II)-*p*-cymene flavone complexes

4.2.1.1. 5, 7-Dihydroxy-4'-chlorophenyl Ru(II) complexes (**19** and **20**)

The novel Ru(II) (η^6 -*p*-cymene) flavone complexes **19** and **20** were synthesized via the reaction of their parent flavones **11** and **13**, respectively, with the commercially available bis[Ru(η^6 -*p*-cymene)Cl₂]. Deprotonation of the 5-OH group in flavone **11** or **13** was achieved using 1.05 equivalents sodium methoxide (NaOMe) in methanol, based on the reported method [318] (**Scheme 4. 1**). The 4-C=S and 4-C=O Ru(II) derivatives (**19** and **20**) were purified by crystallization in 9:1 EtOAc:CHCl₃ or EtOAc:ACN, and were obtained in 46 and 30% yields, respectively.



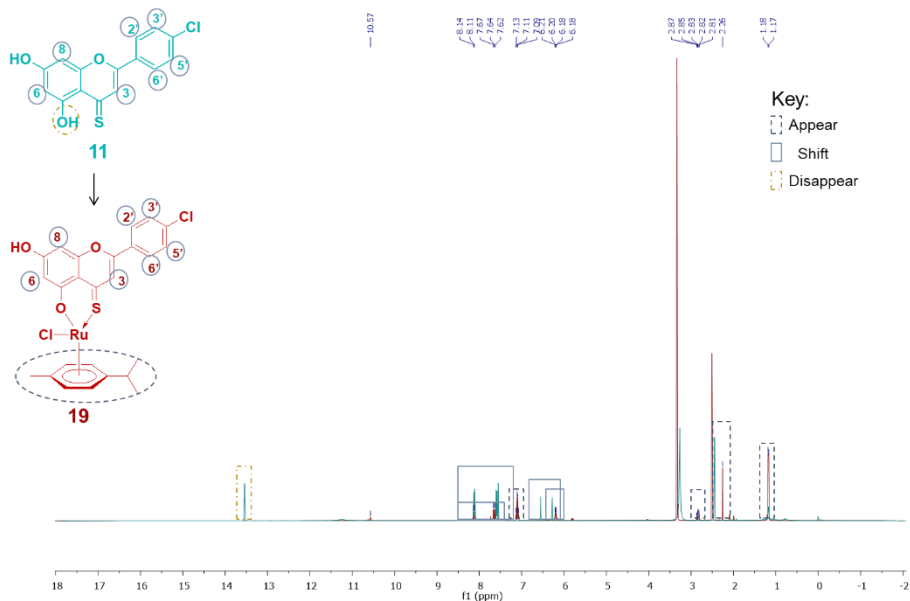
Scheme 4. 1. Synthesis of Ru(II) complexes **19** and **20**

Various techniques may be employed to confirm the structure of metal complexes, as outlined in **Table 4. 1, Section 4.1** [117]. The structures of the synthesized organometallic complexes **19** and **20** were confirmed by ¹H and ¹³C NMR spectroscopic analysis, IR spectroscopy, mass spectrometry, and elemental analysis. It has been reported that IR spectroscopy provides data that can be used to identify the functional groups involved in metal coordination [319]. Complexation of the metal atom with the C=O group, for instance, causes an increase in the bond length, which is manifested as a decrease in the frequency of the C=O peak. The disappearance of the characteristic flavonoid OH broad peaks at 3600–3200 cm⁻¹ in IR spectra indicates their involvement in metal chelation. Nevertheless, removal of the OH peaks in IR spectra can be concealed by the existence of additional OH groups in the flavonoid composition and in the H₂O molecules

that are integrated into the metal sphere during complexation. In this study, the IR spectrum for compound **13** showed a reduction in the frequency of the 4-C=O upon complexation with Ru from 1680 to 1633 cm^{-1} , indicating interaction with the metal atom. The OH peaks of **11** and **13** were shifted from 3358 and 3350 cm^{-1} to 3141 and 3231 cm^{-1} , respectively, after Ru chelation. ^1H NMR spectroscopy also indicated Ru chelation at the 4,5 positions. The ^1H NMR spectrum of **11** shows a sharp signal for the 5-OH proton at δ 13.54 ppm due to its intramolecular HB with the 4-C=S group [320,321]. The ^1H NMR spectrum of complex **19** showed a slight shift of the protons of the thioflavone moiety, and the 5-OH proton was no longer present indicating chelation at this position (**Figure 4. 3A**). Likewise, the peak of the 5-OH group proton where the chelation occurred was no longer present in the ^1H NMR spectrum of **20** as seen in **Figure 4. 3B**. Ru(II)-*p*-cymene complexation of **11** was evident by the appearance of the *p*-cymene CH_3 proton peaks at δ 1.16, 1.18 and 2.26 ppm in addition to a multiplet corresponding to the CH proton at δ 2.83 ppm. Furthermore, aromatic protons of the cymene ring appeared as two doublets at δ 7.07 and 7.11 ppm ($J=8.4$ Hz) (**Figure 4. 3A**). The ^1H NMR spectrum of **20** exhibited the same patterns demonstrating successful complexation where signals of the *p*-cymene protons appeared at δ 1.29, 1.30 ($2\times\text{CH}_3$), 2.17 (CH_3), 2.84 (CH), 5.37 and 5.66 (Ar-CH) ppm (**Figure 4. 3B**). Successful chelation of **13** and Ru(II)-*p*-cymene was also reinforced by the upfield shift of all of the proton signals of compound **13** with the ring A protons (H-6 and 8) seeing the highest shifts by 0.3 and 0.5 ppm, respectively. The carbon signals for the *p*-cymene ring were visible in both the aliphatic and aromatic regions along with the *p*-chlorophenyl ring carbons of the flavone moiety in the ^{13}C NMR spectra of both complexes (**Figure 4. 4**). For instance, the ^{13}C NMR spectrum of complex **20** showed peaks corresponding to the CH_3 and CH groups of cymene at δ 17.92, 22.52 and 30.89 ppm in addition to the aromatic cymene carbons at δ 102.70, 106.34 and 129.81 ppm whereas an upfield shift of the flavone peaks was observed especially with ring A and C carbons (C8, 5, 6 and 3). The 4-C=O group signal also shifted from δ 181.83 to 177.55 ppm in the ^{13}C NMR spectrum of **20**. Finally, mass spectrometry and elemental analysis confirmed the proposed molecular formulas of the resultant compounds. For example, the % of Ru content measured for complexes **19** ($\text{C}_{25}\text{H}_{22}\text{O}_3\text{SCl}_2\text{Ru}$) and **20**

(C₂₅H₂₂O₄Cl₂Ru) were 17.3 and 17.72 compared to calculated % of 17.59 and 18.10, respectively.

(A)



(B)

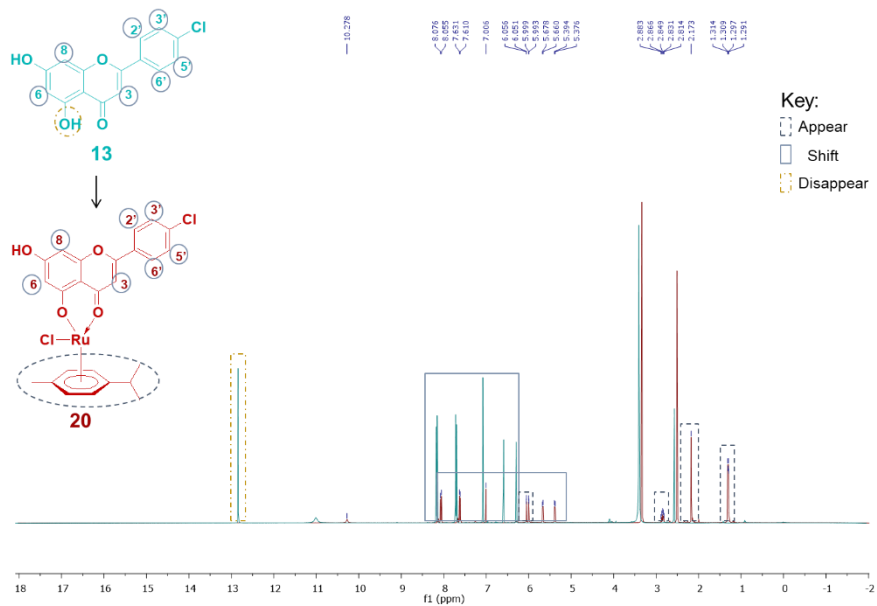
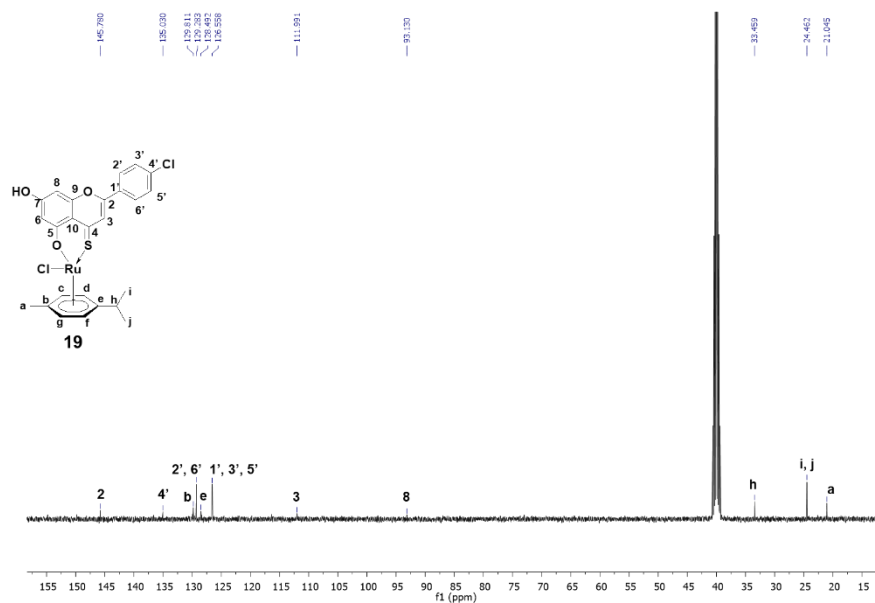


Figure 4. 3. Stacked ¹H NMR spectra of (A) 11 and 19; (B) 13 and 20

(A)



(B)

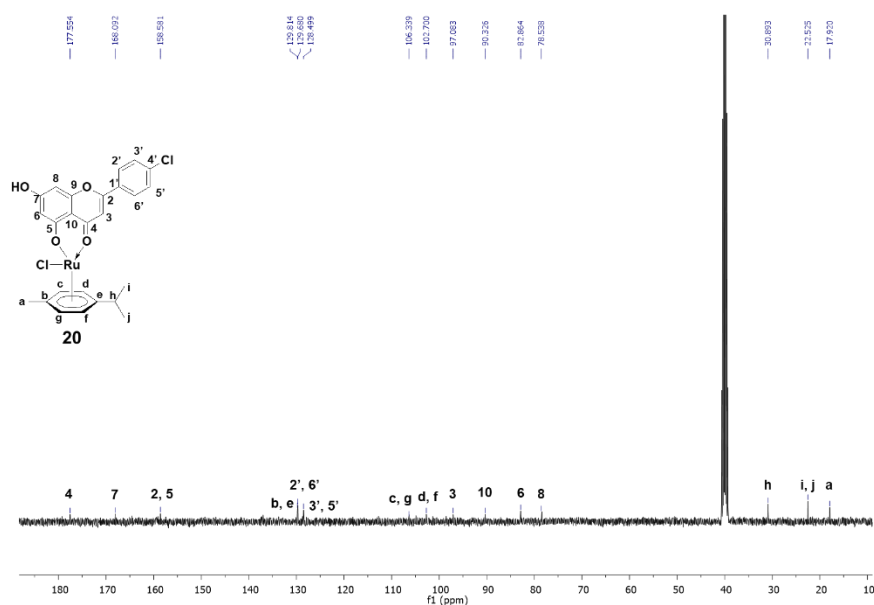


Figure 4. 4. ^{13}C NMR spectra of complexes (A) **19**; (B) **20**

Stability of complexes **19** and **20**

UV-Vis spectroscopy was used to determine the stability of the novel complexes **19** and **20** in aqueous solution (0.1% DMSO/ddH₂O) in order to ensure their stability under the experimental conditions employed in the ensuing biological experiments. The measurements were taken at temperatures ranging from 20 to 80 °C, which covers the

temperatures employed in the cell-based (37 °C) and DNA binding experiments (20-80 °C) described in **Chapter 5**. As shown in **Figure 4. 5** and **Table 4. 2**, the UV-Vis profiles of complexes **19** and **20** showed minor changes upon the applied temperature increments. The variations in the absorbance at a wavelength of 260 nm (λ_{260}) varied from 2 and 1.6% at 40 °C for **19** and **20**, respectively, to 9% at the highest temperature (80 °C) for both complexes (**Table 4. 2**). Flavonoid metal complexes with a 1:1 metal to flavonoid ratio, such as the synthesized Ru complexes, typically exhibit moderate ($5 < \log \beta$ (equilibrium constant for the formation of complex in solution) < 10) to high ($\log \beta > 10$) stability [322]. Moreover, several reports have demonstrated that similar flavonoid Ru(II) arene complexes remain stable in aqueous solution for more than 24 hours, as evaluated by ^1H NMR and UV-Vis spectroscopic analysis [110,144,313].

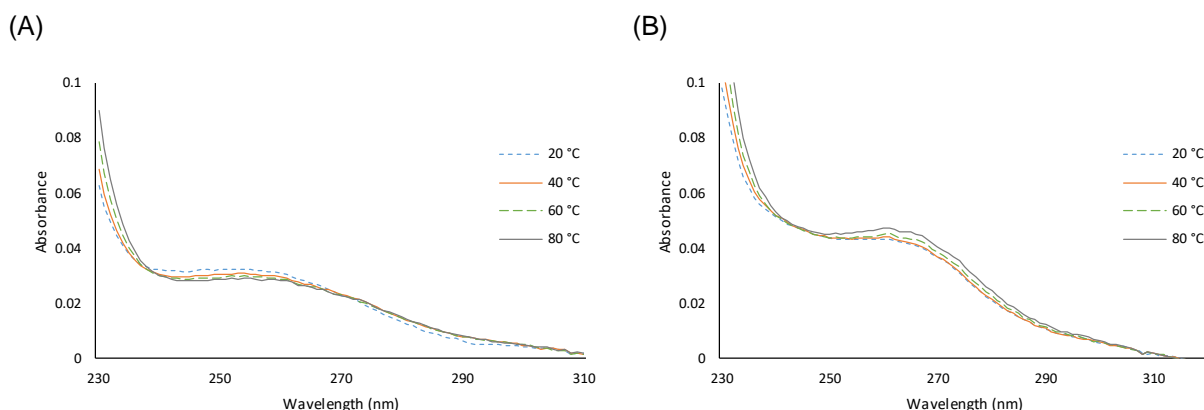


Figure 4. 5. Temperature dependent UV-Vis spectra of (A) **19** and (B) **20** in 0.1%DMSO/ddH₂O solution recorded over a 6 h time interval

Table 4. 2. λ_{260}^a and $\Delta \lambda_{260}^b$ of complexes **19** and **20** at 20 – 80 °C

19	λ_{260}	$\Delta \lambda_{260}$	20	λ_{260}	$\Delta \lambda_{260}$
20 °C	0.03108	0	20 °C	0.0435	0
40 °C	0.02973	0.0013	40 °C	0.04422	0.00072
60 °C	0.02902	0.0021	60 °C	0.04525	0.00174
80 °C	0.02832	0.0028	80 °C	0.04738	0.00388

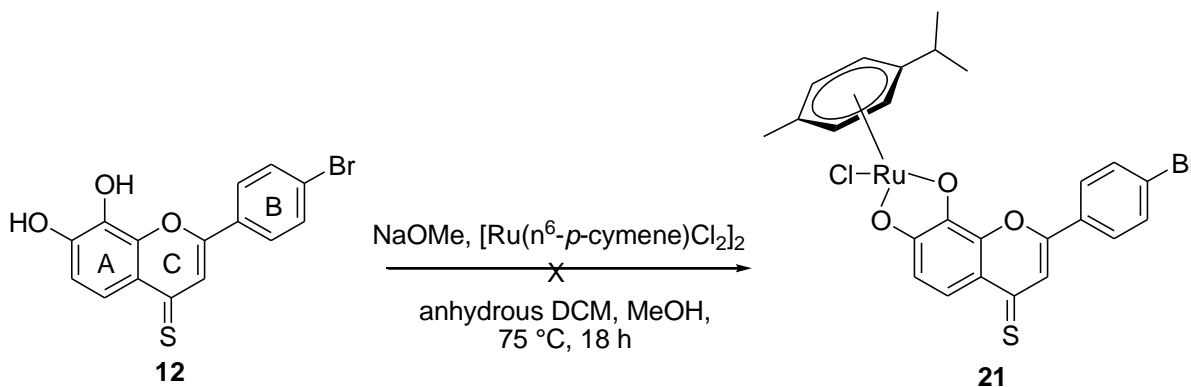
a, λ_{260} is the absorbance at 260 nm; b, $\Delta \lambda_{260} = \lambda_{260}$ (40, 60 or 80 °C) - λ_{260} (20 °C)

The overall stability observed in similar metal complexes, along with the minor changes in the UV-Vis profiles of **19** and **20** at elevated temperatures, indicate that these complexes are expected to retain their stability during the subsequent biological assays

conducted under similar experimental conditions with respect to the cell-based and DNA binding studies (**Chapter 5**).

4.2.1.2. 7, 8-Dihydroxy-4'-bromophenyl Ru(II) complexes (**21** and **22**)

Synthesis of the Ru(II) 7,8-O chelated 4-thioflavone (**21**) was pursued using 2 equivalents of NaOMe in order to deprotonate both of the OH groups in the catechol, followed by addition of 0.55 equivalents of $[\text{Ru}(\eta^6\text{-}p\text{-cymene})\text{Cl}_2]_2$ in anhydrous DCM and MeOH (**Scheme 4. 2**).



Scheme 4. 2. Attempted synthesis of Ru(II) complex **21**

The ^1H NMR spectrum of the crude product showed a downfield shift of the CH_3 protons of *p*-cymene and those of rings A, B and C of the thioflavone scaffold. The crude product was subsequently dissolved in $\text{CHCl}_3\text{:MeOH}$ (9:1, v/v) with the addition of EtOAc to facilitate purification. The resulting black precipitate was then filtered and air dried. The pure product was subjected to mass spectrometric and elemental analysis in order to confirm its structure. The desired peak for complex **21** ($(\text{C}_{25}\text{H}_{21}\text{O}_3^{79}\text{BrRuS})$ calculated $m/z = 581.944$) was detectable on MALDI-TOF MS as $\text{M}+\text{H}-\text{Cl}$ at 582.950 (**Figure 4. 6**). However, neither the elemental analysis nor the ESI-MS spectrometric results correlated with the calculated values for **21**, its free metal ligand or a combination of both. Since, MALDI-TOF MS was inconclusive on its own to prove effective chelation and synthesis, the product was not used in subsequent biological evaluations.

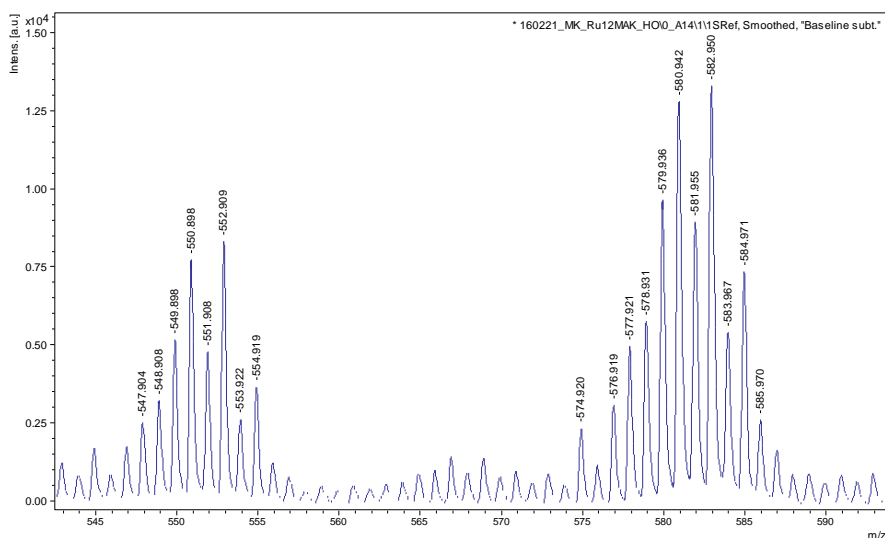
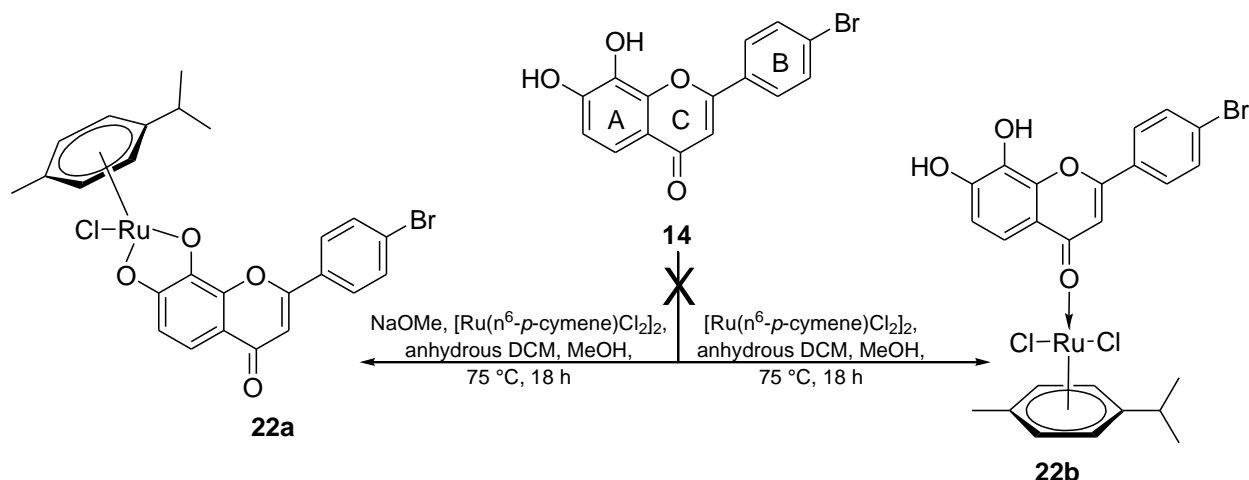


Figure 4. 6. MALDI-TOF MS of **21**

Meanwhile, synthesis of the 4-C=O Ru(II) complex **22** was attempted several times (**Scheme 4. 3**). As shown in **Table 4. 3**, the first two attempts to synthesize **22a** were carried out using 1.05 equivalents of NaOMe, however even after increasing the temperature of the reaction during the deprotonation step, and the duration of the reaction, ^1H NMR spectroscopic analysis showed no reaction to have occurred.



Scheme 4. 3. Attempted synthesis of Ru(II) complexes **22a** and **22b**

Ru(II)-*p*-cymene chelation to flavone **14** was subsequently attempted using 2.1 instead of 1.05 equivalents of NaOMe in order to deprotonate both OH groups at positions 7 and 8 and achieve a 7,8-O chelation (**Scheme 4. 3**). Here, the ^1H NMR spectroscopic data of the crude product exhibited a slight upfield shift in the cymene $2\times\text{CH}_3$ peaks from δ 1.19 and 1.21 to 1.17 and 1.18 ppm and a high upfield shift of the signals corresponding to *p*-

bromophenyl ring of the flavone scaffold (H-2', 6' and H-3', 5' shifted from δ 7.84 and 8.16 to 7.09 and 7.38 ppm, respectively) (**Figure 4. 7**). An upfield shift of the proton signals from the flavone moiety is expected for chelation at position 7, as previously reported by Yang *et al* for a chrysin-7-O-germanium(IV) complex [299]. However, the remaining cymene ring protons appeared at their unchelated positions at δ 2.09 (CH₃), 2.84 (CH) and 5.78-5.83 (H-2,3,5 and 6) ppm (**Figure 4. 7**). Furthermore, some signals were difficult to correlate to specific protons. Despite these conflicting results, free OH signals were absent from the ¹H NMR spectrum of **22a**. Additionally, mass spectrometric analysis showed a M-Cl peak representative of **22a** ((C₂₅H₂₁O₄⁷⁹BrRu) requires 565.406, found 565.083) which gave evidence of successful complexation. In that regard, elemental analysis of the purified product after crystallization by 9:1 EtOAc:CHCl₃ (v/v) was conducted to provide a clear answer for whether or not complexation had occurred. A mixture of equal amounts of Ru(II) chelated flavone (**22a**) and [Ru(η 6-*p*-cymene)Cl₂]₂ was the closest match to the elemental analysis results which explained the presence of proton peaks corresponding to both **22a** and the Ru(II)-*p*-cymene reagent in the ¹H NMR spectroscopy results. However, due to the impurity of the final product, it was not used in further biological evaluations studies.

Table 4. 3. Attempted optimization of the deprotonation step for the synthesis of **22a** or **22b**

NaOMe equivalence	Deprotonation step conditions		Result
	Temperature (°C)	Time (min)	
1.05	Room temperature	15	No reaction
1.05	30	30	No reaction
2.1	30	50	22a complex + residual starting material
0	----	----	No reaction

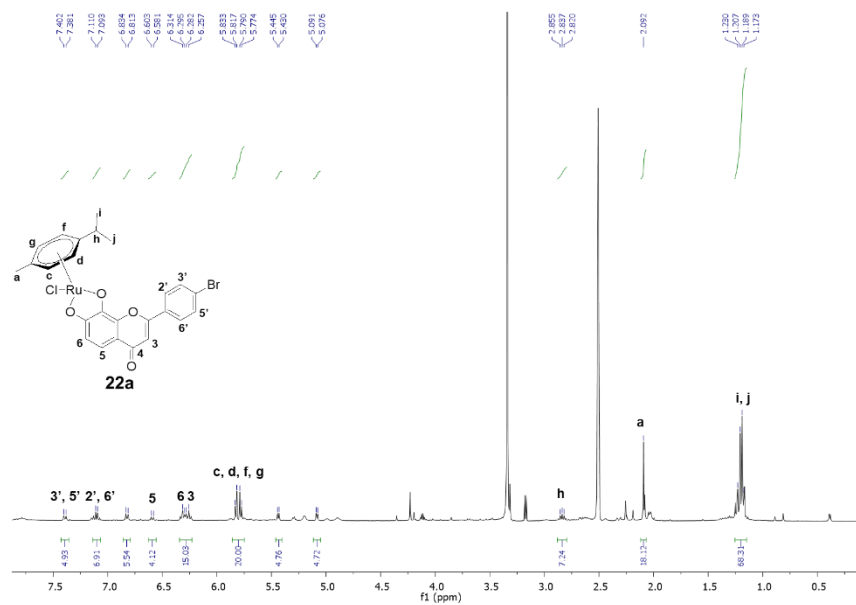


Figure 4. 7. ^1H NMR spectrum of attempted Ru(II)-*p*-cymene complexation of **14** with 2.1 eq. NaOMe. Due to the difficulties in obtaining a pure bidentate product for flavone **14**, the reaction was carried out in the absence of NaOMe to ascertain whether synthesizing a monodentate complex at the 4-C=O position was possible (**Scheme 4. 3**). Interestingly, the ^1H NMR spectrum of the resulting product showed a downfield shift of both the *p*-cymene protons and the H-3, 6 and *p*-bromophenyl ring protons for compound **14** by approximately 0.057, 0.014, 0.015, and 0.01 ppm, respectively. Moreover, two signals corresponding to the 7, 8-OH groups appeared at δ 9.6 and 10.42 ppm indicating no complexation at these sites. On analyzing the integration of the assigned proton peaks it became clear that the signals corresponding to *p*-cymene were 13 fold higher than those of the flavone moiety which negates the presence of a **22b** complex (**Figure 4. 8**). Therefore, this complexation attempt was also deemed unsuccessful.

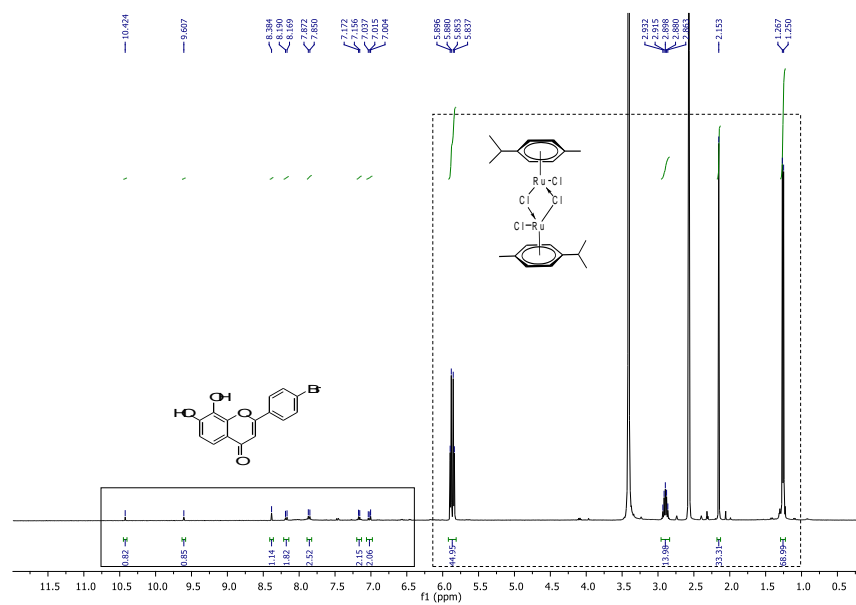
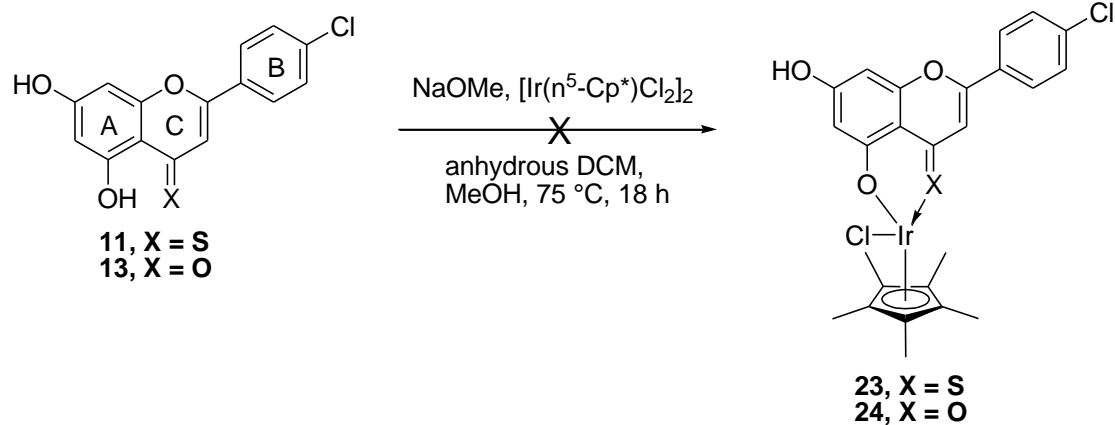


Figure 4. 8. ^1H NMR spectrum of attempted Ru(II)-*p*-cymene complexation of **14** without NaOMe

4.2.2. Attempted synthesis and structural characterization of Ir(III) Cp* flavone complexes

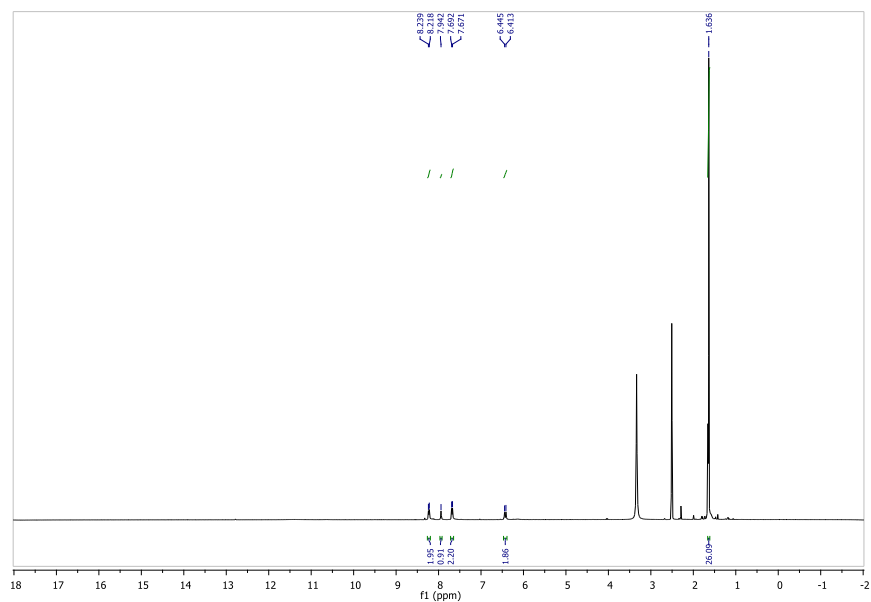
4.2.2.1. 5, 7-Dihydroxy-4'-chlorophenyl Ir(III) complexes (**23** and **24**)

Attempts to synthesize the corresponding Ir(III) derivatives of flavones **11** and **13** did not afford the desired products. Following the same synthetic route detailed for the successful synthesis of Ru complexes **19** and **20**, **11** and **13** were activated by deprotonation with NaOMe and this was followed by the addition of bis[$\text{Ir}(\eta^5\text{-Cp}^*)\text{Cl}_2$] *in situ* (Scheme 4.4). Although ^1H NMR spectroscopic analysis of the 4-thioflavone complex (**23**) demonstrated successful chelation with a singlet signal for the $5\times\text{CH}_3$ protons of the Cp* ring at δ 1.64 ppm, in addition to the expected flavone moiety proton peaks (Figure 4. 9A), its elemental analysis data mainly corresponded to the bisdichlorido($\eta^5\text{-Cp}^*$)Ir(III) starting material indicating failed complexation. Interestingly, the ^1H NMR spectrum of **24** showed 2 signals for the $5\times\text{CH}_3$ protons of the Cp* ring at δ 1.55 and 1.64 ppm as well as those corresponding to the flavone scaffold (Figure 4. 9B). This finding was previously reported for the related Ir(III)chrysin [323] and indicates the afforded product is a mixture of complex **24** and starting material, or a mixture of the bidentate and monodentate Ir(III)-flavone complexes making its purification attempts unsuccessful.



Scheme 4. 4. Attempted synthesis of Ir(III) complexes **23** and **24**

(A)



(B)

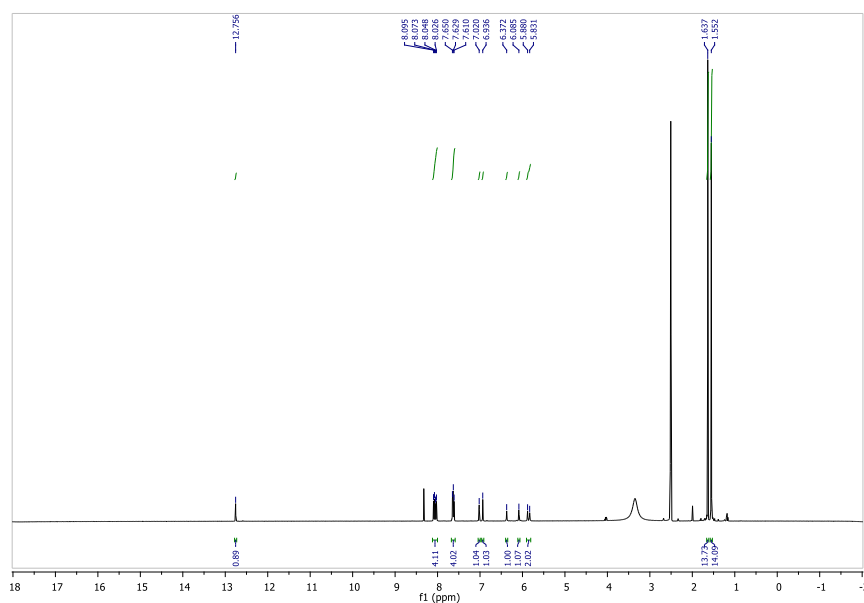
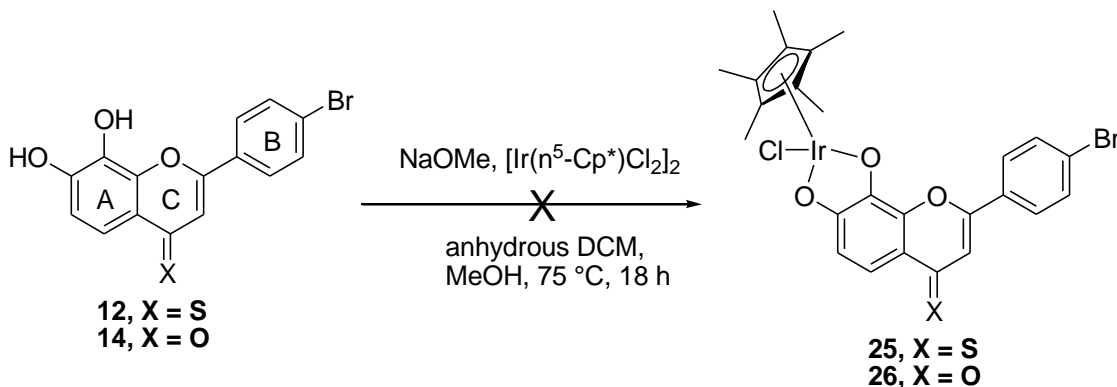


Figure 4. 9. ^1H NMR spectra of attempted Ir(III)Cp* complexation of (A) **11** and (B) **13**

4.2.2.2. 7, 8-Dihydroxy-4'-bromophenyl Ir(III) complexes (**25** and **26**)

Following the same general procedure, **12** or **14** were reacted with 0.55 equivalents of Ir(III) cyclopentadienyl ($\eta^5\text{-Cp}^*$) ligand after deprotonation with 2 equivalents of NaOMe (**Scheme 4. 5**).



Scheme 4. 5. Attempted synthesis of Ir(III) complexes **25** and **26**

^1H NMR spectroscopic analysis of the crude product of the reaction of Ir(III)Cp* ligand and the thio derivative (**12**) exhibited some signs of complexation represented in the downfield shift of Cp* $5\times\text{CH}_3$ from δ 1.64 to 1.65 ppm and the H-6 and 3', 5' proton of **12** signals from δ 6.98 and 7.77 to δ 7.16 and 7.89 ppm, respectively. However, the ^1H NMR spectrum of **25** showed many signals indicative of impurities especially around the Cp*

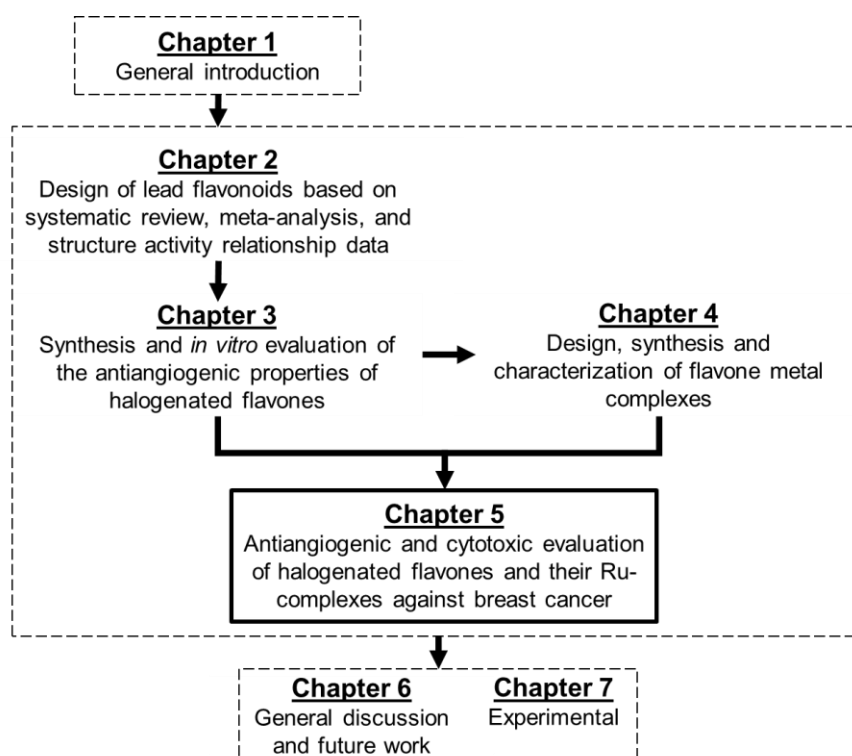
peak in the aliphatic region (δ 1.46-2.00 ppm) which might indicate breakdown of the Ir(III)Cp* starting material. Meanwhile, ^1H NMR spectroscopic analysis of the crude product of the reaction of Ir(III) metal ligand and flavone **14** showed no signs of chelation. Based on these unpromising findings these syntheses were not further pursued.

4.3. Conclusions and future perspectives

Chelation of the synthesized flavones to Ru(II)-*p*-cymene and Ir(III) Cp* metal ligands were adopted in this project as a structural optimization strategy in order to improve the antiangiogenic and cytotoxic properties of the lead flavones. Two novel Ru(II)-*p*-cymene complexes (**19** and **20**) were effectively synthesized and characterized with 46 and 30% yields, respectively. The remaining Ru(II)-*p*-cymene or Ir(III) Cp* complexation attempts either failed to chelate or showed some degree of complexation, but often with the presence of residual starting material and/or byproducts. Hence, crystallization was ineffective for separating a pure product from these materials. Several strategies could be adopted in the future to ensure successful complexation in yields sufficient for effective purification. For instance, further optimization for the reaction conditions could be attempted using varied mole equivalents of NaOMe (1.10, 1.25 and 2) [323] or other bases such as trimethylamine or NH_3 solution as reported in the literature (**Table 4. 1, Section 4.1**). On the other hand, alternative purification methods such as column chromatography could be explored although its less preferable for metal complexes as it comes with the risk of damaging the formed complex due to the presence of acidic sites in silica that can bind to metal ions. In this regard, other stationary phase options like neutral alumina can be investigated although this could still lead to challenges as alumina has high affinity for polyphenols which may result in insufficient yields of the desired products.

Chapter 5

Antiangiogenic and cytotoxic evaluation of halogenated flavones and their Ru-complexes against breast cancer

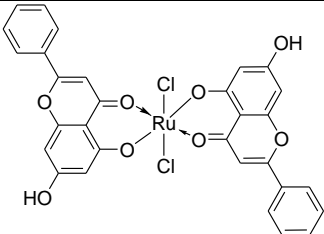
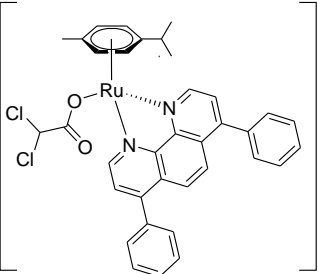
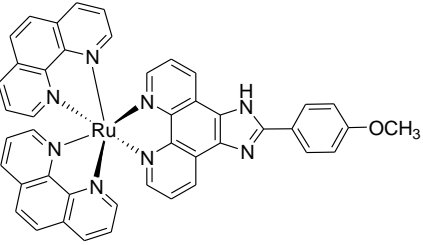
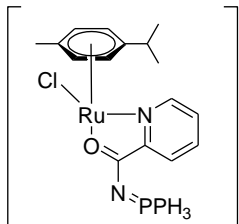


5.1. Introduction

The primary goal of this project is to develop novel anticancer agents that possess both antiangiogenic and cytotoxic properties. Within this thesis it has been discussed how lead thioflavone **11** has demonstrated significant antiangiogenic properties which was comparable to those reported for sunitinib (42% tube formation inhibition at 1 μM versus 50% for sunitinib at 1 μM [266]) by interfering with the VEGF/VEGFR2 pathway (**Chapter 3**). Additionally, Ru(II) complexation to **11** and its 4-oxo derivative **13** was carried out based on the hypothesis that it would enhance their antiangiogenic and cytotoxic properties (**Chapter 4**). Hence, this chapter is comprised of two components. The first details the *in vitro* evaluation of the proposed bi-modal antiangiogenic and cytotoxic activities of lead **11** and its 4-oxo derivative **13** on endothelial and breast cancer cells. The second determines the impact of Ru(II) complexation on the measured biological activities of **11** and **13**.

VEGF is the most predominantly overexpressed proangiogenic factor in breast cancer [324], and is negatively associated with the overall survival of breast cancer patients [325,326]. As outlined in **Table 5. 1**, organometallic Ru(II) complexes have demonstrated strong cytotoxic and antimetastatic activities against breast cancer both *in vitro* and [320,327,328] *in vivo* [329]. Moreover, Ru complexes have shown enhanced accumulation in breast cancer cells and tissues [327–329] (**Table 5. 1**). For example, an iminophosphorane Ru(II) complex showed $<5 \mu\text{g/g}$ tissue weight in liver and kidney while its tumor concentration was $40 \mu\text{g/g}$ ($p < 0.05$) in triple negative breast cancer (TNBC) mice xenografts [329]. Taken together with the inhibitory activities of flavones **11** and **13** against VEGF-induced angiogenesis, it is hypothesized herein that compounds (**11**, **13**, **19** and **20**) will exhibit potent anticancer effects against breast cancer. Accordingly, the cytotoxic and antimigratory activities of the test compounds were evaluated against the estrogen receptor positive (MCF-7) and the triple negative (MDA-MB-231) breast cancer cell lines.

Table 5. 1. Summary of antiangiogenic and cytotoxic activities reported for Ru(II) complexes against breast cancer

Complex	Antiangiogenic activity	Cytotoxic activity	Tumor selectivity	Ref
	VEGF downregulation (100 μ M)	<ul style="list-style-type: none"> DNA intercalation (10 μM) 55% inhibition of MCF-7 viability (100 μM, $p < 0.01$) 29.3% increase in MCF-7 apoptosis (100 μM, $p < 0.01$) 	n/a	[320]
	<ul style="list-style-type: none"> 52% decrease in MDA-MB-231 invasion (3.44 μM, $p < 0.05$) 30% decrease in MDA-MB-231 migration (0.55 μM, $p < 0.01$) 50% decrease in MMP-9 (1.72 μM, $p < 0.01$) 	IC ₅₀ =0.86 μ M on MDA-MB-231	IC ₅₀ =9.4 and > 50 μ M on HEK293 and skin fibroblast cell lines, respectively	[327]
	<ul style="list-style-type: none"> 85% decrease in MDA-MB-231 migration (4 μM, $p < 0.01$) 90% decrease in MDA-MB-231 invasion (4 μM, $p < 0.01$) 40% decrease in MMP-9 expression (4 μM) 40% decrease in VEGF (4 μM) 	IC ₅₀ =28 and 14.6 μ M on MCF-7 and MDA-MB-231, respectively	<ul style="list-style-type: none"> IC₅₀=143 μM on HK2 Cellular uptake efficacy =2.5 and 3 μM/10⁸ cells for MCF-7 and MDA-MB-231, respectively. 35% decrease in MDA-MB-231 cellular uptake % ($p < 0.05$) upon pretreatment with 2 mg/mL transferrin (i.e. transferrin receptor blocker) 	[328]
		<ul style="list-style-type: none"> IC₅₀=2.6 μM on MDA-MB-231 56% decrease in tumor size at 5 mg/kg/every other day for 28 days in MDA-MB-231 injected mice 	<ul style="list-style-type: none"> IC₅₀=2.8 μM on HEK-293T <5 μg/g tissue weight in liver and kidney, tumor concentration = 40 μg/g ($p < 0.05$) 	[329]

n/a, not available; MCF-7, estrogen receptor positive breast cancer cell line; MDA-MB-231, triple negative breast cancer cell line; HEK293, normal human embryonic kidney cell line; HK-2, immortalized human renal proximal tubular epithelial cell line.

The need for research investigating the effects of individual metal atoms on the cytotoxic abilities of structurally similar flavonoids has been highlighted by our recent study (**Appendix B**) [117]. Analysis of the cytotoxic effects of various metal complexes of flavonoids on different cancer cell lines indicated that 64% exhibited superior cytotoxic properties compared to their parent flavonoid, whereas 11% retained the same level of activity, and 25% exhibited decreased activity [117]. However, evidence on the influence of the type of metal on the measured biological activities was insufficient to conclude whether one class was superior to another. Hence, this study can bring new insight on the particular role of Ru complexation on the tested antiangiogenic and cytotoxic properties. Additionally, inclusion of the 4-oxo analogue (**13**) of **11** and its Ru(II) complex (**20**) will determine the impact of the functional group at C-4 on the activity of the free flavonoid and the Ru(II) complex.

I-motif DNA binding

Binding interactions of the test flavones with the non-canonical i-motif DNA structures (VEGF and c-myc) were studied herein as novel anticancer targets. I-motifs are cytosine rich tetraplex DNA structures (**Figure 5. 1**) reported to be capable of regulating oncogene expression and therefore are of interest for their anticancer applications [330–334]. VEGF and c-myc are ideal targets for i-motif ligands due to the presence of cytosine-rich regions in their promoter regions, playing crucial roles in their transcription [330]. Moreover, VEGF and c-myc i-motif sequences are prevalent in oncogene promoter regions in many cancers including breast cancer and as such their ligands have potential anticancer roles [333,335,336]. The ability of flavonoids and Ru compounds to interact with i-motifs has been documented [330,333]. The flavonol fisetin has been shown to selectively attach to the VEGF i-motif, stabilizing its hairpin conformation and restoring VEGF's normal replication [333]. Shi *et al* reported the ability of two polypyridyl Ru-based complexes to interact with an i-motif sequence (22CT) with binding affinities of 5.6 and 1.2 μM [337,338].

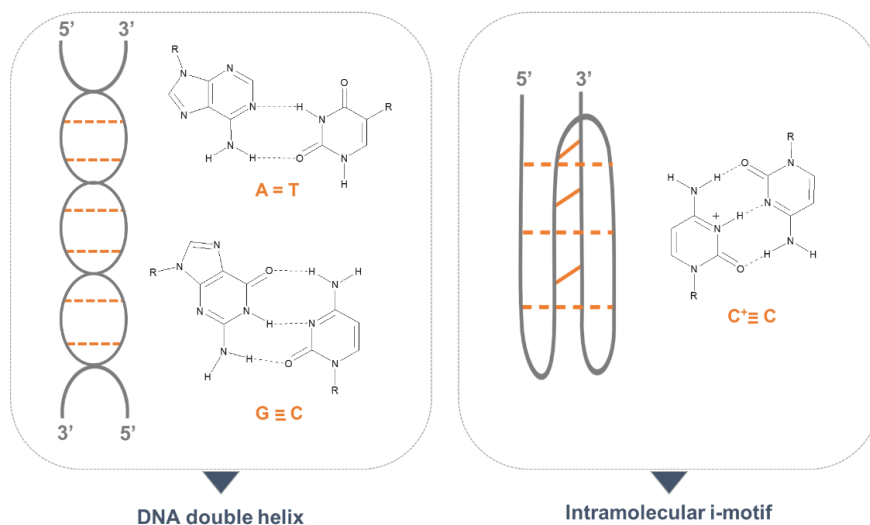


Figure 5. 1. Standard double helix DNA and non-canonical i-motif structures

To summarize, in this chapter the test compounds (**11**, **13**, **19** and **20**) were first evaluated for their toxicity on ECs before the antiangiogenic and cytotoxic activities were determined for ECs and MCF-7 and MDA-MB-231 breast cancer cells using the *in vitro* tube formation and MTT assays, respectively. A scratch assay was conducted in order to assess the efficacy of the tested library of compounds to suppress breast cancer cell migration as a fundamental step in metastasis. Furthermore, binding interactions of the test compounds with the i-motif DNA structures (VEGF and c-myc) were preliminary investigated as a potential novel mechanism of action, using UV-Vis and DNA melting spectroscopic techniques.

5.2. Results and discussion

5.2.1. *In vitro* antiangiogenic evaluation of Ru(II) complexes (**19** and **20**)

5.2.1.1. Cytotoxicity against endothelial cells

The biocompatibility of the flavone Ru(II) complexes (**19** and **20**) with HUVEC cells was determined by conducting a trypan blue exclusion assay. The same protocol was followed as for **11** and **13**, using a concentration of 40 μM [253,339]. As demonstrated in **Figure 5. 2**, almost 100% viability of the cells was retained, and there were no significant statistical changes compared to the control group ($p > 0.05$).

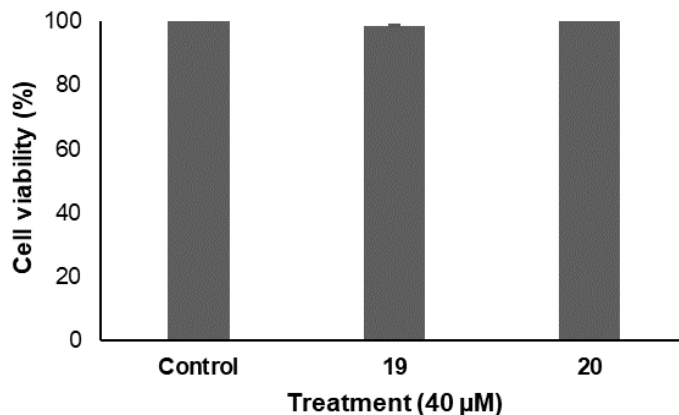
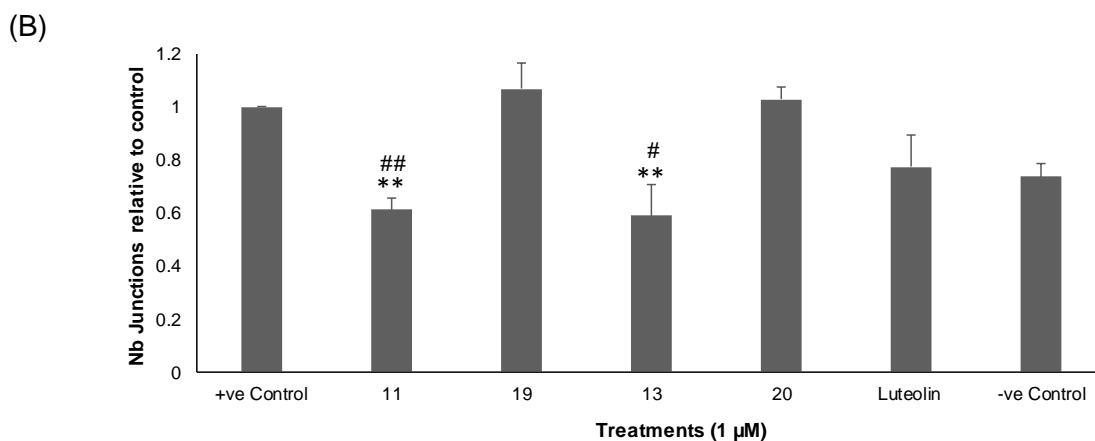
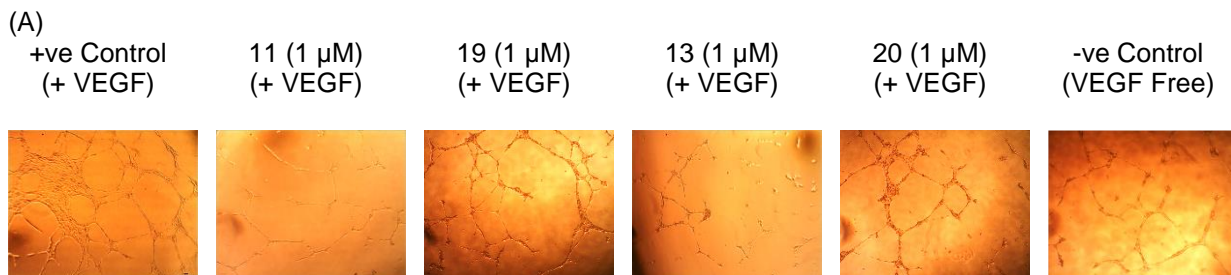


Figure 5. 2. Cell viability of HUVECs after 24 h of treatment with 40 μM of the flavone Ru(II) complexes (**19** and **20**). Data are expressed as mean ± standard error of the mean (SEM), n = 3.

5.2.1.2. Inhibition of endothelial cells tube formation

The impact of complexation with the Ru(II)-*p*-cymene metal ligand on the antiangiogenic activities of **11** and **13** was investigated, using the Matrigel tube formation assay as previously outlined in **Section 3.2.2.2, Chapter 3**. Inhibition of VEGF-mediated tube formation by the substrates was measured after 12 h of treatment on HUVECs at 1 and 10 μM concentrations [253,339].



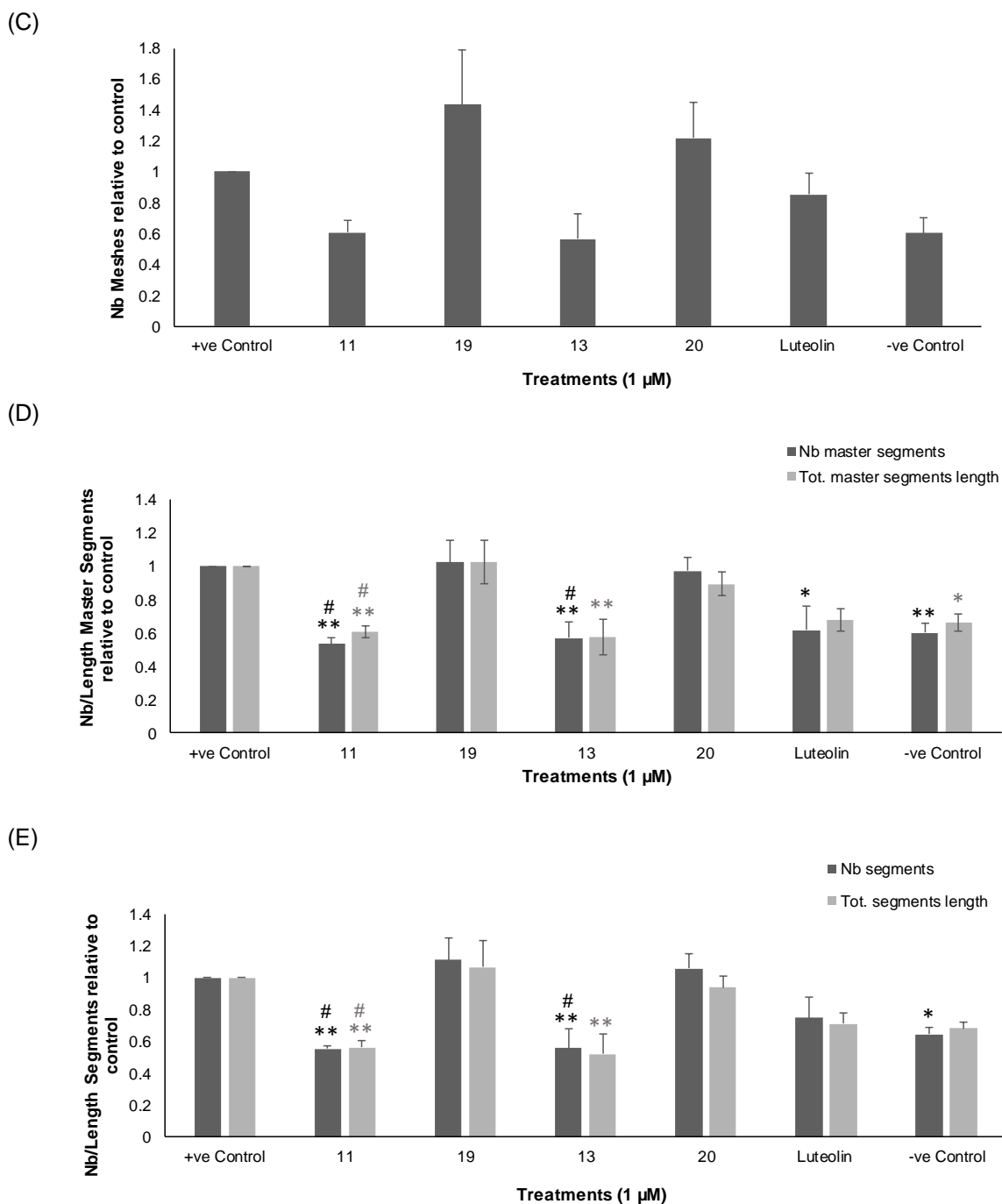
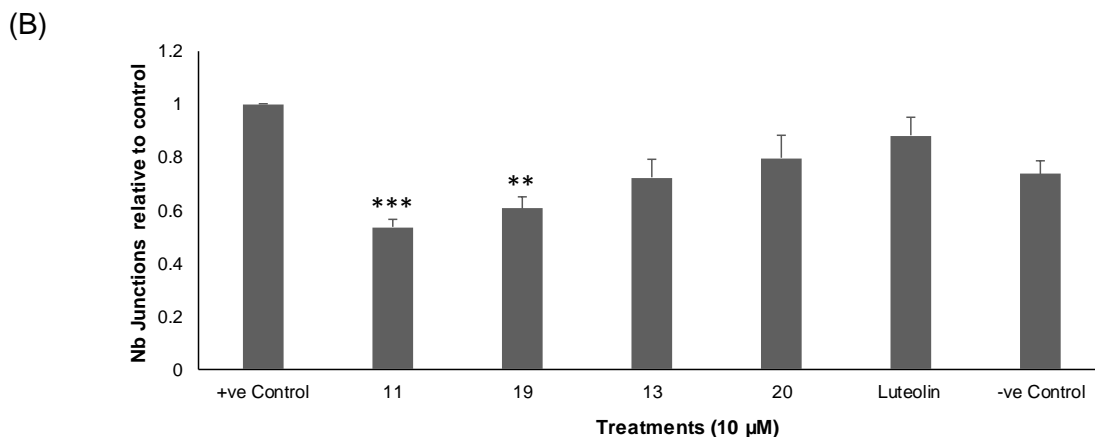
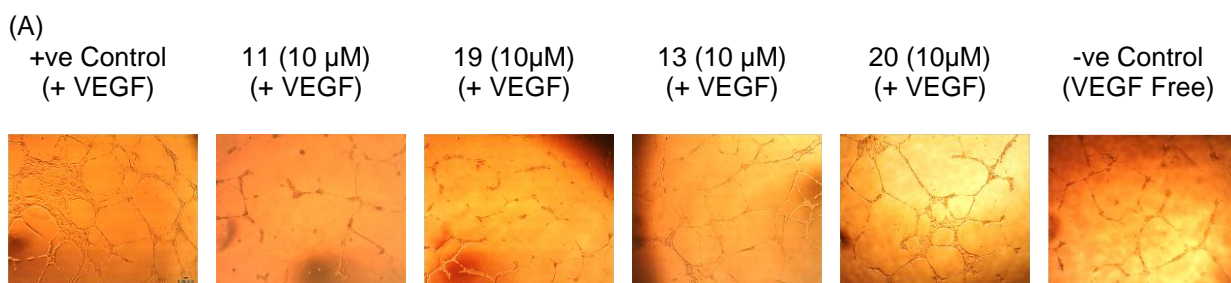


Figure 5. 3. Antiangiogenic activity of flavone Ru(II) complexes (**19** and **20**) and their free flavones **11** and **13** (added for comparison) on *in vitro* HUVEC tube formation after 12 h of treatment with 1 μM, expressed as a ratio to the +ve control (10 ng/mL VEGF-enriched media). (A) Representative images of tube formation assay at 4X magnification. Images were analyzed using Angiogenesis Analyzer macro in ImageJ software; (B) number of junctions, (C) number of meshes, (D) number and length of master segments and (E) number and length of segments. Data are expressed as mean ± standard error of the mean (SEM), n = 3. Statistical significance was estimated with respect to the +ve control (*) by one-way ANOVA, followed by Dunnett's multiple comparison test (*, $p < 0.05$, ** $p < 0.01$). Statistical pairwise significance (**11** versus **19** and **13** versus **20**) was estimated by one-way ANOVA (#), followed by Tukey's multiple comparison test, as recommended for pairwise comparisons [267] (# $p < 0.05$, ## $p < 0.01$).

As shown in **Figure 5. 3**, both complexes **19** and **20** showed a significant loss of the tube formation inhibitory activity compared to their free derivatives at 1 μM ($p < 0.05$). However, at a concentration of 10 μM , Ru(II) complexation retained the antiangiogenic activity of the free flavone **11** ($p > 0.05$), except for the number of master segments component ($p < 0.05$) (**Figure 5. 4**). The 4-C=S Ru(II) complex **19** demonstrated a significant decrease in the number of junctions (40%, $p < 0.01$) as well as both the number and length of master segments (35%, $p < 0.05$) compared to the control at 10 μM . The 4-C=O derivative **13** exhibited a statistically negligible antiangiogenic activity ($p > 0.05$) for all the evaluated aspects of tube formation compared to the control group at 10 μM . Similarly, complex **20** showed no antiangiogenic activity at the 10 μM concentration, and hence did not change the antiangiogenic action of free flavone **13** ($p > 0.05$) at the same concentration (**Figure 5. 4**).



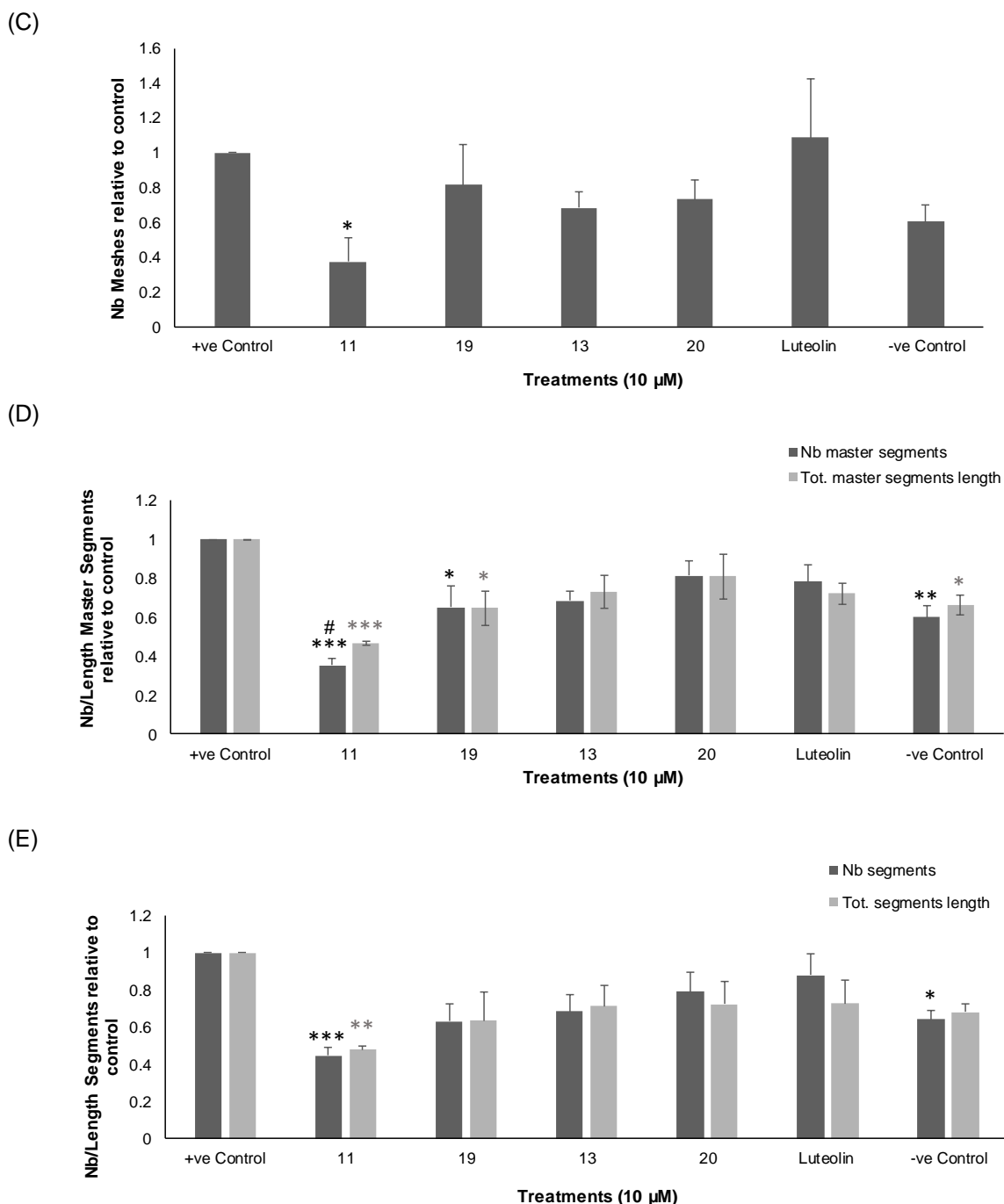


Figure 5. 4. Antiangiogenic activity of flavone Ru(II) complexes (**19** and **20**) and their free flavones (added for comparison) on *in vitro* HUVEC tube formation after 12 h of treatment with 10 μM , expressed as a ratio to the +ve control (10 ng/mL VEGF-enriched media). (A) Representative images of tube formation assay at 4X magnification. Images were analyzed using Angiogenesis Analyzer macro in ImageJ software; (B) number of junctions, (C) number of meshes, (D) number and length of master segments and (E) number and length of segments. Data are expressed as mean \pm standard error of the mean (SEM), $n = 3$. Statistical significance was estimated with respect to the +ve control (*) by one-way ANOVA, followed by Dunnett's multiple comparison test (* $p < 0.05$, ** $p < 0.01$, *** $p < 0.001$). Statistical pairwise significance (11 versus 19 and 13 versus 20) was estimated by one-way ANOVA (#), followed by Tukey's multiple comparison test, as recommended for pairwise comparisons [267] (# $p < 0.05$).

In **Chapter 3 (Section 3.2.2.4)**, it was demonstrated that interaction with the VEGF/VEGFR2 pathway was involved in the antiangiogenic effects observed for flavone **11** [253]. The 4-C=S group performed a pivotal role in the preferable vertical alignment of **11** inside the ATP binding site of VEGFR2 by directly facing the solvent-exposed surface [253]. Due to its high lipophilicity, the *p*-cymene moiety may have been directed preferentially inside the receptor's cavity rather than facing the solvent surface which could account for the reduction in the antiangiogenic activity of **11** following complexation. This proposed orientation of the Ru(II)-*p*-cymene moiety was indeed reported by Bhattacharyya *et al* for a Ru(II)-*p*-cymene benzimidazole complex inside VEGFR2's binding site [340]. In that context, future investigations of the interactions of the Ru(II) complexes **19** and **20** with VEGFR2 via molecular modelling and immunostaining assays are still needed.

As a whole, complexation with Ru(II)-*p*-cymene to afford derivatives (**19** and **20**) did not augment the EC antiangiogenic activity of their respective flavones. Nevertheless, the thionated complex exhibited notable disruption to certain components of angiogenesis. Furthermore, **19** demonstrated superior activity compared to the oxygenated complex **20**, consistent with the activity pattern observed in their parent flavones.

5.2.2. In vitro anticancer evaluation on breast cancer cell lines

5.2.2.1. Cytotoxicity against breast cancer cells

The cytotoxic effects and IC₅₀ values of flavones (**11** and **13**) and their corresponding Ru(II) complexes (**19** and **20**) were assessed using a 72-hour MTT test, with a maximum concentration of 100 μM. Thioflavone **11** exhibited potent cytotoxicity (IC₅₀=1.2 ± 0.8 μM) against MCF-7 cell line, consistent with previously reported data [219] (**Figure 5. 5** and **Table 5. 2**). Compound **11** also demonstrated a modest level of activity (IC₅₀=43.06 ± 1.29 μM) against the triple negative MDA-MB-231 cell line. The Ru(II) complex **19** showed diminished inhibitory effects compared with **11** on the proliferation of both MCF-7 and MDA-MB-231 cells (**Figure 5. 5**).

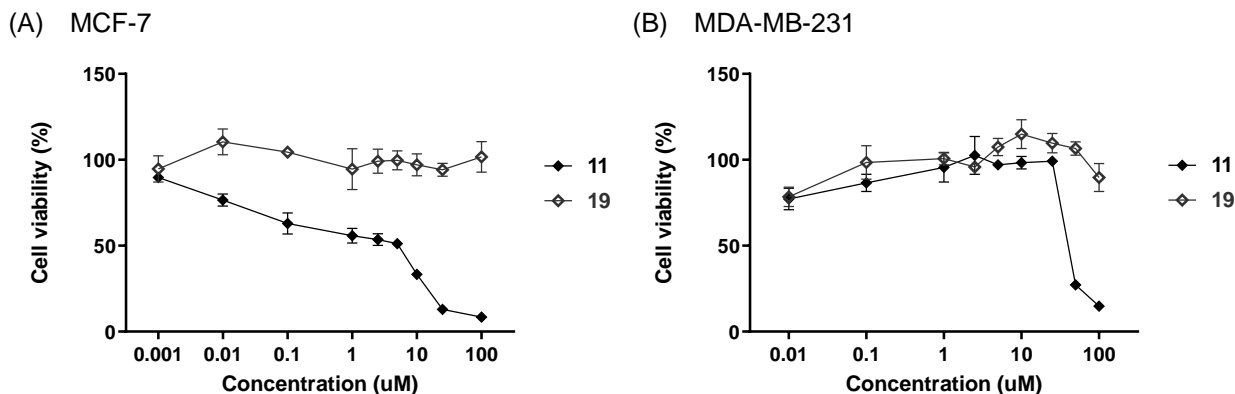


Figure 5. 5. Cytotoxic activity of flavone **11** and its Ru(II) complex **19** against (A) MCF-7 and (B) MDA-MB-231 cancer cell lines. Data are expressed as mean \pm standard error of the mean (SEM), $n = 3$.

Conversely, the free flavone (**13**) did not exhibit any cytotoxic effects on the two breast cancer cell lines at concentrations higher than 100 μM (**Figure 5. 6**). However, its Ru(II) complex (**20**) showed an increased ability to inhibit proliferation, but only on the MCF-7 cell line ($\text{IC}_{50} = 66.15 \pm 5 \mu\text{M}$) (**Table 5. 2**).

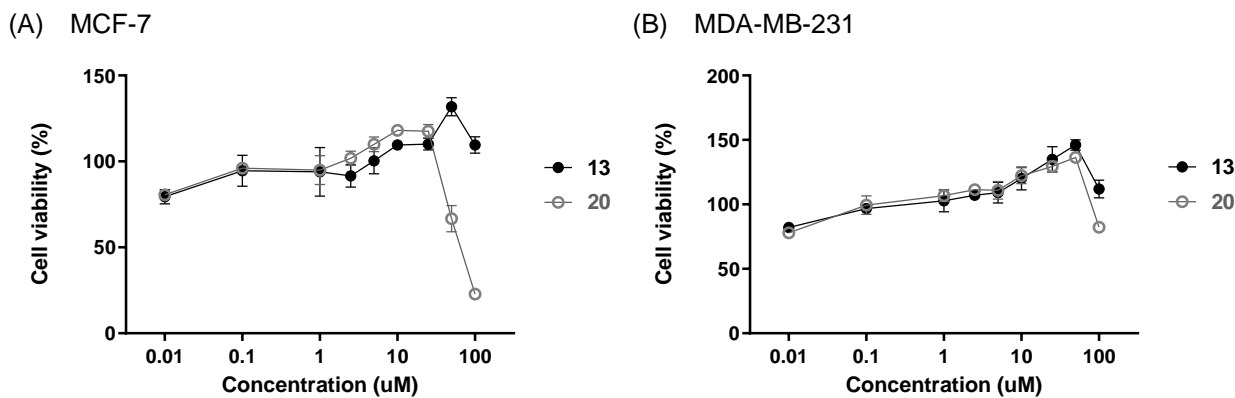


Figure 5. 6. Cytotoxic activity of flavone derivative **13** and its Ru(II) complex **20** against (A) MCF-7 and (B) MDA-MB-231 cancer cell lines. Data are expressed as mean \pm standard error of the mean (SEM), $n = 3$.

Table 5. 2. Determined IC_{50} for flavone derivatives (**11** and **13**) and their Ru(II) complexes (**19** and **20**) against MCF-7 and MDA-MB-231. Data are expressed as mean \pm standard error of the mean (SEM), $n = 3$

Compound	IC_{50} (μM)	
	MCF-7	MDA-MB-231
11	1.2 ± 0.8	43.06 ± 1.29
19	>100	>100
13	>100	>100
20	66.15 ± 5	>100

Given that the sole variation in structure between compounds **11** and **13** is the replacement of the 4-C=O group with a 4-C=S group, it is likely that the presence of the

S atom plays a crucial role in the cytotoxic action of compound **11**. This observation may also explain the decrease in cytotoxic activity upon complexation with Ru(II) in complex **19**, since complexation may have impeded the S atom's capacity for interaction with its cellular target(s). The detrimental effect of masking the 4-C=S group was also observed while investigating the antiangiogenic action of **19** using the tube formation assay (**Section 5.2.1.2**). Ru organometallic complexes, such as NAMI-A, have demonstrated a lack of effectiveness in *in vitro* cytotoxic studies, while displaying exceptional abilities to inhibit the metastasis of cancer cells *in vivo* [118]. Within this context, Montani *et al* observed significant *in vivo* antitumor effects for a Ru(II)-*p*-cymene pyrazolyl derivative, while demonstrating poor *in vitro* activity on the MDA-MB-231 cell line ($IC_{50}=409.89 \mu\text{M}$) [341]. The Ru(II) complex attained a tumor size of 3 mm, whereas the control group of TNBC-injected mice had a growth size of 7 mm ($p<0.01$) [341]. Although the Ru(II) complexes studied herein did not show substantial antiangiogenic or cytotoxic effects, based on the aforementioned reports, they are predicted to have potent antimetastatic properties, which were assessed in the following section.

5.2.2.2. Inhibition of breast cancer cells migration

Tumor invasion and metastasis rely on the key process of malignant cell migration [342]. Hence, the inhibitory effect of the synthesized flavones (**11** and **13**) and their Ru(II) metal complexes (**19** and **20**) on the migration of breast cancer cells (MCF-7 and MDA-MB-231) were evaluated using a 24-hour *in vitro* scratch experiment. This utilized low, subcytotoxic doses of 1, 10, and 20 μM for the test flavones. Due to the cytotoxicity of lead **11** on the MCF-7 cell line ($IC_{50}=1.2 \pm 0.8 \mu\text{M}$), it was not feasible to assess its antimigratory effects on this cell line. The thioflavone Ru(II) complex **19**, exhibited 55% suppression of cell migration in MCF-7 cells at a concentration of 20 μM ($p<0.001$). This is the most potent effect recorded on MCF-7 cells compared to the other tested leads, as illustrated in **Figure 5.7**. The strong activity of **19** remained significant even at lower doses of 1 and 10 μM , with inhibition rates of 52 and 49%, respectively ($p<0.01$). Complex **20** demonstrated a substantial decrease ($p<0.01$) in the migration of MCF-7 cells at all doses examined, resulting in inhibitions of 50, 42, and 41% at 1, 10, and 20 μM , respectively. In contrast, no effects were found for the original flavone **13** at any of the tested concentrations. Hence, Ru(II)-*p*-cymene complexation improved the antimigratory activity of compound

13, with the strongest impact observed at the 1 μM concentration ($p < 0.05$). The antimigratory effects of **19** and **20** complexes on MCF-7 cells are comparable to those reported for the TKI medicines sorafenib and axitinib. Sorafenib and axitinib showed 70 and 57% migration inhibition at 10 μM in a 48-hour scratch experiment [343] and at 5 μM in a 24-hour assay [344], respectively.

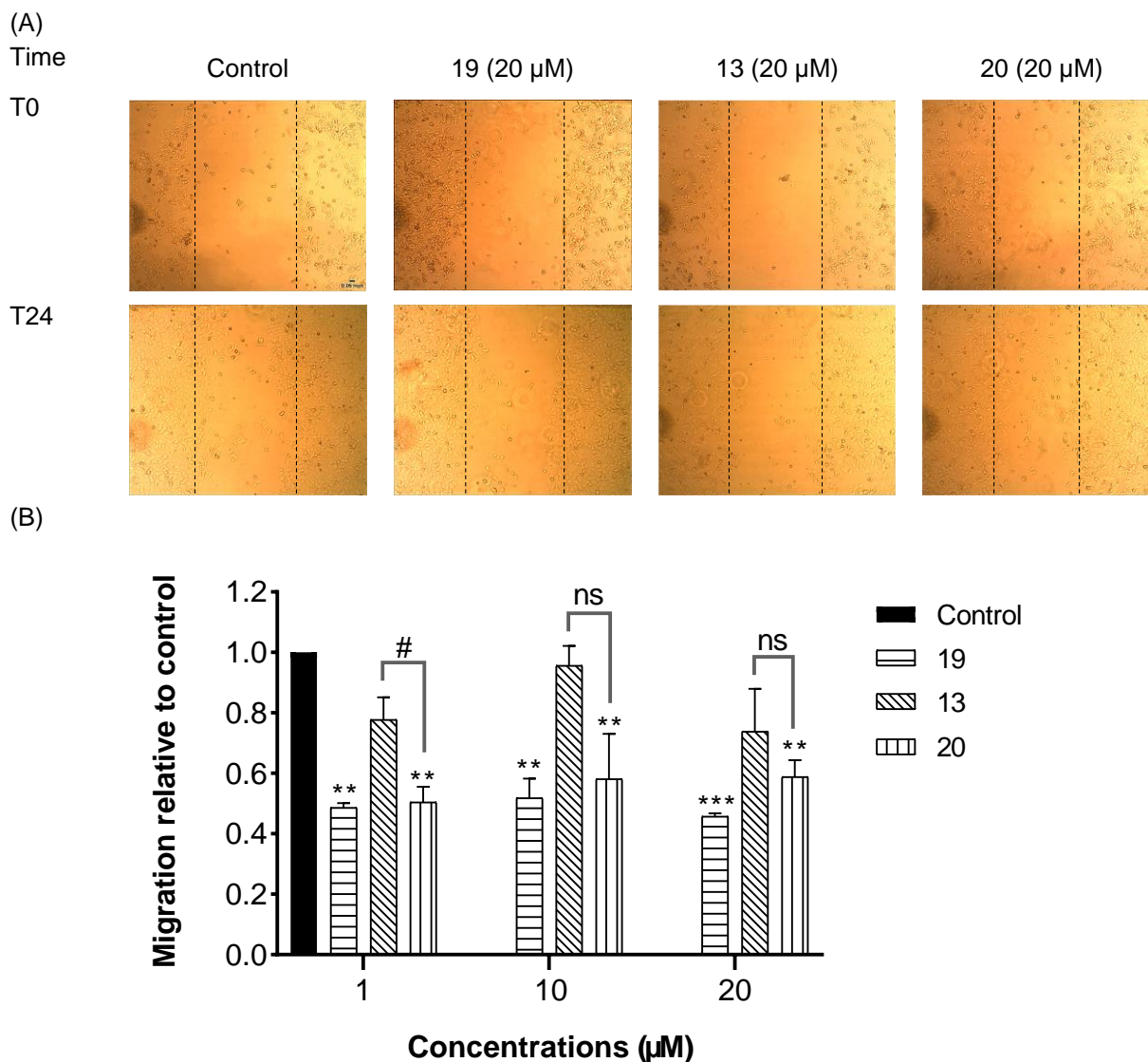
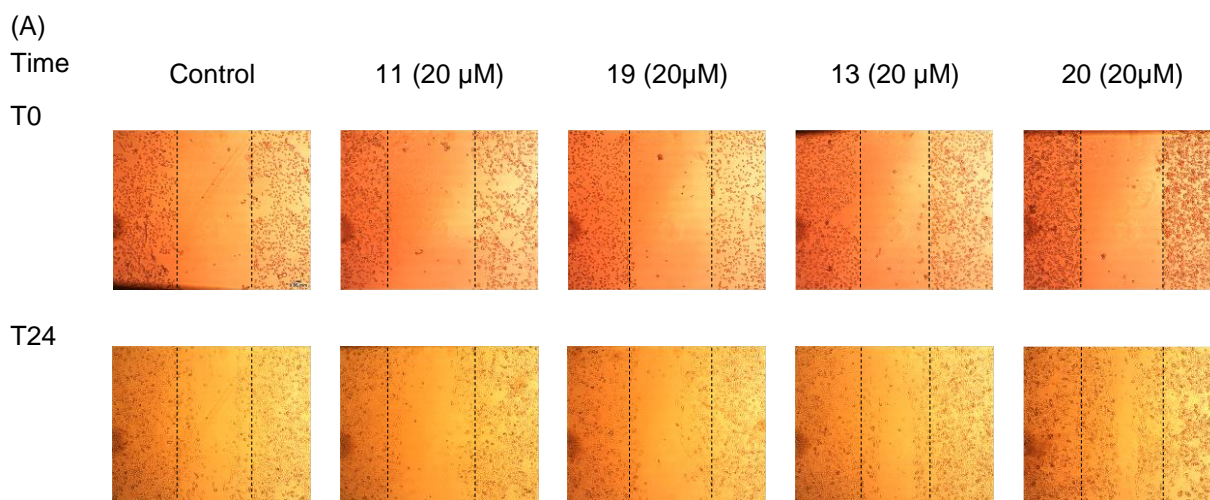


Figure 5. 7. *In vitro* MCF-7 migration (wound closure) inhibition activity of flavone derivative (**13**) and the Ru(II) complexes (**19** and **20**) expressed as a ratio to control. (A) Representative images of scratch assay at 0 h and 24 h at 4X Magnification. Images were analyzed using ImageJ software; (B) Migration after 24 h as a ratio to the control. Data are expressed as mean \pm standard error of the mean (SEM), $n = 3$. Statistical significance was estimated with respect to the control (*) by one-way ANOVA, followed by Dunnett's multiple comparison test (** $p < 0.01$, *** $p < 0.001$). Statistical pairwise significance for **13** versus **20** was estimated by one-way ANOVA (#), followed by Tukey's multiple comparison test, as recommended for pairwise comparisons [267] (# $p < 0.05$).

Results of the scratch assay on the invasive breast cancer cell line (MDA-MB 231) demonstrated the strong antimigratory effects of thioflavone **11** (Figure 5. 8). MDA-MB-231's migration decreased by 43 and 39% ($p < 0.01$) compared to the control upon treatment with 1 and 10 μM of **11**, respectively. Similar to its parent, the Ru(II) complex **19** exhibited potent antimigratory effects at a concentration of 1 μM , resulting in a 47% inhibition ($p < 0.001$) (Figure 5. 8). These effects persisted at higher concentrations of 10 and 20 μM (migration inhibition of 44%, $p < 0.01$ and 36%, $p < 0.05$, respectively). For context, the anticancer drug sorafenib is reported to result in 50% inhibition of MDA-MB-231 cells' migration at 10 μM [343]. Both the 4-carbonyl derivative (**13**) and its Ru(II) complex (**20**) did not have any impact on the migration of MDA-MB-231 breast cancer cells. However, **20** showed significantly better effects at 1 μM compared to **13** ($p < 0.01$), highlighting the positive influence of Ru(II) chelation.



(B)

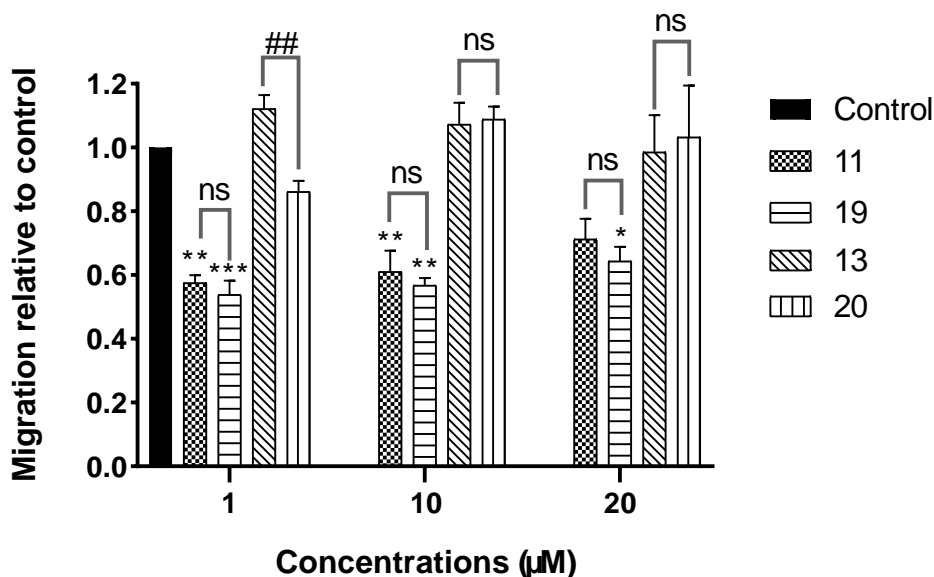


Figure 5. 8. *In vitro* MDA-MB-231 migration (wound closure) inhibition activity of flavone derivatives (**11** and **13**) and the Ru(II) complexes (**19** and **20**) expressed as a ratio to control. (A) Representative images of scratch assay at 0 h and 24 h at 4X Magnification. Images were analyzed using ImageJ software; (B) Migration after 24 h as a ratio to the control. Data are expressed as mean \pm standard error of the mean (SEM), $n = 3$. Statistical significance was estimated with respect to the +ve control (*) by one-way ANOVA, followed by Dunnett's multiple comparison test (* $p < 0.05$, ** $p < 0.01$, *** $p < 0.001$). Statistical pairwise significance (**11** versus **19** and **13** versus **20**) was estimated by one-way ANOVA (#), followed by Tukey's multiple comparison test, as recommended for pairwise comparisons [267] (## $p < 0.01$).

Altogether, these findings emphasize the beneficial effect of including the 4-thio group in the design of lead compounds. As rationalized in **Section 2.2.4, Chapter 2**, substituting the 4-C=O with a 4-C=S group has been extensively documented to improve various pharmacological effects associated with flavones [230,231], particularly their cytotoxic actions [155,219,232,233]. As hypothesized, the Ru(II) complexes elicited strong antimigratory effects against the breast cancer cell lines. Inclusion of the Ru(II)-*p*-cymene ligand particularly enhanced the antimigratory efficacy of the 4-C=O derivative **13**.

5.2.3. I-motif DNA binding

UV-Vis absorption spectroscopy is a sensitive, simple and reproducible technique to detect DNA interactions [345]. The chromophoric groups in purine and pyrimidine residues of DNA undergo electronic transitions, leading to a peak absorption at 260 nm (λ_{\max}) [345]. Variations in λ_{\max} reflect changes in DNA base stacking and, as a result, molecular interactions [345]. The transition temperature (T_m) denotes the stability of the DNA structure and is the point at which 50% of the DNA is folded and 50% is unfolded

[345]. An increase in the T_m value shows enhanced stability whereas a decrease in the T_m value shows decreased stability. Hence, shifts in λ_{\max} and T_m values of VEGF and c-myc i-motifs upon addition of the test compounds would indicate molecular interactions, suggesting possible regulatory impacts on the expression of the related genes [345,346]. Such interactions with VEGF and c-myc i-motifs could have detrimental effects on cancer growth and propagation [346]. **Figure 5.9** displays the UV-Vis absorption spectra of VEGF and c-myc i-motif sequences, both with and without flavones (**11** and **13**), as well as with their Ru(II) complexes (**19** and **20**) in equimolar ratios. The majority of measured λ_{\max} shifts were hyperchromic (i.e. demonstrating an increase in absorbance) in nature. Thioflavone **11** had a strong effect, resulting in an increase of 16 and 18% of λ_{\max} for VEGF and c-myc i-motifs, respectively. The remaining absorption changes were minor ranging from 2 to 8%. Nevertheless, the inclusion of **19** resulted in a decrease in the VEGF i-motif's λ_{\max} from 272 to 271 nm, causing a hypsochromic shift of 1 nm. In contrast to the general hyperchromic trend, the detected λ_{\max} changes of the VEGF i-motif with the 4-oxo flavone **13** and its Ru(II) complex **20** were characterized by a decrease in absorbance (hypochromic).

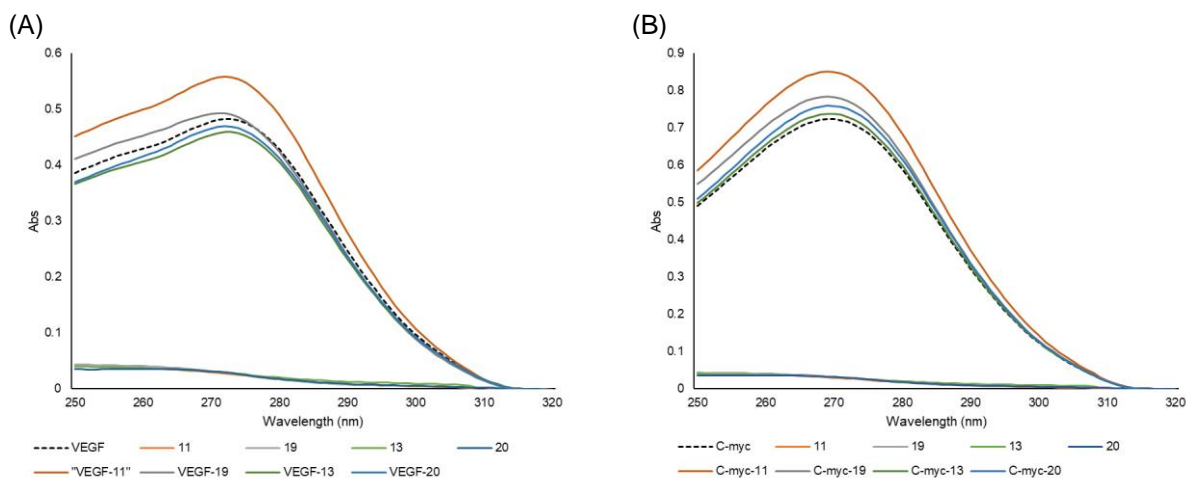


Figure 5. 9. Absorption spectra of VEGF and c-myc i-motif DNA with the flavone derivatives (**11** and **13**) and their Ru(II) complexes (**19** and **20**) in 1:1 ratio. (A) VEGF i-motif interactions; (B) C-myc i-motif interactions

As seen in **Figure 5. 10**, the test flavones resulted in trivial changes on the thermal stability of VEGF and c-myc i-motif sequences ($\Delta T_m < 20$ °C) [330]. **Table 5. 3** shows that the T_m transitions were generally in agreement with λ_{\max} shifts. For example, **11** showed a higher hyperchromic shift (18%) and stabilizing effect ($\Delta T_m = 2$ °C) for c-myc i-motif

compared to the VEGF one (16%, $\Delta T_m=1$ °C). **13** and **20** exhibited the same trends in the magnitude of both the λ_{max} and T_m shifts (Table 5. 3). On the contrary, complex **19** demonstrated a higher increase in λ_{max} with the c-myc i-motif (8%) than with VEGF (2%) while having a more pronounced effect on VEGF stability ($\Delta T_m= -4$ °C) than on c-myc's ($\Delta T_m= -1$ °C) (Table 5. 3).

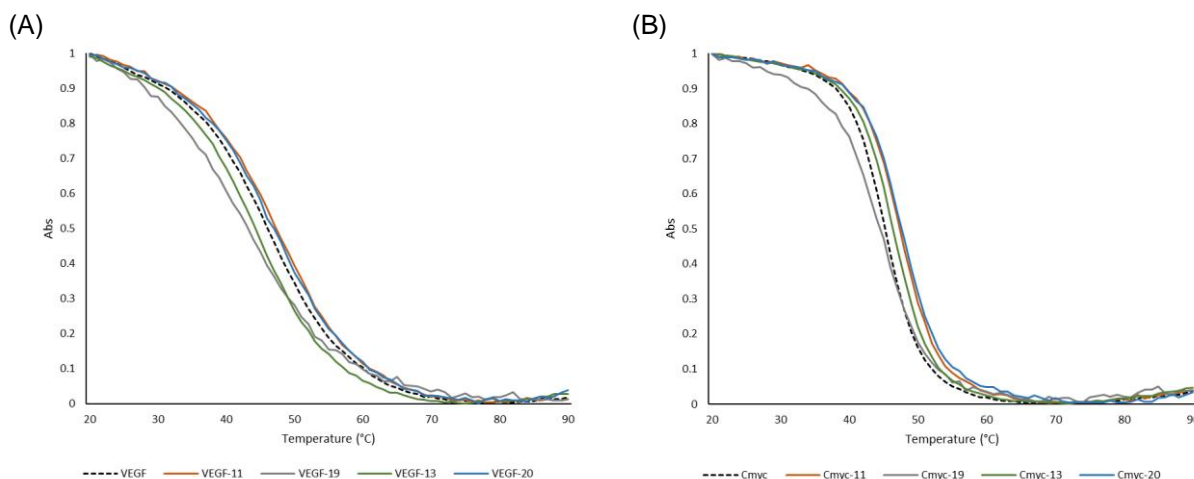


Figure 5. 10. Normalized UV melting curves for VEGF and c-myc i-motif DNA the flavone derivatives (**11** and **13**) and their Ru(II) complexes (**19** and **20**) at 295 nm at 1:1 ratio. (A) VEGF i-motif melt; (B) C-myc i-motif melt

Table 5. 3. Summary of UV-Vis data of VEGF and c-myc i-motifs in the presence of the flavone derivatives (**11** and **13**) and their Ru(II) complexes (**19** and **20**) at 1:1 ratio

Compound	VEGF i-motif		C-myc i-motif	
	λ_{max} shift (%)	ΔT_m (°C)	λ_{max} shift (%)	ΔT_m (°C)
11	16	1	18	2
19	2	-4	8	-1
13	5	-2	2	1
20	3	1	5	3

T_m , midpoint of the transition from each melting experiment; $\Delta T_m = T_m$ (DNA-flavone) - T_m (DNA)
 Orange color, hyperchromic; green color, hypochromic; blue color, stabilizing effect; black color, destabilizing effect.

Findings of the UV-Vis analysis on the interaction of flavones **11**, **13** and complexes **19** and **20** with VEGF and c-myc i-motif sequences suggest a predominantly non-intercalative binding mode. This is supported by the following: First, intercalative DNA binding is a result of higher binding affinity and hence causes bigger shifts in λ_{max} and T_m values of the interacting DNA [347,348]. Consequently, marginal augmentation or reduction in λ_{max} and T_m , such as the one demonstrated for this group of flavone derivatives, is frequently ascribed to a non-intercalative or external binding mode to DNA.

Secondly, intercalation of ligands within the i-motif structure is often challenging especially for planar molecules, such as the tested flavones herein, due to the narrow spatial features of i-motifs (minor grooves are 3.1 Å wide versus 5.7 Å for ds-DNA) [331,334]. Finally, earlier studies reported the ability of Ru complexes to attach to external DNA due to the metal atom's capacity to engage in electrostatic interactions with the negatively charged phosphate groups of DNA base pairs [117,337,338,347]. For example, Shi *et al* demonstrated a non-intercalative binding mode of a polypyridyl-Ru complex with the telomeric i-motif sequence denoted as 22CT via UV-Vis, fluorescence quenching and electron polarization techniques [338]. The tested Ru complex exhibited a 13.9% hypochromic change in 22CT's λ_{\max} in addition to a negligible 0.03 °C increase in T_m . The limited impact demonstrated by the polypyridyl-Ru complex on the absorbance and thermal stability of i-motif is similar to the marginal effects observed for the evaluated flavones in this study.

Overall, this preliminary analysis showed that the lead flavones could interact with VEGF and c-myc i-motifs. Nevertheless, the small magnitude of the observed effects suggests a non-intercalative form of interaction. Further research is required to explore the effects of varying experimental variables, such as pH and test compound concentrations, on the stability of i-motifs and their interactions with the designated molecules. Additionally, spectroscopic methods such as circular dichroism, nuclear magnetic resonance (NMR), and fluorescence emission spectroscopy can provide complementary data on the localization of the tested flavones within the i-motif structures [345].

5.3. Conclusions and future perspectives

The lead flavone **11** exhibited significant cytotoxic ($IC_{50}=1.2 \pm 0.8$ and $43.06 \pm 1.29 \mu\text{M}$ on MCF-7 and MDA-MB-231, respectively) and antimigratory effects (43% inhibition at 1 μM , $p<0.01$ on MDA-MB-231) on breast cancer cell lines *in vitro*, in addition to notable antiangiogenic action on ECs (42% tube formation inhibition at 1 μM , $p<0.05$). The importance of the 4-C=S group was demonstrated by the absence of cytotoxic and antimetastatic actions compared with the 4-C=O analogue, **13** ($IC_{50}>100 \mu\text{M}$ and null inhibition, respectively).

Ru(II) complexation caused varied impact with the different biological activities measured in this study. The Ru(II)-*p*-cymene complex **19** significantly inhibited migration in breast cancer cells, showing comparable activity to its parent **11** on the MDA-MB-231 cell line (47% inhibition at 1 μ M). **20** exhibited superior antimigratory effects on the MCF-7 and MDA-MB-231 cell lines compared with flavone **13** at 1 μ M (50 and 14% versus 33% and null inhibition, respectively, $p < 0.05$). Nonetheless, **19** had lower antiangiogenic and cytotoxic effects than **11**. Similarly, **20** showed reduced antiangiogenic efficacy compared to **13**, however, it enhanced **13**'s cytotoxic activity on the MCF-7 cell line ($IC_{50} = 66.15 \pm 5$ versus $>100 \mu$ M). The SAR findings summarized in **Figure 5. 11** emphasize the constructive contribution of metal complexation on flavones' antimetastatic activities, and the fundamental role of the ligand's chelating atom as well as the nature of the studied pharmacological effect on the biological outcome.

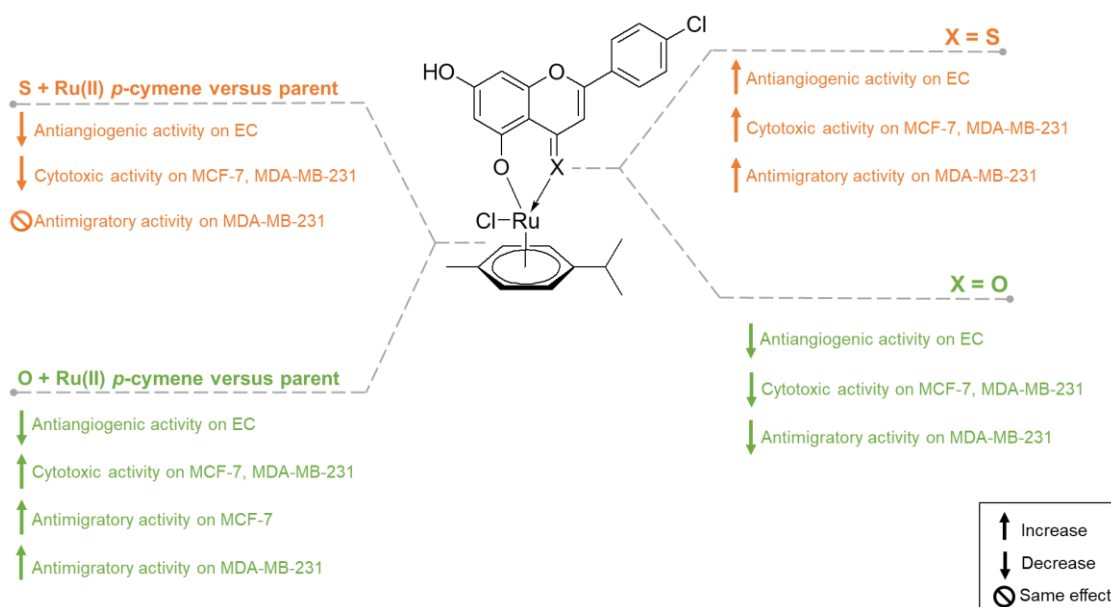


Figure 5. 11. Summary of SARs for the anticancer effects of the flavone derivatives (**11** and **13**) and their Ru(II) complexes (**19** and **20**). EC, endothelial cell; MCF-7, estrogen receptor positive breast cancer cell line; MDA-MB-231, triple negative breast cancer cell line.

UV-Vis spectroscopic techniques were used to further investigate the interactions of flavones (**11** and **13**) and their Ru(II) complexes (**19** and **20**) with VEGF and c-myc i-motif DNA. The evaluated derivatives caused minor shifts in the absorption maxima and the transition temperatures of the i-motif sequences, mostly suggesting a non-intercalative binding mechanism. Despite the small magnitude of the measured UV-Vis properties, the

tested compounds may show good i-motif binding affinity in future studies using different concentrations and pH values. Previous research has found that terbium (Tb) and Ru complexes had only minor effects on the T_m value of i-motif sequences, while having a good binding affinity for the target i-motif DNA [338,349]. The Tb complexes were shown to bind to i-motif at 22 and 30 μM while having ΔT_m of -0.5 and -4 $^\circ\text{C}$, respectively [349]. The polypyridyl-Ru complex also showed good affinity to i-motif DNA at ~ 2 μM while showing 0.03 $^\circ\text{C}$ increase in T_m [338].

In conclusion, this study identified compound **11** as a novel bi-modal antiangiogenic/cytotoxic lead against breast cancer. In order to contextualize the significance of **11**'s anticancer effects relative to existing drugs on the market, its *in vitro* antiangiogenic, cytotoxic and antimigratory activities were compared to reported data for the multi-target TKIs sunitinib and sorafenib. As demonstrated in **Table 5. 4**, **11** is more cytotoxic to MCF-7 cells compared to sunitinib and sorafenib, yet less cytotoxic to the MDA-MB-231 cell line. Nonetheless, **11** showed comparable antiangiogenic and antimigratory effects to both drugs against endothelial HUVECs and MDA-MB-231, respectively. TKIs are associated with clinically limiting cardiovascular side effects such as hypertension and thromboembolism due to their high vascular toxicity [350]. Sunitinib exhibits high cytotoxic activity on HUVECs with an IC_{50} of 9 μM [266]. In contrast, lead **11** did not exhibit cytotoxic effects on HUVECs at 40 μM , which might be indicative of a good toxicity profile subject to further evaluations [6]. Taken together, this work lays the foundation for the development of novel anticancer agents capable of simultaneously addressing tumor growth and propagation with low systemic toxicity.

Table 5. 4. Anticancer effects of lead **11** as evaluated in this study compared to reported data for sunitinib and sorafenib taken from references as indicated

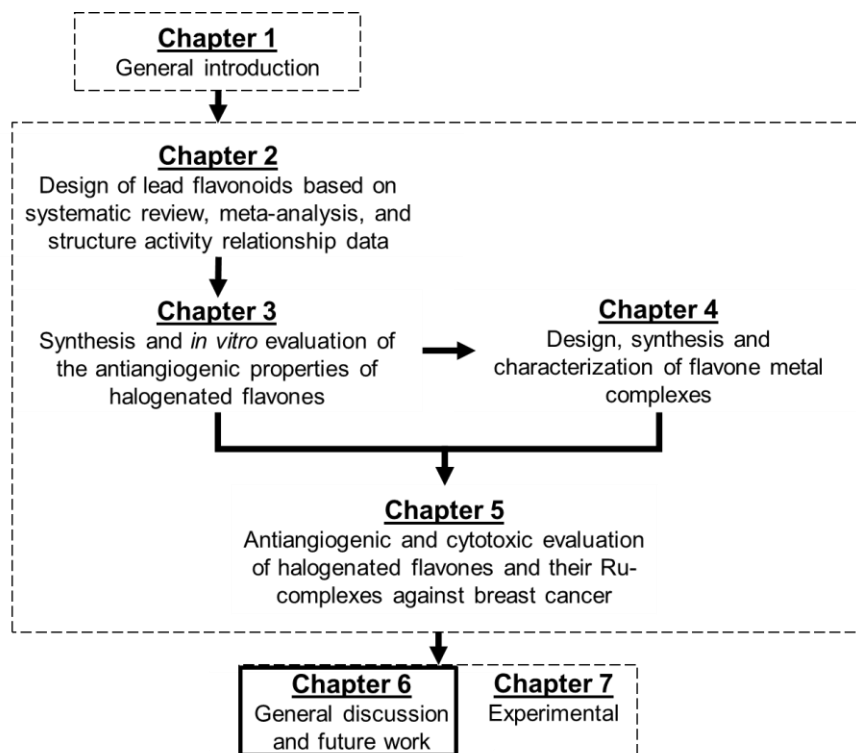
Compound	Antiangiogenic activity against HUVECs (tube formation inhibition)	Cytotoxicity against MCF-7 (IC_{50})	Cytotoxicity against MDA-MB-231 (IC_{50})	Antimigratory activity against MDA-MB-231 (wound closure inhibition)
11	42% at 1 μM	1.2 μM	43.06 μM	43% at 1 μM
Sunitinib	50% at 1 μM [266]	5 μM [351] 7.3 μM [352] 25.41 μM [353]	6.09 μM [352]	74 % at 5 μM [354]
Sorafenib	50% at 2.5 μM [355]	3.0 μM [356] 7.26 μM [357]	5.20 μM [357] 11.66 μM [358]	50% at 10 μM [343]

14.59 μM [358]

HUVECs, human umbilical cord vascular endothelial cells; MCF-7, estrogen receptor positive breast cancer cell line; MDA-MB-231, triple negative breast cancer cell line.

Chapter 6

General discussion and future work



6.1. Introduction

This chapter begins with a summary of the work presented in this thesis focusing on its key findings (**Section 6.2**). This is then followed by a general discussion of the key findings and suggestions for future work (presented in the style of a Case for Support for potential funding) **Section (6.3)**.

6.2. Summary of the thesis

A brief summary of the main findings of this thesis is presented in **Figure 6. 1**. Given the breadth of reported studies on the antiangiogenic activities of flavonoids and the lack of subsequent clinical progression, a robust systematic evaluation of the available data was needed. The thesis therefore commenced with a novel systematic analysis of 402 research and review articles providing an outlook on the progression of the angiogenic evaluations of flavonoids from the year 1997 until 2020 (**Chapter 2**). This demonstrated the interest of researchers in flavones (40%) and anticancer applications (82%), and indicated that 45% of the conducted research utilized a combination of *in vitro* and *in vivo* assays in their angiogenic assessments of flavonoids. Meta-analyses of the antiangiogenic activities of flavonoids, reported by quality assessed studies, based on two sets of data (comparing antiangiogenic effects against normal (set 1) and cancer cell induced CAM vascularization (set2)) were thereafter undertaken and reported in **Chapter 2**. Findings of these meta-analyses suggested the suitability of flavonoids for fulfilling the aim of this project and for antiangiogenic clinical progression, in terms of their antiangiogenic effectiveness (64-80% CAM vessel inhibition versus 40% for the clinical comparator aflibercept at 100 μ M and >40% CAM vessel inhibition of breast, ovarian and prostatic cancer cell lines from 3-40 μ M). A large scale antiangiogenic SAR study was subsequently conducted, mainly identifying the 4-C=O and 5,7-diOH functionalities as key for the antiangiogenic activity of flavonoids (**Chapter 2**). Based on the aforementioned findings, a library of 4-oxo/thio/seleno-4'-halophenyl flavones was designed combining the extrapolated antiangiogenic SAR findings with reported cytotoxic SARs and pharmacokinetic enhancing structural features as a common limitation of flavonoids (**Chapter 2**).

While synthesis of the 4-selenoflavones did not yield the desired products, the 4-oxo and thio derivatives were successfully synthesized using a Baker-Venkataraman approach (yields:60-97%) and were characterized using ^1H and ^{13}C NMR and, IR and mass spectrometry. Purities as determined by HPLC were >90% (**Chapter 3**). The synthesized flavones (**7-14**) indeed showed strong *in vitro* antiangiogenic inhibition of VEGF-induced EC tube formation at 1 (37-55%) and 10 μM (30-65%) after 12 h (50% inhibition reported for sunitinib at 1 μM using the same assay at 48 h) (**Chapter 3**). The most active flavones (**9**, **11**, **12** and **14**) additionally displayed significant reduction in VEGF-induced EC migration at 10 μM (25-37%). Interaction with VEGFR2 was explored for the most active flavones as a possible main target where only the 4-thio-diOH-substituted derivatives (**11** and **12**) showed significant decrease in its phosphorylation at 10 μM (57 and 37%, respectively, $p < 0.05$) in a western blotting assay (**Chapter 3**). Molecular docking simulations revealed a better orientation of **11** and **12** inside the ATP-binding cavity of VEGFR2 (proposing a type-I VEGFR inhibition) relative to the diOCH₃-substituted and the 4-oxo derivatives **9** and **14**, respectively, as well as the remaining 4-oxo compounds **7**, **8** and **13** (**Chapter 3**).

It was further hypothesized (based on literature data) that modification of our library of leads with Ru(II) or Ir(III) metal ligands would enhance their target antiangiogenic and cytotoxic pharmacological properties [146]. In order to test this hypothesis, complexation of Ru(II)-*p*-cymene or Ir(III)-Cp* ligands with flavones **7-14** was attempted in **Chapter 4**. Synthesis and structural characterization of two novel Ru(II)-*p*-cymene complexes (**19** and **20**) of compounds **11** and **13** was successful. Spectroscopic analysis of the remaining Ru(II)-*p*-cymene or Ir(III) Cp* complexation attempts often indicated the presence of a mixture of flavone complexes and residual starting material and/or byproducts, which made their purification via crystallization unsuccessful, hence not yielding those target compounds (**Chapter 4**).

The proposed bi-modal antiangiogenic and cytotoxic activity of lead compound **11** was assessed in **Chapter 5**. In addition to the EC antiangiogenic effects demonstrated by **11**, cytotoxic effects were evident against breast cancer MCF-7 and MDA-MB-231 cell lines ($\text{IC}_{50} = 1.2 \pm 0.8$ and 43.06 ± 1.29 μM , respectively) whereas no cytotoxicity was observed for the 4-oxo derivative **13**. Moreover, **11** exhibited significant reduction in the migration

of the invasive MDA-MB-231 cells at 1 μM (43% inhibition, $p < 0.01$). The *in vitro* anticancer profile of **11** is promising in comparison to the reported activities for the multi-target anticancer drugs sunitinib and sorafenib (e.g. IC_{50} on MCF-7 = 5 and 3 μM , respectively). The hypothesized positive impact of Ru(II) complexation to flavones **11** and **13** was also tested in **Chapter 5**. Whereas a negative impact was observed on the antiangiogenic activities, a positive effect was measured on the cytotoxic effects of compound **13** on the MCF-7 cell line ($\text{IC}_{50} = 66.15 \pm 5$ versus $>100 \mu\text{M}$) and on its antimigratory effects on the MCF-7 and MDA-MB-231 cell lines (50 and 14% versus 33% and null inhibition, respectively at 1 μM , $p < 0.05$). Complex **19** also showed equivalent inhibition to its parent **11** on the migration of MDA-MB-231 cells, besides its notable suppression of MCF-7 cells' migration (47 and 52% inhibition, respectively, at 1 μM).

The interaction with non-canonical i-motif VEGF and c-myc DNA sequences were explored for **11**, **13**, **19** and **20**, as a promising novel anticancer mechanism of action using UV-Vis spectroscopic studies. In general, the observed effects were marginal, mostly suggesting a non-intercalative interaction, however this needs further investigations (**Chapter 5**).

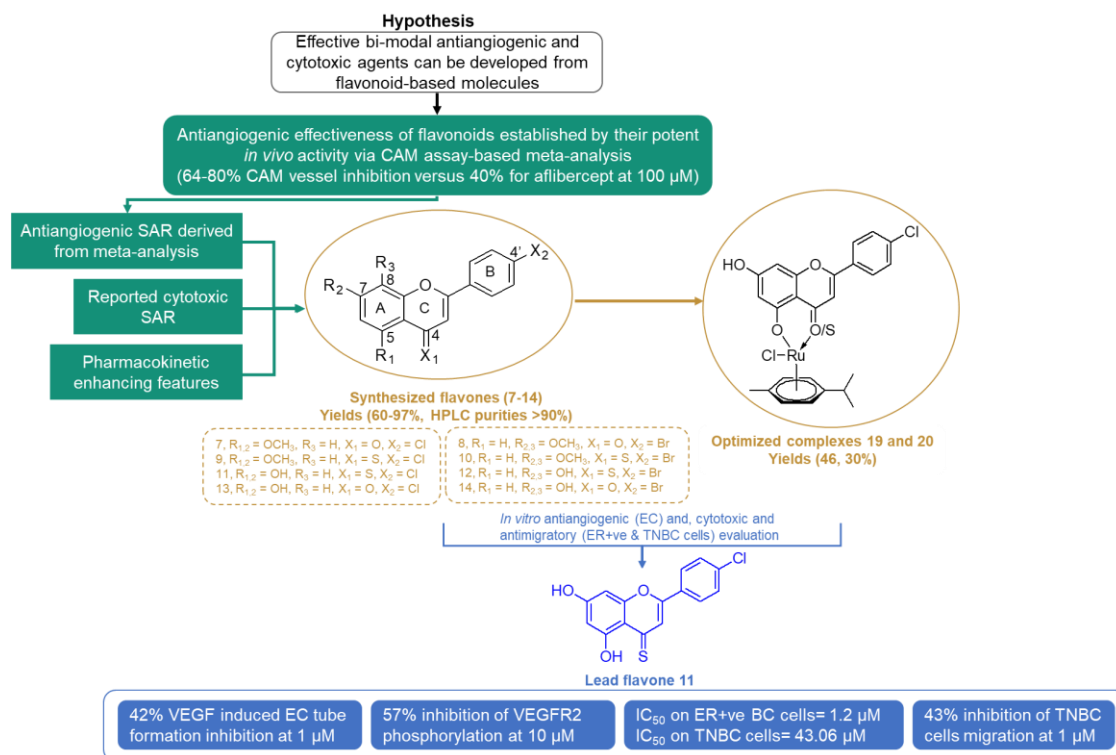


Figure 6. 1. Summary of the key findings of the thesis

6.3. General discussion and future work

This general discussion appraises the findings of the thesis from the standpoint of the clinical prospects of the two primary themes, flavonoids and antiangiogenic agents.

6.3.1. Clinical prospects for the use of flavonoids in cancer therapy

The poor bioavailability and target specificity of flavonoids have been identified as the two key limitations preventing their effective clinical advancement [103], and hence were regarded in the work conducted in this thesis.

a) Enhancing flavonoids bioavailabilities

In this work, structural modification strategies such as the use of Cl/Br atoms as opposed to OH groups in the B ring and methylation of the free OH groups in the A ring were applied in the design of the library of evaluated flavonoids (**Section 2.2.4, Chapter 2**) in order to enhance their lipophilic character and lower their susceptibility to metabolism. The predicted $\log P$ values of the designed flavones ranged from 3.27 to 4.19 in comparison to 2.9 for the natural flavone apigenin. Additionally, complexation with a Ru(II)-*p*-cymene ligand was implemented as a means to enhance aqueous solubility (**Chapter 4**). However, future investigations of the absorption, distribution, metabolism, excretion and toxicity (ADMET) profiles of the presented flavonoids are still required in order to assess whether these structural optimization efforts are effective in addressing the encountered bioavailability challenges.

The low bioavailability of flavonoids is the subject of extensive research in which multiple approaches, such as prodrug-based structural modifications and nanoformulations, have shown substantial improvements in the pharmacokinetic behavior of flavonoids in *in vivo* and clinical settings [10]. Perhaps the most elaborate example is the phosphate prodrug TP-1287, which is developed to allow the oral administration of flavopiridol (alvocidib®) that exhibits low aqueous solubility in neutral and basic conditions [96,97]. TP-1287 showed improved aqueous solubility (9.5 mg/mL versus 0.02 mg/mL for flavopiridol at pH 6.8) and oral bioavailability in mice (% of administered dose that reaches the systemic circulation, %F=182.3 compared to intravenous flavopiridol) [359]. The recommended dose for TP-1287 in patients with advanced solid tumors was identified as 11 mg twice

daily in a recent phase I study [98]. These efforts suggest promising clinical prospects for flavonoids, in terms of overcoming their oral bioavailability limitations, especially with the continuous advancements in the field of drug delivery systems [103].

b) Enhancing flavonoids' target specificity

The reported interaction of individual flavonoids with several kinases and intracellular receptors (**Sections 1.3.1 and 1.3.2, Chapter 1**) complicates their clinical application due to off-target interactions. In this regard, target specific mechanistic and SAR studies need to be identified in order to design optimal flavonoids that are clinically competent. Such data for flavonoids is currently limited, particularly in terms of antiangiogenic activity. This project focused on establishing useful SAR studies for the evaluated antiangiogenic activities including target specific VEGFR2 SARs. **Table 6. 1** summarizes the antiangiogenic SAR findings of this project in comparison to those available in the literature [154,155]. In **Chapter 2**, structural features affecting the antiangiogenic activities of different subclasses of flavonoids from multiple angles was extrapolated in a large scale study (**Table 6. 1**) [162]. Some of the effects measured across the reported studies were in good agreement, such as enhanced antiangiogenic activity upon conversion of OH groups to OCH₃ at positions 5, 7 and 4', which mirrors one of our findings that the presence of 4'-OCH₃ increases activity. With regards to the anti-VEGFR2 activities, a small set of halogenated flavones were evaluated using western blotting and molecular docking studies in **Chapter 3 (Table 6. 1)**. Ravashinkar *et al* similarly derived anti-VEGFR2 SAR conclusions for a set of 4-thio and/or OCH₃ derivatives of quercetin and luteolin [155]. While Ravashinkar *et al* reported a detrimental effect of the replacement of the 4-oxo group by a 4-thio group for VEGFR2 inhibitory activity, our observations suggested that the 4-thio substitution was key for the tested flavones in order to exert a significant anti-VEGFR2 activity. However, these SAR findings cannot be generalized on other sets of flavonoid derivatives for several reasons. First, the generated SARs were based on a limited number of compounds. Secondly, the tested libraries often possess unique structural features with regards to flavonoid subclass and type of functional groups. These structural features could have great influence on the behavior of a molecule in a biochemical space, hence might not correlate well to each other (for instance presence of 4'-OH group (electron donating) as opposed to a halogen (electron

withdrawing) or no 4'-substitution. Additionally, the impact of certain structural features, such as a single OH or OCH₃ substitution and the type of halogen in position 4' (Br or Cl), was not studied in isolation from other functional modalities in the same molecule. In brief, the reported SAR conclusions so far provided valuable insights for future lead optimization, however, further larger scale evaluations are still needed to fully explore the effect of the different involved structural features.

Table 6. 1. Summary of antiangiogenic SAR conclusions of flavonoids available in the literature compared to SAR findings of this project

Measured activity [Ref]	Flavonoid subclass	SAR conclusions
<ul style="list-style-type: none"> • <i>In vitro</i> HUVECs proliferation [154] • <i>In vivo</i> zebrafish vessel formation [154] 	<ul style="list-style-type: none"> • Flavanones • Flavones 	<ul style="list-style-type: none"> • 7-O glycosylation reduced activity • 8-H to OCH₃ reduced activity • 3'-H to OCH₃ increased activity • 5, 6, 7, 4'-OH to OCH₃ might increase activity
<ul style="list-style-type: none"> • <i>In vitro</i> HUVECs scratch assay [155] • <i>In vitro</i> VEGFR2 interaction (western blotting & molecular docking) [155] 	<ul style="list-style-type: none"> • Flavonols • Flavones 	<ul style="list-style-type: none"> • 3, 5, 7, 3', 4'-OH to OCH₃ increased activity • 4-C=O to C=S reduced activity
<i>In vivo</i> CAM assay meta-analysis [162] (Chapter 2)	<ul style="list-style-type: none"> • Flavonols • Flavanols • Flavanones • Flavones • Isoflavones • Anthocyanidins 	<ul style="list-style-type: none"> • C2-C3 unsaturation increased activity • No correlation between number of OHs and activity • 3, 5 and 7 and/or 4'-OHs increased activity • 7-H to OCH₃ reduced activity • 4'-H to OCH₃ increased activity • 3, 7-glycosylation unclear effect
<i>In vitro</i> HUVECs tube formation [253,339] (Chapters 3 & 5)	<ul style="list-style-type: none"> • 4'-Cl/Br phenyl flavones 	<ul style="list-style-type: none"> • 4-C=O to C=S increased activity • 8-OH increased activity • 5, 7 & 8-OH to OCH₃ unclear effect • Ru(II) complexation reduced activity
<i>In vitro</i> VEGFR2 interaction (western blotting & molecular docking) [253] (Chapter 3)	<ul style="list-style-type: none"> • 4'-Cl/Br phenyl flavones 	<ul style="list-style-type: none"> • 4-C=O to C=S enhanced VEGFR2 interaction • 5-OH enhanced VEGFR2 interaction • 5, 7-OH to OCH₃ reduced VEGFR2 interaction

6.3.2. Clinical prospects for the use of antiangiogenic agents in cancer therapy

The *in vitro* inhibitory activities of the library of flavonoids developed in this study on VEGF mediated EC angiogenesis was demonstrated in **Chapters 3** and **5**. Interference of lead flavones **11** and **12** with the phosphorylation of VEGF's cognate receptor VEGFR2 was

additionally established by western blotting studies (**Section 3.2.2.4, Chapter 3**). The focus on targeting the VEGF/VEGFR2 axis herein was motivated by its critical downstream effects on the survival, proliferation, permeability and migration of ECs (**Figure 1.1, Section 2.1, Chapter 1**), driving the progression of tumor angiogenesis [18,29]. In breast cancer, VEGF is the most predominantly overexpressed proangiogenic factor [324]. Rykala and colleagues found significantly higher levels of VEGF in 127 primary breast cancer patients relative to 54 benign breast lesion patients, with a notable association with the majority of breast cancer pathological features, especially distant metastasis [360] (**Table 6. 2**). Many studies have additionally revealed a negative association between the expression of VEGF and the OS of breast cancer patients [325,326,361]. Moreover, individuals diagnosed with TNBC exhibited markedly elevated levels of VEGF in comparison to non-TNBC patients (8.2 pg/ μ g DNA vs 2.7 pg/ μ g DNA, $p < 0.001$) [362].

Table 6. 2. Statistical significance (expressed as p -values) of levels of VEGF, PDGF and ICAM-1 factors in tumor (T) and serum (S) of primary breast cancer relative to T and S of benign breast lesions [360]

Measured characteristic	Angiogenic factor		
	VEGF	PDGF	ICAM-1
Average level in T, S	0.04, 0.009	0.02, 0.02	0.06, 0.008
Relation to positive lymph node status in T, S	0.003, 0.0007	—	0.004, 0.004
Relation to estrogen receptor	0.003, —	—	—
Relation to distant metastasis in T, S	0.02, —	—	—
Relation to tumor size in T, S	—	—, 0.003	0.001
Relation to MVD in T, S	0.018, —	0.004, 0.002	0.01, —

In that context, lead flavone (**11**) showed *in vitro* antiangiogenic effects on ECs as well as cytotoxic and antimigratory effects on estrogen receptor positive and triple negative breast cancer cells comparable to those reported by others for the VEGFR inhibitors sorafenib [343,355] and sunitinib [266,354] using the same assays (**Table 5.4, Section 5.3, Chapter 5**). However, the relation between the cytotoxic and antimigratory effects of compound **11** on breast cancer cells and its interference with the VEGF/VEGFR2 pathway has not been established in this work.

In general, VEGF/VEGFR2 targeting did not result in the expected anticancer efficacy in clinical practice. Patients receiving antiangiogenic medications suffer from relapse and

unresponsiveness to antiangiogenic therapy after a transient period of tumor regression as a result of tumor resistance that occur via both angiogenic (e.g. proangiogenic redundancy) and non-angiogenic pathways (e.g. vessel co-option) (**Figure 1.3, Section 1.2, Chapter 1**). Hence, researchers have focused on a broader context for the clinical utilization of antiangiogenic agents [29] by exploring the following approaches:

a) Targeting multiple pathways associated with angiogenesis

The simultaneous targeting of VEGF/VEGFRs and other targets that have a role in the development of resistance is explored as a means to enhance the effectiveness of antiangiogenic drugs. The role of HIF-1 α , in the development of resistance has been established [24,363]. HIF-1 α increases the expression of proangiogenic and metastatic genes such as VEGF, MMPs 2 and 9 and E-Cadherin, in response to inhibiting the VEGF pathway and the consequent oxygen deprivation [364]. The reduction of sunitinib induced lung carcinoma metastasis in mice by the anticancer drug topotecan (total number of metastases decreased from 101 to 12, $p < 0.001$) via decreasing HIF-1 α expression [44], reflects the potential role of HIF-1 α targeting in overcoming the disease relapse resulting from antiangiogenic drugs.

While VEGFR2 was explored as the primary target for the developed leads in this project, the need to investigate other potential antiangiogenic targets for the tested panel was acknowledged. In fact, the measured antiangiogenic activities of the diOCH₃ substituted and/or 4-oxo flavone derivatives presented in **Chapter 3** were found to be VEGFR2 independent. In **Section 2.2.2.2, Chapter 2**, results of the meta-analysis highlighted the ability of several flavonoids, such as acacetin and kaempferol, to inhibit HIF-1 α in reported tumor induced CAM vascularization assays. Hence, the test flavonoids herein might as well affect other proangiogenic factors with important roles in the development of resistance such as HIF-1 α , which can be investigated in the future using high throughput screening strategies followed by cell based immunoblotting/fluorescence assays.

b) Antiangiogenic and cytotoxic combinations

Antiangiogenic agents fail to elicit a response in cancers demonstrating non-angiogenic resistance abilities (i.e. vessel co-option and vasculogenic mimicry) [21]. For instance, liver metastatic CRC was unresponsive to bevacizumab due to the maintained tumor

growth via vessel co-option [21]. Cancer cells displaying vasculogenic mimicry were not sensitive to antiangiogenic treatments compared to ECs, as shown for melanoma cells in an *in vitro* study [365]. Vasculogenic mimicry was upregulated after treatment with bevacizumab or the induction of hypoxia in multiple preclinical studies [21]. The positive effects of chemotherapy on these angiogenesis independent resistance mechanisms was demonstrated in **Table 1.4, Section 1.2.3, Chapter 1** where the clinical benefits of antiangiogenic and cytotoxic drug combinations were discussed. In this context, the main objective of this project was to develop dual antiangiogenic and cytotoxic compounds. Within this framework, compound **11** exhibited strong cytotoxic effects against the MCF-7 breast cancer cell line ($IC_{50}=1.2 \pm 0.8 \mu\text{M}$) (**Section 5.2.2.1, Chapter 5**) concomitant with an antiangiogenic effect also displayed at $1 \mu\text{M}$ (**Chapter 3**), which could be of future clinical value in terms of targeting the mentioned resistance mechanisms.

c) Vascular normalization

The excessive vessel regression resulting from high doses of antiangiogenic therapy aggravates the hypoxic and acidic conditions in the tumor microenvironment leading to resistance and relapse. In contrast, low doses of anti-VEGF/VEGFR2 therapy can result in vascular remodeling effects which has been associated with enhanced antitumor efficacy especially when combined with chemotherapy, immunotherapy or radiotherapy [24]. Remarkably, recent reports indicate a dynamic crosstalk between vessel normalization and immunomodulation [366]. As shown in **Figure 6. 2**, the abnormal tumor angiogenesis favors an immunosuppressive microenvironment by negatively regulating T-cell function and infiltration through the vessel lining to the tumor bed. On the other hand, normalized vessels allow the re-activation of T-cells which in turn accentuates vessel re-modelling via an IFN- γ mediated antiangiogenic pathway (e.g. by reducing VEGF and Notch signaling) [366].

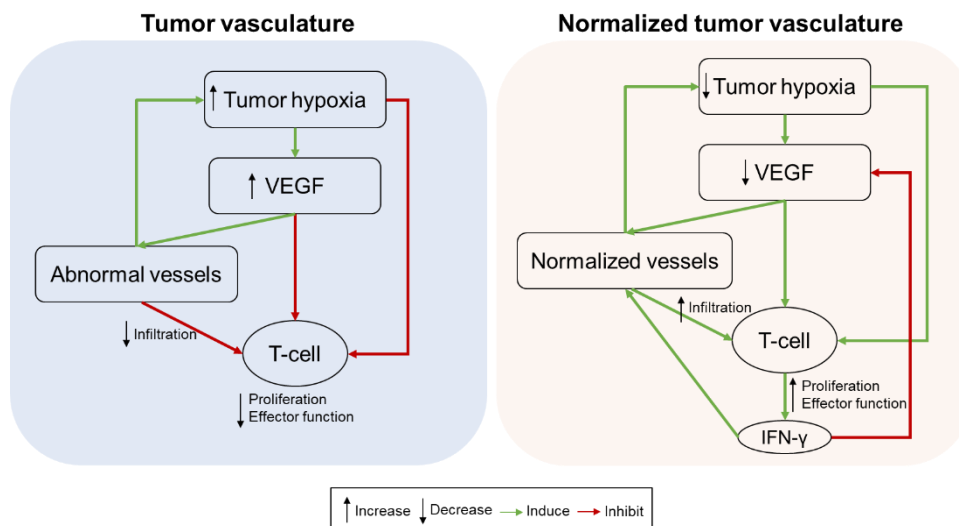


Figure 6. 2. Schematic diagram of the angiogenic-immune crosstalk

The immune checkpoint inhibitor (programmed cell death ligand, PD-L1), expressed on cancer and ECs, plays a vital role in suppressing T-cell function by binding to its T-cell receptor PD-1. Accordingly, combined immune checkpoint blockade (ICB) and VEGF/VEGFR inhibition has shown synergistic anticancer effects with multiple combinations gaining FDA approval (e.g. bevacizumab/atezolizumab (PD-L1 inhibitor) in unresectable HCC and axitinib/pembrolizumab (PD-1 inhibitor) or avelumab (PD-L1 inhibitor) in RCC) [24]. Interestingly, several reports have presented *in vitro* and *in vivo* findings supporting an ICB activity for flavonoids mostly via PD-L1 binding and inhibition [367–371]. This presents a promising clinical prospect for the flavonoids presented in this thesis especially with their proposed anti-VEGF/VEGFR2 activity. In this context, a Case for Support exploring the dual anti-VEGF/VEGFR2 and anti-PD-L1 activities of synthetic flavonoid derivatives is provided below as a possible future development for this work.

Exploring the dual anti-VEGF/VEGFR2 and anti-PD-L1 activities of synthetic flavonoid derivatives

1. Background

Our research aims to investigate the anticancer efficacy of targeting the interplay between tumor angiogenesis and immune suppression ^[1,2] using a single flavonoid-based agent that inhibits the relevant targets (VEGFR2 and PD-L1). The vascular endothelial growth factor (VEGF) is upregulated in most cancers ^[3], promoting tumor angiogenesis and facilitating the evasion of cancer cells to the body's immunosurveillance ^[1,2]. The immunosuppressive consequences of VEGF increase occur in part via the hypoxia-induced upregulation of the negative immune checkpoint regulator (programmed cell death receptor, PD-1) on the surface of T-cells ^[4]. PD-1's binding to its main ligand PD-L1, expressed on the surface of cancer cells, suppresses T-cell function.

The combination of PD-1/PD-L1 inhibition with low doses of anti-VEGF/VEGFR2 drugs has enhanced antitumor efficacy in several clinical trials ^[5], with combinations like bevacizumab/atezolizumab and axitinib/pembrolizumab gaining the FDA approval for hepatocellular and advanced renal cancer, respectively ^[3]. Low doses of anti-VEGF/VEGFR2 drugs are postulated to normalize the tumor vasculature and reactivate the immunosuppressed lymphocytes, whereas high doses cause excessive vessel regression, aggravating the tumor's hypoxic and immunosuppressive environment ^[1,6].

In contrast to the currently approved antibody PD-1/PD-L1 modulators, small molecule inhibitors (SMI) could have fewer immune-related adverse events due to their shorter half-lives. This motivated the search for PD-1/PD-L1 SMIs which was first led by Bristol-Myers Squibb (BMS). Preclinical evidence suggests that PD-1/PD-L1 SMIs can elicit similar biological effects to antibody based inhibitors. For example, the PD-L1 inhibitor INCB086550 (phase II clinical trial ^[7]) blocked the binding of the anti-PD-L1 antibody atezolizumab in cells expressing human PD-L1 ($p < 0.05$) and showed equivalent triple negative breast cancer (TNBC) tumor growth inhibition (55%) in mice ^[8]. In that regard, flavonoids have recently been shown to elicit antitumor effects by directly inhibiting PD-L1 in *in vitro* and *in vivo* studies ^[4,9-12]. In our recent study, *in vitro* data demonstrated an antiangiogenic VEGFR2 inhibitory effect of a synthetic lead flavonoid with a promising anticancer profile. Hence, we aim to combine these two underpinning studies to develop a single molecule capable of inhibiting VEGFR2 and PD-L1 derived from our synthetic lead molecule. A single molecule targeting both VEGF/VEGFR2 and PD-1/PD-L1 axes could bring potential benefits (compared to drug combinations) like predictable pharmacokinetics, higher patient adherence, and a single clinical approval process. We hypothesize that our developed inhibitor can induce vessel normalization and immunomodulatory antitumor effects with minimum toxicity (flavonoids display good tolerability, e.g. no increase in adverse events after flavonoid intake relative to control in a systematic meta-analysis of 30 randomized clinical trials ^[13]). We propose that TNBC can benefit from such pharmacological combination as it is hard to treat ^[4] and characterized by a high level of VEGF (8.2 pg/ μ g DNA versus 2.7 pg/ μ g DNA for non-TNBC patients, $p < 0.001$ ^[14]) and PD-L1 expression (higher mRNA PD-L1 expression versus non-TNBC patients, $p < 0.001$ ^[15]).

2. Preliminary evidence

Outlined below are representative examples of the evidence supporting the different components of the presented hypothesis.

2.a. Evidence from the literature

Low dose anti-VEGFR2 therapy alleviates tumor immunosuppressive effects via vessel normalization: Low dose (60 mg/kg) of the VEGFR2 inhibitor apatinib significantly increased ($p < 0.05$) pericyte coverage (indicator of vessel maturity) in Lewis lung carcinoma mice models and exhibited immunologic effects, significantly increasing the percentage of infiltrating CD8⁺ T-cells relative to the control ($p < 0.001$) and the high apatinib dose of 180 mg/kg ($p < 0.01$) [16].

Combined anti-VEGFR and PD-L1 therapy is clinically effective: The FDA approved the combination of a low dose of the anti-VEGFRs axitinib (10 mg/day) and the anti-PD-1 pembrolizumab as first-line therapy for advanced renal cell cancer patients, based on their significantly increased PFS (15.4 months) compared to 50 mg/day of sunitinib alone (11 months, $p < 0.0001$) in the KEYNOTE-426 phase III trial (n=432) [5].

Flavonoids inhibit PD-L1: Several flavonoids are reported to inhibit PD-1/PD-L1 interaction and/or bind to PD-L1 *in vitro* at low μM ranges (**Table 1**). Quercetin and Salvia plebeia extract (SBE) decreased tumor volumes ($p < 0.01$) and increased CD8⁺ T-cell and IFN- γ cytokine levels in TNBC and colon cancer mice xenografts, respectively.

Table 1. Summary of reported PD-L1 activity for flavonoids. n/a, not available

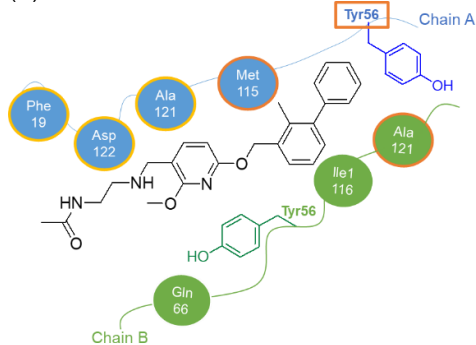
Flavonoid	PD-1/PD-L1 interaction inhibition	PD-L1 binding (K_D)
Quercetin [9]	IC ₅₀ = 0.19 μM	4.53 μM
Apigenin from SBE [10]	40% at 2.5 μM	n/a
Cosmosiin from SBE [10]	70% at 2.5 μM	0.85 μM
Eriodictyol [17]	IC ₅₀ = 0.04 μM	n/a
Fisetin [17]	IC ₅₀ = 0.04 μM	n/a
Kaempferol [18]	IC ₅₀ = 7.79 μM	n/a
Kaempferol 7-O-rhamnoside [18]	n/a	0.19 μM
BMS SMIs [19]	IC ₅₀ range (18-200 nM)	n/a

SAR aspects of flavonoids for PD-L1 inhibition:

Flavonoids with anti-PD-L1 activity (**Table 1**) were shown to induce PD-L1 dimerization, creating a druggable pocket by interacting

with ^ATyr56, ^AMet115, and ^AAsp122 hotspots (similar to BMS identified inhibitors) in molecular dynamic and docking simulation studies [12] (**Figure 1**). PD-L1 dimerization inhibits its ligation to PD-1 which only binds to a PD-L1 monomer [7]. SAR analysis revealed that 3-OH and 7-sugar moieties increased binding with PD-L1 dimer via hydrogen bonding (HB), while a 3'-OH group clashes with the narrowest hydrophobic region of the pocket [10,12] (**Figure 1B**).

(A)



(B)

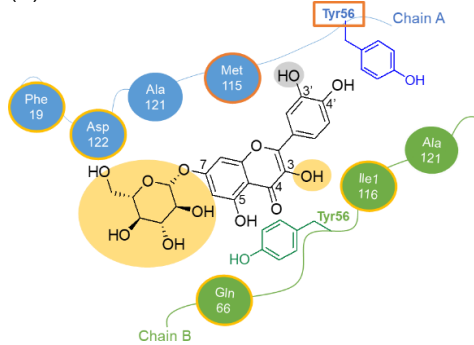


Figure 1. Cartoon representation of binding of PD-L1 dimer with (A) BMS-202 and (B) flavonoids. Hydrophobic interaction, orange outline; polar interaction, yellow outline; favorable functionality, yellow highlight; unfavorable functionality, grey highlight.

2.b. Evidence from our studies

Compound **1** demonstrated strong *in vitro* inhibitory activities against endothelial cell VEGF-induced angiogenesis (42% tube formation inhibition at 1 μM and 25% migration

inhibition at 10 μM compared to control) which was hypothesized to occur via VEGFR2 interaction based on western blotting (57% VEGFR2 phosphorylation inhibition at 10 μM) and molecular docking studies (**Figure 2**). Compound **1** showed cytotoxic ($\text{IC}_{50}=43 \mu\text{M}$) and antimigratory effects (43% inhibition at 1 μM , $p<0.01$) on the TNBC cell line MDA-MB-231. Accordingly, **1** is a suitable starting point for the design of the target VEGFR2/PD-L1 inhibitors effective against TNBC.

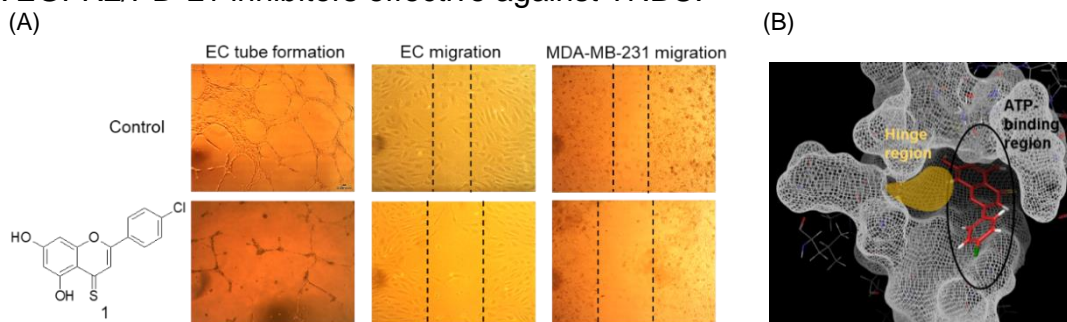


Figure 2. (A) Antiangiogenic and antimigratory effects of **1**; (B) **1** occupying the ATP-binding region of VEGFR2

3. Proposed work

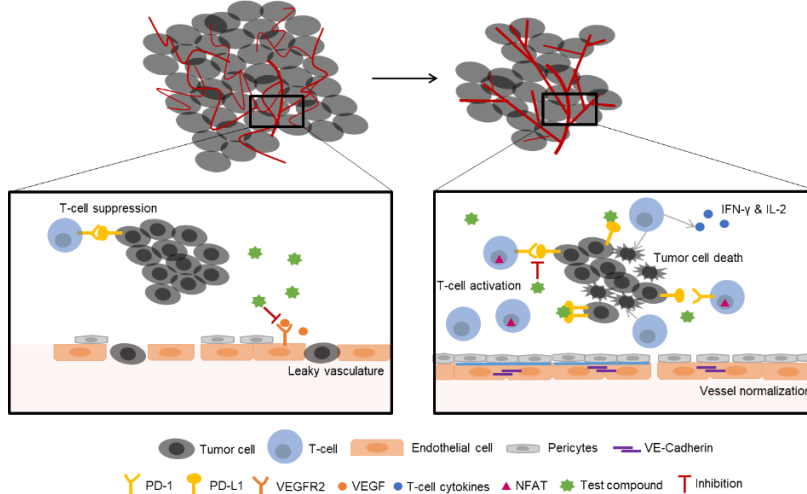
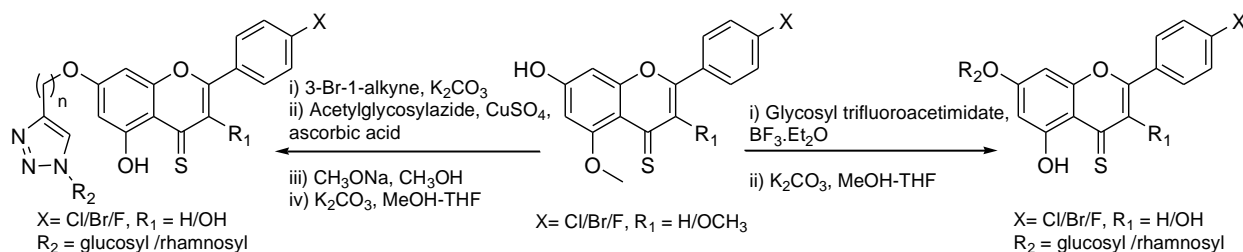


Figure 3. Overarching representation of the proposed work color coded relative to the corresponding work packages

Work package 1 (Design and synthesis of test compounds)

The hydrophobicity of the PD-L1 dimer pocket suggests that compound **1**'s 4-thio and 4'-chloro groups would enhance binding compared to natural flavonoid counterparts ($1 \log P = 4.17$ versus 2.98 for natural analogue apigenin). We aim to diversify the main structure by substituting the 4'-C with other halogens (Br and F). To

boost HB with $_{\text{B}}\text{Ile116}$ and the $_{\text{A}}\text{Phe19}$, $_{\text{A}}\text{Ala121}$ and $_{\text{A}}\text{Asp122}$ amino acids, 3-OH and 7-O-glycoside groups will be introduced, respectively. PD-L1 and VEGFR2 inhibitors often contain N-substituted heterocycles that form HB interactions, hence, a triazole linker of different alkyl chain lengths can be added between the sugar and C-7. This will allow for full burial inside the PD-L1 dimer^[12] and occupying new areas (i.e. the hinge region, **Figure 2B**) within VEGFR2. Design of the proposed ligands (~50) will be validated via molecular docking into VEGFR2 and PD-L1 structures. The basic flavonoid framework will be synthesized using our reported Baker-Venkatarman based method^[20] combined with a reported regioselective 7-O-deprotection method^[21]. The 7-O-substitutions will be added using the reported methods outlined in **Scheme 1**^[21,22]. The synthesized flavonoids will be spectroscopically characterized and their purities determined using HPLC and elemental analysis.



Scheme 1. Synthesis of flavonoids test library

Work package 2 (*In vitro* detection of antiangiogenic vessel normalization effects via inhibition of VEGF/VEGFR2)

This work package aims to determine whether a VEGF/VEGFR2 mediated vessel normalizing effect is possible using the test compounds (20 compounds showing best VEGFR2/PD-L1 interaction in docking studies) and if so, at which concentrations. The VEGFR2 inhibitor apatinib will be used as a positive control in this work package.

2.a) Inhibition of VEGF /VEGFR2 interaction

The VEGF/VEGFR2 inhibitory activities of the test library of flavonoids shall be probed by assessing their ATP-competitive VEGFR2 binding, using a competitive enzyme-linked immunosorbent (ELISA) assay. This will confirm whether there is direct interaction of the test compounds with VEGFR2. Affinity to VEGFR2 (K_D values) will be determined using the surface plasmon resonance (SPR) technique which is a label free biophysical assay that measures the kinetics of protein interactions with high sensitivity. Relevant SARs will also be extrapolated to be used in the design of the next series of compounds.

2.b) Detection of vessel normalization

Vessel normalization comprises a vessel pruning effect accompanied by normalization of the remaining vessels which are characterized by wider lumens, tight endothelial junctions and more pericyte coverage. In our previous work, we showed that **1** significantly decreased tube formation of human umbilical vein endothelial cells (HUVECs) at 1 and 10 μM using a 2D Matrigel-based assay (**Figure 2A**). Herein, we will use a 3D fibrin bead model, which allows for lumen formation in HUVEC tubules [23], to determine the ability of the test compounds to normalize vessels. A range of low and high concentrations (0.1-10 μM), as guided by results from our previous experiments, shall be tested to determine vessel normalizing doses. These will be refined based on the IC_{50} values obtained from the ELISA assay. Clustering of the endothelial cell adhesion molecule (VE-Cadherin) at cellular junctions will be inspected by immunostaining with anti-VE-cadherin in HUVEC monolayers as another vessel normalizing indicator [23].

Work package 3 (*In vitro* detection of mechanism of PD-1/PD-L1 inhibition)

3.a) Detection of PD-1/PD-L1 interaction inhibition

The ability of the test compounds to inhibit the PD-1/PD-L1 complex formation (by which they can halt the tumor induced suppression of T-cells) will be evaluated using different biochemical assays. First, dissociation of the ^{15}N -labeled PD-1/PD-L1 complex upon titration of the test compounds shall be monitored via 2D HSQC NMR (600 MHz), where narrowing of the 1H - ^{15}N signals is indicative of complex dissociation [19]. Next, the interference with PD-1/PD-L1 interaction will be demonstrated using the homogenous time-resolved fluorescence (HTRF) assay [8,19]. Finally, blocking of PD-1/PD-L1 binding by the test compounds will be validated by competitive ELISA. The clinical candidate PD-L1 inhibitor INCB086550 will be used as reference standard.

3.b) Detection of the PD-L1 dimerization induction

This step aims to provide the mechanistic and structural information regarding the constitutive target protein (i.e. whether it is PD-1 or PD-L1) responsible for the observed activities. Here, we focus on the direct binding of test compounds with recombinant PD-L1 protein as the proposed target, using INCB086550 (PD-L1 dimerization inducer) as a reference standard. Initially, direct binding of test compounds with PD-L1 will be detected through signal shifts of the ^{15}N -labeled protein upon the addition of increasing amounts of test material using HSQC NMR [19]. Binding with PD-1 and PD-L2 will be measured to evaluate the PD-L1 selectivity of the test compounds. The test compounds' affinities to PD-L1 can be determined by a differential scanning fluorimetry (DSF)-based thermal stability analysis illustrated as melting temperature (T_m , ~ 34.2 to 35.4°C reported for PD-L1). T_m increases proportionally with ligand binding affinity [19,24] with SMIs typically having T_m shifts between 19 and 4°C [24]. Moreover, the SPR technique will be utilized to determine the K_D values of the test compounds with PD-L1.

To provide physiological context, the ability of the test compounds to induce PD-L1 dimerization will be assessed in solution via size exclusion chromatography. PD-L1 induced dimerization by INCB086550 is reported to shift its retention time from 33 kDa to 69 kDa [8]. A similar behavior observed for our test compounds would confirm their ability to halt PD-1/PD-L1 interaction by inducing PD-L1 dimerization.

Work package 4 (*In vitro* detection of T-cell activation)

In this work package, we aim to determine whether PD-1/PD-L1 inhibition by the test compounds translates into an immunological activity through T-cell activation. Cytotoxicity of the test compounds against the used cell lines will be measured first using cell counting kit-8 to define their maximum tolerated doses. The T-cell activation analysis shall include three main indicators: **4.a) Increased T-cell proliferation** which will be measured for antigen stimulated peripheral blood mononuclear cells (PBMC) using CellTrace CFSE labelling. Proliferating CD4⁺ and CD8⁺ cells will be quantified by flow cytometry using fluorescein appropriate emission filters [10,24]. **4.b) Activity of the nuclear factor of activated T-cells (NFAT)** transcription factor family which plays an important role in T-cell activation and is attenuated upon PD-1/PD-L1 ligation [10]. PD-1 expressing T-lymphocyte Jurkat cells with NFAT reporter luciferase will be co-cultured with the high PD-L1 expressing TNBC (MDA-MB-231) cells [9] for this assay in order to simulate the *in vivo* effector:target immunogenic system [8,18,24]. **4.c) Increased IL-2 and IFN- γ secretion** (as major T-cell activation markers) shall be analyzed by flow cytometry in antigen stimulated PBMC and MDA-MB-231 co-cultures upon addition of test compounds [8,24].

Work package 5 (Target based structural optimization)

At this stage, we will use our novel data sets and test compounds will be optimized further based on the extrapolated SAR conclusions, expanding on structural features showing the highest effectiveness against the evaluated biological activities. The new library will undergo the same *in vitro* assessments in WP 1 to 4 to determine their effectiveness.

Work package 6 (Antitumor effect in preclinical *in vivo* mice models)

We will determine the *in vivo* antitumor efficacy of the 1-2 compounds showing equivalent/better activity than reference standards in *in vitro* assays, via a combined vessel normalizing and immunomodulatory effect. MDA-MB-231 tumor bearing NSG female mice groups engrafted with human CD34⁺ stem cells [8] (n=9/group, based on $p < 0.05$ and 90% power calculations and relevant published data [1,2]) will be randomized

to receive IgG, 50 mg/kg axitinib + 10 mg/kg pembrolizumab, 50 or 150 mg/kg test compounds (as reported for anti-VEGFR2 and related flavonoids in similar models ^[1,9]).

6.a) Antitumor effects: The tumor volumes and masses of the treated mice groups will be monitored, replicating the same conditions with immunodeficient (CD34⁺ lacking) mice to confirm if the observed effects are immunomediated ^[8].

6.b) Vessel normalization effects: Tumors from sacrificed animals will be immunohistochemically stained to detect vessel normalization. Higher doses should result in significant vessel regression (a drop in tumor vessel density) whereas lower doses should increase pericyte coverage and vessel normalization as measured by CD31 (endothelial cell adhesion molecule) and NG2 (pericyte activation marker) immunostaining ^[1].

6.c) Immunomodulatory effects: Increased levels of infiltrating CD8⁺ T-cells and IFN- γ in dissected tumors shall be quantified by flow cytometry as indicators for the immunomodulatory tumor suppressing effects resulting from the vessel normalization and PD-L1 inhibitory activities of the test compounds ^[1,9].

4. Timeliness

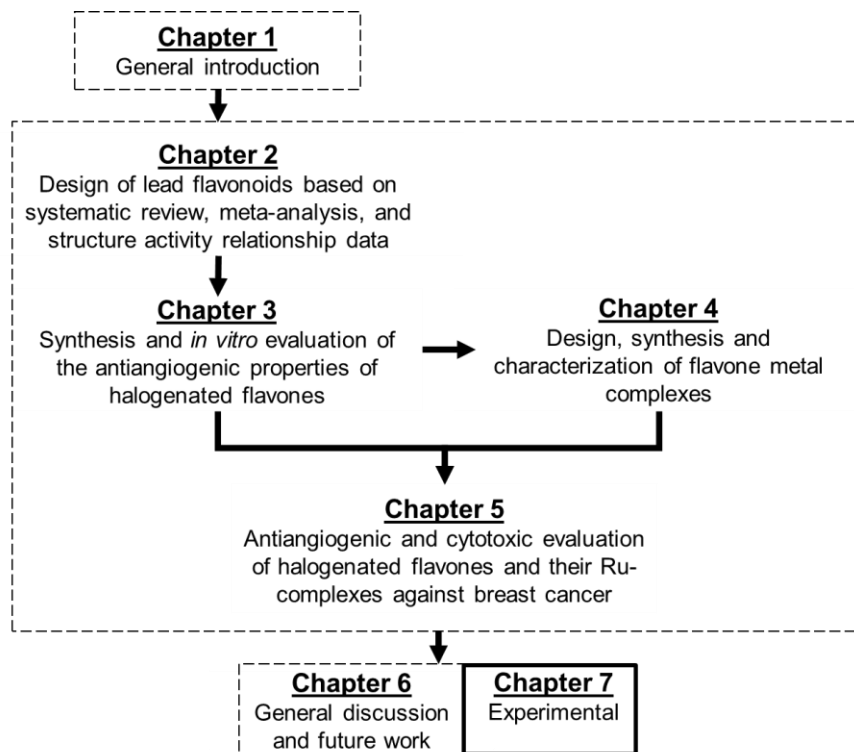
The understanding of the molecular dynamics of cancer has greatly evolved, opening up new and specific targets that can halt the disease progression. Significant clinical improvements were lately achieved by pairing the suppression of tumor vasculature with immune re-activation largely by targeting VEGFR2 and PD-L1 proteins. Here, we aim to combine these effects in a single molecule, a strategy yet to be explored within this research area. Such SMIs may represent an alternative to the currently used antibody and multi-drug therapy that has shown several toxicity and production complexities. Our comprehensive *in vitro* and *in vivo* evaluation approach could provide novel information on the doses, mechanisms of action and structural requisites by which these effects can be achieved using one compound.

References

- [1] Li, Q.; Wang, Y.; Jia, W.; Deng, H.; Li, G.; et al. *Clin. Cancer Res.* 2020, 26 (7), 1712–1724. [2] Allen, E.; Jabouille, A.; Rivera, L. B.; Lodewijckx, I.; Missiaen, R.; et al. *Sci. Transl. Med.* 2017, 9 (385), 9679. [3] Ghalehbandi, S.; Yuzugulen, J.; Pranjol, M. Z. I.; Pourgholami, M. H. *Eur. J. Pharmacol.* 2023, 949 (Jan), 175586. [4] Messeha, S. S.; Zarmouh, N. O.; Soliman, K. F. A. *Nutrients* 2021, 13 (5), 1718. [5] Powles, T.; Plimack, E. R.; Soulières, D.; Waddell, T.; Stus, V.; et al. *Lancet Oncol.* 2020, 21 (12), 1563–1573. [6] Yang, T.; Xiao, H.; Liu, X.; Wang, Z.; Zhang, Q.; et al. *Front. Oncol.* 2021, 11 (Aug), 1–20. [7] Sasikumar, P. G.; Ramachandra, M. *Front. Immunol.* 2022, 13, 752065. [8] Koblisch, H. K.; Wu, L.; Wang, L. C. S.; Liu, P. C. C.; Wynn, R.; et al. *Cancer Discov.* 2022, 12 (6), 1482–1499. [9] Jing, L.; Lin, J.; Yang, Y.; Tao, L.; Li, Y.; et al. *Phyther. Res.* 2021, 35 (11), 6441–6451. [10] Choi, J. G.; Kim, Y. S.; Kim, J. H.; Kim, T. I.; Li, W.; et al. *Front. Immunol.* 2020, 11 (Nov), 1–15. [11] Coombs, M. R. P.; Harrison, M. E.; Hoskin, D. W. *Cancer Lett.* 2016, 380 (2), 424–433. [12] Sartori, G. R.; Albuquerque, A. de O.; Santos-Costa, A. H.; Andrade, L. M.; Almeida, D. da S.; et al. *Front. Drug Discov.* 2022, 2 (Dec), 1–22. [13] Yao, J.; Zhang, Y.; Wang, X. Z.; Zhao, J.; Yang, Z. J.; et al. *Front. Public Heal.* 2022, 10, 814669. [14] Linderholm, B. K.; Hellborg, H.; Johansson, U.; Elmberger, G.; Skoog, L.; et al. *Ann. Oncol.* 2009, 20, 1639–1646. [15] Mittendorf, E. A.; Philips, A. V.; Meric-Bernstam, F.; Qiao, N.; Wu, Y.; et al. *Cancer Immunol. Res.* 2014, 2 (4), 361–370. [16] Zhao, S.; Ren, S.; Jiang, T.; Zhu, B.; Li, X.; et al. *Cancer Immunol. Res.* 2019, 7 (4), 630–643. [17] Li, Wei; Kim, Tae In; Kim, Ji Hye; Chung, H. S. *Molecules* 2019, 24, 4062. [18] Kim, J. H.; Kim, Y. S.; Choi, J. G.; Li, W.; Lee, E. J.; et al. *Int. J. Mol. Sci.* 2020, 21 (9), 1–11. [19] Zak, K. M.; Grudnik, P.; Guzik, K.; Zieba, B. J.; Musielak, B.; et al. *Oncotarget* 2016, 7 (21), 30323–30335. [20] Ravishankar, D.; Watson, K. A.; Greco, F.; Osborn, H. M. I. *RSC Adv.* 2016, 6 (69), 64544–64556. [21] Li, M.; Han, X.; Yu, B. *J. Org. Chem.* 2003, 68 (17), 6842–6845. [22] Wang, G. Q.; Yan, L. L.; Wang, Q. A. *Heterocycl. Commun.* 2018, 24 (2), 119–124. [23] Zhang, W.; Wang, L. J.; Xiao, F.; Wei, Y.; Ke, W.; et al. *Arterioscler. Thromb. Vasc. Biol.* 2012, 32 (11), 2721–2732. [24] Ganesan, A.; Ahmed, M.; Okoye, I.; Arutyunova, E.; Babu, D.; et al. *Sci. Rep.* 2019, 9 (1), 1–19.

Chapter 7

Experimental



7.1. Materials

7.1.1. Chemistry

Chemicals, reagents and analytical grade solvents were purchased from Sigma-Aldrich (Gillingham, UK) unless specified. Gallacetophenone 3',4'-dimethyl ether was purchased from Apollo Scientific (Stockport, UK) and (pentamethylcyclopentadienyl)iridium(III) chloride dimer was purchased from Fischer Scientific (Loughborough, UK). Merck TLC Silica gel 60 F254 aluminium backed plates and silica gel 60 (particle size 35-70 µm) were supplied by Sigma Aldrich (Gillingham, UK).

7.1.2. Cell culture

HUVECs were purchased from Sigma-Aldrich (ECACC) (Gillingham, UK) and cultured in EGM-2 medium (EBM with SingleQuotes™ kit: foetal bovine serum (FBS), fibroblast growth factor B, epidermal growth factor, VEGF, insulin-like growth factor-1, heparin, hydrocortisone) (Lonza, Belgium). MCF-7 (estrogen receptor +ve breast cancer cell line, wild type) was purchased from Sigma-Aldrich (ECACC) (Gillingham, UK) and cultured in RPMI 1640 medium supplemented with 5% FBS (Fischer Scientific, Loughborough, UK). MDA-MB-231 (triple -ve breast cancer cell line) was purchased from Sigma-Aldrich (ECACC) (Gillingham, UK) and cultured in DMEM medium (1g/L glucose, without L-glutamine) supplemented with 2% L-glutamine (200 mM) and 10% FBS (Fischer Scientific, Loughborough, UK). Bovine serum albumin (BSA) was purchased from Sigma-Aldrich (Gillingham, UK). Recombinant human VEGFR-A₁₆₅ was purchased from Peprotech (London, UK). Corning™ Matrigel™ growth factor reduced (GFR) Membrane Matrix was purchased from Fischer Scientific (Loughborough, UK). DC™ Protein Assay Kit II for Lowry assay was purchased from Bio-Rad (Watford, UK). Radioimmunoprecipitation assay (RIPA) lysis buffer, protease and phosphatase inhibitor cocktail, ammonium persulfate (APS), sodium dodecyl sulfate (SDS), glycine, tris Base and tween 20 were purchased from Fischer Scientific (Loughborough, UK). 30% acrylamide and N,N,N',N'-tetramethyl ethylenediamine (Temed) were purchased from Sigma-Aldrich (Gillingham, UK). The primary antibodies directed against phosphorylated Tyr-1175 site in the VEGFR2 (KDR), total VEGFR2, actin and Horseradish peroxidase-conjugated secondary antibody were purchased from Cell Signalling (UK). Laemmli buffer, 2-mercaptoethanol and enhanced chemiluminescence (ECL) detection solutions

were purchased from Bio-Rad (Watford, UK). The 0.45 μm polyvinylidene difluoride (PVDF) membrane was purchased from Fisher Scientific (Loughborough, UK). 3-(4, 5-dimethylthiazol-2-yl)-diphenyl-2*H*-tetrazolium bromide used for MTT assay, DMSO (sterile) used for freezing cells and trypan blue dye were obtained from Sigma-Aldrich (Gillingham, UK). NaCl, Na₂HPO₄ and NaH₂PO₄ reagents used for phosphate buffered saline (PBS) preparation were purchased from Sigma-Aldrich (Gillingham, UK).

7.1.3. I-motif DNA binding

VEGF and c-myc i-motif DNA (5'-3' sequences (CCCCGCCCCCGGCCCGCCCC) and (CCTTCCCCACCCTCCCCACCCTCCCCA), respectively) were purchased from Sigma-Aldrich (Gillingham, UK).

7.2. Equipment

7.2.1. Chemistry

Thin layer chromatography was run on Merck silica 60 F254 aluminium backed plates of 0.2 mm depth. Compounds on the plate were visualized using UV light ($\lambda=254$ nm).

Column chromatography was carried out using Silica gel 60 (particle size 35-70 μm).

Melting points were determined on an Electrothermal Digital Melting Point apparatus and are uncorrected.

¹H NMR and ¹³C NMR spectra were recorded using a Bruker DPX 400 (400 MHz) spectrometer, a Bruker DPX 400 (400 MHz) spectrometer or a Bruker Avance III AV 500 (500 MHz) spectrometer.

Mass spectrometry data were recorded on a Thermo Fisher LTQ Orbitrap XL instrument. Molecular ions and molecular fragments are reported as mass/charge (*m/z*) ratios.

Infrared spectra were recorded on a Perkin Elmer precisely spectrum 100 FT-IR spectrometer.

High Performance Liquid Chromatography (HPLC) analysis was performed using an Agilent-1100 series HPLC equipped with Column: C-18 (ACE-221-2546; 4.6 mm x 250 mm; 5 μm).

CHN elemental analyses for metal compounds were obtained from MEDAC LTD (Woking, UK), analytical and consultancy services.

7.2.2. Cell culture

Tissue culture experiments were carried out in a class II laminar flow hood (Hera Safe, Thermo Electron Corporation, UK). An incubator (Binder, Germany), centrifuge (Biofuge primo, Heraeus instrument, UK), water bath (Griffin & Gerorge, UK), and inverted microscope Nikon Eclipse TS 100 were used for tissue culture procedures. A haemocytometer (Marienfield, Germany) was used for cell counting.

Images of the cells were taken using a 1.3 M Microscope Digital Eyepiece Camera. ImageJ software was used to quantify tube formation and cell migration.

The UV absorbance for the MTT assay was read on a SPECTRA max UV spectrometer.

Tissue culture disposable items; flasks (growth area 25 cm², 75 cm²), disposable pipettes (5, 10, 25 and 50 mL), Gilson pipette-tips (20-200 µL and 100-1000 µL), falcon tubes (15 and 50 mL), 96 well plates, eppendorfs and the 7 mL bijoux were purchased from Greiner Bio-One (Gloucestershire, UK). Sterile disposable syringes (5, 10 and 50 mL) and needles were purchased from Terumo (Surrey, UK). Sterile syringe filters (Minisart, 0.02 µM) were obtained from Sartorius Biotech (UK).

Western blotting equipment used for gel preparation, running the protein samples and transfer of proteins into the PVDF membrane, which includes the minitanks, glass, plates, combs, casting frame, casting stand in addition to the blotting case were from BioRad (Hertfordshire, UK). ImageJ software was used to quantify western blot bands' densities.

7.2.3. I-motif DNA binding

UV-visible absorbance measurements and *DNA UV melting studies* were performed on a Cary 300 C (Varian USA) UV visible spectrophotometer.

7.3. Methods

7.3.1. Systematic review and meta-analysis

The systematic review and meta-analysis presented in **Sections 2.2.1** and **2.2.2**, **Chapter 2** were conducted according to PRISMA guidelines [163] (**Table 7. 1**).

Table 7. 1. PRISMA-P 2015 Checklist. This checklist has been adapted for use with protocol submissions to Systematic Reviews from Table 3 in Moher D et al: Preferred reporting items for systematic review and meta-analysis protocols (PRISMA-P) 2015 statement. Systematic Reviews 2015 4:1.

Section/topic	#	Checklist item	Information reported		Line number(s)
			Yes	No	
ADMINISTRATIVE INFORMATION					
Title					
Identification	1a	Identify the report as a protocol of a systematic review	<input checked="" type="checkbox"/>	<input type="checkbox"/>	659
Update	3	If the protocol is for an update of a previous systematic review, identify as such	<input type="checkbox"/>	<input type="checkbox"/>	n/a
Registration	2	If registered, provide the name of the registry (e.g., PROSPERO) and registration number in the Abstract	<input type="checkbox"/>	<input type="checkbox"/>	n/a
Authors					
Contact	3a	Provide name, institutional affiliation, and e-mail address of all protocol authors; provide physical mailing address of corresponding author	<input type="checkbox"/>	<input type="checkbox"/>	n/a
Contributions	7	Describe contributions of protocol authors and identify the guarantor of the review	<input type="checkbox"/>	<input type="checkbox"/>	n/a
Amendments	4	If the protocol represents an amendment of a previously completed or published protocol, identify as such and list changes; otherwise, state plan for documenting important protocol amendments	<input type="checkbox"/>	<input type="checkbox"/>	n/a
Support					
Sources	5a	Indicate sources of financial or other support for the review	<input checked="" type="checkbox"/>	<input type="checkbox"/>	Acknowledgments
Sponsor	11	Provide name for the review funder and/or sponsor	<input checked="" type="checkbox"/>	<input type="checkbox"/>	Acknowledgments
Role of sponsor/funder	12	Describe roles of funder(s), sponsor(s), and/or institution(s), if any, in developing the protocol	<input type="checkbox"/>	<input type="checkbox"/>	n/a
INTRODUCTION					
Rationale	6	Describe the rationale for the review in the context of what is already known	<input checked="" type="checkbox"/>	<input type="checkbox"/>	638-642
Objectives	7	Provide an explicit statement of the question(s) the review will address with reference to participants, interventions, comparators, and outcomes (PICO)	<input checked="" type="checkbox"/>	<input type="checkbox"/>	683-686, 748-749, 792

Section/topic	#	Checklist item	Information reported		Line number(s)
			Yes	No	
METHODS					
Eligibility criteria	8	Specify the study characteristics (e.g., PICO, study design, setting, time frame) and report characteristics (e.g., years considered, language, publication status) to be used as criteria for eligibility for the review	<input checked="" type="checkbox"/>	<input type="checkbox"/>	3150-3172
Information sources	9	Describe all intended information sources (e.g., electronic databases, contact with study authors, trial registers, or other grey literature sources) with planned dates of coverage	<input checked="" type="checkbox"/>	<input type="checkbox"/>	3132-3138
Search strategy	10	Present draft of search strategy to be used for at least one electronic database, including planned limits, such that it could be repeated	<input checked="" type="checkbox"/>	<input type="checkbox"/>	Tables 7.2, 7.3
STUDY RECORDS					
Data management	11a	Describe the mechanism(s) that will be used to manage records and data throughout the review	<input checked="" type="checkbox"/>	<input type="checkbox"/>	3165-3166, 3175-3176
Selection process	13	State the process that will be used for selecting studies (e.g., two independent reviewers) through each phase of the review (i.e., screening, eligibility, and inclusion in meta-analysis)	<input checked="" type="checkbox"/>	<input type="checkbox"/>	3163-3165
Data collection process	14	Describe planned method of extracting data from reports (e.g., piloting forms, done independently, in duplicate), any processes for obtaining and confirming data from investigators	<input checked="" type="checkbox"/>	<input type="checkbox"/>	1365-3172, 3174-3183
Data items	12	List and define all variables for which data will be sought (e.g., PICO items, funding sources), any pre-planned data assumptions and simplifications	<input checked="" type="checkbox"/>	<input type="checkbox"/>	3166-3172
Outcomes and prioritization	13	List and define all outcomes for which data will be sought, including prioritization of main and additional outcomes, with rationale	<input checked="" type="checkbox"/>	<input type="checkbox"/>	3189-3190
Risk of bias in individual studies	14	Describe anticipated methods for assessing risk of bias of individual studies, including whether this will be done at the outcome or study level, or both; state how this information will be used in data synthesis	<input checked="" type="checkbox"/>	<input type="checkbox"/>	3216-3229
DATA					

Section/topic	#	Checklist item	Information reported		Line number(s)
			Yes	No	
Synthesis	15a	Describe criteria under which study data will be quantitatively synthesized	<input checked="" type="checkbox"/>	<input type="checkbox"/>	3174-3214
	111	If data are appropriate for quantitative synthesis, describe planned summary measures, methods of handling data, and methods of combining data from studies, including any planned exploration of consistency (e.g., I^2 , Kendall's tau)	<input checked="" type="checkbox"/>	<input type="checkbox"/>	3174-3214
	112	Describe any proposed additional analyses (e.g., sensitivity or subgroup analyses, meta-regression)	<input checked="" type="checkbox"/>	<input type="checkbox"/>	3174-3214,3227-3229
	15d	If quantitative synthesis is not appropriate, describe the type of summary planned	<input checked="" type="checkbox"/>	<input type="checkbox"/>	858-860
Meta-bias(es)	16	Specify any planned assessment of meta-bias(es) (e.g., publication bias across studies, selective reporting within studies)	<input checked="" type="checkbox"/>	<input type="checkbox"/>	3225-3227, Table 7.4
Confidence in cumulative evidence	17	Describe how the strength of the body of evidence will be assessed (e.g., GRADE)	<input checked="" type="checkbox"/>	<input type="checkbox"/>	3227-3229

7.3.1.1. Search strategy

For the systematic review (**Section 2.2.1, Chapter 2**), a literature search was conducted using ScienceDirect, PubMed and Web of Science databases between 3 April 2020 and 23 April 2020 with no time limits [164]. The first set of keywords (flavonoid, flavone, flavonol, flavanol, anthocyanidin, polyphenol) was combined systematically using the Boolean operator AND with the second set (angiogenesis, antiangiogenic, proangiogenic, “cell migration”, “wound healing”) in all databases (**Table 7. 2**).

Table 7. 2. Search strategy used to conduct the systematic review on ScienceDirect, PubMed and Web of Science electronic databases

Database	Search Terms	Field	Limited to	Number of Items found
ScienceDirect	All possible combinations of 1 keyword from (flavonoid, flavone, flavonol, flavanol, anthocyanidin, polyphenol) AND	Title, abstract or author-specified keywords	Research articles, review articles, mini reviews and short communications	1277
PubMed	1 keyword from (angiogenesis, antiangiogenic,	Title/Abstract	Journal articles, meta-analysis, review and	1984

	proangiogenic, “cell migration”, “wound healing”)		systematic reviews	
Web of Science		Title	Article, review	119
				Total = 3380

With regards to the meta-analysis (**Section 2.2.2, Chapter 2**), the literature search was carried out using ScienceDirect, PubMed, Web of Science and Google Scholar databases between 8 June 2020 and 10 June 2020 with no time limits [164]. The first set of keywords, (flavonoid, flavone, flavonol, flavanol, anthocyanidin, polyphenol) was combined systematically using the Boolean operator AND with the second set, (angiogenesis, “chick chorioallantoic membrane”, “in vivo angiogenesis”) in all databases (**Table 7. 3**).

Table 7. 3. Search strategy used to conduct the meta-analysis on ScienceDirect, PubMed, Web of Science and Google Scholar electronic databases

Database	Search Terms	Field	Limited to	Number of Items found
ScienceDirect	All possible combinations of 1 keyword from (flavonoid, flavone, flavonol, flavanol, anthocyanidin, polyphenol) AND 1 keyword from (angiogenesis, “Chick Chorioallantoic Membrane”, “in vivo angiogenesis”)	Title, abstract or author-specified keywords	Research articles, review articles, mini reviews and short communications	347
PubMed		Title/Abstract	Journal articles, meta-analysis, review and systematic reviews	495
Web of Science		Title	Article, review	38
Google Scholar		allintitle	Articles	17
				Total = 897

7.3.1.2. Inclusion and exclusion criteria

Studies were included in the systematic review search if they met the following eligibility criteria:

- (i) Natural or synthetic flavonoids
- (ii) *In vitro*, *in vivo* and/or *ex vivo* angiogenesis assays
- (iii) Focus on cancer, diabetes, bone regeneration or eye diseases.

For the meta-analysis, the inclusion criteria were:

- (i) Natural or synthetic flavonoids
- (ii) *In vivo* CAM angiogenesis assays.

Articles not written in English and/or focusing on chalcones, plant extracts/total flavonoids content, combination of compounds, nanoformulations, prodrugs, neurological disorders or cardiovascular diseases were excluded from both searches.

7.3.1.3. Data extraction

In both cases of the systematic review and meta-analysis, articles' titles and abstracts were initially screened based on relevance and inclusion/exclusion criteria. Full texts were checked in some cases when abstracts failed to provide a detailed description. Eligible articles were retrieved and data extracted into a specially designed form on Microsoft Excel 2016. For the systematic review, data was extracted from 402 research and review articles and included title, publication type, year of publication, flavonoid, disease of focus and conducted *in vitro* and/or *in/ex vivo* angiogenesis assays. The second set of data was extracted for the meta-analysis study from 25 research articles and included title, year of publication, flavonoid, angiogenesis promotor, cancer cell line, concentration, time and duration of flavonoid treatment, results representation and number of CAMs used for each test concentration (n).

7.3.1.4. Data analysis

The data analysis for the systematic review was performed using Microsoft Excel 2016. Initially, the data was entered into a table using the aforementioned extracted attributes as column headers. In order to enhance data visualization and analysis, distinct color-coded slicers were added. Subsequently, the filter functionality inside the generated slicers was employed to exclusively display the data pertaining to the present field of investigation, (e.g. *in vivo* studies throughout the years 2013 to 2017). The filter function was employed once again to methodically choose items lying under each distinct category. The quantity of investigations was thereafter counted and recorded in distinct tables designated for each type of analysis. Ultimately, the data was represented utilizing the suitable Excel chart.

For the meta-analysis, the study characteristics mentioned in the preceding section were extracted in a tabular form. Final concentrations of flavonoids reported in μM were used without additional computations. The concentrations reported in mg/mL were converted to μM using the equation:

$$\text{Concentration } (\mu\text{M}) = [\text{Concentration } (\text{mg/mL}) / \text{molecular weight } (\text{mg/mmol})] \times 10^6$$

The outcome measure selected for set 1 of this study was the comparison of means of the number of blood vessels in a CAM relative to the control. The results expressed as a ratio to control were used in their reported form. Results reported as number of new blood vessels in treatment CAM, were divided by the number of blood vessels of control as extracted from the study. Studies conducted by Gacche *et al* quantified their findings using the equation $(1-T/C)$ where T denoted the number of vessels observed in the sample and C the number of vessels in the control [180–182]. In this instance, the outcome that was documented was deducted from 1 in order to transform the data into a representation of the number of blood vessels in relation to the control. Ultimately, the outcomes, which were expressed as percentages relative to the control group, were converted into ratios by dividing them by 100. For studies reporting standard deviation (SD), the standard error of means (SEM) was calculated by dividing SD by the square root of the corresponding study sample size. The aforementioned calculations were performed using Microsoft Excel 2016. Forest plots were generated using Review Manager (RevMan) Version 5.1 (The Nordic Cochrane Centre, The Cochrane Collaboration, Copenhagen, Denmark). The studies that were incorporated into the analysis were identified by their study ID, which consists of the lead author's name and the year of publication for Cochrane reviews. The previously calculated values for the number of vessels relative to control and SEM of each study were added into RevMan in the log scale in accordance with the Cochrane guidelines [210]. Studies were categorized according to the flavonoids' subclasses and pool effect size was expressed as means ratio with 95% confidence interval (CI) as calculated by the inverse variance (IV) method. The random effects model was used because it accounts for between study variability. Heterogeneity was assessed using Higgins' I^2 measure, which was automatically calculated by RevMan. Details on the integrated calculations and equations used by

RevMan are indicated in the Cochrane Handbook for Systematic Reviews of Interventions [210].

7.3.1.5. Quality assessment

The methodological quality and RoB of the studies included in the meta-analysis were evaluated via a specifically designed novel checklist (**Table 7. 4**). The robustness of the meta-analysis findings of set 1 was additionally verified by a sensitivity analysis. The checklist presented combines the relevant criteria derived from established prestructured tools and technical aspects that have the potential to influence the quality of the CAM assay [167–169,171,209]. The highlighted elements in **Table 7. 4** were considered critical for a high-quality CAM test, hence, studies from set 1 that did not adhere to any of these critical criteria underwent additional examination in the sensitivity analysis, provided they present a low RoB. The sensitivity analysis was applied to evaluate the effect of each flavonoid on summary effect size. It is based on the sequential removal of one study at a time (**Tables 3-5, Appendix A**). For set 2, studies that failed to comply with the critical criteria were excluded from the results.

Studies were considered of high RoB if they either failed to report ≥ 2 of RoB criteria, failed to report ≥ 1 of RoB criteria and were unclear ≥ 2 of RoB criteria or were unclear ≥ 3 of RoB criteria.

Table 7. 4. CAM assay methodological quality and risk of bias assessment checklist

Criteria	Question	Notes	SYRCLE [207]	Cochrane Risk of Bias [202]	ToxRTool [203]	CONSORT [208]	OHAT [204]	
Study design	Were experimental conditions reported?				+			
	Was the time between shell opening and addition of test substance ≥ 3 days? [169,171] OR Were negative controls included? [171,209]	Provides time to check for any inflammatory reaction resulting from the shell opening Ensures experimental conditions does not cause CAM irritation and provides a common baseline for all interventions			+		+	
	Was the method of test substance application described?				+			
	Is the full data on dose/concentration of test substance given?				+			
	Is the time between tumor implantation and vessel quantification ≥ 72 h? (set 2) [168,171]	Tumors vascular infiltration starts 72 h after implantation						
	Was an inert substance carrier used? [167,169,171]	Irregular carriers like filter paper can cause inflammation and angiogenesis						
	Was the experiment carried out before day 18? (set 2) [168,169]	CAM lacks a fully development immune system until day 18 which avoids immune reactions that can trigger angiogenesis. Additionally, this helps the implanted cells in preserving their						

		immunogenic characteristics					
	Were positive controls (reference standard) included? [171,209]					+	+
	Is the sample size reasonable (≥ 3 eggs/intervention)? [209]					+	
Data collection	Was the quantification process carried out between days 10-15? (set 2) [168]	CAM neovascularization decreases between days 10-15 making it easier to distinguish between pre-existing CAM and tumor vasculature					
	Were two independent observers used to count blood vessels? [169]	Increases the ability to differentiate between pre-existing vessels and those newly formed	+	+		+	+
	Was the quantification method described? [168,171]					+	
	Are the statistical methods for data analysis given?					+	
Risk of bias	Was there a similar baseline for the different intervention groups? (age of CAMs was the same)		+				
	Was the quantification carried out in a blinded manner?		+	+		+	+
	Were the full results reported?		+	+			+
	Was there any form of selective outcome reporting?		+	+			
	Were there any conflicts of interest declared?		+	+			

Criteria in red color are of critical importance; +, item included in checklist

7.3.2. Chemistry

7.3.2.1. Structural characterization

^1H NMR and ^{13}C NMR chemical shifts (δ) were recorded in either deuterated chloroform (CDCl_3) or deuterated dimethyl sulfoxide ($\text{DMSO-}d_6$) and reported as parts per million (ppm) values relative to tetramethylsilane (TMS) as an internal standard. Coupling constants (J) are reported in Hertz (Hz) and multiplicities are reported as follows: s (singlet), d (doublet) or m (multiplet).

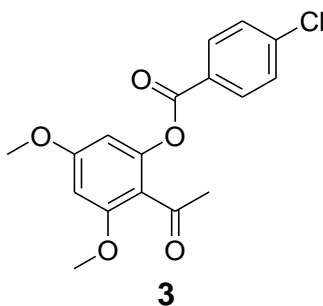
IR absorptions are quoted in wavenumbers [cm^{-1}]. The symbol ν indicate stretching vibrations and band intensities are classified as w, weak; m, medium; s, strong; br, broad.

HPLC was used to determine the purity of final compounds at $\lambda=258$ nm, using a gradient of 1.0 mL/min flowrate; 20 min gradient of 1% acetic acid in acetonitrile [organic mobile phase (A)] and 1% acetic acid in water [aqueous mobile phase (B)] from 5% A at 0 min, 20% A at 2 min, 40% A at 6 min, 60% A at 8 min, 95% A at 10 min, 5% A at 20 min. Purity is reported as percentage area.

7.3.2.2. Synthesis

7.3.2.2.1. Synthesis of 4-oxo/thioflavones (7-14) [219]

Synthesis of 2-Acetyl-3,5-dimethoxyphenyl 4-chlorobenzoate (3)

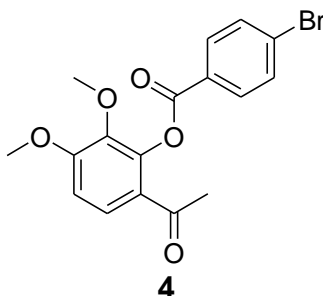


1-(2-Hydroxy-4, 6-dimethoxyphenyl) ethanone (1.96 g, 10 mmol) was dissolved in anhydrous pyridine (6 mL) and heated to 50 °C. DBU (0.06 mL, 1% v/v of pyridine) was added to the mixture and the solution was stirred at 50 °C for 30 min. 4-Chlorobenzoyl chloride (7.9 mL, 15 mmol, 1.5 eq.) was added slowly over 15 min, the mixture was then heated to 75 °C and stirred for 2 h. The reaction was cooled to room temperature, acidified to pH 5 with 2 M HCl and extracted with EtOAc (2 x 20 mL). The organic layers were

combined, dried over anhydrous magnesium sulfate and concentrated *in vacuo* to yield the crude product. The pure compound was obtained as a white solid after purification by column chromatography [Hexane:CHCl₃:EtOAc (6:3:1 v/v/v)].

Yield: 98%; **m.p.:** 112-114 °C (lit.[219] 124-126 °C); **¹H NMR:** (CDCl₃, 400 MHz) δ 2.47 (3H, s, CH₃), 3.83 (3H, s, -OCH₃), 3.87 (3H, s, -OCH₃), 6.35 (1H, s, H-4), 6.41 (1H, s, H-6), 7.45 (2H, d, *J* = 8 Hz, H-3',5'), 8.06 (2H, d, *J* = 8 Hz, H-2',6'); **¹³C NMR:** (CDCl₃, 100 MHz) δ 31.98 (-CH₃), 55.69 (-OCH₃), 55.95 (-OCH₃), 96.76 (C6), 100.11 (C4), 117.06 (C2), 127.71 (C1'), 128.95 (C3', C5'), 131.67 (C2', C6'), 140.19 (C4'), 149.79 (C1), 159.38 (C5), 162.34 (C3), 164.26 (COO-Ar), 199.16 (COCH₃); **IR v_{max} [cm⁻¹]:** 1684 (C=O, v, s), 1609 (C=O, v, m), 1251 (-OCH₃, v, s), 1113 (O-C=O, s, m); **m/z (FTMS+ESI):** [M+H]⁺ (C₁₇H₁₆O₅³⁵Cl) requires 335.0681, found 335.0672.

Synthesis of 6-Acetyl-2,3-dimethoxyphenyl 4-bromobenzoate (4)

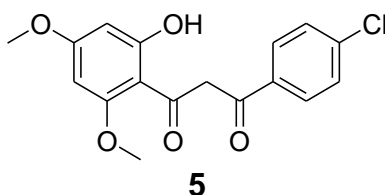


[1-(2-Hydroxy-3, 4-dimethoxyphenyl) ethanone] (1.96 g, 10 mmol) was dissolved in anhydrous pyridine (6 mL) and heated to 50 °C. DBU (0.06 mL, 1% v/v of pyridine) was added to the mixture and the solution was stirred at 50 °C for 30 min. 4-Bromobenzoyl chloride (3.3 g, 15 mmol, 1.5 eq.) was added slowly over 15 min, the mixture was then heated to 75 °C and stirred for 2 h. The reaction was cooled to room temperature, acidified to pH 5 with 2 M HCl and extracted with EtOAc (2 x 20 mL). The organic layers were combined, dried over anhydrous magnesium sulfate and concentrated *in vacuo* to yield the crude product. The pure compound was obtained as a white solid after purification by column chromatography [Hexane:CHCl₃:EtOAc (5:4:1 v/v/v)].

Yield: 97%; **m.p.:** 101-102 °C (lit.[219] 117-119 °C); **¹H NMR:** (CDCl₃, 400 MHz) δ 2.48 (3H, s, -CH₃), 3.81 (3H, s, -OCH₃), 3.95 (3H, s, -OCH₃), 6.88 (1H, d, *J* = 8 Hz, H-4), 7.67 (1H, d, *J* = 8 Hz, H-5), 7.98 (2H, d, *J* = 8 Hz, H-3',5'), 8.08 (2H, d, *J* = 8 Hz, H-2',6'); **¹³C**

NMR: (CDCl₃, 100 MHz) δ 29.53 (CH₃), 56.20 (-OCH₃), 61.01 (- OCH₃), 109.18 (C4), 124.38 (C6), 126.16 (C5), 128.18 (C4'), 128.99 (C1'), 131.87 (C3', C5'), 132.06 (C2', C6'), 141.58 (C2), 144.14 (C1), 157.27 (C3), 164.10 (COO-Ar), 195.66 (COCH₃); **IR** ν_{\max} [cm⁻¹]: 1726 (C=O, v, s), 1670 (C=O, v, s), 1263 (-OCH₃, v, s), 1094 (O-C=O, v, m); **m/z** (**FTMS+ESI**): [M+H]⁺ (C₁₇H₁₆O₅⁷⁹Br) requires 379.0176, found 379.0171.

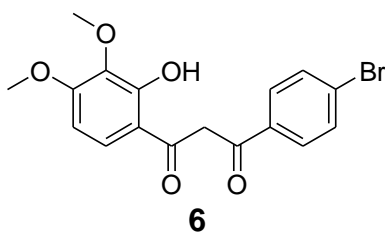
Synthesis of 1-(4-Chlorophenyl)-3-(2-hydroxy-4,6-dimethoxyphenyl) propane-1,3- dione (5)



The 2-acetyl-3, 5-dimethoxyphenyl 4-chlorobenzoate (**3**) (3.4 g, 10 mmol) was dissolved in anhydrous pyridine (40 mL) and heated to 50 °C for 1 h. Powdered anhydrous KOH (1.12 g, 20 mmol, 2 eq.) was added to the solution and the mixture was heated to 75 °C. After 90 min, the reaction mixture was cooled to room temperature, acidified to pH 5 with 2 M HCl and extracted with EtOAc (2 x 20 mL). The organic layers were combined, dried over anhydrous magnesium sulfate and concentrated *in vacuo* to yield the crude 1,3-diketone. The crude product was washed with glacial acetic acid to obtain compound (**5**) as a yellow solid which was used in the next step without further purification.

Yield: 80%; **¹H NMR:** (CDCl₃, 400 MHz) [The compound exists as a mixture of keto-enol tautomers] δ 3.47 (3H, s, -OCH₃), 3.88 (3H, s, -OCH₃), 4.68 (2H, s, CH₂), 6.10 (1H, s, H-5), 6.20 (1H, s, H-3), 7.20 (1H, s, -CH of enol form), 7.63 (2H, d, *J* = 8 Hz, H-3',5'), 7.99 (2H, d, *J* = 8 Hz, H-2',6'), 13.24 (1H, s, OH), 13.65 (1H, s, OH of enol form).

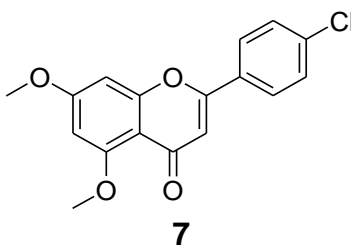
Synthesis of 1-(4-Bromophenyl)-3-(2-hydroxy-3,4-dimethoxyphenyl) propane-1,3- dione (6)



The 6-acetyl-2, 3-dimethoxyphenyl 4-bromobenzoate (**4**) (3.8 g, 10 mmol) was dissolved in anhydrous pyridine (40 mL) and heated to 50 °C for 1 h. Powdered anhydrous KOH (1.12 g, 20 mmol, 2 eq.) was added to the solution and the mixture was heated to 75 °C. After 90 min, the reaction mixture was cooled to room temperature, acidified to pH 5 with 2 M HCl and extracted with EtOAc (2 x 20 mL). The organic layers were combined, dried over anhydrous magnesium sulfate and concentrated *in vacuo* to yield the crude 1,3-diketone. The crude product was washed with glacial acetic acid to obtain compound (**6**) as a yellow solid which was used in the next step without further purification.

Yield: 87%; **¹H NMR:** (CDCl₃, 400 MHz) [The compound exists as a mixture of keto-enol tautomers] δ 3.92 (3H, s, -OCH₃), 3.94 (2H, s, CH₂), 3.95 (3H, s, -OCH₃), 6.52 (1H, d, *J* = 9 Hz, H-5), 6.71 (1H, =CH of enol form), 7.53 (1H, d, *J* = 9 Hz, H-6), 7.61 (2H, d, *J* = 8 Hz, H-3',5'), 7.78 (2H, d, *J* = 8 Hz, H-2',6'), 12.26 (1H, s, OH), 12.56 (1H, s, OH of enol form).

Synthesis of 2-(4-Chlorophenyl)-5,7-dimethoxy-4H-chromen-4-one (7)

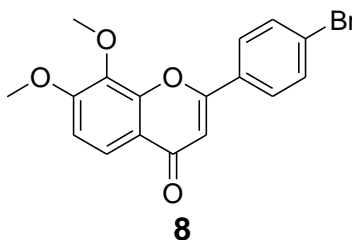


1-(4-Chlorophenyl)-3-(2-hydroxy-4,6-dimethoxyphenyl) propane-1,3- dione (**5**) (2 g, 6 mmol) was dissolved in acetic acid (18 mL) and heated to 90 °C for 1 h. Concentrated sulfuric acid (0.18 mL, 1% v/v of acetic acid) was added to the solution and the mixture was heated at 110 °C for 90 min. The reaction mixture was cooled to room temperature, diluted with deionized water (30 mL) and the organic layer was extracted with EtOAc (2 x 20 mL). The organic layers were combined, dried over anhydrous magnesium sulfate and concentrated *in vacuo* to obtain the crude product. The pure compound was obtained as a white solid after purification by column chromatography [EtOAc (100%) followed by 5% MeOH in EtOAc].

Yield: 77%; **m.p:** 174-175 °C (lit.[219] 188-192 °C); **¹H NMR:** (CDCl₃, 400 MHz) δ 3.91 (3H, s, -OCH₃), 3.95 (3H, s, -OCH₃), 6.37 (1H, s, H-6), 6.55 (1H, s, H-8), 6.64 (1H, s, H-

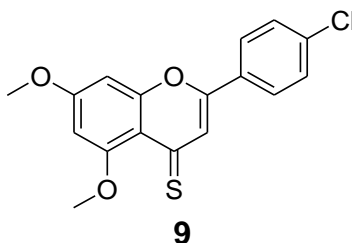
3), 7.45 (2H, d, $J = 8$ Hz, H-2',6'), 7.78 (2H, d, $J = 8$ Hz, H-3',5'); ^{13}C NMR: (CDCl_3 , 100 MHz) δ 55.79 (-OCH₃), 56.43 (-OCH₃), 92.79 (C8), 96.26 (C6), 109.14 (C3), 127.17 (C3',5',1'), 129.23 (C2', C6'), 129.97 (C10), 137.36 (C4'), 159.47 (C9), 159.78 (C5), 160.91 (C2), 164.16 (C7), 177.38 (C=O); IR ν_{max} [cm^{-1}]: 1673 (C=O, v, s), 1175 (-OCH₃, v, m), 1110 (C-O, v, m); m/z (FTMS+ESI): $[\text{M}+\text{H}]^+$ ($\text{C}_{17}\text{H}_{14}\text{O}_4^{35}\text{Cl}$) requires 317.0575, found 317.0573. HPLC Purity: >96.4% ($R_t = 13.19$ min).

Synthesis of 2-(4-Bromophenyl)-7,8-dimethoxy-4H-chromen-4-one (8)



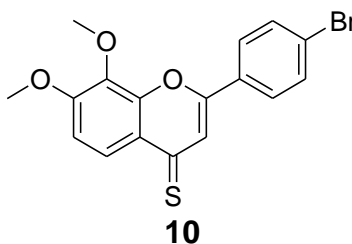
1-(4-Bromophenyl)-3-(2-hydroxy-3,4-dimethoxyphenyl) propane-1,3- dione (**6**) (2.3 g, 6 mmol) was dissolved in acetic acid (18 mL) and heated to 90 °C for 1 h. Concentrated sulfuric acid (0.18 mL, 1% v/v of acetic acid) was added to the solution and the mixture was heated at 110 °C for 90 min. The reaction mixture was cooled to room temperature, diluted with deionized water (30 mL) and the organic layer was extracted with EtOAc (2 x 20 mL). The organic layers were combined, dried over anhydrous magnesium sulfate and concentrated *in vacuo* to obtain the crude product. The pure compound was obtained as a white solid after purification by column chromatography [CHCl_3 :Hexane:EtOAc (5:3:2 v/v/v)].

Yield: 88%; **m.p.:** 198-198.5 °C (lit.[219] 197-199 °C); ^1H NMR: (CDCl_3 , 400 MHz) δ 4.01 (3H, s, -OCH₃), 4.03 (3H, s, -OCH₃), 6.75 (1H, s, H-3), 7.05 (1H, d, $J = 9$ Hz, H-6), 7.66 (2H, d, $J = 8$ Hz, H-2',6'), 7.81 (2H, d, $J = 8$ Hz, H-3',5'), 7.95 (1H, d, $J = 9$ Hz, H-5); ^{13}C NMR: (CDCl_3 , 100 MHz) δ 56.47 (-OCH₃), 61.63 (-OCH₃), 107.06 (C3), 110.06 (C6), 118.62 (C10), 121.12 (C5), 126.24 (C4'), 127.65 (C2', C6'), 130.93 (C1), 132.40 (C3', C5'), 136.97 (C8), 150.52 (C9), 156.82 (C7), 161.95 (C2), 177.95 (C=O); IR ν_{max} [cm^{-1}]: 1641 (C=O, v, m), 1288 (-OCH₃, v, s) 1093 (C-O, v, m); m/z (FTMS+ESI): $[\text{M}+\text{H}]^+$ ($\text{C}_{17}\text{H}_{14}\text{O}_4^{79}\text{Br}$) requires 361.0070, found 361.0066. HPLC Purity: >99.4% ($R_t = 13.59$ min)

Synthesis of 2-(4-Chlorophenyl)-5,7-dimethoxy-4H-chromene-4-thione (**9**)

2-(4-Chlorophenyl)-5,7-dimethoxy-4H-chromen-4-one (**7**) (316.74 mg, 1 mmol) was dissolved in anhydrous toluene (1.5 mL), and Lawesson's reagent (404.47 mg, 1 mmol, 1 eq.) was added to the solution and the mixture was heated to 110 °C for 4 h. The reaction mixture was cooled to room temperature and concentrated *in vacuo*. The pure compound was obtained as a green solid after purification by column chromatography [CHCl₃ (100%)].

Yield: 77%; **m.p:** 173.1-173.8 °C (lit.[219] 170-172 °C); **¹H NMR:** (CDCl₃, 400 MHz) δ 3.91 (3H, s, -OCH₃), 3.93 (3H, s, -OCH₃), 6.40 (1H, d, *J* = 2 Hz, H-6), 6.55 (1H, d, *J* = 2 Hz, H-8), 7.44 (2H, d, *J* = 8 Hz, H-2',6'), 7.48 (1H, s, H-3), 7.81 (2H, d, *J* = 8.5 Hz, H-3',5'); **¹³C NMR:** (CDCl₃, 100 MHz) δ 55.87 (-OCH₃), 55.89 (-OCH₃), 92.73 (C8), 96.90 (C6), 117.83 (C10), 122.30 (C3), 127.30 (C2', 6'), 129.30 (C3', 5'), 129.48 (C1'), 137.44 (C4'), 148.49 (C2), 155.59 (C9), 161.56 (C7), 163.94 (C5), 200.36 (C=S); **IR v_{max} [cm⁻¹]:** 1295 (C=S, v, s), 1091 (-OCH₃, v, m), 1044 (C-O, v, s); ***m/z* (FTMS+ESI):** [M+H]⁺ (C₁₇H₁₄O₃³⁵ClS) requires 333.0347 found 333.0344. HPLC Purity: >93.5 % (R_t= 14.22 min).

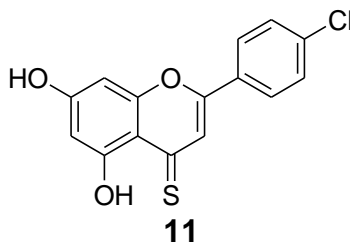
Synthesis of 2-(4-Bromophenyl)-7,8-dimethoxy-4H-chromene-4-thione (**10**)

2-(4-Bromophenyl)-7,8-dimethoxy-4H-chromen-4-one (**8**) (361.19 mg, 1 mmol) was dissolved in anhydrous toluene (1.5 mL), and Lawesson's reagent (404.47 mg, 1 mmol, 1 eq.) was added to the solution and the mixture was heated to 110 °C for 4 h. The

reaction mixture was cooled to room temperature and concentrated *in vacuo*. The pure compound was obtained as an orange solid after purification by column chromatography [CHCl_3 (100%)].

Yield: 88%; **m.p.:** 214-216 °C (lit.[219] 216-218 °C); **$^1\text{H NMR}$:** (CDCl_3 , 400 MHz) δ 4.02 (3H, s, $-\text{OCH}_3$), 4.03 (3H, s, $-\text{OCH}_3$), 7.07 (1H, d, $J = 9.5$ Hz, H-6), 7.66 (1H, s, H-3), 7.67 (2H, d, $J = 8.5$ Hz, H-2',6'), 7.87 (2H, d, $J = 8$ Hz, H-3',5'), 8.33 (1H, d, $J = 9$ Hz, H-5); **$^{13}\text{C NMR}$:** (CDCl_3 , 100 MHz) δ 56.54 ($-\text{OCH}_3$), 61.74 ($-\text{OCH}_3$), 111.14 (C6), 119.08 (C3), 124.19 (C5, C10), 125.52 (C4'), 126.56 (C1'), 127.88 (C2', C6'), 132.59 (C3', C5'), 137.27 (C8), 145.90 (C9), 152.41 (C7), 157.39 (C2), 201.33 (C=S); **IR ν_{max} [cm^{-1}]:** 1288 (C=S, v, s), 1091 ($-\text{OCH}_3$, v, m), 1040 (C-O, v, s); **m/z (FTMS+ESI):** $[\text{M}+\text{H}]^+$ ($\text{C}_{17}\text{H}_{14}\text{O}_3^{79}\text{BrS}$) requires 376.9842, found 376.9840. HPLC Purity: >92.3% ($R_t = 13.36$ min).

Synthesis of 2-(4-Chlorophenyl)-5,7-dihydroxy-4H-chromene-4-thione (11)

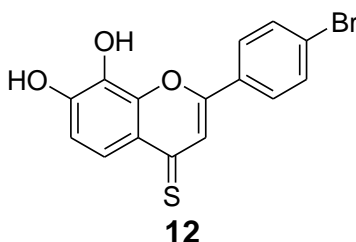


2-(4-Chlorophenyl)-5,7-dimethoxy-4H-chromene-4-thione (**9**) (166.4 mg, 0.5 mmol) was dissolved in anhydrous DCM (1 mL). 1 M BBr_3 in anhydrous DCM (2.5 mL, 2.5 mmol) was added to the solution and the mixture was stirred at 30 °C for 4 h. The reaction mixture was cooled to room temperature and diluted with deionized water (50 mL). The pH was adjusted to 6 with 5% Na_2HPO_4 and the organic layer was extracted with EtOAc (2 x 10 mL). The organic layers were combined, dried over anhydrous magnesium sulfate and concentrated *in vacuo* to obtain the crude product. The pure compound was obtained as a bright yellow solid after purification by column chromatography [CHCl_3 :Hexane:EtOAc (8:1:1) v/v/v].

Yield: 64%; **m.p.:** 247.7-248 °C (lit.[219] 249-252 °C); **$^1\text{H NMR}$:** ($\text{DMSO}-d_6$, 400 MHz) δ 6.28 (1H, s, H-6), 6.55 (1H, s, H-8), 7.55 (1H, s, H-3), 7.58 (2H, d, $J = 8$ Hz, H-2',6'), 8.11 (2H, d, $J = 8$ Hz, H-3',5'), 11.24 (1H, s, OH), 13.54 (1H, s, OH); **$^{13}\text{C NMR}$:** ($\text{DMSO}-d_6$, 100 MHz) δ 95.28 (C8), 101.30 (C6), 113.13 (C10), 118.00 (C3), 129.84 (C1', 3', 5'),

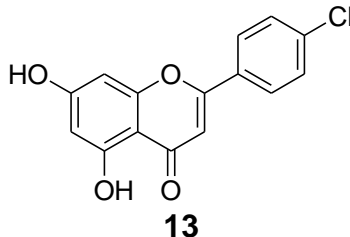
129.84 (C2', C6'), 137.63 (C4'), 153.62 (C2), 154.55(C9), 162.32 (C7), 165.19 (C5), 196.52 (C=S); IR ν_{\max} [cm^{-1}]: 3358 (OH, w, b), 1170 (C=S, v, m), 1135(c-O, v, m); **m/z (FTMS+ESI)**: $[\text{M}+\text{H}]^+$ ($\text{C}_{15}\text{H}_{10}\text{O}_3^{35}\text{ClS}$) requires 305.0034, found 305.0034. HPLC Purity: >98.6% (R_t = 14.17 min)

Synthesis of 2-(4-Bromophenyl)-7,8-dihydroxy-4H-chromene-4-thione (12)



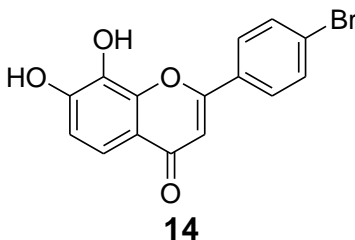
2-(4-Bromophenyl)-7,8-dimethoxy-4H-chromene-4-thione (**10**) (188.62 mg, 0.5 mmol) was dissolved in anhydrous DCM (1 mL). 1 M BBr_3 in anhydrous DCM (2.5 mL, 2.5 mmol) was added to the solution and the mixture was stirred at 30 °C for 4 h. The reaction mixture was cooled to room temperature and diluted with deionized water (50 mL). The pH was adjusted to 6 with 5% Na_2HPO_4 and the organic layer was extracted with EtOAc (2 x 10 mL). The organic layers were combined, dried over anhydrous magnesium sulfate and concentrated *in vacuo* to obtain the crude product. The pure compound was obtained as an orange solid after purification by column chromatography [EtOAc (100%)].

Yield: 85%; **m.p.:** 223.8-224 °C (lit.[219] 235-237 °C); **$^1\text{H NMR}$:** (DMSO- d_6 , 400 MHz) δ 6.98 (1H, d, J = 8.5 Hz, H-6), 7.70 (1H, s, H-3), 7.74 (2H, d, J = 8 Hz, H-2',6'), 7.77 (2H, d, J = 9 Hz, H-3',5'), 8.12 (1H, d, J = 8.5 Hz, H-5), 9.62 (1H, s, OH), 10.57 (1H, s, OH); **$^{13}\text{C NMR}$:** (DMSO- d_6 , 100 MHz) δ 116.23 (C6), 118.25 (C4'), 119.00 (C3), 124.44 (C5), 126.14 (C10), 129.22 (C2', C6'), 130.54 (C1'), 132.69 (C3', C5'), 133.53 (C8), 142.85 (C7), 152.27 (C9), 152.69 (C2), 200.36 (C=S); IR ν_{\max} [cm^{-1}]: 3501 (OH, v, s), 1279 (C=S, v, s), 1174 (C-O, v, m); **m/z (FTMS+ESI)**: $[\text{M}+\text{H}]^+$ ($\text{C}_{15}\text{H}_{10}\text{O}_3^{79}\text{BrS}$) requires 348.9529, found 348.9529. HPLC Purity: >90.5% (R_t = 13.01 min).

Synthesis of 2-(4-Chlorophenyl)-5,7-dihydroxy-4H-chromen-4-one (**13**)

2-(4-Chlorophenyl)-5,7-dimethoxy-4H-chromen-4-one (**7**) (316.74 mg, 1 mmol) was dissolved in anhydrous DCM (1.5 mL). 1 M BBr₃ in anhydrous DCM (5 mL, 5 mmol) was added to the solution and the mixture was stirred at 40 °C overnight. The reaction mixture was cooled to room temperature and diluted with deionized water (50 mL). The pH was adjusted to 6 with 5% Na₂HPO₄ and the organic layer was extracted with EtOAc (2 x 10 mL). The organic layers were combined, dried over anhydrous magnesium sulfate and concentrated *in vacuo* to obtain the crude product. The pure compound was obtained as a pale yellow solid after purification by column chromatography [EtOAc (100%)].

Yield: 97%; **m.p:** 250 °C (lit.[219] 294-296 °C); **¹H NMR:** (DMSO- *d*₆, 400 MHz) δ 6.29 (1H, s, H-6), 6.59 (1H, s, H-8), 7.08 (1H, s, H-3), 7.62 (2H, d, *J* = 8.5 Hz, H-2',6'), 7.99 (2H, d, *J* = 8.5 Hz, H-3',5'), 12.20 (1H, s, OH), 12.84 (1H, s, OH); **¹³C NMR:** (DMSO- *d*₆, 100 MHz) δ 93.98 (C8), 99.04 (C6), 105.51 (C3, C10), 128.22 (C1'), 128.70 (C3', C5'), 129.18 (C2', C6'), 131.93 (C4'), 157.36 (C9), 161.39 (C5), 161.94 (C2), 166.41 (C7), 181.83 (C=O); **IR ν_{max} [cm⁻¹]:** 3350 (OH, w, b), 1680 (C=O, v, m), 1091 (C-O, v, s); ***m/z* (FTMS+ESI):** [M+H]⁺ (C₁₅H₁₀O₄³⁵Cl) requires 289.0262, found 289.0260. HPLC Purity: >99.4% (R_t= 13.06 min).

Synthesis of 2-(4-Bromophenyl)-7,8-dihydroxy-4H-chromen-4-one (**14**)

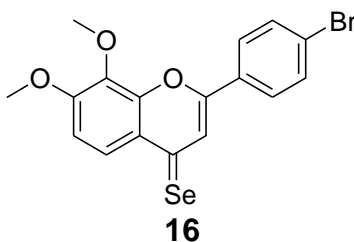
2-(4-Bromophenyl)-7,8-dimethoxy-4H-chromen-4-one (**8**) (361.19 mg, 1 mmol) was dissolved in anhydrous DCM (1.5 mL). 1 M BBr₃ in anhydrous DCM (5 mL, 5 mmol) was

added to the solution and the mixture was stirred at 40 °C for 18 h. The reaction mixture was cooled to room temperature and diluted with deionized water (50 mL). The pH was adjusted to 6 with 5% Na₂HPO₄ and the organic layer was extracted with EtOAc (2 x 10 mL). The organic layers were combined, dried over anhydrous magnesium sulfate and concentrated *in vacuo* to obtain the crude product. The pure compound was obtained as a pale green solid after purification by column chromatography [EtOAc (100%)].

Yield: 60%; **m.p.:** 275-280 °C (lit.[219] 285-290 °C); **¹H NMR:** (DMSO- *d*₆, 400 MHz) δ 6.99 (1H, s, H-3), 7.00 (1H, d, *J* = 8.5 Hz, H-6), 7.44 (1H, d, *J* = 8.5 Hz, H-5), 7.84 (2H, d, *J* = 8 Hz, H-2',6'), 8.16 (2H, d, *J* = 8.5 Hz, H-3',5'); **¹³C NMR:** (DMSO- *d*₆, 100 MHz) δ 106.32 (C3), 114.10 (C6), 115.08 (C5), 116.84 (C10), 125.16 (C4'), 128.29 (C2', C6'), 130.70 (C1'), 131.98 (C3', C5'), 133.07 (C8), 146.50 (C9), 150.62 (C7), 160.61 (C2), 176.77 (C=O); **IR ν_{max} [cm⁻¹]:** 3365 (OH, w, b), 1618 (C=O, v, m), 1066 (C-O, v, s); ***m/z*** (**FTMS+ESI**): [M+H]⁺ (C₁₅H₁₀O₄⁷⁹Br) requires 332.9757, found 332.9754. HPLC Purity: >98.8% (R_t= 11.22 min).

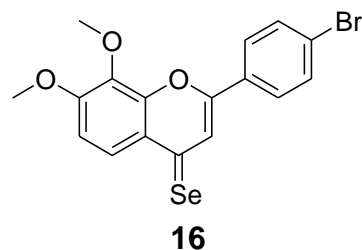
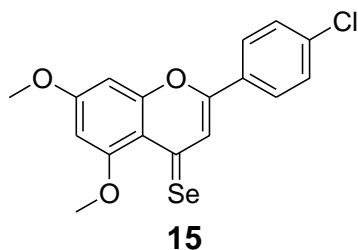
7.3.2.2.2. Attempted synthesis of 4-selenoflavones (15-18)

Microwave assisted synthesis of 2-(4-bromophenyl)-7,8-dimethoxy-4H-chromene-4-selenone (16)



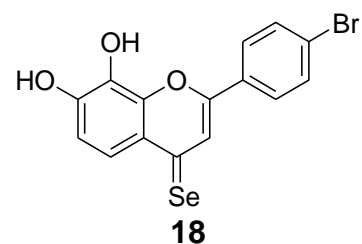
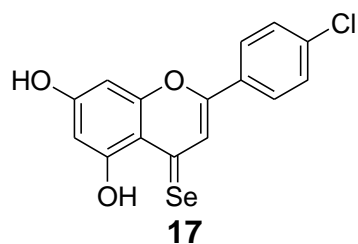
2-(4-Bromophenyl)-7,8-dimethoxy-4H-chromen-4-one (**8**) (50.4 mg, 140 μmol) was dissolved in anhydrous ACN (3 mL) in a sealed microwave vial. Woollin's reagent (30 mg, 56 μmol, 0.4 eq.) was added and the suspension was heated by microwave irradiation at 150 °C (MW power 175 W, 7 min). The solvent was evaporated *in vacuo* and the residue purified by column chromatography [100% DCM followed by 1:1 DCM:MeOH (v/v)].

General procedure using conventional heating for synthesis of 4-selenoflavones 2-(4-chlorophenyl)-5,7-dimethoxy-4H-chromene-4-selenone (15) and 2-(4-bromophenyl)-7,8-dimethoxy-4H-chromene-4-selenone (16)



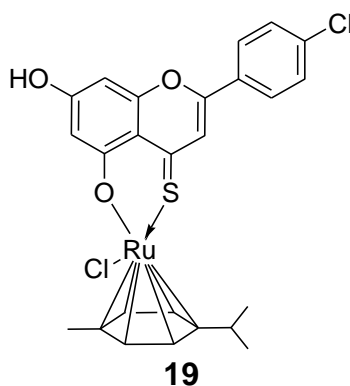
2-(4-Chlorophenyl)-5,7-dimethoxy-4H-chromen-4-one (**7**) (158.37 mg, 0.5 mmol) or 2-(4-bromophenyl)-7,8-dimethoxy-4H-chromen-4-one (**8**) (180.6 mg, 0.5 mmol) were dissolved in anhydrous toluene (1 mL). Woollin's reagent (213 mg, 0.4 mmol, 0.8 eq.) was added to the solution and heated at 130 °C for 4h. The solvent was evaporated *in vacuo* after the addition of a few mLs of CHCl_3 several times to help evaporate the toluene. The obtained residue was purified by column chromatography [100% DCM followed by 1:1 DCM:MeOH (v/v)].

Synthesis of subsequent compounds **17** and **18** was not possible due to unsuccessful synthesis of precursors **15** and **16**.



7.3.2.2.3. Synthesis of ruthenium and iridium metal complexes (19-26)

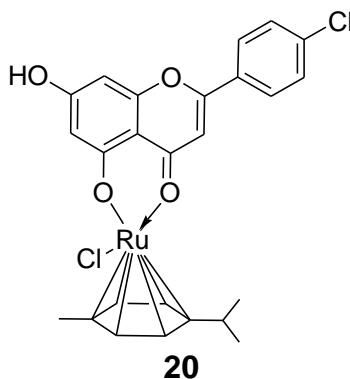
Synthesis of chlorido [(5-oxo- κO)-7-hydroxy-2-(4'-chlorophenyl)-4H-chromen-4-thionato- κO] (η^6 -*p*-cymene) ruthenium(II) (**19**)



A solution of NaOMe (28 mg, 0.525 mmol, 1.05 eq.) in anhydrous MeOH (10 mL) was added to 2-(4-chlorophenyl)-5,7-dihydroxy-4H-chromene-4-thione (**11**) (152.37 mg, 0.5 mmol) and the suspension was stirred at 50 °C for 30 min. $[\text{Ru}(\eta^6\text{-}p\text{-cymene})\text{Cl}_2]_2$ (303 mg, 0.495 mmol, 0.9 eq.) in anhydrous DCM (10 mL) was added to the reaction mixture and stirred at 75 °C overnight under argon atmosphere. The solvent was evaporated *in vacuo* and the residue was dissolved in warm $\text{CHCl}_3\text{:MeOH}$ (9:1) (15 mL) and filtered to remove any salts and impurities formed during the reaction. The filtrate was concentrated *in vacuo* to 2–3 mL and the product was precipitated by the addition of few drops of EtOAc. The formed precipitate was filtered, air dried and recrystallized from EtOAc: CHCl_3 (9:1) to give a dark reddish brown powder.

Yield: 46%; **m.p.:** >360 °C; **$^1\text{H NMR}$:** (DMSO- d_6 , 400 MHz) δ 1.16 (3H, s, CH_3 cym), 1.18 (3H, s, CH_3 cym), 2.26 (3H, s, CH_3 cym), 2.81–2.87 (1H, m, CH cym), 6.18 (1H, d, $J = 2.4$ Hz, H-6), 6.2 (1H, d, $J = 2.4$ Hz, H-8), 7.07 (2H, d, $J = 8.4$ Hz, H-2, 6 cym), 7.11 (2H, d, $J = 8.4$ Hz, H-3, 5 cym), 7.62 (1H, s, H-3), 7.64 (2H, d, $J = 8.8$ Hz, H-2', 6'), 8.11 (2H, d, $J = 8.8$ Hz, H-3', 5'), 10.57 (1H, s, OH); **$^{13}\text{C NMR}$:** (DMSO- d_6 , 100 MHz) δ 21.04 (CH_3 cym), 24.46 (2x CH_3 cym), 33.45 (CH cym), 93.00 (C8), 111.99 (C3), 126.56 (C1', 3', 5'), 128.49 (C4 cym), 129.28 (C2', 6'), 129.81 (C1 cym), 135.03 (C4'), 145.78 (C2); **IR ν_{max} [cm^{-1}]:** 3141 (OH, w, b), 1173 (C=S, v, m), 1088 (C–O, v, m); **m/z (FTMS+ESI):** M-Cl ($\text{C}_{25}\text{H}_{22}\text{O}_3\text{S}^{35}\text{ClRu}$) requires 539.0022, found 539.0062; **Elemental analysis:** $\text{C}_{25}\text{H}_{22}\text{O}_3\text{S}\text{Cl}_2\text{Ru}$, calculated: C, 52.27; H, 3.86; Ru, 17.59; found: C, 51.58; H, 3.85; Ru, 17.30 (% of C content is >0.4% due to the presence of traces of CHCl_3).

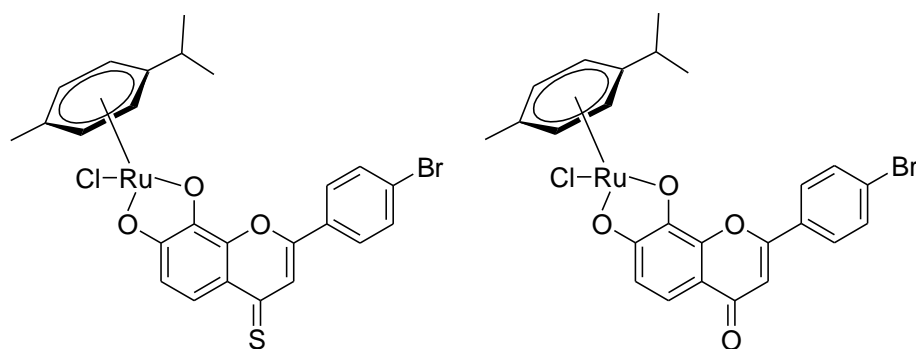
*Synthesis of chlorido [(5-oxo- κO)-7-hydroxy-2-(4'-chlorophenyl)-4H-chromen-4-onato- κO] (η^6 -*p*-cymene) ruthenium(II) (**20**)*

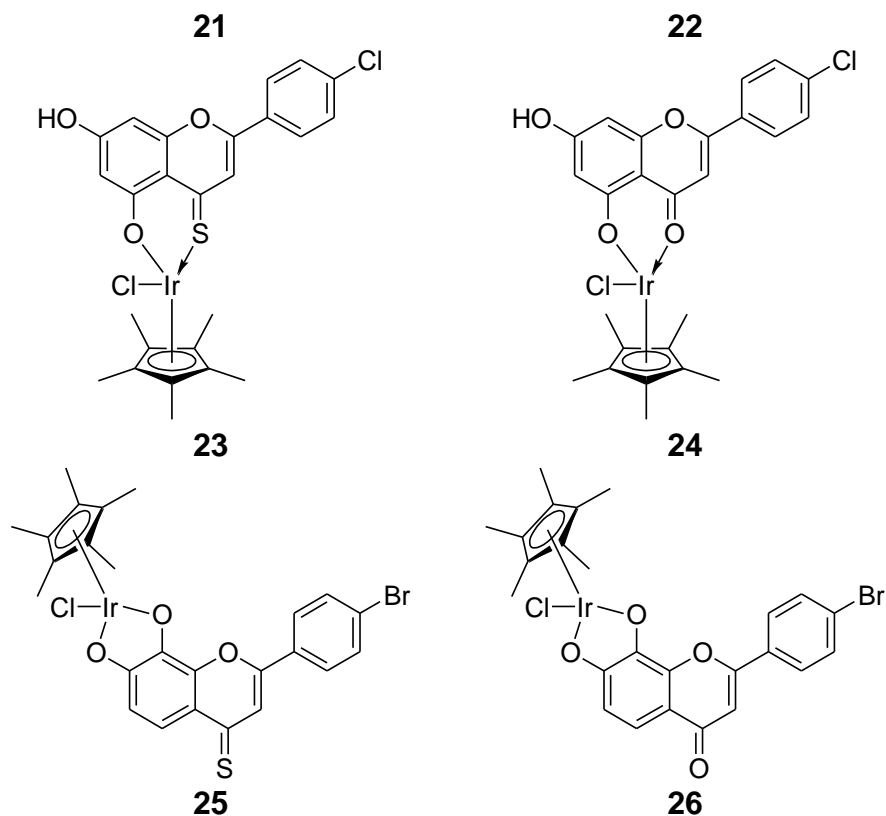


A solution of NaOMe (28 mg, 0.525 mmol, 1.05 eq.) in anhydrous MeOH (10 mL) was added to 2-(4-chlorophenyl)-5,7-dihydroxy-4H-chromen-4-one (**13**) (144 mg, 0.5 mmol) and the suspension was stirred at 50 °C for 30 min. $[\text{Ru}(\eta^6\text{-}p\text{-cymene})\text{Cl}_2]_2$ (168 mg, 0.275 mmol, 0.55 eq.) in anhydrous DCM (10 mL) was added to the reaction mixture and this was stirred at 75 °C overnight under an argon atmosphere. The solvent was evaporated *in vacuo* and the residue was dissolved in warm $\text{CHCl}_3\text{:MeOH}$ (9:1) (15 mL) and filtered to remove any salts and impurities formed during the reaction. The filtrate was concentrated *in vacuo* to 2–3 mL and the product was precipitated by the addition of few drops of EtOAc. The formed precipitate was filtered, air dried and recrystallized from EtOAc:ACN (9:1) to give a bright red powder.

Yield: 30%; **m.p.:** decompose 230 °C; **$^1\text{H NMR}$:** (DMSO- d_6 , 400 MHz) δ 1.29 (3H, d, J = 2.4 Hz, CH_3 cym), 1.30 (3H, d, J = 2 Hz, CH_3 cym), 2.17 (3H, s, CH_3 cym), 2.81–2.88 (1H, m, CH cym), 5.37 (2H, d, J = 7.2 Hz, H-2, 6 cym), 5.66 (2H, d, J = 7.2 Hz, H-3, 12ym), 5.99 (1H, d, J = 2.4 Hz, H-6), 6.05 (1H, d, J = 2 Hz, H-8), 7.00 (1H, s, H-3), 7.61 (2H, d, J = 8.4 Hz, H-2', 6'), 8.05 (2H, d, J = 8.4 Hz, H-3', 5'), 10.27 (1H, s, OH); **$^{13}\text{C NMR}$:** (DMSO- d_6 , 100 MHz) δ 17.92 (CH_3 cym), 22.52 (2x CH_3 cym), 30.89 (CH cym), 78.54 (C8), 82.86 (C6), 90.33 (C10), 97.08 (C3), 102.70 (C3, 5 cym), 106.34 (C2, 6 cym), 128.49 (C3', 5'), 129.68 (C2', 6'), 129.81 (C1, 4 cym), 158.58 (C2, 5), 168.09 (C7), 177.55 ($\text{C}=\text{O}$); **IR ν_{max} [cm^{-1}]:** 3231 (OH, w, b), 1633 ($\text{C}=\text{O}$, v, s), 1094 ($\text{C}-\text{O}$, v, s); **m/z (FTMS+ESI):** M-Cl ($\text{C}_{25}\text{H}_{22}\text{O}_4^{35}\text{ClRu}$) requires 523.0250, found 523.0233; **Elemental analysis:** $\text{C}_{25}\text{H}_{22}\text{O}_4\text{Cl}_2\text{Ru}$, calculated: C, 53.77; H, 3.97; Ru, 18.10; found: C, 53.45; H, 4.12; Ru, 17.72.

General procedure for the attempted synthesis of ruthenium and iridium flavone complexes (21-26)





A solution of NaOMe (1.05 eq. for 4,5-chelation or 2 eq. for 7,8-chelation) in anhydrous MeOH (10 mL) was added to the free flavone (1 eq.) and the suspension was stirred at 50 °C for 30 min. $[\text{Ru}(\eta^6\text{-}p\text{-cymene})\text{Cl}_2]_2$ or $[\text{Ir}(\eta^5\text{-Cp}^*)\text{Cl}_2]_2$ (0.55 eq.) in anhydrous DCM (10 mL) was added to the reaction mixture and this was stirred at 75 °C overnight under an argon atmosphere. The solvent was evaporated *in vacuo* and the residue was dissolved in warm $\text{CHCl}_3\text{:MeOH}$ (9:1) (15 mL) and filtered to remove any salts and impurities formed during the reaction. The filtrate was concentrated *in vacuo* to 2-3 mL and the product was precipitated by the addition of few drops of EtOAc.

7.3.2.3. Stability of complexes 19 and 20

The absorbance spectra of Ru(II)-*p*-cymene complexes (**19** and **20**) were recorded using 1.0 cm matched quartz cuvettes (600 μL). First, the stock solutions of the test compounds (20 mM) were prepared in 100% sterile DMSO. These stocks were then appropriately diluted with HPLC grade water, and DMSO levels were maintained below 0.1%, in the test concentrations. Absorbance spectra were recorded in the range of 200-320 nm at a heating rate of 1 °C/min from 20 to 90 °C. Measurements recorded at 260 nm from two

individual experiments were normalized to the minimum and maximum measurements (set at 0 and 1, respectively) and their mean used to generate the melting curves.

7.3.3. Cell culture

7.3.3.1. General methods

7.3.3.1.1. Preparation of phosphate buffer saline (PBS)

PBS (1 L) was prepared as follows: Na₂HPO₄ (7.5 g), NaCl (4.4 g) and NaH₂PO₄.H₂O₂ (2.1 g) were stirred in 800 mL double distilled water until dissolution was complete. The pH was checked to ensure it was 7.4 then the volume was adjusted to 1 L by the addition of ultra-pure water. The buffer was then aliquoted in small glass bottles (50-100 mL) before sterilization.

7.3.3.1.2. Preparation of EGM-2 medium

HUVECs were cultured in EGM-2 medium which was supplied as basal medium (EBM™, 500 mL) with a kit of nutrients and growth factors (FBS, VEGF, fibroblast growth factor B, insulin like growth factor-1, epidermal growth factor, hydrocortisone, heparin, gentamycin, amphotericin-B) (SingleQuotes™, frozen). In order to avoid any kind of cross interference with the activity of the test compounds, these supplements were defrosted and added to the medium prior to use except for the antibiotics (gentamycin, amphotericin-B). For the scratch, tube formation and western blotting assays, VEGF free and serum starvation modified media were prepared as shown in **Table 7. 5**. VEGF enriched medium was prepared as outlined in the next **Section (7.3.3.1.3)**.

Table 7. 5. Components of media used for HUVECs culture and antiangiogenic evaluation

Medium	Base medium	Additives		
		Antibiotics	VEGF	FBS
VEGF free		—	—	2%
Serum starvation	EBM-2 + Growth factors (fibroblast growth factor B, insulin like growth factor-1, epidermal growth factor, hydrocortisone, heparin)	—	0.1%	0.1%
VEGF enriched		—	20 ng/mL	2%
EGM-2		—	0.1%	2%

7.3.3.1.3. Preparation of VEGF and VEGF enriched medium

VEGF (10 µg), supplied in a microvial, was centrifuged for 1 min at 6,000 x g before opening, to collect the small amount of the powder at the bottom of the vial. VEGF was then dissolved in sterile water (100 µL) and 0.1% BSA in PBS (900 µL) was added. After mixing the VEGF solution (10 µg/mL) by vortex, it was aliquoted into 5 eppendorf tubes (2 µg/200 µL of each) to form standard stock solution 1 and stored at -20 °C. In order to prepare standard stock solution 2, 800 µL of 0.1% BSA were added to a vial of standard stock solution 1 (2 µg/200 µL VEGF), this was mixed and further aliquoted into 10 eppendorf tubes (0.2 µg/100 µL of each) and stored at -20 °C. For the experiments, an aliquot of standard stock solution 2 of VEGF (100 µL, 2 µg/mL) was defrosted and added to 9.9 mL of complete medium (EGM-2) to obtain a final concentration of 20 ng/mL of VEGF enriched medium (working solution). This was sterilized by filtration (0.2 µm).

7.3.3.1.4. Maintenance of cell lines

Defrosting cells

A frozen vial of HUVECs, MCF-7 or MDA-MB-231 stocks (1 mL) containing a suspension of approximately 10^6 cells was thawed in a water bath at 37 °C. The thawed cell suspension was then added to a falcon tube containing 9 mL of freshly prepared pre-warmed complete medium (**Table 7. 6**), mixed and centrifuged for 5 min at 125 x g (HUVECs) or 215 x g (MCF-7 and MDA-MB-231). The supernatant was aspirated and cells were re-suspended in 10 or 5 mL of appropriate fresh complete media, mixed and transferred into a 75 or 25 cm² flasks for HUVECs and MCF-7 and MDA-MB-231, respectively. The flask was incubated for 24 h in order to allow the cells to adhere, followed by replacement of the medium with a fresh one. The cells were then allowed to reach 70-80% confluency.

Cell maintenance and passaging

HUVECs are primary cells that are cultured for only a couple of passages (1-2) while purchased. HUVECs were maintained according to the following procedure:

- (i) HUVECs were received from the supplier, defrosted and cultured in a 75 cm² flask until confluent (passage 1)
- (ii) The monolayer of HUVECs was split and transferred into three different 75 cm² flasks, where they were allowed to grow until confluent (passage 2)
- (iii) HUVECs from each 75 cm² flask were split, frozen and kept in liquid nitrogen vapor until used (passage 3).

Before starting an experiment, HUVECs (passage 3) were defrosted, cultured in EGM-2 medium in a 75 cm² flask until 70-90% confluent, then harvested and used. HUVECs were not further sub-cultured.

Breast cancer MCF-7 cells were cultured in RPMI 1640 (with L-glutamine) supplemented with 5% FBS while MDA-MB-231 cells were cultured in DMEM (1g/L glucose, without L-glutamine) supplemented with 2% L-glutamine (200 mM) and 10% FBS.

HUVEC cells, and MCF-7 and MDA-MB-231 cell lines were maintained at 37 °C in humidified atmosphere with 5% CO₂. Cells were passaged/sub-cultured into 25 or 75 cm² flasks when reached 70-90% confluency as follows:

- (i) The spent medium was aspirated and cells washed with 5 or 10 mL PBS to remove any residual serum.
- (ii) 0.5 or 2 mL of trypsin EDTA was then added and incubated for no more than 5 min to detach the cells
- (iii) 4.5 or 8 mL of the appropriate complete medium was then added to the detached cells and the solution (5 or 10 mL) was transferred to a falcon tube
- (iv) The cell suspension (5 or 10 mL) was then centrifuged at 125 x g (HUVECs) or 215 x g (MCF-7 and MDA-MB-231) for 5 min
- (v) The supernatant was discarded and 5 or 10 mL of the appropriate complete medium were added to the cell pellets and mixed gently
- (vi) 4.5 or 9 mL of the appropriate complete medium were added to 0.5 or 1 mL of the cell suspension prepared in step (v), respectively, and cultured into a new 25 or 75 cm² flask and maintained as described in **Table 7. 6**.

Table 7. 6. Culture conditions for the cell lines used in this project

Cell line	Origin	Culture medium	Freezing medium
HUVEC	Human umbilical vein endothelial cells	EGM-2	90% FBS + 10% DMSO
MCF-7	Human breast cancer cell line (ER +ve)	RPMI1640 + 5% FBS	90% FBS + 10% DMSO
MDA-MB-231	Human breast cancer cell line (Triple negative, ER -ve, PR -ve and HER2 -ve)	DMEM + 2% L-glutamine + 10% FBS	Complete Medium + 5% DMSO

FBS, foetal bovine serum; ER, estrogen receptor; PR, progesterone; HER2, human epidermal growth factor receptor 2.

Counting and seeding cells

The determination of the number of cells in a cell suspension followed the following procedure:

- (i) Confluent cells were detached from the culture flask using trypsin EDTA and re-suspended in fresh medium as mentioned in the previous section
- (ii) An aliquot (100 μ L) of the cell suspension was mixed with TB 0.2% v/v (100 μ L, prepared from 0.4% trypan blue in saline diluted with PBS) and allowed to stand for 1 min to stain the dead cells
- (iii) The TB cell suspension was placed in the two chambers of a Neubauer haemocytometer covered with a glass cover-slip and visualized under the microscope. Each chamber of the haemocytometer has two grids of five squares each with a volume of $0.1 \text{ mm}^3 = 10^{-4} \text{ mL}$ ($0.1 \text{ (D)} \times \text{surface area of each square (1 mm (L)} \times 1 \text{ (W) mm} = 1 \text{ mm}^2)$)
- (iv) The number of non-stained living cells was counted in ten of the grid squares of the haemocytometer (five from each chamber)
- (v) The arithmetic mean of the ten squares was calculated and the cell concentration was determined according to the formula:

$$\text{Concentration of cells/mL} = \text{Cells per square (Mean)} \times 2 \times 10^4$$

where 2 is the trypan blue dilution factor and the 10^4 is the correction factor for each square in mL

- (vi) The calculated concentration of cells was used to determine the appropriate volume of medium needed to dilute the cell suspension to obtain the required cell density.

Preservation of cells (freezing)

Reserves of the cell lines under investigation were maintained by cryogenic preservation. Cells were detached (trypsinized) from culture flasks and suspended in the corresponding culture medium. Cell concentration was then determined from an aliquot of the cell suspension. A suspension of 10^6 cells/mL was then prepared in the appropriate freezing medium (**Table 7. 6**) and aliquoted (1 mL) into cryogenic vials. Vials were then stored at -20 °C for 1 h followed by freezing at -80 °C overnight before they were transferred to liquid nitrogen vapor for storage until subsequent use.

Preparation of test compounds

The stock solutions (20 mM) of the test compounds were prepared by dissolving appropriate quantity of the compound in 100% DMSO. The prepared stock solutions were then stored at -20 °C until further use. At the time of experiment, stock solutions were defrosted and diluted to the desired concentration using the appropriate medium/reagent for each experiment. DMSO levels were maintained below 1% in the test concentrations.

7.3.3.2. Antiangiogenic evaluation

7.3.3.2.1. Cytotoxicity on endothelial cells (trypan blue exclusion assay)

Cytotoxic activity of treatments on HUVECs was assessed using the trypan blue exclusion assay [261]. The principle of this method is based on the ability of the living cells to exclude the uptake of the blue dye due to their intact cell membrane. For the experiment, HUVECs were seeded in 96 well plates at 1×10^5 cells/mL (100 μ L/well) and cultured for 24 h. Cells were then treated with either luteolin, one of the synthesized derivatives at 40 μ M or EGM-2 culture medium (control) for 24 h. After 24 h, solutions were removed and cells washed with 100 μ L PBS followed by the addition of 50 μ L trypsin–EDTA and incubation for no more than 5 min to detach the cells. 50 μ L of EGM-2 media was then added to the wells and mixed gently. 50 μ L aliquots of the cell suspension were mixed with equal volume of trypan blue 0.2% v/v in PBS then the cells were counted using a haemocytometer. The numbers of viable and dead cells were counted manually and % cell viability of each treatment was expressed as % of control using the equation:

$$\% \text{ Cell Viability} = (\text{Cell viability in treatment} / \text{Cell viability in control}) \times 100$$

where Cell Viability = Number of viable cells/Total number of cells (viable and dead).

The data was represented as the % cell viability mean of three individual experiments \pm SEM.

7.3.3.2.2. Endothelial cell Matrigel tube formation assay

The endothelial tube formation assay was used to evaluate the overall antiangiogenic activity of the test compounds *in vitro*. Corning Matrigel Matrix GFR is a solubilized basement membrane preparation extracted from the Engelbreth-Holm-Swarm mouse sarcoma, a tumor rich in extracellular matrix proteins. It mainly consists of laminin, followed by collagen IV and heparan sulfate proteoglycans [372,373]. Corning Matrigel Matrix GFR also contains important growth factors such as, TGF-beta, epidermal growth factor, insulin-like growth factor, fibroblast growth factor and others which occur naturally in the EHS tumor [251].

Optimization of seeding density

The appropriate seeding density for the experiment was guided by the reported methods in the literature [173,374,375] and further optimized through experimental trials. Seeding densities of either 1×10^4 , 1.5×10^4 or 2×10^4 cells/well were well reported and hence were selected for the optimization trials [173,374,375]. HUVECs were cultured and seeded on the solidified matrigel, as described in the next section, at the three densities then treated with VEGF enriched medium (10 ng/mL). After 12 h incubation, photos of the wells were taken using 4X magnification power of an inverted light microscope. As shown in **Figure 7. 1**, the 1×10^4 cells/well density was too low while the 2×10^4 cells/well concentration resulted in heavily condensed clusters of cells. Meanwhile the 1.5×10^4 cells/well seeding resulted in an optimum density and hence was used in the experiments.

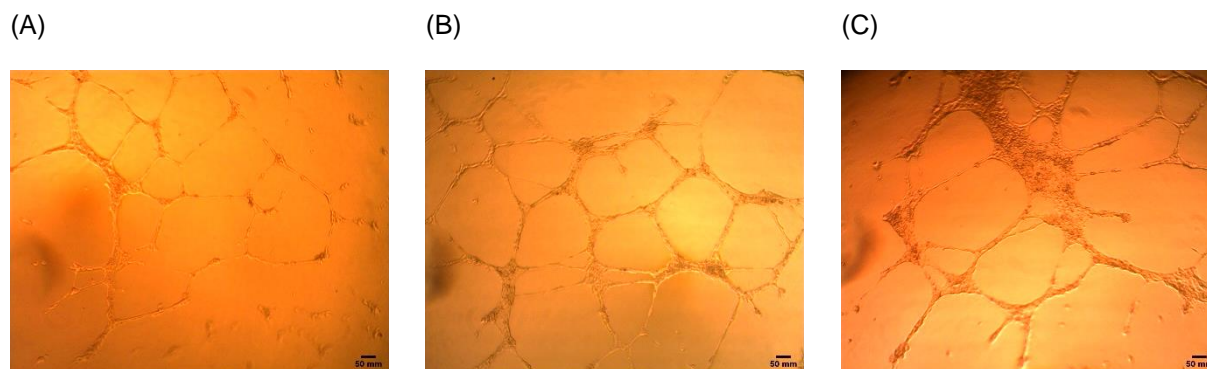


Figure 7. 1. Representative images of *in vitro* HUVEC tube formation assay optimization after 12 h in VEGF enriched media (10 ng/mL) at 4X magnification. (A) 1×10^4 cells/well density; (B) 1.5×10^4 cells/well density; (C) 2×10^4 cells/well density

Tube formation experiment

The experiment followed the reported method [376]. Passage 3 HUVECs were defrosted and cultured in EGM-2 medium until 70-90% confluent. EGM-2 medium was then replaced by serum starvation medium (0.1% FBS) and cells were incubated for 24 h. This helps synchronize the cells at the same stage of the cell cycle [377] and also mimics the unproliferative state of quiescent ECs under normal conditions. The matrix Matrigel was thawed overnight at 4 °C and 96 well plates, pipettes and tips needed for the experiment were also pre-cooled overnight at 4 °C. Afterwards, 96 well plates were coated with 50 μ L of the Matrigel matrix at 4 °C and incubated at 37 °C for 1–2 h to solidify. Serum starved HUVECs were collected and counted as described previously. Calculated volumes needed to prepare cell suspensions of densities: 3×10^5 cells/mL (for treatments and positive control) and 1.5×10^5 cells/mL (for negative control), were transferred into falcon tubes (**a** and **b**), respectively. The two falcons were then centrifuged at 125 x g for 5 min, and the supernatant medium was aspirated from each. Cells in **tube a** were re-suspended in VEGF enriched medium (20 ng/mL) while cells in **tube b** were re-suspended in VEGF free medium. 50 μ L of the cell suspension in **tube a** were seeded onto the solidified Matrigel in the designated treatments and positive control wells. This was followed by the addition of 50 μ L of either luteolin or one of the synthesized derivatives (at 1 or 10 μ M). 100 μ L of the cell suspension in **tube b** were seeded onto the solidified Matrigel in the designated negative control wells. Plates were incubated for 12 h and photos covering the whole well area were taken using 4X magnification power of

an inverted light microscope. Each treatment was carried out in duplicate in each experiment and the experiments were carried out in triplicates. The Angiogenesis Analyzer plugin proved to be an efficient tool in characterizing the branching of ECs into tube networks as well as identifying various elements of endothelial tube formation [264]. Number of junctions, number of meshes, number and length of master segments and segments were quantified from the taken images via the Angiogenesis Analyzer plugin [264] in ImageJ software [265]. Data was represented as a ratio to the positive control (VEGF enriched) as the mean of the three individual experiments \pm SEM.

7.3.3.2.3. Endothelial cell scratch assay

The scratch (wound healing assay) was carried out to assess the effect of the most active test compounds (**9**, **11**, **12** and **14**) on VEGF induced migration of HUVECs. Passage 3 HUVECs were defrosted and cultured in EGM-2 medium until 70-90% confluent. HUVECs were seeded into 12 well plates at 3×10^4 cells/mL/well and cultured until 80-90% confluent. EGM-2 medium was then removed and replaced by serum starvation medium. This helps synchronize the cells at the same stage of the cell cycle [377] and ensures wound closure is mainly due to cell migration not proliferation. After 24 h of serum starvation, a scratch was performed on the cell monolayers using a 200 μ L pipette tip. The spent medium was then removed and cells were washed twice with PBS. HUVECs were treated with 1 mL of either of the following treatments:

- VEGF enriched medium (10 ng/mL) (positive control)
- VEGF enriched medium (10 ng/mL) + **9**, **11**, **12** or **14** (at 1 μ M or 10 μ M).
- VEGF free medium (negative control)

Images of the scratches were taken immediately after performing the scratch (t=0 h) and after 12 h incubation (t=12 h) at the 10X magnification power of an inverted light microscope. The area not covered by the cells was quantified using ImageJ software. The % wound closure (migration) was calculated using the following equation:

$$100 \times (\text{Area of scratch at } t_0 - \text{Area of scratch at } t_{12} / \text{Area of scratch at } t_0)$$

and expressed as a ratio to the positive control. The data was represented as the mean of three individual experiments \pm SEM.

7.3.3.2.4. Western blotting

Western blotting is a technique widely used to separate proteins for analysis and purification. Its based on the migration of negatively charged proteins within an electric field (electrophoresis) through polyacrylamide gels that act as size-selective sieves [378]. The resolved proteins are then transferred to specific membranes (blotting) were they can be immunologically stained using protein specific antibodies and visualized by chemiluminescent reagents [378]. In this project, western blotting was used to detect the ability of the most active compounds to inhibit VEGFR2 phosphorylation at the Tyr1175 position.

Preparation of cell lysates

Passage 3 HUVECs were cultured in 6 well plates at 1×10^5 cells/well (2 mL) and cultured for 48 h. After 48 h, the spent medium was removed and serum starvation medium (2 mL) was added for 24 h to inhibit cell proliferation. The serum starvation medium was afterwards replaced with complete medium with or without the test compounds (at 1 μ M or 10 μ M) and incubated for 1 h. The treatments were then removed and the cells were washed twice with PBS. This was followed by the addition of medium with 10 ng/mL of VEGF and incubation for 50 min to activate VEGFR2. Afterward, the cells were washed twice with ice-cold PBS and lysed by the addition of 100 μ L RIPA lysis buffer with 1% protease inhibitor and phosphatase inhibitor. The cells were then scraped with cell scrapper, collected into eppendorfs and preserved at -80 °C until use.

Protein content determination

Protein content determination is an important step in quantitative western blotting in order to ensure that the same amount of protein is loaded in the gel for each sample, hence allow proper comparison. It also ensures that the amount of loaded protein is appropriate for the selected lane dimension [378]. Herein, the quantity of protein in each sample was determined using Bio-Rad DC Protein assay adapted from Lowry assay [379]. Lowry assay is a colorimetric assay that is based on the reaction of peptide bonds with cupric acid under alkaline conditions followed by reaction of the reduced Cu^+ with folin reagent (a mixture of phosphotungstic acid and phosphomolybdic acid). A final color is produced that can be measured spectrophotometrically at a maximum absorbance of $\lambda=750$ nm

[379]. First, a standard calibration curve was set up, using BSA as a standard protein, as follows:

- (i) Five standard solutions (0.2, 0.4, 0.8, 1.25 and 2.5 mg/mL) of BSA were prepared in the lysis buffer
- (ii) 500 μL of reagent A' (20 μL of reagent S: 1 mL of reagent A) were added to a 100 μL of the standard BSA solutions as well as the test samples and vortexed to mix
- (iii) 4 mL of reagent B were then added to each solution, vortexed and left for 15 m at room temperature
- (iv) The absorbance of each solution was measured at $\lambda=750$ nm
- (v) The concentration of protein in each sample was determined using the plotted BSA calibration curve (**Figure 7.2**). The data was represented as the mean of three individual experiments.

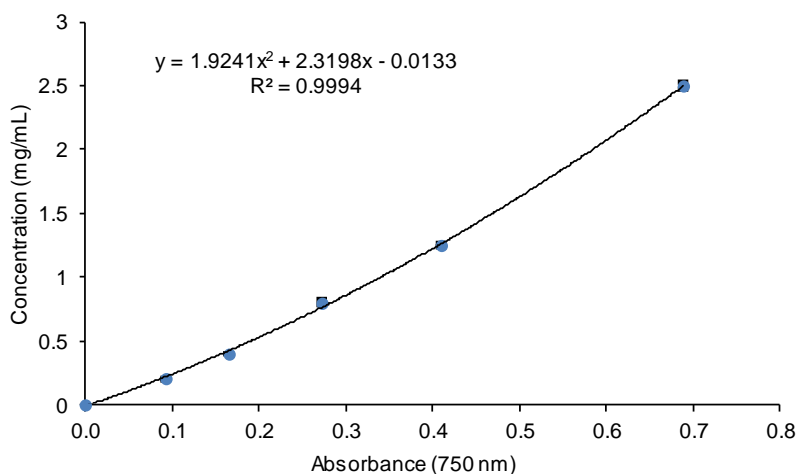


Figure 7.2. BSA standard calibration curve used for HUVEC lysate protein content determination

SDS PAGE

Gel casts were prepared by loading 7% resolving gel (**Table 7. 7**) into 1.5 mm spacers and leaving them to polymerize for 30 min. 3% Stacking gel (**Table 7. 8**) was then loaded on top of the solidified resolving gel and a 10 well comb was immediately inserted into the cast. After 20 min, gel casts were placed in an electrophoresis tank filled with 1X running buffer (100 mL of 10X running buffer + 900 mL ddH₂O) (**Table 7. 9**) and the comb was removed. Protein samples (15 μg /well) were prepared by mixing an appropriate quantity with 5 μL of loading buffer (270 μL Laemmli buffer + 30 μL 2-mercaptoethanol). Samples

were heated at 100 °C to denature the proteins, vortexed and loaded (25 µL) into the wells of the prepared polyacrylamide gel casts. 5 µL of the precision plus protein marker (molecular weight marker, 10-250 kDa) were loaded in the gel along the protein samples. The loaded gels were then run in 1X running buffer at 50 V until the protein bands migrated to the resolving gel then at 100 V for 1 h.

Table 7. 7. Composition of 7% resolving gel

Reagents	Amount
ddH ₂ O	17.5 mL
30% Acrylamide	7 mL
1.5 M Tris pH 8.8	5 mL
10% SDS	300 µL
10 % APS	150 µL
Temed	24 µL

Table 7. 8. Composition of 3% stacking gel

Reagents	Amount
ddH ₂ O	15.4 mL
30% Acrylamide	2.4 mL
0.5 M Tris pH 6.8	6 mL
10% SDS	108 µL
10 % APS	250 µL
Temed	24 µL

Table 7. 9. Composition of 10X running buffer

Reagents	Amount (g)
Glycine	144
Tris base	30.3
SDS	10
Dissolved in 1L ddH ₂ O	

Gel transfer (blotting)

PVDF membranes and filter paper were cut to the same size of the transfer cassette. PVDF membranes were activated by soaking in MeOH for 1 min followed by soaking the activated membranes, filter paper and transfer sponges in 1X transfer buffer (100 mL of 10X transfer buffer + 100 mL MeOH + 800 mL ddH₂O) (**Table 7. 10**). Gels were removed from the electrophoresis tank and carefully detached from the glass plates. The transfer cassettes were prepared by layering the different components on the anode (black) side in the following order: sponge, two filter papers, gel, PVDF membrane, two filter papers and sponge. The prepared cassettes were run in 1X transfer buffer at 90 V for 2 h.

Table 7. 10. Composition of 10X transfer buffer

Reagents	Amount (g)
Glycine	112.6
Tris base	24.2
Dissolved in 1L ddH ₂ O	

Analysis and visualization of blotting membrane

After the transfer run was finished, the PVDF membrane was taken out of the transfer cassette and blocked with 5% w/v BSA in tris buffer saline-tween (100 mL 10X TBS + 900 mL ddH₂O + 0.1% (1 mL) tween[®] 20) for 1 h at room temperature (**Table 7. 11**). The membrane was then cut into two pieces, from 250 kDa to 50 kDa (for VEGFR2 detection) and from 50 kDa to 10 kDa (for actin detection). Each of these membranes were incubated with their primary antibodies (P^{Tyr1175}-VEGFR2 and actin, respectively) at 1:1000 dilutions at 4°C overnight. Following incubation with primary antibodies, the membranes were washed thrice (5-10 min each) with PBS-T (100 mL 10X PBS + 900 mL ddH₂O + 0.1% (1 mL) tween[®]20). The membranes were afterwards incubated with horseradish peroxidase-conjugated secondary antibodies (1:5000) for 1 h at room temperature, then washed thrice (15 min each) with PBS-T. Finally, the membranes were incubated for 1 min with enzyme linked enhanced chemiluminescent reagent (reagent A: reagent B, 1:1) and bands visualized using Image Quant LAS 4000 (GE Healthcare, Hatfield, UK). In order to detect the T-VEGFR2, P^{Tyr1175}-VEGFR2 membranes were stripped according to Abcam's protocol [380] by incubation with the stripping buffer (**Table**

7. 12) twice (5 min each) at room temperature. The stripped membranes were washed twice (10 min each) with 1X PBS, then twice (5 min each) with TBS-T. The stripped membranes were then probed for total VEGFR2 (1:1000). The density of the bands was measured using ImageJ software. T-VEGFR2 was normalized to β -actin to ensure no significant differences exist in the total levels of T-VEGFR2 among the evaluated groups. P-VEGFR2 was normalized to T-VEGFR2 and was represented as a ratio to the positive control (VEGF enriched). All data was represented as the mean of three individual experiments \pm SEM, except for compound **14** (1 μ M) where only two replicates are presented (**Figure 7. 3**).

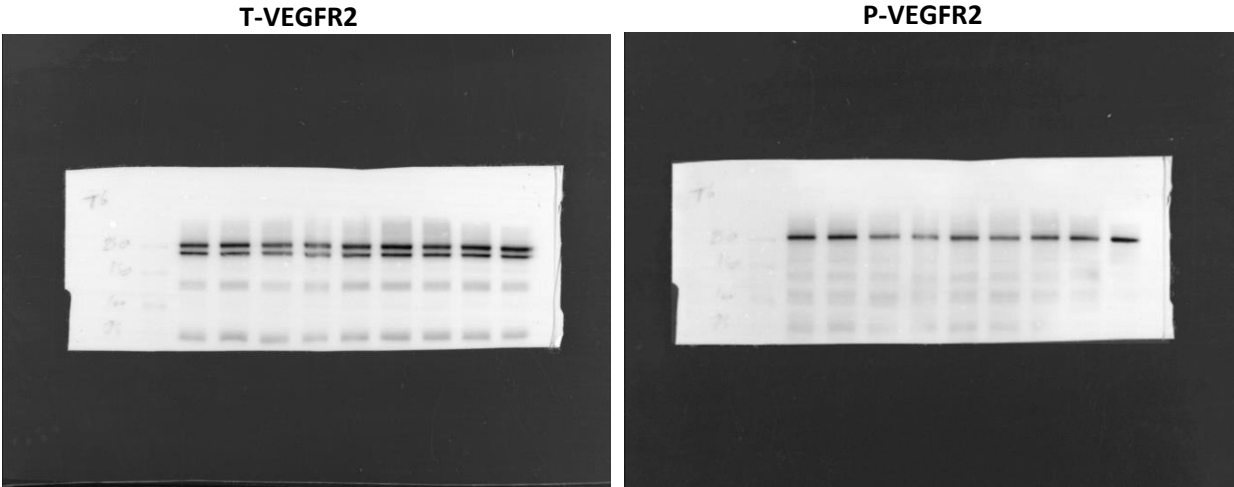
Table 7. 11. Composition of 10X tris buffer

Reagents	Amount (g)
Tris base	24.2
NaCl	80
Dissolved in 1L ddH ₂ O	

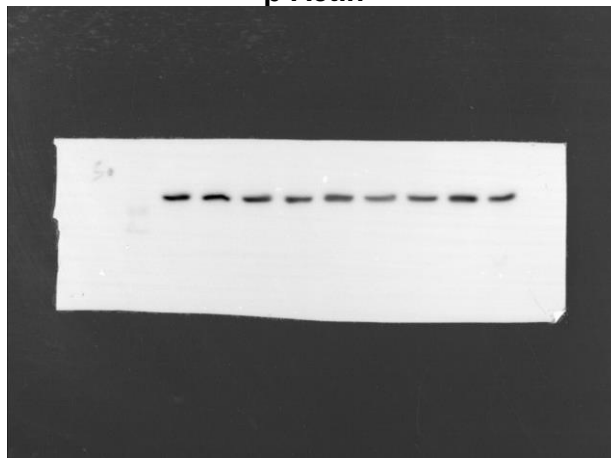
Table 7. 12. Composition of stripping buffer (pH 2.2)

Reagents	Amount
Glycine	15 g
SDS	1 g
Tween®20	10 mL
Dissolved in 1 L ddH ₂ O	

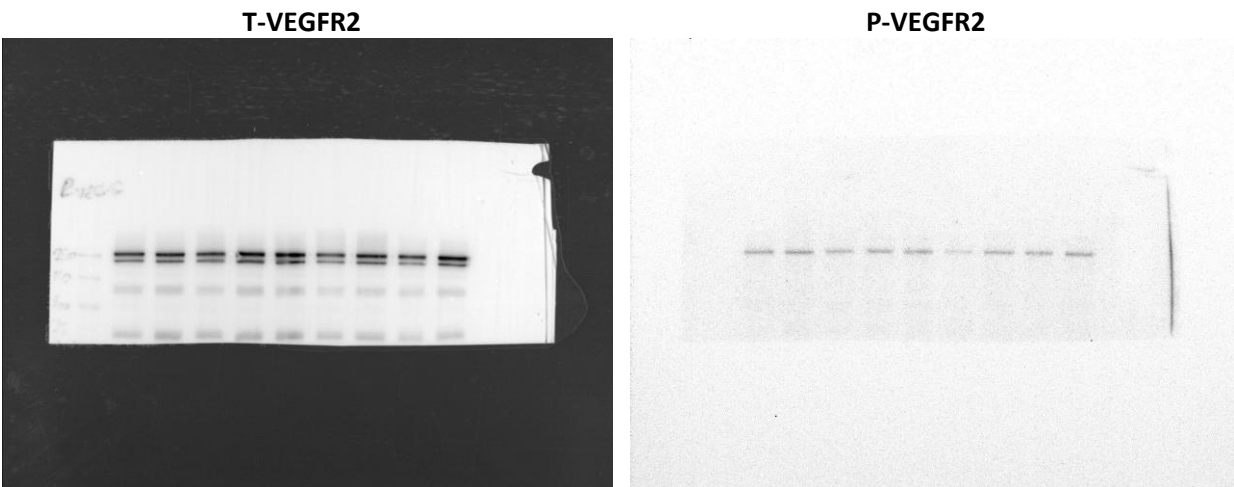
(A) N1: +veC 9(10 μ M) 9(1 μ M) 12(10 μ M) 12(1 μ M) 11(10 μ M) 11(1 μ M) 14(10 μ M) 14(1 μ M)



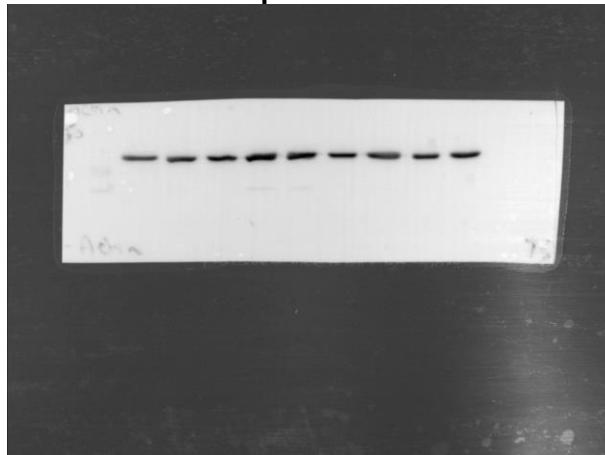
β -Actin



(B) N2: +veC 9(10 μ M) 9(1 μ M) 12(10 μ M) 12(1 μ M) 11(10 μ M) 11(1 μ M) 14(10 μ M) 14(1 μ M)

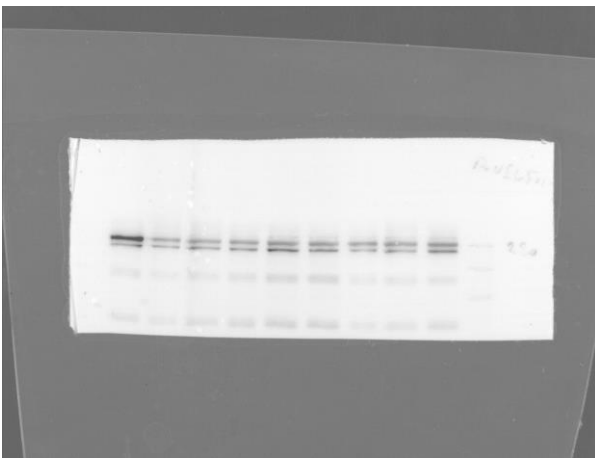


β -Actin



(C) N3: n/a 11(10 μ M) 12(10 μ M) 9(10 μ M) 14(10 μ M) +veC 11(1 μ M) 12(1 μ M) 9(1 μ M)

T-VEGFR2



P-VEGFR2



β -Actin

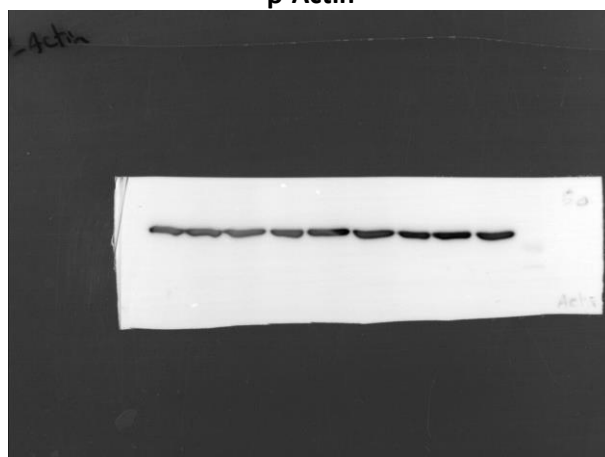


Figure 7. 3. Raw western blot membrane for trials N1- N3

7.3.3.3. Anticancer evaluation against breast cancer cells

7.3.3.3.1. Cytotoxicity on breast cancer cells (MTT assay)

The MTT assay was used to determine the cell viability of the estrogen receptor positive (MCF-7) and the triple negative (MDA-MB-231) breast cancer cell lines upon treatment with flavones (**11** and **13**) as well as their respective Ru(II)-*p*-cymene metal derivatives (**19** and **20**). The MTT assay is a quantitative colorimetric assay based on the ability of mitochondrial dehydrogenases of metabolically active cells to reduce 3-(4, 5-dimethylthiazol-2-yl)-diphenyl-2*H*-tertrazolium bromide (MTT) into insoluble purple formazan crystals [381].

MCF-7 and MDA-MB-231 cells were seeded at a density of 4×10^4 and 2×10^4 cells/mL, respectively, into 96 well plates and incubated to allow the attachment for 24 h. After 24 h, the cells were treated with one of the synthesized derivatives at range of concentrations (0–100 μ M) for 67 h. After 67 h, 20 μ L of MTT solution in PBS (5 mg/mL) was added to each well and the cells were incubated for 5 h. The supernatant was then removed and the purple crystals formed were dissolved in 100 μ L of DMSO. After 30 min incubation, the plates were read at 560 nm using a SPECTRA max UV spectrometer (Bio-Rad). The cytotoxicity of compounds was determined as the percentage of cell survival assuming 100% cell viability for the control (blank). Percentage cell survival was plotted against the log concentration of the compound to obtain a sigmoidal curve. IC₅₀ values were obtained using GraphPad Prism 8 Software. The data was represented as the mean of three individual experiments \pm SEM.

7.3.3.3.2. Breast cancer cells scratch assay

The scratch assay was used to evaluate the antimigratory effects of flavones (**11** and **13**) and their respective Ru(II)-*p*-cymene derivatives (**19** and **20**) on breast cancer cell lines (MCF-7 and MDA-MB-231). MCF-7 or MDA-MB-231 cells were seeded in 12 well plates at 2×10^5 or 1×10^5 cells/mL, respectively, and cultured until 70–80% confluency. Afterwards, they were serum-starved (0% serum) for 24 h to inactivate the cell proliferation. A scratch was performed on the cell monolayers using a 200 μ L pipette tip. Cells were then washed twice with PBS and treated with complete medium and one of the synthesized derivatives at 1, 10 or 20 μ M. Compound **11** was not tested on MCF-7

cell line due to cytotoxicity ($IC_{50}=1.2 \mu\text{M}$). Images of the scratches were taken immediately after performing the scratch ($t = 0 \text{ h}$) and at 24 h ($t = 24 \text{ h}$). The area not covered by the cells was quantified using ImageJ software. % of wound closure (migration) was calculated using the following equation:

$$100 \times (\text{Area of scratch at } t_0 - \text{Area of scratch at } t_{24} / \text{Area of scratch at } t_0)$$

and expressed as a ratio to the positive control as the mean of three individual experiments \pm SEM.

7.3.3.4. Molecular docking

Molecular docking studies were carried out in order to simulate the interactions of the test compounds with VEGFR2 active site as a possible mode of antiangiogenic action. Docking studies for the new compounds of interest were performed using the program Surflex-Dock (SFXC) [382] as provided by Sybyl-X 2.1.

Preparation of the ligands

The 2D structures of the test flavones were built using ChemDraw Ultra 8 software, then transformed into their 3D structures using SYBYL2.1 molecular modelling program. Energy minimization was performed on the library of test compounds as well as the original ligand extracted from the receptor's coordinate files, taken from PDBid: 1YWN, using the MMFF94 force field, employing a conjugate gradient algorithm [383].

Receptor preparation

The X-ray crystallographic structure of VEGFR2 in complex with 4-amino-furo[2,3-d]pyrimidine ligand was obtained from the Protein Data Bank (PDBid: 1YWN, 1.71 Å resolution) [279]. The co-crystallized ligand was extracted from the coordinate file of the VEGFR2 receptor (1YWN) and prepared as described above. The protein structure was prepared for docking using the Biopolymer Structure Preparation Tool with the implemented default settings provided in the SYBYL program suite. Hydrogens were added to the protein structure in idealized geometries, and an overall energy minimization of the protein was performed using the MMFF94 force field, employing a conjugate gradient algorithm [383] with a convergence criterion of 0.5 kcal/mol/Å and up to 5000 iterations. Finally, before the docking run, all water molecules, except molecule number

163 (previously shown to be involved in water-mediated ligand protein interactions) were removed.

Docking procedure

A standard guided docking protocol was used in this study in which a protomol, representing the receptor's catalytic site, was generated using reported literature data on the amino acids outlining the binding site [269,271,272,279–282]. The Surflex-X docking algorithm docks a given ligand to a receptor using a flexible ligand and a semi-flexible receptor algorithm; in this case, the compounds were allowed to be fully flexible while the receptor was semi-flexible. This allows for the optimization of potentially favorable molecular interactions, such as those defined by hydrogen bond and van der Waal forces. Visualization and analyses of the docking results as well as the molecular interactions of the docked ligands were performed using the program Maestro [384]. Potential hydrogen bonds were assigned if the distance between two electronegative atoms was less than 3.5 Å, whereas any separation greater than 3.5 Å, but less than 4.5 Å, was considered a van der Waal interaction.

Validation of the docking procedure

The docking procedure was validated by re-docking of the original pyrimidine ligand into the prepared protein structure. Superimposition of the ligand conformation resulting from docking and the original ligand co-crystallized with the protein structure, resulted in a RMSD value of 0.97 Å calculated by Maestro program V13.1 [384]. This RMSD value and the reproducible ligand-protein contacts indicated that the docking procedure is valid and reliable as are the results, which are well within the 2 Å grid spacing used in the docking procedure [285].

7.3.3.5. I-motif DNA binding

The interaction of flavones (**11** and **13**) and their respective Ru(II)-*p*-cymene metal derivatives (**19** and **20**) with VEGF and c-myc i-motif DNA was carried out using UV-Vis spectroscopy.

Determination of DNA concentration

The supplied DNA were reconstituted with ddH₂O to make 1 mM stock solutions. 1 μ L of the DNA stock solution was added to 597 μ L of ddH₂O and the absorbance was measured at 260 nm at 80 °C in a 1 cm quartz cuvette. Another 1 μ L of the DNA stock solution was added to the 598 μ L solution and the absorbance was re-measured. A final 1 μ L of the DNA stock solution was added to the cuvette and the absorbance was measured for a third time. DNA concentrations were then determined by using the molar extinction coefficient supplied by the manufacturer (**Table 7. 13**), using the equation:

$$\text{DNA concentration (mM)} = (\text{Absorbance}/E) \times 1000 \times 600$$

Table 7. 13. Supplier's data for VEGF and c-myc i-motif oligonucleotides

DNA	Sequence (5'-3')	MW	Amount (μ g)	Epsilon 1/(mMcm)
VEGF	(CCCCGCCCCCGGCCCGCCCC)	5882	572.8	154
C-myc	(CCTTCCCCACCCTCCCCACCCTCCCCA)	7878	735.8	215.2

UV-Vis scans

The absorbance spectra of VEGF and c-myc i-motif sequences with or without flavones (**11** and **13**) and their Ru(II)-*p*-cymene complexes (**19** and **20**) were recorded in a 1:1 ratio (2 μ M:2 μ M). First, the stock solutions of the test compounds (20 mM) were prepared in 100% sterile DMSO. These stocks were then appropriately diluted with HPLC grade water and DMSO levels were maintained below 0.1% in the test concentrations. VEGF and c-myc i-motifs were prepared by diluting with Na cacodylate buffer (20 mM, pH 5.5), then annealed by heating with or without the flavonoid at 95 °C for 5 min followed by gentle cooling to room temperature. UV-visible absorbance measurements were then recorded using 1.0 cm matched quartz cuvettes (600 μ L). Initially, the spectra were recorded in the range of 200–500 nm to determine the relevant wavelength range. No peaks were observed above 320 nm, hence subsequent spectra were recorded in the range of 200–320 nm at 25 °C. The data was represented as the mean of two individual experiments.

Thermal stability

The effect of flavones (**11** and **13**) and their Ru(II)-*p*-cymene complexes (**19** and **20**) on the thermal stability of VEGF and c-myc i-motif sequences was measured in 1:1 ratio (2 μ M:2 μ M) using 1.0 cm matched quartz cuvettes (600 μ L). VEGF and c-myc i-motifs were prepared by diluting with Na cacodylate buffer (20 mM, pH 5.5), then annealed by heating with or without the flavonoid at 95 °C for 5 min followed by gentle cooling to room temperature. Absorbance spectra were recorded in the range of 200-320 nm at a heating rate of 1 °C/min from 20 to 90 °C. Measurements recorded at 295 nm from two individual experiments were normalized to the minimum and maximum measurements (set at 0 and 1, respectively) and their mean used to generate the melting curves. T_m was calculated by non-linear fitting of the sigmoidal curve obtained from the mean of two measurements at 295 nm using Microsoft Excel 2016.

7.3.3.6. Statistical analysis

Statistical analysis was carried out against the control group by one-way ANOVA followed by Dunnett's *post hoc* test (*) using Graphpad Prism 6. Statistical analysis for pairwise comparisons were carried out by one-way ANOVA followed by Tukey's *post hoc* test (#) [267] using Graphpad Prism 6. Statistical significance value was set at *, # p <0.05, **, ## p <0.01, ***, ### p <0.001.

References

1. Weinberg, R. A. *The Biology of Cancer*, Garland Science, Taylor & Francis: New York, 2016.
2. Debela, D. T.; Muzazu, S. G.; Heraro, K. D.; Ndalama, M. T.; Mesele, B. W.; et al. New Approaches and Procedures for Cancer Treatment: Current Perspectives: *SAGE open Med.* **2021**, *9*, 205031212110343.
3. Gasparini, G.; Longo, R.; Fanelli, M.; Teicher, B. A. Combination of Antiangiogenic Therapy with Other Anticancer Therapies: Results, Challenges, and Open Questions. *J. Clin. Oncol.* **2005**, *23* (6), 1295–1311.
4. Pottier, C.; Fresnais, M.; Gilon, M.; Jérusalem, G.; Longuespée, R.; et al. Tyrosine Kinase Inhibitors in Cancer: Breakthrough and Challenges of Targeted Therapy. *Cancers (Basel)*. **2020**, *12* (3), 731.
5. Raghavendra, N. M.; Pingili, D.; Kadasi, S.; Mettu, A.; Prasad, S. V. U. M. Dual or Multi-Targeting Inhibitors: The next Generation Anticancer Agents. *Eur. J. Med. Chem.* **2018**, *143*, 1277–1300.
6. LopezLazaro, M. Flavonoids as Anticancer Agents: Structure-Activity Relationship Study. *Curr. Med. Chem. - Anti-Cancer Agents* **2002**, *2* (6), 691–714.
7. Diniz, C.; Suliburska, J.; Ferreira, I. M. New Insights into the Antiangiogenic and Proangiogenic Properties of Dietary Polyphenols. *Mol. Nutr. Food Res.* **2017**, *61* (6), 1–17.
8. Mirossay, L.; Varinská, L.; Mojžiš, J. Antiangiogenic Effect of Flavonoids and Chalcones: An Update. *Int. J. Mol. Sci.* **2018**, *19* (1), 27.
9. Mojzis, J.; Varinska, L.; Mojzisova, G.; Kostova, I.; Mirossay, L. Antiangiogenic Effects of Flavonoids and Chalcones. *Pharmacol. Res.* **2008**, *57* (4), 259–265.
10. Zhao, J.; Yang, J.; Xie, Y. Improvement Strategies for the Oral Bioavailability of Poorly Water-Soluble Flavonoids: An Overview. *Int. J. Pharm.* **2019**, *570* (June), 118642.
11. Ferlay, J.; Colombet, M.; Soerjomataram, I.; Parkin, D. M.; Piñeros, M.; et al. Cancer Statistics for the Year 2020: An Overview. *Int. J. Cancer* **2021**, *149* (4), 778–789.
12. Bray, F.; Ferlay, J.; Soerjomataram, I.; Siegel, R. L.; Torre, L. A.; et al. Global Cancer Statistics 2018: GLOBOCAN Estimates of Incidence and Mortality Worldwide for 36 Cancers in 185 Countries. *CA. Cancer J. Clin.* **2018**, *68* (6), 394–424.
13. Cancer mortality statistics | Cancer Research UK
<https://www.cancerresearchuk.org/health-professional/cancer-statistics/mortality#heading-Zero> (accessed Jul 11, 2024).
14. Cancer deaths - Health, United States
<https://www.cdc.gov/nchs/hus/topics/cancer-deaths.htm> (accessed Apr 5, 2024).

15. Pucci, C.; Martinelli, C.; Ciofani, G. Innovative Approaches for Cancer Treatment: Current Perspectives and New Challenges. *Ecancermedicalscience* **2019**, *13*.
16. Ucuzian, A. A.; Gassman, A. A.; East, A. T.; Greisler, H. P. Molecular Mediators of Angiogenesis. *J. Burn Care Res.* **2010**, *31* (1), 158.
17. Wang, X.; Bove, A. M.; Simone, G.; Ma, B. Molecular Bases of VEGFR-2-Mediated Physiological Function and Pathological Role. *Front. Cell Dev. Biol.* **2020**, *8*, 1314–1325.
18. Elebiyo, T. C.; Rotimi, D.; Evbuomwan, I. O.; Maimako, R. F.; Iyobhebhe, M.; et al. Reassessing Vascular Endothelial Growth Factor (VEGF) in Anti-Angiogenic Cancer Therapy. *Cancer Treat. Res. Commun.* **2022**, *32* (August), 100620.
19. Hanahan, D.; Folkman, J. Patterns and Emerging Mechanisms of the Angiogenic Switch during Tumorigenesis. *Cell* **1996**, *86* (3), 353–364.
20. Zetter, B. R. Angiogenesis and Tumor Metastasis. *Annu. Rev. Med.* **1998**, *49* (1), 407–424.
21. Haibe, Y.; Kreidieh, M.; El Hajj, H.; Khalifeh, I.; Mukherji, D.; et al. Resistance Mechanisms to Anti-Angiogenic Therapies in Cancer. *Front. Oncol.* **2020**, *10*, 221–243.
22. Modi, S. J.; Kulkarni, V. M. Vascular Endothelial Growth Factor Receptor (VEGFR-2)/KDR Inhibitors: Medicinal Chemistry Perspective. *Med. Drug Discov.* **2019**, *2*, 100009.
23. Folkman, J. Role of Angiogenesis in Tumor Growth and Metastasis. *Semin. Oncol.* **2002**, *29* (6), 15–18.
24. Ghalehbandi, S.; Yuzugulen, J.; Pranjol, M. Z. I.; Pourgholami, M. H. The Role of VEGF in Cancer-Induced Angiogenesis and Research Progress of Drugs Targeting VEGF. *Eur. J. Pharmacol.* **2023**, *949* (January), 175586.
25. Kerbel, R.; Folkman, J. Clinical Translation of Angiogenesis Inhibitors. *Nat. Rev. Cancer* **2002**, *2* (10), 727–739.
26. Ge, H.; Luo, H. Overview of Advances in Vasculogenic Mimicry—a Potential Target for Tumor Therapy. *Cancer Manag. Res.* **2018**, *10*, 2429–2437.
27. Maniotis, A. J.; Folberg, R.; Hess, A.; Seftor, E. A.; Gardner, L. M. G.; et al. Vascular Channel Formation by Human Melanoma Cells in Vivo and in Vitro: Vasculogenic Mimicry. *Am. J. Pathol.* **1999**, *155* (3), 739–752.
28. Chen, C.; Hung, M. Beyond Anti-VEGF: Dual-Targeting Antiangiogenic and Antiproliferative Therapy. *Am. J. Transl. Res.* **2013**, *5* (4), 393–403.
29. Zhao, Y.; Adjei, A. A. Targeting Angiogenesis in Cancer Therapy: Moving Beyond Vascular Endothelial Growth Factor. *Oncologist* **2015**, *20* (6), 660–673.
30. Griffioen, A. W.; Mans, L. A.; De Graaf, A. M. A.; Nowak-Sliwinska, P.; De Hoog, C. L. M. M.; et al. Rapid Angiogenesis Onset after Discontinuation of Sunitinib Treatment of Renal Cell Carcinoma Patients. *Clin. Cancer Res.* **2012**, *18* (14), 3961–3971.

31. Vafopoulou, P.; Kourti, M. Anti-Angiogenic Drugs in Cancer Therapeutics: A Review of the Latest Preclinical and Clinical Studies of Anti-Angiogenic Agents with Anticancer Potential. *J. Cancer Metastasis Treat.* **2022**, *8*, 18.
32. Palazzo, A.; Dellapasqua, S.; Munzone, E.; Bagnardi, V.; Mazza, M.; et al. Phase II Trial of Bevacizumab Plus Weekly Paclitaxel, Carboplatin, and Metronomic Cyclophosphamide With or Without Trastuzumab and Endocrine Therapy as Preoperative Treatment of Inflammatory Breast Cancer. *Clin. Breast Cancer* **2018**, *18* (4), 328–335.
33. Lan, C.-Y.; Wang, Y.; Xiong, Y.; Li, J.-D.; Shen, J.-X. Apatinib Combined with Oral Etoposide in Patients with Platinum-Resistant or Platinum-Refractory Ovarian Cancer (AEROC): A Phase 2, Single-Arm, Prospective Study. *Lancet Oncol.* **2018**, *19* (9), 1239–1246.
34. Gangjee, A.; Pavana, R. K.; Ihnat, M. A.; Thorpe, J. E.; Disch, B. C.; et al. Discovery of Antitubulin Agents with Antiangiogenic Activity as Single Entities with Multitarget Chemotherapy Potential. *ACS Med. Chem. Lett.* **2014**, *5* (5), 480–484.
35. Chi, Y.; Fang, Z.; Hong, X.; Yao, Y.; Sun, P.; et al. Safety and Efficacy of Anlotinib, a Multikinase Angiogenesis Inhibitor, in Patients with Refractory Metastatic Soft-Tissue Sarcoma. *Clin. Cancer Res.* **2018**, *24* (21), 5233–5238.
36. Han, B.; Li, K.; Wang, Q.; Zhang, L.; Shi, J.; et al. Effect of Anlotinib as a Third-Line or Further Treatment on Overall Survival of Patients With Advanced Non-Small Cell Lung Cancer: The ALTER 0303 Phase 3 Randomized Clinical Trial. *JAMA Oncol.* **2018**, *4* (11), 1569–1575.
37. Xu, J.; Shen, L.; Bai, C.; Wang, W.; Li, J.; et al. Surufatinib in Advanced Pancreatic Neuroendocrine Tumours (SANET-p): A Randomised, Double-Blind, Placebo-Controlled, Phase 3 Study. *Lancet Oncol.* **2020**, *21* (11), 1489–1499.
38. Riechelmann, R. P.; Leite, L. S.; Bariani, G. M.; Glasberg, J.; Rivelli, T. G.; et al. Regorafenib in Patients with Antiangiogenic-Naïve and Chemotherapy-Refractory Advanced Colorectal Cancer: Results from a Phase IIb Trial. *Oncologist* **2019**, *24* (9), 1180–1187.
39. Taylor, M. H.; Lee, C. H.; Makker, V.; Rasco, D.; Dutcus, C. E.; et al. Phase IB/II Trial of Lenvatinib Plus Pembrolizumab in Patients With Advanced Renal Cell Carcinoma, Endometrial Cancer, and Other Selected Advanced Solid Tumors. *J. Clin. Oncol.* **2020**, *38* (11), 1154.
40. Atkins, M. B.; Plimack, E. R.; Puzanov, I.; Fishman, M. N.; McDermott, D. F.; et al. Axitinib in Combination with Pembrolizumab in Patients with Advanced Renal Cell Cancer: A Non-Randomised, Open-Label, Dose-Finding, and Dose-Expansion Phase 1b Trial. *Lancet Oncol.* **2018**, *19* (3), 405–415.
41. Powles, T.; Plimack, E. R.; Soulières, D.; Waddell, T.; Stus, V.; et al. Pembrolizumab plus Axitinib versus Sunitinib Monotherapy as First-Line Treatment of Advanced Renal Cell Carcinoma (KEYNOTE-426): Extended Follow-up from a Randomised, Open-Label, Phase 3 Trial. *Lancet Oncol.* **2020**, *21* (12), 1563–1573.

42. Tong, R. T.; Boucher, Y.; Kozin, S. V.; Winkler, F.; Hicklin, D. J.; et al. Vascular Normalization by Vascular Endothelial Growth Factor Receptor 2 Blockade Induces a Pressure Gradient Across the Vasculature and Improves Drug Penetration in Tumors. *Cancer Res.* **2004**, *64* (11), 3731–3736.
43. Zeng, F.; Ju, R. J.; Liu, L.; Xie, H. J.; Mu, L. M.; et al. Application of Functional Vincristine plus Dasatinib Liposomes to Deletion of Vasculogenic Mimicry Channels in Triple-Negative Breast Cancer. *Oncotarget* **2015**, *6* (34), 36625.
44. Roviida, A.; Castiglioni, V.; Decio, A.; Scarlato, V.; Scanziani, E.; et al. Chemotherapy Counteracts Metastatic Dissemination Induced by Antiangiogenic Treatment in Mice. *Mol. Cancer Ther.* **2013**, *12* (10), 2237–2247.
45. Hertog, M. G. L.; Feskens, E. J. M.; Kromhout, D.; Hertog, M. G. L.; Hollman, P. C. H.; et al. Dietary Antioxidant Flavonoids and Risk of Coronary Heart Disease: The Zutphen Elderly Study. *Lancet* **1993**, *342* (8878), 1007–1011.
46. Keli, S. O.; Hertog, M. G. L.; Feskens, E. J. M.; Kromhout, D. Dietary Flavonoids, Antioxidant Vitamins, and Incidence of Stroke: The Zutphen Study. *Arch. Intern. Med.* **1996**, *156* (6), 637–642.
47. Knekt, P.; Järvinen, R.; Seppänen, R.; Heliövaara, M.; Teppo, L.; et al. Dietary Flavonoids and the Risk of Lung Cancer and Other Malignant Neoplasms. *Am. J. Epidemiol.* **1997**, *146* (3), 223–230.
48. Xu, K.; Ren, X.; Wang, J.; Zhang, Q.; Fu, X.; et al. Clinical Development and Informatics Analysis of Natural and Semi-Synthetic Flavonoid Drugs: A Critical Review. *J. Adv. Res.* **2023**.
49. Raffa, D.; Maggio, B.; Raimondi, M. V.; Plescia, F.; Daidone, G. Recent Discoveries of Anticancer Flavonoids. *Eur. J. Med. Chem.* **2017**, *142*, 213–228.
50. Alzaabi, M. M.; Hamdy, R.; Ashmawy, N. S.; Hamoda, A. M.; Alkhayat, F.; et al. Flavonoids Are Promising Safe Therapy against COVID-19. *Phytochem. Rev.* **2022**, *21* (1), 291–312.
51. Shoskes, D. A.; Zeitlin, S. I.; Shahed, A.; Rajfer, J. Quercetin in Men with Category III Chronic Prostatitis: A Preliminary Prospective, Double-Blind, Placebo-Controlled Trial. *Urology* **1999**, *54* (6), 960–963.
52. Dallas, C.; Gerbi, A.; Elbez, Y.; Caillard, P.; Zamaria, N.; et al. Clinical Study to Assess the Efficacy and Safety of a Citrus Polyphenolic Extract of Red Orange, Grapefruit, and Orange (Sinetrol-XPur) on Weight Management and Metabolic Parameters in Healthy Overweight Individuals. *Phyther. Res.* **2014**, *28* (2), 212–218.
53. Yao, J.; Zhang, Y.; Wang, X. Z.; Zhao, J.; Yang, Z. J.; et al. Flavonoids for Treating Viral Acute Respiratory Tract Infections: A Systematic Review and Meta-Analysis of 30 Randomized Controlled Trials. *Front. Public Heal.* **2022**, *10*, 814669.
54. Greeff, J.; Joubert, J.; Malan, S. F.; Van Dyk, S. Antioxidant Properties of 4-Quinolones and Structurally Related Flavones. *Bioorg. Med. Chem.* **2012**, *20* (2),

- 809–818.
55. Peluso, I.; Raguzzini, A.; Serafini, M. Effect of Flavonoids on Circulating Levels of TNF- α and IL-6 in Humans: A Systematic Review and Meta-Analysis. *Mol. Nutr. Food Res.* **2013**, *57* (5), 784–801.
 56. Guz, N. R.; Stermitz, F. R.; Johnson, J. B.; Beeson, T. D.; Willen, S.; et al. Flavonolignan and Flavone Inhibitors of a Staphylococcus Aureus Multidrug Resistance Pump: Structure-Activity Relationships. *J. Med. Chem.* **2001**, *44* (2), 261–268.
 57. Li, G.; Zhu, Y.; Zhang, Y.; Lang, J.; Chen, Y.; et al. Estimated Daily Flavonoid and Stilbene Intake from Fruits, Vegetables, and Nuts and Associations with Lipid Profiles in Chinese Adults. *J. Acad. Nutr. Diet.* **2013**, *113* (6), 786–794.
 58. Spencer, J. P. E.; Vafeiadou, K.; Williams, R. J.; Vauzour, D. Neuroinflammation: Modulation by Flavonoids and Mechanisms of Action. *Mol. Aspects Med.* **2012**, *33* (1), 83–97.
 59. Wang, T. yang; Li, Q.; Bi, K. shun. Bioactive Flavonoids in Medicinal Plants: Structure, Activity and Biological Fate. *Asian J. Pharm. Sci.* **2018**, *13* (1), 12–23.
 60. Kopustinskiene, D. M.; Jakstas, V.; Savickas, A.; Bernatoniene, J. Flavonoids as Anticancer Agents. *Nutrients* **2020**, *12* (2), 1–25.
 61. Bao, L.; Liu, F.; Guo, H. bin; Li, Y.; Tan, B. bo; et al. Naringenin Inhibits Proliferation, Migration, and Invasion as Well as Induces Apoptosis of Gastric Cancer SGC7901 Cell Line by Downregulation of AKT Pathway. *Tumor Biol.* **2016**, *37* (8), 11365–11374.
 62. Jiang, Z. Q.; Li, M. H.; Qin, Y. M.; Jiang, H. Y.; Zhang, X.; et al. Luteolin Inhibits Tumorigenesis and Induces Apoptosis of Non-Small Cell Lung Cancer Cells via Regulation of MicroRNA-34a-5p. *Int. J. Mol. Sci.* **2018**, *19* (2), 447.
 63. Sirico, M.; D'Angelo, A.; Gianni, C.; Casadei, C.; Merloni, F.; et al. Current State and Future Challenges for PI3K Inhibitors in Cancer Therapy. *Cancers (Basel)*. **2023**, *15* (3), 703.
 64. Bruning, A. Inhibition of MTOR Signaling by Quercetin in Cancer Treatment and Prevention. *Anticancer. Agents Med. Chem.* **2013**, *13* (7), 1025–1031.
 65. Granato, M.; Rizzello, C.; Montani, M. S. G.; Cuomo, L.; Vitillo, M.; et al. Quercetin Induces Apoptosis and Autophagy in Primary Effusion Lymphoma Cells by Inhibiting PI3K/AKT/MTOR and STAT3 Signaling Pathways. *J. Nutr. Biochem.* **2017**, *41*, 124–136.
 66. Zhu, Y.; Mao, Y.; Chen, H.; Lin, Y.; Hu, Z.; et al. Apigenin Promotes Apoptosis, Inhibits Invasion and Induces Cell Cycle Arrest of T24 Human Bladder Cancer Cells. *Cancer Cell Int.* **2013**, *13* (1), 1–7.
 67. Chen, Y.; Wang, S.; Geng, B.; Yi, Z. Pelargonidin Induces Antitumor Effects in Human Osteosarcoma Cells via Autophagy Induction, Loss of Mitochondrial Membrane Potential, G2/M Cell Cycle Arrest and Downregulation of PI3K/AKT Signalling Pathway. *JBUON* **2018**, *23* (3), 735–740.

68. Ai, X.-Y.; Qin, Y.; Liu, H.-J.; Cui, Z.-H.; Li, M.; et al. Apigenin Inhibits Colonic Inflammation and Tumorigenesis by Suppressing STAT3-NF-KB Signaling. *Oncotarget* **2017**, *8* (59), 100216–100226.
69. Lim, W.; Song, G. Inhibitory Effects of Delphinidin on the Proliferation of Ovarian Cancer Cells via PI3K/AKT and ERK 1/2 MAPK Signal Transduction. *Oncol. Lett.* **2017**, *14* (1), 810–818.
70. Zhang, X. H.; Hsiang, J.; Rosen, S. T. Flavopiridol (Alvocidib), a Cyclin-Dependent Kinases (CDKs) Inhibitor, Found Synergy Effects with Niclosamide in Cutaneous T-Cell Lymphoma. *J. Clin. Haematol.* **2021**, *2* (2), 48–61.
71. Kelland, L. R. Flavopiridol, the First Cyclin-Dependent Kinase Inhibitor to Enter the Clinic: Current Status. *Expert Opin. Investig. Drugs* **2000**, *9* (12), 2903–2911.
72. Bonvini, P.; Zorzi, E.; Mussolin, L.; Monaco, G.; Pigazzi, M.; et al. The Effect of the Cyclin-Dependent Kinase Inhibitor Flavopiridol on Anaplastic Large Cell Lymphoma Cells and Relationship with NPM-ALK Kinase Expression and Activity. *Haematologica* **2009**, *94* (7), 944.
73. Li, J.; Cheng, Y.; Qu, W.; Sun, Y.; Wang, Z.; et al. Fisetin, a Dietary Flavonoid, Induces Cell Cycle Arrest and Apoptosis through Activation of P53 and Inhibition of NF-Kappa B Pathways in Bladder Cancer Cells. *Basic Clin. Pharmacol. Toxicol.* **2011**, *108* (2), 84–93.
74. Choi, E. J.; Kim, G. H. Apigenin Causes G2/M Arrest Associated with the Modulation of P21Cip1 and Cdc2 and Activates P53-Dependent Apoptosis Pathway in Human Breast Cancer SK-BR-3 Cells. *J. Nutr. Biochem.* **2009**, *20* (4), 285–290.
75. Engeland, K. Cell Cycle Regulation: P53-P21-RB Signaling. *Cell Death Differ.* **2022**, *29* (5), 946–960.
76. Boege, F.; Straub, T.; Kehr, A.; Boesenberg, C.; Christiansen, K.; et al. Selected Novel Flavones Inhibit the DNA Binding or the DNA Religation Step of Eukaryotic Topoisomerase I. *J. Biol. Chem.* **1996**, *271* (4), 2262–2270.
77. Chowdhury, A. R.; Sharma, S.; Mandal, S.; Goswami, A.; Mukhopadhyay, S.; et al. Luteolin, an Emerging Anti-Cancer Flavonoid, Poisons Eukaryotic DNA Topoisomerase I. *Biochem. J.* **2002**, *366* (2), 653–661.
78. Wei, Q.; Zhang, Y. H. Flavonoids with Anti-Angiogenesis Function in Cancer. *Molecules* **2024**, *29* (7), 1570.
79. Yang, Y.; Sun, M.; Wang, L.; Jiao, B. HIFs, Angiogenesis, and Cancer. *J. Cell. Biochem.* **2013**, *114* (5), 967–974.
80. Song, X.; Yao, J.; Wang, F.; Zhou, M.; Zhou, Y.; et al. Wogonin Inhibits Tumor Angiogenesis via Degradation of HIF-1 α Protein. *Toxicol. Appl. Pharmacol.* **2013**, *271* (2), 144–155.
81. Chen, J.; Chen, A. Y.; Huang, H.; Ye, X.; Rollyson, W. D.; et al. The Flavonoid Nobiletin Inhibits Tumor Growth and Angiogenesis of Ovarian Cancers via the Akt Pathway. *Int. J. Oncol.* **2015**, *46* (6), 2629–2638.

82. Lu, N.; Gao, Y.; Ling, Y.; Chen, Y.; Yang, Y.; et al. Wogonin Suppresses Tumor Growth in Vivo and VEGF-Induced Angiogenesis through Inhibiting Tyrosine Phosphorylation of VEGFR2. *Life Sci.* **2008**, *82* (17–18), 956–963.
83. Jiang, H.; Wu, D.; Xu, D.; Yu, H.; Zhao, Z.; et al. Eupafolin Exhibits Potent Anti-Angiogenic and Antitumor Activity in Hepatocellular Carcinoma. *Int. J. Biol. Sci.* **2017**, *13* (6), 701–711.
84. Pratheeshkumar, P.; Budhraj, A.; Son, Y. O.; Wang, X.; Zhang, Z.; et al. Quercetin Inhibits Angiogenesis Mediated Human Prostate Tumor Growth by Targeting VEGFR- 2 Regulated AKT/MTOR/P70S6K Signaling Pathways. *PLoS One* **2012**, *7* (10), e47516.
85. Pratheeshkumar, P.; Son, Y. O.; Budhraj, A.; Wang, X.; Ding, S.; et al. Luteolin Inhibits Human Prostate Tumor Growth by Suppressing Vascular Endothelial Growth Factor Receptor 2-Mediated Angiogenesis. *PLoS One* **2012**, *7* (12), 52279.
86. Lin, C.; Wu, M.; Dong, J. Quercetin-4'-o- β -d-Glucopyranoside (QODG) Inhibits Angiogenesis by Suppressing VEGFR2-Mediated Signaling in Zebrafish and Endothelial Cells. *PLoS One* **2012**, *7* (2), 31708.
87. Chin, H. K.; Horng, C. T.; Liu, Y. S.; Lu, C. C.; Su, C. Y.; et al. Kaempferol Inhibits Angiogenic Ability by Targeting VEGF Receptor-2 and Downregulating the PI3K/AKT, MEK and ERK Pathways in VEGF-Stimulated Human Umbilical Vein Endothelial Cells. *Oncol. Rep.* **2018**, *39* (5), 2351–2357.
88. Li, Q.; Wang, Y.; Zhang, L.; Chen, L.; Du, Y.; et al. Naringenin Exerts Anti-Angiogenic Effects in Human Endothelial Cells: Involvement of ERR α /VEGF/KDR Signaling Pathway. *Fitoterapia* **2016**, *111*, 78–86.
89. Qiu, J. G.; Wang, L.; Liu, W. J.; Wang, J. F.; Zhao, E. J.; et al. Apigenin Inhibits IL-6 Transcription and Suppresses Esophageal Carcinogenesis. *Front. Pharmacol.* **2019**, *10*, 474288.
90. Chang, G.-D.; Tsai, P.-H.; Cheng, C.-H.; Lin, C.-Y.; Huang, Y.-T.; et al. Dietary Flavonoids Luteolin and Quercetin Suppressed Cancer Stem Cell Properties and Metastatic Potential of Isolated Prostate Cancer Cells. *Anticancer Res.* **2016**, *36* (12), 6367–6380.
91. Cheng, H.; Hsieh, M.; Yang, J.; Lin, C.; Oncotarget, K. L.-; et al. Nobiletin Inhibits Human Osteosarcoma Cells Metastasis by Blocking ERK and JNK-Mediated MMPs Expression. *Oncotarget* **2016**, *7* (23), 35208.
92. Liskova, A.; Koklesova, L.; Samec, M.; Varghese, E.; Abotaleb, M.; et al. Implications of Flavonoids as Potential Modulators of Cancer Neovascularity. *J. Cancer Res. Clin. Oncol.* **2020**, *146* (12), 3079–3096.
93. Bisol, Â.; De Campos Paloma, Santos Lamers, M. L. Flavonoids as Anticancer Therapies: A Systematic Review of Clinical Trials. *Phyther. Res.* **2020**, *34* (3), 568–582.
94. Gupta, P.; Narayanan, S.; Yang, D.-H. CDK Inhibitors as Sensitizing Agents for

- Cancer Chemotherapy. In *Protein Kinase Inhibitors as Sensitizing Agents for Chemotherapy*; Academic Press, 2019; pp 125–149.
95. Karp, J. E.; Blackford, A.; Smith, B. D.; Alino, K.; Seung, A. H.; et al. Clinical Activity of Sequential Flavopiridol, Cytosine Arabinoside, and Mitoxantrone for Adults with Newly Diagnosed, Poor-Risk Acute Myelogenous Leukemia. *Leuk. Res.* **2010**, *34* (7), 877–882.
 96. Senderowicz, A. M. Flavopiridol: The First Cyclin-Dependent Kinase Inhibitor in Human Clinical Trials. **1999**, *17* (3), 313–320.
 97. Cicenas, J.; Simkus, J. CDK Inhibitors and FDA: Approved and Orphan. *Cancers (Basel)*. **2024**, *16* (8), 1555.
 98. Vogelzang, N. J.; George, B.; Ashenbamer, N.; Edenfield, W. J.; Richards, D.; et al. Phase 1, First-in-Human, Dose-Escalation Study of Oral TP-1287, a Cyclin Dependent Kinase 9 (CDK9) Inhibitor, in Patients (Pts) with Advanced Solid Tumors (ASTs) [Abstract]. In *Proceedings of the American Association for Cancer Research Annual Meeting*; American Association for Cancer Research, 2022; Vol. 82, pp CT191–CT191.
 99. Dey, J.; Deckwerth, T. L.; Kerwin, W. S.; Casalini, J. R.; Merrell, A. J.; et al. Voruciclib, a Clinical Stage Oral CDK9 Inhibitor, Represses MCL-1 and Sensitizes High-Risk Diffuse Large B-Cell Lymphoma to BCL2 Inhibition. *Sci. Rep.* **2017**, *7* (1), 18007.
 100. FDA approval of lymphoma medicine Ukoniq (umbralisib) is withdrawn due to safety concerns | FDA <https://www.fda.gov/drugs/drug-safety-and-availability/fda-approval-lymphoma-medicine-ukoniq-umbralisib-withdrawn-due-safety-concerns> (accessed Apr 22, 2024).
 101. Zhang, C.; Sui, X.; Jiang, Y.; Wang, X.; Wang, S. Antitumor Effects of Icaritin and the Molecular Mechanisms. *Discov. Med.* **2020**, *29* (156), 5–16.
 102. Liu, X.; Yang, F.; Jia, D.; Dong, X.; Zhang, Y.; et al. Case Report: A Case Study on the Treatment Using Icaritin Soft Capsules in Combination with Lenvatinib Achieving Impressive PR and Stage Reduction in Unresectable Locally Progressive Pancreatic Cancer and a Literature Review. *Front. Genet.* **2023**, *14*, 1167470.
 103. Safe, S.; Jayaraman, A.; Chapkin, R. S.; Howard, M.; Mohankumar, K.; et al. Flavonoids: Structure–Function and Mechanisms of Action and Opportunities for Drug Development. *Toxicol. Res.* **2021**, *37* (2), 147–162.
 104. Hostetler, G. L.; Ralston, R. A.; Schwartz, S. J. Flavones: Food Sources, Bioavailability, Metabolism, and Bioactivity. *Adv. Nutr. An Int. Rev. J.* **2017**, *8* (3), 423–435.
 105. Teng, H.; Zheng, Y.; Cao, H.; Huang, Q.; Xiao, J.; et al. Enhancement of Bioavailability and Bioactivity of Diet-Derived Flavonoids by Application of Nanotechnology: A Review. *Crit. Rev. Food Sci. Nutr.* **2021**, *June* (27), 1–16.
 106. Loftsson, T. Drug Solubilization by Complexation. *Int. J. Pharm.* **2017**, *531* (1),

- 276–280.
107. Ross, D. L.; Riley, C. M. Physicochemical Properties of the Fluoroquinolone Antimicrobials. III. Complexation of Lomefloxacin with Various Metal Ions and the Effect of Metal Ion Complexation on Aqueous Solubility. *Int. J. Pharm.* **1992**, *87* (1–3), 203–213.
 108. Manning, T. J.; Ogburn, R. N.; Ledwith, K. V.; Philips, D. R.; Wylie, G. P. Copper Ion Delivery Platform for Pharmaceutical Agents. *13/418,235*, 2013.
 109. Sareen, R.; Jain, N.; Dhar, K. L. Curcumin–Zn(II) Complex for Enhanced Solubility and Stability: An Approach for Improved Delivery and Pharmacodynamic Effects. *Pharm. Dev. Technol.* **2016**, *21* (5), 630–635.
 110. Kurzwernhart, A.; Kandioller, W.; Bächler, S.; Bartel, C.; Martic, S.; et al. Structure-Activity Relationships of Targeted Ru(II)- η^6 -P-Cymene Anticancer Complexes with Flavonol-Derived Ligands. *J. Med. Chem.* **2012**, *55* (23), 10512–10522.
 111. Nishijima, T.; Iwai, K.; Saito, Y.; Takida, Y. Chronic Ingestion of Apple Pectin Can Enhance the Absorption of Quercetin. *J. Agric. Food Chem.* **2009**, *57* (6), 2583–2587.
 112. Qian, J.; Meng, H.; Xin, L.; Xia, M.; Shen, H.; et al. Self-Nanoemulsifying Drug Delivery Systems of Myricetin: Formulation Development, Characterization, and in Vitro and in Vivo Evaluation. *Colloids Surfaces B Biointerfaces* **2017**, *160*, 101–109.
 113. Jain, S.; Jain, A.; Pohekar, M.; Thanki, K. Novel Self-Emulsifying Formulation of Quercetin for Improved in Vivo Antioxidant Potential: Implications for Drug-Induced Cardiotoxicity and Nephrotoxicity. *Free Radic. Biol. Med.* **2013**, *65*, 117–130.
 114. Hollman, P. C. H. Absorption, Bioavailability, and Metabolism of Flavonoids. *Pharm. Biol.* **2004**, *42* (SUP1), 74–83.
 115. Walle, T.; Ta, N.; Kawamori, T.; Wen, X.; Tsuji, P. A.; et al. Cancer Chemopreventive Properties of Orally Bioavailable Flavonoids-Methylated versus Unmethylated Flavones. *Biochem. Pharmacol.* **2007**, *73* (9), 1288–1296.
 116. Martau, G. A.; Mihai, M.; Vodnar, D. C. The Use of Chitosan, Alginate, and Pectin in the Biomedical and Food Sector—Biocompatibility, Bioadhesiveness, and Biodegradability. *Polymers (Basel)*. **2019**, *11* (11), 1837.
 117. Khater, M.; Ravishankar, D.; Greco, F.; Osborn, H. M. I. Metal Complexes of Flavonoids: Their Synthesis, Characterization and Enhanced Antioxidant and Anticancer Activities. *Future Med. Chem.* **2019**, *11* (21), 2845–2867.
 118. Zeng, L.; Gupta, P.; Chen, Y.; Wang, E.; Ji, L.; et al. The Development of Anticancer Ruthenium(II) Complexes: From Single Molecule Compounds to Nanomaterials. *Chem. Soc. Rev.* **2017**, *46* (19), 5771–5804.
 119. Muhammad, N.; Guo, Z. Metal-Based Anticancer Chemotherapeutic Agents. *Curr. Opin. Chem. Biol.* **2014**, *19* (1), 144–153.

120. Lin, K.; Zhao, Z. Z.; Bo, H. Ben; Hao, X. J.; Wang, J. Q. Applications of Ruthenium Complex in Tumor Diagnosis and Therapy. *Front. Pharmacol.* **2018**, *9* (NOV), 1323–1332.
121. Antonarakis, E. S.; Emadi, A. Ruthenium-Based Chemotherapeutics: Are They Ready for Prime Time? *Cancer Chemother. Pharmacol.* **2010**, *66* (1), 1–9.
122. Das, U.; Kar, B.; Pete, S.; Paira, P. Ru (II), Ir (III), Re (I) and Rh (III) Based Complexes as next Generation Anticancer Metallopharmaceuticals. *Dalton* **2021**, *50* (32), 11259–11290.
123. Chen, H.; Parkinson, J. A.; Morris, R. E.; Sadler, P. J. Highly Selective Binding of Organometallic Ruthenium Ethylenediamine Complexes to Nucleic Acids: Novel Recognition Mechanisms. *J. Am. Chem. Soc.* **2003**, *125* (1), 173–186.
124. Luo, Z.; Yu, L.; Yang, F.; Zhao, Z.; Yu, B.; et al. Ruthenium Polypyridyl Complexes as Inducer of ROS-Mediated Apoptosis in Cancer Cells by Targeting Thioredoxin Reductase. *Metallomics* **2014**, *6* (8), 1480–1490.
125. Bregman, H.; Carroll, P. J.; Meggers, E. Rapid Access to Unexplored Chemical Space by Ligand Scanning around a Ruthenium Center: Discovery of Potent and Selective Protein Kinase Inhibitors. *J. Am. Chem. Soc.* **2006**, *128* (3), 877–884.
126. Feng, L.; Geisselbrecht, Y.; Blanck, S.; Wilbuer, A.; Atilla-Gokcumen, G. E.; et al. Structurally Sophisticated Octahedral Metal Complexes as Highly Selective Protein Kinase Inhibitors. *J. Am. Chem. Soc.* **2011**, *133* (15), 5976–5986.
127. Alessio, E.; Messori, L.; Alessio, E.; Messori, L. NAMI-A and KP1019/1339, Two Iconic Ruthenium Anticancer Drug Candidates Face-to-Face: A Case Story in Medicinal Inorganic Chemistry. *Molecules* **2019**, *24* (10), 1995.
128. Coverdale, J. P. C.; Laroia-McCarron, T.; Romero-Canelón, I. Designing Ruthenium Anticancer Drugs: What Have We Learnt from the Key Drug Candidates? *Inorganics* **2019**, *7* (3), 31.
129. Kenny, R. G.; Marmion, C. J. Toward Multi-Targeted Platinum and Ruthenium Drugs - A New Paradigm in Cancer Drug Treatment Regimens? *Chem. Rev.* **2019**, *119* (2), 1058–1137.
130. Fan, C.; Wu, Q.; Chen, T.; Zhang, Y.; Zheng, W.; et al. Arene Ruthenium (II) Complexes Induce S-Phase Arrest in MG-63 Cells through Stabilization of c-Myc G-Quadruplex DNA. *Medchemcomm* **2014**, *5* (5), 597–602.
131. Du, J.; Zhang, E.; Zhao, Y.; Zheng, W.; Zhang, Y.; et al. Discovery of a Dual-Targeting Organometallic Ruthenium Complex with High Activity Inducing Early Stage Apoptosis of Cancer Cells. *Metallomics* **2015**, *7* (12), 1573–1583.
132. Thota, S.; Rodrigues, D. A.; Crans, D. C.; Barreiro, E. J. Ru(II) Compounds: Next-Generation Anticancer Metallotherapeutics? *J. Med. Chem.* **2018**, *61* (14), 5805–5821.
133. Vaidya, S. P.; Gadre, S.; Kamiseti, R. T.; Patra, M. Challenges and Opportunities in the Development of Metal-Based Anticancer Theranostic Agents. *Biosci. Rep.* **2022**, *42* (5), 20212160.

134. Liu, Z.; Romero-Canelón, I.; Qamar, B.; Hearn, J. M.; Habtemariam, A.; et al. The Potent Oxidant Anticancer Activity of Organoiridium Catalysts. *Angew. Chemie* **2014**, *126* (15), 4022–4027.
135. Poth, T.; Paulus, H.; Elias, H.; Dücker-Benfer, C.; Van Eldik, R. Kinetics and Mechanism of Water Substitution at Half-Sandwich Iridium(III) Aqua Cations $Cp^*Ir(A-B)(H_2O)_2^{2+}$ in Aqueous Solution ($Cp^* = H_5$ -Pentamethylcyclopentadienyl Anion; A-B = Bidentate N₉N or N,O Ligand). *Eur. J. Inorg. Chem.* **2001**, No. 5, 1361–1369.
136. Liu, Z.; Habtemariam, A.; Pizarro, A. M.; Fletcher, S. A.; Kisova, A.; et al. Organometallic Half-Sandwich Iridium Anticancer Complexes. *J. Med. Chem.* **2011**, *54* (8), 3011–3026.
137. Liu, Z.; Sadler, P. J. Organoiridium Complexes: Anticancer Agents and Catalysts. *Acc. Chem. Res.* **2014**, *47* (4), 1174–1185.
138. Habtemariam, A.; Zhe, L.; Soldevila, J.; Pizarro, A. Novel Iridium/Rhodium Anti-Cancer Compounds. CA2797921A1, 2013.
139. Ouyang, M.; Zeng, L.; Huang, H.; Jin, C.; Liu, J.; et al. Fluorinated Cyclometalated Iridium(III) Complexes as Mitochondria-Targeted Theranostic Anticancer Agents. *Dalt. Trans.* **2017**, *46* (20), 6734–6744.
140. Yellol, J.; Pérez, S. A.; Buceta, A.; Yellol, G.; Donaire, A.; et al. Novel C,N-Cyclometalated Benzimidazole Ruthenium(II) and Iridium(III) Complexes as Antitumor and Antiangiogenic Agents: A Structure-Activity Relationship Study. *J. Med. Chem.* **2015**, *58* (18), 7310–7327.
141. Gadre, S.; Manikandan, M.; Chakraborty, G.; Rayrikar, A.; Paul, S.; et al. Development of a Highly In Vivo Efficacious Dual Antitumor and Antiangiogenic Organoiridium Complex as a Potential Anti-Lung Cancer Agent. *J. Med. Chem.* **2023**, *66* (19), 13481–13500.
142. Wilbuer, A.; Vlecken, D. H.; Schmitz, D. J.; Kräling, K.; Harms, K.; et al. Iridium Complex with Antiangiogenic Properties. *Angew. Chemie - Int. Ed.* **2010**, *49* (22), 3839–3842.
143. Wang, F.; Habtemariam, A.; Van Der Geer, E. P. L.; Fernández, R.; Melchart, M.; et al. Controlling Ligand Substitution Reactions of Organometallic Complexes: Tuning Cancer Cell Cytotoxicity. *Proc. Natl. Acad. Sci. U. S. A.* **2005**, *102* (51), 18269–18274.
144. Kurzwernhart, A.; Kandioller, W.; Bartel, C.; Bächler, S.; Trondl, R.; et al. Targeting the DNA-Topoisomerase Complex in a Double-Strike Approach with a Topoisomerase Inhibiting Moiety and Covalent DNA Binder. *Chem. Commun.* **2012**, *48* (40), 4839.
145. Singh, A. K.; Saxena, G.; Sahabjada; Arshad, M. Synthesis, Characterization and Biological Evaluation of Ruthenium Flavanol Complexes against Breast Cancer. *Spectrochim. Acta - Part A Mol. Biomol. Spectrosc.* **2017**, *180*, 97–104.
146. Rubio, A. R.; González, R.; Busto, N.; Vaquero, M.; Iglesias, A. L.; et al.

- Anticancer Activity of Half-Sandwich Ru, Rh and Ir Complexes with Chrysin Derived Ligands: Strong Effect of the Side Chain in the Ligand and Influence of the Metal. *Pharmaceutics* **2021**, *13* (10), 1540.
147. Abotaleb, M.; Samuel, S. M.; Varghese, E.; Varghese, S.; Kubatka, P.; et al. Flavonoids in Cancer and Apoptosis. **2018**, *11* (1), 28.
 148. DerSimonian, R.; Laird, N. Meta-Analysis in Clinical Trials. *Control. Clin. Trials* **1986**, *7* (3), 177–188.
 149. Abe, O.; Abe, R.; Enomoto, K.; Kikuchi, K.; Koyama, H.; et al. Effects of Chemotherapy and Hormonal Therapy for Early Breast Cancer on Recurrence and 15-Year Survival: An Overview of the Randomised Trials. *Lancet* **2005**, *365* (9472), 1687–1717.
 150. Siddaway, A. P.; Wood, A. M.; Hedges, L. V. How to Do a Systematic Review: A Best Practice Guide for Conducting and Reporting Narrative Reviews, Meta-Analyses, and Meta-Syntheses. *Annu. Rev. Psychol.* **2019**, *70*, 747–770.
 151. Baumeister, R. F. Writing a Literature Review. *The Portable Mentor* **2013**, 119–132.
 152. Baumeister, R. F.; Leary, M. R. Writing Narrative Literature Reviews. *Rev. Gen. Psychol.* **1997**, *1* (3), 311–320.
 153. Cumming, G. The New Statistics: Why and How. *Psychol. Sci.* **2014**, *25* (1), 7–29.
 154. Lam, I. K.; Alex, D.; Wang, Y. H.; Liu, P.; Liu, A. L.; et al. In Vitro and in Vivo Structure and Activity Relationship Analysis of Polymethoxylated Flavonoids: Identifying Sinensetin as a Novel Antiangiogenesis Agent. *Mol. Nutr. Food Res.* **2012**, *56* (6), 945–956.
 155. Ravishankar, D.; Watson, K. A.; Boateng, S. Y.; Green, R. J.; Greco, F.; et al. Exploring Quercetin and Luteolin Derivatives as Antiangiogenic Agents. *Eur. J. Med. Chem.* **2015**, *97*, 259–274.
 156. Carvalho, M. T. B.; Araújo-Filho, H. G.; Barreto, A. S.; Quintans-Júnior, L. J.; Quintans, J. S. S.; et al. Wound Healing Properties of Flavonoids: A Systematic Review Highlighting the Mechanisms of Action. *Phytomedicine* **2021**, *90*, 153636.
 157. Jung, Y.; Jerng, U.; Lee, S. A Systematic Review of Anticancer Effects of Radix Astragali. *Chin. J. Integr. Med.* **2016**, *22* (3), 225–236.
 158. Ghanbari-Movahed, M.; Jackson, G.; Farzaei, M. H.; Bishayee, A. A Systematic Review of the Preventive and Therapeutic Effects of Naringin Against Human Malignancies. *Front. Pharmacol.* **2021**, *12*, 29.
 159. Parvareh, A.; Razavi, R.; Rafie, N.; Ghiasvand, R.; Pourmasoumi, M.; et al. Quercetin and Ovarian Cancer: An Evaluation Based on a Systematic Review. *J. Res. Med. Sci.* **2016**, *21* (2).
 160. Khan, Y. H.; Uttra, A. M.; Qasim, S.; Mallhi, T. H.; Alotaibi, N. H.; et al. Potential Role of Phytochemicals Against Matrix Metalloproteinase Induced Breast Cancer; An Explanatory Review. *Frontiers in Chemistry*. Frontiers Media S.A. January 15,

- 2021, p 592152.
161. Khuayjarernpanishk, T.; Sookying, S.; Duangjai, A.; Saokaew, S.; Sanbua, A.; et al. Anticancer Activities of Polygonum Odoratum Lour.: A Systematic Review. *Front. Pharmacol.* **2022**, *13*, 875016.
 162. Khater, M.; Greco, F.; Osborn, H. M. I. Antiangiogenic Activity of Flavonoids: A Systematic Review and Meta-Analysis. *Molecules* **2020**, *25* (20), 4712–4742.
 163. Moher, D.; Shamseer, L.; Clarke, M.; Ghersi, D.; Liberati, A.; et al. Preferred Reporting Items for Systematic Review and Meta-Analysis Protocols (PRISMA-P) 2015 Statement. *Rev. Esp. Nutr. Humana y Diet.* **2016**, *20* (2), 148–160.
 164. International Agency for Research on Cancer. GLOBOCAN https://gco.iarc.fr/overtime/en/dataviz/bars?cancers=0&mode=cancer&sexes=1_2&years=2019&types=1 (accessed Jul 10, 2024).
 165. Staton, C. A.; Stribbling, S. M.; Tazzyman, S.; Hughes, R.; Brown, N. J.; et al. Current Methods for Assaying Angiogenesis in Vitro and in Vivo. *Int. J. Experimental Biol.* **2004**, *85* (5), 233–248.
 166. Nguyen, M.; Shing, Y.; Folkman, J. Quantitation of Angiogenesis and Antiangiogenesis in the Chick Embryo Chorioallantoic Membrane. *Microvasc. Res.* **1994**, *47* (1), 31–40.
 167. Ribatti, D.; Vacca, A.; Roncali, L.; Dammacco, F. The Chick Embryo Chorioallantoic Membrane as a Model for in Vivo Research on Angiogenesis. *Int. J. Dev. Biol.* **1996**, *40* (6), 1189–1197.
 168. Chu, P. Y.; Koh, A. P. F.; Antony, J.; Huang, R. Y. J. Applications of the Chick Chorioallantoic Membrane as an Alternative Model for Cancer Studies. *Rev. Artic. Cells Tissues Organs* **2022**, *211* (2), 222–237.
 169. Norrby, K. In Vivo Models of Angiogenesis. *J. Cell. Mol. Med.* **2006**, *10* (3), 588–612.
 170. Ribatti, D.; Vacca, A. Models for Studying Angiogenesis in Vivo. *Int. J. Biol. Markers* **1999**, *14* (4), 207–213.
 171. Kennedy, D. C.; Coen, B.; Wheatley, A. M.; McCullagh, K. J. A. Microvascular Experimentation in the Chick Chorioallantoic Membrane as a Model for Screening Angiogenic Agents Including from Gene-Modified Cells. *Int. J. Mol. Sci.* **2022**, *23* (1), 452.
 172. Lee, Y. H. An Overview of Meta-Analysis for Clinicians. *Korean J. Intern. Med.* **2018**, *33* (2), 277.
 173. Zhao, K.; Yuan, Y.; Lin, B.; Miao, Z.; Li, Z.; et al. LW-215 , a Newly Synthesized Flavonoid , Exhibits Potent Anti-Angiogenic Activity in Vitro and in Vivo. *Gene* **2018**, *642*, 533–541.
 174. Chen, Y.; Lu, N.; Ling, Y.; Wang, L.; You, Q.; et al. LYG-202, a Newly Synthesized Flavonoid, Exhibits Potent Anti-Angiogenic Activity in Vitro and in Vivo. *J. Pharmacol. Sci.* **2010**, *112* (1), 37–45.

175. Hattori, H.; Okuda, K.; Murase, T.; Shigetsura, Y.; Narise, K.; et al. Isolation, Identification, and Biological Evaluation of HIF-1-Modulating Compounds from Brazilian Green Propolis. *Bioorganic Med. Chem.* **2011**, *19* (18), 5392–5401.
176. Tan, W. F.; Lin, L. P.; Li, M. H.; Zhang, Y. X.; Tong, Y. G.; et al. Quercetin, a Dietary-Derived Flavonoid, Possesses Antiangiogenic Potential. *Eur. J. Pharmacol.* **2003**, *459* (2–3), 255–262.
177. Favot, L.; Martin, S.; Keravis, T.; Andriantsitohaina, R.; Lugnier, C. Involvement of Cyclin-Dependent Pathway in the Inhibitory Effect of Delphinidin on Angiogenesis. *Cardiovasc. Res.* **2003**, *59* (2), 479–487.
178. Panda, S. P.; Panigrahy, U. P.; Prasanth, D. S. N. B. K.; Gorla, U. S.; Guntupalli, C.; et al. A Trimethoxy Flavonoid Isolated from Stem Extract of *Tabebuia Chrysantha* Suppresses Angiogenesis in Angiosarcoma. *J. Pharm. Pharmacol.* **2020**, *72*, 990–999.
179. Chen, Y.; Lu, N.; Ling, Y.; Gao, Y.; Wang, L.; et al. Wogonoside Inhibits Lipopolysaccharide-Induced Angiogenesis in Vitro and in Vivo via Toll-like Receptor 4 Signal Transduction. *Toxicology* **2009**, *259* (1–2), 10–17.
180. Gacche, R. N.; Shegokar, H. D.; Gond, D. S.; Yang, Z.; Jadhav, A. D. Evaluation of Selected Flavonoids as Antiangiogenic, Anticancer, and Radical Scavenging Agents: An Experimental and In Silico Analysis. *Cell Biochem. Biophys.* **2011**, *61* (3), 651–663.
181. Gacche, R. N.; Meshram, R. J.; Shegokar, H. D.; Gond, D. S.; Kamble, S. S.; et al. Flavonoids as a Scaffold for Development of Novel Anti-Angiogenic Agents: An Experimental and Computational Enquiry. *Arch. Biochem. Biophys.* **2015**, *577*, 35–48.
182. Rajesh, G.; Harshala, S.; Dhananjay, G.; Jadhav, A.; Vikram, G. Effect of Hydroxyl Substitution of Flavone on Angiogenesis and Free Radical Scavenging Activities: A Structure-Activity Relationship Studies Using Computational Tools. *Eur. J. Pharm. Sci.* **2010**, *39* (1–3), 37–44.
183. Meng, G.; Chai, K.; Li, X.; Zhu, Y.; Huang, W. Luteolin Exerts Pro-Apoptotic Effect and Anti-Migration Effects on A549 Lung Adenocarcinoma Cells through the Activation of MEK/ERK Signaling Pathway. *Chem. Biol. Interact.* **2016**, *257*, 26–34.
184. Viegas, O.; Faria, M. A.; Sousa, J. B.; Vojtek, M.; Gonçalves-Monteiro, S.; et al. Delphinidin-3-O-Glucoside Inhibits Angiogenesis via VEGFR2 Downregulation and Migration through Actin Disruption. *J. Funct. Foods* **2019**, *54*, 393–402.
185. Bhat, T. A.; Nambiar, D.; Tailor, D.; Pal, A.; Agarwal, R.; et al. Acacetin Inhibits in Vitro and in Vivo Angiogenesis and Downregulates Stat Signaling and VEGF Expression. *Cancer Prev. Res.* **2013**, *6* (10), 1–7.
186. Oh, S. J.; Kim, O.; Lee, J. S.; Kim, J. A.; Kim, M. R.; et al. Inhibition of Angiogenesis by Quercetin in Tamoxifen-Resistant Breast Cancer Cells. *Food Chem. Toxicol.* **2010**, *48* (11), 3227–3234.

187. Liu, L. Z.; Jing, Y.; Jiang, L. L.; Jiang, X. E.; Jiang, Y.; et al. Acacetin Inhibits VEGF Expression, Tumor Angiogenesis and Growth through AKT/HIF-1 α Pathway. *Biochem. Biophys. Res. Commun.* **2011**, *413* (2), 299–305.
188. Huang, H.; Chen, A. Y.; Rojanasakul, Y.; Ye, X.; Rankin, G. O.; et al. Dietary Compounds Galangin and Myricetin Suppress Ovarian Cancer Cell Angiogenesis. *J. Funct. Foods* **2015**, *15*, 464–475.
189. Huang, Y.; Fang, J.; Lu, W.; Wang, Z.; Wang, Q.; et al. A Systems Pharmacology Approach Uncovers Wogonoside as an Angiogenesis Inhibitor of Triple-Negative Breast Cancer by Targeting Hedgehog Signaling. *Cell Chem. Biol.* **2019**, *26* (8), 1143–1158.
190. Huang, Y.; Zhao, K.; Hu, Y.; Zhou, Y.; Luo, X.; et al. Wogonoside Inhibits Angiogenesis in Breast Cancer via Suppressing Wnt/ β -Catenin Pathway. *Mol. Carcinog.* **2016**, *55* (11), 1598–1612.
191. Fang, J.; Zhou, Q.; Liu, L. Z.; Xia, C.; Hu, X.; et al. Apigenin Inhibits Tumor Angiogenesis through Decreasing HIF-1 α and VEGF Expression. *Carcinogenesis* **2007**, *28* (4), 858–864.
192. Luo, H.; Rankin, G. O.; Liu, L.; Daddysman, M. K.; Jiang, B. H.; et al. Kaempferol Inhibits Angiogenesis and VEGF Expression through Both HIF Dependent and Independent Pathways in Human Ovarian Cancer Cells. *Nutr. Cancer* **2009**, *61* (4), 554–563.
193. Lin, C. M.; Chang, H.; Chen, Y. H.; Li, S. Y.; Wu, I. H.; et al. Protective Role of Wogonin against Lipopolysaccharide-Induced Angiogenesis via VEGFR-2, Not VEGFR-1. *Int. Immunopharmacol.* **2006**, *6* (11), 1690–1698.
194. Lin, C. M.; Chang, H.; Chen, Y. H.; Wu, I. H.; Chiu, J. H. Wogonin Inhibits IL-6-Induced Angiogenesis via down-Regulation of VEGF and VEGFR-1, Not VEGFR-2. *Planta Med.* **2006**, *72* (14), 1305–1310.
195. Li, X.; Chen, M.; Lei, X.; Huang, M.; Ye, W.; et al. Luteolin Inhibits Angiogenesis by Blocking Gas6/Axl Signaling Pathway. *Int. J. Oncol.* **2017**, *51* (2), 677–685.
196. Ciombor, K. K.; Berlin, J.; Chan, E. Aflibercept. *Clin. Cancer Res.* **2013**, *19* (8), 1920–1925.
197. Sak, K. Cytotoxicity of Dietary Flavonoids on Different Human Cancer Types. *Pharmacogn. Rev.* **2014**, *8* (16), 122–146.
198. Nowak-Sliwinska, P.; Weiss, A.; Van Beijnum, J. R.; Wong, T. J.; Kilarski, W. W.; et al. Photoactivation of Lysosomally Sequestered Sunitinib after Angiostatic Treatment Causes Vascular Occlusion and Enhances Tumor Growth Inhibition. *Cell Death Dis.* **2015**, *6* (2), 1641.
199. Gao, Y.; Rankin, G. O.; Tu, Y.; Chen, Y. C. Theaflavin-3, 3'-Digallate Decreases Human Ovarian Carcinoma OVCAR-3 Cell-Induced Angiogenesis via Akt and Notch-1 Pathways, Not via MAPK Pathways. *Int. J. Oncol.* **2016**, *48* (1), 281–292.
200. Kim, M. R.; Choi, H. S.; Heo, T. H.; Hwang, S. W.; Kang, K. W. Induction of Vascular Endothelial Growth Factor by Peptidyl-Prolyl Isomerase Pin1 in Breast

- Cancer Cells. *Biochem. Biophys. Res. Commun.* **2008**, 369 (2), 547–553.
201. Han, L.; Fu, Q.; Deng, C.; Luo, L.; Xiang, T.; et al. Immunomodulatory Potential of Flavonoids for the Treatment of Autoimmune Diseases and Tumour. *Scand. J. Immunol.* **2022**, 95 (1), 1–19.
202. Higgins, J.; Altman, D.; Gøtzsche, P.; Jüni, P.; Moher, D.; et al. The Cochrane Collaboration’s Tool for Assessing Risk of Bias in Randomised Trials. *BMJ* **2011**, 343.
203. Schneider, K.; Schwarz, M.; Burkholder, I.; Kopp-Schneider, A.; Edler, L.; et al. “ToxRTool”, a New Tool to Assess the Reliability of Toxicological Data. *Toxicol. Lett.* **2009**, 189 (2), 138–144.
204. NTP. *OHAT Risk of Bias Rating Tool for Human and Animal Studies*; 2015.
205. Tran, L.; Ngoc Hien Tam, D.; Elshafay, A.; Dang, T.; Hirayama, K.; et al. Quality Assessment Tools Used in Systematic Reviews of in Vitro Studies: A Systematic Review. *BMC Med. Res. Methodol.* **2021**, 21 (2), 101.
206. Paiva Barbosa, V.; Bastos Silveira, B.; Amorim dos Santos, J.; Monteiro, M. M.; Coletta, R. D.; et al. Critical Appraisal Tools Used in Systematic Reviews of in Vitro Cell Culture Studies: A Methodological Study. *Res. Synth. Methods* **2023**.
207. Hooijmans, C. R.; Rovers, M. M.; De Vries, R. B. M.; Leenaars, M.; Ritskes-Hoitinga, M.; et al. SYRCLE’s Risk of Bias Tool for Animal Studies. *BMC Med. Res. Methodol.* **2014**, 14 (1), 1–9.
208. Schulz, K. F.; Altman, D. G.; Moher, D. CONSORT 2010 Statement: Updated Guidelines for Reporting Parallel Group Randomised Trials. *BMC Med.* **2010**, 8 (1), 1–9.
209. ICCVAM-Recommended Test Method Protocol: Hen’s Egg Test-Chorioallantoic Membrane (HET-CAM) Test Method.
210. Higgins, J. P.; Green, S. Cochrane Handbook for Systematic Reviews of Interventions: Cochrane Book Series. *Cochrane Handb. Syst. Rev. Interv. Cochrane B. Ser.* **2008**, 1–649.
211. Von Hippel, P. T. The Heterogeneity Statistic I² Can Be Biased in Small Meta-Analyses. *BMC Med. Res. Methodol.* **2015**, 15 (1), 1–8.
212. Inthout, J.; Ioannidis, J. P. A.; Borm, G. F.; Goeman, J. J. Small Studies Are More Heterogeneous than Large Ones: A Meta-Meta-Analysis. *J. Clin. Epidemiol.* **2015**, 68 (8), 860–869.
213. Rücker, G.; Schwarzer, G.; Carpenter, J. R.; Schumacher, M. Undue Reliance on I² in Assessing Heterogeneity May Mislead. *BMC Med. Res. Methodol.* **2008**, 8 (1), 1–9.
214. Singh, M.; Kaur, M.; Silakari, O. Flavones: An Important Scaffold for Medicinal Chemistry. *Eur. J. Med. Chem.* **2014**, 84, 206–239.
215. Chidambara Murthy, K. N.; Kim, J.; Vikram, A.; Patil, B. S. Differential Inhibition of Human Colon Cancer Cells by Structurally Similar Flavonoids of Citrus. *Food*

- Chem.* **2012**, *132* (1), 27–34.
216. Chang, H.; Mi, M.; Ling, W.; Zhu, J.; Zhang, Q.; et al. Structurally Related Cytotoxic Effects of Flavonoids on Human Cancer Cells in Vitro. *Arch. Pharm. Res.* **2008**, *31* (9), 1137–1144.
217. Plochmann, K.; Korte, G.; Koutsilieri, E.; Richling, E.; Riederer, P.; et al. Structure–Activity Relationships of Flavonoid-Induced Cytotoxicity on Human Leukemia Cells. *Arch. Biochem. Biophys.* **2007**, *460* (1), 1–9.
218. Li, N.; Liu, J. H.; Zhang, J.; Yu, B. Y. Comparative Evaluation of Cytotoxicity and Antioxidative Activity of 20 Flavonoids. *J. Agric. Food Chem.* **2008**, *56* (10), 3876–3883.
219. Ravishankar, D.; Watson, K. A.; Greco, F.; Osborn, H. M. I. Novel Synthesised Flavone Derivatives Provide Significant Insight into the Structural Features Required for Enhanced Anti-Proliferative Activity. *RSC Adv.* **2016**, *6* (69), 64544–64556.
220. Haupt, V. J.; Daminelli, S.; Schroeder, M. Drug Promiscuity in PDB: Protein Binding Site Similarity Is Key. *PLoS One* **2013**, *8* (6), 65894.
221. Conseil, G.; Baubichon-Cortay, H.; Dayan, G.; Jault, J. M.; Barron, D.; et al. Flavonoids: A Class of Modulators with Bifunctional Interactions at Vicinal ATP- and Steroid-Binding Sites on Mouse P-Glycoprotein. *Proc. Natl. Acad. Sci. U. S. A.* **1998**, *95* (17), 9831–9836.
222. Wijnen, R.; Pecoraro, C.; Carbone, D.; Fuji, H.; Avan, A.; et al. Cyclin Dependent Kinase-1 (Cdk-1) Inhibition as a Novel Therapeutic Strategy against Pancreatic Ductal Adenocarcinoma (Pdac). *Cancers (Basel)*. **2021**, *13* (17).
223. Bose, S.; Sarkar, D.; Bose, A.; Subhash, & Mandal, C. Natural Flavonoids and Its Pharmaceutical Importance. *pharma Rev.* **2018**, *94*, 61–75.
224. López-Lázaro, M.; Gálvez, M.; Martín-Cordero, C.; Ayuso, M. J. Cytotoxicity of Flavonoids on Cancer Cell Lines. Structure-Activity Relationship. *Stud. Nat. Prod. Chem.* **2002**, *27*, 891–932.
225. Salehi, B.; Venditti, A.; Sharifi-Rad, M.; Kręgiel, D.; Sharifi-Rad, J.; et al. The Therapeutic Potential of Apigenin. *Int. J. Mol. Sci.* **2019**, *20* (6), 1305.
226. ADMETlab 3.0 <https://admetlab3.scbdd.com/> (accessed May 15, 2024).
227. Le Bail, J. C.; Varnat, F.; Nicolas, J. C.; Habrioux, G. Estrogenic and Antiproliferative Activities on MCF-7 Human Breast Cancer Cells by Flavonoids. *Cancer Lett.* **1998**, *130* (1–2), 209–216.
228. Fang, Y.; Cao, W.; Xia, M.; Pan, S.; Nutrients, X. X.-; et al. Study of Structure and Permeability Relationship of Flavonoids in Caco-2 Cells. *Nutrients* **2017**, *9* (12), 1301.
229. Moridani, M. Y.; Siraki, A.; Chevaldina, T.; Scobie, H.; O'Brien, P. J. Quantitative Structure Toxicity Relationships for Catechols in Isolated Rat Hepatocytes. *Chem. Biol. Interact.* **2004**, *147* (3), 297–307.

230. Murai, T. The Construction and Application of C=S Bonds. *Top. Curr. Chem.* **2018**, 376 (4), 1–21.
231. Mughal, E. U.; Sadiq, A.; Ashraf, J.; Zafar, M. N.; Sumrra, S. H.; et al. Flavonols and 4-Thioflavonols as Potential Acetylcholinesterase and Butyrylcholinesterase Inhibitors: Synthesis, Structure-Activity Relationship and Molecular Docking Studies. *Bioorg. Chem.* **2019**, 91, 103124.
232. Kataoka, T.; Watanabe, S. I.; Mori, E.; Kadomoto, R.; Tanimura, S.; et al. Synthesis and Structure-Activity Relationships of Thioflavone Derivatives as Specific Inhibitors of the ERK-MAP Kinase Signaling Pathway. *Bioorganic Med. Chem.* **2004**, 12 (9), 2397–2407.
233. Li, W.; Li, X.; Liu, M.; Wang, Q. Synthesis and Antiproliferative Activity of Thioxoflavones Mannich Base Derivatives. *Arch. Pharm. (Weinheim)*. **2017**, 350 (7), 1–7.
234. Ramos-Inza, S.; Plano, D.; Sanmartín, C. Metal-Based Compounds Containing Selenium: An Appealing Approach towards Novel Therapeutic Drugs with Anticancer and Antimicrobial Effects. *Eur. J. Med. Chem.* **2022**, 244, 114834.
235. Fernandes, A. P.; Gandin, V. Selenium Compounds as Therapeutic Agents in Cancer. *Biochim. Biophys. Acta - Gen. Subj.* **2015**, 1850 (8), 1642–1660.
236. Gandin, V.; Khalkar, P.; Braude, J.; Fernandes, A. P. Organic Selenium Compounds as Potential Chemotherapeutic Agents for Improved Cancer Treatment. *Free Radic. Biol. Med.* **2018**, 127 (April), 80–97.
237. Martins, I. L.; Charneira, C.; Gandin, V.; Ferreira Da Silva, J. L.; Justino, G. C.; et al. Selenium-Containing Chrysin and Quercetin Derivatives: Attractive Scaffolds for Cancer Therapy. *J. Med. Chem.* **2015**, 58 (10), 4250–4265.
238. Zhang, J.; Wu, Y.; Zhao, X.; Luo, F.; Li, X.; et al. Chemopreventive Effect of Flavonoids from Ougan (*Citrus Reticulata* Cv. *Suavissima*) Fruit against Cancer Cell Proliferation and Migration. *J. Funct. Foods* **2014**, 10, 511–519.
239. Yun, B. H.; Lee, Y. H.; Park, K. T.; Jung, S. J.; Lee, Y. S. Synthesis of Novel Flavone Derivatives Possessing Substituted Benzamides and Their Biological Evaluation against Human Cancer Cells. *Bioorg. Med. Chem. Lett.* **2016**, 26 (17), 4170–4173.
240. Wen, X.; Walle, T. Methylation Protects Dietary Flavonoids from Rapid Hepatic Metabolism. *Xenobiotica* **2006**, 36 (5), 387–397.
241. Wen, X.; Walle, T. Methylated Flavonoids Have Greatly Improved Intestinal Absorption and Metabolic Stability. *Drug Metab. Dispos.* **2006**, 34 (10), 1786–1792.
242. Walle, T. Methylation of Dietary Flavones Greatly Improves Their Hepatic Metabolic Stability and Intestinal Absorption. *Mol. Pharm.* **2007**, 4 (6), 826–832.
243. Mahal, H. S.; Rai, H. S.; Venkataraman, K. Synthetical Experiments in the Chromone Group. Part XVI. Chalkones and Flavanones and Their Oxidation to Flavones by Means of Selenium Dioxide. *J. Chem. Soc.* **1935**, No. 0, 866.

244. Baker, W. Molecular Rearrangement of Some O-Acyloxyacetophenones. *J. Chem. Soc.* **1933**, 1381–1389.
245. Saxena, S.; Makarandi, J. K.; Grover, S. K. Synthesis of 5- and/or 7-Hydroxyflavones Using a Modified Phase Transfer-Catalysed Baker-Venkataraman Transformation. *Synthesis (Stuttg)*. **1985**, No. 6–7, 697.
246. Verma, A. K.; Pratap, R. Chemistry of Biologically Important Flavones. *Tetrahedron* **2012**, *68* (41), 8523–8538.
247. Kshatriya, R.; Jejurkar, V. P.; Saha, S. In Memory of Prof. Venkataraman: Recent Advances in the Synthetic Methodologies of Flavones. *Tetrahedron* **2018**, *74* (8), 811–833.
248. Barbuceanu, S.-F.; Olaru, O. T.; Leonte, D.; Ungureanu, D.; Zaharia, V. Flavones and Related Compounds: Synthesis and Biological Activity. *Molecules* **2023**, *28* (18), 6528.
249. Stryker, Z. I.; Rajabi, M.; Davis, P. J.; Mousa, S. A. Evaluation of Angiogenesis Assays. *Biomedicines* **2019**, *7* (2), 37.
250. Jain, R. K.; Schlenger, K.; Höckel, M.; Yuan, F. Quantitative Angiogenesis Assays: Progress and Problems. *Nat. Med.* **1997**, *3* (11), 1203–1208.
251. Vukicevic, S.; Kleinman, H. K.; Luyten, F. P.; Roberts, A. B.; Roche, N. S.; et al. Identification of Multiple Active Growth Factors in Basement Membrane Matrigel Suggests Caution in Interpretation of Cellular Activity Related to Extracellular Matrix Components. *Exp. Cell Res.* **1992**, *202* (1), 1–8.
252. Goodwin, A. M. In Vitro Assays of Angiogenesis for Assessment of Angiogenic and Anti-Angiogenic Agents. *Microvasc. Res.* **2007**, *74* (2–3), 172–183.
253. Khater, M.; Watson, K. A.; Boateng, S. Y.; Greco, F.; Osborn, H. M. I. Halogenated Flavonoid Derivatives Display Antiangiogenic Activity. *Molecules* **2022**, *27* (15), 4757–4778.
254. Zaid, M. E. A.; Belboukhari, N.; Sekkoum, K.; Ibtissam, B.; Enein, H. Y. A. Synthesis and Chiral Separation of Some 4-Thioflavones. *J. Chromatogr. Sci.* **2021**, *59* (9), 856–862.
255. Basavanag Unnamatla, M. V; Montaña, R. G. Efficient and Rapid Conversion of 3-Amino-Imidazo [1,2-a]Pyridin-2-Yl-4H-Chromene-4-Ones to Its Corresponding Thio Analogues Using Lawesson's Reagent. In *Proceedings*; 2018; Vol. 2.
256. López-García, M. Á. Woollins' Reagent. *Synlett* **2009**, *2009* (14), 2373–2374.
257. Martins, I. L.; Miranda, J. P.; Oliveira, N. G.; Fernandes, A. S.; Gonçalves, S.; et al. Synthesis and Biological Activity of 6-Selenocaffeine: Potential Modulator of Chemotherapeutic Drugs in Breast Cancer Cells. *Molecules* **2013**, *18* (5), 5251–5264.
258. Spiegel, M. T.; Hoogerbrugge, A.; Truksa, S.; Smith, A. G.; Shuford, K. L.; et al. Synthesis of First Row Transition Metal Selenomaltol Complexes. *Dalt. Trans.* **2018**, *47* (27), 9030–9037.

259. Angeli, A.; Trallori, E.; Carta, F.; Di Cesare Mannelli, L.; Ghelardini, C.; et al. Heterocoumarins Are Selective Carbonic Anhydrase IX and XII Inhibitors with Cytotoxic Effects against Cancer Cells Lines. *ACS Med. Chem. Lett.* **2018**, *9* (9), 947–951.
260. Kim, J. D.; Liu, L.; Guo, W.; Meydani, M. Chemical Structure of Flavonols in Relation to Modulation of Angiogenesis and Immune-Endothelial Cell Adhesion. *J. Nutr. Biochem.* **2006**, *17* (3), 165–176.
261. Acton, A. L.; Fante, C.; Flatley, B.; Burattini, S.; Hamley, I. W.; et al. Janus PEG-Based Dendrimers for Use in Combination Therapy: Controlled Multi-Drug Loading and Sequential Release. *Biomacromolecules* **2013**, *14* (2), 564–574.
262. Jain, R. K. Normalization of Tumor Vasculature: An Emerging Concept in Antiangiogenic Therapy. *Science (80-.)*. **2005**, *307* (5706), 58–62.
263. Carpentier, G.; Berndt, S.; Ferratge, S.; Rasband, W.; Cuendet, M.; et al. Angiogenesis Analyzer for ImageJ — A Comparative Morphometric Analysis of “Endothelial Tube Formation Assay” and “Fibrin Bead Assay.” *Sci. Rep.* **2020**, *10* (1), 1–13.
264. Angiogenesis Analyzer for ImageJ - Gilles Carpentier Research Web Site: Computer Image Analysis <http://image.bio.methods.free.fr/ImageJ/?Angiogenesis-Analyzer-for-ImageJ> (accessed Oct 18, 2021).
265. Rasband, W. S. ImageJ. U.S. National Institutes of Health: Bethesda, Maryland, U.S.A.
266. Ferreira, A. K.; Freitas, V. M.; Levy, D.; Ruiz, J. L. M.; Bydlowski, S. P.; et al. Anti-Angiogenic and Anti-Metastatic Activity of Synthetic Phosphoethanolamine. *PLoS One* **2013**, *8* (3), 57937–57951.
267. Prasad Kumar Mahapatra, A.; Nanda, A.; Bhusan Mohapatra, B.; Prasada Kumar Mahapatra, A.; Prasad Kumar Mahapatra BALVIKAS, A.; et al. Multiple Comparison Test by Tukey’s Honestly Significant Difference (HSD): Do the Confident Level Control Type I Error. *Int. J. Stat. Appl. Math.* **2021**, *6* (1), 59–65.
268. Tribolo, S.; Lodi, F.; Connor, C.; Suri, S.; Wilson, V. G.; et al. Comparative Effects of Quercetin and Its Predominant Human Metabolites on Adhesion Molecule Expression in Activated Human Vascular Endothelial Cells. *Atherosclerosis* **2008**, *197* (1), 50–56.
269. Modi, S. J.; Kulkarni, V. M. Vascular Endothelial Growth Factor Receptor (VEGFR-2)/KDR Inhibitors: Medicinal Chemistry Perspective-NC-ND License ([Http://creativecommons.org/licenses/by-nc-nd/4.0/](http://creativecommons.org/licenses/by-nc-nd/4.0/)). **2019**.
270. Lemmon, M. A.; Schlessinger, J. Cell Signaling by Receptor-Tyrosine Kinases. *Cell* **2010**, *141* (7), 1117.
271. Moradi, M.; Mousavi, A.; Emamgholipour, Z.; Giovannini, J.; Moghimi, S.; et al. Quinazoline-Based VEGFR-2 Inhibitors as Potential Anti-Angiogenic Agents: A Contemporary Perspective of SAR and Molecular Docking Studies. *Eur. J. Med. Chem.* **2023**, *259*, 115626.

272. Abd El-Meguid, E. A.; Naglah, A. M.; Moustafa, G. O.; Awad, H. M.; El Kerdawy, A. M. Novel Benzothiazole-Based Dual VEGFR-2/EGFR Inhibitors Targeting Breast and Liver Cancers: Synthesis, Cytotoxic Activity, QSAR and Molecular Docking Studies. *Bioorg. Med. Chem. Lett.* **2022**, *58*, 128529.
273. Hou, D. X.; Kumamoto, T. Flavonoids as Protein Kinase Inhibitors for Cancer Chemoprevention: Direct Binding and Molecular Modeling. *Antioxid. Redox Signal.* **2010**, *13* (5), 691–719.
274. Baby, B.; Antony, P.; Vijayan, R. Interactions of Quercetin with Receptor Tyrosine Kinases Associated with Human Lung Carcinoma. *Nat. Prod. Res.* **2018**, *32* (24), 2928–2931.
275. Basha, S. H.; Bethapudi, P.; Rambabu, M.; Firoz, A.; Viswanadha, N. V. S. M.; et al. Anti-Angiogenesis Property by Quercetin Compound Targeting VEGFR2 Elucidated in a Computational Approach. *Eur. J. Biotechnol. Biosci.* **2014**, *2* (6), 30–46.
276. Sarkar, D.; Ganguly, A. Molecular Docking Studies with Garlic Phytochemical Constituents To Inhibit The Human EGFR Protein For Lung Cancer Therapy. *Int. J. Pharm. Sci.* **2022**, *13* (2), 1–14.
277. Mahmoud, M.; Ali, M. A.; Albohy, A.; Zada, S. K.; Tolba, M. F.; et al. Molecular Modeling Studies on Biochanin-A as a Potential Dual Inhibitor for VEGFR-2 and Cyclin D1-CDK-4 Complex. *Arch. Pharm. Sci.* **2021**, *5* (1), 16–32.
278. Walker, E. H.; Pacold, M. E.; Perisic, O.; Stephens, L.; Hawkins, P. T.; et al. Structural Determinants of Phosphoinositide 3-Kinase Inhibition by Wortmannin, LY294002, Quercetin, Myricetin, and Staurosporine. *Mol. Cell* **2000**, *6* (4), 909–919.
279. Miyazaki, Y.; Matsunaga, S.; Tang, J.; Maeda, Y.; Nakano, M.; et al. Novel 4-Amino-Furo[2,3-d]Pyrimidines as Tie-2 and VEGFR2 Dual Inhibitors. *Bioorg. Med. Chem. Lett.* **2005**, *15* (9), 2203–2207.
280. Chitranshi, N.; Gupta, V.; Kumar, S.; Graham, S. L. Exploring the Molecular Interactions of 7,8-Dihydroxyflavone and Its Derivatives with TrkB and VEGFR2 Proteins. *Int. J. Mol. Sci.* **2015**, *16* (9), 21087–21108.
281. Okamoto, K.; Ikemori-Kawada, M.; Jestel, A.; Von König, K.; Funahashi, Y.; et al. Distinct Binding Mode of Multikinase Inhibitor Lenvatinib Revealed by Biochemical Characterization. *ACS Med. Chem. Lett.* **2015**, *6* (1), 89–94.
282. El-Adl, K.; El-Helby, A. G. A.; Sakr, H.; El-Hddad, S. S. A. Design, Synthesis, Molecular Docking, and Anticancer Evaluations of 1-Benzylquinazoline-2,4(1H,3H)-Dione Bearing Different Moieties as VEGFR-2 Inhibitors. *Arch. Pharm. (Weinheim)*. **2020**, *353* (8), 2000068–2000081.
283. Zuccotto, F.; Ardini, E.; Casale, E.; Angiolini, M. Through the “Gatekeeper Door”: Exploiting the Active Kinase Conformation. *J. Med. Chem.* **2010**, *53* (7), 2681–2694.
284. Kornev, A. P.; Haste, N. M.; Taylor, S. S.; Ten Eyck, L. F. Surface Comparison of

- Active and Inactive Protein Kinases Identifies a Conserved Activation Mechanism. *Proc. Natl. Acad. Sci. U. S. A.* **2006**, *103* (47), 17783–17788.
285. Wang, R.; Lu, Y.; Wang, S. Comparative Evaluation of 11 Scoring Functions for Molecular Docking. *J. Med. Chem.* **2003**, *46* (12), 2287–2303.
286. Abdelgawad, M. A.; Hayallah, A. M.; Bukhari, S. N. A.; Musa, A.; Elmowafy, M.; et al. Design, Synthesis, Molecular Modeling, and Anticancer Evaluation of New VEGFR-2 Inhibitors Based on the Indolin-2-One Scaffold. *Pharmaceuticals* **2022**, *15* (11), 1416.
287. Hekal, M. H.; Farag, P. S.; Hemdan, M. M.; El-Sayed, W. M. New N-(1,3,4-Thiadiazol-2-Yl)Furan-2-Carboxamide Derivatives as Potential Inhibitors of the VEGFR-2. *Bioorg. Chem.* **2021**, *115*, 105176.
288. Sangande, F.; Julianti, E.; Tjahjono, D. H. Ligand-Based Pharmacophore Modeling, Molecular Docking, and Molecular Dynamic Studies of Dual Tyrosine Kinase Inhibitor of EGFR and VEGFR2. *Int. J. Mol. Sci.* **2020**, *21* (20), 7779.
289. Krych, J.; Gebicka, L. Catalase Is Inhibited by Flavonoids. *Int. J. Biol. Macromol.* **2013**, *58*, 148–153.
290. Giuliani, C.; Bucci, I.; Santo, S. Di; Rossi, C.; Grassadonia, A.; et al. The Flavonoid Quercetin Inhibits Thyroid-Restricted Genes Expression and Thyroid Function. *Food Chem. Toxicol.* **2014**, *66*, 23–29.
291. Lamy, S.; Akla, N.; Ouanouki, A.; Lord-Dufour, S.; Béliveau, R. Diet-Derived Polyphenols Inhibit Angiogenesis by Modulating the Interleukin-6/STAT3 Pathway. *Exp. Cell Res.* **2012**, *318* (13), 1586–1596.
292. Lin, C. M.; Shyu, K. G.; Wang, B. W.; Chang, H.; Chen, Y. H.; et al. Chrysin Suppresses IL-6-Induced Angiogenesis via down-Regulation of JAK1/STAT3 and VEGF: An in Vitro and Inzovo Approach. *J. Agric. Food Chem.* **2010**, *58* (11), 7082–7087.
293. Wang, J.; Liao, Y.; Fan, J.; Ye, T.; Sun, X.; et al. Apigenin Inhibits the Expression of IL-6, IL-8, and Icam-1 in Dehp-Stimulated Human Umbilical Vein Endothelial Cells and in Vivo. *Inflammation* **2012**, *35* (4), 1466–1476.
294. Tan, J.; Zhu, L.; Wang, B. DNA Binding and Cleavage Activity of Quercetin Nickel(II) Complex. *Dalt. Trans.* **2009**, *2* (24), 4722–4728.
295. Tan, J.; Wang, B.; Zhu, L. DNA Binding and Oxidative DNA Damage Induced by a Quercetin Copper(II) Complex: Potential Mechanism of Its Antitumor Properties. *J. Biol. Inorg. Chem.* **2009**, *14* (5), 727–739.
296. Zhou, J.; Wang, L. fang; Wang, J. yi; Tang, N. Synthesis, Characterization, Antioxidative and Antitumor Activities of Solid Quercetin Rare Earth(III) Complexes. *J. Inorg. Biochem.* **2001**, *83* (1), 41–48.
297. Tabassum, S.; Zaki, M.; Afzal, M.; Arjmand, F. New Modulated Design and Synthesis of Quercetin-Cull/Zn II-Sn2IV Scaffold as Anticancer Agents: In Vitro DNA Binding Profile, DNA Cleavage Pathway and Topo-I Activity. *Dalt. Trans.*

- 2013**, 42 (27), 10029–10041.
298. Naso, L.; Ferrer, E. G.; Lezama, L.; Rojo, T.; Etcheverry, S. B.; et al. Role of Oxidative Stress in the Antitumoral Action of a New Vanadyl(IV) Complex with the Flavonoid Chrysin in Two Osteoblast Cell Lines: Relationship with the Radical Scavenger Activity. *J. Biol. Inorg. Chem.* **2010**, 15 (6), 889–902.
299. Yang, F.; Jin, H.; Pi, J.; Jiang, J. H.; Liu, L.; et al. Anti-Tumor Activity Evaluation of Novel Chrysin-Organogermanium(IV) Complex in MCF-7 Cells. *Bioorganic Med. Chem. Lett.* **2013**, 23 (20), 5544–5551.
300. Zeng, Y. B.; Yang, N.; Liu, W. S.; Tang, N. Synthesis, Characterization and DNA-Binding Properties of La(III) Complex of Chrysin. *J. Inorg. Biochem.* **2003**, 97 (3), 258–264.
301. Roy, S.; Mallick, S.; Chakraborty, T.; Ghosh, N. Synthesis, Characterisation and Antioxidant Activity of Luteolin–Vanadium (II) Complex. *Food Chem.* **2015**, 173, 1172–1178.
302. Naso, L. G.; Lezama, L.; Valcarcel, M.; Salado, C.; Villacé, P.; et al. Bovine Serum Albumin Binding, Antioxidant and Anticancer Properties of an Oxidovanadium(IV) Complex with Luteolin. *J. Inorg. Biochem.* **2016**, 157, 80–93.
303. Dong, H.; Yang, X.; He, J.; Cai, S.; Xiao, K. Enhanced Antioxidant Activity, Antibacterial Activity and Hypoglycemic Effect of Luteolin by Complexation with Manganese (II) and Its Inhibition Kinetics on Xanthine Oxidase. *RSC Adv.* **2017**, 7 (84), 53385–53395.
304. Etcheverry, S. B.; Ferrer, E. G.; Naso, L.; Rivadeneira, J.; Salinas, V.; et al. Antioxidant Effects of the VO(IV) Hesperidin Complex and Its Role in Cancer Chemoprevention. *J. Biol. Inorg. Chem.* **2008**, 13 (3), 435–447.
305. Wang, H.; Tan, M.; Zhu, J.; Pan, Y.; Chen, Z.; et al. Synthesis, Cytotoxic Activity, and DNA Binding Properties of Copper (II) Complexes with Hesperetin, Naringenin, and Apigenin. *Bioinorg. Chem. Appl.* **2009**, 2009 (lii).
306. Pereira, R. M. S.; Andrades, N. E. D.; Paulino, N.; Sawaya, A. C. H. F.; Eberlin, M. N.; et al. Synthesis and Characterization of a Metal Complex Containing Naringin and Cu, and Its Antioxidant, Antimicrobial, Antiinflammatory and Tumor Cell Cytotoxicity. *Molecules* **2007**, 12 (7), 1352–1366.
307. Naso, L. G.; Ferrer, E. G.; Butenko, N.; Cavaco, I.; Lezama, L.; et al. Antioxidant, DNA Cleavage, and Cellular Effects of Silibinin and a New Oxovanadium(IV)/Silibinin Complex. *J. Biol. Inorg. Chem.* **2011**, 16 (4), 653–668.
308. Naso, L. G.; Lezama, L.; Rojo, T.; Etcheverry, S. B.; Valcarcel, M.; et al. Biological Evaluation of Morin and Its New Oxovanadium(IV) Complex as Antio-Xidant and Specific Anti-Cancer Agents. *Chem. Biol. Interact.* **2013**, 206 (2), 289–301.
309. Tu, L. Y.; Pi, J.; Jin, H.; Cai, J. Y.; Deng, S. P. Synthesis, Characterization and Anticancer Activity of Kaempferol-Zinc(II) Complex. *Bioorganic Med. Chem. Lett.* **2016**, 26 (11), 2730–2734.
310. Manolov, I.; Kostova, I.; Konstantinov, S.; Karaivanova, M. Synthesis,

- Physicochemical Characterization and Cytotoxic Screening of New Complexes of Cerium, Lanthanum and Neodymium with Nifflcoumar Sodium Salt. *Eur. J. Med. Chem.* **1999**, *34* (10), 853–858.
311. Kostova, I.; Manolov, I.; Karaivanova, M. Synthesis, Physicochemical Characterization, and Cytotoxic Screening of New Zirconium Complexes with Coumarin Derivatives. *Arch. Pharm. (Weinheim)*. **2001**, *334* (5), 157–162.
312. Pi, J.; Zeng, J.; Luo, J. J.; Yang, P. H.; Cai, J. Y. Synthesis and Biological Evaluation of Germanium(IV)-Polyphenol Complexes as Potential Anti-Cancer Agents. *Bioorganic Med. Chem. Lett.* **2013**, *23* (10), 2902–2908.
313. Pastuszko, A.; Majchrzak, K.; Czyz, M.; Kupcewicz, B.; Budzisz, E. The Synthesis, Lipophilicity and Cytotoxic Effects of New Ruthenium(II) Arene Complexes with Chromone Derivatives. *J. Inorg. Biochem.* **2016**, *159*, 133–141.
314. Pastuszko, A.; Niewinna, K.; Czyz, M.; Jóźwiak, A.; Małecka, M.; et al. Synthesis, X-Ray Structure, Electrochemical Properties and Cytotoxic Effects of New Arene Ruthenium(II) Complexes. *J. Organomet. Chem.* **2013**, *745–746*, 64–70.
315. Wang, B. D.; Yang, Z. Y.; Wang, Q.; Cai, T. K.; Crewdson, P. Synthesis, Characterization, Cytotoxic Activities, and DNA-Binding Properties of the La(III) Complex with Naringenin Schiff-Base. *Bioorganic Med. Chem.* **2006**, *14* (6), 1880–1888.
316. Kostova, I.; Kostova, R.; Momekov, G. Antineoplastic Activity of New Lanthanide (Cerium, Lanthanum and Neodymium) Complex Compounds. *J. Trace Elem. Med. Biol.* **2005**, *18* (3), 219–226.
317. Ciesielska, E.; Studzian, K.; Zyner, E.; Ochocki, J.; Szmigiero, L. DNA Damage and Apoptosis Induction in L1210 Cells by Cis-Diamminedichloroplatinum (II) and Its New Aminoflavone Analogue. *Cell. Mol. Biol. Lett.* **2000**, *5* (2), 235.
318. Ravishankar, D.; Salamah, M.; Attina, A.; Pothi, R.; Vallance, T. M.; et al. Ruthenium-Conjugated Chrysin Analogues Modulate Platelet Activity, Thrombus Formation and Haemostasis with Enhanced Efficacy. *Sci. Rep.* **2017**, *7* (1), 1–16.
319. Samsonowicz, M.; Regulska, E.; Kalinowska, M. Hydroxyflavone Metal Complexes - Molecular Structure, Antioxidant Activity and Biological Effects. *Chem. Biol. Interact.* **2017**, *273*, 245–256.
320. Roy, S.; Sil, A.; Chakraborty, T. Potentiating Apoptosis and Modulation of P53, Bcl2, and Bax by a Novel Chrysin Ruthenium Complex for Effective Chemotherapeutic Efficacy against Breast Cancer. *J. Cell. Physiol.* **2019**, *234* (4), 4888–4909.
321. Exarchou, V.; Troganis, A.; Gerothanassis, I. P.; Tsimidou, M.; Boskou, D. Do Strong Intramolecular Hydrogen Bonds Persist in Aqueous Solution? Variable Temperature Gradient 1H, 1H–13C GE-HSQC and GE-HMBC NMR Studies of Flavonols and Flavones in Organic and Aqueous Mixtures. *Tetrahedron* **2002**, *58* (37), 7423–7429.
322. Kasprzak, M. M.; Erxleben, A.; Ochocki, J. Properties and Applications of

- Flavonoid Metal Complexes. *RSC Adv.* **2015**, *5* (57), 45853–45877.
323. Ravishankar, D. Design, Synthesis and Biological Evaluation of Novel Flavone Derivatives, University of Reading, 2015.
324. Madu, C. O.; Wang, S.; Madu, C. O.; Lu, Y. Angiogenesis in Breast Cancer Progression, Diagnosis, and Treatment. *J. Cancer* **2020**, *11* (15), 4474.
325. Gasparini, G.; Toi, M.; Gion, M.; Verderio, P.; Dittadi, R.; et al. Prognostic Significance of Vascular Endothelial Growth Factor Protein in Node-Negative Breast Carcinoma. *J. Natl. Cancer Inst.* **1997**, *89* (2), 139–147.
326. Gasparini, G.; Toi, M.; Miceli, R.; Vermeulen, P. Clinical Relevance of Vascular Endothelial Growth Factor and Thymidine Phosphorylase in Patients with Node-Positive Breast Cancer Treated with Either Adjuvant. *Cancer J. Sci. Am.* **1999**, *5* (2), 101–111.
327. Pracharova, J.; Novohradsky, V.; Kostrhunova, H.; Štarha, P.; Trávníček, Z.; et al. Half-Sandwich Os(II) and Ru(II) Bathophenanthroline Complexes: Anticancer Drug Candidates with Unusual Potency and a Cellular Activity Profile in Highly Invasive Triple-Negative Breast Cancer Cells. *Dalt. Trans.* **2018**, *47* (35), 12197–12208.
328. Cao, W.; Zheng, W.; Chen, T. Ruthenium Polypyridyl Complex Inhibits Growth and Metastasis of Breast Cancer Cells by Suppressing FAK Signaling with Enhancement of TRAIL-Induced Apoptosis. *Sci. Rep.* **2015**, *5* (1), 9157.
329. Frik, M.; Martínez, A.; Elie, B. T.; Gonzalo, O.; Ramírez De Mingo, D.; et al. In Vitro and in Vivo Evaluation of Water-Soluble Iminophosphorane Ruthenium (II) Compounds. A Potential Chemotherapeutic Agent for Triple Negative Breast Cancer. *ACS Publ.* **2014**, *57* (23), 9995–10012.
330. Day, H. A.; Pavlou, P.; Waller, Z. A. E. I-Motif DNA: Structure, Stability and Targeting with Ligands. *Bioorganic Med. Chem.* **2014**, *22* (16), 4407–4418.
331. Assi, H. A.; Garavís, M.; González, C.; Damha, M. J. I-Motif DNA: Structural Features and Significance to Cell Biology. *Nucleic Acids Res.* **2018**, *46* (16), 8038–8056.
332. Huppert, J. L.; Balasubramanian, S. G-Quadruplexes in Promoters throughout the Human Genome. *Nucleic Acids Res.* **2007**, *35* (2), 406–413.
333. Takahashi, S.; Bhattacharjee, S.; Ghosh, S.; Sugimoto, N.; Bhowmik, S. Preferential Targeting Cancer-Related i-Motif DNAs by the Plant Flavonol Fisetin for Theranostics Applications. *Sci. Rep.* **2020**, *10* (1), 1–13.
334. Benabou, S.; Aviñó, A.; Eritja, R.; González, C.; Gargallo, R. Fundamental Aspects of the Nucleic Acid I-Motif Structures. *RSC Adv.* **2014**, *4* (51), 26956–26980.
335. Duffy, M. J.; O’Grady, S.; Tang, M.; Crown, J. MYC as a Target for Cancer Treatment. *Cancer Treat. Rev.* **2021**, *94*, 102154.
336. Xu, J.; Chen, Y.; Olopade, O. I. MYC and Breast Cancer. *Genes Cancer* **2010**, *1*

- (6), 629–640.
337. Shi, S.; Geng, X.; Zhao, J.; Yao, T.; Wang, C.; et al. Interaction of [Ru(Bpy)₂(Dppz)]²⁺ with Human Telomeric DNA: Preferential Binding to G-Quadruplexes over i-Motif. *Biochimie* **2010**, *92* (4), 370–377.
338. Shi, S.; Zhao, J.; Geng, X.; Yao, T.; Huang, H.; et al. Molecular “Light Switch” for G-Quadruplexes and i-Motif of Human Telomeric DNA: [Ru(Phen)₂(Dppz)]²⁺. *Dalt. Trans.* **2010**, *39* (10), 2490–2493.
339. Khater, M.; Brazier, J. .; Greco, F.; Osborn, H. M. . Anticancer Evaluation of New Organometallic Ruthenium(II) Flavone Complexes. *RSC Med. Chem.* **2023**, *14* (2), 253–267.
340. Bhattacharyya, S.; Purkait, K.; Mukherjee, A. Ruthenium(II) p-Cymene Complexes of a Benzimidazole-Based Ligand Capable of VEGFR2 Inhibition: Hydrolysis, Reactivity and Cytotoxicity Studies. *Dalt. Trans.* **2017**, *46* (26), 8539–8554.
341. Montani, M.; Badillo Pazmay, G. V; Hysi, A.; Lupidi, G.; Pettinari, R.; et al. The Water Soluble Ruthenium (II) Organometallic Compound CI Suppresses Triple Negative Breast Cancer. *Pharmacol. Res.* **2016**, *107*, 282–290.
342. Entschladen, F.; Drell VI, T. L.; Lang, K.; Joseph, J.; Zaenker, K. S. Tumour-Cell Migration, Invasion, and Metastasis: Navigation by Neurotransmitters. *Lancet Oncol.* **2004**, *5* (4), 254–258.
343. Dattachoudhury, S.; Sharma, R.; Kumar, A.; Jaganathan, B. G. Sorafenib Inhibits Proliferation, Migration and Invasion of Breast Cancer Cells. *Oncology* **2020**, *98* (7), 478–486.
344. Alaseem, A. M.; Alhazzani, K.; Alanazi, A. Z.; Alqarni, Y.; Algahtani, M. M.; et al. Preclinical In Vitro Investigation of MDM2 Inhibition in Combination with Antiangiogenic Therapy for Breast Cancer Treatment. *Sci. Pharm.* **2023**, *91* (1), 12.
345. González-Ruiz, V.; Olives, A. I.; Martín, M. A.; Ribelles, P.; Ramos, M. T.; et al. An Overview of Analytical Techniques Employed to Evidence Drug-DNA Interactions. Applications to the Design of Genosensors. *Biomed. Eng. trends, Res. Technol.* **2011**, *32*, 215–219.
346. Masoud, S. S.; Nagasawa, K. I-Motif-Binding Ligands and Their Effects on the Structure and Biological Functions of I-Motif. *Chem. Pharm. Bull.* **2018**, *66* (12), 1091–1103.
347. Biver, T. Use of UV-Vis Spectrometry to Gain Information on the Mode of Binding of Small Molecules to DNAs and RNAs. *Appl. Spectrosc. Rev.* **2012**, *47* (4), 272–325.
348. Hassani, L.; Fazeli, Z.; Safaei, E.; Rastegar, H.; Akbari, M. A Spectroscopic Investigation of the Interaction between C-MYC DNA and Tetrapyridinoporphyrazinatozinc(II). *J. Biol. Phys.* **2014**, *40* (3), 275–283.
349. Xu, H.; Zhang, H.; Qu, X. Interactions of the Human Telomeric DNA with

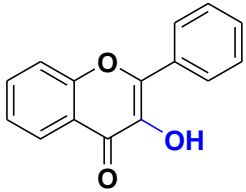
- Terbium–Amino Acid Complexes. *J. Inorg. Biochem.* **2006**, *100* (10), 1646–1652.
350. Neves, K. B.; Montezano, A. C.; Lang, N. N.; Touyz, R. M. Vascular Toxicity Associated with Anti-Angiogenic Drugs. *Clin. Sci.* **2020**, *134* (18), 2503–2520.
351. Bousquet, G.; Varna, M.; Ferreira, I.; Wang, L.; Mongiat-Artus, P.; et al. Differential Regulation of Sunitinib Targets Predicts Its Tumor-Type-Specific Effect on Endothelial and/or Tumor Cell Apoptosis. *Cancer Chemother. Pharmacol.* **2013**, *72* (6), 1183–1193.
352. Shah, S.; Lee, C.; Choi, H.; Gautam, J.; Jang, H.; et al. 5-Hydroxy-7-Azaindolin-2-One, a Novel Hybrid of Pyridinol and Sunitinib: Design, Synthesis and Cytotoxicity against Cancer Cells. *Org. Biomol. Chem.* **2016**, *14* (21), 4829–4841.
353. Wang, M.; Ye, C.; Liu, M.; Wu, Z.; Li, L.; et al. Synthesis and Antitumor Activity of 5-(5-Halogenated-2-Oxo-1H-Pyrrolo[2,3-b]Pyridin-(3Z)-Ylidenemethyl)-2,4-Dimethyl-1H-Pyrrole-3-Carboxamides. *Bioorg. Med. Chem. Lett.* **2015**, *25* (14), 2782–2787.
354. Stalker, L.; Pemberton, J.; Moorehead, R. A. Inhibition of Proliferation and Migration of Luminal and Claudin-Low Breast Cancer Cells by PDGFR Inhibitors. *Cancer Cell Int.* **2014**, *14* (1), 1–9.
355. Yu, P.; Ye, L.; Wang, H.; Du, G.; Zhang, J.; et al. NSK-01105, a Novel Sorafenib Derivative, Inhibits Human Prostate Tumor Growth via Suppression of VEGFR2/EGFR-Mediated Angiogenesis. *PLoS One* **2014**, *9* (12), e115041.
356. Babic, Ž.; Crkvencic, M.; Rajic, Z.; Mikecin, A. M.; Kralj, M.; et al. New Sorafenib Derivatives: Synthesis, Antiproliferative Activity Against Tumour Cell Lines and Antimetabolic Evaluation. *Molecules* **2012**, *17* (1), 1124–1137.
357. Ismail, M. M. F.; Husseiny, E. M.; Ibrahim, M. H. Mimicry of Sorafenib: Novel Diarylureas as VEGFR2 Inhibitors and Apoptosis Inducers in Breast Cancer. *New J. Chem.* **2023**, *47* (24), 11565–11576.
358. Wang, H. L.; Ma, X.; Guan, X. Y.; Song, C.; Li, G. B.; et al. Potential Synthetic Lethality for Breast Cancer: A Selective Sirtuin 2 Inhibitor Combined with a Multiple Kinase Inhibitor Sorafenib. *Pharmacol. Res.* **2022**, *177*, 106050.
359. Kim, W.; Haws, H.; Peterson, P.; Whatcott, C. J.; Weitman, S.; et al. TP-1287, an Oral Prodrug of the Cyclin-Dependent Kinase-9 Inhibitor Alvocidib. In *Cancer Research*; American Association for Cancer Research, 2017; Vol. 77, pp 5133–5133.
360. Rykala, J.; Przybylowska, K.; Majsterek, I.; Pasz-Walczak, G.; Sygut, A.; et al. Angiogenesis Markers Quantification in Breast Cancer and Their Correlation with Clinicopathological Prognostic Variables. *Pathol. Oncol. Res.* **2011**, *17* (4), 809–817.
361. Micheie, R.; LeJeune, S.; Scott, P. A. E.; Fox, S. Expression of the Angiogenic Factors Vascular Endothelial Cell Growth Factor, Acidic and Basic Fibroblast Growth Factor, Tumor Growth Factor β -1, Platelet-Derived Endothelial Cell Growth Factor, Placenta Growth Factor, and Pleiotrophin in Human Primary Br.

- Cancer Res.* **1997**, *57* (5), 963–969.
362. Linderholm, B. K.; Hellborg, H.; Johansson, U.; Elmberger, G.; Skoog, L.; et al. Significantly Higher Levels of Vascular Endothelial Growth Factor (VEGF) and Shorter Survival Times for Patients with Primary Operable Triple-Negative Breast Cancer. *Ann. Oncol.* **2009**, *20*, 1639–1646.
363. Itatani, Y.; Kawada, K.; Yamamoto, T.; Sakai, Y. Resistance to Anti-Angiogenic Therapy in Cancer—Alterations to Anti-VEGF Pathway. *Int. J. Mol. Sci.* **2018**, *19* (4), 1232.
364. Muz, B.; de la Puente, P.; Azab, F.; Azab, A. K. The Role of Hypoxia in Cancer Progression, Angiogenesis, Metastasis, and Resistance to Therapy. *Hypoxia* **2015**, 83–92.
365. Van Der Schaft, D. W. J.; Seftor, R. E. B.; Seftor, E. A.; Hess, A. R.; Gruman, L. M.; et al. Effects of Angiogenesis Inhibitors on Vascular Network Formation by Human Endothelial and Melanoma Cells. *J. Natl. Cancer Inst.* **2004**, *96* (16), 1437–1477.
366. Yang, T.; Xiao, H.; Liu, X.; Wang, Z.; Zhang, Q.; et al. Vascular Normalization: A New Window Opened for Cancer Therapies. *Front. Oncol.* **2021**, *11* (August), 1–20.
367. Jing, L.; Lin, J.; Yang, Y.; Tao, L.; Li, Y.; et al. Quercetin Inhibiting the PD-1/PD-L1 Interaction for Immune-Enhancing Cancer Chemopreventive Agent. *Phyther. Res.* **2021**, *35* (11), 6441–6451.
368. Choi, J. G.; Kim, Y. S.; Kim, J. H.; Kim, T. I.; Li, W.; et al. Anticancer Effect of *Salvia plebeia* and Its Active Compound by Improving T-Cell Activity via Blockade of PD-1/PD-L1 Interaction in Humanized PD-1 Mouse Model. *Front. Immunol.* **2020**, *11* (November), 1–15.
369. Messeha, S. S.; Zarmouh, N. O.; Soliman, K. F. A. Polyphenols Modulating Effects of Pd-L1/Pd-1 Checkpoint and Emt-Mediated Pd-L1 Overexpression in Breast Cancer. *Nutrients* **2021**, *13* (5), 1718.
370. Coombs, M. R. P.; Harrison, M. E.; Hoskin, D. W. Apigenin Inhibits the Inducible Expression of Programmed Death Ligand 1 by Human and Mouse Mammary Carcinoma Cells. *Cancer Lett.* **2016**, *380* (2), 424–433.
371. Sartori, G. R.; Albuquerque, A. de O.; Santos-Costa, A. H.; Andrade, L. M.; Almeida, D. da S.; et al. In Silico Mapping of the Dynamic Interactions and Structure-Activity Relationship of Flavonoid Compounds against the Immune Checkpoint Programmed-Cell Death 1 Pathway. *Front. Drug Discov.* **2022**, *2* (December), 1–22.
372. Kleinman, H. K.; McGarvey, M. L.; Liotta, L. A.; Robey, P. G.; Tryggvason, K.; et al. Isolation and Characterization of Type IV Procollagen, Laminin, and Heparan Sulfate Proteoglycan from the EHS Sarcoma. *Biochemistry* **1982**, *21* (24), 6188–6193.
373. Simoni, R. D.; Hays, J. B.; Nakazawa, T.; Roseman, S.; Stein, R.; et al. Basement

- Membrane Complexes with Biological Activity. *Proc. Natl. Acad. Sci. U.S.A* **1986**, 25, 616.
374. Choi, J.; Lee, D.; Park, S.; Seol, J. Diosmetin Inhibits Tumor Development and Block Tumor Angiogenesis in Skin Cancer. *Biomed. Pharmacother.* **2019**, 117 (Sep), 109091–109099.
375. Yue, M.; Zeng, N.; Xia, Y.; Wei, Z.; Dai, Y. Morin Exerts Anti-Arthritic Effects by Attenuating Synovial Angiogenesis via Activation of Peroxisome Proliferator Activated Receptor- γ . *Mol. Nutr. Food Res.* **2018**, 62 (21), 1–13.
376. Endothelial Cell Tube Formation Assay | Thermo Fisher Scientific - UK <https://www.thermofisher.com/uk/en/home/references/protocols/cell-and-tissue-analysis/cell-proliferation-assay-protocols/angiogenesis-protocols/endothelial-cell-tube-formation-assay.html#prot4> (accessed Oct 18, 2021).
377. Bhattacharya, R.; Kwon, J.; Li, X.; Wang, E.; Patra, S.; et al. Distinct Role of PLC β 3 in VEGF-Mediated Directional Migration and Vascular Sprouting. *J. Cell Sci.* **2009**, 122 (7), 1025–1034.
378. Laboratories Bio-Rad. *A Guide to Polyacrylamide Gel Electrophoresis and Detection*; 2012.
379. Classics Lowry, O., Rosebrough, N., Farr, A. and Randall, R. Protein Measurement with the Folin Phenol Reagent. *J. Biol. Chem.* **1951**, 193 (1), 265–275.
380. Western blot membrane stripping for restaining protocol | Abcam <https://www.abcam.com/protocols/western-blot-membrane-stripping-for-restaining-protocol> (accessed Mar 28, 2022).
381. Mosmann, T. Rapid Colorimetric Assay for Cellular Growth and Survival: Application to Proliferation and Cytotoxicity Assays. *J. Immunol. Methods* **1983**, 65 (1–2), 55–63.
382. Jain, A. N. Surflex: Fully Automatic Flexible Molecular Docking Using a Molecular Similarity-Based Search Engine. *J. Med. Chem.* **2003**, 46 (4), 499–511.
383. Powell, M. J. D. Restart Procedures for the Conjugate Gradient Method. *Math. Program.* **1977**, 12 (1), 241–254.
384. Schrödinger Release 2022-1: Maestro, Schrödinger, LLC, New York, NY, 2021. Schrödinger, LLC: New York.

Appendix A

Table 1. Characteristics of the studies included in the systematic review for 9 subclasses of flavonoids

Class	Flavonoid	Disease	<i>In vitro</i> tests	<i>In/ex vivo</i> tests	Author, year
 <p>Flavonols</p>	Beturetol	Angiogenesis		CAM	Hisanori Hattori, 2011 [1]
	Casticin	Cancer	Review		Shanaya Ramchandani, 2020 [2]
	Denticulatain	Lung Cancer		ZFM	Da Song Yang, 2015 [3]
	Dihydrokaempferide	Angiogenesis		CAM	Hisanori Hattori, 2011 [1]
	Fisetin	Cancer	Review		Dharambir Kashyap, 2018 [4]
	Cancer	Review			Thamaraiselvan Rengarajan, 2016 [5]
	Cancer	Review			Deeba N.Syed, 2016 [6]
	Cancer	Review			Lall K. Rahul, 2016 [7]
	Breast Cancer	In			Cheng Fang Tsai, 2018 [8]
	Breast Cancer	WH, In			Xu Sun, 2018 [9]
	Breast Cancer	WH, In		Mets in mice	Jie Li, 2018 [10]
	Cervical Cancer	In			Ruey Hwang Chou, 2013 [11]
	Glioma	In			Chien Min Chen, 2015 [12]
	Hepatic Cancer	In			Xiang Feng Liu, 2017 [13]
	Leukemia	In			Anna Klimaszewska-Wiśniewska, 2019 [14]
	Lung Cancer	WH, In			Saba Tabasum, 2019 [15]
	Lung Cancer	WH, In, Ad			Junjian Wang, 2018 [16]
Prostate Cancer	WH, In, Ad			Chi Sheng Chien, 2010 [17]	

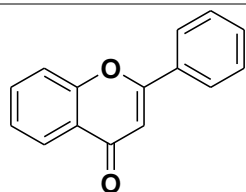
	Renal Cancer	In		Yih Shou Hsieh, 2019 [18]
	Retinopathy		RbCN	A M Joussem, 2000 [19]
Galangin	Hepatic Cancer	Review		Dengyang Fang, 2019 [20]
	Angiogenesis	TF, Ad		Jong Deog Kim, 2006 [21]
	Glioma	TF, In	CAM, MD in mice	Daliang Chen, 2019 [22]
	Glioma	In		Deqiang Lei, 2018 [23]
	Hepatic Cancer	WH, In, Ad		Shang Tao Chien, 2015 [24]
	Ovarian Cancer	TF	CAM	Haizhi Huang, 2015 [25]
	Renal Cancer	WH, In		Jingyi Cao, 2016 [26]
	Renal Cancer	In		Yun Zhu, 2018 [27]
Gossypin	Gastric Cancer	In		Wang Li, 2019 [28]
Herbacetin	Melanoma	In		Lei Li, 2019 [29]
Hyperoside	Arthritis	WH, In	CIAM in mice	Xiang Nan Jin, 2016 [30]
Icariin	Bone disease	Review		Xin Zhang, 2014 [31]
	Cancer	Review		Meixia Chen, 2016 [32]
	Angiogenesis	TF, In	RAR	Byung Hee Chung, 2008 [33]
	Esophageal Cancer	In		Zhen Fang Gu, 2017 [34]
	Ovarian Cancer	WH		Pengzhen Wang, 2019 [35]
	Wound healing		EWM in rats	Wangkheirakpam Ramdas Singh, 2019 [36]
Icariside	Cancer	Review		Meixia Chen, 2016 [32]
	Glioma	WH, In		Kai Quan, 2017 [37]
Isoviolanthin	Hepatic Cancer	WH, In		Shangping Xing, 2018 [38]
Isosakuranetin	Angiogenesis		CAM	Hisanori Hattori, 2011 [1]
Kaempferol	Cancer	Review		Allen Y. Chen, 2013 [39]

Cancer	Review		Dharambir Kashyap, 2017 [40]	
Angiogenesis	WH, TB, In		Hsien Kuo Chin, 2018 [41]	
Angiogenesis	WH, TB	ZFM	Fang Liang, 2015 [42]	
Angiogenesis		CAM	Shigenori Kumazawa, 2013 [43]	
Angiogenesis	TF, Ad		Jong Deog Kim, 2006 [21]	
Diabetes		EWM in rats	Yusuf Özay, 2019 [44]	
Glioma	WH		Vivek Sharma, 2007 [45]	
Glioma	In	Mets in mice	S.C. Shen, 2006 [46]	
Hepatic Cancer	WH, In	Mets in mice	Youyou Qin, 2015 [47]	
Hepatic Cancer	In		Genglong Zhu, 2018 [48]	
Lung Cancer	WH, In		Eunji Jo, 2015 [49]	
Medulloblastoma	Ad		David Labbé, 2009 [50]	
Oral Cancer	In		Chiao Wen Lin, 2013 [51]	
Osteosarcoma	WH, In, Ad		Hui Jye Chen, 2013 [52]	
Ovarian Cancer		CAM	Haitao Luo, 2009 [53]	
Pancreatic Cancer	In		Jungwhoi Lee, 2016 [54]	
Renal Cancer	WH, In	Mets in mice	Tung Wei Hung, 2017 [55]	
Retinal Vascularization	WH, In		Hsiang Wen Chien, 2019 [56]	
kaempferol-3-O-[(6-caffeoyl)- β -glucopyranosyl (1 \rightarrow 3) α -rhamnopyranoside]-7- O- α -rhamnopyranoside	Angiogenesis	WH	Marco Clericuzio, 2012 [57]	
Kaempferide	Angiogenesis	CAM	Hisanori Hattori, 2011 [1]	
Morin	Arthritis	WH, TB	CIAM in rats	Ni Zeng, 2015 [58]
	Arthritis	WH, TB	CIAM in rats	Mengfan Yue, 2018 [59]

	Leukemia	Ad		Nagaja Capitani, 2019 [60]
	Melanoma	WH		Hua Wen Li, 2016 [61]
Myricetin	Melanoma	Review		Nam Joo Kang, 2011 [62]
	Angiogenesis	TF, Ad		Jong Deog Kim, 2006 [21]
	Breast Cancer	In	CAM, MD in mice, RAR	Zhiqing Zhou, 2019 [63]
	Breast Cancer	WH, In, Ad	Mets in mice	Yingqian Ci, 2018 [64]
	Glioma	WH, In		Wen Ta Chiu, 2010 [65]
	Hepatic Cancer	In		Noriko Yamada, 2020 [66]
	Hepatic Cancer	WH, In		Hongxin Ma, 2019 [67]
	Lung Cancer	WH, In, Ad		Yuan Wei Shih, 2009 [68]
	Medulloblastoma	In, Ad		David Labbé, 2009 [50]
	Ovarian Cancer	TF	CAM	Haizhi Huang, 2015 [25]
Quercetin	Breast Cancer	Review		Maryam Ezzati, 2020 [69]
	Cancer	Review		Si-min Tang, 2020 [70]
	Cancer	Review		Dharambir Kashyap, 2016 [71]
	Colorectal Cancer	Review		Saber G. Darband, 2018 [72]
	Angiogenesis	WH, In		Nu Ry Song, 2014 [73]
	Angiogenesis	WH, TB	ZFM	Chen Lin, 2012 [74]
	Angiogenesis	TF, Ad		Jong Deog Kim, 2006 [21]
	Bladder Cancer	WH, In		Yu Hsiang Lee, 2019 [75]
	Breast Cancer	WH		Divyashree Ravishankar, 2015 [76]
	Breast Cancer		MD in mice	Xin Zhao, 2016 [77]
	Breast Cancer		CAM	Soo Jin Oh, 2010 [78]
	Breast Cancer	WH, In		Asha Srinivasan, 2016 [79]

Breast Cancer	WH, In		Cheng Wei Lin, 2008 [80]
Breast Cancer	In		Amilcar Rivera Rivera, 2016 [81]
Cancer	TF	ZFM	Daxian Zhao, 2014 [82]
Cancer	TF, In	CAM	Wen Fu Tan, 2003 [83]
Cancer		MD in mice	Xiangpei Zhao, 2012 [84]
Cancer	WH, In		Lung Ta Lee, 2004 [85]
Cancer	WH		Dong Eun Lee, 2013 [86]
Colorectal Cancer	WH, In	Mets in mice	Ji Ye Kee, 2016 [87]
Glioma	WH		Hong Chao Pan, 2015 [88]
Glioma	WH, In		Wen Ta Chiu, 2010 [65]
Glioma	WH, In		Yue Liu, 2017 [89]
Glioma	In		Jonathan Michaud-Levesque, 2012 [90]
Glioma	WH		Alessandra Bispo da Silva, 2020 [91]
Glioma	WH, TB, In		Yue Liu, 2017 [92]
Hepatic Cancer	In		Noriko Yamada, 2020 [66]
Hepatic Cancer	WH, In		Jun Lu, 2018 [93]
Lung Cancer	WH		Anna Klimaszewska-Wiśniewska, 2017 [94]
Lung Cancer	In		Tzu Chin Wu, 2018 [95]
Lung Cancer	In		Yo Chuen Lin, 2013 [96]
Medulloblastoma	In, Ad		David Labbé, 2009 [50]
Melanoma	In		Mun Kyung Hwang, 2009 [97]
Melanoma	In		Hui Hui Cao, 2015 [98]
Melanoma	WH, In	Mets in mice	Hui Hui Cao, 2014 [99]

	Oral Cancer	In		Junfang Zhao, 2019 [100]	
	Osteoblasts	In		Tae Wook Nam, 2008 [101]	
	Osteosarcoma	WH, In, Ad		Shenglong Li, 2019 [102]	
	Osteosarcoma	WH, In	Mets in mice	Haifeng Lan, 2017 [103]	
	Osteosarcoma	WH, Ad		Kersten Berndt, 2013 [104]	
	Pancreatic Cancer	WH, In		Ying Tang Huang, 2005 [105]	
	Pancreatic Cancer	WH, In		Yu Dinglai 2017 [106]	
	Prostate Cancer	WH, In		Firdous Ahmad Bhat, 2014 [107]	
	Prostate Cancer	TF, In	MD in mice	Feiya Yang, 2016 [108]	
	Retinoblastoma	In		Wei Song, 2017 [109]	
	Quercetin-3-O-[(6-caffeoyl)- β -glucopyranosyl(1 \rightarrow 3) α -rhamnopyranoside]-7-O- α -rhamnopyranoside	Angiogenesis	WH	Marco Clericuzio, 2012 [57]	
	Rutin	Angiogenesis	CAM	César Muñoz Camero, 2018 [110]	
		Angiogenesis	CAM	Shigenori Kumazawa, 2013 [43]	
		Cancer	WH, In, Ad	Mohamed ben Sghaier, 2016 [111]	
		Glioma	WH	Alessandra Bispo da Silva, 2020 [91]	
		Neuroblastoma	WH, In	Hongyan Chen, 2013 [112]	
	3-Hydroxy flavone	Angiogenesis	TF	Myoung H. Kim, 2003 [113]	
		Osteosarcoma	WH, In, Ad	Mets in mice	Ko Hsiu Lu, 2016 [114]
	5-Hydroxy flavone	Oral Cancer	CAM	Shun Fa Yang, 2008 [115]	
	7-Hydroxy flavone				
	5, 6, 7-Trihydroxy flavone				



Flavones

4', 5, 7 -Trihydroxy flavone				
5,6,7-Trimethoxy flavonoid salicylate	Gastric Cancer	WH		Renbo Liu, 2020 [116]
7,8-Dihydroxyflavone	Melanoma	WH, In		Deok Yong Sim, 2016 [117]
Acacetin	Angiogenesis		CAM	Ling Zhi Liu, 2011[118]
	Cancer	TF, In	CAM, MPA in mice, RAR	Tariq A. Bhat, 2014 [119]
	Lung Cancer	In, Ad		Yaou Fong, 2010 [120]
	Lung cancer	WH, In, Ad		Shang Tao Chien, 2011 [121]
	Prostate Cancer	WH, In		Kun Hung Shen, 2010 [122]
Apigenin	Cancer		Review	Dharambir Kashyap, 2018 [123]
	Cancer		Review	Deendayal Patel, 2007 [124]
	Gastric Cancer		Review	Émilie C.Lefort, 2013 [125]
	Angiogenesis	TF, In		Sylvie Lamy, 2012 [126]
	Angiogenesis	TF		Myoung H. Kim, 2003 [113]
	Breast Cancer	In, Ad		F. Lindenmeyer, 2011 [127]
	Breast Cancer	WH, In, Ad		Wei Jiunn Lee, 2008 [128]
	Cancer		CAM, MPA in mice	Jing Fang, 2007 [129]
	Cancer	WH, In		Lei Wang, 2013 [130]
	Cancer	WH		Cornelia Spoerlein, 2013 [131]
	Cervical Cancer	In		Jaroslav Czyz, 2005 [132]
	Choriocarcinoma	In		Whasun Lim, 2016 [133]
	Colorectal Cancer	WH, In	Mets in mice	Li Chunhua, 2013 [134]
	Colorectal Cancer	WH, In	Mets in mice	Jin Dai, 2016 [135]
Glioma	WH		Paulo L.C. Coelho, 2016 [136]	

	Glioma	WH		Paulo L.C. Coelho, 2019 [137]
	Lung Cancer		MPA in mice	Ling Zhi Liu, 2005 [138]
	Melanoma	In		Md Abul Hasnat, 2015 [139]
	Melanoma	WH, In		Guangming Zhao, 2017 [140]
	Melanoma	WH, In, Ad	Mets in mice	Hui Hui Cao, 2016 [141]
	Melanoma	WH	CAM	Alexandra Ghițu, 2019 [142]
	Ovarian Cancer	TF		Jing Fang, 2005 [143]
	Ovarian Cancer	WH, In, Ad	Mets in mice	Xiao Men Hu, 2008 [144]
	Pancreatic Cancer	WH		Jing He, 2015 [145]
	Prostate Cancer	WH		Suat Erdogan, 2016 [146]
	Prostate Cancer	WH, In	Mets in mice	Ming Hsien Chien, 2019 [147]
	Prostate Cancer	WH, In, Ad		Carrie A. Franzen, 2019 [148]
	Prostate Cancer	WH	MPA in mice	Sanjeev Shukla, 2015 [149]
Apigenin-7-O-glucoside	Angiogenesis		CAM	César Muñoz Camero, 2018 [110]
Artocarpin	Wound healing	WH, TB, In	EWM in mice	Chung Ju Yeh, 2017 [150]
Baicalein	Cancer		Review	Gao Ying, 2016 [151]
	Angiogenesis	WH, TB	CAM, RAR	Yun Ling, 2011 [152]
	Breast Cancer	WH, In	Mets in mice	Xing Cong Ma, 2016 [153]
	Breast Cancer	WH, In, Ad		Ling Wang, 2010 [154]
	Breast Cancer	WH, In, Ad		Dandan Shang, 2015 [155]
	Breast Cancer	In		Heesung Chung, 2015 [156]
	Colorectal Cancer	In		Yuxia Chai, 2017 [157]
	Colorectal Cancer	In		C. Lalou, 2013 [158]
	Gastric Cancer	WH, In		Fenglin Chen, 2014 [159]

	Glioma	WH, In		Wen Ta Chiu, 2010 [65]
	Hepatic Cancer	WH, In, Ad		Yung Wei Chiu, 2011 [160]
	Hepatic Cancer	In		Xiaolan Yu, 2018 [161]
	Lung Cancer	WH, TB	Mets in mice	Yang Gyu Park, 2017 [162]
	Melanoma	WH, In		Eun Ok Choi, 2017 [163]
	Osteosarcoma	In		Jian Zhang, 2018 [164]
	Osteosarcoma	In, Ad		Yi Zhang, 2013 [165]
	Pancreatic Cancer	WH, In		Rong Tao Zhou, 2017 [166]
	Wound healing		SF in rats	Renjin Lin, 2018 [167]
Baicalin	Breast Cancer	In		Heesung Chung, 2015 [156]
	Breast Cancer	WH, In		Tao Zhou, 2017 [168]
	Colorectal Cancer	WH, In, Ad	Mets in mice	Bolin Yang, 2020 [169]
	Glioma	In		Yihao Zhu, 2018 [170]
	Hepatic Cancer	In		Xiongjian Wu, 2018 [171]
	Lung Cancer	WH, In		Jiawen You, 2018 [172]
	Ovarian Cancer	WH, In		Chen Gao, 2017 [173]
	Retinopathy		RRN	Hyoung Jo, 2015 [174]
Chrysin	Cancer		Review	Eshvendar Reddy Kasala, 2015 [175]
	Angiogenesis	WH	MAR	Sha-sha Tian, 2014 [176]
	Breast Cancer	WH, In		Bing Yang, 2014 [177]
	Cancer		MD in mice	Xiangpei Zhao, 2012 [84]
	Cancer	WH		Cornelia Spoerlein, 2013 [131]
	Colorectal Cancer	In		C. Lalou, 2013 [158]
	Gastric Cancer	In		Yong Xia, 2015 [178]

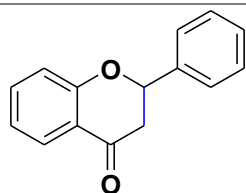
	Lung Cancer	In		Tzu Chin Wu, 2018 [95]
	Prostate Cancer		MPA in mice	Beibei Fu, 2007 [179]
	Retinopathy		MRN	Min Kyung Kang, 2016 [180]
Chrysoeriol	Breast Cancer	In		K. Amrutha, 2014 [181]
Cirsiliol	Melanoma	WH, In		Priyanka Prasad, 2019 [182]
Didymin	Angiogenesis	WH, TB, In	MPA in mice, MAR	Kirtikar Shukla, 2019 [183]
	Neuroblastoma	WH		Jyotsana Singhal, 2012 [184]
Diosmetin	Glioma	WH, In		Yuli Yan, 2020 [185]
	Lung Cancer	WH		Yuli Yan, 2020 [186]
	Melanoma	WH, TB	MD in mice, RAR	Jawun Choi, 2019 [187]
Eupafolin	Hepatic Cancer	WH, TB, In	MPA in mice, MD in mice	Honglei Jiang, 2017 [188]
Eupatilin	Gastric Cancer	TF		Jae Ho Cheong, 2011 [189]
	Glioma	WH, In		Xiaowei Fei, 2019 [190]
Eupatorin	Cancer	WH, TB		Iva Dolečková, 2012 [191]
Flavone-6-C- β -D-glucopyranoside	Ovarian Cancer	In		Yuanda Du, 2015 [192]
Flavopiridol	Lung Cancer	WH		Irem Dogan Turacli, 2019 [193]
GL-V9	Breast Cancer	WH, In, Ad		Liwen Li, 2011 [194]
Hispidulin	Colon Cancer	WH, In	E-cadherin level inhibition in mice tumor	Jing Xie, 2015 [195]
	Hepatic Cancer	WH, In	Mets in mice	Mei Han, 2018 [196]
	Pancreatic Cancer	WH, TB, In	MCN,MD in mice, RAR	Lijun He, 2011 [197]
	Renal Cancer	In	Mets in mice	Ming Quan Gao, 2017 [198]
LFG-500	Breast Cancer	WH, In, Ad	Mets in mice	Chenglin Li, 2014 [199]

Linarin	Glioma	WH, In		Zi Gang Zhen, 2017 [200]
Luteolin	Breast Cancer		Review	Matthew T Cook, 2018 [201]
	Angiogenesis	WH, TB, In	CAM, RAR	Xiaobo Li, 2017 [202]
	Angiogenesis	In		Manyi Zhu, 2013 [203]
	Angiogenesis	TF, In		Sylvie Lamy, 2012 [126]
	Breast Cancer	WH		Divyashree Ravishankar, 2015 [76]
	Breast Cancer	WH, In	Mets in mice	Hongyuan Li, 2017 [204]
	Cancer (breast and colon)	WH, In, Ad	Mets in mice	Luciana G.Naso, 2016 [205]
	Cancer	WH, In		Lung Ta Lee, 2004 [85]
	Cancer	WH, In		Samir Attoub, 2011 [206]
	Cancer (epidermal)		RbCN, MD in mice	Eleni Bagli, 2004 [207]
	Colorectal	WH, In	Mets in mice	Yuanyuan Yao, 2019 [208]
	Diabetes		EWM in rats	Santram Lodhi, 2013 [209]
	Gastric Cancer	In		Jun Lu, 2015 [210]
	Gastric Cancer	In		Ming de Zang, 2017 [211]
	Gastric Cancer	In	Mets in mice	Yansong Pu, 2018 [212]
	Glioma	WH		Qiang Wang, 2017 [213]
	Glioma	WH		Ruthrotha B.Selvi, 2015 [214]
	Glioma	WH, In		Wen Yu Cheng, 2013 [215]
	Glioma	WH		Yollanda E. M. Franco, 2020 [216]
	Hepatic Cancer	In		Wei Jiunn Lee, 2006 [217]
	Lung Caner	WH, In		Guanmin Meng, 2016 [218]
	Lung Cancer	In, Ad		Junshan Ruan, 2012 [219]

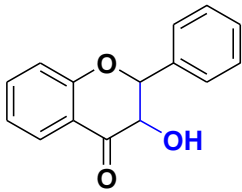
	Lung Cancer	In		Yo Chuen Lin, 2013 [96]
	Melanoma	WH, TB, In, Ad		Chunyu Li, 2019 [220]
	Melanoma	WH, In		Xin Yao, 2019 [221]
	Melanoma	In, Ad	Mets in mice	Jun Shan Ruan, 2012 [222]
	Oral Cancer	WH, In		Bharath Kumar Velmurugan, 2020 [223]
	Pancreatic Cancer	WH, In		Ying Tang Huang, 2005 [105]
	Prostate Cancer	WH, TB, In	CAM, RAR	Poyil Pratheeshkumar, 2012 [224]
	Retinopathy		RbCN	A M Joussem, 2000 [19]
	Ovarian Cancer	In		Yuanda Du, 2015 [192]
	Hepatic Cancer	WH, In	Mets in mice	Shao Hua Fan, 2014 [225]
	Angiogenesis	TF, In	CAM, RAR	Kai Zhao, 2018 [226]
	Angiogenesis	TF, In	CAM, RAR	Yan Chen, 2010 [227]
	Breast Cancer	TF, In	CAM, MPA in mice, MD in mice, RAR	Kai Zhao, 2018 [228]
	Hepatic Cancer	WH, In, Ad	Mets in mice	Wea Lung Lin, 2015 [229]
	Angiogenesis	TF	ZFM	Kai Heng Lam, 2011 [230]
	Breast Cancer	WH, TB, In		S. P. Nipin, 2017 [231]
	Breast Cancer	WH, TB, In		S. P. Nipin, 2018 [232]
	Breast Cancer	WH		Jianli Liu, 2018 [233]
	Gastric Cancer	WH, In, Ad		Yi Chieh Lee, 2011 [234]
	Glioma	WH, In		Li Ming Lien, 2016 [235]
	Glioma	WH, In		Xiang Zhang, 2017 [236]
	Hepatic Cancer	In, Ad		Ming Der Shi, 2013 [237]

	Lung Cancer	In, Ad	Mets in mice	Chunli Da, 2016 [238]
	Ovarian Cancer		CAM	Jianchu Chen, 2015 [239]
	Renal Cancer	In		Feng Liu, 2019 [240]
	Wound healing		SF in mice	Renhao Jiang, 2020 [241]
Orientin	Breast Cancer	WH		Soo Jin Kim, 2018 [242]
Isoorientin	Lung Cancer	WH		Hsu Kai Huang, 2020 [243]
Oroxylin	Breast Cancer	WH, In, Ad	Mets in mice	Zhijian Lu, 2012 [244]
	Colorectal Cancer	In		C.Lalou, 2013 [158]
Oroxylin A 7 β -glucuronomide	Colorectal Cancer	In		C.Lalou, 2013 [158]
Pectolinarigenin	Breast Cancer	WH, In	Mets in mice	Yali Li, 2019 [245]
	Colorectal	WH, In	Mets in mice	Cailing Gan, 2019 [246]
	Hepatic Cancer	WH, In		Sheng Liu, 2020 [247]
Radix Tetrastigma hemsleyani flavone (RTHF)	Colorectal Cancer	WH, In		Xiaowei Wu, 2018 [248]
Scutellarin	Angiogenesis	WH, TB		Zhong Xiu Zi Gao, 2010 [249]
	Bladder Cancer	In	Mets in mice	Wei Ling Lv, 2019 [250]
	Glioma	In		Shi Lei Tang, 2019 [251]
	Hepatic Cancer	WH, In	Mets in mice	Yang Ke, 2017 [252]
	Melanoma	WH, TB, In, Ad		Chun Yu Li, 2019 [253]
	Renal Cancer	In		Wenting Deng, 2018 [254]
Scutellarein	Cancer		CAM, RCN	Prabhu Thirusangu, 2017 [255]
Tricetin	Oral Cancer	In		Tsung Te Chung, 2017 [256]
	Osteosarcoma	WH, In		Pin Yu Chang, 2017 [257]
Tricin	Glioma	WH, In		Dai Jung Chung, 2018 [258]

	Hepatic Cancer	In		Naoko Seki, 2012 [259]
VI-14	Breast Cancer	WH, In, Ad		Fanni Li, 2012 [260]
Vicenin	Lung Cancer	WH, In		Yingyi Luo, 2019 [261]
Vitexin	Pheochromocytoma	TF, In		Hwa Jung Choi, 2006 [262]
Wogonin	Cancer	Review		Do Luong Huynh, 2017 [263]
	Angiogenesis	WH	MAR	Sha-sha Tian, 2014 [176]
	Angiogenesis	TF, In	CAM	Chiu Mei Lin, 2006 [264]
	Cancer	TF, In	CAM, MD in mice, RAR	Xiuming Song, 2013 [265]
	Glioma	In	Mets in mice	S. C. Shen, 2006 [46]
	Myeloma	WH, TB, In	MD in mice	Rong Fu, 2016 [266]
	Pancreatic Cancer	WH, In		Ying Tang Huang, 2005 [105]
Wogonoside	Angiogenesis	WH, TB	CAM, RAR	Yan Chen, 2009 [267]
	Breast Cancer	WH, TB	CAM, MD in mice, RAR	Yujie Huang, 2016 [268]
	Endometrial Cancer	In	Mets in mice	Shaorong Chen, 2019 [269]
WYC02-9	Cervical Cancer	WH, TB, In	ZFM, MPA in mice, MD in mice	Yun-ju Chen, 2013 [270]
2'-Hydroxy flavanone	Breast Cancer	WH		Jyotsana Singhal, 2017 [271]
	Prostate Cancer	WH, In		Shiqi Wu, 2018 [272]
7,2',4'-Trihydroxy-5-methoxy-8-dimethylallyl flavanone	Angiogenesis	WH, TB, Ad		Xiu Li Zhang, 2013 [273]
Alpinetin	Ovarian Cancer	WH		Xuezhi Zhao, 2018 [274]
Chamaejasmenin	Breast Cancer	WH, In	Mets in mice	Qi Li, 2016 [275]
Eriodictyol	Glioma	WH, In		Wenjun Li, 2020 [276]
Hesperidin	Diabetes		EWM in rats	Wenbin Li, 2018 [277]

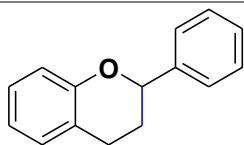


Flavanones

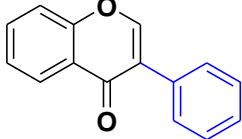
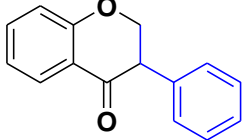
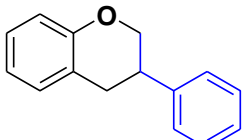
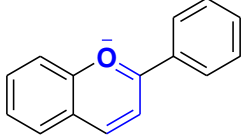
	Melanoma	WH	Mets in mice	Eui Baek Byun, 2019 [278]
HLBT-100	Cancer		RAR	Henry I.C. Lowe, 2017 [279]
HMFRR	Lung Cancer	WH, In, Ad		Qing Shi, 2017 [280]
Liquiritigenin	Cervical Cancer	TF		Si Rou Xie, 2012 [281]
Naringin	Glioma	WH, In		Sonia Aroui, 2016 [282]
	Glioma	In		Sonia Aroui, 2016 [283]
Naringenin	Angiogenesis	TF	MPA in mice	Irene Pafumi, 2017 [284]
	Cancer		MD in mice	Xiangpei Zhao, 2012 [84]
Pinocembrin	Retinoblastoma	In, Ad		Kun Shiang Chen, 2014 [285]
 <p>Flavanols</p>	Epigallocatechin gallate	Angiogenesis	Review	Daniel Karas, 2017 [286]
	Cancer	Review	Zhe Hou, 2004 [287]	
	Cancer	Review	Vidushi S. Neergheen, 2010 [288]	
	Cancer	Review	Animesh Chowdhury, 2016 [289]	
	Cancer	Review	Michael Xavier Doss, 2005 [290]	
	Cancer/Diabetes	Review	Layth Abdulmajeed Abdulkhaleq, 2017 [291]	
	Melanoma	Review	Suchitra Katiyar, 2007 [292]	
	Miscellaneous diseases	Review	Muhammad Saeed, 2017 [293]	
	Angiogenesis	TF	MPA in mice	A. K.Singh, 2002 [294]
	Angiogenesis	TF, In		Jun Shi, 2017 [295]
	Bladder Cancer	WH, In		Ke Wang Luo, 2017 [296]
	Bladder Cancer	WH, In		Ke Wang Luo, 2018 [297]
	Breast Cancer	WH, In		Yimin Zhang, 2009 [298]
	Cancer	TF, In	DASM in mice	Satoru Yamakawa, 2004 [299]

Cervical Cancer	In, Ad		Oana Tudoran, 2012 [300]
Glioma	In		Borhane Annabi, 2002 [301]
Glioma	In		Hong Li, 2014 [302]
Hepatic Cancer	WH, In		Mao Chuan Zhen, 2006 [303]
Kaposi Sarcoma	In	MPA in mice, MD in mice	Gianfranco Fassina, 2004 [304]
Lung Cancer	TF	MPA in mice	Xiangyong Li, 2013 [305]
Lung Cancer	WH, In		Jingli Shi, 2015 [306]
Lung Cancer	In		Yea Tzy Deng, 2011 [307]
Medulloblastoma	In, Ad		Anthony Pilorget, 2003 [308]
Melanoma	In	MD in mice	Noritaka Ohga, 2009 [309]
Nasopharyngeal Carcinoma	WH, In		Chien Hung Lin, 2012 [310]
Nasopharyngeal Carcinoma	In		Chih Yeu Fang, 2015 [311]
Nasopharyngeal Carcinoma	WH		Chien Hung Lin, 2020 [312]
Neuroblastoma	TF, In		Md Motarab Hossain, 2012 [313]
Neuroblastoma	In		Spiridione Garbisa, 2001 [314]
Oral Cancer	In		Yung Chuan Ho, 2007 [315]
Oral Cancer	WH, In, Ad		Pei Ni Chen, 2011 [316]
Osteoblasts	WH, In		Tetsu Kawabata, 2018 [317]
Osteoblasts	WH, In		Tetsu Kawabata, 2018 [318]
Ovarian Cancer	In	MD in mice	Francesca Spinella, 2006 [319]
Pancreatic Cancer	In		Atsushi Masamune, 2005 [320]
Prostate Cancer	In		Damian Duhon, 2010 [321]
Retinopathy	In, Ad		Chi Ming Chan, 2010 [322]

	Retinopathy	TF	MCN	Hak Sung Lee, 2014 [323]	
Epicatechin-3-gallate	Diabetes		IWM in rats	Kelly J. McKelvey, 2012 [324]	
	Lung Cancer	WH, In, Ad		Shu Fang Huang, 2016 [325]	
Silymarin	Breast/Prostate Cancer	TF		Cheng Jiang, 2000 [326]	
Silibinin	Prostate Cancer		Review	Harold Ting, 2013 [327]	
	Bladder Cancer	In	Mets in mice	Kaijie Wu, 2013 [328]	
	Bladder Cancer	WH, In		Feng Li, 2018 [329]	
	Breast Cancer	In		Mohadeseh Dastpeyman, 2012 [330]	
	Breast Cancer	WH, In		Hyo Joo Byun, 2017 [331]	
	Colon Cancer	In		Chiu Mei Lin, 2012 [332]	
	Glioma	In		Kwang Won Kim, 2009 [333]	
	Prostate Cancer	In	Mets in mice	Harold Ting, 2013 [334]	
	Prostate Cancer	TF		Gagan Deep, 2017 [335]	
	Prostate Cancer	In, Ad		Mohammad Javad Mokhtari, 2008 [336]	
	Renal Cancer	In		Liang Liang, 2012 [337]	
	Retinopathy		RRN	C. H. Lin, 2013 [338]	
	Taxifolin	Osteosarcoma	In		Xin Chen, 2018 [339]
BAS1 & BAS4	Glioma	WH		L. A.L. Maués, 2019 [340]	
Flavanes	Alpinumisoflavone	Melanoma	WH, In	Mets in mice	Ming Gao, 2017 [341]
	Biochanin	Lung Cancer	WH, In		Yan Wang, 2018 [342]
	Corylin	Hepatic Cancer	WH, In		Chi Yuan Chen, 2018 [343]



Flavanes

 <p>Isoflavones</p>	DCMF	Wound healing	WH	EWM in mice	Phorl Sophors, 2016 [344]	
	Furowanin	Colorectal Cancer	WH, In	Mets in mice	Jinxia Zhao, 2019 [345]	
	Genistein	Cancer		Review		Janet M. Pavese, 2010 [346]
		Angiogenesis	TF			Myoung H.Kim, 2003 [113]
		Breast Cancer	In		MD in mice	Z.Shao, 2000 [347]
		Cancer	WH			Cornelia Spoerlein, 2013 [131]
		Hepatic Cancer	WH			Qian Zhang, 2019 [348]
		Retinopathy			RbCN	A M Jousen, 2000 [19]
4', 6, 7-trimethoxyisoflavone (TMF)	Angiogenesis			CAM	Siva Prasad Panda, 2020 [349]	
	Wound healing	WH			Ngoc Thuy Bui, 2014 [350]	
 <p>Isoflavanones</p>	Deguelin	Cancer		Review	Ying Wang, 2013 [351]	
		Angiogenesis	TF, In		MPA in mice	Raffaella Dell'Eva, 2007 [352]
		Pancreatic Cancer	WH, In			Wen Zheng, 2016 [353]
 <p>Isoflavanes</p>	Glabridin	Breast Cancer	WH, TB, In	MPA in mice	Ya Ling Hsu, 2011 [354]	
		Lung Cancer	WH, TB, In		MPA in mice	Ying Ming Tsai, 2011 [355]
 <p>Anthocyanidins</p>	Cyanidin	Angiogenesis	TF		Matsunaga Nozomu, 2010 [356]	
	Delphinidin	Angiogenesis		Review		Kanika Patel, 2013 [357]
		Angiogenesis	TF, In		MPA in mice	Sylvie Lamy, 2006 [358]
		Angiogenesis	WH		CAM	Laure Favot, 2003 [359]
		Angiogenesis	TF, In			Sylvie Lamy, 2012 [126]
	Angiogenesis	TF			Matsunaga Nozomu, 2010 [356]	

	Breast Cancer		CAM	Olga Viegas, 2019 [360]
	Colorectal Cancer	In, Ad	Mets in mice	Chi Chou Huang, 2019 [361]
	Lung Cancer		MPA in mice	Mun Hyeon Kim, 2017 [362]
	Osteosarcoma	WH, In		Hae Mi Kang, 2018 [363]
Malvidin	Angiogenesis	TF		Matsunaga Nozomu, 2010 [356]
Miscellaneous (articles with > 4 Flavonoids)	Angiogenesis		Review	Lucia Morbidelli, 2016 [364]
	Angiogenesis		Review	Ladislav Mirossay, 2018 [365]
	Angiogenesis		Review	Józef Dulak, 2005 [366]
	Angiogenesis		Review	Carmen Diniz, 2017 [367]
	Breast Cancer		Review	Andrea Kapinova, 2017 [368]
	Cancer		Review	J.Mojzis, 2008 [369]
	Cancer		Review	Divyashree Ravishankar, 2013 [370]
	Cancer		Review	Yihai Cao, 2002 [371]
	Cancer		Review	Loïc Le Marchand, 2002 [372]
	Cancer		Review	Vijayalakshmi Nandakumar, 2008 [373]
	Cancer		Review	Maria Angeles Martin, 2013 [374]
	Cancer		Review	Jian Ping Zhang, 2016 [375]
	Cancer		Review	Mirza Aghazadeh-Attari, 2020 [376]
	Cancer		Review	Nam Joo Kang, 2011 [377]
	Cancer		Review	Suleman S.Hussain, 2016 [378]
Cancer		Review	Hanna Lewandowska, 2016 [379]	
Cancer		Review	Ching Shu Lai, 2011 [380]	
Cancer		Review	Chithan Kanadaswami, 2005 [381]	

Cancer		Review	Gary David Stoner, 2008 [382]
Colon Cancer		Review	Jasleen Kaur, 2015 [383]
Colorectal Cancer		Review	João R. Araújo, 2011 [384]
Eye disease		Review	Zhihan Xu, 2017 [385]
Hepatic Cancer		Review	Dimitrios Stagos, 2012 [386]
Hepatic Cancer		Review	Estefanny Ruiz García, 2018 [387]
Myeloma		Review	F.Pojero, 2019 [388]
Ocular angiogenesis		Review	Rania S. Sulaiman, 2014 [389]
Angiogenesis		CAM	Gacche Rajesh, 2010 [390]
Angiogenesis		ZFM	In Kei Lam, 2012 [391]
Angiogenesis	In		Theodore Fotsis, 1997 [392]
Angiogenesis	WH		Chalermnat Suktap, 2018 [393]
Cancer		CAM	R. N.Gacche, 2015 [394]
Cancer	WH		Jiukai Zhang, 2014 [395]
Cancer		CAM	Rajesh N.Gacche, 2011 [396]
Glioma	WH		Balbino L.Santos, 2015 [397]
Glioma	In		Amira Ouanouki, 2017 [398]
Hepatic Cancer	WH, TB		Ning Li, 2015 [399]
Lung Cancer	WH		Chun Gu Wang, 2018 [400]
Lung Cancer	In, Ad	Mets in mice	Yung Chin Hsiao, 2007 [401]

TB, Tube Formation; WH, Wound Healing; In, Invasion; Ad, Adhesion; Mets, Metastasis; CAM, Chick Chorioallantoic Membrane; MPA, Matrigel Plug Assay; RAR, Rat Aortic Ring; EWM, Excision Wound Model; SF, Skin Flap; RRN, Rat Retinal Neovascularization; MAR, Mice Aortic Ring; MD, Microvessel Density; MRN, Mice Retinal Neovascularization; MCN, Mice Corneal Neovascularization; RbCN, Rabbit Corneal Neovascularization; ZFM, Zebra Fish Model; RCN, Rat Corneal Neovascularization; CIAM, Collagen Induced Arthritis Model; DASM, Dorsal air Sac Model; IWM, Incision Wound Model.

Table 2. Characteristics of studies included in the meta-analysis

Author, Year	Flavonoid	Angiogenesis promoter	Cell line	Concentration	Time, duration of treatment	Results representation	n
Soo Jin Oh, 2010 [78]	Quercetin	n/a	TAMR-MCF-7	3, 10, 30 μ M	10 th day, 72 h	Number of branches	5 to 7
Chiu-Mei Lin, 2006 [264]	Wogonin	LPS (1 μ g/mL)	NA	10 ⁻⁵ , 10 ⁻⁶ , 10 ⁻⁷ , 10 ⁻⁸ M	10 th day, 48 h	Percentage of vascular counts (%)	3
Ling-Zhi Liu, 2011 [118]	Acacetin	n/a	OVCAR-3	10 μ M	9 th day, 4 days	Relative angiogenesis	5
Kai Zhao, 2018 [226]	Wogonin, LW-215	n/a	n/a	Wogonin: 80 ng/CAM, LW-215: 2, 4, 8 ng/CAM	10 th day, 48 h	The number of new vessels (% of control)	3
Haizhi Huang, 2015 [25]	Galangin, myricetin	n/a	OVCAR-3	G: 40 μ M, M: 20 μ M	9 th day, 5 days	Blood vessels (%)	6
Olga Viegas, 2019 [360]	Cyanidin, C-3-O-glucoside, delphinidin, D-3-O-glucoside	n/a	n/a	20, 40, 80, 100, 200 μ M	11 th day, 48 h	% of control	5
Wen-fu Tan, 2003 [83]	Quercetin	n/a	n/a	25, 50, 100 nmol/10 μ L/CAM	10 th day, 48 h	Microscopic pictures	10
Rajesh Gacche, 2010 [390]	Flavone, 3/5/6/7/-Hydroxy flavone	n/a	n/a	10, 50, 100 μ M	10 th day, 48 h	Antiangiogenic activity (%) of selected flavonoids	8
R.N. Gacche, 2011 [396]	3, 6-DHF, 3, 7-DHF, 5, 7-DHF, apigenin, genistein, kaempferol, luteolin, fisetin, rutin, quercetin	n/a	n/a	10, 50, 100 μ M in 0.05% DMSO/20 μ L/CAM	10 th day, 48 h	Antiangiogenic activity (%) of selected flavonoids	8
R.N. Gacche, 2015 [394]	4'-Methoxy flavone, 3-Hydroxy-7-methoxy flavone, Formononetin,	n/a	n/a	10, 50, 100 μ M in 0.05% DMSO/20 μ L/CAM	10 th day, 48 h	Antiangiogenic activity (%) of selected flavonoids	8

	Biochanin-A, Diosmin, Hesperitin, Hesperidin, 2'- Hydroxy flavanone, 4'- Hydroxy flavanone, 7- Hydroxy flavanone, Myricetin, Taxifolin, Silibinin, Silymarin, Naringenin, Naringin, Catechin						
Yan Chen, 2010 [227]	LYG-202	n/a	n/a	2.4, 12, 60 ng/CAM	10 th day, 48 h	Percentage of vascular counts (% of control)	10
Hisanori Hattori, 2011 [1]	Beturetol, isosakuranetin	n/a	n/a	300 ng/CAM	5 th day, 7 days	Inhibition % of angiogenesis at 300 ng/CAM.	10
Yujie Huang, 2019 [402]	Wogonoside	n/a	MDA-MB- 231, MDA-MB- 468	50, 100, 200 ng/CAM	10 th day, 48 h	Number of new vessels (% cells)	3
Yan Chen, 2009 [267]	Wogonoside	LPS (1µg/mL)	n/a	1.5, 15, 150 ng/CAM	10 th day, 48 h	Number of vessels (% of LPS)	10
Xiaobo Li, 2017 [202]	Luteolin	Gas6 (300 ng/mL)	n/a	10, 20 µM	6 th day, 48 h	Relative vascular density (% of control)	3
Siva Prasad Panda, 2020 [349]	TMF	n/a	EAT	10, 17, 25 µg/mL	5 th day, 11 days	Microscopic pictures	5
Yujie Huang, 2016 [268]	Wogonoside	n/a	MCF-7	50, 100, 200 ng/CAM	10 th day, 48 h	Number of new vessels (% MCF- 7)	3

Tariq A. Bhat, 2013 [119]	Acacetin	n/a	n/a	50 µM	6 th day, (every 48 h for 8 days)	% capillary formation	5 independent areas on CAMs for each treatment
Jing Fang, 2007 [129]	Apigenin	n/a	OVCAR-3, PC-3	OVCAR-3: 7.5, 15 µM, PC-3: 10, 20 µM	9 th day, 4 days	Quantification of blood vessels on the CAM	8
Jianchu Chen, 2015 [239]	Nobiletin	n/a	A2780	20 µM	9 th day, 5 days	Blood vessel count	10
Poyil Pratheeshkumar, 2012 [224]	Luteolin	n/a	n/a	20, 40 µM	8 th day, 48 h	Relative vascular density	3
Chiu-Mei Lin, 2006 [403]	Wogonin	IL-6 (10 ng/mL)	n/a	10 ⁻⁵ , 10 ⁻⁶ , 10 ⁻⁷ , 10 ⁻⁸ M	10 th day, 48 h	Percentage of vascular count (%)	3
Dongqing Zhu, 2016 [404]	Baicalin, baicalein	n/a	n/a	0.5, 2, 10, 50 µg/mL and 0.2, 1, 5 mg/mL	7.5 th day, 48 h	Number of new blood vessels	30
Haitao Luo, 2009 [53]	Kaempferol	n/a	OVCAR-3	20 µM	9 th day, 5 days	Blood vessel count	5
Laure Favot, 2003 [359]	Delphinidin	n/a	n/a	2, 10, 25, 50 µg	8 th day, 48 h	Microscopic pictures	5
Mercedes Peña, 2023 [405]	Aflibercept (Zaltrap®)	n/a	n/a	10 mg/mL	7 th day, 72 h	Vascular density	10

n/a, not available; DHF, Dihydroxyflavone; TMF, Trimethoxyflavonoid; TMAR, Tamoxifen breast cancer resistant cell line; MCF-7, Breast cancer cell line; LPS, Lipopolysaccharide; OVCAR-3, Ovarian cancer cell line; MDA-MB-231, MDA-MB-468, Triple negative breast cancer cell lines; Gas6, Growth arrest specific 6; EAT, Mouse breast carcinoma (Ehrlich-Lettre Ascites); PC-3, Prostate cancer cell line; A2780, ovarian cancer cell line; IL-6, Interleukin 6.

Table 3. Low concentration range (10 -20 µM) sensitivity analysis

Subgroup	Before Overall summary (95%CI X - Y, P)	After Overall summary (95%CI X - Y, P)	Left-out-study
Isoflavones	0.71 (0.66 - 0.76, 99%)	0.73 (0.71 – 0.76, 93%)	Gacche 2011 (Genistein)
		0.70 (0.62 – 0.80, 99%)	Gacche 2015 (Biochanin-A)
		0.69 (0.63 – 0.75, 98%)	Gacche 2015 (Formononetin)
Flavones	0.73 (0.70 – 0.77, 98%)	0.73 (0.69 – 0.76, 98%)	Gacche 2010 (5-Hydroxyflavone)
		0.72 (0.69 – 0.76, 97%)	Gacche 2010 (6-Hydroxyflavone)

		0.73 (0.70 – 0.77, 98%)	Gacche 2010 (7-Hydroxyflavone)
		0.74 (0.71 – 0.77, 97%)	Gacche 2010 (Flavone)
		0.74 (0.70 – 0.77, 98%)	Gacche 2011 (5,7-Dihydroxyflavone)
		0.74 (0.71 – 0.77, 97%)	Gacche 2011 (Apigenin)
		0.74 (0.70 – 0.77, 98%)	Gacche 2011 (Luteolin)
		0.73 (0.69 – 0.76, 97%)	Gacche 2015 (4'-Methoxyflavone)
		0.73 (0.69 – 0.77, 98%)	Gacche 2015 (Diosmin)
		0.73 (0.70 – 0.77, 98%)	Pratheeshkumar 2012 (Luteolin)
		0.73 (0.70 – 0.77, 98%)	Zhu 2016 (Baicalein)
		0.73 (0.70 – 0.77, 98%)	Zhu 2016 (Baicalin)
Flavonols	0.74 (0.69 – 0.79, 99%)	0.75 (0.70 – 0.80, 99%)	Gacche 2010 (3-Hydroxyflavone)
		0.72 (0.68 – 0.77, 99%)	Gacche 2011 (3,6-Dihydroxyflavone)
		0.73 (0.68 – 0.78, 99%)	Gacche 2011 (3,7-Dihydroxyflavone)
		0.74 (0.70 – 0.79, 99%)	Gacche 2011 (Fisetin)
		0.75 (0.70 – 0.79, 99%)	Gacche 2011 (Kaempferol)
		0.75 (0.70 – 0.79, 99%)	Gacche 2011 (Quercetin)
		0.74 (0.69 – 0.79, 99%)	Gacche 2011 (Rutin)
		0.73 (0.68 – 0.78, 99%)	Gacche 2015 (3-Hydroxy-7-methoxy flavone)
Flavanols	0.74 (0.55 – 0.99, 100%)	0.74 (0.69 – 0.79, 99%)	Gacche 2015 (Myricetin)
		0.86 (0.84 – 0.88, n/a)	Gacche 2015 (Silibinin)
		0.64 (0.63 – 0.65, n/a)	Gacche 2015 (Taxifolin)
Flavanones	0.84 (0.80 – 0.89, 98%)	0.84 (0.79 – 0.90, 98%)	Gacche 2015 (2'-Hydroxyflavanone)
		0.84 (0.79 – 0.89, 98%)	Gacche 2015 (4'-Hydroxyflavanone)
		0.84 (0.79 – 0.89, 98%)	Gacche 2015 (7-Hydroxyflavanone)
		0.84 (0.79 – 0.89, 98%)	Gacche 2015 (Hesperidin)
		0.84 (0.79 – 0.90, 98%)	Gacche 2015 (Hesperitin)
		0.86 (0.81 – 0.91, 98%)	Gacche 2015 (Naringenin)
		0.86 (0.83 – 0.90, 96%)	Gacche 2015 (Naringin)
Anthocyanidins	1.07 (0.86 – 1.33, 81%)	1.14 (0.87 – 1.48, 84%)	Viegas 2019 (Cyanidin)
		0.99 (0.81 – 1.22, 70%)	Viegas 2019 (Cyanidin-3-O-glucoside)
		1.02 (0.79 – 1.31, 85%)	Viegas 2019 (Delphinidin)
		1.14 (0.89 – 1.47, 79%)	Viegas 2019 (Delphinidin-3-O-glucoside)

n/a, not applicable; results highlighted in red showed >10% change in re-pooled summary estimates.

Table 4. Medium concentration range (40-50 µM) sensitivity analysis

Subgroup	Before Overall summary (95%CI X - Y, P)	After Overall summary (95%CI X - Y, P)	Left-out-study
----------	--	---	----------------

Isoflavones	0.46 (0.44 – 0.49, 92%)	0.47 (0.41 – 0.55, 88%)	Gacche 2011 (Genistein)
		0.48 (0.44 – 0.53, 68%)	Gacche 2015 (Biochanin-A)
		0.45 (0.43 – 0.48, 94%)	Gacche 2015 (Formononetin)
Flavonols	0.50 (0.46 – 0.56, 100%)	0.53 (0.48 – 0.58, 100%)	Gacche 2010 (3-Hydroxyflavone)
		0.49 (0.44 – 0.54, 100%)	Gacche 2011 (3,6-Dihydroxyflavone)
		0.50 (0.45 – 0.56, 100%)	Gacche 2011 (3,7-Dihydroxyflavone)
		0.50 (0.45 – 0.56, 100%)	Gacche 2011 (Fisetin)
		0.51 (0.45 – 0.57, 100%)	Gacche 2011 (Kaempferol)
		0.50 (0.45 – 0.57, 100%)	Gacche 2011 (Quercetin)
		0.50 (0.45 – 0.56, 100%)	Gacche 2011 (Rutin)
		0.50 (0.44 – 0.56, 100%)	Gacche 2015 (3-Hydroxy-7-methoxy flavone)
Flavanols	0.53 (0.27 – 1.02, 100%)	0.52 (0.48 – 0.57, 100%)	Gacche 2015 (Myricetin)
		0.74 (0.73 – 0.76, n/a)	Gacche 2015 (Silibinin)
		0.38 (0.37 – 0.39, n/a)	Gacche 2015 (Taxifolin)
Flavones	0.55 (0.45 – 0.67, 100%)	0.59 (0.51 – 0.68, 100%)	Bhat 2013 (Acacetin)
		0.52 (0.44 – 0.61, 100%)	Gacche 2010 (5-Hydroxyflavone)
		0.54 (0.43 – 0.67, 100%)	Gacche 2010 (6-Hydroxyflavone)
		0.54 (0.44 – 0.66, 100%)	Gacche 2010 (7-Hydroxyflavone)
		0.56 (0.45 – 0.69, 100%)	Gacche 2010 (Flavone)
		0.55 (0.44 – 0.69, 100%)	Gacche 2011 (5,7-Dihydroxyflavone)
		0.55 (0.44 – 0.69, 100%)	Gacche 2011 (Apigenin)
		0.55 (0.44 – 0.69, 100%)	Gacche 2011 (Luteolin)
		0.54 (0.44 – 0.67, 100%)	Gacche 2015 (4'-Methoxyflavone)
		0.56 (0.45 – 0.69, 100%)	Gacche 2015 (Diosmin)
0.55 (0.45 – 0.68, 100%)	Pratheeshkumar 2012 (Luteolin)		
Flavanones	0.74 (0.68 – 0.80, 99%)	0.55 (0.45 – 0.67, 100%)	Zhu 2016 (Baicalein)
		0.73 (0.67 – 0.80, 100%)	Gacche 2015 (2'-Hydroxyflavanone)
		0.74 (0.67 – 0.81, 99%)	Gacche 2015 (4'-Hydroxyflavanone)
		0.73 (0.66 – 0.81, 100%)	Gacche 2015 (7-Hydroxyflavanone)
		0.72 (0.66 – 0.79, 99%)	Gacche 2015 (Hesperidin)
		0.72 (0.66 – 0.80, 99%)	Gacche 2015 (Hesperitin)
		0.75 (0.69 – 0.82, 99%)	Gacche 2015 (Naringenin)
0.76 (0.71 – 0.81, 99%)	Gacche 2015 (Naringin)		
Anthocyanidins	1.00 (0.94 – 1.07, 0%)	1.00 (0.94 – 1.07, 0%)	Viegas 2019 (Cyanidin)
		1.00 (0.92 – 1.09, 0%)	Viegas 2019 (Cyanidin-3-O-glucoside)
		0.99 (0.93 – 1.06, 0%)	Viegas 2019 (Delphinidin)
		1.01 (0.93 – 1.10, 0%)	Viegas 2019 (Delphinidin-3-O-glucoside)

n/a, not applicable; results highlighted in red showed >10% change re-pooled summary estimates.

Table 5. High concentration (100 µM) sensitivity analysis

Subgroup	Before Overall summary (95%CI X - Y, P)	After Overall summary (95%CI X - Y, P)	Left-out-study
Isoflavones	0.20 (0.14 - 0.29, 100%)	0.25 (0.19 – 0.33, 100%)	Gacche 2011 (Genistein)
		0.19 (0.09 – 0.42, 100%)	Gacche 2015 (Biochanin-A)
		0.17 (0.10 – 0.28, 100%)	Gacche 2015 (Formononetin)
		0.26 (0.18 – 0.38, 100%)	Gacche 2010 (3-Hydroxyflavone)
		0.24 (0.18 – 0.32, 100%)	Gacche 2011 (3,6-Dihydroxyflavone)
		0.24 (0.18 – 0.34, 100%)	Gacche 2011 (3,7-Dihydroxyflavone)
		0.25 (0.18 – 0.36, 100%)	Gacche 2011 (Fisetin)
Flavonols	0.26 (0.19 – 0.35, 100%)	0.28 (0.21 – 0.36, 100%)	Gacche 2011 (Kaempferol)
		0.27 (0.19 – 0.39, 100%)	Gacche 2011 (Quercetin)
		0.26 (0.18 – 0.37, 100%)	Gacche 2011 (Rutin)
		0.25 (0.18 – 0.35, 100%)	Gacche 2015 (3-Hydroxy-7-methoxy flavone)
		0.26 (0.18 – 0.36, 100%)	Gacche 2015 (Myricetin)
		0.57 (0.56 – 0.58, n/a)	Gacche 2015 (Silibinin)
		0.14 (0.14 – 0.14, n/a)	Gacche 2015 (Taxifolin)
Flavanols	0.28 (0.07 – 1.12, 100%)	0.35 (0.28 – 0.45, 100%)	Gacche 2010 (5-Hydroxyflavone)
		0.35 (0.28 – 0.44, 100%)	Gacche 2010 (6-Hydroxyflavone)
		0.34 (0.27 – 0.43, 100%)	Gacche 2010 (7-Hydroxyflavone)
		0.36 (0.28 – 0.46, 100%)	Gacche 2010 (Flavone)
		0.36 (0.28 – 0.45, 100%)	Gacche 2011 (5,7-Dihydroxyflavone)
		0.37 (0.29 – 0.47, 100%)	Gacche 2011 (Apigenin)
		0.39 (0.32 – 0.47, 100%)	Gacche 2011 (Luteolin)
		0.34 (0.27 – 0.42, 100%)	Gacche 2015 (4'-Methoxyflavone)
		0.37 (0.29 – 0.49, 100%)	Gacche 2015 (Diosmin)
		0.34 (0.27 – 0.43, 100%)	Zhu 2016 (Baicalin)
Flavones	0.36 (0.29 – 0.44, 100%)	0.58 (0.52 – 0.66, 99%)	Gacche 2015 (2'-Hydroxyflavanone)
		0.58 (0.52 – 0.64, 99%)	Gacche 2015 (4'-Hydroxyflavanone)
		0.58 (0.51 – 0.65, 99%)	Gacche 2015 (7-Hydroxyflavanone)
		0.57 (0.51 – 0.63, 99%)	Gacche 2015 (Hesperidin)
		0.57 (0.51 – 0.64, 99%)	Gacche 2015 (Hesperitin)
		0.59 (0.53 – 0.66, 99%)	Gacche 2015 (Naringenin)
		0.60 (0.56 – 0.65, 99%)	Gacche 2015 (Naringin)
Anthocyanidins	0.82 (0.74 – 0.90, 40%)	0.83 (0.72 – 0.95, 60%)	Viegas 2019 (Cyanidin)
		0.81 (0.72 – 0.91, 54%)	Viegas 2019 (Cyanidin-3-O-glucoside)
		0.77 (0.71 – 0.84, 0%)	Viegas 2019 (Delphinidin)

0.87 (0.78 – 0.96, 0%) Viegas 2019 (Delphinidin-3-O-glucoside)

n/a, not applicable; results highlighted in red showed >10% in re-pooled summary estimates

Table 6. Reported cytotoxic SAR effects of flavonoids (most common features highlighted in bold)

Structural feature	Effect	Example	Cell line	Ref
C2-C3 double bond	Enhance activity	Proliferation inhibition of naringenin (10%) versus apigenin (46%) at 200 μ M	Colon cancer (SW480)	[406]
OH at C-6	Enhance activity	Proliferation inhibition of apigenin (46%) versus quercetagenin (63%) at 200 μ M		
OH at C-3	Reduce activity	Proliferation inhibition of apigenin (46%) versus kaempferol (increase proliferation by 20%) at 200 μ M		
Replacement of OH with OCH₃ at C-4	No effect	Proliferation inhibition of hesperidin (0%) versus naringin (15%) at 200 μ M		
Replacement of OH with OCH₃ at C-5	Reduce activity	Proliferation inhibition of 5-demethylnobiletin (75%) versus nobiletin (20%) at 20 μ g/ml	Triple negative breast cancer (MDA-MB-231)	[395]
OCH₃ at C-8	Enhance activity	IC ₅₀ of nobiletin (6.8 \pm 1.7 μ g/ml) versus sinensetin (88.9 \pm 32.3 μ g/ml)	Human liver cancer (HepG2)	
C2-C3 double bond	Enhance activity	EC ₅₀ of naringenin (81.2 μ M) versus apigenin (29.6 μ M)	Colorectal carcinoma (DLD-1)	[407]
Number of OHs between 2 and 4	Enhance activity	EC ₅₀ of 6-hydroxyflavone (1OH, 47.7 μ M) and morin (5OHs, NA) versus 3,6-dihydroxyflavone (2OHs, 17.3 μ M)	Prostatic cancer (PC3)	
Attachment of ring B at C2	Enhance activity	EC ₅₀ of genistein (promoted cell viability) versus apigenin (36.4 μ M)	Breast cancer (MCF-7)	
OH at C-3	Enhance activity	EC ₅₀ galangin (67.8 μ M) versus 3,7-dihydroxy flavone (40.1 μ M)	Colorectal carcinoma (LoVo)	
OH at C-5	Reduce activity	EC ₅₀ of fisetin (22.4 μ M) versus quercetin (41.2 μ M)	Triple negative breast cancer (MDA-MB-231)	
OH at C-6	Enhance activity	EC ₅₀ of flavone (>100 μ M) versus 6-OH flavone (38.6 μ M)	Colorectal carcinoma (DLD-1)	
OH at C-7	Enhance activity	EC ₅₀ of chrysin (>100 μ M) versus 7-hydroxyflavone (37.5 μ M)	Triple negative breast cancer (MDA-MB-231)	
Ortho-diOH on ring B	Enhance activity	EC ₅₀ of chrysin (>100 μ M) versus luteolin (23.5 μ M)	Prostatic cancer (PC3)	

Replacement of OH with OCH₃ at C-5	Reduce activity	GI ₅₀ of N-methoxybenzoyl amine-5-hydroxy-6,7-dimethoxyflavone (1.83 μM) versus N-methoxybenzoyl amine-5,6,7-trimethoxyflavone (15.29 μM)	Breast cancer (MCF-7)	[408]
C2-C3 double bond	Enhance activity	EC ₅₀ of naringenin (617.7 μM) versus luteolin (78.1 μM)	Human leukemia (Jurkat E6-1)	[409]
OH at C-3	Reduce activity	EC ₅₀ of apigenin (72.7 μM) versus kaempferol (163.1 μM)		
Ortho-diOH on ring B	Enhance activity	EC ₅₀ of morin (680.3 μM) versus quercetin (354.7 μM)		
OCH₃ at C-7	Enhance activity	EC ₅₀ of baicalein (213.3 μM) versus 7-methoxy-baicalein (91 μM)		
Replacement of OH with OCH₃ at C-7	Enhance activity	EC ₅₀ of hispidulin (153.1 μM) versus cirsimaritin (66.8 μM)		
Replacement of OH with OCH₃ at C-6	Enhance activity	EC ₅₀ of scutellarein (501.9 μM) versus hispidulin (153.1 μM)		
Replacement of OH with OCH₃ at C-5'	Enhance activity	EC ₅₀ of quercetin (354.7 μM) versus isorhamnetin (116.8 μM)		
Glycosylation at C-7	Enhance activity	EC ₅₀ of baicalein (213.3 μM) versus baicalein-glucuronide (137 μM)		
4-C=O	Enhance activity	EC ₅₀ of catechin (4410 μM) versus taxifolin (2247 μM)		
C2-C3 double bond	Enhance activity	IC ₅₀ of naringenin (NA) versus apigenin (79.77 μM)	Human liver cancer (HepG2)	[410]
OH at C-3	Reduce activity	IC ₅₀ of luteolin (78.95 μM) versus quercetin (188.84 μM)		
Replacement of OH with OCH₃ at C-7, 3' and/or 4'	Reduce activity	IC ₅₀ of apigenin (79.77 μM) versus apigenin-4',7-dimethyl ether (NA) and luteolin (78.95 μM) versus luteolin-3',4',7-trimethyl ether (NA)		
Glycosylation at C-3	Reduce activity	IC ₅₀ of quercetin (188.84 μM) versus rutin (NA)		
Attachment of ring B at C2	Enhance activity	IC ₅₀ of genistein (135.95 μM) versus apigenin (79.77 μM)		
Number of OHs in 4-C=O	No effect	IC ₅₀ of tetrahydroxy flavone (21.6 μM) versus dihydroxy flavone (25.6 μM)	Breast cancer (MCF-7)	[411]
Lower number of OHs in 4-C=S	Enhance activity	IC ₅₀ of pentahydroxy-4-thioflavone (102.6 μM) vs tetrahydroxy-4-thioflavone (27.3 μM) versus dihydroxy-4-thioflavone (7.9 μM)		

OH at C-5, 7	Enhance activity	IC ₅₀ of 7,8,3',4'-tetrahydroxyflavone (97.5 μM) versus 5,7,3',4'-tetrahydroxyflavone (21.6 μM)		
Replacement of OH with OCH₃	Reduce activity	IC ₅₀ of 5,7,3',4'-tetrahydroxy flavone (21.6 μM) versus 5,7,3',4'-tetramethoxy flavone (>250 μM)		
Cl or Br at C-4'	Enhance activity	IC ₅₀ of 4-thio-5,7-dihydroxy flavone (7.9 μM) versus 4-thio-5,7-dihydroxy-4'-chlorophenyl flavone (1 μM) and 4-thio-7,8-dihydroxy flavone (14.7 μM) versus 4-thio-7,8-dihydroxy-4'-bromophenyl flavone (4.9 μM)		
4-C=S	Enhance activity	IC ₅₀ of 4-oxo-5,7-dihydroxy flavone (25.6 μM) versus 4-thio-5,7-dihydroxy flavone (7.9 μM)		
C2-C3 double bond	Enhance activity	n/a	Review article	[412]
OH at C-5, 7	Enhance activity			
OH at C-6	Enhance activity			
Ortho-di-OH on ring B	Enhance activity			
OH at C-3	Enhance activity			
OH at C-5, 4'	Enhance activity	n/a	Review article	[413]
OCH₃ at C-3, 3', 5'	Enhance activity			
Cl at C-6, 2'	Enhance activity			
OH at C-5, 7	Enhance activity	n/a	Review article	[414]
Ortho-diOH on ring B	Enhance activity			
C2-C3 double bond	Enhance activity	n/a	Review article	[415]
Replacement of OH with OCH₃	Enhance activity			
OH at C-5, 7	Enhance activity			
OH at C-6	Enhance activity			
OH at C-3	Enhance activity			

n/a, not applicable; IC₅₀, half maximal inhibitory concentration; EC₅₀, half maximal effective concentration

References

1. Hattori, H.; Okuda, K.; Murase, T.; Shigetsura, Y.; Narise, K.; et al. Isolation, Identification, and Biological Evaluation of HIF-1-Modulating Compounds from Brazilian Green Propolis. *Bioorganic Med. Chem.* **2011**, *19* (18), 5392–5401.
2. Ramchandani, S.; Naz, I.; Lee, J. H.; Khan, M. R.; Ahn, K. S. An Overview of the Potential Antineoplastic Effects of Casticin. *Molecules* **2020**, *25* (6), 1287.
3. Yang, D. S.; Li, Z. L.; Peng, W. B.; Yang, Y. P.; Wang, X.; et al. Three New Prenylated Flavonoids from *Macaranga Denticulata* and Their Anticancer Effects. *Fitoterapia* **2015**, *103*, 165–170.
4. Kashyap, D.; Sharma, A.; Sak, K.; Tuli, H. S.; Buttar, H. S.; et al. Fisetin: A Bioactive Phytochemical with Potential for Cancer Prevention and Pharmacotherapy. *Life Sci.* **2018**, *194*, 75–87.
5. Rengarajan, T.; Yaacob, N. S. The Flavonoid Fisetin as an Anticancer Agent Targeting the Growth Signaling Pathways. *Eur. J. Pharmacol.* **2016**, *789*, 8–16.
6. Syed, D. N.; Adhami, V. M.; Khan, N.; Khan, M. I.; Mukhtar, H. Exploring the Molecular Targets of Dietary Flavonoid Fisetin in Cancer. *Semin. Cancer Biol.* **2016**, *40*, 130–140.
7. Rahul K. Lall, Vaqar Mustafa Adhami, and H. M. Dietary Flavonoid Fisetin for Cancer Prevention and Treatment. *Mol. Nutr. Food Res.* **2016**, *60* (6), 1396–1405.
8. Tsai, C. F.; Chen, J. H.; Chang, C. N.; Lu, D. Y.; Chang, P. C.; et al. Fisetin Inhibits Cell Migration via Inducing HO-1 and Reducing MMPs Expression in Breast Cancer Cell Lines. *Food Chem. Toxicol.* **2018**, *120*, 528–535.
9. Sun, X.; Ma, X.; Li, Q.; Yang, Y.; Xu, X.; et al. Anti-cancer Effects of Fisetin on Mammary Carcinoma Cells via Regulation of the PI3K/Akt/MTOR Pathway: In Vitro and in Vivo Studies. *Int. J. Mol. Med.* **2018**, *42* (2), 811–820.
10. Li, J.; Gong, X.; Jiang, R.; Lin, D.; Zhou, T.; et al. Fisetin Inhibited Growth and Metastasis of Triple-Negative Breast Cancer by Reversing Epithelial-to-Mesenchymal Transition via PTEN/Akt/GSK3 β Signal Pathway. *Front. Pharmacol.* **2018**, *9*, 1–14.

11. Chou, R. H.; Hsieh, S. C.; Yu, Y. L.; Huang, M. H.; Huang, Y. C.; et al. Fisetin Inhibits Migration and Invasion of Human Cervical Cancer Cells by Down-Regulating Urokinase Plasminogen Activator Expression through Suppressing the P38 MAPK-Dependent NF-KB Signaling Pathway. *PLoS One* **2013**, *8* (8), 1–12.
12. Chen, C. M.; Hsieh, Y. H.; Hwang, J. M.; Jan, H. J.; Hsieh, S. C.; et al. Fisetin Suppresses ADAM9 Expression and Inhibits Invasion of Glioma Cancer Cells through Increased Phosphorylation of ERK1/2. *Tumor Biol.* **2015**, *36* (5), 3407–3415.
13. Liu, X. F.; Long, H. J.; Miao, X. Y.; Liu, G. L.; Yao, H. L. Fisetin Inhibits Liver Cancer Growth in a Mouse Model: Relation to Dopamine Receptor. *Oncol. Rep.* **2017**, *38* (1), 53–62.
14. Klimaszewska-Wiśniewska, A.; Grzanka, D.; Czajkowska, P.; Hałas-Wiśniewska, M.; Durślewicz, J.; et al. Cellular and Molecular Alterations Induced by Low-dose Fisetin in Human Chronic Myeloid Leukemia Cells. *Int. J. Oncol.* **2019**, *55* (6), 1261–1274.
15. Tabasum, S.; Singh, R. P. Fisetin Suppresses Migration, Invasion and Stem-Cell-like Phenotype of Human Non-Small Cell Lung Carcinoma Cells via Attenuation of Epithelial to Mesenchymal Transition. *Chem. Biol. Interact.* **2019**, *303*, 14–21.
16. Wang, J.; Huang, S. Fisetin Inhibits the Growth and Migration in the A549 Human Lung Cancer Cell Line via the ERK1/2 Pathway. *Exp. Ther. Med.* **2018**, *15* (3), 2667–2673.
17. Chien, C. S.; Shen, K. H.; Huang, J. S.; Ko, S. C.; Shih, Y. W. Antimetastatic Potential of Fisetin Involves Inactivation of the PI3K/Akt and JNK Signaling Pathways with Downregulation of MMP-2/9 Expressions in Prostate Cancer PC-3 Cells. *Mol. Cell. Biochem.* **2010**, *333* (1–2), 169–180.
18. Hsieh, Y. S.; Tsai, Yang; Chiou; Lin; et al. Fisetin Suppresses the Proliferation and Metastasis of Renal Cell Carcinoma through Upregulation of MEK/ERK-Targeting CTSS and ADAM9. *Cells* **2019**, *8* (9), 948.
19. Joussen, A. M. Treatment of Corneal Neovascularization with Dietary Isoflavonoids and Flavonoids. *Exp. Eye Res.* **2000**, *71* (5), 483–487.
20. Fang, D.; Xiong, Z.; Xu, J.; Yin, J.; Luo, R. Chemopreventive Mechanisms of Galangin against Hepatocellular

Carcinoma: A Review. *Biomed. Pharmacother.* **2019**, *109*, 2054–2061.

21. Kim, J. D.; Liu, L.; Guo, W.; Meydani, M. Chemical Structure of Flavonols in Relation to Modulation of Angiogenesis and Immune-Endothelial Cell Adhesion. *J. Nutr. Biochem.* **2006**, *17* (3), 165–176.
22. Chen, D.; Li, D.; Xu, X. bing; Qiu, S.; Luo, S.; et al. Galangin Inhibits Epithelial-Mesenchymal Transition and Angiogenesis by Downregulating CD44 in Glioma. *J. Cancer* **2019**, *10* (19), 4499–4508.
23. Lei, D.; Zhang, F.; Yao, D.; Xiong, N.; Jiang, X.; et al. Galangin Increases ERK1/2 Phosphorylation to Decrease ADAM9 Expression and Prevents Invasion in A172 Glioma Cells. *Mol. Med. Rep.* **2018**, *17* (1), 667–673.
24. Chien, S. T.; Shi, M. Der; Lee, Y. C.; Te, C. C.; Shih, Y. W. Galangin, a Novel Dietary Flavonoid, Attenuates Metastatic Feature via PKC/ERK Signaling Pathway in TPA-Treated Liver Cancer HepG2 Cells. *Cancer Cell Int.* **2015**, *15* (1), 1–11.
25. Huang, H.; Chen, A. Y.; Rojanasakul, Y.; Ye, X.; Rankin, G. O.; et al. Dietary Compounds Galangin and Myricetin Suppress Ovarian Cancer Cell Angiogenesis. *J. Funct. Foods* **2015**, *15*, 464–475.
26. Cao, J.; Wang, H.; Chen, F.; Fang, J.; Xu, A.; et al. Galangin Inhibits Cell Invasion by Suppressing the Epithelial-Mesenchymal Transition and Inducing Apoptosis in Renal Cell Carcinoma. *Mol. Med. Rep.* **2016**, *13* (5), 4238–4244.
27. Zhu, Y.; Rao, Q.; Zhang, X.; Zhou, X. Galangin Induced Antitumor Effects in Human Kidney Tumor Cells Mediated via Mitochondrial Mediated Apoptosis, Inhibition of Cell Migration and Invasion and Targeting PI3K/ AKT/MTOR Signalling Pathway. *J. B.U.ON.* **2018**, *23* (3), 795–799.
28. Li Wang, Xiangyu Wang, Hanyong Chen, Xueyin Zu, Fayang Ma, Kangdong Liu, Ann M. Bode, Zigang Dong, and D. J. K. Gossypin Inhibits Gastric Cancer Growth by Direct Targeting AURKA and RSK2. *Phyther. Res.* **2019**, *33* (3), 640–650.
29. Li, L.; Fan, P.; Chou, H.; Li, J.; Wang, K.; et al. Herbacetin Suppressed MMP9 Mediated Angiogenesis of Malignant Melanoma through Blocking EGFR-ERK / AKT Signaling Pathway. *Biochimie* **2019**, *162*, 198–207.

30. Jin, X. N.; Yan, E. Z.; Wang, H. M.; Sui, H. J.; Liu, Z.; et al. Hyperoside Exerts Anti-Inflammatory and Anti-Arthritic Effects in LPS-Stimulated Human Fibroblast-like Synoviocytes in Vitro and in Mice with Collagen-Induced Arthritis. *Acta Pharmacol. Sin.* **2016**, *37* (5), 674–686.
31. Zhang, X.; Liu, T.; Huang, Y.; Wismeijer, D.; Liu, Y. Icariin: Does It Have an Osteoinductive Potential for Bone Tissue Engineering? *Phyther. Res.* **2014**, *28* (4), 498–509.
32. Chen, M.; Wu, J.; Luo, Q.; Mo, S.; Lyu, Y.; et al. The Anticancer Properties of Herba Epimedii and Its Main Bioactive Components icariin and Icariside II. *Nutrients* **2016**, *8* (9), 1–19.
33. Chung, B. H.; Kim, J. D.; Kim, C. K.; Kim, J. W.; Won, M. H.; et al. Icariin Stimulates Angiogenesis by Activating the MEK/ERK- and PI3K/Akt/ENOS-Dependent Signal Pathways in Human Endothelial Cells. *Biochem. Biophys. Res. Commun.* **2008**, *376* (2), 404–408.
34. Gu, Z. F.; Zhang, Z. T.; Wang, J. Y.; Xu, B. Bin. Icariin Exerts Inhibitory Effects on the Growth and Metastasis of KYSE70 Human Esophageal Carcinoma Cells via PI3K/AKT and STAT3 Pathways. *Environ. Toxicol. Pharmacol.* **2017**, *54*, 7–13.
35. Wang, P.; Zhang, J.; Xiong, X.; Yuan, W.; Qin, S.; et al. Icariin Suppresses Cell Cycle Transition and Cell Migration in Ovarian Cancer Cells. *Oncol. Rep.* **2019**, *41* (4), 2321–2328.
36. Singh, W. R.; Devi, H. S.; Kumawat, S.; Sadam, A.; Appukuttan, A. V.; et al. Angiogenic and MMPs Modulatory Effects of Icariin Improved Cutaneous Wound Healing in Rats. *Eur. J. Pharmacol.* **2019**, *858*, 172466.
37. Quan, K.; Zhang, X.; Fan, K.; Liu, P.; Yue, Q.; et al. Icariside II Induces Cell Cycle Arrest and Apoptosis in Human Glioblastoma Cells through Suppressing Akt Activation and Potentiating FOXO3A Activity. *Am. J. Transl. Res.* **2017**, *9* (5), 2508–2519.
38. Xing, S.; Yu, W.; Zhang, X.; Luo, Y.; Lei, Z.; et al. Isoviolanthin Extracted from *Dendrobium Officinale* Reverses TGF- β 1-Mediated Epithelial–Mesenchymal Transition in Hepatocellular Carcinoma Cells via Deactivating the TGF- β /Smad and PI3K/Akt/MTOR Signaling Pathways. *Int. J. Mol. Sci.* **2018**, *19* (6), 1–17.
39. Chen, A. Y.; Chen, Y. C. A Review of the Dietary Flavonoid, Kaempferol on Human Health and Cancer

Chemoprevention. *Food Chem.* **2013**, 138 (4), 2099–2107.

40. Kashyap, D.; Sharma, A.; Tuli, H. S.; Sak, K.; Punia, S.; et al. Kaempferol – A Dietary Anticancer Molecule with Multiple Mechanisms of Action: Recent Trends and Advancements. *J. Funct. Foods* **2017**, 30, 203–219.
41. Chin, H. K.; Horng, C. T.; Liu, Y. S.; Lu, C. C.; Su, C. Y.; et al. Kaempferol Inhibits Angiogenic Ability by Targeting VEGF Receptor-2 and Downregulating the PI3K/AKT, MEK and ERK Pathways in VEGF-Stimulated Human Umbilical Vein Endothelial Cells. *Oncol. Rep.* **2018**, 39 (5), 2351–2357.
42. Liang, F.; Han, Y.; Gao, H.; Xin, S.; Chen, S.; et al. Kaempferol Identified by Zebrafish Assay and Fine Fractionations Strategy from *Dysosma Versipellis* Inhibits Angiogenesis through VEGF and FGF Pathways. *Sci. Rep.* **2015**, 5, 1–10.
43. Kumazawa, S.; Kubota, S.; Yamamoto, H.; Okamura, N.; Sugiyama, Y.; et al. Antiangiogenic Activity of Flavonoids from *Melia Azedarach*. *Nat. Prod. Commun.* **2013**, 8 (12), 1719–1720.
44. Özay, Y.; Güzel, S.; Yumrutaş, Ö.; Pehlivanoğlu, B.; Erdoğan, İ. H.; et al. Wound Healing Effect of Kaempferol in Diabetic and Nondiabetic Rats. *J. Surg. Res.* **2019**, 233, 284–296.
45. Sharma, V.; Joseph, C.; Ghosh, S.; Agarwal, A.; Mishra, M. K.; et al. Kaempferol Induces Apoptosis in Glioblastoma Cells through Oxidative Stress. *Mol. Cancer Ther.* **2007**, 6 (9), 2544–2553.
46. Shen, S. C.; Lin, C. W.; Lee, H. M.; Chien, L. L.; Chen, Y. C. Lipopolysaccharide plus 12-o-Tetradecanoylphorbol 13-Acetate Induction of Migration and Invasion of Glioma Cells in Vitro and in Vivo: Differential Inhibitory Effects of Flavonoids. *Neuroscience* **2006**, 140 (2), 477–489.
47. Qin, Y.; Cui, W.; Yang, X.; Tong, B. Kaempferol Inhibits the Growth and Metastasis of Cholangiocarcinoma in Vitro and in Vivo. *Acta Biochim. Biophys. Sin. (Shanghai)*. **2015**, 48 (3), 238–245.
48. Zhu, G.; Liu, X.; Li, H.; Yan, Y.; Hong, X.; et al. Kaempferol Inhibits Proliferation, Migration, and Invasion of Liver Cancer HepG2 Cells by down-Regulation of MicroRNA-21. *Int. J. Immunopathol. Pharmacol.* **2018**, 32, 2058738418814341.

49. Jo, E.; Park, S. J.; Choi, Y. S.; Jeon, W. K.; Kim, B. C. Kaempferol Suppresses Transforming Growth Factor-B1-Induced Epithelial-to-Mesenchymal Transition and Migration of A549 Lung Cancer Cells by Inhibiting Akt1-Mediated Phosphorylation of Smad3 at Threonine-179. *Neoplasia* **2015**, *17* (7), 525–537.
50. Labbé, D.; Provençal, M.; Lamy, S.; Boivin, D.; Gingras, D.; et al. The Flavonols Quercetin, Kaempferol, and Myricetin Inhibit Hepatocyte Growth. *J. Nutr. Biochem. Mol. Genet. Mech.* **2009**, *139*, 646–652.
51. Lin, C. W.; Chen, P. N.; Chen, M. K.; Yang, W. E.; Tang, C. H.; et al. Kaempferol Reduces Matrix Metalloproteinase-2 Expression by down-Regulating ERK1/2 and the Activator Protein-1 Signaling Pathways in Oral Cancer Cells. *PLoS One* **2013**, *8* (11), 80883.
52. Chen, H. J.; Lin, C. M.; Lee, C. Y.; Shih, N. C.; Peng, S. F.; et al. Kaempferol Suppresses Cell Metastasis via Inhibition of the ERK-P38-JNK and AP-1 Signaling Pathways in U-2 OS Human Osteosarcoma Cells. *Oncol. Rep.* **2013**, *30* (2), 925–932.
53. Luo, H.; Rankin, G. O.; Liu, L.; Daddysman, M. K.; Jiang, B. H.; et al. Kaempferol Inhibits Angiogenesis and VEGF Expression through Both HIF Dependent and Independent Pathways in Human Ovarian Cancer Cells. *Nutr. Cancer* **2009**, *61* (4), 554–563.
54. Lee, J.; Kim, J. H. Kaempferol Inhibits Pancreatic Cancer Cell Growth and Migration through the Blockade of EGFR-Related Pathway in Vitro. *PLoS One* **2016**, *11* (5), 1–14.
55. Hung, T. W.; Chen, P. N.; Wu, H. C.; Wu, S. W.; Tsai, P. Y.; et al. Kaempferol Inhibits the Invasion and Migration of Renal Cancer Cells through the Downregulation of AKT and FAK Pathways. *Int. J. Med. Sci.* **2017**, *14* (10), 984–993.
56. Chien, H. W.; Wang, K.; Chang, Y. Y.; Hsieh, Y. H.; Yu, N. Y.; et al. Kaempferol Suppresses Cell Migration through the Activation of the ERK Signaling Pathways in ARPE-19 Cells. *Environ. Toxicol.* **2019**, *34* (3), 312–318.
57. Clericuzio, M.; Tinello, S.; Burlando, B.; Ranzato, E.; Martinotti, S.; et al. Flavonoid Oligoglycosides from *Ophioglossum Vulgatum* L. Having Wound Healing Properties. *Planta Med.* **2012**, *78* (15), 1639–1644.
58. Zeng, N.; Tong, B.; Zhang, X.; Dou, Y.; Wu, X.; et al. Antiarthritis Effect of Morin Is Associated with Inhibition of

- Synovial Angiogenesis. *Drug Dev. Res.* **2015**, 76 (8), 463–473.
59. Yue, M.; Zeng, N.; Xia, Y.; Wei, Z.; Dai, Y. Morin Exerts Anti-Arthritic Effects by Attenuating Synovial Angiogenesis via Activation of Peroxisome Proliferator Activated Receptor- γ . *Mol. Nutr. Food Res.* **2018**, 62 (21), 1–13.
 60. Capitani, N.; Lori, G.; Paoli, P.; Patrussi, L.; Troilo, A.; et al. LMW-PTP Targeting Potentiates the Effects of Drugs Used in Chronic Lymphocytic Leukemia Therapy. *Cancer Cell Int.* **2019**, 19 (1), 1–9.
 61. Li, H. W.; Zou, T. Bin; Jia, Q.; Xia, E. Q.; Cao, W. J.; et al. Anticancer Effects of Morin-7-Sulphate Sodium, a Flavonoid Derivative, in Mouse Melanoma Cells. *Biomed. Pharmacother.* **2016**, 84, 909–916.
 62. Kang, N. J.; Jung, S. K.; Lee, K. W.; Lee, H. J. Myricetin Is a Potent Chemopreventive Phytochemical in Skin Carcinogenesis. *Ann. N. Y. Acad. Sci.* **2011**, 1229 (1), 124–132.
 63. Zhou, Z.; Mao, W.; Li, Y.; Qi, C.; He, Y. Myricetin Inhibits Breast Tumor Growth and Angiogenesis by Regulating VEGF/VEGFR2 and P38MAPK Signaling Pathways. *Anat. Rec.* **2019**, 302 (12), 2186–2192.
 64. Ci, Y.; Zhang, Y.; Liu, Y.; Lu, S.; Cao, J.; et al. Myricetin Suppresses Breast Cancer Metastasis through Down-Regulating the Activity of Matrix Metalloproteinase (MMP)-2/9. *Phyther. Res.* **2018**, 32 (7), 1373–1381.
 65. Chiu, W. T.; Shen, S. C.; Chow, J. M.; Lin, C. W.; Shia, L. T.; et al. Contribution of Reactive Oxygen Species to Migration/Invasion of Human Glioblastoma Cells U87 via ERK-Dependent COX-2/PGE2 Activation. *Neurobiol. Dis.* **2010**, 37 (1), 118–129.
 66. Yamada, N.; Matsushima-Nishiwaki, R.; Kozawa, O. Quercetin Suppresses the Migration of Hepatocellular Carcinoma Cells Stimulated by Hepatocyte Growth Factor or Transforming Growth Factor- α : Attenuation of AKT Signaling Pathway. *Arch. Biochem. Biophys.* **2020**, 682, 108296.
 67. Ma, H.; Zhu, L.; Ren, J.; Rao, B.; Sha, M.; et al. Myricetin Inhibits Migration and Invasion of Hepatocellular Carcinoma MHCC97H Cell Line by Inhibiting the EMT Process. *Oncol. Lett.* **2019**, 18 (6), 6614–6620.
 68. Shih, Y. W.; Wu, P. F.; Lee, Y. C.; Shi, M. Der; Chiang, T. A. Myricetin Suppresses Invasion and Migration of Human Lung Adenocarcinoma A549 Cells: Possible Mediation by Blocking the Erk Signaling Pathway. *J. Agric.*

Food Chem. **2009**, 57 (9), 3490–3499.

69. Ezzati, M.; Yousefi, B.; Velaei, K.; Safa, A. A Review on Anti-Cancer Properties of Quercetin in Breast Cancer. *Life Sci.* **2020**, 248, 117463.
70. Tang, S. M.; Deng, X. T.; Zhou, J.; Li, Q. P.; Ge, X. X.; et al. Pharmacological Basis and New Insights of Quercetin Action in Respect to Its Anti-Cancer Effects. *Biomed. Pharmacother.* **2020**, 121, 109604.
71. Kashyap, D.; Mittal, S.; Sak, K.; Singhal, P.; Tuli, H. S. Molecular Mechanisms of Action of Quercetin in Cancer: Recent Advances. *Tumor Biol.* **2016**, 37 (10), 12927–12939.
72. Darband, S. G.; Kaviani, M.; Yousefi, B.; Sadighparvar, S.; Pakdel, F. G.; et al. Quercetin: A Functional Dietary Flavonoid with Potential Chemo-Preventive Properties in Colorectal Cancer. *J. Cell. Physiol.* **2018**, 233 (9), 6544–6560.
73. Song, N. R.; Chung, M. Y.; Kang, N. J.; Seo, S. G.; Jang, T. S.; et al. Quercetin Suppresses Invasion and Migration of H-Ras-Transformed MCF10A Human Epithelial Cells by Inhibiting Phosphatidylinositol 3-Kinase. *Food Chem.* **2014**, 142, 66–71.
74. Lin, C.; Wu, M.; Dong, J. Quercetin-4'-o- β -d-Glucopyranoside (QODG) Inhibits Angiogenesis by Suppressing VEGFR2-Mediated Signaling in Zebrafish and Endothelial Cells. *PLoS One* **2012**, 7 (2), 31708.
75. Lee, Y. H.; Tuyet, P. T. Synthesis and Biological Evaluation of Quercetin–Zinc (II) Complex for Anti-Cancer and Anti-Metastasis of Human Bladder Cancer Cells. *Vitr. Cell. Dev. Biol. - Anim.* **2019**, 55 (6), 395–404.
76. Ravishankar, D.; Watson, K. A.; Boateng, S. Y.; Green, R. J.; Greco, F.; et al. Exploring Quercetin and Luteolin Derivatives as Antiangiogenic Agents. *Eur. J. Med. Chem.* **2015**, 97, 259–274.
77. Zhao, X.; Wang, Q.; Yang, S.; Chen, C.; Li, X.; et al. Quercetin Inhibits Angiogenesis by Targeting Calcineurin in the Xenograft Model of Human Breast Cancer. *Eur. J. Pharmacol.* **2016**, 781, 60–68.
78. Oh, S. J.; Kim, O.; Lee, J. S.; Kim, J. A.; Kim, M. R.; et al. Inhibition of Angiogenesis by Quercetin in Tamoxifen-Resistant Breast Cancer Cells. *Food Chem. Toxicol.* **2010**, 48 (11), 3227–3234.

79. Srinivasan, A.; Thangavel, C.; Liu, Y.; Shoyele, S.; Den, R. B.; et al. Quercetin Regulates β -Catenin Signaling and Reduces the Migration of Triple Negative Breast Cancer. *Mol. Carcinog.* **2016**, *55* (5), 743–756.
80. Lin, C. W.; Hou, W. C.; Shen, S. C.; Juan, S. H.; Ko, C. H.; et al. Quercetin Inhibition of Tumor Invasion via Suppressing PKC δ /ERK/ AP-1-Dependent Matrix Metalloproteinase-9 Activation in Breast Carcinoma Cells. *Carcinogenesis* **2008**, *29* (9), 1807–1815.
81. Rivera Rivera, A.; Castillo-Pichardo, L.; Gerena, Y.; Dharmawardhane, S. Anti-Breast Cancer Potential of Quercetin via the Akt/AMPK/Mammalian Target of Rapamycin (MTOR) Signaling Cascade. *PLoS One* **2016**, *11* (6), 0157251.
82. Zhao, D.; Qin, C.; Fan, X.; Li, Y.; Gu, B. Inhibitory Effects of Quercetin on Angiogenesis in Larval Zebra Fi Sh and Human Umbilical Vein Endothelial Cells. *Eur. J. Pharmacol.* **2014**, *723*, 360–367.
83. Tan, W. F.; Lin, L. P.; Li, M. H.; Zhang, Y. X.; Tong, Y. G.; et al. Quercetin, a Dietary-Derived Flavonoid, Possesses Antiangiogenic Potential. *Eur. J. Pharmacol.* **2003**, *459* (2–3), 255–262.
84. Zhao, X.; Shu, G.; Chen, L.; Mi, X.; Mei, Z.; et al. A Flavonoid Component from *Docynia Delavayi* (Franch.) Schneid Represses Transplanted H22 Hepatoma Growth and Exhibits Low Toxic Effect on Tumor-Bearing Mice. *Food Chem. Toxicol.* **2012**, *50* (9), 3166–3173.
85. Lee, L. T.; Huang, Y. T.; Hwang, J. J.; Lee, A. Y. L.; Ke, F. C.; et al. Transinactivation of the Epidermal Growth Factor Receptor Tyrosine Kinase and Focal Adhesion Kinase Phosphorylation by Dietary Flavonoids: Effect on Invasive Potential of Human Carcinoma Cells. *Biochem. Pharmacol.* **2004**, *67* (11), 2103–2114.
86. Lee, D. E.; Chung, M. Y.; Lim, T. G.; Huh, W. B.; Lee, H. J.; et al. Quercetin Suppresses Intracellular Ros Formation, MMP Activation, and Cell Motility in Human Fibrosarcoma Cells. *J. Food Sci.* **2013**, *78* (9).
87. Kee, J. Y.; Han, Y. H.; Kim, D. S.; Mun, J. G.; Park, J.; et al. Inhibitory Effect of Quercetin on Colorectal Lung Metastasis through Inducing Apoptosis, and Suppression of Metastatic Ability. *Phytomedicine* **2016**, *23* (13), 1680–1690.
88. Pan, H. C.; Jiang, Q.; Yu, Y.; Mei, J. P.; Cui, Y. K.; et al. Quercetin Promotes Cell Apoptosis and Inhibits the Expression of MMP-9 and Fibronectin via the AKT and ERK Signalling Pathways in Human Glioma Cells.

Neurochem. Int. **2015**, *80*, 60–71.

89. Liu, Y.; Tang, Z. G.; Lin, Y.; Qu, X. G.; Lv, W.; et al. Effects of Quercetin on Proliferation and Migration of Human Glioblastoma U251 Cells. *Biomed. Pharmacother.* **2017**, *92*, 33–38.
90. Michaud-Levesque, J.; Bousquet-Gagnon, N.; Béliveau, R. Quercetin Abrogates IL-6/STAT3 Signaling and Inhibits Glioblastoma Cell Line Growth and Migration. *Exp. Cell Res.* **2012**, *318* (8), 925–935.
91. da Silva, A. B.; Cerqueira Coelho, P. L.; das Neves Oliveira, M.; Oliveira, J. L.; Oliveira Amparo, J. A.; et al. The Flavonoid Rutin and Its Aglycone Quercetin Modulate the Microglia Inflammatory Profile Improving Antiglioma Activity. *Brain. Behav. Immun.* **2020**, *85*, 170–185.
92. Liu, Y.; Tang, Z. G.; Yang, J. Q.; Zhou, Y.; Meng, L. H.; et al. Low Concentration of Quercetin Antagonizes the Invasion and Angiogenesis of Human Glioblastoma U251 Cells. *Onco. Targets. Ther.* **2017**, *10*, 4023–4028.
93. Lu, J.; Wang, Z.; Li, S.; Xin, Q.; Yuan, M.; et al. Quercetin Inhibits the Migration and Invasion of HCCLM3 Cells by Suppressing the Expression of P-Akt1, Matrix Metalloproteinase (MMP) MMP-2, and MMP-9. *Med. Sci. Monit.* **2018**, *24*, 2583–2589.
94. Klimaszewska-Wiśniewska, A.; Hałas-Wiśniewska, M.; Izdebska, M.; Gagat, M.; Grzanka, A.; et al. Antiproliferative and Antimetastatic Action of Quercetin on A549 Non-Small Cell Lung Cancer Cells through Its Effect on the Cytoskeleton. *Acta Histochem.* **2017**, *119* (2), 99–112.
95. Wu, T. C.; Chan, S. T.; Chang, C. N.; Yu, P. S.; Chuang, C. H.; et al. Quercetin and Chrysin Inhibit Nickel-Induced Invasion and Migration by Downregulation of TLR4/NF-KB Signaling in A549 cells. *Chem. Biol. Interact.* **2018**, *292* (110), 101–109.
96. Lin, Y. C.; Tsai, P. H.; Lin, C. Y.; Cheng, C. H.; Lin, T. H.; et al. Impact of Flavonoids on Matrix Metalloproteinase Secretion and Invadopodia Formation in Highly Invasive A431-III Cancer Cells. *PLoS One* **2013**, *8* (8), 71903–71915.
97. Hwang, M. K.; Song, N. R.; Kang, N. J.; Lee, K. W.; Lee, H. J. Activation of Phosphatidylinositol 3-Kinase Is Required for Tumor Necrosis Factor- α -Induced Upregulation of Matrix Metalloproteinase-9: Its Direct Inhibition by

- Quercetin. *Int. J. Biochem. Cell Biol.* **2009**, *41* (7), 1592–1600.
98. Cao, H. H.; Cheng, C. Y.; Su, T.; Fu, X. Q.; Guo, H.; et al. Quercetin Inhibits HGF/c-Met Signaling and HGF-stimulated Melanoma Cell Migration and Invasion. *Mol. Cancer* **2015**, *14* (1), 1–12.
 99. Cao, H. H.; Tse, A. K. W.; Kwan, H. Y.; Yu, H.; Cheng, C. Y.; et al. Quercetin Exerts Anti-Melanoma Activities and Inhibits STAT3 Signaling. *Biochem. Pharmacol.* **2014**, *87* (3), 424–434.
 100. Zhao, J.; Fang, Z.; Zha, Z.; Sun, Q.; Wang, H.; et al. Quercetin Inhibits Cell Viability, Migration and Invasion by Regulating MiR-16/HOXA10 Axis in Oral Cancer. *Eur. J. Pharmacol.* **2019**, *847*, 11–18.
 101. Nam, T. W.; Yoo, C. I.; Kim, H. T.; Kwon, C. H.; Park, J. Y.; et al. The Flavonoid Quercetin Induces Apoptosis and Inhibits Migration through a MAPK-Dependent Mechanism in Osteoblasts. *J. Bone Miner. Metab.* **2008**, *26* (6), 551–560.
 102. Li, S.; Pei, Y.; Wang, W.; Liu, F.; Zheng, K.; et al. Quercetin Suppresses the Proliferation and Metastasis of Metastatic Osteosarcoma Cells by Inhibiting Parathyroid Hormone Receptor 1. *Biomed. Pharmacother.* **2019**, *114*, 108839.
 103. Lan, H.; Hong, W.; Fan, P.; Qian, D.; Zhu, J.; et al. Quercetin Inhibits Cell Migration and Invasion in Human Osteosarcoma Cells. *Cell. Physiol. Biochem.* **2017**, *43* (2), 553–567.
 104. Berndt, K.; Campanile, C.; Muff, R.; Strehler, E.; Born, W.; et al. Evaluation of Quercetin as a Potential Drug in Osteosarcoma Treatment. *Anticancer Res.* **2013**, *33* (4), 1297–1306.
 105. Huang, Y. T.; Lee, L. T.; Lee, P. P. H.; Lin, Y. S.; Lee, M. T. Targeting of Focal Adhesion Kinase by Flavonoids and Small-Interfering RNAs Reduces Tumor Cell Migration Ability. *Anticancer Res.* **2005**, *25* (3 B), 2017–2025.
 106. Dinglai Yu, Tingting Ye, Yukai Xiang, Zhehao Shi, Jie Zhang, Bin Lou, Fan Zhang, Bicheng Chen, and M. Z. Quercetin Inhibits Epithelial–Mesenchymal Transition, Decreases Invasiveness and Metastasis, and Reverses IL-6 Induced Epithelial–Mesenchymal Transition, Expression of MMP by Inhibiting STAT3 Signaling in Pancreatic Cancer Cells. *Onco. Targets. Ther.* **2017**, *10*, 4719–4729.

107. Bhat, F. A.; Sharmila, G.; Balakrishnan, S.; Arunkumar, R.; Elumalai, P.; et al. Quercetin Reverses EGF-Induced Epithelial to Mesenchymal Transition and Invasiveness in Prostate Cancer (PC-3) Cell Line via EGFR/PI3K/Akt Pathway. *J. Nutr. Biochem.* **2014**, *25* (11), 1132–1139.
108. Yang, F.; Jiang, X.; Song, L.; Wang, H.; Mei, Z.; et al. Quercetin Inhibits Angiogenesis through Thrombospondin-1 Upregulation to Antagonize Human Prostate Cancer PC-3 Cell Growth in Vitro and in Vivo. *Oncol. Rep.* **2016**, *35* (3), 1602–1610.
109. Song, W.; Zhao, X.; Xu, J.; Zhang, H. Quercetin Inhibits Angiogenesis–Mediated Human Retinoblastoma Growth by Targeting Vascular Endothelial Growth Factor Receptor. *Oncol. Lett.* **2017**, *14* (3), 3343–3348.
110. Camero, C. M.; Germanò, M. P.; Rapisarda, A.; D'Angelo, V.; Amira, S.; et al. Anti-Angiogenic Activity of Iridoids from Galium Tunetanum. *Brazilian J. Pharmacogn.* **2018**, *28* (3), 374–377.
111. Ben Sghaier, M.; Pagano, A.; Mousslim, M.; Ammari, Y.; Kovacic, H.; et al. Rutin Inhibits Proliferation, Attenuates Superoxide Production and Decreases Adhesion and Migration of Human Cancerous Cells. *Biomed. Pharmacother.* **2016**, *84*, 1972–1978.
112. Chen, H.; Miao, Q.; Geng, M.; Liu, J.; Hu, Y.; et al. Anti-Tumor Effect of Rutin on Human Neuroblastoma Cell Lines through Inducing G2/M Cell Cycle Arrest and Promoting Apoptosis. *Sci. World J.* **2013**, 2013.
113. Kim, M. H. Flavonoids Inhibit VEGF/BFGF-Induced Angiogenesis in Vitro by Inhibiting the Matrix-Degrading Proteases. *J. Cell. Biochem.* **2003**, *89* (3), 529–538.
114. Lu, K. H.; Chen, P. N.; Hsieh, Y. H.; Lin, C. Y.; Cheng, F. Y.; et al. 3-Hydroxyflavone Inhibits Human Osteosarcoma U2OS and 143B Cells Metastasis by Affecting EMT and Repressing u-PA/MMP-2 via FAK-Src to MEK/ERK and RhoA/MLC2 Pathways and Reduces 143B Tumor Growth in Vivo. *Food Chem. Toxicol.* **2016**, *97*, 177–186.
115. Yang, S. F.; Yang, W. E.; Kuo, W. H.; Chang, H. R.; Chu, S. C.; et al. Antimetastatic Potentials of Flavones on Oral Cancer Cell via an Inhibition of Matrix-Degrading Proteases. *Arch. Oral Biol.* **2008**, *53* (3), 287–294.
116. Liu, R.; Deng, X.; Peng, Y.; Feng, W.; Xiong, R.; et al. Synthesis and Biological Evaluation of Novel 5 , 6 , 7-Trimethoxy Flavonoid Salicylate Derivatives as Potential Anti-Tumor Agents. *Bioorg. Chem.* **2020**, *96* (August

2019), 103652.

117. Sim, D. Y.; Jung, H. J. Anticancer Activity of 7,8-Dihydroxyflavone in Melanoma Cells via Downregulation of α -MSH/CAMP/MITF Pathway. *Oncol. Rep.* **2016**, 36 (1), 528–534.
118. Liu, L. Z.; Jing, Y.; Jiang, L. L.; Jiang, X. E.; Jiang, Y.; et al. Acacetin Inhibits VEGF Expression, Tumor Angiogenesis and Growth through AKT/HIF-1 α Pathway. *Biochem. Biophys. Res. Commun.* **2011**, 413 (2), 299–305.
119. Bhat, T. A.; Nambiar, D.; Tailor, D.; Pal, A.; Agarwal, R.; et al. Acacetin Inhibits in Vitro and in Vivo Angiogenesis and Downregulates Stat Signaling and VEGF Expression. *Cancer Prev. Res.* **2013**, 6 (10), 1–7.
120. Fong, Y.; Shen, K. H.; Chiang, T. A.; Shih, Y. W. Acacetin Inhibits TPA-Induced MMP-2 and u-PA Expressions of Human Lung Cancer Cells through Inactivating JNK Signaling Pathway and Reducing Binding Activities of NF-KB and AP-1. *J. Food Sci.* **2010**, 75 (1), 30–38.
121. Chien, S. T.; Lin, S. S.; Wang, C. K.; Lee, Y. Bin; Chen, K. S.; et al. Acacetin Inhibits the Invasion and Migration of Human Non-Small Cell Lung Cancer A549 Cells by Suppressing the P38 α MAPK Signaling Pathway. *Mol. Cell. Biochem.* **2011**, 350 (1–2), 135–148.
122. Shen, K. H.; Hung, S. H.; Yin, L. Te; Huang, C. S.; Chao, C. H.; et al. Acacetin, a Flavonoid, Inhibits the Invasion and Migration of Human Prostate Cancer DU145 Cells via Inactivation of the P38 MAPK Signaling Pathway. *Mol. Cell. Biochem.* **2010**, 333 (1–2), 279–291.
123. Kashyap, D.; Sharma, A.; Singh, H.; Sak, K.; Kumar, V.; et al. Apigenin : A Natural Bioactive Flavone-Type Molecule with Promising Therapeutic Function. **2018**, 48 (April), 457–471.
124. Patel, D.; Shukla, S.; Gupta, S. Apigenin and Cancer Chemoprevention: Progress, Potential and Promise (Review). *Int. J. Oncol.* **2007**, 30 (1), 233–245.
125. Lefort, É. C.; Blay, J. Apigenin and Its Impact on Gastrointestinal Cancers. *Mol. Nutr. Food Res.* **2013**, 57 (1), 126–144.

126. Lamy, S.; Akla, N.; Ouanouki, A.; Lord-Dufour, S.; Béliveau, R. Diet-Derived Polyphenols Inhibit Angiogenesis by Modulating the Interleukin-6/STAT3 Pathway. *Exp. Cell Res.* **2012**, *318* (13), 1586–1596.
127. F. Lindenmeyer, H. Li, S. Menashi, C. Soria, and H. L. Apigenin Acts on the Tumor Cell Invasion Process and Regulates Protease Production. *Nutr. Cancer* **2001**, *39* (1), 139–147.
128. Lee, W. J.; Chen, W. K.; Wang, C. J.; Lin, W. L.; Tseng, T. H. Apigenin Inhibits HGF-Promoted Invasive Growth and Metastasis Involving Blocking PI3K/Akt Pathway and B4 Integrin Function in MDA-MB-231 Breast Cancer Cells. *Toxicol. Appl. Pharmacol.* **2008**, *226* (2), 178–191.
129. Fang, J.; Zhou, Q.; Liu, L. Z.; Xia, C.; Hu, X.; et al. Apigenin Inhibits Tumor Angiogenesis through Decreasing HIF-1 α and VEGF Expression. *Carcinogenesis* **2007**, *28* (4), 858–864.
130. Wang, L.; Kuang, L.; Hitron, J. A.; Son, Y. O.; Wang, X.; et al. Apigenin Suppresses Migration and Invasion of Transformed Cells through Down-Regulation of C-X-C Chemokine Receptor 4 Expression. *Toxicol. Appl. Pharmacol.* **2013**, *272* (1), 108–116.
131. Spoerlein, C.; Mahal, K.; Schmidt, H.; Schobert, R. Effects of Chrysin, Apigenin, Genistein and Their Homoleptic Copper(II) Complexes on the Growth and Metastatic Potential of Cancer Cells. *J. Inorg. Biochem.* **2013**, *127*, 107–115.
132. Czyz, J.; Madeja, Z.; Irmer, U.; Korohoda, W.; Hülser, D. F. Flavonoid Apigenin Inhibits Motility and Invasiveness of Carcinoma Cells in Vitro. *Int. J. Cancer* **2005**, *114* (1), 12–18.
133. Lim, W.; Park, S.; Bazer, F. W.; Song, G. Apigenin Reduces Survival of Choriocarcinoma Cells by Inducing Apoptosis via the PI3K/AKT and ERK1/2 MAPK Pathways. *J. Cell. Physiol.* **2016**, *231* (12), 2690–2699.
134. Chunhua, L.; Donglan, L.; Xiuqiong, F.; Lihua, Z.; Qin, F.; et al. Apigenin Up-Regulates Transgelin and Inhibits Invasion and Migration of Colorectal Cancer through Decreased Phosphorylation of AKT. *J. Nutr. Biochem.* **2013**, *24* (10), 1766–1775.
135. Dai, J.; Van Wie, P. G.; Fai, L. Y.; Kim, D.; Wang, L.; et al. Downregulation of NEDD9 by Apigenin Suppresses Migration, Invasion, and Metastasis of Colorectal Cancer Cells. *Toxicol. Appl. Pharmacol.* **2016**, *311*, 106–112.

136. Coelho, P. L. C.; Oliveira, M. N.; Da Silva, A. B.; Pitanga, B. P. S.; Silva, V. D. A.; et al. The Flavonoid Apigenin from Croton Betulaster Mull Inhibits Proliferation, Induces Differentiation and Regulates the Inflammatory Profile of Glioma Cells. *Anticancer. Drugs* **2016**, *27* (10), 960–969.
137. Coelho, P. L. C.; Amparo, J. A. O.; da Silva, A. B.; da Silva, K. C.; Braga-de-Souza, S.; et al. Apigenin from Croton Betulaster Müll Restores the Immune Profile of Microglia against Glioma Cells. *Phyther. Res.* **2019**, *33* (12), 3191–3202.
138. Liu, L. Z.; Fang, J.; Zhou, Q.; Hu, X.; Shi, X.; et al. Apigenin Inhibits Expression of Vascular Endothelial Growth Factor and Angiogenesis in Human Lung Cancer Cells: Implication of Chemoprevention of Lung Cancer. *Mol. Pharmacol.* **2005**, *68* (3), 635–643.
139. Hasnat, M. A.; Pervin, M.; Lim, J. H.; Lim, B. O. Apigenin Attenuates Melanoma Cell Migration by Inducing Anoikis through Integrin and Focal Adhesion Kinase Inhibition. *Molecules* **2015**, *20* (12), 21157–21166.
140. Zhao, G.; Han, X.; Cheng, W.; Ni, J.; Zhang, Y.; et al. Apigenin Inhibits Proliferation and Invasion, and Induces Apoptosis and Cell Cycle Arrest in Human Melanoma Cells. *Oncol. Rep.* **2017**, *37* (4), 2277–2285.
141. Cao, H. H.; Chu, J. H.; Kwan, H. Y.; Su, T.; Yu, H.; et al. Inhibition of the STAT3 Signaling Pathway Contributes to Apigenin-Mediated Anti-Metastatic Effect in Melanoma. *Sci. Rep.* **2016**, *6* (1), 1–12.
142. Ghițu, A.; Schwiebs, A.; Radeke, H. H.; Avram, S.; Zupko, I.; et al. A Comprehensive Assessment of Apigenin as an Antiproliferative, Proapoptotic, Antiangiogenic and Immunomodulatory Phytocompound. *Nutrients* **2019**, *11* (4), 858–877.
143. Fang, J.; Xia, C.; Cao, Z.; Zheng, J. Z.; Reed, E.; et al. Apigenin Inhibits VEGF and HIF-1 Expression via PI3K/AKT/P70S6K1 and HDM2/P53 Pathways. *FASEB J.* **2005**, *19* (3), 342–353.
144. Hu, X. M.; Meng, D.; Fang, J. Apigenin Inhibited Migration and Invasion of Human Ovarian Cancer A2780 Cells through Focal Adhesion Kinase. *Carcinogenesis* **2008**, *29* (12), 2369–2376.
145. He, J.; Ning, C.; Wang, Y.; Ma, T.; Huang, H.; et al. Natural Plant Flavonoid Apigenin Directly Disrupts Hsp90/Cdc37 Complex and Inhibits Pancreatic Cancer Cell Growth and Migration. *J. Funct. Foods* **2015**, *18*, 10–21.

146. Erdogan, S.; Doganlar, O.; Doganlar, Z. B.; Serttas, R.; Turkekul, K.; et al. The Flavonoid Apigenin Reduces Prostate Cancer CD44+ Stem Cell Survival and Migration through PI3K/Akt/NF-KB Signaling. *Life Sci.* **2016**, *162*, 77–86.
147. Chien, M. H.; Lin, Y. W.; Wen, Y. C.; Yang, Y. C.; Hsiao, M.; et al. Targeting the SPOCK1-Snail/Slug Axis-Mediated Epithelial-to-Mesenchymal Transition by Apigenin Contributes to Repression of Prostate Cancer Metastasis. *J. Exp. Clin. Cancer Res.* **2019**, *38* (1), 1–17.
148. Franzen, C. A.; Amargo, E.; Todorović, V.; Desai, B. V.; Huda, S.; et al. The Chemopreventive Bioflavonoid Apigenin Inhibits Prostate Cancer Cell Motility through the Focal Adhesion Kinase/Src Signaling Mechanism. *Cancer Prev. Res.* **2009**, *2* (9), 830–841.
149. Shukla, S.; Kanwal, R.; Shankar, E.; Datt, M.; Chance, M. R.; et al. Apigenin Blocks IKKa Activation and Suppresses Prostate Cancer Progression. *Oncotarget* **2015**, *6* (31), 31216–31232.
150. Yeh, C. J.; Chen, C. C.; Leu, Y. L.; Lin, M. W.; Chiu, M. M.; et al. The Effects of Artocarpin on Wound Healing: In Vitro and in Vivo Studies. *Sci. Rep.* **2017**, *7* (1), 1–13.
151. Gao, Y.; Snyder, S. A.; Jaclyn N. Smith; Chen, Y. C. Anticancer Properties of Baicalein: A Review. *Med. Chem. Res.* **2016**, *25* (8), 1515–1523.
152. Ling, Y.; Chen, Y.; Chen, P.; Hui, H.; Song, X.; et al. Baicalein Potently Suppresses Angiogenesis Induced by Vascular Endothelial Growth Factor through the P53/Rb Signaling Pathway Leading to G1/s Cell Cycle Arrest. *Exp. Biol. Med.* **2011**, *236* (7), 851–858.
153. Ma, X. C.; Yan, W.; Dai, Z.; Gao, X.; Ma, Y.; et al. Baicalein Suppresses Metastasis of Breast Cancer Cells by Inhibiting EMT via Downregulation of SATB1 and Wnt/ β -Catenin Pathway. *Drug Des. Devel. Ther.* **2016**, *10*, 1419–1441.
154. Wang, L.; Ling, Y.; Chen, Y.; Li, C. L.; Feng, F.; et al. Flavonoid Baicalein Suppresses Adhesion, Migration and Invasion of MDA-MB-231 Human Breast Cancer Cells. *Cancer Lett.* **2010**, *297* (1), 42–48.
155. Shang, D.; Li, Z.; Zhu, Z.; Chen, H.; Zhao, L.; et al. Baicalein Suppresses 17- β -Estradiol-Induced Migration,

- Adhesion and Invasion of Breast Cancer Cells via the G Protein-Coupled Receptor 30 Signaling Pathway. *Oncol. Rep.* **2015**, *33* (4), 2077–2085.
156. Chung, H.; Choi, H. S.; Seo, E. K.; Kang, D. H.; Oh, E. S. Baicalin and Baicalein Inhibit Transforming Growth Factor-B1-Mediated Epithelial-Mesenchymal Transition in Human Breast Epithelial Cells. *Biochem. Biophys. Res. Commun.* **2015**, *458* (3), 707–713.
157. Chai, Y.; Xu, J.; Yan, B. The Anti-Metastatic Effect of Baicalein on Colorectal Cancer. *Oncol. Rep.* **2017**, *37* (4), 2317–2323.
158. Lalou, C.; Basak, A.; Mishra, P.; Mohanta, B. C.; Banik, R.; et al. Inhibition of Tumor Cells Proliferation and Migration by the Flavonoid Furin Inhibitor Isolated From *Oroxylum Indicum*. *Curr. Med. Chem.* **2013**, *20* (4), 583–591.
159. Chen, F.; Zhuang, M.; Peng, J.; Wang, X.; Huang, T.; et al. Baicalein Inhibits Migration and Invasion of Gastric Cancer Cells through Suppression of the TGF- β Signaling Pathway. *Mol. Med. Rep.* **2014**, *10* (4), 1999–2003.
160. Chiu, Y. W.; Lin, T. H.; Huang, W. S.; Teng, C. Y.; Liou, Y. S.; et al. Baicalein Inhibits the Migration and Invasive Properties of Human Hepatoma Cells. *Toxicol. Appl. Pharmacol.* **2011**, *255* (3), 316–326.
161. Yu, X.; Tang, W.; Yang, Y.; Tang, L.; Dai, R.; et al. Long Noncoding RNA NKILA Enhances the Anti-Cancer Effects of Baicalein in Hepatocellular Carcinoma via the Regulation of NF-KB Signaling. *Chem. Biol. Interact.* **2018**, *285*, 48–58.
162. Park, Y. G.; Choi, J.; Jung, H. K.; Kim, B.; Kim, C.; et al. Baicalein Inhibits Tumor Progression by Inhibiting Tumor Cell Growth and Tumor Angiogenesis. *Oncol. Rep.* **2017**, *38* (5), 3011–3018.
163. Choi, E. O.; Cho, E. J.; Jeong, J. W.; Park, C.; Hong, S. H.; et al. Baicalein Inhibits the Migration and Invasion of B16F10 Mouse Melanoma Cells through Inactivation of the Pi3K/Akt Signaling Pathway. *Biomol. Ther.* **2017**, *25* (2), 213–221.
164. Zhang, J.; Yang, W.; Zhou, Y. B.; Xiang, Y. X.; Wang, L. S.; et al. Baicalein Inhibits Osteosarcoma Cell Proliferation and Invasion through the MiR-183/Ezrin Pathway. *Mol. Med. Rep.* **2018**, *18* (1), 1104–1112.

165. Zhang, Y.; Song, L.; Cai, L.; Wei, R.; Hu, H.; et al. Effects of Baicalein on Apoptosis, Cell Cycle Arrest, Migration and Invasion of Osteosarcoma Cells. *Food Chem. Toxicol.* **2013**, *53*, 325–333.
166. Zhou, R. T.; He, M.; Yu, Z.; Liang, Y.; Nie, Y.; et al. Baicalein Inhibits Pancreatic Cancer Cell Proliferation and Invasion via Suppression of NEDD9 Expression and Its Downstream Akt and ERK Signaling Pathways. *Oncotarget* **2017**, *8* (34), 56351–56363.
167. Lin, R.; Lin, J.; Li, S.; Ding, J.; Wu, H.; et al. Effects of the Traditional Chinese Medicine Baicalein on the Viability of Random Pattern Skin Flaps in Rats. *Drug Des. Devel. Ther.* **2018**, *12*, 2267–2276.
168. Zhou, T.; Zhang, A.; Kuang, G.; Gong, X.; Jiang, R.; et al. Baicalin Inhibits the Metastasis of Highly Aggressive Breast Cancer Cells by Reversing Epithelial-to-Mesenchymal Transition by Targeting β -Catenin Signaling. *Oncol. Rep.* **2017**, *38* (6), 3599–3607.
169. Yang, B.; Bai, H.; Sa, Y.; Zhu, P.; Liu, P. Inhibiting EMT, Stemness and Cell Cycle Involved in Baicalin-Induced Growth Inhibition and Apoptosis in Colorectal Cancer Cells. *J. Cancer* **2020**, *11* (8), 2303–2317.
170. Zhu, Y.; Fang, J.; Wang, H.; Fei, M.; Tang, T.; et al. Baicalin Suppresses Proliferation, Migration, and Invasion in Human Glioblastoma Cells via Ca²⁺-Dependent Pathway. *Drug Des. Devel. Ther.* **2018**, *12*, 3247–3261.
171. Wu, X.; Zhi, F.; Lun, W.; Deng, Q.; Zhang, W. Baicalin Inhibits PDGF-BB-Induced Hepatic Stellate Cell Proliferation, Apoptosis, Invasion, Migration and Activation via the MiR-3595/ACSL4 Axis. *Int. J. Mol. Med.* **2018**, *41* (4), 1992–2002.
172. You, J.; Cheng, J.; Yu, B.; Duan, C.; Peng, J. Baicalin, a Chinese Herbal Medicine, Inhibits the Proliferation and Migration of Human Non-Small Cell Lung Carcinoma (NSCLC) Cells, A549 and H1299, by Activating the SIRT1/AMPK Signaling Pathway. *Med. Sci. Monit.* **2018**, *24*, 2126–2133.
173. Gao, C.; Zhou, Y.; Li, H.; Cong, X.; Jiang, Z.; et al. Antitumor Effects of Baicalin on Ovarian Cancer Cells through Induction of Cell Apoptosis and Inhibition of Cell Migration in Vitro. *Mol. Med. Rep.* **2017**, *16* (6), 8729–8734.
174. Jo, H.; Jung, S. H.; Yim, H. Bin; Lee, S. J.; Kang, K. D. The Effect of Baicalin in a Mouse Model of Retinopathy of Prematurity. *BMB Rep.* **2015**, *48* (5), 271–276.

175. Kasala, E. R.; Bodduluru, L. N.; Madana, R. M.; Athira, K. V.; Gogoi, R.; et al. Chemopreventive and Therapeutic Potential of Chrysin in Cancer: Mechanistic Perspectives. *Toxicol. Lett.* **2015**, *233* (2), 214–225.
176. Tian, S.; Jiang, F.; Zhang, K.; Zhu, X.; Jin, B.; et al. Fitoterapia Flavonoids from the Leaves of *Carya Cathayensis* Sarg. Inhibit Vascular Endothelial Growth Factor-Induced Angiogenesis. *Fitoterapia* **2014**, *92*, 34–40.
177. Yang, B.; Huang, J.; Xiang, T.; Yin, X.; Luo, X.; et al. Chrysin Inhibits Metastatic Potential of Human Triple-Negative Breast Cancer Cells by Modulating Matrix Metalloproteinase-10, Epithelial to Mesenchymal Transition, and PI3K/Akt Signaling Pathway. *J. Appl. Toxicol.* **2014**, *34* (1), 105–112.
178. Xia, Y.; Lian, S.; Khoi, P. N.; Yoon, H. J.; Han, J. Y.; et al. Chrysin Inhibits Cell Invasion by Inhibition of Recepteur d'origine Nantais via Suppressing Early Growth Response-1 and NF-KB Transcription Factor Activities in Gastric Cancer Cells. *Int. J. Oncol.* **2015**, *46* (4), 1835–1843.
179. Fu, B.; Xue, J.; Li, Z.; Shi, X.; Jiang, B. H.; et al. Chrysin Inhibits Expression of Hypoxia-Inducible Factor 1- α through Reducing Hypoxia-Inducible Factor-1 α Stability and Inhibiting Its Protein Synthesis. *Mol. Cancer Ther.* **2007**, *6* (1), 220–226.
180. Kang, M. K.; Park, S. H.; Kim, Y. H.; Lee, E. J.; Antika, L. D.; et al. Dietary Compound Chrysin Inhibits Retinal Neovascularization with Abnormal Capillaries in Db/Db Mice. *Nutrients* **2016**, *8* (12).
181. Amrutha, K.; Nanjan, P.; Shaji, S. K.; Sunilkumar, D.; Subhalakshmi, K.; et al. Discovery of Lesser Known Flavones as Inhibitors of NF-KB Signaling in MDA-MB-231 Breast Cancer Cells - A SAR Study. *Bioorganic Med. Chem. Lett.* **2014**, *24* (19), 4735–4742.
182. Prasad, P.; Vasas, A.; Hohmann, J.; Bishayee, A.; Sinha, D. Cirsiliol Suppressed Epithelial to Mesenchymal Transition in B16F10 Malignant Melanoma Cells through Alteration of the PI3K/Akt/NF-Kb Signaling Pathway. *Int. J. Mol. Sci.* **2019**, *20* (3), 19.
183. Shukla, K.; Sonowal, H.; Saxena, A.; Ramana, K. V. Didymin by Suppressing NF- κ B Activation Prevents VEGF-Induced Angiogenesis in Vitro and in Vivo. *Vascul. Pharmacol.* **2019**, *115* (November 2018), 18–25.
184. Singhal, J.; Nagaprashantha, L. D.; Vatsyayan, R.; Ashutosh; Awasthi, S.; et al. Didymin Induces Apoptosis by

- Inhibiting N-Myc and Upregulating RKIP in Neuroblastoma. *Cancer Prev. Res.* **2012**, 5 (3), 473–483.
185. Yan, Y.; Liu, X.; Gao, J.; Wu, Y.; Li, Y. Inhibition of TGF- α Signaling in Gliomas by the Flavonoid Diosmetin Isolated from *Dracocephalum Peregrinum* L. *Molecules* **2020**, 25 (1), 192–204.
186. Ge, A.; Ma, Y.; Liu, Y. N.; Li, Y. S.; Gu, H.; et al. Diosmetin Prevents TGF-B1-Induced Epithelial-Mesenchymal Transition via ROS/MAPK Signaling Pathways. *Life Sci.* **2016**, 153, 1–8.
187. Choi, J.; Lee, D.; Park, S.; Seol, J. Diosmetin Inhibits Tumor Development and Block Tumor Angiogenesis in Skin Cancer. *Biomed. Pharmacother.* **2019**, 117 (Sep), 109091–109099.
188. Jiang, H.; Wu, D.; Xu, D.; Yu, H.; Zhao, Z.; et al. Eupafolin Exhibits Potent Anti-Angiogenic and Antitumor Activity in Hepatocellular Carcinoma. *Int. J. Biol. Sci.* **2017**, 13 (6), 701–711.
189. Cheong, J. H.; Hong, S. Y.; Zheng, Y.; Noh, S. H. Eupatilin Inhibits Gastric Cancer Cell Growth by Blocking STAT3-Mediated VEGF Expression. *J. Gastric Cancer* **2011**, 11 (1), 16–22.
190. Fei, X.; Wang, J.; Chen, C.; Ding, B.; Fu, X.; et al. Eupatilin Inhibits Glioma Proliferation, Migration, and Invasion by Arresting Cell Cycle at G1/S Phase and Disrupting the Cytoskeletal Structure. *Cancer Manag. Res.* **2019**, 11, 4781–4796.
191. Dolečková, I.; Rárová, L.; Grúz, J.; Vondrusová, M.; Strnad, M.; et al. Antiproliferative and Antiangiogenic Effects of Flavone Eupatorin, an Active Constituent of Chloroform Extract of *Orthosiphon Stamineus* Leaves. *Fitoterapia* **2012**, 83 (6), 1000–1007.
192. Du, Y.; Feng, J.; Wang, R.; Zhang, H.; Liu, J. Effects of Flavonoids from *Potamogeton Crispus* L. On Proliferation, Migration, and Invasion of Human Ovarian Cancer Cells. *PLoS One* **2015**, 10 (6), 1–17.
193. Dogan Turacli, I.; Demirtas Korkmaz, F.; Candar, T.; Ekmekci, A. Flavopiridol's Effects on Metastasis in KRAS Mutant Lung Adenocarcinoma Cells. *J. Cell. Biochem.* **2019**, 120 (4), 5628–5635.
194. Li, L.; Chen, P.; Ling, Y.; Song, X.; Lu, Z.; et al. Inhibitory Effects of GL-V9 on the Invasion of Human Breast Carcinoma Cells by Downregulating the Expression and Activity of Matrix Metalloproteinase-2/9. *Eur. J. Pharm. Sci.*

2011, 43 (5), 393–399.

195. Xie, J.; Gao, H.; Peng, J.; Han, Y.; Chen, X.; et al. Hispidulin Prevents Hypoxia-Induced Epithelial-Mesenchymal Transition in Human Colon Carcinoma Cells. *Am. J. Cancer Res.* **2015**, 5 (3), 1047–1061.
196. Han, M.; Gao, H.; Ju, P.; Gao, M. quan; Yuan, Y. ping; et al. Hispidulin Inhibits Hepatocellular Carcinoma Growth and Metastasis through AMPK and ERK Signaling Mediated Activation of PPAR γ . *Biomed. Pharmacother.* **2018**, 103, 272–283.
197. He, L.; Wu, Y.; Lin, L.; Wang, J.; Wu, Y.; et al. Hispidulin, a Small Flavonoid Molecule, Suppresses the Angiogenesis and Growth of Human Pancreatic Cancer by Targeting Vascular Endothelial Growth Factor Receptor 2-Mediated PI3K/Akt/MTOR Signaling Pathway. *Cancer Sci.* **2011**, 102 (1), 219–225.
198. Gao, M. Q.; Gao, H.; Han, M.; Liu, K. L.; Peng, J. J.; et al. Hispidulin Suppresses Tumor Growth and Metastasis in Renal Cell Carcinoma by Modulating Ceramide-Sphingosine 1-Phosphate Rheostat. *Am. J. Cancer Res.* **2017**, 7 (7), 1501–1514.
199. Li, C.; Li, F.; Zhao, K.; Yao, J.; Cheng, Y.; et al. LFG-500 Inhibits the Invasion of Cancer Cells via down-Regulation of PI3K/AKT/NF-KB Signaling Pathway. *PLoS One* **2014**, 9 (3), 1–12.
200. Zhen, Z. G.; Ren, S. H.; Ji, H. M.; Ma, J. H.; Ding, X. M.; et al. Linarin Suppresses Glioma through Inhibition of NF-KB/P65 and up-Regulating P53 Expression in Vitro and in Vivo. *Biomed. Pharmacother.* **2017**, 95, 363–374.
201. Cook, M. T. Mechanism of Metastasis Suppression by Luteolin in Breast Cancer. *Breast Cancer Targets Ther.* **2018**, 10, 89–100.
202. Li, X.; Chen, M.; Lei, X.; Huang, M.; Ye, W.; et al. Luteolin Inhibits Angiogenesis by Blocking Gas6/Axl Signaling Pathway. *Int. J. Oncol.* **2017**, 51 (2), 677–685.
203. Zhu, M.; Chen, D.; Li, D.; Ding, H.; Zhang, T.; et al. Luteolin Inhibits Angiotensin II-Induced Human Umbilical Vein Endothelial Cell Proliferation and Migration through Downregulation of Src and Akt Phosphorylation. *Circ. J.* **2013**, 77 (3), 772–779.

204. Li, H.; Lin, D.; Kuang, G.; Wan, J.; Zhang, X.; et al. Luteolin Suppresses the Metastasis of Triple-Negative Breast Cancer by Reversing Epithelial-to-Mesenchymal Transition via Downregulation of β -Catenin Expression. *Oncol. Rep.* **2017**, *37* (2), 895–902.
205. Naso, L. G.; Badiola, I.; Marquez Clavijo, J.; Valcarcel, M.; Salado, C.; et al. Inhibition of the Metastatic Progression of Breast and Colorectal Cancer in Vitro and in Vivo in Murine Model by the Oxidovanadium(IV) Complex with Luteolin. *Bioorganic Med. Chem.* **2016**, *24* (22), 6004–6011.
206. Attoub, S.; Hassan, A. H.; Vanhoecke, B.; Iratni, R.; Takahashi, T.; et al. Inhibition of Cell Survival, Invasion, Tumor Growth and Histone Deacetylase Activity by the Dietary Flavonoid Luteolin in Human Epithelioid Cancer Cells. *Eur. J. Pharmacol.* **2011**, *651* (1–3), 18–25.
207. Bagli, E.; Stefaniotou, M.; Morbidelli, L.; Ziche, M.; Psillas, K.; et al. Luteolin Inhibits Vascular Endothelial Growth Factor-Induced Angiogenesis; Inhibition of Endothelial Cell Survival and Proliferation by Targeting Phosphatidylinositol 3'-Kinase Activity. *Cancer Res.* **2004**, *64* (21), 7936–7946.
208. Yao, Y.; Rao, C.; Zheng, G.; Wang, S. Luteolin Suppresses Colorectal Cancer Cell Metastasis via Regulation of the MiR-384/Pleiotrophin Axis. *Oncol. Rep.* **2019**, *42* (1), 131–141.
209. Lodhi, S.; Singhai, A. K. Wound Healing Effect of Flavonoid Rich Fraction and Luteolin Isolated from *Martynia Annua* Linn. on Streptozotocin Induced Diabetic Rats. *Asian Pac. J. Trop. Med.* **2013**, *6* (4), 253–259.
210. Lu, J.; Li, G.; He, K.; Jiang, W.; Xu, C.; et al. Luteolin Exerts a Marked Antitumor Effect in CMet-Overexpressing Patient-Derived Tumor Xenograft Models of Gastric Cancer. *J. Transl. Med.* **2015**, *13* (1), 1–11.
211. Zang, M. de; Hu, L.; Fan, Z. yuan; Wang, H. xiao; Zhu, Z. lun; et al. Luteolin Suppresses Gastric Cancer Progression by Reversing Epithelial-Mesenchymal Transition via Suppression of the Notch Signaling Pathway. *J. Transl. Med.* **2017**, *15* (1), 1–11.
212. Pu, Y.; Zhang, T.; Wang, J.; Mao, Z.; Duan, B.; et al. Luteolin Exerts an Anticancer Effect on Gastric Cancer Cells through Multiple Signaling Pathways and Regulating MiRNAs. *J. Cancer* **2018**, *9* (20), 3669–3675.
213. Wang, Q.; Wang, H.; Jia, Y.; Ding, H.; Zhang, L.; et al. Luteolin Reduces Migration of Human Glioblastoma Cell

Lines via Inhibition of the P-IGF-1R/PI3K/AKT/MTOR Signaling Pathway. *Oncol. Lett.* **2017**, 14 (3), 3545–3551.

214. Selvi, R. B.; Swaminathan, A.; Chatterjee, S.; Shanmugam, M. K.; Li, F.; et al. Inhibition of P300 Lysine Acetyltransferase Activity by Luteolin Reduces Tumor Growth in Head and Neck Squamous Cell Carcinoma (HNSCC) Xenograft Mouse Model. *Oncotarget* **2015**, 6 (41), 43806–43818.
215. Cheng, W. Y.; Chiao, M. T.; Liang, Y. J.; Yang, Y. C.; Shen, C. C.; et al. Luteolin Inhibits Migration of Human Glioblastoma U-87 MG and T98G Cells through Downregulation of Cdc42 Expression and PI3K/AKT Activity. *Mol. Biol. Rep.* **2013**, 40 (9), 5315–5326.
216. Franco, Y. E. M.; de Lima, C. A.; Rosa, M. N.; Silva, V. A. O.; Reis, R. M.; et al. Investigation of U-251 Cell Death Triggered by Flavonoid Luteolin: Towards a Better Understanding on Its Anticancer Property against Glioblastomas. *Nat. Prod. Res.* **2020**, 1–7.
217. Lee, W. J.; Wu, L. F.; Chen, W. K.; Wang, C. J.; Tseng, T. H. Inhibitory Effect of Luteolin on Hepatocyte Growth Factor/Scatter Factor-Induced HepG2 Cell Invasion Involving Both MAPK/ERKs and PI3K-Akt Pathways. *Chem. Biol. Interact.* **2006**, 160 (2), 123–133.
218. Meng, G.; Chai, K.; Li, X.; Zhu, Y.; Huang, W. Luteolin Exerts Pro-Apoptotic Effect and Anti-Migration Effects on A549 Lung Adenocarcinoma Cells through the Activation of MEK/ERK Signaling Pathway. *Chem. Biol. Interact.* **2016**, 257, 26–34.
219. Ruan, J.; Zhang, L.; Yan, L.; Liu, Y.; Yue, Z.; et al. Inhibition of Hypoxia-Induced Epithelial Mesenchymal Transition by Luteolin in Non-Small Cell Lung Cancer Cells. *Mol. Med. Rep.* **2012**, 6 (1), 232–238.
220. Li, C.; Wang, Q.; Shen, S.; Wei, X.; Li, G. HIF-1 α /VEGF Signaling-Mediated Epithelial–Mesenchymal Transition and Angiogenesis Is Critically Involved in Anti-Metastasis Effect of Luteolin in Melanoma Cells. *Phyther. Res.* **2019**, 33 (3), 798–807.
221. Yao, X.; Jiang, W.; Yu, D.; Yan, Z. Luteolin Inhibits Proliferation and Induces Apoptosis of Human Melanoma Cells: In Vivo and in Vitro by Suppressing MMP-2 and MMP-9 through the PI3K/AKT Pathway. *Food Funct.* **2019**, 10 (2), 703–712.

222. Ruan, J. S.; Liu, Y. P.; Zhang, L.; Yan, L. G.; Fan, F. T.; et al. Luteolin Reduces the Invasive Potential of Malignant Melanoma Cells by Targeting B3 Integrin and the Epithelial-Mesenchymal Transition. *Acta Pharmacol. Sin.* **2012**, *33* (10), 1325–1331.
223. Velmurugan, B. K.; Lin, J.-T.; Mahalakshmi, B.; Chuang, Y.-C.; Lin, C.-C.; et al. Luteolin-7-O-Glucoside Inhibits Oral Cancer Cell Migration and Invasion by Regulating Matrix Metalloproteinase-2 Expression and Extracellular Signal-Regulated Kinase Pathway. *Biomolecules* **2020**, *10* (4), 502.
224. Pratheeshkumar, P.; Son, Y. O.; Budhraja, A.; Wang, X.; Ding, S.; et al. Luteolin Inhibits Human Prostate Tumor Growth by Suppressing Vascular Endothelial Growth Factor Receptor 2-Mediated Angiogenesis. *PLoS One* **2012**, *7* (12), 52279.
225. Fan, S. H.; Wang, Y. Y.; Lu, J.; Zheng, Y. L.; Wu, D. M.; et al. Luteoloside Suppresses Proliferation and Metastasis of Hepatocellular Carcinoma Cells by Inhibition of NLRP3 Inflammasome. *PLoS One* **2014**, *9* (2), 1–11.
226. Zhao, K.; Yuan, Y.; Lin, B.; Miao, Z.; Li, Z.; et al. LW-215 , a Newly Synthesized Flavonoid , Exhibits Potent Anti-Angiogenic Activity in Vitro and in Vivo. *Gene* **2018**, *642*, 533–541.
227. Chen, Y.; Lu, N.; Ling, Y.; Wang, L.; You, Q.; et al. LYG-202, a Newly Synthesized Flavonoid, Exhibits Potent Anti-Angiogenic Activity in Vitro and in Vivo. *J. Pharmacol. Sci.* **2010**, *112* (1), 37–45.
228. Zhao, K.; Yao, Y.; Luo, X.; Lin, B.; Huang, Y.; et al. LYG-202 Inhibits Activation of Endothelial Cells and Angiogenesis through CXCL12/CXCR7 Pathway in Breast Cancer. *Carcinogenesis* **2018**, *39* (4), 588–600.
229. Lin, W. L.; Lai, D. Y.; Lee, Y. J.; Chen, N. F.; Tseng, T. H. Antitumor Progression Potential of Morusin Suppressing STAT3 and NFκB in Human Hepatoma SK-Hep1 Cells. *Toxicol. Lett.* **2015**, *232* (2), 490–498.
230. Lam, K. H.; Alex, D.; Lam, I. K.; Tsui, S. K. W.; Yang, Z. F.; et al. Nobiletin, a Polymethoxylated Flavonoid from Citrus, Shows Anti-Angiogenic Activity in a Zebrafish in Vivo Model and HUVEC in Vitro Model. *J. Cell. Biochem.* **2011**, *112* (11), 3313–3321.
231. Nipin, S. P.; Kang, D. Y.; Joung, Y. H.; Park, J. H.; Kim, W. S.; et al. Nobiletin Inhibits Angiogenesis by Regulating Src/FAK/STAT3-Mediated Signaling through PXN In ER+ Breast Cancer Cells. *Int. J. Mol. Sci.* **2017**, *18* (5).

232. Sp, N.; Kang, D. Y.; Kim, D. H.; Park, J. H.; Lee, H. G.; et al. Nobiletin Inhibits CD36-Dependent Tumor Angiogenesis, Migration, Invasion, and Sphere Formation through the Cd36/Stat3/Nf-Kb Signaling Axis. *Nutrients* **2018**, *10* (6).
233. Liu, J.; Wang, S.; Tian, S.; He, Y.; Lou, H.; et al. Nobiletin Inhibits Breast Cancer via P38 Mitogen-Activated Protein Kinase, Nuclear Transcription Factor-Kb, and Nuclear Factor Erythroid 2-Related Factor 2 Pathways in MCF-7 Cells. *Food Nutr. Res.* **2018**, *62* (13), 1–10.
234. Lee, Y. C.; Cheng, T. H.; Lee, J. S.; Chen, J. H.; Liao, Y. C.; et al. Nobiletin, a Citrus Flavonoid, Suppresses Invasion and Migration Involving FAK/PI3K/Akt and Small GTPase Signals in Human Gastric Adenocarcinoma AGS Cells. *Mol. Cell. Biochem.* **2011**, *347* (1–2), 103–115.
235. Lien, L. M.; Wang, M. J.; Chen, R. J.; Chiu, H. C.; Wu, J. L.; et al. Nobiletin, a Polymethoxylated Flavone, Inhibits Glioma Cell Growth and Migration via Arresting Cell Cycle and Suppressing MAPK and Akt Pathways. *Phyther. Res.* **2016**, *30* (2), 214–221.
236. Zhang, X.; Zheng, K.; Li, C.; Zhao, Y.; Li, H.; et al. Nobiletin Inhibits Invasion via Inhibiting AKT/GSK3 β / β -Catenin Signaling Pathway in Slug-Expressing Glioma Cells. *Oncol. Rep.* **2017**, *37* (5), 2847–2856.
237. Shi, M. Der; Liao, Y. C.; Shih, Y. W.; Tsai, L. Y. Nobiletin Attenuates Metastasis via Both ERK and PI3K/Akt Pathways in HGF-Treated Liver Cancer HepG2 Cells. *Phytomedicine* **2013**, *20* (8–9), 743–752.
238. Da, C.; Liu, Y.; Zhan, Y.; Liu, K.; Wang, R. Nobiletin Inhibits Epithelial-Mesenchymal Transition of Human Non-Small Cell Lung Cancer Cells by Antagonizing the TGF-B1/Smad3 Signaling Pathway. *Oncol. Rep.* **2016**, *35* (5), 2767–2774.
239. Chen, J.; Chen, A. Y.; Huang, H.; Ye, X.; Rollyson, W. D.; et al. The Flavonoid Nobiletin Inhibits Tumor Growth and Angiogenesis of Ovarian Cancers via the Akt Pathway. *Int. J. Oncol.* **2015**, *46* (6), 2629–2638.
240. Liu, F.; Zhang, S.; Yin, M.; Guo, L.; Xu, M.; et al. Nobiletin Inhibits Hypoxia-Induced Epithelial-Mesenchymal Transition in Renal Cell Carcinoma Cells. *J. Cell. Biochem.* **2019**, *120* (2), 2039–2046.
241. Jiang, R.; Lin, C.; Jiang, C.; Huang, Z.; Gao, W.; et al. Nobiletin Enhances the Survival of Random Pattern Skin Fl

Aps : Involvement of Enhancing Angiogenesis and Inhibiting Oxidative Stress. *Int. Immunopharmacol.* **2020**, *78*, 106010.

242. Kim, S. J.; Pham, T. H.; Bak, Y.; Ryu, H. W.; Oh, S. R.; et al. Orientin Inhibits Invasion by Suppressing MMP-9 and IL-8 Expression via the PKC α / ERK/AP-1/STAT3-Mediated Signaling Pathways in TPA-Treated MCF-7 Breast Cancer Cells. *Phytomedicine* **2018**, *50*, 35–42.
243. Huang, H. K.; Lee, S. Y.; Huang, S. F.; Lin, Y. S.; Chao, S. C.; et al. Isoorientin Decreases Cell Migration via Decreasing Functional Activity and Molecular Expression of Proton-Linked Monocarboxylate Transporters in Human Lung Cancer Cells. *Am. J. Chin. Med.* **2020**, *48* (1), 201–222.
244. Lu, Z.; Lu, N.; Li, C.; Li, F.; Zhao, K.; et al. Oroxylin A Inhibits Matrix Metalloproteinase-2/9 Expression and Activation by up-Regulating Tissue Inhibitor of Metalloproteinase-2 and Suppressing the ERK1/2 Signaling Pathway. *Toxicol. Lett.* **2012**, *209* (3), 211–220.
245. Li, Y.; Gan, C.; Zhang, Y.; Yu, Y.; Fan, C.; et al. Inhibition of Stat3 Signaling Pathway by Natural Product Pectolinarigenin Attenuates Breast Cancer Metastasis. *Front. Pharmacol.* **2019**, *10*, 1–13.
246. Gan, C.; Li, Y.; Yu, Y.; Yu, X.; Liu, H.; et al. Natural Product Pectolinarigenin Exhibits Potent Anti-Metastatic Activity in Colorectal Carcinoma Cells in Vitro and in Vivo. *Bioorganic Med. Chem.* **2019**, *27* (21).
247. Liu, S.; Zhang, J.; Yang, H.; Zhang, Q.; Chen, M. Pectolinarigenin Flavonoid Exhibits Selective Anti-Proliferative Activity in Cisplatin-Resistant Hepatocellular Carcinoma, Autophagy Activation, Inhibiting Cell Migration and Invasion, G2/M Phase Cell Cycle Arrest and Targeting ERK1/2 MAP Kinases. *J. B.U.ON.* **2020**, *25* (1), 415–420.
248. Wu, X.; Yu, N.; Zhang, Y.; Ye, Y.; Sun, W.; et al. Radix Tetrastigma Hemsleyani Flavone Exhibits Antitumor Activity in Colorectal Cancer via Wnt/ β -Catenin Signaling Pathway. *Onco. Targets. Ther.* **2018**, *11*, 6437–6446.
249. Gao, Z. X. Z.; Huang, D. Y.; Li, H. X.; Zhang, L. N.; Lv, Y. H.; et al. Scutellarin Promotes in Vitro Angiogenesis in Human Umbilical Vein Endothelial Cells. *Biochem. Biophys. Res. Commun.* **2010**, *400* (1), 151–156.
250. Lv, W. L.; Liu, Q.; An, J. H.; Song, X. Y. Scutellarin Inhibits Hypoxia-Induced Epithelial-Mesenchymal Transition in Bladder Cancer Cells. *J. Cell. Physiol.* **2019**, *234* (12), 23169–23175.

251. Tang, S. L.; Gao, Y. L.; Hu, W. Z. Scutellarin Inhibits the Metastasis and Cisplatin Resistance in Glioma Cells. *Onco. Targets. Ther.* **2019**, *12*, 587–598.
252. Ke, Y.; Bao, T.; Wu, X.; Tang, H.; Wang, Y.; et al. Scutellarin Suppresses Migration and Invasion of Human Hepatocellular Carcinoma by Inhibiting the STAT3/Girdin/Akt Activity. *Biochem. Biophys. Res. Commun.* **2017**, *483* (1), 509–515.
253. Li, C. Y.; Wang, Q.; Wang, X.; Li, G.; Shen, S.; et al. Scutellarin Inhibits the Invasive Potential of Malignant Melanoma Cells through the Suppression Epithelial-Mesenchymal Transition and Angiogenesis via the PI3K/Akt/MTOR Signaling Pathway. *Eur. J. Pharmacol.* **2019**, *858* (22), 172463.
254. Deng, W.; Han, W.; Fan, T.; Wang, X.; Cheng, Z.; et al. Scutellarin Inhibits Human Renal Cancer Cell Proliferation and Migration via Upregulation of PTEN. *Biomed. Pharmacother.* **2018**, *107*, 1505–1513.
255. Thirusangu, P.; Vigneshwaran, V.; Vijay Avin, B. R.; Rakesh, H.; Vikas, H. M.; et al. Scutellarein Antagonizes the Tumorigenesis by Modulating Cytokine VEGF Mediated Neoangiogenesis and DFF-40 Actuated Nucleosomal Degradation. *Biochem. Biophys. Res. Commun.* **2017**, *484* (1), 85–92.
256. Chung, T. Te; Chuang, C. Y.; Teng, Y. H.; Hsieh, M. J.; Lai, J. C.; et al. Tricetin Suppresses Human Oral Cancer Cell Migration by Reducing Matrix Metalloproteinase-9 Expression through the Mitogen-Activated Protein Kinase Signaling Pathway. *Environ. Toxicol.* **2017**, *32* (11), 2392–2399.
257. Chang, P. Y.; Hsieh, M. J.; Hsieh, Y. S.; Chen, P. N.; Yang, J. S.; et al. Tricetin Inhibits Human Osteosarcoma Cells Metastasis by Transcriptionally Repressing MMP-9 via P38 and Akt Pathways. *Environ. Toxicol.* **2017**, *32* (8), 2032–2040.
258. Chung, D. J.; Wang, C. J.; Yeh, C. W.; Tseng, T. H. Inhibition of the Proliferation and Invasion of C6 Glioma Cells by Tricin via the Upregulation of Focal-Adhesion-Kinase-Targeting MicroRNA-7. *J. Agric. Food Chem.* **2018**, *66* (26), 6708–6716.
259. Seki, N.; Toh, U.; Kawaguchi, K.; Ninomiya, M.; Koketsu, M.; et al. Tricin Inhibits Proliferation of Human Hepatic Stellate Cells in Vitro by Blocking Tyrosine Phosphorylation of PDGF Receptor and Its Signaling Pathways. *J. Cell. Biochem.* **2012**, *113* (7), 2346–2355.

260. Li, F.; Li, C.; Zhang, H.; Lu, Z.; Li, Z.; et al. VI-14, a Novel Flavonoid Derivative, Inhibits Migration and Invasion of Human Breast Cancer Cells. *Toxicol. Appl. Pharmacol.* **2012**, *261* (2), 217–226.
261. Luo, Y.; Ren, Z.; Du, B.; Xing, S.; Huang, S.; et al. Structure Identification of ViceninII Extracted from *Dendrobium Officinale* and the Reversal of TGF-B1-Induced Epithelial–Mesenchymal Transition in Lung Adenocarcinoma Cells through TGF- β /Smad and PI3K/Akt/MTOR Signaling Pathways. *Molecules* **2019**, *24* (1), 1–17.
262. Choi, H. J.; Eun, J. S.; Kim, B. G.; Kim, S. Y.; Jeon, H.; et al. Vitexin, an HIF-1 α Inhibitor, Has Anti-Metastatic Potential in PC12 Cells. *Mol. Cells* **2006**, *22* (3), 291–299.
263. Huynh, D. L.; Sharma, N.; Kumar Singh, A.; Singh Sodhi, S.; ZHANG, J. J.; et al. Anti-Tumor Activity of Wogonin, an Extract from *Scutellaria Baicalensis*, through Regulating Different Signaling Pathways. *Chin. J. Nat. Med.* **2017**, *15* (1), 15–40.
264. Lin, C. M.; Chang, H.; Chen, Y. H.; Li, S. Y.; Wu, I. H.; et al. Protective Role of Wogonin against Lipopolysaccharide-Induced Angiogenesis via VEGFR-2, Not VEGFR-1. *Int. Immunopharmacol.* **2006**, *6* (11), 1690–1698.
265. Song, X.; Yao, J.; Wang, F.; Zhou, M.; Zhou, Y.; et al. Wogonin Inhibits Tumor Angiogenesis via Degradation of HIF-1 α Protein. *Toxicol. Appl. Pharmacol.* **2013**, *271* (2), 144–155.
266. Fu, R.; Chen, Y.; Wang, X.; An, T.; Tao, L.; et al. Wogonin Inhibits Multiple Myeloma-Stimulated Angiogenesis via c-Myc / VHL / HIF-1 α Signaling Axis. *Oncotarget* **2016**, *7* (5), 5715–5727.
267. Chen, Y.; Lu, N.; Ling, Y.; Gao, Y.; Wang, L.; et al. Wogonoside Inhibits Lipopolysaccharide-Induced Angiogenesis in Vitro and in Vivo via Toll-like Receptor 4 Signal Transduction. *Toxicology* **2009**, *259* (1–2), 10–17.
268. Huang, Y.; Zhao, K.; Hu, Y.; Zhou, Y.; Luo, X.; et al. Wogonoside Inhibits Angiogenesis in Breast Cancer via Suppressing Wnt/ β -Catenin Pathway. *Mol. Carcinog.* **2016**, *55* (11), 1598–1612.
269. Chen, S.; Wu, Z.; Ke, Y.; Shu, P.; Chen, C.; et al. Wogonoside Inhibits Tumor Growth and Metastasis in Endometrial Cancer via ER Stress-Hippo Signaling Axis. *Acta Biochim. Biophys. Sin. (Shanghai)*. **2019**, *51* (11), 1096–1105.

270. Chen, Y.; Cheng, Y.; Hung, A. C.; Wu, Y.; Hou, M. The Synthetic Flavonoid WYC02-9 Inhibits Cervical Cancer Cell Migration / Invasion and Angiogenesis via MAPK14 Signaling. *Gynecol. Oncol.* **2013**, *131* (3), 734–743.
271. Singhal, J.; Nagaprashantha, L.; Chikara, S.; Awasthi, S.; Horne, D.; et al. 2'-Hydroxyflavanone: A Novel Strategy for Targeting Breast Cancer. *Oncotarget* **2017**, *8* (43), 75025–75037.
272. Wu, S.; Huang, J.; Hui, K.; Yue, Y.; Gu, Y.; et al. 2'-Hydroxyflavanone Inhibits Epithelial-Mesenchymal Transition, and Cell Migration and Invasion via Suppression of the Wnt/ β -Catenin Signaling Pathway in Prostate Cancer. *Oncol. Rep.* **2018**, *40* (5), 2836–2843.
273. Zhang, X. L.; Cao, M. A.; Pu, L. P.; Huang, S. S.; Gao, Q. X.; et al. A Novel Flavonoid Isolated from *Sophora Flavescens* Exhibited Anti-Angiogenesis Activity, Decreased VEGF Expression and Caused G0/G1 Cell Cycle Arrest in Vitro. *Pharmazie* **2013**, *68* (5), 369–375.
274. Zhao, X.; Guo, X.; Shen, J.; Hua, D. Alpinetin Inhibits Proliferation and Migration of Ovarian Cancer Cells via Suppression of STAT3 Signaling. *Mol. Med. Rep.* **2018**, *18* (4), 4030–4036.
275. Li, Q.; Wang, Y.; Xiao, H.; Li, Y.; Kan, X.; et al. Chamaejasmenin B, a Novel Candidate, Inhibits Breast Tumor Metastasis by Rebalancing TGF-Beta Paradox. *Oncotarget* **2016**, *7* (30), 48180–48192.
276. Li, W.; Du, Q.; Li, X.; Zheng, X.; Lv, F.; et al. Eriodictyol Inhibits Proliferation, Metastasis and Induces Apoptosis of Glioma Cells via PI3K/Akt/NF-KB Signaling Pathway. *Front. Pharmacol.* **2020**, *11*, 1–16.
277. Li, W.; Kandhare, A. D.; Mukherjee, A. A.; Bodhankar, S. L. Hesperidin, a Plant Flavonoid Accelerated the Cutaneous Wound Healing in Streptozotocin-Induced Diabetic Rats: Role of TGF-B/SMADS and ANG-1/TIE-2 Signaling Pathways. *EXCLI J.* **2018**, *17*, 399–419.
278. Byun, E. B.; Kim, H. M.; Song, H. Y.; Kim, W. S. Hesperidin Structurally Modified by Gamma Irradiation Induces Apoptosis in Murine Melanoma B16BL6 Cells and Inhibits Both Subcutaneous Tumor Growth and Metastasis in C57BL/6 Mice. *Food Chem. Toxicol.* **2019**, *127*, 19–30.
279. Lowe, H. I. C.; Toyang, N. J.; Watson, C. T.; Ayeah, K. N.; Bryant, J. HLBT-100: A Highly Potent Anti-Cancer Flavanone from *Tillandsia Recurvata* (L.) L. *Cancer Cell Int.* **2017**, *17* (1), 1–12.

280. Shi, Q.; Jiang, Z.; Yang, J.; Cheng, Y.; Pang, Y.; et al. A Flavonoid Glycoside Compound from *Murraya Paniculata* (L.) Interrupts Metastatic Characteristics of A549 Cells by Regulating STAT3/NF-KB/COX-2 and EGFR Signaling Pathways. *AAPS J.* **2017**, *19* (6), 1779–1790.
281. Xie, S. R.; Wang, Y.; Liu, C. W.; Luo, K.; Cai, Y. Q. Liquiritigenin Inhibits Serum-Induced HIF-1 α and VEGF Expression via the AKT/MTOR-P70S6K Signalling Pathway in HeLa Cells. *Phyther. Res.* **2012**, *26* (8), 1133–1141.
282. Aroui, S.; Aouey, B.; Chtourou, Y.; Meunier, A. C.; Fetoui, H.; et al. Naringin Suppresses Cell Metastasis and the Expression of Matrix Metalloproteinases (MMP-2 and MMP-9) via the Inhibition of ERK-P38-JNK Signaling Pathway in Human Glioblastoma. *Chem. Biol. Interact.* **2016**, *244*, 195–203.
283. Aroui, S.; Najlaoui, F.; Chtourou, Y.; Meunier, A. C.; Laajimi, A.; et al. Naringin Inhibits the Invasion and Migration of Human Glioblastoma Cell via Downregulation of MMP-2 and MMP-9 Expression and Inactivation of P38 Signaling Pathway. *Tumor Biol.* **2016**, *37* (3), 3831–3839.
284. Pafumi, I.; Festa, M.; Papacci, F.; Lagostena, L.; Giunta, C.; et al. Naringenin Impairs Two-Pore Channel 2 Activity and Inhibits VEGF-Induced Angiogenesis /631/67/2328 /631/80/86/1999 /9/74 /96/34 /64/60 /14/63 /96/63 Article. *Sci. Rep.* **2017**, *7* (1), 1–11.
285. Chen, K. S.; Shi, M. Der; Chien, C. S.; Shih, Y. W. Pinocembrin Suppresses TGF-B1-Induced Epithelial-Mesenchymal Transition and Metastasis of Human Y-79 Retinoblastoma Cells through Inactivating Av β 3 Integrin/FAK/P38 α Signaling Pathway. *Cell Biosci.* **2014**, *4* (1), 1–13.
286. Karas, D.; Ulrichová, J.; Valentová, K. Galloylation of Polyphenols Alters Their Biological Activity. *Food Chem. Toxicol.* **2017**, *105*, 223–240.
287. Hou, Z.; Lambert, J. D.; Chin, K. V.; Yang, C. S. Effects of Tea Polyphenols on Signal Transduction Pathways Related to Cancer Chemoprevention. *Mutat. Res. - Fundam. Mol. Mech. Mutagen.* **2004**, *555* (1–2), 3–19.
288. Neergheen, V. S.; Bahorun, T.; Taylor, E. W.; Jen, L. S.; Aruoma, O. I. Targeting Specific Cell Signaling Transduction Pathways by Dietary and Medicinal Phytochemicals in Cancer Chemoprevention. *Toxicology* **2010**, *278* (2), 229–241.

289. Chowdhury, A.; Sarkar, J.; Chakraborti, T.; Pramanik, P. K.; Chakraborti, S. Protective Role of Epigallocatechin-3-Gallate in Health and Disease: A Perspective. *Biomed. Pharmacother.* **2016**, *78*, 50–59.
290. Doss, M. X.; Potta, S. P.; Hescheler, J.; Sachinidis, A. Trapping of Growth Factors by Catechins: A Possible Therapeutical Target for Prevention of Proliferative Diseases. *J. Nutr. Biochem.* **2005**, *16* (5), 259–266.
291. Abdulkhaleq, L. A.; Assi, M. A.; Noor, M. H. M.; Abdullah, R.; Saad, M. Z.; et al. Therapeutic Uses of Epicatechin in Diabetes and Cancer. *Vet. World* **2017**, *10* (8), 869–872.
292. Katiyar, S.; Elmets, C. A.; Katiyar, S. K. Green Tea and Skin Cancer: Photoimmunology, Angiogenesis and DNA Repair. *J. Nutr. Biochem.* **2007**, *18* (5), 287–296.
293. Saeed, M.; Naveed, M.; Arif, M.; Kakar, M. U.; Manzoor, R.; et al. Green Tea (*Camellia Sinensis*) and L-Theanine: Medicinal Values and Beneficial Applications in Humans—A Comprehensive Review. *Biomed. Pharmacother.* **2017**, *95*, 1260–1275.
294. Singh, A. K.; Seth, P.; Anthony, P.; Husain, M. M.; Madhavan, S.; et al. Green Tea Constituent Epigallocatechin-3-Gallate Inhibits Angiogenic Differentiation of Human Endothelial Cells. *Arch. Biochem. Biophys.* **2002**, *401* (1), 29–37.
295. Shi, J.; Deng, H.; Pan, H.; Xu, Y.; Zhang, M. Epigallocatechin-3-Gallate Attenuates Microcystin-LR Induced Oxidative Stress and Inflammation in Human Umbilical Vein Endothelial Cells. *Chemosphere* **2017**, *168*, 25–31.
296. Luo, K. W.; Wei Chen; Lung, W. Y.; Wei, X. Y.; Cheng, B. H.; et al. EGCG Inhibited Bladder Cancer SW780 Cell Proliferation and Migration Both in Vitro and in Vivo via Down-Regulation of NF-KB and MMP-9. *J. Nutr. Biochem.* **2017**, *41*, 56–64.
297. Luo, K. W.; Lung, W. Y.; Chun-Xie; Luo, X. Le; Huang, W. R. EGCG Inhibited Bladder Cancer T24 and 5637 Cell Proliferation and Migration via PI3K/AKT Pathway. *Oncotarget* **2018**, *9* (15), 12261–12272.
298. Zhang, Y.; Han, G.; Fan, B.; Zhou, Y.; Zhou, X.; et al. Green Tea (-)-Epigallocatechin-3-Gallate down-Regulates VASP Expression and Inhibits Breast Cancer Cell Migration and Invasion by Attenuating Rac1 Activity. *Eur. J. Pharmacol.* **2009**, *606* (1–3), 172–179.

299. Yamakawa, S.; Asai, T.; Uchida, T.; Matsukawa, M.; Akizawa, T.; et al. (-)-Epigallocatechin Gallate Inhibits Membrane-Type 1 Matrix Metalloproteinase, MT1-MMP, and Tumor Angiogenesis. *Cancer Lett.* **2004**, *210* (1), 47–55.
300. Tudoran, O.; Soritau, O.; Balacescu, O.; Balacescu, L.; Braicu, C.; et al. Early Transcriptional Pattern of Angiogenesis Induced by EGCG Treatment in Cervical Tumour Cells. *J. Cell. Mol. Med.* **2012**, *16* (3), 520–530.
301. Annabi, B.; Lachambre, M. P.; Bousquet-Gagnon, N.; Pageé, M.; Gingras, D.; et al. Green Tea Polyphenol (-)-Epigallocatechin 3-Gallate Inhibits MMP-2 Secretion and MT1-MMP-Driven Migration in Glioblastoma Cells. *Biochim. Biophys. Acta - Mol. Cell Res.* **2002**, *1542* (1–3), 209–220.
302. Li, H.; Li, Z.; Xu, Y. M.; Wu, Y.; Yu, K. K.; et al. Epigallocatechin-3-Gallate Induces Apoptosis, Inhibits Proliferation and Decreases Invasion of Glioma Cell. *Neurosci. Bull.* **2014**, *30* (1), 67–73.
303. Zhen, M. C.; Huang, X. H.; Wang, Q.; Sun, K.; Liu, Y. J.; et al. Green Tea Polyphenol Epigallocatechin-3-Gallate Suppresses Rat Hepatic Stellate Cell Invasion by Inhibition of MMP-2 Expression and Its Activation. *Acta Pharmacol. Sin.* **2006**, *27* (12), 1600–1607.
304. Fassina, G.; Venè, R.; Morini, M.; Minghelli, S.; Benelli, R.; et al. Mechanisms of Inhibition of Tumor Angiogenesis and Vascular Tumor Growth by Epigallocatechin-3-Gallate. *Clin. Cancer Res.* **2004**, *10* (14), 4865–4873.
305. Li, X.; Feng, Y.; Liu, J.; Feng, X.; Zhou, K.; et al. Epigallocatechin-3-Gallate Inhibits IGF-I-Stimulated Lung Cancer Angiogenesis through Downregulation of HIF-1 α and VEGF Expression. *lifestyle Genomics* **2013**, *6* (3), 169–178.
306. Shi, J.; Liu, F.; Zhang, W.; Liu, X.; Lin, B.; et al. Epigallocatechin-3-Gallate Inhibits Nicotine-Induced Migration and Invasion by the Suppression of Angiogenesis and Epithelial-Mesenchymal Transition in Non-Small Cell Lung Cancer Cells. *Oncol. Rep.* **2015**, *33* (6), 2972–2980.
307. Deng, Y. T.; Lin, J. K. EGCG Inhibits the Invasion of Highly Invasive CL1-5 Lung Cancer Cells through Suppressing MMP-2 Expression via JNK Signaling and Induces G2/M Arrest. *J. Agric. Food Chem.* **2011**, *59* (24), 13318–13327.
308. Pilorget, A.; Berthet, V.; Luis, J.; Moghrabi, A.; Annabi, B.; et al. Medulloblastoma Cell Invasion Is Inhibited by Green Tea (-)Epigallocatechin-3-Gallate. *J. Cell. Biochem.* **2003**, *90* (4), 745–755.

309. Ohga, N.; Hida, K.; Hida, Y.; Muraki, C.; Tsuchiya, K.; et al. Inhibitory Effects of Epigallocatechin-3 Gallate, a Polyphenol in Green Tea, on Tumor-Associated Endothelial Cells and Endothelial Progenitor Cells. *Cancer Sci.* **2009**, *100* (10), 1963–1970.
310. Lin, C. H.; Shen, Y. A.; Hung, P. H.; Yu, Y. Bin; Chen, Y. J. Epigallocatechin Gallate, Polyphenol Present in Green Tea, Inhibits Stem-like Characteristics and Epithelial-Mesenchymal Transition in Nasopharyngeal Cancer Cell Lines. *BMC Complement. Altern. Med.* **2012**, *12* (1), 1.
311. Fang, C. Y.; Wu, C. C.; Hsu, H. Y.; Chuang, H. Y.; Huang, S. Y.; et al. EGCG Inhibits Proliferation, Invasiveness and Tumor Growth by up-Regulation of Adhesion Molecules, Suppression of Gelatinases Activity, and Induction of Apoptosis in Nasopharyngeal Carcinoma Cells. *Int. J. Mol. Sci.* **2015**, *16* (2), 2530–2558.
312. Lin, C. H.; Wang, H. H.; Chen, T. H.; Chiang, M. C.; Hung, P. H.; et al. Involvement of MicroRNA-296 in the Inhibitory Effect of Epigallocatechin Gallate against the Migratory Properties of Anoikis-Resistant Nasopharyngeal Carcinoma Cells. *Cancers (Basel)*. **2020**, *12* (4), 973.
313. Hossain, M. M.; Banik, N. L.; Ray, S. K. Survivin Knockdown Increased Anti-Cancer Effects of (-)-Epigallocatechin-3-Gallate in Human Malignant Neuroblastoma SK-N-BE2 and SH-SY5Y Cells. *Exp. Cell Res.* **2012**, *318* (13), 1597–1610.
314. Garbisa, S.; Sartor, L.; Biggin, S.; Salvato, B.; Benelli, R.; et al. Tumor Gelatinases and Invasion Inhibited by the Green Tea Flavanol Epigallocatechin-3-Gallate. *Cancer* **2001**, *91* (4), 822–832.
315. Ho, Y. C.; Yang, S. F.; Peng, C. Y.; Chou, M. Y.; Chang, Y. C. Epigallocatechin-3-Gallate Inhibits the Invasion of Human Oral Cancer Cells and Decreases the Productions of Matrix Metalloproteinases and Urokinase-Plasminogen Activator. *J. Oral Pathol. Med.* **2007**, *36* (10), 588–593.
316. Chen, P. N.; Chu, S. C.; Kuo, W. H.; Chou, M. Y.; Lin, J. K.; et al. Epigallocatechin-3 Gallate Inhibits Invasion, Epithelial-Mesenchymal Transition, and Tumor Growth in Oral Cancer Cells. *J. Agric. Food Chem.* **2011**, *59* (8), 3836–3844.
317. Kawabata, T.; Otsuka, T.; Fujita, K.; Sakai, G.; Matsushima-Nishiwaki, R.; et al. (-)-Epigallocatechin Gallate but Not Chlorogenic Acid Suppresses EGF-Stimulated Migration of Osteoblasts via Attenuation of P38 MAPK Activity. *Int. J.*

Mol. Med. **2018**, *42* (6), 3149–3156.

318. Kawabata, T.; Tokuda, H.; Sakai, G.; Fujita, K.; Matsushima-Nishiwaki, R.; et al. Repression of IGF-I-Induced Osteoblast Migration by (-)-Epigallocatechin Gallate through P44/P42 MAP Kinase Signaling. *Biomed. Reports* **2018**, *9* (4), 318–326.
319. Spinella, F.; Rosanò, L.; Di Castro, V.; Decandia, S.; Albini, A.; et al. Green Tea Polyphenol Epigallocatechin-3-Gallate Inhibits the Endothelin Axis and Downstream Signaling Pathways in Ovarian Carcinoma. *Mol. Cancer Ther.* **2006**, *5* (6), 1483–1492.
320. Masamune, A.; Kikuta, K.; Satoh, M.; Suzuki, N.; Shimosegawa, T. Green Tea Polyphenol Epigallocatechin-3-Gallate Blocks PDGF-Induced Proliferation and Migration of Rat Pancreatic Stellate Cells. *World J. Gastroenterol.* **2005**, *11* (22), 3368–3374.
321. Duhon, D.; Bigelow, R. L. H.; Coleman, D. T.; Steffan, J. J.; Yu, C.; et al. The Polyphenol Epigallocatechin-3-Gallate Affects Lipid Rafts to Block Activation of the c-Met Receptor in Prostate Cancer Cells. *Mol. Carcinog.* **2010**, *49* (8), 739–749.
322. Chan, C. M.; Huang, J. H.; Chiang, H. S.; Wu, W. Bin; Lin, H. H.; et al. Effects of (-)-Epigallocatechin Gallate on Rpe Cell Migration and Adhesion. *Mol. Vis.* **2010**, *16* (510), 586–595.
323. Lee, H. S.; Jun, J. H.; Jung, E. H.; Koo, B. A.; Kim, Y. S. Epigallocatechin-3-Gallate Inhibits Ocular Neovascularization and Vascular Permeability in Human Retinal Pigment Epithelial and Human Retinal Microvascular Endothelial Cells via Suppression of MMP-9 and VEGF Activation. *Molecules* **2014**, *19* (8), 12150–12172.
324. Appleton, K. J. M. I. Epicatechin Gallate Improves Healing and Reduces Scar Formation of Incisional Wounds in Type 2 Diabetes Mellitus Rat Model. *Wounds* **2012**, *24* (3), 55–57.
325. Huang, S. F.; Horng, C. T.; Hsieh, Y. S.; Hsieh, Y. H.; Chu, S. C.; et al. Epicatechin-3-Gallate Reverses TGF-B1-Induced Epithelial-to-Mesenchymal Transition and Inhibits Cell Invasion and Protease Activities in Human Lung Cancer Cells. *Food Chem. Toxicol.* **2016**, *94*, 1–10.

326. Jiang, C.; Agarwal, R.; Lü, J. Anti-Angiogenic Potential of a Cancer Chemopreventive Flavonoid Antioxidant, Silymarin: Inhibition of Key Attributes of Vascular Endothelial Cells and Angiogenic Cytokine Secretion by Cancer Epithelial Cells. *Biochem. Biophys. Res. Commun.* **2000**, *276* (1), 371–378.
327. Ting, H.; Deep, G.; Agarwal, R. Molecular Mechanisms of Silibinin-Mediated Cancer Chemoprevention with Major Emphasis on Prostate Cancer. *AAPS J.* **2013**, *15* (3), 707–716.
328. Wu, K.; Ning, Z.; Zeng, J.; Fan, J.; Zhou, J.; et al. Silibinin Inhibits β -Catenin/ZEB1 Signaling and Suppresses Bladder Cancer Metastasis via Dual-Blocking Epithelial-Mesenchymal Transition and Stemness. *Cell. Signal.* **2013**, *25* (12), 2625–2633.
329. Li, F.; Sun, Y.; Jia, J.; Yang, C.; Tang, X.; et al. Silibinin Attenuates TGF- β 1-Induced Migration and Invasion via EMT Suppression and Is Associated with COX-2 Downregulation in Bladder Transitional Cell Carcinoma. *Oncol. Rep.* **2018**, *40* (6), 3543–3550.
330. Dastpeyman, M.; Motamed, N.; Azadmanesh, K.; Mostafavi, E.; Kia, V.; et al. Inhibition of Silibinin on Migration and Adhesion Capacity of Human Highly Metastatic Breast Cancer Cell Line, MDA-MB-231, by Evaluation of B1-Integrin and Downstream Molecules, Cdc42, Raf-1 and D4GDI. *Med. Oncol.* **2012**, *29* (4), 2512–2518.
331. Byun, H. J.; Darvin, P.; Kang, D. Y.; Sp, N.; Joung, Y. H.; et al. Silibinin Downregulates MMP2 Expression via Jak2/STAT3 Pathway and Inhibits the Migration and Invasive Potential in MDA-MB-231 Cells. *Oncol. Rep.* **2017**, *37* (6), 3270–3278.
332. Lin, C. M.; Chen, Y. H.; Ma, H. P.; Wang, B. W.; Chiu, J. H.; et al. Silibinin Inhibits the Invasion of IL-6-Stimulated Colon Cancer Cells via Selective JNK/AP-1/MMP-2 Modulation in Vitro. *J. Agric. Food Chem.* **2012**, *60* (51), 12451–12457.
333. Kim, K. W.; Choi, C. H.; Kim, T. H.; Kwon, C. H.; Woo, J. S.; et al. Silibinin Inhibits Glioma Cell Proliferation via Ca²⁺/Ros/Mapk- Dependent Mechanism in Vitro and Glioma Tumor Growth in Vivo. *Neurochem. Res.* **2009**, *34* (8), 1479–1490.
334. Deep, G.; Kumar, R.; Jain, A. K.; Agarwal, C.; Agarwal, R. Silibinin Inhibits Fibronectin Induced Motility, Invasiveness and Survival in Human Prostate Carcinoma PC3 Cells via Targeting Integrin Signaling. *Mutat. Res.* -

Fundam. Mol. Mech. Mutagen. **2014**, 768 (C), 35–46.

335. Deep, G.; Kumar, R.; Nambiar, D. K.; Jain, A. K.; Ramteke, A. M.; et al. Silibinin Inhibits Hypoxia-Induced HIF-1 α -Mediated Signaling, Angiogenesis and Lipogenesis in Prostate Cancer Cells: In Vitro Evidence and in Vivo Functional Imaging and Metabolomics. *Mol. Carcinog.* **2017**, 56 (3), 833–848.
336. Mokhtari, M. J.; Motamed, N.; Shokrgozar, M. A. Evaluation of Silibinin on the Viability, Migration and Adhesion of the Human Prostate Adenocarcinoma (PC-3) Cell Line. *Cell Biol. Int.* **2008**, 32 (8), 888–892.
337. Liang, L.; Li, L.; Zeng, J.; Gao, Y.; Chen, Y. Le; et al. Inhibitory Effect of Silibinin on EGFR Signal-Induced Renal Cell Carcinoma Progression via Suppression of the EGFR/MMP-9 Signaling Pathway. *Oncol. Rep.* **2012**, 28 (3), 999–1005.
338. Lin, C. H.; Li, C. H.; Liao, P. L.; Tse, L. S.; Huang, W. K.; et al. Silibinin Inhibits VEGF Secretion and Age-Related Macular Degeneration in a Hypoxia-Dependent Manner through the PI-3 Kinase/Akt/MTOR Pathway. *Br. J. Pharmacol.* **2013**, 168 (4), 920–931.
339. Chen, X.; Gu, N.; Xue, C.; Li, B. R. Plant Flavonoid Taxifolin Inhibits the Growth, Migration and Invasion of Human Osteosarcoma Cells. *Mol. Med. Rep.* **2018**, 17 (2), 3239–3245.
340. Maués, L. A. L.; Alves, G. M.; Couto, N. M. G.; da Silva, B. J. M.; Arruda, M. S. P.; et al. Flavonoids from the Amazon Plant *Brosimum Acutifolium* Induce C6 Glioma Cell Line Apoptosis by Disrupting Mitochondrial Membrane Potential and Reducing AKT Phosphorylation. *Biomed. Pharmacother.* **2019**, 113, 108728.
341. Gao, M.; Chang, Y.; Wang, X.; Ban, C.; Zhang, F. Reduction of COX-2 through Modulating MiR-124/ SPHK1 Axis Contributes to the Antimetastatic Effect of Alpinumisoflavone in Melanoma. *Am. J. Transl. Res.* **2017**, 9 (3), 986–998.
342. Wang, Y.; Li, J. J.; Chen, Y. M. Biochanin A Extirpates the Epithelial-Mesenchymal Transition in a Human Lung Cancer. *Exp. Ther. Med.* **2018**, 15 (3), 2830–2836.
343. Chen, C. Y.; Chen, C. C.; Shieh, T. M.; Hsueh, C.; Wang, S. H.; et al. Corylin Suppresses Hepatocellular Carcinoma Progression via the Inhibition of Epithelial-Mesenchymal Transition, Mediated by Long Noncoding RNA GAS5. *Int.*

J. Mol. Sci. **2018**, *19* (2), 1–13.

344. Sophors, P.; Kim, Y. M.; Seo, G. Y.; Huh, J. S.; Lim, Y.; et al. A Synthetic Isoflavone, DCMF, Promotes Human Keratinocyte Migration by Activating Src/FAK Signaling Pathway. *Biochem. Biophys. Res. Commun.* **2016**, *472* (2), 332–338.
345. Zhao, J.; Xu, J.; Lv, J. Identification of Profilin 1 as the Primary Target for the Anti-Cancer Activities of Furowanin A in Colorectal Cancer. *Pharmacol. Reports* **2019**, *71* (5), 940–949.
346. Pavese, J. M.; Farmer, R. L.; Bergan, R. C. Inhibition of Cancer Cell Invasion and Metastasis by Genistein. *Cancer Metastasis Rev.* **2010**, *29* (3), 465–482.
347. Shao, Z.; Wu, J.; Shen, Z. Genistein Exerts Multiple Suppressive Effects on Human Breast Carcinoma Cells. *Zhonghua Zhong Liu Za Zhi* **2000**, *22* (5), 362–365.
348. Zhang, Q.; Bao, J.; Yang, J. Genistein-Triggered Anticancer Activity against Liver Cancer Cell Line HepG2 Involves ROS Generation, Mitochondrial Apoptosis, G2/M Cell Cycle Arrest and Inhibition of Cell Migration and Inhibition of Cell Migration. *Arch. Med. Sci.* **2019**, *15* (4), 1001–1009.
349. Panda, S. P.; Panigrahy, U. P.; Prasanth, D. S. N. B. K.; Gorla, U. S.; Guntupalli, C.; et al. A Trimethoxy Flavonoid Isolated from Stem Extract of *Tabebuia Chrysantha* Suppresses Angiogenesis in Angiosarcoma. *J. Pharm. Pharmacol.* **2020**, *72*, 990–999.
350. Bui, N. T.; Ho, M. T.; Kim, Y. M.; Lim, Y.; Cho, M. Flavonoids Promoting HaCaT Migration: II. Molecular Mechanism of 4',6,7-Trimethoxyisoflavone via NOX2 Activation. *Phytomedicine* **2014**, *21* (4), 570–577.
351. WANG, Y.; MA, W.; ZHENG, W. Deguelin, a Novel Anti-Tumorigenic Agent Targeting Apoptosis, Cell Cycle Arrest and Anti-Angiogenesis for Cancer Chemoprevention. *Mol. Clin. Oncol.* **2013**, *1* (2), 215–219.
352. Dell'Eva, R.; Minghelli, S.; Minghelli, S.; Noonan, D. M.; Albini, A.; et al. The Akt Inhibitor Deguelin, Is an Angiopreventive Agent Also Acting on the NF-KB Pathway. *Carcinogenesis* **2007**, *28* (2), 404–413.
353. Zheng, W.; Lu, S.; Cai, H.; Kang, M.; Qin, W.; et al. Deguelin Inhibits Proliferation and Migration of Human

- Pancreatic Cancer Cells in Vitro Targeting Hedgehog Pathway. *Oncol. Lett.* **2016**, *12* (4), 2761–2765.
354. Hsu, Y. L.; Wu, L. Y.; Hou, M. F.; Tsai, E. M.; Lee, J. N.; et al. Glabridin, an Isoflavan from Licorice Root, Inhibits Migration, Invasion and Angiogenesis of MDA-MB-231 Human Breast Adenocarcinoma Cells by Inhibiting Focal Adhesion Kinase/Rho Signaling Pathway. *Mol. Nutr. Food Res.* **2011**, *55* (2), 318–327.
355. Tsai, Y. M.; Yang, C. J.; Hsu, Y. L.; Wu, L. Y.; Tsai, Y. C.; et al. Glabridin Inhibits Migration, Invasion, and Angiogenesis of Human Non-Small Cell Lung Cancer A549 Cells by Inhibiting the FAK/Rho Signaling Pathway. *Integr. Cancer Ther.* **2011**, *10* (4), 341–349.
356. Nozomu Matsunaga, Kazuhiro Tsuruma, Masamitsu Shimazawa, Shigeru Yokota and Hara, H. Inhibitory Actions of Bilberry Anthocyanidins on Angiogenesis. *Phyther. Res.* **2010**, *24*, S42–S47.
357. Patel, K.; Jain, A.; Patel, D. K. Medicinal Significance, Pharmacological Activities, and Analytical Aspects of Anthocyanidins ‘Delphinidin’: A Concise Report. *J. Acute Dis.* **2013**, *2* (3), 169–178.
358. Lamy, S.; Blanchette, M.; Michaud-Levesque, J.; Lafleur, R.; Durocher, Y.; et al. Delphinidin, a Dietary Anthocyanidin, Inhibits Vascular Endothelial Growth Factor Receptor-2 Phosphorylation. *Carcinogenesis* **2006**, *27* (5), 989–996.
359. Favot, L.; Martin, S.; Keravis, T.; Andriantsitohaina, R.; Lugnier, C. Involvement of Cyclin-Dependent Pathway in the Inhibitory Effect of Delphinidin on Angiogenesis. *Cardiovasc. Res.* **2003**, *59* (2), 479–487.
360. Viegas, O.; Faria, M. A.; Sousa, J. B.; Vojtek, M.; Gonçalves-Monteiro, S.; et al. Delphinidin-3-O-Glucoside Inhibits Angiogenesis via VEGFR2 Downregulation and Migration through Actin Disruption. *J. Funct. Foods* **2019**, *54*, 393–402.
361. Huang, C. C.; Hung, C. H.; Hung, T. W.; Lin, Y. C.; Wang, C. J.; et al. Dietary Delphinidin Inhibits Human Colorectal Cancer Metastasis Associating with Upregulation of MiR-204-3p and Suppression of the Integrin/FAK Axis. *Sci. Rep.* **2019**, *9* (1), 1–11.
362. Kim, M. H.; Jeong, Y. J.; Cho, H. J.; Hoe, H. S.; Park, K. K.; et al. Delphinidin Inhibits Angiogenesis through the Suppression of HIF-1 α and VEGF Expression in A549 Lung Cancer Cells. *Oncol. Rep.* **2017**, *37* (2), 777–784.

363. Kang, H. M.; Park, B. S.; Kang, H. K.; Park, H. R.; Yu, S. Bin; et al. Delphinidin Induces Apoptosis and Inhibits Epithelial-to-Mesenchymal Transition via the ERK/P38 MAPK-Signaling Pathway in Human Osteosarcoma Cell Lines. *Environ. Toxicol.* **2018**, 33 (6), 640–649.
364. Morbidelli, L. Polyphenol-Based Nutraceuticals for the Control of Angiogenesis: Analysis of the Critical Issues for Human Use. *Pharmacol. Res.* **2016**, 111, 384–393.
365. Mirossay, L.; Varinská, L.; Mojžiš, J. Antiangiogenic Effect of Flavonoids and Chalcones: An Update. *Int. J. Mol. Sci.* **2018**, 19 (1), 27.
366. Dulak, J. Nutraceuticals as Anti-Angiogenic Agents: Hopes and Reality. *J. Physiol. Pharmacol.* **2005**, 56 (1), 51–67.
367. Diniz, C.; Suliburska, J.; Ferreira, I. M. New Insights into the Antiangiogenic and Proangiogenic Properties of Dietary Polyphenols. *Mol. Nutr. Food Res.* **2017**, 61 (6), 1–17.
368. Kapinova, A.; Stefanicka, P.; Kubatka, P.; Zubor, P.; Uramova, S.; et al. Are Plant-Based Functional Foods Better Choice against Cancer than Single Phytochemicals? A Critical Review of Current Breast Cancer Research. *Biomed. Pharmacother.* **2017**, 96, 1465–1477.
369. Mojzis, J.; Varinska, L.; Mojzisova, G.; Kostova, I.; Mirossay, L. Antiangiogenic Effects of Flavonoids and Chalcones. *Pharmacol. Res.* **2008**, 57 (4), 259–265.
370. Ravishankar, D.; Rajora, A. K.; Greco, F.; Osborn, H. M. I. Flavonoids as Prospective Compounds for Anti-Cancer Therapy. *Int. J. Biochem. Cell Biol.* **2013**, 45 (12), 2821–2831.
371. Cao, Y.; Cao, R.; Bråkenhielm, E. Antiangiogenic Mechanisms of Diet-Derived Polyphenols. *J. Nutr. Biochem.* **2002**, 13 (7), 380–390.
372. Le Marchand, L. Cancer Preventive Effects of Flavonoids - A Review. *Biomed. Pharmacother.* **2002**, 56 (6), 296–301.
373. Nandakumar, V.; Singh, T.; Katiyar, S. K. Multi-Targeted Prevention and Therapy of Cancer by Proanthocyanidins. *Cancer Lett.* **2008**, 269 (2), 378–387.

374. Martin, M. A.; Goya, L.; Ramos, S. Potential for Preventive Effects of Cocoa and Cocoa Polyphenols in Cancer. *Food Chem. Toxicol.* **2013**, *56*, 336–351.
375. Zhang, J. P.; Tian, X. H.; Yang, Y. X.; Liu, Q. X.; Wang, Q.; et al. Gleditsia Species: An Ethnomedical, Phytochemical and Pharmacological Review. *J. Ethnopharmacol.* **2016**, *178*, 155–171.
376. Mirza-Aghazadeh-Attari, M.; Ekrami, E. M.; Aghdas, S. A. M.; Mihanfar, A.; Hallaj, S.; et al. Targeting PI3K/Akt/MTOR Signaling Pathway by Polyphenols: Implication for Cancer Therapy. *Life Sci.* **2020**, 117481.
377. Kang, N. J.; Shin, S. H.; Lee, H. J.; Lee, K. W. Polyphenols as Small Molecular Inhibitors of Signaling Cascades in Carcinogenesis. *Pharmacol. Ther.* **2011**, *130* (3), 310–324.
378. Hussain, S. S.; Kumar, A. P.; Ghosh, R. Food-Based Natural Products for Cancer Management: Is the Whole Greater than the Sum of the Parts? *Semin. Cancer Biol.* **2016**, *40*, 233–246.
379. Lewandowska, H.; Kalinowska, M.; Lewandowski, W.; Stepkowski, T. M.; Brzóška, K. The Role of Natural Polyphenols in Cell Signaling and Cytoprotection against Cancer Development. *J. Nutr. Biochem.* **2016**, *32*, 1–19.
380. Lai, C. S.; Pan, M. H. Mechanism for Possible Chemopreventive Effects of Natural Dietary Compounds on Smoking-Induced Tumorigenesis. *J. Exp. Clin. Med.* **2011**, *3* (6), 262–271.
381. Kanadaswami, C.; Lee, L. T.; Lee, P. P. H.; Hwang, J. J.; Ke, F. C.; et al. The Antitumor Activities of Flavonoids. *In Vivo (Brooklyn)*. **2005**, *19* (5), 895–910.
382. Stoner, G. D.; Wang, L. S.; Casto, B. C. Laboratory and Clinical Studies of Cancer Chemoprevention by Antioxidants in Berries. *Carcinogenesis* **2008**, *29* (9), 1665–1674.
383. Kaur, J.; Kaur, G. An Insight into the Role of Citrus Bioactives in Modulation of Colon Cancer. *J. Funct. Foods* **2015**, *13*, 239–261.
384. Araújo, J. R.; Gonçalves, P.; Martel, F. Chemopreventive Effect of Dietary Polyphenols in Colorectal Cancer Cell Lines. *Nutr. Res.* **2011**, *31* (2), 77–87.

385. Xu, Z.; Sun, T.; Li, W.; Sun, X. Inhibiting Effects of Dietary Polyphenols on Chronic Eye Diseases. *J. Funct. Foods* **2017**, *39*, 186–197.
386. Stagos, D.; Amoutzias, G. D.; Matakos, A.; Spyrou, A.; Tsatsakis, A. M.; et al. Chemoprevention of Liver Cancer by Plant Polyphenols. *Food Chem. Toxicol.* **2012**, *50* (6), 2155–2170.
387. García, E. R.; Gutierrez, E. A.; Melo, F. C. S. A. De; Novaes, R. D.; Gonçalves, R. V. Flavonoids Effects on Hepatocellular Carcinoma in Murine Models: A Systematic Review. *Evidence-based Complement. Altern. Med.* **2018**, *2018*.
388. Pojero, F.; Poma, P.; Spanò, V.; Montalbano, A.; Barraja, P.; et al. Targeting Multiple Myeloma with Natural Polyphenols. *Eur. J. Med. Chem.* **2019**, *180*, 465–485.
389. Sulaiman, R. S.; Basavarajappa, H. D.; Corson, T. W. Natural Product Inhibitors of Ocular Angiogenesis. *Exp. Eye Res.* **2014**, *129*, 161–171.
390. Rajesh, G.; Harshala, S.; Dhananjay, G.; Jadhav, A.; Vikram, G. Effect of Hydroxyl Substitution of Flavone on Angiogenesis and Free Radical Scavenging Activities: A Structure-Activity Relationship Studies Using Computational Tools. *Eur. J. Pharm. Sci.* **2010**, *39* (1–3), 37–44.
391. Lam, I. K.; Alex, D.; Wang, Y. H.; Liu, P.; Liu, A. L.; et al. In Vitro and in Vivo Structure and Activity Relationship Analysis of Polymethoxylated Flavonoids: Identifying Sinensetin as a Novel Antiangiogenesis Agent. *Mol. Nutr. Food Res.* **2012**, *56* (6), 945–956.
392. Fotsis, T.; Pepper, M. S.; Aktas, E.; Breit, S.; Rasku, S.; et al. Flavonoids, Dietary-Derived Inhibitors of Cell Proliferation and in Vitro Angiogenesis. *Cancer Res.* **1997**, *57* (14), 2916–2921.
393. Suktap, C.; Lee, H. K.; Amnuaypol, S.; Suttisri, R.; Sukrong, S. Wound Healing Effect of Flavonoid Glycosides from *Afgekia Mahidolae* B.L.Burt & Chermisr. Leaves. *Rec. Nat. Prod.* **2018**, *12* (4), 391–396.
394. Gacche, R. N.; Meshram, R. J.; Shegokar, H. D.; Gond, D. S.; Kamble, S. S.; et al. Flavonoids as a Scaffold for Development of Novel Anti-Angiogenic Agents: An Experimental and Computational Enquiry. *Arch. Biochem. Biophys.* **2015**, *577*, 35–48.

395. Zhang, J.; Wu, Y.; Zhao, X.; Luo, F.; Li, X.; et al. Chemopreventive Effect of Flavonoids from Ougan (Citrus Reticulata Cv. Suavissima) Fruit against Cancer Cell Proliferation and Migration. *J. Funct. Foods* **2014**, *10*, 511–519.
396. Gacche, R. N.; Shegokar, H. D.; Gond, D. S.; Yang, Z.; Jadhav, A. D. Evaluation of Selected Flavonoids as Antiangiogenic, Anticancer, and Radical Scavenging Agents: An Experimental and In Silico Analysis. *Cell Biochem. Biophys.* **2011**, *61* (3), 651–663.
397. Santos, B. L.; Oliveira, M. N.; Coelho, P. L. C.; Pitanga, B. P. S.; Da Silva, A. B.; et al. Flavonoids Suppress Human Glioblastoma Cell Growth by Inhibiting Cell Metabolism, Migration, and by Regulating Extracellular Matrix Proteins and Metalloproteinases Expression. *Chem. Biol. Interact.* **2015**, *242*, 123–138.
398. Ouanouki, A.; Lamy, S.; Annabi, B. Anthocyanidins Inhibit Epithelial–Mesenchymal Transition through a TGF β /Smad2 Signaling Pathway in Glioblastoma Cells. *Mol. Carcinog.* **2017**, *56* (3), 1088–1099.
399. Li, N.; Zhang, P.; Wu, H.; Wang, J.; Liu, F.; et al. Natural Flavonoids Function as Chemopreventive Agents from Gancao (Glycyrrhiza Inflata Batal). *J. Funct. Foods* **2015**, *19*, 563–574.
400. Wang, C. G.; Yao, W. N.; Zhang, B.; Hua, J.; Liang, D.; et al. Lung Cancer and Matrix Metalloproteinases Inhibitors of Polyphenols from Selaginella Tamariscina with Suppression Activity of Migration. *Bioorganic Med. Chem. Lett.* **2018**, *28* (14), 2413–2417.
401. Hsiao, Y. C.; Kuo, W. H.; Chen, P. N.; Chang, H. R.; Lin, T. H.; et al. Flavanone and 2'-OH Flavanone Inhibit Metastasis of Lung Cancer Cells via down-Regulation of Proteinases Activities and MAPK Pathway. *Chem. Biol. Interact.* **2007**, *167* (3), 193–206.
402. Huang, Y.; Fang, J.; Lu, W.; Wang, Z.; Wang, Q.; et al. A Systems Pharmacology Approach Uncovers Wogonoside as an Angiogenesis Inhibitor of Triple-Negative Breast Cancer by Targeting Hedgehog Signaling. *Cell Chem. Biol.* **2019**, *26* (8), 1143–1158.
403. Lin, C. M.; Chang, H.; Chen, Y. H.; Wu, I. H.; Chiu, J. H. Wogonin Inhibits IL-6-Induced Angiogenesis via down-Regulation of VEGF and VEGFR-1, Not VEGFR-2. *Planta Med.* **2006**, *72* (14), 1305–1310.

404. Zhu, D.; Wang, S.; Lawless, J.; He, J.; Zheng, Z. Dose Dependent Dual Effect of Baicalin and Herb Huang Qin Extract on Angiogenesis. *PLoS One* **2016**, *11* (11), 1–18.
405. Peña, M.; Mesas, C.; Perazzoli, G.; Martínez, R.; Porres, J. M.; et al. Antiproliferative, Antioxidant, Chemopreventive and Antiangiogenic Potential of Chromatographic Fractions from *Anemonia Sulcata* with and without Its Symbiont *Symbiodinium* in Colorectal Cancer Therapy. *Int. J. Mol. Sci.* **2023**, *24* (14), 11249.
406. Chidambara Murthy, K. N.; Kim, J.; Vikram, A.; Patil, B. S. Differential Inhibition of Human Colon Cancer Cells by Structurally Similar Flavonoids of Citrus. *Food Chem.* **2012**, *132* (1), 27–34.
407. Chang, H.; Mi, M.; Ling, W.; Zhu, J.; Zhang, Q.; et al. Structurally Related Cytotoxic Effects of Flavonoids on Human Cancer Cells in Vitro. *Arch. Pharm. Res.* **2008**, *31* (9), 1137–1144.
408. Yun, B. H.; Lee, Y. H.; Park, K. T.; Jung, S. J.; Lee, Y. S. Synthesis of Novel Flavone Derivatives Possessing Substituted Benzamides and Their Biological Evaluation against Human Cancer Cells. *Bioorg. Med. Chem. Lett.* **2016**, *26* (17), 4170–4173.
409. Plochmann, K.; Korte, G.; Koutsilieris, E.; Richling, E.; Riederer, P.; et al. Structure–Activity Relationships of Flavonoid-Induced Cytotoxicity on Human Leukemia Cells. *Arch. Biochem. Biophys.* **2007**, *460* (1), 1–9.
410. Li, N.; Liu, J. H.; Zhang, J.; Yu, B. Y. Comparative Evaluation of Cytotoxicity and Antioxidative Activity of 20 Flavonoids. *J. Agric. Food Chem.* **2008**, *56* (10), 3876–3883.
411. Ravishankar, D.; Watson, K. A.; Greco, F.; Osborn, H. M. I. Novel Synthesised Flavone Derivatives Provide Significant Insight into the Structural Features Required for Enhanced Anti-Proliferative Activity. *RSC Adv.* **2016**, *6* (69), 64544–64556.
412. Bose, S.; Sarkar, D.; Bose, A.; Subhash, & Mandal, C. Natural Flavonoids and Its Pharmaceutical Importance. *pharma Rev.* **2018**, *94*, 61–75.
413. Singh, M.; Kaur, M.; Silakari, O. Flavones: An Important Scaffold for Medicinal Chemistry. *Eur. J. Med. Chem.* **2014**, *84*, 206–239.

414. LopezLazaro, M. Flavonoids as Anticancer Agents: Structure-Activity Relationship Study. *Curr. Med. Chem. - Anti-Cancer Agents* **2002**, 2 (6), 691–714.
415. Wang, T. yang; Li, Q.; Bi, K. shun. Bioactive Flavonoids in Medicinal Plants: Structure, Activity and Biological Fate. *Asian J. Pharm. Sci.* **2018**, 13 (1), 12–23.

Appendix B

Khater, M.; Ravishankar, D.; Greco, F.; Osborn, H. M. I. Metal Complexes of Flavonoids: Their Synthesis, Characterization and Enhanced Antioxidant and Anticancer Activities. *Future Med. Chem.* **2019**, *11* (21), 2845–2867.

<https://doi.org/10.4155/fmc-2019-0237>